

The persistence of rapid exhumation in the eastern Himalayan syntaxis

Karl A. Lang

A dissertation

Submitted in partial fulfillment of the
Requirements for the degree of

Doctor of Philosophy

University of Washington

2014

Reading Committee:

Katharine W. Huntington, Chair

David R. Montgomery

Bernard Hallet

Program Authorized to Offer Degree:

Earth and Space Sciences

©Copyright 2014

Karl A. Lang

University of Washington

Abstract

The persistence of rapid exhumation in the eastern Himalayan syntaxis

Karl A. Lang

Chair of the Supervisory Committee:

Assistant Professor Katharine W. Huntington

Department of Earth and Space Sciences

At the eastern margin of the Indian-Eurasian plate collision, margin-normal plate convergence transitions to dextral strike-slip motion, warping tectonic units southward to form the eastern Himalayan syntaxis. Large southeast Asian rivers (e.g., the Yangtze, Salween and Mekong rivers) closely following the periphery of this syntaxis reflect the accumulation of crustal strain from the ongoing collision. In contrast, the Yarlung-Siang-Brahmaputra River bisects the syntaxis, abruptly dropping over two kilometers from the Tibetan Plateau through the steep Tsangpo Gorge. Along this reach, surface erosion rates increase sharply, contributing nearly half of the erosional efflux to the foreland from only ~3% of the river's drainage area. Curiously, this intense erosion directly coincides with the Namche Barwa metamorphic massif, a crustal-scale antiform that has been rapidly exhumed in the Late Pliocene and Pleistocene.

Thermo-mechanical modeling indicates that if erosion has remained focused in this area over a multi-million year timescale, the continuous removal of upper crustal material

may have resulted in the local exhumation of a crustal-scale structure. This consequential rock uplift would have maintained a steep topographic gradient at the southeastern margin of the Tibetan Plateau, such that the high relief and elevated erosional fluxes observed today may in fact have persisted for many millions of years in the eastern Himalayan landscape. This idea presents an interesting concept in landscape evolution – that the legacy of processes shaping the surface of the Earth may extend much deeper to directly influence the dynamics of the Earth's crust.

This thesis specifically evaluates the circumstances by which rapid exhumation of the eastern syntaxis initiated and has been sustained in the Late Cenozoic. To do this, I extend the existing Late Pliocene and Pleistocene exhumation history by interpreting detrital evidence from syntaxis-proximal foreland basin deposits. First, I reconstruct continental-scale river drainage patterns from detrital analyses of foreland basin units, demonstrating a connection of the Yarlung-Siang-Brahmaputra River prior to the Middle or Early Miocene. Second, I document the potential of glacial ice and debris dam-burst flood events to exacerbate Quaternary erosion rates within this connected river system. Finally, I interpret the cooling histories of detrital minerals in the same foreland basin units to constrain the onset of rapid exhumation rates in the Late Miocene.

I conclude from this work that an antecedent river has locally sustained rapid exhumation of the eastern syntaxis since the Late Miocene. In the Late Miocene, localized tectonic uplift accelerated exhumation where an antecedent river crossed the southeastern Tibetan Plateau margin. By the Early Pliocene, thermo-mechanical feedbacks between surface erosion and rock uplift may have developed to sustain rapid exhumation rates at the plateau margin to the present day.

ACKNOWLEDGMENTS

There are many people without which this research would not exist. I will acknowledge and thank some here, but I am grateful for them all. Chiefly, I thank my thesis advisor: Dr. Katharine W. Huntington, as well as my thesis committee: Dr. David R. Montgomery and Dr. Bernard Hallet, for their guidance, patience and inspiration. Another point of inspiration has been the seminal work of the late Dr. Richard J. Stewart.

I also thank the institutions supporting my research, including: the Department of Earth and Space Sciences and Quaternary Research Center at the University of Washington, the Geological Society of America, the National Aeronautics and Space Administration, and the National Science Foundation. As well, I thank the many institutions with which I have collaborated on this work: the Indian National Fission-track laboratory at Kurukshetra University, LaserChron center at the University of Arizona, Noble Gas Geochronology and Geochemistry laboratory at Arizona State University, Western Washington University, and Apatite to Zircon, Inc.

Of course, I also thank the many colleagues who have helped me during the course of my study: Vikas Adlakha, Katy Atakturk, Katu Bage, Adam Barker, Sarah Bergman, Russ Burmister, Gabe Casale, Darrel Cowan, Ray Donelick, Alison Duvall, Nicky Giesler, Harvey Greenberg, Bernie Housen, Rachel Headley, Amanda Henck, Arvind Jain, Peter Kamp, Isaac Larsen, Graham Messe, Beth Novak, Paul O'Sullivan, Mark Pecha, Charles Plummer, Kristina Sumner, Oken Tayeng, Mike Turzewski, Jo-Anne Wartho, and the many, many wonderful graduate students at the University of Washington.

Finally, I thank my parents, who first introduced to me to the Earth.

for science

TABLE OF CONTENTS

CHAPTER 1. Introduction

- 1.0 Abstract
- 1.1 A take home message
- 1.2 Background
 - 1.2.1 Uplift, exhumation and erosion
 - 1.2.2 Landscape evolution
 - 1.2.3 Feedbacks in the Himalayan syntaxes
- 1.3 Research objectives
- 1.4 Motivation for study
 - 1.4.1 Interpretation of the sedimentary record
 - 1.4.2 Connection to global climate
- 1.5 Course of study
- 1.6 Presentation of results
- 1.7 References

CHAPTER 2. Antecedence of the Yarlung-Siang-Brahmaputra River, eastern Himalaya

- 2.0 Abstract
- 2.1 Introduction
- 2.2 Background
 - 2.2.1 Sedimentary units of the eastern Himalayan foreland basin
 - 2.2.2 Provenance constrains from detrital zircon U-Pb geochronology
 - 2.2.3 Previous constraints on Siwalik provenance in the eastern Himalaya
- 2.3 Sampling and analytical methods
- 2.4 Results of detrital zircon U-Pb dating and provenance interpretations
- 2.5 Discussion
 - 2.5.1 Antecedence of the Yarlung-Siang-Brahmaputra River
 - 2.5.2 Capture and reversal of the Parlung River
 - 2.5.3 Exhumation of the Namche Barwa massif
- 2.6 Conclusions
- 2.7 Acknowledgements
- 2.8 References
- 2.9 Figures
 - 2.9.1 Study area in the eastern Himalayan syntaxis
 - 2.9.2 Drainage evolution patterns
 - 2.9.3 Published bedrock and detrital geochronology
 - 2.9.4 New detrital geochronology of Siwalik units
 - 2.9.5 Proposed drainage evolution
- 2.10 Tables
 - 2.10.1 Detrital zircon (U-Th)/Pb analyses
 - 2.10.2 Compilation of bedrock geochronology
 - 2.10.3 Compilation of detrital geochronology
- 2.11 Appendix
 - 2.11.1 Analytical details

CHAPTER 3. Erosion of the Tsangpo Gorge by megafloods, eastern Himalaya

- 3.0 Abstract
- 3.1 Introduction
- 3.2 Methods
 - 3.2.1 Sampling
 - 3.2.2 U-Pb and petrographic analyses
 - 3.2.3 Synthetic CDF mixture modeling
 - 3.2.4 Estimating bed shear stress during peak discharges
- 3.3 Discussion
 - 3.3.1 Slackwater deposits
 - 3.3.2 Tsangpo Gorge erosion
 - 3.3.3 The role of megafloods
- 3.4 Acknowledgements
- 3.5 References
- 3.6 Figures
 - 3.6.1 Location map and river profile
 - 3.6.2 Detrital analyses
 - 3.6.3 Mixture modeling
 - 3.6.4 Shear stress calculations
- 3.7 Tables
 - 3.7.1 Detrital zircon U-Pb data
 - 3.7.2 Sample locations and new petrographic data
- 3.8 Appendix
 - 3.8.1 U-Pb analytical details
 - 3.8.2 Variables used in shear stress calculations

CHAPTER 4. Late Miocene exhumation of the Namche Barwa massif, eastern Himalaya

- 4.0 Abstract
- 4.1 Introduction
- 4.2 Background
 - 4.2.1 Tectonic and geomorphic setting of the eastern Himalayan syntaxis
 - 4.2.2 The easternmost Himalayan foreland basin
 - 4.2.2.1 Constraints on depositional age
 - 4.2.2.2 Constraints on sedimentary provenance
- 4.3 Methods
 - 4.3.1 Mapping and stratigraphic surveying
 - 4.3.2 Magnetostratigraphy
 - 4.3.3 Detrital thermochronology
 - 4.3.3.1 Muscovite $^{40}\text{Ar}/^{39}\text{Ar}$
 - 4.3.3.2 Zircon fission-track
- 4.4 Results
 - 4.4.1 Stratigraphy of the Siji River section
 - 4.4.1.1 Middle Siwalik
 - 4.4.1.2 Upper Siwalik
 - 4.4.1.3 Interpretation of depositional environment
 - 4.4.2 Structure of the Siji River region

- 4.4.3 Magnetostratigraphy
 - 4.4.3.1 New constraints on depositional age
- 4.4.4 Detrital thermochronology
 - 4.4.4.1 New $^{40}\text{Ar}/^{39}\text{Ar}$ analyses of river sediment
 - 4.4.4.1.1 Samples from Himalayan tributaries
 - 4.4.4.1.2 Samples from the Siang River
 - 4.4.4.2 New analyses of Siwalik units
 - 4.4.4.2.1 Coupled zircon fission track and U-Pb analyses
 - 4.4.4.2.2 Muscovite $^{40}\text{Ar}/^{39}\text{Ar}$ analyses
- 4.5 Discussion
 - 4.5.1 Interpretation of thermochronologic lag time
 - 4.5.1 Thermal modeling with PECUBE
 - 4.5.2 A mechanism to initiate rapid exhumation
 - 4.5.3 Lag time across the Himalaya
- 4.6 Summary and conclusions
- 4.7 Acknowledgments
- 4.8 References
- 4.9 Figures
 - 4.9.1 Study area in the eastern syntaxis and foreland basin
 - 4.9.2 Detailed geology of the Siji River area
 - 4.9.3 Upper and Middle Siwalik stratigraphy in the study area
 - 4.9.4 Magnetostratigraphy of lower Middle Siwalik exposures
 - 4.9.5 Detrital muscovite $^{40}\text{Ar}/^{39}\text{Ar}$ thermochronology of river sediment
 - 4.9.6 Detrital muscovite $^{40}\text{Ar}/^{39}\text{Ar}$ thermochronology of Siwalik units
 - 4.9.7 Coupled detrital zircon fission-track and U-Pb analyses of Siwalik units
 - 4.9.8 Correlation of the Siji River and Bhalukpong sections
 - 4.9.9 Thermochronologic lag time from Siwalik samples
 - 4.9.10 Quantitative constraints from thermal modeling
 - 4.9.11 Exhumation history of the Namche Barwa massif
 - 4.9.12 Compilation of Himalayan lag time data
- 4.10 Tables
 - 4.10.1 Sample data
 - 4.10.2 Magnetostartigraphy
 - 4.10.3 Detrital zircon fission track analyses
 - 4.10.4 Zircon fission track peak decomposition
 - 4.10.5 Detrital muscovite $^{40}\text{Ar}/^{39}\text{Ar}$ analyses
 - 4.10.6 Model parameters

CHAPTER 5. Conclusions

- 5.0 Summary and suggestions for future work
 - 5.0.1 Chapter 2
 - 5.0.2 Chapter 3
 - 5.0.3 Chapter 4
- 5.1 Synthesis of results
 - 5.1.1 Comparison across the Himalaya

5.2 Loose ends

5.3 A note on persistence

5.4 References

CHAPTER 1: Introduction

1.0 Abstract

At the eastern margin of the Indian-Eurasian plate collision, margin-normal plate convergence transitions to dextral strike-slip motion, warping tectonic units southward to form the eastern Himalayan syntaxis. Large southeast Asian rivers (e.g., the Yangtze, Salween and Mekong rivers) closely following the periphery of this syntaxis reflect the accumulation of crustal strain from the ongoing collision. In contrast, the Yarlung-Siang-Brahmaputra River bisects the syntaxis, abruptly dropping over two kilometers from the Tibetan Plateau through the steep Tsangpo Gorge. Along this reach, surface erosion rates increase sharply, contributing nearly half of the erosional efflux to the foreland from only ~3% of the river's drainage area. Curiously, this intense erosion directly coincides with the Namche Barwa metamorphic massif, a crustal-scale antiform that has been rapidly exhumed in the Late Pliocene and Pleistocene.

Thermo-mechanical modeling indicates that if erosion has remained focused in this area over a multi-million year timescale, the continuous removal of upper crustal material may have resulted in the local exhumation of a crustal-scale structure. This consequential rock uplift would have maintained a steep topographic gradient at the southeastern margin of the Tibetan Plateau, such that the high relief and elevated erosional fluxes observed today may in fact have persisted for many millions of years in the eastern Himalayan landscape. This idea presents an interesting concept in landscape evolution – that the legacy of processes shaping the surface of the Earth may extend much deeper to directly influence the dynamics of the Earth's crust.

This thesis specifically evaluates the circumstances by which rapid exhumation of

the eastern syntaxis initiated and has been sustained in the Late Cenozoic. To do this, I extend the existing Late Pliocene and Pleistocene exhumation history by interpreting detrital evidence from syntaxis-proximal foreland basin deposits. First, I reconstruct continental-scale river drainage patterns from detrital analyses of foreland basin units, demonstrating a connection of the Yarlung-Siang-Brahmaputra River prior to the Middle or Early Miocene. Second, I document the potential of glacial ice and debris dam-burst flood events to exacerbate Quaternary erosion rates within this connected river system. Finally, I interpret the cooling histories of detrital minerals in the same foreland basin units to constraining the onset of rapid exhumation rates in the Late Miocene.

I conclude from this work that an antecedent river has locally sustained rapid exhumation of the eastern syntaxis since the Late Miocene. In the Late Miocene, localized tectonic uplift accelerated exhumation where an antecedent river crossed the southeastern Tibetan Plateau margin. By the Early Pliocene, thermo-mechanical feedbacks between surface erosion and rock uplift may have developed to sustain rapid exhumation rates at the plateau margin to the present day.

1.1 A take home message

A wise advisor once told her student to begin their argument with the most important message, a single message the audience should take home with them, if nothing else. The message to take home from this thesis is that quite a lot can be learned about a landscape from the byproducts of its destruction, perhaps even more than can be gleaned from its present exposure. The landscape investigated herein, the eastern Himalayan syntaxis, is full of superlatives: mountains that are arguably as steep as they

can be (e.g., Larsen and Montgomery, 2012) beside one of Earth's deepest river gorges. The prodigious sediment evacuation resulting from the erosion of this landscape dominates the downstream sediment flux that feeds the great Brahmaputra River (e.g., Stewart et al., 2008) itself one of the largest contributors of terrestrial sediment to the global oceans (Milliman and Farnsworth, 2011).

This landscape is anomalous even in comparison to the broader Himalaya (Finlayson et al., 2002) the largest mountain range on Earth, and so it seems natural that it may have similarly anomalous origins. Current hypotheses invoke the taming of a large Tibetan torrent by a trifling Himalayan tributary (e.g., Clark et al., 2004), or of the rapid invasion of icy dams to steal a mighty river's bite (e.g., Korup and Montgomery, 2008). Yet, though the present landscape is not unfamiliar to catastrophe, the adjacent foreland contains a long history of dramatic change. I interpret this sedimentary record grain-by-grain, literally digging into the archives to unearth the secrets of this unique landscape.

1.2 Background

1.2.1 Uplift, exhumation and erosion

Terms referring to the displacement of earth materials with respect to a constant (perhaps conceptual) reference elevation should be precisely defined (England and Molnar, 1990). Within this text, rock or tectonic "uplift" is defined as the movement of crustal material in the opposite direction of gravity and rock "exhumation" is defined as the movement of crustal material toward the Earth's surface (England and Molar, 1990). Within this framework, a change in the elevation of the Earth's surface is simply the difference between rock uplift and rock exhumation.

Rock uplift is primarily accomplished within the Himalaya by tectonic processes of folding and reverse faulting, although isostatic compensation of eroded material is also important regional component (Montgomery, 1994). Rock exhumation results from normal faulting, ductile thinning within the lithosphere or surface erosion (Ring et al. 1999). Within this text, I consider only exhumation by surface erosion (primarily glacial, fluvial and hillslope erosion), which is considered to be the dominant process exhuming the region of interest (Zeitler et al., 2001) as evidence for significant normal displacement on local structures is atypical (Kidd et al., 2006; Zeitler et al., 2014).

1.2.2 Landscape evolution

Geologists have long looked to the mountains to understand the processes shaping Earth's surface. Early models of landscape evolution conceptualized a geomorphic cycle of periodic rejuvenation and decay (e.g., Davis, 1899; Penck, 1953) wherein landscapes originate from, and inevitably return to a low relief surface. Hack (1975) is often credited with formally introducing the concept of a dynamic equilibrium to discussions of landscape evolution (this could perhaps be better attributed to Gilbert, 1880) by proposing that topography will reflect a balance between surface erosion and rock uplift provided sufficiently long spans of geological time. Generally, this steady state is anticipated from the strong dependence of erosional efficacy on topographic relief (Ahnert, 1970) and elevation (through glacial erosion, e.g., Hallet et al., 1996), which function as a negative feedback on the growth of topography.

Either conceptualization may be an accurate characterization of Earth surface processes depending on the temporal and spatial scale considered. In this thesis, I

consider the evolution of a portion of an active tectonic plate boundary ($\sim 100,000 \text{ km}^2$) over a Late Cenozoic timescale ($< 23 \text{ Myr}$). At these scales, tectonic convergence between the Indian and Eurasian plates has been sustained (Molnar and Stock, 2009) and the tectonic addition of crustal material to the Himalayan orogen has progressively uplifted rocks, generating topography along the convergence zone (e.g., Harrison et al., 1992; Fielding, 1996) such that this orogenic growth presents a dynamic system that would similarly tend toward an steady state (e.g., Adams, 1980).

This steady state condition itself requires additional clarification. Willet and Brandon (2002) specify four distinct types of steady states, largely defined by the type of data used to interpret them. Of these, a flux steady state is achieved when the tectonic accretionary flux and erosional flux (often sediment flux from mountain rivers) are equal. A thermal steady state is satisfied when the thermal structure of an orogen becomes time-insensitive. This thermal steady state may only be achieved when the rate of material flux through the orogen becomes constant, as advection of crustal heat may steepen near surface geothermal gradients (Stuwe et al., 1994). Ultimately an exhumational steady state may be documented with radiometric cooling ages, such as from low-temperature thermochronometry, which may be interpreted to record constant exhumation rates over an extended period of time (Reiners and Brandon, 2006).

A growing body of research suggests that an exhumational steady state may have characterized portions of the main Himalayan front during the Late Cenozoic (e.g., Bernet et al., 2006; Chirouze et al., 2013), however these observations are not readily extended to the ends of the Himalayan orogen, where the transition from convergent to strike-slip motion warps the plate boundary southward. The Himalayan syntaxes

experience extremely rapid and focused exhumation that may exert an additional positive feedback on rock uplift (Zeitler et al., 2001), accelerating rock uplift and exhumation over time (e.g., Cervery et al. 1988; Bernet and Garver, 2005).

1.2.3 Feedbacks in the Himalayan syntaxes

Numerical (e.g., Beaumont et al., 1992), analog (e.g., Malavielle, 2010) and analytical (Dahlen and Suppe, 1988) experiments demonstrate that rapid, focused surface erosion of convergent orogens may localize regional strain gradients, concentrating exhumation within the area of rapid erosion. When rapid surface erosion is prolonged and sufficient upper crustal material is removed, a thermo-mechanical relationship may develop wherein the rock uplifted from lower lithospheric levels advects heat into the upper crust, steepening the near surface geothermal gradient (Stuwe et al., 1994) and increasing the susceptibility of the upper crust to subsequent deformation (Koons et al., 2002). In this situation, the rate of rock exhumation increases over time such that neither a thermal nor exhumational steady state is maintained. In such a region, topographic relief should increase to a maximum value limited only by internal rock strength and valley spacing (Montgomery and Brandon, 2002). Ultimately, these feedbacks lead to localized “hot spots” of very steep topography, high geothermal gradients and rapidly exhumed, crustal-scale structures (Zeitler et al., 2001).

Such a relationship between surface erosion and rock exhumation is best observed within the Himalayan syntaxes (Zeitler et al., 2001; Koons et al., 2013). Both regions exemplify the predicted final condition of thermo-mechanical feedbacks, with the coincidence of efficient erosional systems, steep topography and rapidly exhumed

metamorphic massifs (Finlayson et al., 2002). However, a detailed exhumation history of the syntaxes remains elusive. Abundant bedrock and detrital thermochronology from both syntaxes detail extremely rapid rock exhumation rates since the Late Pliocene or Pleistocene (e.g., Winslow et al., 1996; Burg et al., 1998), but this rapid cooling associated with this exhumation restricts interpretation prior to this time. Similarly, while antecedence of syntaxial rivers has long been speculated (e.g., Harrison et al., 1992) remarkably few data constrain the Late Cenozoic evolution of these drainage systems.

Presently, the exhumation history of the western syntaxis is best constrained and the existing data support the interpretation of a positive feedback between surface erosion and rock uplift in the Late Cenozoic. While Brookfield et al. (1998) speculated that the Indus River may have once drained northwestward into the Gilgit valley, a more recent study by Clift et al. (2001) favors the early establishment of an antecedent Indus River in the Paleogene. Moreover, the highly influential work by Cervený et al. (1988) documents increased rates of rock exhumation within the western syntaxis since at least the Middle Miocene (Bernet and Garver, 2005).

This thesis focuses on the exhumation history of the eastern syntaxis. Some preexisting evidence indicates that the Brahmaputra River may have connected through to Tibet since at least the Late Miocene (Galy et al., 2010), however the location of this connection through the eastern syntaxis is disputed (e.g., Clark et al., 2004; Cina et al., 2009). Moreover, the erosional efficacy of an antecedent river through the syntaxis may have been dramatically altered in the Quaternary by glacial and landslide damming (Montgomery et al., 2004), potentially focusing exhumation within the Tsango Gorge region (Korup and Montgomery, 2008). The only detrital record of syntaxial exhumation

is interpreted from Siwalik foreland units over 200 km downstream from the Brahmaputra River headwaters (Chirouze et al., 2013) and do not apparently support increasing Late Cenozoic exhumation rates within the eastern syntaxis.

To better constrain the Late Cenozoic exhumation history, drainage reorganization, and the potential influence of Quaternary glacial damming upstream of the eastern syntaxis this thesis applies a diverse suite of field observations and laboratory analyses to interpret Quaternary and Neogene foreland basin units from locations proximal to the syntaxis.

1.3 Research objectives

This thesis has three research objectives, each addressed in the following chapters. First, to determine when a river initially drained through the eastern Himalayan syntaxis. I accomplish this by interpreting the sedimentary provenance of Neogene foreland basin units with detrital zircon geochronology at several locations proximal to the eastern syntaxis. Second, to assess the potential impact of Quaternary ice and debris damming in the headwaters of a syntaxial drainage, I similarly interpret the sedimentary provenance of Quaternary flood deposits along the Siang River valley. I use a simple mixture model to evaluate the potential impact of a dam-burst flood event to determine if such events may have had an important erosional impact on the landscape. Third, to extend the exhumation history of the eastern syntaxis before the Pleistocene and Late Pliocene, I interpret detrital mineral cooling ages from the best studied foreland basin units proximal to the Brahmaputra River confluence. I use simple thermal modeling to interpret mineral cooling as a proxy for paleo-exhumation rate, to evaluate if an exhumational equilibrium

characterized the eastern syntaxis in the Neogene.

1.4 Motivations for study

1.4.1 Interpretation of the sedimentary record

Feedbacks between surface erosion and rock uplift could hypothetically sustain prodigious sediment discharges from the eastern syntaxis. Today, nearly half of the sediment carried into the foreland by the Yarlung-Siang River originates in only ~3% of the drainage area. If similar conditions were typical of the Neogene, this rapid sediment production may have profoundly influence proximal deposition within the basin, potentially complicating interpretations of proximal and distal basin records.

The flux of sediment from an eroding upland is one of the most important variables controlling the development of sedimentary basins (Allen et al., 2013). Terrestrial sedimentary basins are significant sources of freshwater, fossil fuel, and agricultural resources as well as popular dwellings for a large portion of humanity (the eastern Himalayan foreland is no exception to this). Moreover, these basins are valuable archives of Earth history, recording global tectonic (e.g., Copeland and Harrison, 1990) and climatic (e.g., France-Lanord and Derry, 1997) change in the Late Cenozoic. In the conceptual model I investigate, localization and acceleration of rock exhumation may profoundly influence interpretation of these sedimentary records by biasing sediment provenance to rapid erosion of the syntaxes. Moreover, understanding of source region exhumation and the development of continental scale drainage patterns elucidates the age and distribution of large distal basins (e.g., Métivier et al., 1999).

1.4.2 Connection to global climate

Mountain exhumation may have played an important role in global climate regulation during the Late Cenozoic (Raymo and Ruddiman, 1992). Development of high topography, such as that resulting from uplift of the Tibetan Plateau physically disrupts atmospheric circulation, focusing erosion to the windward sides of orogens (e.g. Ruddiman and Kutzbach, 1989; Willet, 1999). Enhanced erosion promotes the physical disintegration and comminution of rocks, exposing silicate mineral surfaces to chemical dissolution. Ultimately, this may result in net sequestration of atmospheric carbon, as well as the rapid burial of organic carbon. Carbon trapped in large sedimentary basins (e.g., the Bengal fan) is effectively removed from the atmosphere over a geological timescale, ultimately cooling the planet.

Furthermore, mountain exhumation may feed back on the development of mountainous topography, as erosion is isostatically (e.g., Molnar and England, 1990) or dynamically (e.g., Beaumont et al., 2001) compensated with increased rock uplift. Within this context, definition and documentation of the feedbacks between surface erosion and rock uplift are critical steps toward a broader understanding of the Earth's climatic history, offering some explanation of the geological contributions to observed fluctuations in atmospheric temperature and ocean chemistry.

1.5 Course of study

This research presented in this thesis was carried out over a period of six years between 2008 and 2014. During this time, three field expeditions in Spring 2008, Winter 2010-2011 and Winter 2012-2013 provided the opportunities for field observation,

measurement, and sample collection for the interpretations made herein. This research employs field mapping and stratigraphic surveying, magnetostratigraphy, modal analysis, detrital zircon U-Pb geochronology and fission-track thermochronology, and detrital muscovite $^{40}\text{Ar}/^{39}\text{Ar}$ thermochronology of modern river sediment, Quaternary alluvial deposits and a Quaternary-Neogene depositional sequence. All mineral separation and sample preparation were conducted at the University of Washington, and geochronological and thermochronological analyses were carried out at various collaborative institutions between 2010 and 2014 (details for each dataset are presented in their respective chapter). Data analysis and interpretation was subsequently carried out by the author at the University of Washington, often in consultation with members of the thesis committee and other members of the graduate students and faculty.

1.6 Presentation of results

This research is presented in three parts. First, to determine if connection of the Yarlung and Brahmaputra rivers through the Siang River predated Late Pliocene and Pleistocene exhumation of the Namche Barwa massif, I used detrital zircon U-Pb geochronology to determine the sedimentary provenance of Neogene units in the easternmost portion of the eastern foreland basin. This work, entitled *Antecedence of the Yarlung-Siang-Brahmaputra River, eastern Himalaya* has been published in *Earth and Planetary Science Letters*.

Second, to determine if glacial ice and debris damming of rivers draining into the Tsangpo Gorge may have focused Quaternary exhumation at the margin of the Tibetan Plateau, I use detrital zircon U-Pb geochronology and modal analysis to determine the

provenance of enigmatic slackwater flood deposits along the Siang River valley. I use a simple analytical model to constrain the amount of material a hypothetical dam-burst flood might transport in a worst-case, catastrophic scenario. This work, entitled *Erosion of the Tsangpo Gorge by Megafloods, eastern Himalaya* has been published in *Geology*.

Lastly, to extend the exhumation history of the eastern syntaxis region before the Late Pliocene, I combine detrital zircon fission-track and muscovite $^{40}\text{Ar}/^{39}\text{Ar}$ thermochronology with previous zircon U-Pb analyses from the same Neogene units investigated in the second chapter. I used a simple thermal model to constrain the timing and magnitude of an increase in syntaxial exhumation rate. This work, entitled *Late Miocene exhumation of the eastern Himalayan syntaxis from analysis of foreland basin deposits* has been prepared for submission to the *Geological Society of America Bulletin*.

1.7 References

- Adams, J. 1980; Contemporary uplift and erosion of the Southern Alps, New Zealand. *Geol. Soc. Am. Bull.*, 91, 1-114.
- Ahnert, F., 1970. Functional relationships between denudation, relief and uplift in large mid-latitude drainage basins. *Am. J. Sci.* 268, 243-263.
- Allen, P.A., Armitage, J.J., Carter, A., Duller, R.A., Michael, N.A., Sinclair, H.D., Whitchurch, A.L., Whittaker, A.C., 2013. The Qs problem: Sediment volumetric balance of proximal foreland basin systems. *Sedimentology*, 60, 102-130.
- Beaumont, C., Fullsack, P., Hamilton, J., 1992. Erosional control of active compressional orogens. In McClak, K.J.R. (ed.) *Thrust tectonics*, Chapman and Hall, London, 1-18.

- Beaumont, C., Jamieson, R.A., Nguyen, M.H., Lee, B., 2001. Himalayan tectonics explained by extrusion of a low-viscosity crustal channel coupled to focused surface denudation. *Nature*. 414, 738-742.
- Bernet, M., Garver, J.I., 2005. Fission-track analysis of detrital zircon, in Reiners, P.W., Ehlers, T.A., (eds.), *Reviews in Mineralogy and Geochemistry, Low-Temperature Thermochronology: Techniques, Interpretations and Applications*, 58, 205-238.
- Bernet, M., van der Beek, P., Pik, R., Huyghe, P., Mugnier, J-L., Labrin, E., Szulc, A., 2006. Miocene to recent exhumation of the central Himalaya determined from combined detrital zircon fission-track and U/Pb analysis of Siwalik sediments, western Nepal. *Basin Res.* 18, 393-412.
- Brookfield, M.E., 1998. The evolution of the great river systems of southern Asia during the Cenozoic India-Asia collision: Rivers draining southwards. *Geomorph.* 22, 285-312.
- Burg, J.-P., Nievergelt, P., Oberli, F., Seward, D., Davy, P., Mairing, J.-C., Diao, Z., Meier, M., 1998. The Namche Barwa syntaxis: Evidence for exhumation related to compressional crustal folding. *J. Asian Earth Sci.* 16, 239–252.
- Cerveny, P.F., Naeser, N.D., Zeitler, P.K., Naeser, C.W., Johnson, N.M., 1988. History of uplift and relief of the Himalaya during the past 18 million years: Evidence from fission-track ages of detrital zircons from sandstones of the Siwalik Group, in Kleinspehn, K.L., Paola, C. (eds.), *New perspectives in basin analysis*, Springer, New York. 43-61.
- Chirouze, F., Huyghe, P., van der Beek, P., Chauvel, C., Chakraborty, T., Dupont-Nivet, G., Bernet, M., 2013. Tectonics, exhumation and drainage evolution of the eastern

- Himalaya since 13 Ma from detrital geochemistry and thermochronology, Kameng River section, Arunachal Pradesh. *Geol. Soc. Am. Bull.* 125, 523-538.
- Cina, S.E., Yin, A., Grove, M., Dubey, C.S., Shukla, D.P., Lovera, O.M., Kelty, T.K., Gehrels, G.E., Foster, D.A., 2009. Gangdese arc detritus within the eastern Himalayan Neogene foreland basin: Implications for the Neogene evolution of the Yalu-Brahmaputra River system. *Earth Planet. Sci. Lett.* 285, 150-162.
- Clark, M.K., Schoenbohm, L.M., Royden, L.H., Whipple, K.X., Burchfiel, B.C., Zhang, X., Tang, W., Wang, E., Chen, L., 2004. Surface uplift, tectonics and erosion of eastern Tibet from large-scale drainage patterns. *Tectonics*, v. 23, TC1006.
- Clift, P.D., Zhimizu, N., Layne, G.D., Blusztajn, J.S., Gaedicke, C., Schluter, H-U., Clark, M.K., Amjad, S., 2001. Development of the Indus fan and its significance for the erosional history of the Western Himalaya and Karakoram. *Geol. Soc. Am. Bull.* 113, 1039-1051.
- Copeland, P., Harrison, T.M., 1990. Episodic rapid uplift in the Himalaya revealed by $^{40}\text{Ar}/^{39}\text{Ar}$ analysis of detrital K-feldspar and muscovite, Bengal fan. *Geology*. 18, 354-357.
- Dahlen, F.A., Suppe, J., 1988. Mechanics, growth, and erosion of mountain belts. In Clark, S.P.J., Burchfiel, B.C., Suppe, J. (eds), *Processes in Continental Lithospheric Deformation*. Geological Society of America, Boulder, 161-178.
- Davis, W.M., 1899. The geographical cycle. *Geog. J.*, 1, 481-504.
- England, P., Molnar, P., 1990. Surface uplift, uplift of rocks, and exhumation of rocks. *Geology*, 18, 1173-1177.
- Fielding, E., 1996. Tibet uplift and erosion. *Tectonophysics*. 260, 55-84.

- Finlayson, D.P., Montgomery, D.R., Hallet, B., 2002. Spatial coincidence of rapid inferred erosion with young metamorphic massifs in the Himalayas. *Geology*. 30, 219-222.
- France-Lanord, C., Derry, L.A., 1997. Organic carbon burial forcing of the carbon cycle from Himalayan erosion. *Nature*, 390, 65-67.
- Galy, V., France-Lanord, C., Peucker-Ehrenbrink, B., Huyghe, P., 2010. Sr-Nd-Os evidence for a stable erosion regime in the Himalaya during the past 12 Myr. 290, 3-4, 474-480.
- Gilbert, G.K., 1880. Report on the Geology of the Henry Mountains. US Government Printing office, 2nd ed, 170 pp.
- Hack, J.T., 1975. Dynamic equilibrium and landscape evolution. In Melhorn, W.N., Fleman, R.C. (eds), *Theories of landform Evolution*. Allen and Unwin, Boston, p. 87-102.
- Hallet, B., Hunter, L., Bogen, J., 1996. Rates of erosion and sediment evacuation by glaciers: A review of field data and their implications. *Global Planet. Change*, 12, 213-235.
- Harrison, T.M., Copeland, P., Kidd, W.S.F., Yin, A., 1992. Raising Tibet. *Science*. V. 255, 1663-1670.
- Kidd, W.S., Lim, C., Zeitler, P.K., Enkelmann, E., Booth, A.L., Chamberlain, C.P., Tang, W., Liu, Y., and Craw, D., 2006, Structural and tectonic geology of the Namche Barwa–Gyala Peri antiform, southeastern Tibet: Eos (Transactions, American Geophysical Union), 87 Abstract T23-0480.

- Koons, P.O., Zeitler, P.K., Chamberlain, C.P., Craw, D., Meltzer, A.S., 2002. Mechanical links between erosion and metamorphism in Nanga Parbat, Pakistan Himalaya. *Am. J. Sci.* 302, 749-773.
- Koons, P.O., Zeitler, P.K., Hallet, B., 2013. Tectonic aneurysms and mountain building, in: *Treatise on Geomorphology*. Owen, L.A., (ed.), 5, Elsevier, Amsterdam, 32 pp.
- Korup, O., and Montgomery, D.R., 2008. Tibetan plateau river incision inhibited by glacial stabilization of the Tsangpo gorge. *Nature*, v. 455, p. 786–789.
- Larsen, I.J., Montgomery, D.R., 2012. Landslide erosion coupled to tectonics and river incision. *Nature Geos.* 5, 468-473.
- Malavielle, J., 2010. Impact of erosion, sedimentation, and structural heritage on the structure and kinematics of orogenic wedges: analog models and case studies. *GSA Today*, 20, 1, 4-10.
- Métivier, F., Gaudemer, Y., Tapponier, P., 1999. Mass accumulation rates in Asia during the Cenozoic. *Geophys. J. Int.*, 137, 280-318.
- Molnar, P., England, P., 1990. Late Cenozoic uplift of mountain ranges and global climate change: chicken or egg? *Nature*. 346, 29-34.
- Molnar, P., Stock, J.M., 2009. Slowing of India's convergence with Eurasia since 20 Ma and its implications for Tibetan mantle dynamics. *Tectonics*, 28, 3, TC3001.
- Montgomery, D.R., 1994. Valley incision and the uplift of mountain peaks. *J. Geophys. Res. Solid Earth*. 99, B7, 13913-13921.
- Montgomery, D.R., Brandon, M.T., 2002. Topographic controls on erosion rates in tectonically active mountain ranges. *Earth and Planet. Sci. Lett.* 201, 481-489.

- Montgomery, D.R., Hallet, B., Yuping, L., Finnegan, N., Anders, A., Gillespie, A., Greenberg, H.M., 2004. Evidence for Holocene megafloods down the Tsangpo River gorge, southeastern Tibet. *Quat. Res.* 62, 201-207.
- Milliman, J.D., Farnsworth, K.L., 2011. River discharge to the coastal ocean: a global synthesis. Cambridge University Press, Cambridge. pp. 392.
- Penck, W., 1953. Morphological analysis of landforms. St. Martin's Press, New York.
- Raymo, M.E., Ruddiman, W.F., 1992. Tectonic forcing of late Cenozoic climate change. *Nature*, 359, 117-122.
- Reiners, P.W., Brandon, M.T., 2006. Using thermochronology to understand orogenic erosion. *Ann. Rev. Earth. Planet. Sci.* 34, 419-466.
- Ring, U., Brandon, M.T., Willett, S.D., Lister, G.S., 1999. Exhumation processes. *Geol. Soc. London Spec. Publ.*, 154, 1-27.
- Ruddiman, W.F., Kutzback, J.E., 1989. Forcing of late Cenozoic Northern hemisphere climate by plateau uplift in southern Asia and the American west. *J. Geophys. Res. Atmospheres*, 94, D15, 18409-18427.
- Stewart, R.J., Hallet, B., Zeitler, P.K., Malloy, M.A., Allen, C.M., Trippett, D., 2008. Brahmaputra sediment flux dominated by highly localized rapid erosion from the easternmost Himalaya. *Geology*. 36, 711-714.
- Stuwe, K., White, L., Brown, R., 1994. The influence of eroding topography on steady state isotherms. Application to fission-track analysis. *Earth Planet. Sci. Lett.*, 124, 63-74.
- Willet, S. 1999. Orogeny and orography. *J. Geophys. Res. Solid Earth*. 104, B12, 28957-28981.

Willet, S., Brandon, M.T., 2002. On steady states in mountain belts. *Geology*. 30, 175-178.

Winslow, D.M., Zeitler, P.K., Chamberlain, C.P., Williams, I.S., 1996. Geochronologic constraints on syntaxial development in the Nanga Parbat region, Pakistan. *Tectonics*. 15, 6, 1292-1308.

Zeitler, P.K., Meltzer, A.S., Koons, P.O., Craw, D., Hallet, B., Chamberlain, C.P., Kidd, W.S.F., Park, S.K., Seeber, L., Bishop, M., Shroder, J., 2001. Erosion, Himalayan geodynamics, and the geomorphology of metamorphism, *GSA Today*, 11(1), 4–9.

Zeitler, P.K., Meltzer, A.S., Brown, L., Kidd, W.S.F., Lim, C., Enkelmann, E., 2014. Tectonics and topographic evolution of Namche Barwa and the easternmost Lhasa block, Tibet. *Geol. Soc. Am. Special Paper 507*, 23.

CHAPTER 2: Antecedence of the Yarlung-Siang-Brahmaputra River, eastern Himalaya

Coauthors: Katharine W. Huntington, David R. Montgomery

2.0 Abstract

At the eastern terminus of the Himalayan orogen, distortion and capture of southeast Asian drainage basins reflects regional patterns of crustal strain due to the indentation of the Indian Plate into Eurasia. After flowing eastward >1000 km along the southern margin of Tibet, the Yarlung–Siang–Brahmaputra River turns abruptly southward through the eastern Himalayan syntaxis rapidly exhuming a crustal scale antiform in an impressive >2 km knickpoint. This conspicuous drainage pattern and coincidence of focused fluvial incision and rapid rock exhumation has been explained by the capture of an ancestral, high-elevation Yarlung River by headward erosion of a Himalayan tributary. However, recent observation of Tibetan detritus in Neogene foreland basin units complicates this explanation, requiring a connection from Tibet to the foreland prior to the estimated onset of rapid rock exhumation. We constrain the sedimentary provenance of foreland basin units deposited near the Brahmaputra River confluence in the eastern Himalayan foreland basin using detrital zircon U–Pb geochronology. We interpret the significant presence of Gangdese-age detritus in each foreland basin unit to indicate that connection of the Yarlung–Siang–Brahmaputra River was established during, or prior to foreland deposition in the Early Miocene. Our results indicate that connection of the Yarlung–Siang–Brahmaputra River precedes exhumation of the syntaxis, demonstrating the potential for the progressive coevolution of rock uplift and rapid erosion of the Namche Barwa massif.

2.1 Introduction

The peculiar drainage patterns of large southeast Asian rivers reflect a complex history of crustal deformation and river reorganization. For example, distortion of the upper Salween, Mekong and Yangtze rivers may be explained by warping of antecedent drainage basins (e.g., Burrard and Hayden, 1907; Brookfield, 1998; Hallet and Molnar, 2001) from collision of the eastern Indian Plate margin with the Eurasian Plate (e.g., Peltzer and Tapponier, 1988; Holt et al., 1991; Royden et al., 1997; Sol et al., 2007) beginning in the Early Eocene (Searle et al., 1987; Garzanti and Van Haver, 1988; Yin, 2006; Najman, 2006). Near the Indian indentor corner in the eastern Himalayan syntaxis (Figure 1), locally steepened river channels (e.g., Seeber and Gornitz, 1983), barbed tributaries (e.g., Burrard and Hayden, 1907; Burchfiel et al., 2000; Clark et al., 2004) and low drainage divides within the Yarlung–Siang–Brahmaputra drainage basin provide evidence that such distortion can culminate in drainage reorganization by capture and reversal (e.g., Clark et al., 2004; Clift et al., 2006).

Of particular interest is a ~100 km reach where the Yarlung–Siang–Brahmaputra River abruptly bends southward through the eastern syntaxis after flowing eastward >1000 km along terrane boundaries (Brookfield, 1998), dropping >2 km from the Tibetan plateau between >7 km Himalayan peaks. This anomalously steep (Seeber and Gornitz, 1983) and narrow (Montgomery, 2004) reach (i.e. knickzone) known as the Tsangpo gorge, is a locus of extremely rapid and focused erosion (e.g., Finlayson et al., 2002; Finnegan et al., 2008; Stewart et al., 2008; Larsen and Montgomery, 2012) coincident with an active crustal-scale antiform, the Namche Barwa massif (Figure 2A;

e.g., Burg et al., 1997, 1998; Ding et al., 2001; Kidd et al., 2006; Quanru et al., 2009; Xu et al., 2012a). Thermochronological, geochronological and petrological analyses of metamorphic and anatectic bedrock in the core of the massif constrain rapid exhumation rates exceeding 5 km/Myr since at least the Pliocene (Burg et al., 1998; Malloy, 2004; Seward and Burg, 2008) or Late Miocene (Ding et al., 2001; Booth et al., 2009; Xu et al., 2012a), and analyses of erosional efflux further indicate that modern erosion rates are also high (e.g., Galy and France-Lanord, 2001; Singh and France-Lanord, 2002; Garzanti et al., 2004; Pik et al., 2005), potentially exceeding 10 mm/yr (Stewart et al., 2008; Enkelmann et al., 2011).

Initiation of such rapid exhumation has been explained by the capture of a high elevation, ancestral Yarlung drainage basin via headward erosion of a steep Himalayan tributary (Figure 2B; e.g., Burrard and Hayden, 1907; Gregory and Gregory, 1925; Seeber and Gornitz, 1983; Brookfield, 1998; Clark et al., 2004). The resulting increase in drainage area and discharge to a knickzone at the point of capture would have increased the river's erosional potential, causing the knickzone to propagate upstream in a wave of incision. However, this knickzone has not relaxed into the Tibetan plateau as predicted by a simple model of upstream propagation (Finnegan et al., 2008), but has instead remained at the margin of the Tibetan plateau in the vicinity of the Namche Barwa massif.

Alternatively, connection of the Yarlung and Siang Rivers may predate uplift of the Namche Barwa massif (e.g., Harrison et al., 1992; Seward and Burg, 2008), in which case the Tsangpo gorge would represent a stationary knickzone resulting from localized uplift of the massif due to lithospheric buckling (e.g., Burg et al., 1998; Burg and Podladchikov, 1999) or geometric stiffening of the indenting margin of the Indian Plate

(e.g., Ehlers and Bendick, 2013). Localized rock uplift will steepen the equilibrium channel profile of rivers crossing the massif, locally increasing the potential for fluvial incision (Whipple and Tucker, 1999) and it has been proposed that rapid incision of an uplifting massif may eventually lead to a thermo-mechanical feedback (e.g., Koons, 1995, 1998; Koons et al., 2013; Zeitler et al., 2001) sustaining rapid rock exhumation and explaining the locally high topography (Finlayson et al., 2002; Finnegan et al., 2008), elevated geothermal gradient (Craw et al., 2005) and antiformal structure (Koons et al., 2002; Simpson, 2004) observed in the vicinity of the Tsangpo gorge. Seward and Burg (2008) noted that if the Yarlung–Siang connection predated uplift of the massif, the geomorphic evidence for reversal of the Parlung River (e.g., barbed tributaries to the Parlung River and the low divide in Figure 1; Burchfiel et al., 2000; Clark et al., 2004) may indicate that lateral propagation of the antiform forced the capture of an ancestral Yigong–Parlung River by the Yarlung–Siang–Brahmaputra (Figure 2C).

In this paper, we investigate the integration of the Yarlung–Siang–Brahmaputra River with new detrital zircon U–Pb provenance constraints from sedimentary units deposited along the eastern extent of the Himalayan foreland basin. Provenance analysis allows us to constrain the timing of Yarlung–Siang–Brahmaputra integration from the proximal sedimentary record, expanding on the prior work from sedimentary sections south of the Subansiri River (Cina et al., 2009; Chirouze et al., 2013) to determine when the Yarlung and Brahmaputra Rivers connected through the Siang. We use the collective dataset to interpret the Neogene evolution of rivers draining into the eastern Himalayan foreland, placing new constraints on the relationship between fluvial incision and tectonic deformation in this dynamic region.

2.2 Background

2.2.1 Sedimentary units of the eastern Himalayan foreland basin

Our study focuses on samples from three sedimentary sections exposed in the Himalayan foothills along the margin of the eastern Himalayan foreland basin near the town of Pasighat and the villages of Likabali and Kimin (Figure 1). Of these three sections, the two near Likabali and Pasighat are upstream of the Subansiri-Brahmaputra River confluence, and the one near Kimin is downstream of the confluence.

Beginning in the Pleistocene (Kumar, 1997; Chirouze et al., 2013), movement on the Tipi Thrust and Main Frontal Thrust has uplifted a sequence of sedimentary rocks estimated to be at least ~6 km (Jain et al., 1974; Agarwal et al., 1991; Chirouze et al., 2012) and as much as ~10 km thick (Karunakaran and Ranga Rao, 1976; Ranga Rao, 1983; Kumar, 1997). GPS data indicate that convergence across the eastern Himalaya is dominantly perpendicular to the mountain front with a maximum of 6–7 mm/yr of sinistral movement in the eastern Himalaya (see compilation in Burgess et al., 2012). If convergence was similar throughout the Neogene (e.g., Molnar and Stock, 2009), the foreland basin units exhumed at the mountain front should have originally been deposited near the orthogonal position of their present exposure.

The sedimentary rocks exposed in these sections comprise an upward-coarsening clastic sequence broadly interpreted to represent filling of a peripheral foreland basin with detritus shed from the rising Himalaya (e.g., Ranga Rao, 1983; Kumar, 1997; Najman, 2006). Three lithologically distinct units are observed within this sequence (Jain et al., 1974; Ranga Rao, 1983; Agarwal et al., 1991); progressing up-section these are: (1)

alternating beds of fine grained sandstone with carbonaceous shale, followed by (2) very thickly bedded, massive and cross-bedded medium to coarse grained sandstone with coalified logs, centimeter to meter scale calcareous nodules and gravel to cobble channel lag deposits, and (3) interbedded siltstone, sandstone, and clast supported gravel to cobble conglomerate with coarse to very coarse grained sand and silt lenses. The ages of the depositional contacts between each unit are paleontologically (Ranga Rao, 1983; Kumar, 1997) and magnetostratigraphically (Chirouze et al., 2012) constrained to ~10–11 Ma between the lower and middle units, and ~2–3 Ma between the middle and upper units.

Regional literature classifies these three units as the Dafla, Subansiri and Kimin formations, respectively (e.g., Ranga Rao, 1983; Kumar, 1997; Cina et al., 2009; Burgess et al., 2012); however, the units are loosely correlated to the Lower, Middle and Upper Siwalik units in the Western and Central Himalaya (e.g., Ranga Rao, 1983; Kumar, 1997; Najman, 2006; Chirouze et al., 2012), a terminology we adopt for consistency with the broader Himalayan literature.

Field observations from the Likabali section provide some indication of the sedimentary provenance of the units. Clast lithologies of conglomeratic beds in the Upper Siwalik unit contain variously colored quartzite (red, green, white, gray), volcanic rocks including amygdular basalt, high-grade metamorphic rocks including gneiss and schist, and dolomite (Jain et al., 1974). We observed these clast lithologies in conglomerate beds across the Upper-Middle Siwalik transition as well as in channel lag gravels within the Middle Siwalik unit, where amygdular basalt, gneiss, volcanic breccia, quartzite (red, purple, white, gray), vein quartz, and dolomite first appear. These clast lithologies are

generally characteristic of Lesser Himalayan metasedimentary units in the eastern Himalaya (e.g., Singh, 1993; Kumar, 1997; Acharyya, 2007; Yin et al., 2010; Kesari, 2010), but the distinct presence of volcanic rocks suggests a specific source region from the 'Abor volcanics' exposed along the Siang River (e.g., Jain and Thakur, 1978; Ali et al., 2012).

Paleocurrent indicators from multiple sections in the eastern Himalaya consistently show either south or southwest paleoflow directions, indicating that source areas remained north of sample locations during deposition of this sedimentary sequence. South-directed paleocurrent indicators, have been observed in the Upper Siwalik unit from imbricate pebbles near Itanagar (Cina et al., 2009) and cobbles near Likabali (Jain et al., 1974) and Bhalukpong (Kesari, 2010). Paleocurrent indicators in the Middle Siwalik unit indicate a variable (Chirouze et al., 2013), but dominantly southwest-directed paleoflow direction as measured on cross-bedding in pebbly conglomerate lag deposits near Itanagar (Cina et al., 2009) and Bhalukpong (Kesari, 2010; Chirouze et al., 2013). A dominantly southwest-directed paleoflow is also interpreted from cross-bedding in the Lower Siwalik unit near Bhalukpong (Chirouze et al., 2013).

Collectively, field observations support the interpretation of a fluvial depositional environment for the Lower and Middle Siwalik units and an alluvial-fan environment in the Upper Siwalik unit (e.g., Karunakaran and Ranga Rao, 1976; Kumar, 1997; Chirouze et al., 2012). The presence of Himalayan-derived clasts including volcanic rocks observed by us and by Jain et al. (1974) near Likabali suggests some component of basin detritus was derived from the Siang valley during the deposition of the Middle and Upper Siwalik units. The transition from southwest to south-directed paleoflow directions

observed from the Middle to Upper Siwalik units may represent transition from deposition in an expansive southwest directed fluvial braidplain (similar to the modern Brahmaputra River) to local deposition by south directed tributaries (e.g., the Subansiri River) and alluvial fans proximal to the mountain front. Alternatively, this change could represent natural variability within an expansive braidplain (Cina et al., 2009) or post-depositional counter-clockwise rotation of these units (Chirouze et al., 2012).

2.2.2 Provenance constrains from detrital zircon U-Pb geochronology

Single-grain U–Pb dating of detrital zircon cores provides a useful approach to assess sedimentary provenance in the Himalayan foreland basin (e.g., DeCelles et al., 1998; Bernet et al., 2006; Cina et al., 2009). This approach is particularly useful in the eastern Himalayan syntaxis, where published bedrock and detrital ages characterize the range of ages from specific source terranes (e.g., Stewart et al., 2008; Liang et al., 2008; Cina et al., 2009; Zhang et al., 2012; Lang et al., 2013; Robinson et al., 2013). We compiled published datasets from Himalayan and Tibetan source terranes within the eastern syntaxial region to constrain the range of ages contributed from each terrane (Figure 3).

Zircons older than 300 Ma most often represent inherited or detrital grains characteristic of Himalayan and Tibetan units (e.g., DeCelles et al., 2000; Yin et al., 2010; Gehrels et al., 2011; Zhang et al., 2012; Webb et al., 2012), with the important exceptions of some Early Cretaceous-Triassic zircons reported in the Lhasa Terrane (e.g., Leier et al., 2007; Zhu et al., 2011; Li et al., 2013; Lin et al., 2013a), Tethyan Himalaya (e.g., Zhu et al., 2008; Aikman et al., 2008, 2012; Li et al., 2010; Zeng et al., 2011; Webb

et al., 2012), and Indus-Tsangpo Suture Zone and adjacent basins (e.g., Wu et al., 2010; Aitchison et al., 2011; Wang et al., 2011; Cai et al., 2012).

Zircons younger than 300 Ma most often represent primary grains from Paleogene–Cretaceous igneous units in Tibet; they may also represent contributions from Neogene–Paleogene igneous units in Tethyan and Greater Himalayan sequences in the Arunachal Himalaya (e.g., Aikman et al., 2008; Hu et al., 2010; McQuarrie et al., 2008; Yin et al., 2010; Zeng et al., 2011; Hou et al., 2012) and Neogene metamorphic units within the vicinity of the Namche Barwa massif (e.g., Ding et al., 2001; Chung et al., 2003, 2009; Booth et al., 2004; Xu et al., 2010, 2012a; Zhang et al., 2010b, 2010c; Guo et al., 2012; Su et al., 2011; Zeng et al., 2012; Lin et al., 2013a; Xu et al., 2013). While these <300 Ma zircons are rare in detrital populations from sediment samples collected in Himalayan tributaries (<5% of the Kameng and Subansiri Rivers, Cina et al., 2009), they dominate sediment samples from Tibetan rivers (Figure 3).

Multiple source regions contribute <300 Ma zircons from north of the Indus Yarlung Suture Zone in Tibet (Figure 3). Gangdese plutons and volcanic units west of the Namche Barwa massif yield primarily Paleogene–Late Cretaceous zircons (e.g., Booth et al., 2004; Wen et al., 2008; Zhang et al., 2010a, 2012; Zhu et al., 2011; Guo et al., 2011, 2012; Ji et al., 2012; Guan et al., 2012; Zheng et al., 2012), while Bomi–Chayu igneous sources east of the Namche Barwa massif yield primarily Early Cretaceous zircons (e.g., Booth et al., 2004; Chiu et al., 2009; Liang et al., 2008; Xu et al., 2012b; Zhang et al., 2012; Lin et al., 2013b). Jurassic–Permian zircons are also observed from units in the Nyingoh River headwaters (e.g., Chu et al., 2006; Zhu et al., 2009, 2011; Guo et al., 2011; Zhang et al., 2012; Li et al., 2013; Lin et al., 2013c), and a few published zircon

U–Pb analyses from the Lohit Plutonic Suite suggest that this terrane may be a source of Early Cretaceous (Lin et al., 2013b; Haproff et al., 2013) as well as Late Cretaceous zircons (e.g., Lohit River sample of Cina et al., 2009). However, the limited data available for this particular region make this a source of uncertainty in our provenance analysis.

Source region is not the only factor influencing the relative density of detrital zircon U–Pb age probability. For example, age distributions may be strongly influenced by localized, short-term patterns of sediment delivery (e.g., Ruhl and Hodges, 2005; Stock et al., 2006; Avdeev et al., 2011), downstream dilution by contribution from local sources (Zhang et al., 2012), and the heterogeneous distribution of target minerals (i.e. zircon) in source terranes (e.g., Amidon et al., 2005; Duvall et al., 2012). Thus even when a large number of detrital grains is analyzed, the absence of a specific age component does not necessarily exclude the possibility that the corresponding source area was within the contributing area of the sample (Vermeesch, 2004). However, the presence of specific age components is a robust indicator of sedimentary provenance, requiring source terranes to have been within the contributing area of the basin concurrent with or prior to the time of sample deposition. With these considerations, we focus our provenance interpretations on the presence of distinct age components in Siwalik samples.

2.2.3 Previous constraints on Siwalik provenance in the eastern Himalaya

Coupled detrital zircon U–Pb and ϵ Hf analyses, as well as bulk ϵ Nd data constrain Siwalik Group provenance downstream of the modern Subansiri–Brahmaputra River confluence. Cina et al. (2009) have interpreted the presence of Paleogene–Early

Cretaceous zircons with ϵHf signatures similar to Gangdese sources as Gangdese detritus in Upper, Middle and Lower Siwalik units. The authors discuss that the presence of this detritus could be explained by either connection of the lower Yarlung River to the Siang River or the upper Yarlung River to the Subansiri River prior to capture by the Siang at some time during deposition of the Middle Siwalik unit, estimated to be before ~ 4 Ma (Clark et al., 2004). They prefer connection of the Yarlung and Subansiri rivers prior to ~ 4 Ma, given additional observations of changing paleoflow directions (from southwest to south) between deposition of the Middle and Upper Siwalik units.

Alternatively, the presence of Gangdese detritus and the change in paleocurrent direction in the Upper Siwaliks could be explained by recycling of Lower and Middle Siwalik units (as observed in the modern Subansiri River samples of Cina et al., 2009). Additional ϵNd isotopic work near Bhalukpong by Chirouze et al. (2013) demonstrates that the Middle Siwalik unit was sourced from a longitudinal river system draining Tibetan sources like the modern Brahmaputra since ~ 7 Ma, but indicates that this source changed to a transverse Himalayan river like the Kameng River during deposition of the Upper Siwalik unit. Pleistocene faulting at the mountain front (Kumar, 1997; Chirouze et al., 2013) would have exposed the Lower and Middle Siwalik units to erosion during deposition of the Upper Siwalik unit, providing an additional source of Gangdese detritus—an interpretation corroborated by evidence of growth strata in the uppermost portion of the Upper Siwalik formation near Bhalukpong (Burgess et al., 2012).

Determining when the Yarlung–Siang River connection was established is important for evaluating explanations for rapid exhumation of the Namche Barwa massif (e.g., initiation in response to rapid, focused river incision following capture of the

Yarlung by headward erosion of the Siang). As Cina et al. (2009) point out, if the Yarlung River connected to the Subansiri prior to capture by the Siang ~4 Ma, Upper Miocene foreland basin units east of the Subansiri River should not contain Gangdese-age detrital zircons. To test this prediction, we analyzed additional samples from Siwalik units exposed east of the Itanagar section and more proximal to the Siang–Brahmaputra River confluence.

2.3 Sampling and analytical methods

We collected 15 samples from the three sedimentary sections investigated. The approximate stratigraphic position of each sample is illustrated in Figure 4. At the section near Likabali we focused on detailing provenance changes with multiple samples from each Siwalik unit, and we evaluated variability of a single unit along strike of the Himalaya with additional Middle Siwalik samples collected near Kimin and Pasighat.

Near Likabali, we sampled compact fine-grained sandstones of the Lower Siwalik unit exposed between the Tipi Thrust and the Main Boundary Thrust. We collected six Middle Siwalik samples from medium to coarse sandstones exposed along the Siji River and in road exposures, where the unit is uninterrupted by faulting (Jain et al., 1974; Agarwal et al., 1991) between the Main Frontal Thrust and the conformable Upper-Middle Siwalik contact. We collected three samples from the Upper Siwalik unit including one from a medium sandstone interbedded with siltstone and gravel conglomerate beds above the Middle Siwalik contact, one from a coarse sandstone interbedded with cobble conglomerate in the middle of the unit, and one from a sand lens within the conspicuous boulder conglomerate at the top of the section near the Tipi

Thrust.

Additional Middle Siwalik samples were collected near Kimin and Pasighat from massive medium and coarse sandstones. The two Kimin samples were collected in river exposures between the Tipi Thrust and the Upper-Middle Siwalik contact, and the two Pasighat samples were collected in road exposures along the mountain front.

In preparation for isotopic analysis, sedimentary rock samples were manually disaggregated in a dilute HCl solution and wet sieved to isolate the 63–250 μm size fraction. Zircons were separated from this fraction by standard magnetic and heavy liquid techniques, mounted in epoxy, polished and imaged using high-resolution electron backscatter detection and cathodoluminescence prior to isotopic analysis. U–Th–Pb analyses of a random selection of zircon cores by laser ablation, multicollector inductively coupled plasma mass spectrometry were carried out in two locations: at the University of Arizona LaserChron center and by Apatite to Zircon, Inc. Analyses at the University of Arizona LaserChron center were conducted on a Nu high resolution mass spectrometer coupled to a Photon Machines 193 nm excimer laser with a ~ 30 μm spot size (Gehrels et al., 2006, 2008). Analyses at Apatite to Zircon, Inc. were conducted on an Agilent 7700 $\circ\phi$ quadrupole mass spectrometer coupled to a Resonetics RESOLUTION M-50 193 nm excimer laser with a ~ 30 μm spot size (Donelick et al., 2005; Chew and Donelick, 2012).

We analyzed at least 50 grains per sample (and many more when possible) with the goal of identifying the presence of <300 Ma zircons. Zircons of this age represent $\sim 25\%$ of detrital populations sampled in river sediment near Pasighat (Stewart et al., 2008) and $\sim 10\%$ of detrital populations sampled from Brahmaputra River sediment downstream

(Cina et al., 2009); by analyzing 50 grains we can be 95% confident that our analyses did not miss an age component representing >10% of the total (Vermeesch, 2004). The analytical data and details of standard calibration and isotopic corrections are presented in the Supplementary Material.

2.4 Results of detrital zircon U-Pb dating and provenance interpretations

A total of 1222 detrital zircon U–Pb analyses produced ages that range from 15 Ma to 3.3 Ga and confirm the presence of a significant component of <300 Ma zircons in each Siwalik unit (Figure 4). In the section near Likabali, about 20% of zircons in both of the Lower Siwalik samples and in the lowest Middle Siwalik sample are younger than 300 Ma. The three Upper Siwalik samples from this section contain a similar proportion of younger zircons (20–24%). The remaining five samples from this section may suggest an increase in the proportion of <300 Ma zircons during Middle Siwalik deposition—the young zircon population makes up >30% of each sample, and 70% of sample 5b. The additional four Middle Siwalik samples from Pasighat and Kimin are more variable (12–33% young zircons).

In all samples, <300 Ma zircons (333 of the total 1222 grains) are dominantly Paleogene–Late Cretaceous in age, similar to Gangdese bedrock from west of the Namche Barwa massif and detrital zircons from rivers draining that area (Figure 3). Early Cretaceous zircons characteristic of Bomi–Chayu sources are present in most samples in relatively smaller abundance, with the exception of one Middle Siwalik sample and one Lower Siwalik sample collected near Likabali that lack zircons of this age. Neogene zircons characteristic of young anatectic units from the Namche Barwa massif are rare.

We interpret the provenance of detrital zircons based on U–Pb age (although complimentary isotopic and modal analysis may further evaluate these interpretations), such that zircons with Paleogene–Late Cretaceous U–Pb ages represent Gangdese detritus and zircons with Early Cretaceous ages represent detritus from a Bomi–Chayu source. Older grains are not as diagnostic, but likely represent Jurassic and Triassic units observed within the Gangdese source area. When observed, Neogene zircons may represent sources in the Arunachal Himalaya or Namche Barwa specifically.

It is possible that some zircons in this age range could come from other sources. Paleogene zircons (specifically ~40–50 Ma) could alternatively represent igneous units in the Tethyan Himalaya; however these rocks are presently exposed over a very small region of the Himalaya and do not represent a significant component of modern Himalayan detrital sediments (e.g., Subansiri and Kameng River samples of Cina et al. (2009) shown in Figure 3). It is also possible that Paleogene and Cretaceous zircons may represent unobserved sources within the Lohit Plutonic Suite (Early Cretaceous ages in Lohit River sample may be evidence for this), but additional sampling of this region, specifically of the Dibang River drainage, is necessary to confirm this.

Sediment recycling could potentially introduce another source of uncertainty in provenance analysis. Recycling of exposed Siwalik units is an important source of detrital zircons in modern sediment samples (e.g., Cina et al., 2009) and may have been an additional source of zircons once Siwalik units were exhumed along the Himalayan mountain front in the Pleistocene. However, the absence of growth strata in all but the uppermost Upper Siwalik unit indicates that recycling was not likely to be an additional source of zircons until the very end of this depositional sequence, and thus is not a

potential source of the zircons observed in Lower and Middle Siwalik units.

2.5 Discussion

Our results broadly corroborate previous observations of Gangdese detritus within eastern Himalayan foreland basin units (e.g., Cina et al., 2009; Chirouze et al., 2013), and place new constraints on the organization of rivers carrying this detritus into the basin. In particular, we observe Gangdese detritus in samples from the Middle and Lower Siwalik units upstream of the Subansiri–Brahmaputra River confluence, which we propose indicates a connected drainage system from Gangdese sources west of the Namche Barwa massif through the Siang River to the foreland basin at least since deposition of the Lower Siwalik unit began in the Early Miocene. These observations do not exclude the possibility of additional connections from Tibet through the eastern Himalaya during Siwalik deposition, such as between a transverse river like the Subansiri River and the upper ~2/3 of the present Yarlung drainage (Cina et al., 2009). However, an additional connection is not necessary to explain the collective dataset.

2.5.1 Antecedence of the Yarlung-Siang-Brahmaputra River

The collective detrital zircon U–Pb provenance dataset including the new data presented here, observations from the Siwalik Group sections near Itanagar and Bhalukpong (Cina et al., 2009) and from distal Brahmaputra River deposits (Najman et al., 2008) may be explained by antecedent drainage of the Yarlung–Siang–Brahmaputra River. The Gangdese detritus observed in our Middle and Lower Siwalik samples, as well as the Middle and Lower samples collected near Itanagar and the Middle Siwalik sample

collected near Bhalukpong (Figure 4, Cina et al., 2009) may indicate deposition by a large southwest flowing river system that connected to the ancestral Yarlung River through the Siang River, a landscape similar to the present. This interpretation is consistent with paleocurrent indicators that indicate deposition of the Middle Siwalik by a southwest flowing river, and connection through the Siang River is further supported by the presence of volcanic clasts in the Middle and Upper Siwalik units.

The presence of Gangdese detritus in Upper Siwalik samples with south-directed paleocurrent indicators has been interpreted to indicate prior connection of the upper Yarlung and Subansiri Rivers (Cina et al., 2009). However, recycled detritus from the Lower and Middle Siwalik units may have been an additional source of zircons during deposition of the Upper Siwalik unit. Thus, south directed paleocurrent indicators in the Upper Siwalik unit could represent local deposition by a south-flowing transverse tributary near the mountain front (e.g., the Subansiri River).

Because the Yarlung River presently follows the Indus Yarlung Suture Zone for over 1000 km prior to entering the Tsangpo gorge, we speculate that the Yarlung–Siang–Brahmaputra River originally followed a similar eastern course along the suture (Figure 5A, Brookfield, 1998) after a potential reversal in the Early Miocene (Wang et al., 2013) yet prior to uplift of the Namche Barwa massif. Uplift of the massif progressively warped the suture zone into the distinct U-shape observed today (Figure 5B), and the river may have followed this warping until it eventually captured and reversed flow of the Parlung River (Figure 5C; Seward and Burg, 2008).

Although many of the Siwalik samples contain some Early Cretaceous zircons characteristic of Bomi–Chayu sources in addition to the dominant Gangdese component,

we argue that this does not suggest that the Gangdese source region was connected to the foreland through the ancestral Parlung and Lohit Rivers. Drainage through the ancestral Parlung and Lohit Rivers would have entrained a larger component of Bomi–Chayu detritus immediately prior to entering the basin, yet Early Cretaceous zircons do not dominate the detrital population. Moreover, although this age range is characteristic of Bomi–Chayu igneous sources, it is also possible that Early Cretaceous zircons originated from unobserved northern igneous sources (e.g., the northern igneous belt of Zhang et al., 2012), and thus their presence does not demand routing of Gangdese detritus through the Lohit drainage. Rather, the dominance of Gangdese detritus in every sample we measured suggests that at least during deposition of the Middle and Lower Siwalik units, a river carried Gangdese detritus directly to the basin avoiding a more circuitous route through the ancestral Parlung and Lohit Rivers.

Observations of Gangdese detritus in Burmese basins (Robinson et al., 2013) require drainage from Gangdese sources into Burma prior to ~18 Ma. We propose that a separate, integrated Yigong–Parlung–Irrawaddy river may explain these observations until an Early Miocene capture event rerouted flow into the Lohit River (e.g., Clark et al., 2004; Robinson et al., 2013). The absence of Bomi–Chayu detritus in the lowest Lower Siwalik sample at Likabali may be consistent with this drainage configuration prior to capture by the Lohit, but additional analyses are necessary from the lowest Siwalik strata to confirm this.

2.5.2 Capture and reversal of the Parlung River

The geomorphic evidence for reversal of the Parlung River may be explained by

capture of the ancestral Yigong–Parlung–Lohit River as lateral propagation of the Namche Barwa massif forced the Yarlung–Siang–Brahmaputra northward (Seward and Burg, 2008). Capture of the Yigong and Parlung drainage areas would have added Early Cretaceous zircons with a characteristic Bomi–Chayu provenance to the Yarlung–Siang–Brahmaputra sediment load, as is presently observed in modern river sediment sampled from the Siang River upstream of Siwalik exposures (see Figure 3). If this capture occurred in the Quaternary (Figure 5C), potentially influenced by glacial activity (e.g., drainage divide retreat – Oskin and Burbank, 2005; or temporary damming – Riedel et al., 2007; Korup and Montgomery, 2010), we might expect an increase of Early Cretaceous zircons in the uppermost Upper Siwalik unit. Our youngest sample collected near Likabali may be consistent with this prediction, but does not permit us to test this hypothesis due to the potential influence of sedimentary recycling and low number of analyses. Additional, and more detailed provenance analyses of the proximal Upper Siwalik samples and Late Quaternary terraces (e.g., Srivastava et al., 2008) near the Siang River confluence may further test this hypothesis to constrain the timing of capture and reversal of the Parlung River.

2.5.3 Exhumation of the Namche Barwa massif

Rapid exhumation of the Namche Barwa massif is estimated to have initiated in the Pliocene or Late Miocene. We propose that integration of the Yarlung–Siang–Brahmaputra river was established by at least the Early Miocene, which implies that rapid exhumation did not initiate in response to capture of the ancestral Yarlung River by headward erosion of the Siang. Instead, antecedence of the Yarlung–Siang–Brahmaputra

River demonstrates the potential for the progressive coevolution of rapid rock uplift and erosion of the Namche Barwa massif. Fluvial incision may amplify crustal deformation in the presence of regional compressive stresses (Simpson, 2004) as has been previously observed along Himalayan river anticlines (e.g., Montgomery and Stolar, 2006). We propose that coincident rock uplift associated with folding of the Namche Barwa antiform and erosion in the antecedent river channel locally increased exhumation rates at the margin of the Tibetan plateau without requiring a dramatic increase in drainage area. Sustained exhumation of the plateau margin, perhaps further increased after capture of the Yigong and Parlung Rivers, may have eventually removed enough crustal material to develop a thermo-mechanical feedback producing high topography over hot, weak crust (e.g., Zeitler et al., 2001; Koons et al., 2013).

2.6 Conclusions

We used detrital zircon U–Pb geochronology to determine the sedimentary provenance of Siwalik units exposed in three new locations in the eastern Himalayan foreland basin proximal to where the Yarlung–Siang–Brahmaputra River enters the basin. We observe a significant component of young, Paleogene–Late Cretaceous detrital zircons in all samples throughout the sedimentary sequence and interpret these ages to represent detritus from Gangdese source rocks west of the Namche Barwa massif. These results corroborate previous observations of Gangdese-age detritus within the eastern Himalayan foreland basin and further suggest that connection of the Yarlung–Siang–Brahmaputra River was established by the time deposition of the Lower Siwalik unit began in the Early Miocene. Rapid exhumation of the Namche Barwa massif is thought

to have initiated later, in the Pliocene or Late Miocene, and therefore we propose that exhumation of the massif was not related to capture of an ancestral Yarlung River by headward erosion of the Siang River. Considering this, we prefer the explanation for reversal of the Parlung River via capture by an integrated Yarlung–Siang–Brahmaputra as the rivers were tectonically juxtaposed by lateral propagation of the Namche Barwa massif. Antecedence of the Yarlung–Siang–Brahmaputra River demonstrates the potential for the progressive coevolution of rock uplift, and fluvial incision of the Namche Barwa massif, such that sustained erosion at the plateau margin may have eventually initiated a thermo-mechanical feedback that focused crustal exhumation in the region.

2.7 Acknowledgements

The authors acknowledge funding from the National Science Foundation (NSF-EAR 1349279 and NSF-EAR 0955309 to K.W.H., NSF-EAR 1032156 for support of the Arizona LaserChron Center), the Geological Society of America (Graduate Student Research Grant to K.A.L.), and the Quaternary Research Center at the University of Washington. The authors thank V. Adlakha, K. Bage and O. Tayeng for field assistance, K. Atakturk and K. Sumner for laboratory assistance, and T.M. Harrison for editorial support. This paper greatly benefited from detailed reviews from E. Garzanti, D. Burbank and A. Yin as well as informal reviews and comments by D. Montgomery and B. Hallet.

2.8 References

Acharyya, S.K., 2007. Evolution of the Himalayan Paleogene foreland basin, influence of

- its litho-packet on the formation of thrust-related domes and windows in the Eastern Himalayas – a review. *J. Geol. Soc. India* 31, 1–17.
- Agarwal, R.P., Srivastava, Maithani A, A.K., 1991. Geology of the Eastern Himalayan foothill belt of Bhutan and Arunachal Pradesh: an overview. *J. Himal. Geol.*, 197–205.
- Aikman, A.B., Harrison, T.M., Lin, D., 2008. Evidence for Early (>44 Ma) Himalayan crustal thickening, tethyan Himalaya, southeastern Tibet. *Earth Planet. Sci. Lett.* 274 (1–2), 14–23.
- Aikman, A.B., Harrison, T.M., Hermann, J., 2012. The origin of Eo- and Neo-Himalayan granitoids, Eastern Tibet. *J. Asian Earth Sci.* 58, 143–157.
- Aitchison, J.C., Xia, X., Baxter, A.T., Ali, J.R., 2011. Detrital zircon U–Pb ages along the Yarlung–Tsangpo suture zone, Tibet: implications for oblique convergence and collision between India and Asia. *Gondwana Res.* 20, 691–709.
- Ali, J.R., Aitchison, J.C., Chik, S.Y.S., Baxter, A.T., Bryan, S.E., 2012. Paleomagnetic data support Early Permian age for the Abor Volcanics in the lower Siang Valley, NE India: significance for Gondwana-related break-up models. *J. Asian Earth Sci.* 50, 105–115.
- Amidon, W.H., Burbank, D.W., Gehrels, G.E., 2005. Construction of detrital mineral populations: insights from mixing of U–Pb zircon ages in Himalayan rivers. *Basin Res.* 17 (4), 463–485.
- Armijo, R., Tapponnier, P., Han, T., 1989. Late cenozoic right-lateral strike-slip faulting in Southern Tibet. *J. Geophys. Res.* 94 (B3), 2787–2838.
- Avdeev, B., Niemi, N.A., Clark, M.K., 2011. Doing more with less: Bayesian estimation

- of erosion models with detrital thermochronometric data. *Earth Planet. Sci. Lett.* 305 (3–4), 385–395.
- Bernet, M., van der Beek, P., Pik, R., Huyghe, P., Mugnier, J.-L., Labrin, E., Szulc, A., 2006. Miocene to recent exhumation of the central Himalaya determined from combined detrital zircon fission-track and U/Pb analysis of Siwalik sediments, western Nepal. *Basin Res.* 18, 393–412.
- Booth, A.L., Zeitler, P.K., Kidd, W.S.F., Wooden, J., Lui, Y., Idleman, B., Hren, M., Chamberlain, C.P., 2004. U–Pb zircon constraints on the tectonic evolution of southeastern Tibet, Namche Barwa area. *Am. J. Sci.* 304, 889–929.
- Booth, A.L., Chamberlain, C.P., Kidd, W.S.F., Zeitler, P.K., 2009. Constraints on the metamorphic evolution of the eastern Himalayan syntaxis from geochronologic and petrologic studies of Namche Barwa. *Geol. Soc. Am. Bull.* 121, 385–407.
- Brookfield, M.E., 1998. The evolution of the great river systems of southern Asia during the Cenozoic India–Asia collision: rivers draining southwards. *Geomorphology*, 22, 285–312.
- Burchfiel, B.C., Clark, M.K., Wang, E., Chen, Z., Liu Pan G, Y., 2000. Tectonic framework of the Namche Barwa region, eastern Himalayan syntaxis, SE Tibet. *Abstr. Programs - Geol. Soc. Am.* 32, A-33.
- Burg, J.-P., Podladchikov, Y., 1999. Lithospheric scale folding: numerical modeling and application to the Himalayan syntaxes. *Int. J. Earth Sci.* 88, 190–200.
- Burg, J.-P., Davy, P., Nievergelt, P., Oberli, F., Seward, D., Diao, Z., Meier, M., 1997. Exhumation during folding in the Namche Barwa syntaxis. *Terra Nova* 9, 53–56.
- Burg, J.-P., Nievergelt, P., Oberli, F., Seward, D., Davy, P., Mairing, J.-C., Diao, Z.,

- Meier, M., 1998. The Namche Barwa syntaxis: evidence for exhumation related to compressional crustal folding. *J. Asian Earth Sci.* 16, 239–252.
- Burgess, W.P., Yin, A., Dubey, C.S., Shen, Z.K., Kelty, T.K., 2012. Holocene shortening across the Main Frontal Thrust zone in the eastern Himalaya. *Earth Planet. Sci. Lett.* 357–358, 152–167.
- Burrard, S.G., Hayden, H.H., 1907. *Geography and Geology of Himalayan Mountains and Tibet, Part 3: The Rivers of Himalaya and Tibet.* Government of India Press, Calcutta, pp. 119–230.
- Cai, F., Ding, L., Leary, R.J., Wang, H., Xu, Q., Zhang, L., Yue, Y., 2012. Tectonostratigraphy and provenance of an accretionary complex within the Yarlung–Zangpo suture zone, southern Tibet: insights into subduction–accretion processes in the Neo-Tethys. *Tectonophysics* 574–575, 181–192.
- Chew, D.M., Donelick, R.A., 2012. Combined apatite fission track and U–Pb dating by LA-ICP-MS and its application in apatite provenance analysis. In: Sylvester, P. (Ed.), *Quantitative Mineralogy and Microanalysis of Sediments and Sedimentary Rocks.* Mineralogical Association of Canada Short Course, 42. St. John's, Newfoundland and Labrador, pp. 219–247.
- Chirouze, F., Dupont-Nivet, G., Huyghe, P., van der Beek, P., Chakraborti, T., Bernet, M., Erens, V., 2012. Magnetostratigraphy of the Neogene Siwalik Group of far eastern Himalaya, Kameng section, Arunachal Pradesh, India. *J. Asian Earth Sci.* 44, 117–135.
- Chirouze, F., Huyghe, P., van der Beek, P., Chauvel, C., Chakraborty, T., Dupont-Nivet, G., Bernet, M., 2013. Tectonics, exhumation and drainage evolution of the eastern

- Himalaya since 13 Ma from detrital geochemistry and thermochronology, Kameng River section, Arunachal Pradesh. *Geol. Soc. Am. Bull.* 125, 523–538.
- Chiu, H.-Y., Chung, S.-L., Wu, F.-Y., Liu, D., Liang, Y.-H., Lin, I.-J., Iizuka, Y., Xie, L.-W., Wang, Y., Chu, M.-F., 2009. Zircon U–Pb and Hf isotopic constraints from eastern Transhimalayan batholiths on the precollisional magmatic and tectonic evolution in southern Tibet. *Tectonophysics* 477, 3–19.
- Chu, M.-F., Chung, S.-L., Song, B., Liu, D.-Y., O'Reilly, S.Y., Pearson, N.J., Ji, J.-Q., Wen, D.-J., 2006. Zircon U–Pb and Hf isotope constraints on the Mesozoic tectonics and crustal evolution of southern Tibet. *Geology* 34, 745–748.
- Chung, S.-L., Liu, D., Ji, J., Chu, M.-F., Lee, H.-Y., Wen, D.-J., Lo, C.-H., Lee, T.-Y., Qian, Q., Zhang, Qi., 2003. Adakites from continental collision zones: melting of thickened lower crust beneath southern Tibet. *Geology* 31, 1021–1024.
- Chung, S.-L., Chu, M.-F., Ji, J.-Q., O'Reilly, S.Y., Pearson, N.J., Liu, D.-Y., Lee, T.-Y., Lo, C.-H., 2009. The nature and timing of crustal thickening in southern Tibet: geochemical and zircon Hf isotopic constrains from postcollisional adakites. *Tectonophysics* 477, 36–48.
- Cina, S.E., Yin, A., Grove, M., Dubey, C.S., Shukla, D.P., Lovera, O.M., Kelty, T.K., Gehrels, G.E., Foster, D.A., 2009. Gangdese arc detritus within the eastern Himalayan Neogene foreland basin: implications for the Neogene evolution of the Yalu–Brahmaputra River system. *Earth Planet. Sci. Lett.* 285, 150–162.
- Clark, M.K., Schoenbohm, L.M., Royden, L.H., Whipple, K.X., Burchfiel, B.C., Zhang, X., Tang, W., Wang, E., Chen, L., 2004. Surface uplift, tectonics and erosion of eastern Tibet from large-scale drainage patterns. *Tectonics* 23, TC1006.

- Clift, P.D., Blusztajn, J., Anh Duc, N., 2006. Large-scale drainage capture and surface uplift in eastern Tibet–SW China before 24 Ma inferred from sediments of the Hanoi Basin, Vietnam. *Geophys. Res. Lett.* 33 (19).
<http://dx.doi.org/10.1029/2006GL027772>, L19403.
- Craw, D., Koons, P.O., Zeitler, P.K., Kidd, W.S.F., 2005. Fluid evolution and thermal structure in the rapidly exhuming gneiss complex of Namche Barwa–Gyala Peri, eastern Himalayan syntaxis. *J. Metamorph. Geol.* 23, 829–845.
- DeCelles, P.G., Gehrels, G.E., Quade, J., Ojha, T.P., Kapp, P.A., Upreti, B.N., 1998. Neogene foreland basin deposits, erosional unroofing, and the kinematic history of the Himalayan fold-thrust belt, western Nepal. *Geol. Soc. Am. Bull.* 110, 2–21.
- DeCelles, P.G., Gehrels, G.E., Quade, J., LaReau, B., Spurlin, M., 2000. Tectonic implications of U–Pb zircon ages of the Himalayan orogenic belt in Nepal. *Science* 288, 497–499.
- Ding, L., Zhong, D., Yin, A., Kapp, P., Harrison, T.M., 2001. Cenozoic structural and metamorphic evolution of the eastern Himalayan syntaxis (Namche Barwa). *Earth Planet. Sci. Lett.* 192, 423–438.
- Donelick, R.A., O’Sullivan, P.B., Ketcham, R.A., 2005. Apatite fission-track analysis. In: *Reviews in Mineralogy and Geochemistry*, vol. 58. Mineralogical Society of America, pp. 49–94.
- Duvall, A.R., Clark, M.K., Avdeev, B., Farley, K.A., Chen, Z., 2012. Widespread late Cenozoic increase in erosion rates across the interior of eastern Tibet constrained by detrital low-temperature thermochronometry. *Tectonics* 31, TC3014.
- Ehlers, T., Bendick, R., 2013. “Bottom up” subduction geometry initiation of extreme

- localized exhumation at orogeny syntaxes. *Abstr. Programs - Geol. Soc. Am.* 45, 222.
- Enkelmann, E., Ehlers, T.A., Zeitler, P.K., Hallet, B., 2011. Denudation of the Namche Barwa antiform, eastern Himalaya. *Earth Planet. Sci. Lett.* 307, 323–333.
- Finlayson, D.P., Montgomery, D.R., Hallet, B., 2002. Spatial coincidence of rapid inferred erosion with young metamorphic massifs in the Himalayas. *Geology* 30, 219–222.
- Finnegan, N.J., Hallet, B., Montgomery, D.R., Zeitler, P.K., Stone, J.O., Anders, A.M., Liu, Y., 2008. Coupling of rock uplift and river incision in the Namche Barwa–Gyala Peri massif, Tibet, China. *Geol. Soc. Am. Bull.* 120, 142–155.
- Galy, A., France-Lanord, C., 2001. Higher erosion rates in the Himalaya: geochemical constraints on riverine fluxes. *Geology* 29, 23–26.
- Garzanti, E., Van Haver, T., 1988. The Indus clastics: forearc basin sedimentation in the Ladakh Himalaya (India). *Sediment. Geol.* 59, 237–249.
- Garzanti, E., Vezzoli, G., Ando, S., France-Lanord, C., Singh, S.K., Foster, G., 2004. Sand petrology and focused erosion in collision orogens: the Brahmaputra case. *Earth Planet. Sci. Lett.* 220, 157–174.
- Gehrels, G.E., Valencia, V., Pullen, A., 2006. Detrital zircon geochronology by Laser-Ablation Multicollector ICPMS at the Arizona LaserChron Center. In: Loszewski, T., Huff, W. (Eds.), *Geochronology: Emerging Opportunities*. In: *Paleontology Society Short Course: Paleontology Society Papers*, vol. 11. 10 pp.
- Gehrels, G.E., Valencia, V., Ruiz, J., 2008. Enhanced precision, accuracy, efficiency, and spatial resolution of U–Pb ages by laser ablation–multicollector–inductively

- coupled plasma–mass spectrometry. *Geochem. Geophys. Geosyst.* 9, Q03017.
- Gehrels, G.E., Kapp, P., DeCelles, P., Pullen, A., Blakey, R., Weislogel, A., Ding, L., Guynn, J., Martin, A., McQuarrie, N., Yin, A., 2011. Detrital zircon geochronology of pre-Tertiary strata in the Tibetan–Himalayan orogeny. *Tectonics* 30, TC5016.
- Gregory, J.W., Gregory, C.J., 1925. The geology and physical geography of Chinese Tibet, and its relations to the mountain system of south-eastern Asia, from observations made during the Percy Sladen Expedition 1922. *Philos. Trans. R. Soc. Lond., Ser. B* 213, 171–298.
- Guan, Q., Zhu, D.-C., Zhao, Z.-D., Dong, G.-C., Zhang, L.-L., Li, X.-W., Liu, M., Mo, X.-X., Liu, Y.-S., Yuan, H.-L., 2012. Crustal thickening prior to 38 Ma in southern Tibet: evidence from lower crust-derived adakitic magmatism in the Gangdese Batholith. *Gondwana Res.* 21 (1), 88–99.
- Guo, L., Zhang, H.-F., Harris, N., Pan, F.-B., Xu, W.-C., 2011. Origin and evolution of multi-stage felsic melts in eastern Gangdese belt: constraints from U–Pb zircon dating and Hf isotopic composition. *Lithos* 127, 54–67.
- Guo, L., Zhang, H.-F., Harris, N., Parrish, R., Xu, W.-C., Shi, Z.-L., 2012. Paleogene crustal anatexis and metamorphism in Lhasa terrane, eastern Himalayan syntaxis: evidence from U–Pb zircon ages and Hf isotopic compositions of the Nyingchi Complex. *Gondwana Res.* 21, 100–111.
- Hallet, B., Molnar, P., 2001. Distorted drainage basins as markers of crustal strain east of the Himalaya. *J. Geophys. Res.* 106, 13697–13709.
- Haproff, P.J., Yin, A., Dubey, C.S., 2013. Tectonic framework of the eastern Himalayan

- region based on U–Pb zircon geochronology and detailed geologic mapping, NE India. *Eos Trans. AGU. Abstract T11A 2422.*
- Harrison, T.M., Copeland, P., Kidd, W.S.F., Yin, A., 1992. Raising Tibet. *Science* 255, 1663–1670.
- Holt, W.E., Ni, J.F., Wallace, T.C., Haines, A.J., 1991. The active tectonics of the eastern Himalayan syntaxis and surrounding regions. *J. Geophys. Res., Solid Earth* 96, 14595–14632.
- Hou, Z.-Q., Zheng, Y.-C., Zeng, L.-S., Gao, L.-E., Huang, K.-X., Li, W., Li, Q.-Y., Fu, Q., Liang, W., Sun, Q.-Z., 2012. Eocene-Oligocene granitoids in southern Tibet: constraints on crustal anatexis and tectonic evolution of the Himalayan orogen. *Earth Planet. Sci. Lett.* 349–350, 35–52.
- Hu, X., Jansa, L., Chen, L., Griffin, W.L., O'Reilly, S.Y., Wang, J., 2010. Provenance of lower cretaceous Wolong volcanoclastics in the Tibetan Tethyan Himalaya: implications for the final breakup of Eastern Gondwana. *Sediment. Geol.* 233, 193–205.
- Jain, A.K., Thakur, V.C., 1978. Abor volcanics of Arunachal Himalaya. *J. Geol. Soc. India* 8, 335–349.
- Jain, A.K., Thakur, V.C., Tandon, S.K., 1974. Stratigraphy and structure of the Siang District, Arunachal (NEFA) Himalaya. *Himal. Geol.* 4, 28–60.
- Ji, W.-Q., Wu, F.-Y., Liu, C.-Z., Chung, S.-L., 2012. Early Eocene crustal thickening in southern Tibet: new age and geochemical constraints from the Gangdese batholith. *J. Asian Earth Sci.* 53, 82–95.
- Karunakaran, C., Ranga Rao, A., 1976. Status of exploration for hydrocarbons in the

- Himalayan region-contributions to stratigraphy and structure. Misc. Publ. Geol. Surv. India 41, 1–66.
- Kesari, G.K., 2010. Geology and mineral resources of Arunachal Pradesh. Misc. Publ. Geol. Soc. India 30, 60. p. IV, vol. 1.
- Kidd, W.S., Lim, C., Zeitler, P.K., Enkelmann, E., Booth, A.L., Chamberlain, C.P., Tang, W., Liu, Y., Craw, D., 2006. Structural and tectonic geology of the Namche Barwa–Gyala Peri antiform, southeastern Tibet. Eos Trans. AGU 87, Abstract T23-0480.
- Koons, P.O., 1995. Modeling the topographic evolution of collisional belts. Annu. Rev. Earth Planet. Sci. 23, 375–408.
- Koons, P.O., 1998. Big mountains, big rivers and hot rocks: beyond isostasy. Eos Trans. AGU 79, Abstract F908.
- Koons, P.O., Zeitler, P.K., Chamberlain, C.P., Craw, D., Meltzer, A.S., 2002. Mechanical links between erosion and metamorphism in Nanga Parbat, Pakistan Himalaya. Am. J. Sci. 302, 749–773.
- Koons, P.O., Zeitler, P.K., Hallet, B., 2013. Tectonic aneurysms and mountain building. In: Owen, L.A. (Ed.), Treatise on Geomorphology, vol. 5. 32 pp.
- Korup, O., Montgomery, D.R., 2010. Glacier and landslide feedbacks to topographic relief in the Himalayan syntaxes. Proc. Natl. Acad. Sci. USA 107, 5317–5322.
- Kumar, D., 1997. Geology of Arunachal Pradesh. Geol. Soc. India, Bangalore. 217 pp.
- Lang, K.A., Huntington, K.W., Montgomery, D.R., 2013. Erosion of the Tsangpo Gorge by megafloods, eastern Himalaya. Geology 41, 1003–1006.
- Larsen, I.J., Montgomery, D.R., 2012. Landslide erosion coupled to tectonics and river

- incision. *Nat. Geosci.* 5, 468–473.
- Leier, A.L., Kapp, P., Gehrels, G.E., DeCelles, P.G., 2007. Detrital zircon geochronology of Carboniferous–Cretaceous strata in the Lhasa terrane, Southern Tibet. *Basin Res.* 19, 361–378. <http://dx.doi.org/10.1111/j.1365-2117.2007.00330.x>.
- Li, G., Liu, X., Pullem, A., Wei, J., Liu, X., Huang, F., Zhou, X., 2010. In-situ detrital zircon geochronology and Hf isotopic analyses from upper Triassic Tethys sequence strata. *Earth Planet. Sci. Lett.* 297 (3–4), 461–470.
- Li, G., Sandiford, M., Liu, X., Xu, Z., Wei, L., Li, H., 2013. Provenance of Late Triassic sediments in central Lhasa terrane, Tibet and its implication. *Gondwana Res.* 25, 1680–1689.
- Liang, Y.-H., Chung, S.-L., Liu, D., Xu, Y., Wu, F.-Y., Yang, J.-H., Wang, Y., Lo, C.-H., 2008. Detrital zircon evidence from Burma for reorganization of the eastern Himalayan river system. *Am. J. Sci.* 308, 618–638.
- Lin, Y.-H., Zhang, Z.-M., Gond, X., Xiang, H., Yan, R., 2013a. Early Mesozoic metamorphism and tectonic significance of the eastern segment of the Lhasa Terrane, south Tibet. *J. Asian Earth Sci.* 78, 160–183.
- Lin, T.-H., Chung, S.-L., Kumar, A., Wu, F.-Y., Chiu, H.-Y., Lin, I.-J., 2013b. Linking a prolonged Neo-Tethyan magmatic arc in South Asia: zircon U–Pb and Hf isotopic constraints from the Lohit Batholith, NE India. *Terra Nova* 25 (6), 453–458.
- Lin, Y.-H., Zhang, Z.-M., Dong, X., Shen, K., Lu, X., 2013c. Precambrian evolution of the Lhasa terrane, Tibet: constraint from the zircon U–Pb geochronology of the gneisses. *Precambrian Res.* 237, 64–77.
- Malloy, M., 2004. Rapid erosion at the Tsangpo knickpoint and exhumation of

- southeastern Tibet. M.S. thesis. Lehigh University, Bethlehem, Pennsylvania. 67 pp.
- McQuarrie, N., Robinson, D., Long, S., Tobgay, T., Grujic, D., Gehrels, G., Ducea, M., 2008. Preliminary stratigraphic and structural architecture of Bhutan: implications for the along-strike architecture of the Himalayan system. *Earth Planet. Sci. Lett.* 272, 105–117.
- Misra, D.K., 2009. Litho-tectonic sequence and their regional correlation along the Lohit and Dibang valleys, eastern Arunachal Pradesh. *J. Geol. Soc. India* 73, 213–219.
- Molnar, P., Stock, J.M., 2009. Slowing of India's convergence with Eurasia since 20 Ma and its implications for Tibetan mantle dynamics. *Tectonics* 28, TC3001.
- Montgomery, D.R., 2004. Observations on the role of lithology in strath terrace formation and bedrock channel width. *Am. J. Sci.* 304, 454–476.
- Montgomery, D.R., Stolar, D.B., 2006. Reconsidering Himalayan river anticlines. *Geomorphology* 82, 4–15.
- Najman, Y., 2006. The detrital record of orogenesis: a review of approaches and techniques used in the Himalayan sedimentary basins. *Earth-Sci. Rev.* 74, 1–72.
- Najman, Y., Bickle, M., BouDagher-Fadel, M., Carter, A., Garzanti, E., Paul, M., Wijbrans, J., Willett, E., Oliver, G., Parrish, R., Akhter, S.H., Allen, R., Ando, S., Chisty, E., Reisberg, L., Zevvoli, G., 2008. The Paleogene record of Himalayan erosion: Bengal Basin, Bangladesh. *Earth Planet. Sci. Lett.* 273, 1–14.
- Oskin, M., Burbank, D.W., 2005. Alpine landscape evolution dominated by cirque retreat. *Geology* 33, 933–936.
- Pan, G., Ding, J., Yao, D., Wang, L., 2004. Geological map of Qinghai-Xizang (Tibet)

- and adjacent areas: Chengdu Cartographic Publishing House, scale 1:1,500,000, 6 sheets.
- Peltzer, G., Tapponier, P., 1988. Formation and evolution of strike-slip faults, rifts, and basins during the India-Asia collision: an experimental approach. *J. Geophys. Res.* 93 (B12), 15085–15117.
- Pik, R., France-Lanord, C., Carignan, J., 2005. Extreme uplift and erosion rates in eastern Himalayas (Siang–Brahmaputra basin) revealed by detrital (U–Th)/He thermochronology. *Geophys. Res. Abstr.* 7, Abstract 09421.
- Quanru, G., Guitang, P., Zheng, L., Chen, Z., Fisher, R.D., Sun, Z., Ou, C., Dong, H., Wang, X., Li, S., Lou, X., Fu, H., 2009. The Eastern Himalayan Syntaxis: major tectonic domains, ophiolitic mélanges and geological evolution. *J. Asian Earth Sci.* 27, 265–285.
- Ranga Rao, A., 1983. Geology and hydrocarbon potential of a part of Assam–Arakan basin and its adjacent region. In: Bhandari, L.L., Venkatachala, B.S., Kumar, R., Swamy, S.N., Garga, P., Srivastava, D.C. (Eds.), *Petroliferous Basins of India*. *Pet. Asia J.* 6, 112–127.
- Riedel, J.L., Haugerud, R.A., Clague, J.J., 2007. Geomorphology of a Cordilleran Ice Sheet drainage network through breached divides in the North Cascades Mountains of Washington and British Columbia. *Geomorphology* 91, 1–18.
- Robinson, R.A.J., Brezina, C.A., Parrish, R.R., Horstwood, M.S.A., Oo, N.W., Bird, M.I., Thein, M., Walters, A.S., Oliver, G.J.H., Zaw, K., 2013. Large rivers and orogens: the evolution of the Yarlung Tsangpo–Irrawaddy system and the eastern Himalayan syntaxis. *Gondwana Res.* <http://dx.doi.org/10.1016/j.gr.2013.07.002>.

- Royden, L.H., Burchfiel, B.C., King, R.W., Wang, E., Chen, Z., Shen, F., Liu, Y., 1997. Surface deformation and lower crustal flow in eastern Tibet. *Science* 276, 788–790.
- Ruhl, K.W., Hodges, K.V., 2005. The use of detrital mineral cooling ages to evaluate steady state assumptions in active orogens: an examples from the central Nepalese Himalaya. *Tectonics* 24, TC4015. <http://dx.doi.org/10.1029/2004TC001712>.
- Searle, M.P., Windley, B.F., Coward, M.P., Cooper, D.J.W., Rex, A.J., Rex, D., Tingdong, L., Xuchang, X., Jan, M.Q., Thakur, V.C., Kuman, S., 1987. The closing of the Tethys and the tectonics of the Himalaya. *Geol. Soc. Am. Bull.* 98, 678–701.
- Seeber, L., Gornitz, V., 1983. River profiles along the Himalayan arc as indicators of active tectonics. *Tectonophysics* 92, 335–367.
- Seward, D., Burg, J.-P., 2008. Growth of the Namche Barwa Syntaxis and associated evolution of the Tsangpo Gorge: constraints from structural and thermochronological data. *Tectonophysics* 451, 282–289.
- Simpson, G., 2004. Role of river incision in enhancing deformation. *Geology* 32, 341–344.
- Singh, S., 1993. Geology and Tectonics of the Eastern Syntaxial Bend, Arunachal Himalaya. *J. Him. Geol.* 4 (2), 149–163.
- Singh, S., France-Lanord, C., 2002. Tracing the distribution of erosion in the Brahmaputra watershed from isotopic compositions of stream sediments. *Earth Planet. Sci. Lett.* 252, 645–662.
- Sol, S., Meltzer, A., Burgmann, R., van der Hilst, R.D., King, R., Chen, Z., Koons, P.O.,

- Lev, E., Liu, Y.P., Zeitler, P.K., Zhang, X., Zhang, J., Zurek, B., 2007. Geodynamics of the southeastern Tibetan Plateau from seismic anisotropy and geodesy. *Geology* 35, 563–566.
- Srivastava, P., Bhakuni, S.S., Luirei, K., Misra, D.K., 2008. Morpho-sedimentary records at the Brahmaputra River exit, NE Himalaya: climate-tectonic interplay during the Late Pleistocene–Holocene. *J. Quat. Sci.* <http://dx.doi.org/10.1002/jqs.1190>.
- Stewart, R.J., Hallet, B., Zeitler, P.K., Malloy, M.A., Allen, C.M., Trippett, D., 2008. Brahmaputra sediment flux dominated by highly localized rapid erosion from the easternmost Himalaya. *Geology* 36, 711–714.
- Stock, G.M., Ehlers, T.A., Farley, K.A., 2006. Where does sediment come from? Quantifying catchment erosion with detrital apatite (U–Th)/He thermochronometry. *Geology* 34, 725–728.
- Su, W., Zhang, M., Liu, X., Lin, J., Ye, K., Liu, X., 2011. Exact timing of granulite metamorphism in the Namche–Barwa, eastern Himalayan syntaxis: new constraints from SIMS U–Pb zircon age. *Int. J. Earth Sci.* 101, 239–252.
- Vermeesch, P., 2004. How many grains are needed for a provenance study? *Earth Planet. Sci. Lett.* 224, 441–451.
- Vermeesch, P., 2012. On the visualisation of detrital age distributions. *Chem. Geol.* 312–313, 190–194.
- Wang, J., Hu, X., Jansa, L., Huang, Z., 2011. Provenance of the Upper Cretaceous–Eocene Deep-Water Sandstones in Sangdanlin, Southern Tibet: constraints on the timing of Initial India–Asia Collision. *J. Geol.* 119 (3), 293–309.
- Wang, J.-G., Hu, X.-M., Garzanti, E., Wu, F.-Y., 2013. Upper oligocene-lower Miocene

- gangrinboche conglomerate in the Xigaze area, Southern Tibet: implications for Himalayan uplift and Paleo–Yarlung–Zangbo initiation. *J. Geol.* 121 (4), 425–444.
- Webb, A.A.G., Yin, A., Dubey, C.S., 2012. U–Pb zircon geochronology of major lithologic units in the eastern Himalaya: implications for the origin and assembly of Himalayan rocks. *Geol. Soc. Am. Bull.* 125, 499–522.
- Wen, D.-R., Liu, D.-Y., Chung, S.-L., Chu, M.-F., Ji, J.-Q., Zhang, Q., Song, B., Lee, T.-Y., Yeh, M.-W., Lo, C.-H., 2008. Zircon SHRIMP U–Pb ages of the Gangdese batholith and implications for Neotethyan subduction in southern Tibet. *Chem. Geol.* 252, 191–201.
- Whipple, K.X., Tucker, G.E., 1999. Dynamics of the stream-power river incision model: implications for height limits of mountain ranges, landscape response timescales, and research needs. *J. Geophys. Res.* 104, 17661–17674.
- Wu, F.-Y., Ji, W.-Q., Liu, C.-Z., Chung, S.-L., 2010. Detrital zircon U–Pb and Hf isotopic data from the Xigaze fore-arc basin: constraints on Transhimalayan magmatic evolution in southern Tibet. *Chem. Geol.* 271, 13–25.
- Xu, W.-C., Zhang, H.-F., Parrish, R., Harris, N., Guo, L., Yuan, H.-L., 2010. Timing of granulite-facies metamorphism in the eastern Himalayan syntaxis and its tectonic implications. *Tectonophysics* 485, 231–244.
- Xu, Z., Ji, S., Cai, Z., Zeng, L., Geng, Q., Cao, H., 2012a. Kinematics and dynamics of the Namche Barwa Syntaxis, eastern Himalaya: constraints from deformation, fabrics and geochronology. *Gondwana Res.* 21, 19–36.
- Xu, Y.-G., Yang, Q.-J., Lan, J.-B., Luo, Z.-Y., Huang, X.-L., Shi, Y.-R., Xie, L.-W., 2012b. Temporal–spatial distribution and tectonic implications of the batholiths in

- the Gaoligong–Tengliang–Yinjiang area, western Yunnan: constraints from zircon U–Pb ages and Hf isotopes. *J. Asian Earth Sci.* 53, 151–175.
- Xu, W.-C., Zhang, H.-F., Harris, N., Gu, L., Pan, F.-B., Wang, S., 2013. Geochronology and geochemistry of Mesoproterozoic granitoids in the Lhasa terrane, south Tibet: implications for the early evolution of Lhasa Terrane. *Precambrian Res.* 236, 46–58.
- Yin, A., 2006. Cenozoic tectonic evolution of the Himalayan orogen as constrained by along-strike variation of structural geometry, exhumation history, and foreland sedimentation. *Earth-Sci. Rev.* 76 (1), 1–131.
- Yin, A., Dubey, C.S., Kelty, T.K., Webb, A.A.G., Harrison, T.M., Chou, C.Y., Celerier, J., 2010. Geologic correlation of the Himalayan orogeny and Indian craton: Part 2. Structural geology, geochronology and tectonic evolution of the Eastern Himalaya. *Geol. Soc. Am. Bull.* 122, 360–395.
- Zeitler, P.K., Meltzer, A.S., Koons, P.O., Craw, D., Hallet, B., Chamberlain, C.P., Kidd, W.S.F., Park, S.K., Seeber, L., Bishop, M., Shroder, J., 2001. Erosion, Himalayan geodynamics, and the geomorphology of metamorphism. *GSA Today* 11 (1), 4–9.
- Zeng, L., Gao, L.-E., Xue, K., Liu-Zeng, J., 2011. Mid-Eocene high Sr/Y granites in the Northern Himalayan Gneiss Domes: melting thickened lower continental crust. *Earth Planet. Sci. Lett.* 303 (3–4), 251–266.
- Zeng, L., Gao, L.-E., Dong, C., Tang, S., 2012. High-pressure melting of metapelite and the formation of Ca-rich granitic melts in the Namche Barwa Massif, southern Tibet. *Gondwana Res.* 21, 138–151.
- Zhang, Z.-M., Zhao, G.-C., Santosh, M., Wang, J.-L., Dong, X., Shen, K., 2010a. Late

- Cretaceous charnockite with adakitic affinities from the Gangdese batholith, southeastern Tibet: evidence for Neo-Tethyan mid-ocean ridge subduction? *Gondwana Res.* 17, 615–631.
- Zhang, Z.-M., Zhao, G.C., Santosh, M., Wang, J.L., Dong, X., Liou, J.G., 2010b. Two stages of granulite facies metamorphism in the eastern Himalayan syntaxis, south Tibet: petrology, zircon geochronology and implications for the subduction of Neo-Tethys and the Indian continent beneath Asia. *J. Metamorph. Geol.* 28, 719–733.
- Zhang, H.-F., Harris, N., Guo, L., Xu, W., 2010c. The significance of Cenozoic magmatism from the western margin of the eastern syntaxis, southeast Tibet. *Contrib. Mineral. Petrol.* 160, 83–98.
- Zhang, J.Y., Yin, A., Liu, W.C., Wu, F.Y., Lin, D., Grove, M., 2012. Coupled U–Pb dating and Hf isotopic analysis of detrital zircon of modern river sand from the Yalu River (Yarlung Tsangpo) drainage system in southern Tibet: constraints on the transport processes and evolution of Himalayan rivers. *Geol. Soc. Am. Bull.* 124, 1449–1473.
- Zheng, Y.-C., Hou, Z.-Q., Li, Q.-Y., Sun, Q.-Z., Liang, W., Fu, Q., Li, W., Huang, K.-X., 2012. Origin of Late Oligocene adakitic intrusives in the southeastern Lhasa terrane: evidence from in situ zircon U–Pb dating, Hf–O isotopes, and whole rock geochemistry. *Lithos* 148, 296–311.
- Zhu, D.-C., Mo, Y.-X., Pan, G.-T., Zhao, Z., Dong, G.-C., Shi, Y., Liao, Z., Wang, L.-Q., Zhou, C.-Y., 2008. Petrogenesis of the earliest Early Cretaceous mafic rocks from the Cona area of the eastern Tethyan Himalaya in South Tibet: interaction

between the incubating Kerguelen plume and the eastern Greater India

Lithosphere? *Lithos* 100 (1–4), 147–173.

Zhu, D.-C., Mo, X.-X., Niu, Y., Zhao, Z.-D., Wang, L.-Q., Pan, G.-T., Wu, F.-Y., 2009.

Zircon U–Pb dating and in-situ Hf isotopic analysis of Permian peraluminous granite in the Lhasa terrane, southern Tibet: implications for Permian collisional orogeny and paleogeography. *Tectonophysics* 469, 48–60.

Zhu, D.-C., Zhao, Z.-D., Niu, Y., Mo, X.-X., Chung, S.-L., Hou, Z.-Q., Wang, L.-Q., Wu,

F.-Y., 2011. The Lhasa terrane: record of a microcontinent and its histories of drift and growth. *Earth Planet. Sci. Lett.* 301, 241–255.

2.9 Figures

Figure 2.9.1 Study area in the eastern Himalayan syntaxis

Study area in the eastern Himalayan syntaxis. (A) The Yarlung River follows the Indus–Yarlung Suture Zone (IYSZ, dashed) along the southern margin of Tibet before sharply turning southward to flow through the eastern Himalayan syntaxis, becoming the Siang River prior to joining the Brahmaputra River in the eastern Himalayan foreland basin (drainage area shaded). (B) Compilation of regional geological mapping (from Armijo et al., 1989; Agarwal et al., 1991; Kidd et al., 2006; Pan et al., 2004; Acharyya, 2007; Misra, 2009; Yin et al., 2010) illustrates potential source areas for <300 Ma zircons in igneous rocks north of the IYSZ and within the eastern Himalaya. We sampled Siwalik foreland basin units from three new locations (Kimin, Likabali, Pasighat) to constrain sedimentary provenance upstream of previous observations near Bhalukpong and Itanagar (Cina et al., 2009; Chirouze et al., 2013). Major tectonic features are labeled for reference: the Tipi Thrust (TPT), Main Boundary Thrust (MBT), Main Central thrust (MCT), and South Tibetan Detachment (STD).

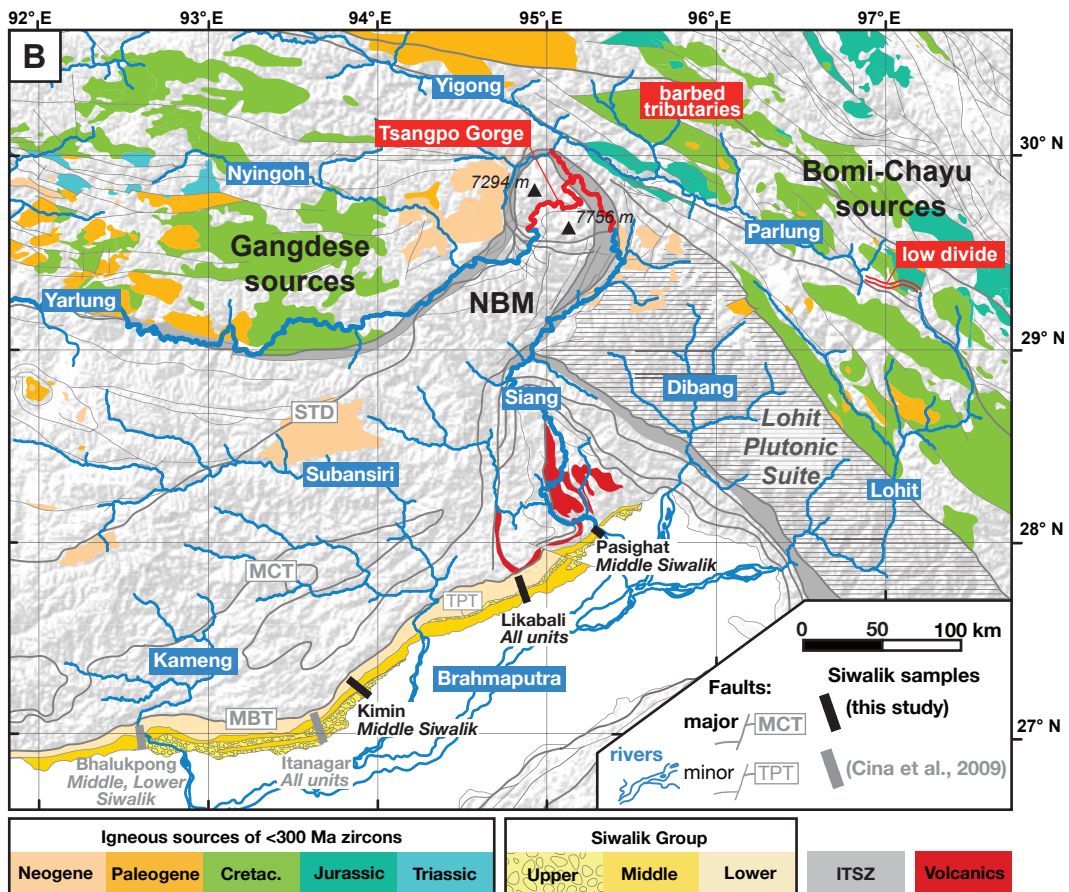
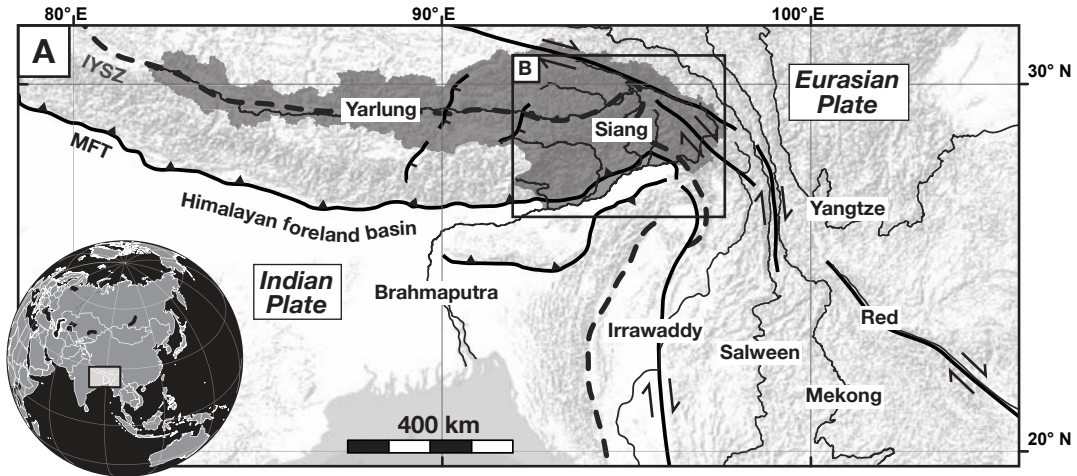
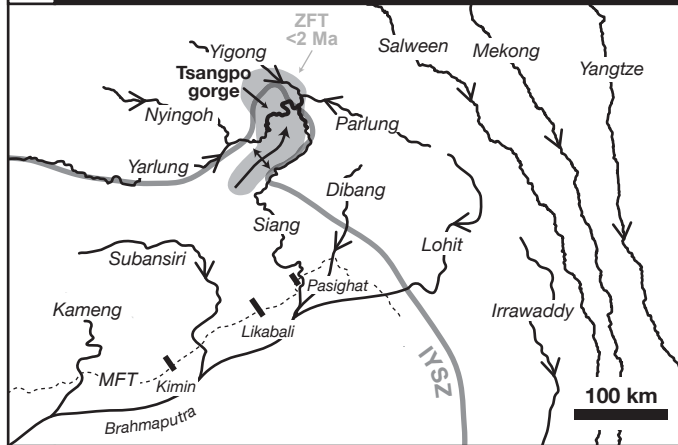


Figure 2.9.2 Drainage evolution patterns

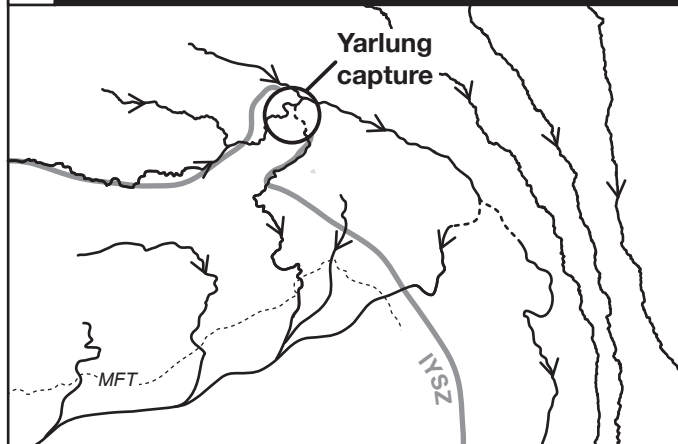
Modern drainage pattern and explanations of river capture and drainage evolution.

(A) The torturous modern route of the Yarlung–Siang–Brahmaputra River across the rapidly exhuming Namche Barwa massif (defined by gray area of zircon fission-track (ZFT) cooling ages <2 Ma, Enkelmann et al., 2011). (B) Headward erosion of a Himalayan tributary may have captured an ancestral east-draining Yarlung River to initiate rapid exhumation at the capture location (e.g., Clark et al., 2004), or (C) lateral propagation of the massif may have forced an integrated Yarlung–Siang–Brahmaputra River to capture an ancestral east-draining Yigong–Parlung River (e.g., Seward and Burg, 2008).

A Drainage pattern in the eastern Himalayan syntaxis



B Capture by headward erosion of a Himalayan tributary



C Capture by propagation of the Namche Barwa massif

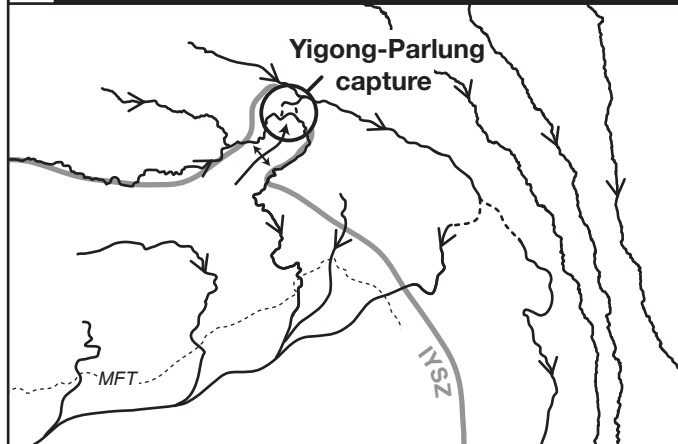
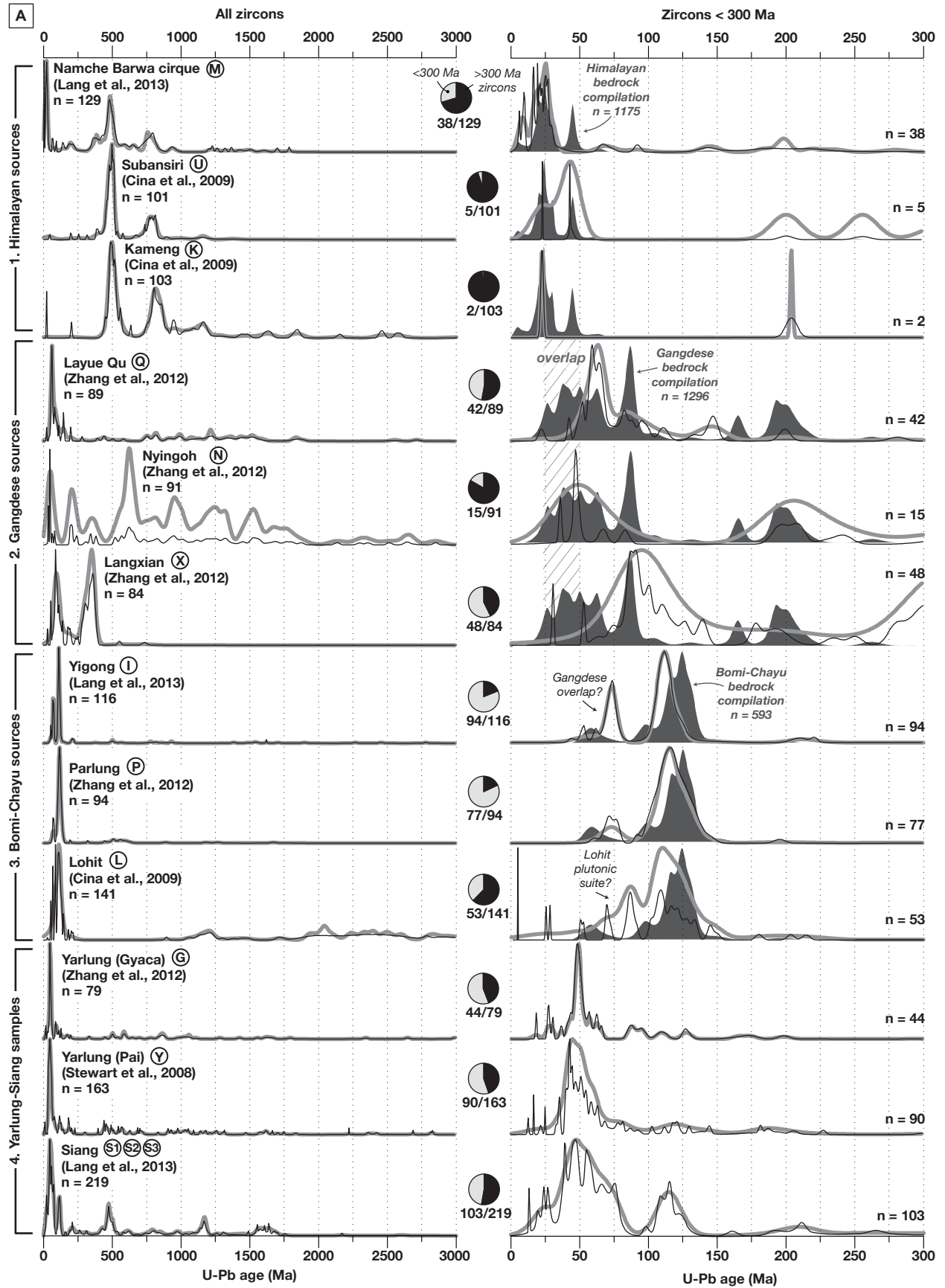
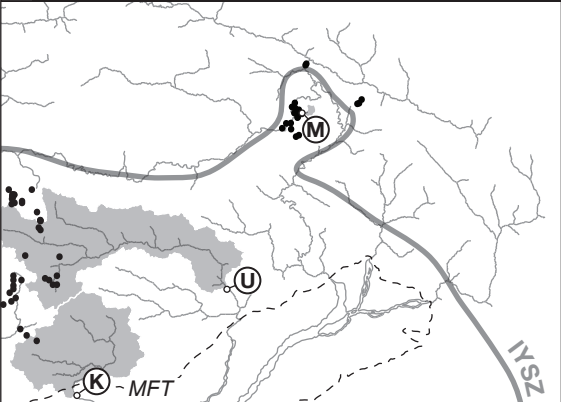


Figure 2.9.3 Published bedrock and detrital geochronology

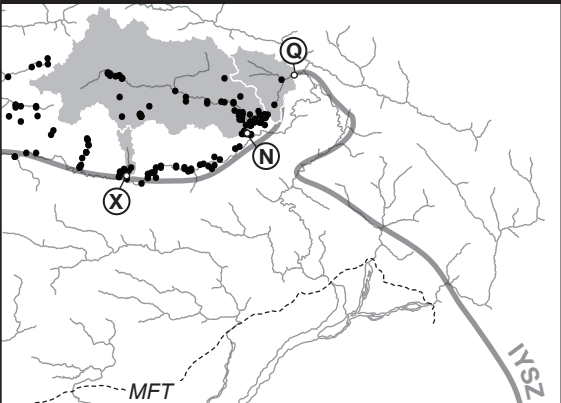
Compilation of published bedrock and detrital zircon U–Pb ages from the eastern syntaxis region. (A) Compiled age data from 1. Himalaya, 2. Gangdese, 3. Bomi–Chayu sources, and 4. modern samples from the Yarlung and Siang rivers (see text for references). Ages from detrital samples are plotted as normalized summed probability density functions (thin black line) and kernel density estimates (thick gray line). Kernel density estimates are locally adapted to age density with a maximum smoothing bandwidth of 30 Ma (generated using the Density Plotter application of Vermeesch, 2012). Bedrock ages (<300 Ma only) are plotted as solid-dark-gray kernel density estimates for comparison with detrital samples. The full range of observed ages from 0–3000 Ma is shown in the left column, and 0–300 Ma ages are shown in detail in the right column. Pie charts show the fraction of zircons <300 Ma. (B) Locations for the bedrock (black dots) and detrital (white dots, with contributing drainage area in gray) samples used in the data compilation in (A).



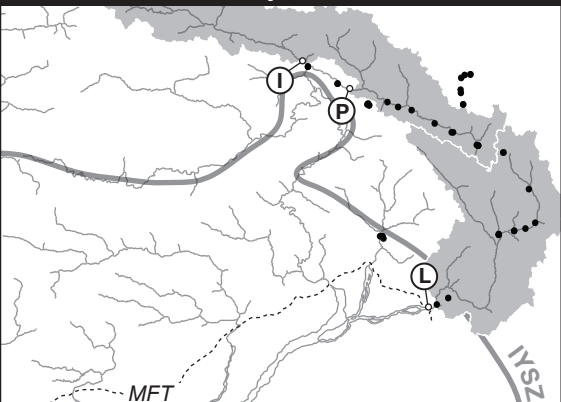
B Himalayan sources



Gangdese sources



Bomi-Chayu sources



Yarlung and Siang river samples

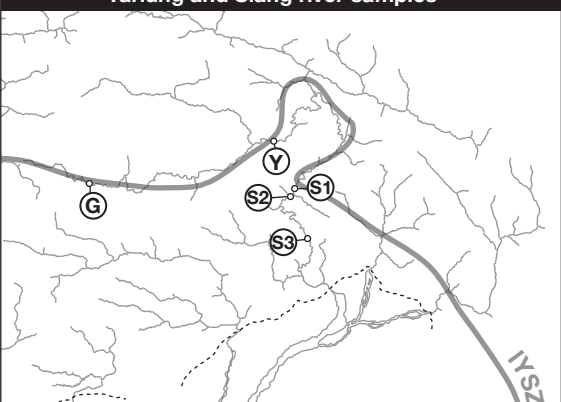
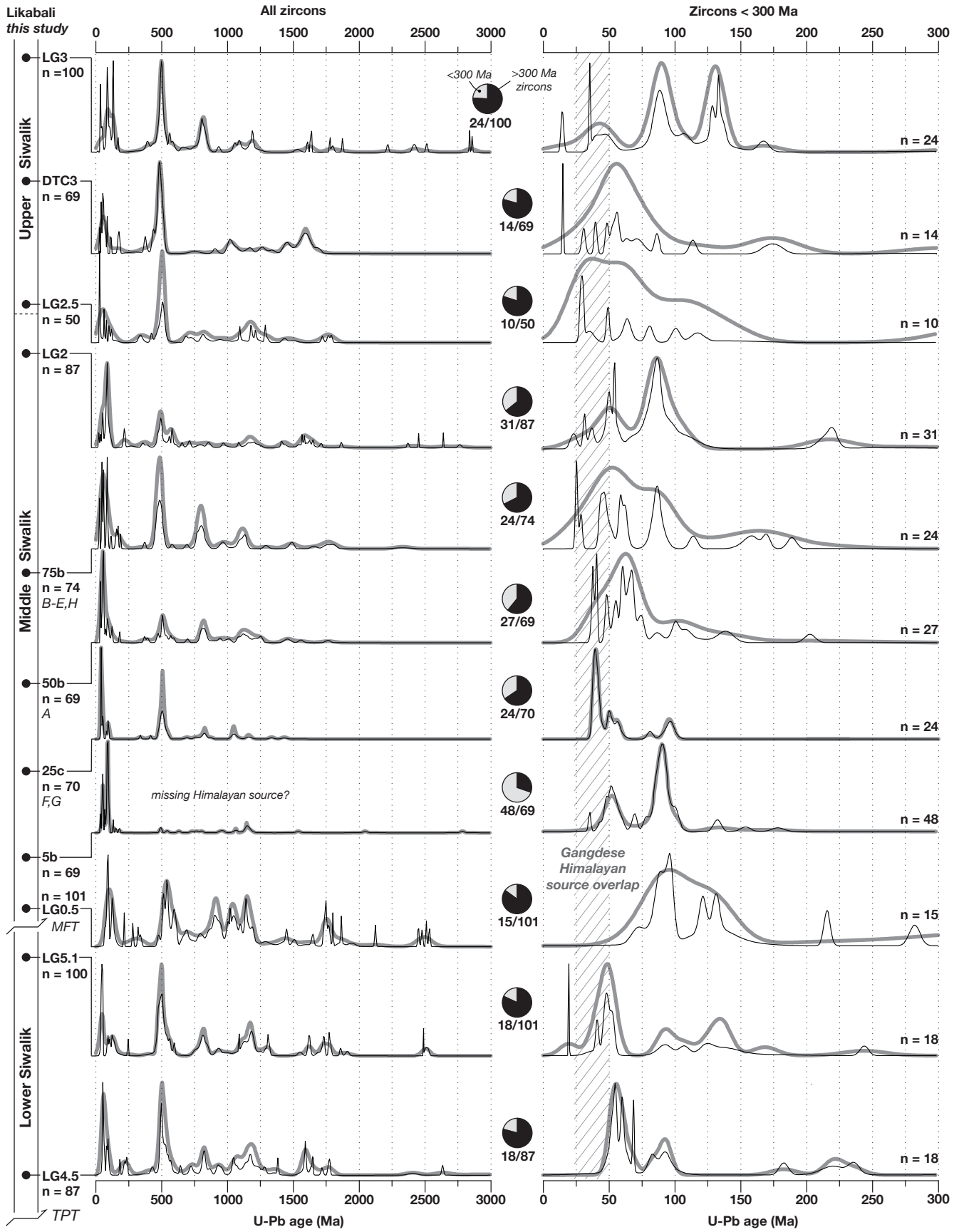


Figure 2.9.4 New detrital geochronology of Siwalik units

Detrital zircon U–Pb data from Siwalik units sampled at the three new locations shown in Figure 1 and data from previously sampled sections at Bhalukpong and Itanagar (Cina et al., 2009) for comparison. Samples are plotted at their approximate stratigraphic position. Paleogene–Late Cretaceous ages characteristic of Gangdese sources west of the Namche Barwa massif are observed in all samples with the exception of the Lower Siwalik unit at Bhalukpong (Cina et al., 2009). Pie charts and age spectra are plotted in the same manner as Figure 3.



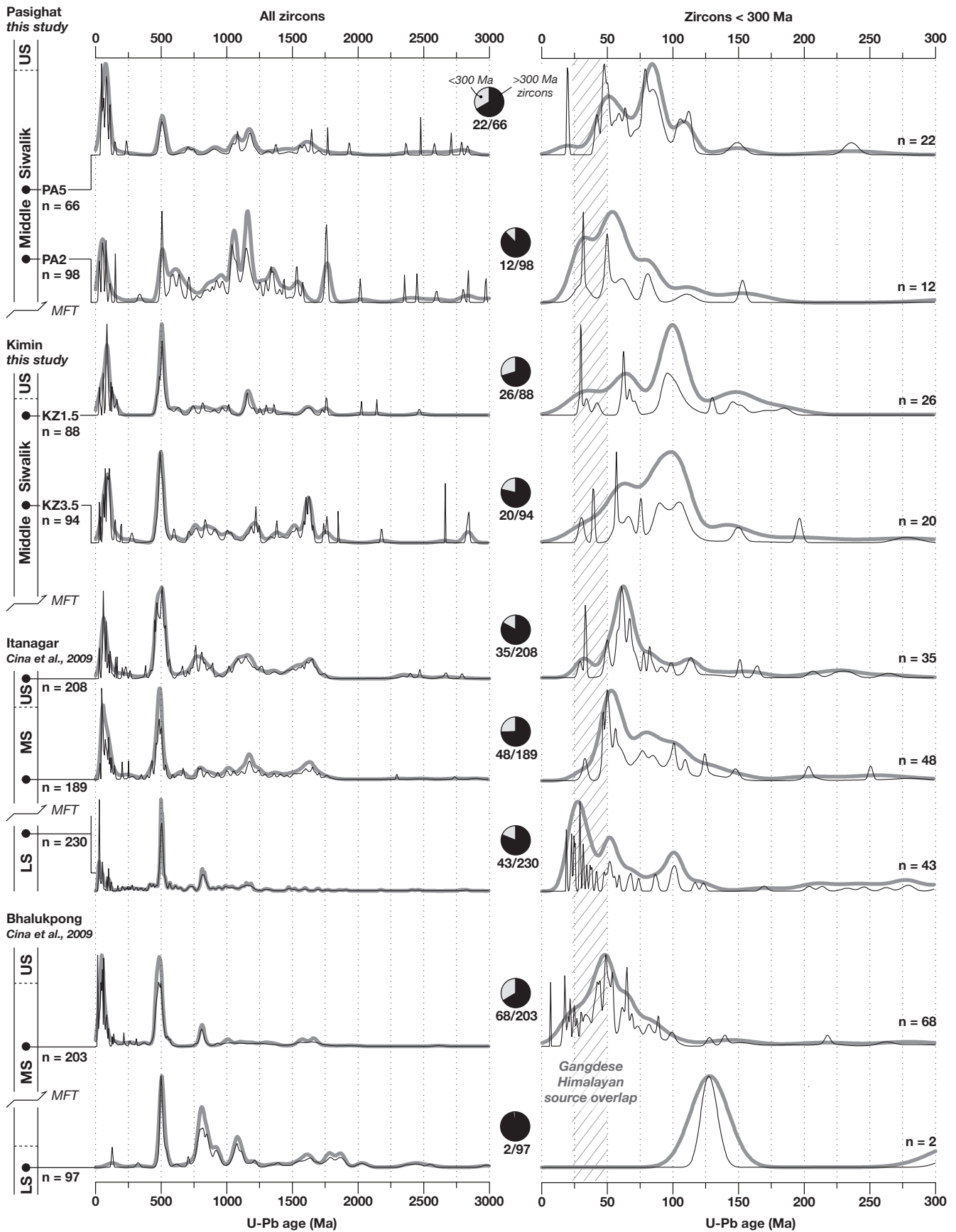
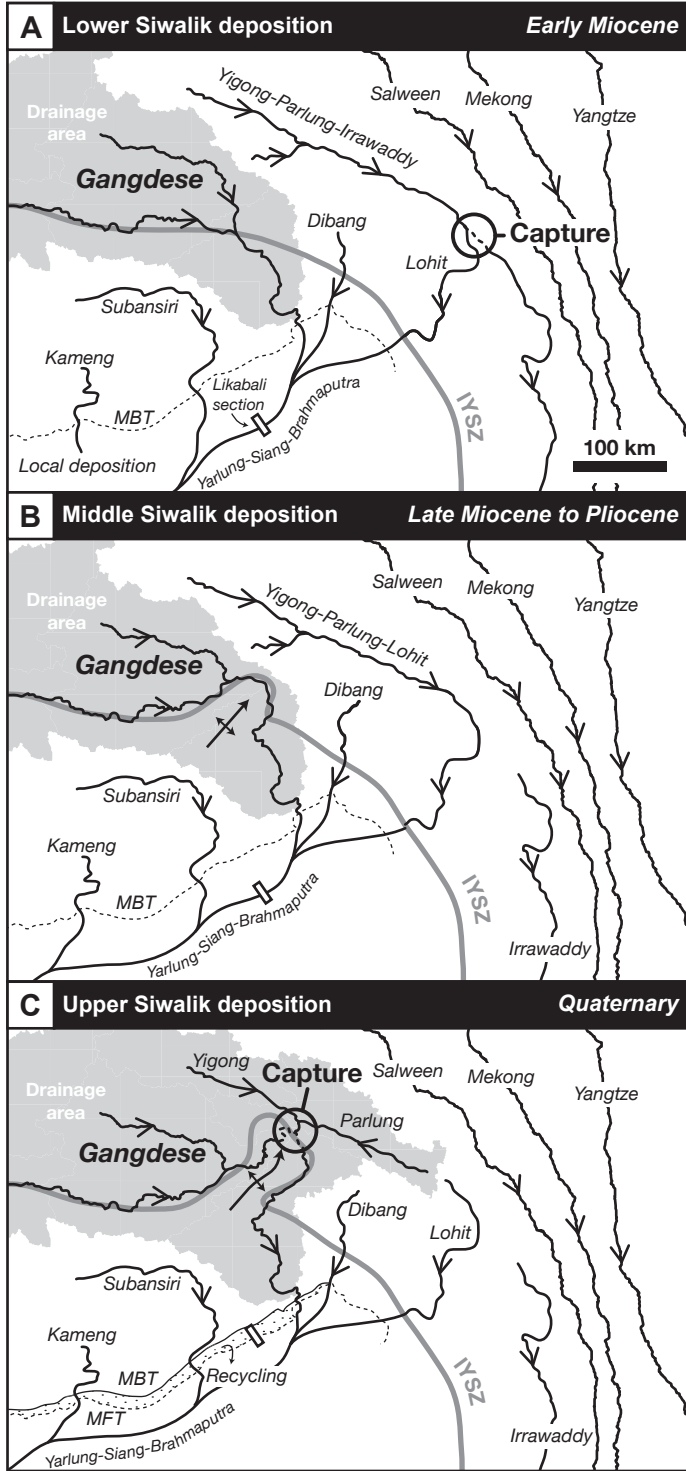


Figure 2.9.5 Proposed drainage evolution

Proposed drainage evolution of rivers flowing into the eastern Himalayan foreland basin. (A) Connection of the Yarlung–Siang–Brahmaputra River was established during or prior to deposition of the Lower Siwalik unit in the Early Miocene. The ancestral Yarlung River may have followed the IYSZ into the basin as an ancestral Yigong–Parlung River connected to the Irrawaddy system prior to capture by the Lohit River at ~18 Ma (Robinson et al., 2013). (B) Uplift of the Namche Barwa massif began to warp the IYSZ into a U-shape, steepening the Yarlung–Siang–Brahmaputra where it crosses the structure and initiating rapid exhumation of the massif. (C) Lateral propagation of the massif eventually led to capture of the Yigong and Parlung Rivers, reversing flow of the Parlung. The timing of this event remains poorly constrained but may have been influenced by glacial activity in the Quaternary Period.



2.10 Tables

2.10.1 Detrital zircon (U-Th)/Pb analyses

TABLE A1. Details of detrital zircon (U-Th)/Pb analyses (1 sigma uncertainties reported). Analyses conducted at University of Arizona LaserChron Center.

NORTHING	EASTING	DIRECTION	LOCATION	UNIT	SAMPLE ID	GRAIN	GRAIN ID	U (ppm)	206Pb*/204Pb	U/Th	Isotope ratios						Apparent ages (Ma)										
											206Pb*/207Pb*	± (%)	207Pb*/235U*	± (%)	206Pb*/238U	± (%)	error corr.	206Pb*/238U*	± (Ma)	207Pb*/235U	± (Ma)	206Pb*/207Pb*	± (Ma)	Preferred age (Ma)	± (Ma)	Conc (%)	
28.13025	95.301267	PASIGHAT	MIDDLE SIAWALK	PA2	1	PA2-01	130	124661	1.3	12.3537	0.8	0.8	2.0639	3.8	0.1849	3.7	0.97	1093.8	± 7.0	1136.9	± 25.8	1220.2	± 16.7	16.7	90		
28.13025	95.301267	PASIGHAT	MIDDLE SIAWALK	PA2	2	PA2-02	191	80606	1.1	17.3402	1.3	0.6532	1.6	0.0822	1.9	0.55	509.0	4.3	510.5	6.3	517.2	28.9	509.0	4.3	98		
28.13025	95.301267	PASIGHAT	MIDDLE SIAWALK	PA2	3	PA2-03	187	76510	2.0	14.2145	0.7	1.5092	1.5	0.1556	1.4	0.90	932.2	11.9	934.1	9.3	938.6	13.5	932.2	11.9	99		
28.13025	95.301267	PASIGHAT	MIDDLE SIAWALK	PA2	4	PA2-04	174	327637	1.4	13.2628	0.7	1.8831	1.5	0.1811	1.3	0.88	1073.2	12.1	1077.2	10.7	1079.2	13.9	1079.2	13.9	99		
28.13025	95.301267	PASIGHAT	MIDDLE SIAWALK	PA2	5	PA2-05	186	150914	2.1	10.2074	0.3	3.7798	1.3	0.2798	1.3	0.97	1550.4	18.8	1558.5	6.4	1585.8	6.4	1585.8	6.4	100		
28.13025	95.301267	PASIGHAT	MIDDLE SIAWALK	PA2	6	PA2-06	150	134297	1.0	13.0266	1.0	1.9882	1.2	0.1878	0.7	0.55	1109.7	6.9	1115.1	8.3	1115.1	20.4	1115.1	20.4	100		
28.13025	95.301267	PASIGHAT	MIDDLE SIAWALK	PA2	7	PA2-07	107	104705	1.0	12.9200	0.7	2.0940	2.0	0.1943	1.9	0.94	1144.5	19.7	1146.9	13.8	1151.3	13.8	1151.3	13.8	99		
28.13025	95.301267	PASIGHAT	MIDDLE SIAWALK	PA2	8	PA2-08	184	73658	1.5	16.4448	0.8	0.8938	2.2	0.1066	2.0	0.94	653.0	12.7	648.4	10.4	632.5	16.2	653.0	12.7	103		
28.13025	95.301267	PASIGHAT	MIDDLE SIAWALK	PA2	9	PA2-09	125	147847	0.8	8.0141	0.3	6.1701	2.0	0.3586	2.0	0.99	1975.7	34.4	2000.2	17.8	2025.7	5.0	2025.7	5.0	98		
28.13025	95.301267	PASIGHAT	MIDDLE SIAWALK	PA2	10	PA2-10	522	207919	5.2	11.6063	0.3	2.7895	2.1	0.2348	2.1	0.99	1359.7	25.4	1352.7	15.6	1341.8	6.0	1341.8	6.0	101		
28.13025	95.301267	PASIGHAT	MIDDLE SIAWALK	PA2	11	PA2-12	166	265841	1.2	9.2759	0.3	4.6752	1.1	0.3145	1.0	0.95	1762.9	15.6	1762.8	9.0	1762.6	6.3	1762.6	6.3	100		
28.13025	95.301267	PASIGHAT	MIDDLE SIAWALK	PA2	12	PA2-13	34	15534	0.8	16.7046	6.9	0.8192	7.2	0.0992	2.0	0.28	610.0	11.7	607.6	33.0	598.7	15.0	610.0	11.7	102		
28.13025	95.301267	PASIGHAT	MIDDLE SIAWALK	PA2	13	PA2-16	193	80675	1.2	12.5509	0.7	2.1881	1.4	0.1992	1.1	0.84	1170.9	12.2	1177.3	9.4	1189.0	14.3	1189.0	14.3	98		
28.13025	95.301267	PASIGHAT	MIDDLE SIAWALK	PA2	14	PA2-17	41	41390	0.7	11.0300	2.6	3.1865	6.2	0.2549	5.6	0.91	1463.7	73.6	1453.9	47.7	1439.5	48.7	1439.5	48.7	102		
28.13025	95.301267	PASIGHAT	MIDDLE SIAWALK	PA2	15	PA2-18	146	437073	2.6	6.2328	0.2	10.0182	1.8	0.4529	1.8	0.99	2408.0	36.3	2436.5	16.8	2460.3	4.1	2460.3	4.1	98		
28.13025	95.301267	PASIGHAT	MIDDLE SIAWALK	PA2	16	PA2-19	233	29870	0.8	17.4200	2.0	0.6515	2.5	0.0823	1.6	0.62	509.9	7.6	509.4	10.0	507.1	43.1	509.9	7.6	101		
28.13025	95.301267	PASIGHAT	MIDDLE SIAWALK	PA2	17	PA2-20	239	444663	1.7	12.1093	0.5	2.4853	1.9	0.2183	1.9	0.97	1272.7	21.6	1287.8	13.9	1259.4	8.9	1259.4	8.9	101		
28.13025	95.301267	PASIGHAT	MIDDLE SIAWALK	PA2	18	PA2-21	111	75919	2.4	15.5538	1.3	1.1351	2.8	0.1280	2.4	0.89	776.7	17.9	770.2	14.8	751.4	26.8	776.7	17.9	103		
28.13025	95.301267	PASIGHAT	MIDDLE SIAWALK	PA2	19	PA2-22	193	89125	1.2	13.9455	0.8	1.6092	1.6	0.1628	1.4	0.88	972.1	13.0	973.8	10.2	977.7	15.5	972.1	13.0	99		
28.13025	95.301267	PASIGHAT	MIDDLE SIAWALK	PA2	20	PA2-23	80	63375	2.8	13.7896	1.7	1.7242	2.3	0.1724	1.6	0.68	1025.5	15.0	1017.6	14.9	1000.5	34.3	1000.5	34.3	102		
28.13025	95.301267	PASIGHAT	MIDDLE SIAWALK	PA2	21	PA2-24	73	111934	0.6	17.8700	3.5	0.6343	3.9	0.0809	1.6	0.41	501.5	7.7	498.7	15.2	486.1	77.7	501.5	7.7	103		
28.13025	95.301267	PASIGHAT	MIDDLE SIAWALK	PA2	22	PA2-25	332	253543	5.8	11.0149	0.3	3.1371	2.9	0.2506	2.9	0.99	1441.6	36.9	1441.8	22.1	1442.1	5.6	1442.1	5.6	100		
28.13025	95.301267	PASIGHAT	MIDDLE SIAWALK	PA2	23	PA2-26	39	15597	0.9	10.9869	7.1	0.7803	7.5	0.0900	2.5	0.33	555.7	13.1	556.7	32.2	561.0	154.7	555.7	13.1	99		
28.13025	95.301267	PASIGHAT	MIDDLE SIAWALK	PA2	24	PA2-27	402	297202	15.4	15.0160	0.4	1.2573	1.4	0.1369	1.8	0.97	824.1	18.4	826.7	18.3	827.3	14.4	827.3	14.4	100		
28.13025	95.301267	PASIGHAT	MIDDLE SIAWALK	PA2	25	PA2-28	546	396911	2.6	15.7506	0.5	1.0211	1.4	0.1166	1.3	0.94	711.2	9.0	714.5	7.3	724.9	9.9	711.2	9.0	98		
28.13025	95.301267	PASIGHAT	MIDDLE SIAWALK	PA2	26	PA2-29	194	349703	1.5	10.4510	0.3	3.5882	0.8	0.2720	0.7	0.93	1550.8	10.2	1546.9	6.4	1541.6	5.6	1541.6	5.6	101		
28.13025	95.301267	PASIGHAT	MIDDLE SIAWALK	PA2	27	PA2-30	119	53420	0.4	16.8311	3.3	0.7658	3.5	0.0935	1.3	0.37	576.1	7.3	577.3	15.6	582.3	71.5	577.3	7.3	99		
28.13025	95.301267	PASIGHAT	MIDDLE SIAWALK	PA2	28	PA2-31	296	1000	0.7	18.5591	13.7	0.0578	13.9	0.0078	2.5	0.18	49.9	1.2	57.0	37.7	366.1	309.8	49.9	1.2	NA		
28.13025	95.301267	PASIGHAT	MIDDLE SIAWALK	PA2	29	PA2-32	145	31331	0.9	17.4288	3.8	0.5592	4.3	0.0833	2.0	0.46	516.0	9.7	514.1	30.0	506.0	83.0	516.0	9.7	102		
28.13025	95.301267	PASIGHAT	MIDDLE SIAWALK	PA2	30	PA2-33	100	242507	2.0	9.2356	0.4	4.7283	1.6	0.3167	1.6	0.97	1773.2	24.7	1772.3	13.8	1770.6	7.6	1770.6	7.6	100		
28.13025	95.301267	PASIGHAT	MIDDLE SIAWALK	PA2	31	PA2-34	78	60727	1.2	10.3743	0.9	3.3002	4.9	0.2483	4.8	0.98	1429.8	61.1	1481.1	37.9	1555.4	17.7	1555.4	17.7	92		
28.13025	95.301267	PASIGHAT	MIDDLE SIAWALK	PA2	32	PA2-35	55	62405	2.5	14.4160	2.5	1.4227	2.7	0.1487	1.2	0.83	893.9	9.7	898.5	16.3	909.7	50.9	893.9	9.7	98		
28.13025	95.301267	PASIGHAT	MIDDLE SIAWALK	PA2	33	PA2-36	217	67101	2.2	9.2287	0.3	4.5382	1.3	0.3038	1.3	0.97	1709.9	19.4	1738.0	11.1	1772.0	5.5	1772.0	5.5	96		
28.13025	95.301267	PASIGHAT	MIDDLE SIAWALK	PA2	34	PA2-37	35	36773	0.5	12.7436	3.8	2.2198	4.3	0.2052	2.0	0.48	1203.0	22.4	1187.3	30.0	1158.8	74.7	1158.8	74.7	104		
28.13025	95.301267	PASIGHAT	MIDDLE SIAWALK	PA2	35	PA2-38	91	5957	1.0	30.8173	75.0	0.0371	75.7	0.0083	10.1	0.13	53.2	5.4	52.1	27.5	52.1	253.2	53.2	5.4	NA		
28.13025	95.301267	PASIGHAT	MIDDLE SIAWALK	PA2	36	PA2-39	52	53838	1.8	13.3326	2.1	1.8560	2.5	0.1795	1.4	0.54	1064.1	13.5	1065.6	16.8	1068.6	42.9	1068.6	42.9	100		
28.13025	95.301267	PASIGHAT	MIDDLE SIAWALK	PA2	37	PA2-40	186	64321	0.6	17.4656	2.0	0.6427	3.2	0.0814	2.5	0.77	504.6	11.9	504.0	12.6	501.4	48.6	504.6	12.6	101		
28.13025	95.301267	PASIGHAT	MIDDLE SIAWALK	PA2	38	PA2-41	87	104742	1.1	12.9634	1.4	2.0167	2.3	0.1896	1.9	0.80	1119.2	19.2	1121.1	15.8	1124.8	47.9	1124.8	27.9	100		
28.13025	95.301267	PASIGHAT	MIDDLE SIAWALK	PA2	39	PA2-42	818	142182	1.4	20.0973	1.9	0.1652	2.4	0.0241	1.5	0.63	153.4	2.3	183.7	3.5	155.2	23.9	153.4	2.3	NA		
28.13025	95.301267	PASIGHAT	MIDDLE SIAWALK	PA2	40	PA2-43	580	584599	1.0	11.1948	0.6	2.9143	3.5	0.2366	3.5	0.98	1369.1	42.6	1385.6	26.5	1411.2	12.3	1411.2	12.3	97		
28.13025	95.301267	PASIGHAT	MIDDLE SIAWALK	PA2	41	PA2-44	168	150939	4.3	14.3627	1.6	1.5463	3.3	0.1611	2.9	0.88	962.7	25.6	949.0	20.1	917.3	33.9	962.7	25.6	105		
28.13025	95.301267	PASIGHAT	MIDDLE SIAWALK	PA2	42	PA2-45	105	11473	0.8	21.0391	13.3	0.1135	14.4	0.0173	5.6	0.39	110.7	6.2	109.2	15.0	75.9	137.4	110.7	6.2	NA		
28.13025	95.301267	PASIGHAT	MIDDLE SIAWALK	PA2	43	PA2-46	43	193007	1.1	4.9239	0.2	15.2408	2.5	0.5443	2.5	1.00	2801.3	56.5	2830.4	23.7	2851.2	2.9	2851.2	2.9	98		
28.13025	95.301267	PASIGHAT	MIDDLE SIAWALK	PA2	44	PA2-47	220	275109	1.1	6.5894	0.3	6.5894	4.7	0.4102	4.7	1.00	2216.0	87.4	2294.8	42.5	2365.8	4.3	2365.8	4.3	94		
28.13025	95.301267	PASIGHAT	MIDDLE SIAWALK	PA2	45	PA2-48	375	420482	7.4	13.4954	0.4	1.7893	3.3	0.1751	3.3	0.99	1040.3	31.5	1041.6	10.0	1044.2	9.0	1044.2	9.0	100		
28.13025	95.301267	PASIGHAT	MIDDLE SIAWALK	PA2	46	PA2-49	1650	2057	0.4	16.5227	26.5	0.0411	32.4	0.0049	18.7	0.58	31.7	5.9	40.9	21.6	102.3	580.3	31.7	5.9	NA		
28.13025	95.301267	PASIGHAT	MIDDLE SIAWALK	PA2	47	PA2-50	70	15335	2.33	0.9	9.2331	195.0	0.0699	172.2	0.09	30.1	5.2	177.0	130.6	177.1	288.8	177.0	130.6	177.1	288.8	5.2	NA
28.13025	95.301267	PASIG																									

28.13025	95.301267	PASIGHAT	MIDDLE SIAWALK	PA2	90	PA2-97	105	134626	1.0	13.4006	0.9	1.7295	2.6	0.1681	2.4	0.94	1001.6	22.3	1019.6	16.5	1058.4	17.7	1058.4	17.7	1058.4	17.7	95
28.13025	95.301267	PASIGHAT	MIDDLE SIAWALK	PA2	91	PA2-98	42	26360	1.0	12.4966	3.6	2.2450	4.1	0.2035	1.9	0.46	1194.0	20.6	1195.2	26.8	1197.5	17.8	1197.5	17.8	1197.5	17.8	100
28.13025	95.301267	PASIGHAT	MIDDLE SIAWALK	PA2	92	PA2-99	152	163658	2.6	11.8337	0.4	2.5434	1.9	0.1783	1.9	0.98	1272.8	21.6	1284.6	13.9	1304.2	7.2	1304.2	7.2	1304.2	7.2	98
28.13025	95.301267	PASIGHAT	MIDDLE SIAWALK	PA2	93	PA2-100	116	190239	2.0	4.2530	0.3	17.2259	2.2	0.5659	2.2	0.99	280.5	92.0	290.5	13.9	294.7	13.9	294.7	13.9	294.7	13.9	97
28.13025	95.301267	PASIGHAT	MIDDLE SIAWALK	PA2	94	PA2-101	221	142650	0.7	13.4689	0.8	1.8364	2.1	0.2194	2.0	0.93	1063.6	19.3	1058.6	13.9	1048.2	15.7	1048.2	15.7	1048.2	15.7	101
28.13025	95.301267	PASIGHAT	MIDDLE SIAWALK	PA2	95	PA2-102	159	160845	1.0	13.4174	0.9	1.8187	1.8	0.1770	1.5	0.87	1050.5	14.8	1052.2	11.5	1055.9	17.5	1055.9	17.5	1055.9	17.5	99
28.13025	95.301267	PASIGHAT	MIDDLE SIAWALK	PA2	96	PA2-103	97	59741	0.7	16.9523	2.0	0.7853	2.6	0.0966	1.6	0.63	594.2	14.3	588.5	11.6	566.7	44.1	594.2	9.3	594.2	9.3	105
28.13025	95.301267	PASIGHAT	MIDDLE SIAWALK	PA2	97	PA2-104	117	154732	2.3	13.2496	0.6	1.9032	4.1	0.1829	4.0	0.99	1082.7	4.0	1082.2	10.2	1081.2	12.9	1081.2	12.9	1081.2	12.9	100
28.13025	95.301267	PASIGHAT	MIDDLE SIAWALK	PA2	98	PA2-105	121	144382	1.3	10.4727	0.6	3.5572	1.3	0.2702	1.2	0.90	1541.7	16.0	1537.7	27.3	1537.7	10.4	1537.7	10.4	1537.7	10.4	100
28.09767	95.271133	PASIGHAT	MIDDLE SIAWALK	PAS	1	PAS-1	256	16618	1.4	25.9649	20.9	0.0393	21.1	0.0074	2.5	0.12	47.5	1.2	39.1	8.1	-449.7	556.3	47.5	1.2	NA	NA	NA
28.09767	95.271133	PASIGHAT	MIDDLE SIAWALK	PAS	2	PAS-2	65	105753	1.2	5.0913	0.4	13.5576	2.5	0.5006	2.4	0.99	2616.5	52.7	2719.3	23.4	2796.6	5.8	2796.6	5.8	2796.6	5.8	94
28.09767	95.271133	PASIGHAT	MIDDLE SIAWALK	PAS	3	PAS-3	351	20991	1.4	20.0580	15.3	0.0547	15.5	0.0080	2.4	0.16	51.1	1.2	54.1	8.2	188.2	359.0	51.1	1.2	NA	NA	NA
28.09767	95.271133	PASIGHAT	MIDDLE SIAWALK	PAS	4	PAS-4	130	132727	1.1	11.7592	1.2	2.5764	2.6	0.2197	2.3	0.89	1280.5	26.4	1294.0	18.7	1316.4	22.6	1316.4	22.6	1316.4	22.6	97
28.09767	95.271133	PASIGHAT	MIDDLE SIAWALK	PAS	5	PAS-5	39	2520	1.3	19.2189	31.0	0.0990	37.1	0.0138	20.5	0.55	88.4	18.0	95.9	34.0	286.8	723.5	88.4	18.0	NA	NA	NA
28.09767	95.271133	PASIGHAT	MIDDLE SIAWALK	PAS	6	PAS-6	262	16240	2.6	20.2133	5.9	0.0857	8.9	0.0126	6.7	0.75	80.5	5.3	83.5	7.2	170.3	138.7	80.5	5.3	NA	NA	NA
28.09767	95.271133	PASIGHAT	MIDDLE SIAWALK	PAS	7	PAS-7	389	87816	1.7	17.3302	1.8	0.6309	2.9	0.0793	2.3	0.78	491.9	10.8	496.6	11.5	518.5	40.4	491.9	10.8	95	95	95
28.09767	95.271133	PASIGHAT	MIDDLE SIAWALK	PAS	8	PAS-8	295	362609	1.0	9.8730	5.5	4.0026	2.1	0.2866	2.0	0.97	1624.6	29.2	1634.7	17.1	1647.8	9.9	1647.8	9.9	1647.8	9.9	99
28.09767	95.271133	PASIGHAT	MIDDLE SIAWALK	PAS	9	PAS-9	352	24056	1.0	24.9900	7.2	0.0418	7.8	0.0076	3.0	0.39	48.6	1.5	41.5	3.2	-349.9	185.2	48.6	1.5	NA	NA	NA
28.09767	95.271133	PASIGHAT	MIDDLE SIAWALK	PAS	10	PAS-10	61	257607	1.3	4.9486	0.5	14.6472	1.7	0.5257	1.6	0.95	2723.3	36.2	2792.6	16.3	2843.0	8.7	2843.0	8.7	2843.0	8.7	96
28.09767	95.271133	PASIGHAT	MIDDLE SIAWALK	PAS	11	PAS-11	260	365197	1.6	10.7838	1.9	3.0670	4.6	0.2399	4.2	0.91	1386.0	52.3	1424.5	35.4	1482.4	36.6	1482.4	36.6	1482.4	36.6	93
28.09767	95.271133	PASIGHAT	MIDDLE SIAWALK	PAS	12	PAS-12	339	89428	1.7	11.3909	0.4	2.8637	2.6	0.2366	2.6	0.99	1368.9	32.0	1372.4	19.8	1377.9	7.8	1377.9	7.8	1377.9	7.8	99
28.09767	95.271133	PASIGHAT	MIDDLE SIAWALK	PAS	13	PAS-14	347	372193	1.2	13.2453	0.6	0.9166	2.0	0.1841	1.9	0.95	1039.4	18.6	1086.9	13.1	1081.8	12.8	1081.8	12.8	1081.8	12.8	101
28.09767	95.271133	PASIGHAT	MIDDLE SIAWALK	PAS	14	PAS-15	431	45808	0.5	20.4250	5.0	0.1193	5.3	0.0177	1.8	0.35	1189.2	2.1	114.5	5.7	145.9	116.6	113.0	2.1	NA	NA	NA
28.09767	95.271133	PASIGHAT	MIDDLE SIAWALK	PAS	15	PAS-16	222	294341	1.7	9.8589	0.2	0.6145	1.9	0.2871	1.9	0.99	1626.8	27.3	1637.1	15.5	1650.5	4.5	1650.5	4.5	99	99	99
28.09767	95.271133	PASIGHAT	MIDDLE SIAWALK	PAS	16	PAS-17	392	168915	0.8	17.2967	1.2	4.0548	3.4	0.0821	3.1	0.93	508.9	15.2	511.4	13.5	522.7	27.4	508.9	15.2	97	97	97
28.09767	95.271133	PASIGHAT	MIDDLE SIAWALK	PAS	17	PAS-18	188	7413	1.2	21.6704	14.6	0.1052	14.8	0.0165	2.8	0.19	105.7	2.9	101.6	5.2	105.7	5.2	105.7	5.2	105.7	5.2	98
28.09767	95.271133	PASIGHAT	MIDDLE SIAWALK	PAS	18	PAS-19	180	247777	1.8	15.2138	1.0	2.1228	1.0	0.2182	1.0	1.86	1156.2	18.3	1169.4	16.8	1169.4	16.8	1169.4	16.8	1169.4	16.8	98
28.09767	95.271133	PASIGHAT	MIDDLE SIAWALK	PAS	19	PAS-20	221	354517	0.5	9.2196	0.2	4.6550	1.3	0.3113	1.3	0.99	1746.9	19.8	1759.2	10.9	1773.8	2.8	1773.8	2.8	1773.8	2.8	98
28.09767	95.271133	PASIGHAT	MIDDLE SIAWALK	PAS	20	PAS-21	201	434159	0.7	6.1442	0.1	10.2232	1.7	0.4556	1.7	1.00	2420.0	33.4	2455.2	15.3	2484.5	1.7	2484.5	1.7	2484.5	1.7	97
28.09767	95.271133	PASIGHAT	MIDDLE SIAWALK	PAS	21	PAS-22	65	3469	0.9	21.1949	40.9	0.0928	41.6	0.0143	7.9	0.19	91.3	7.1	90.1	35.9	58.4	1012.5	91.3	7.1	NA	NA	NA
28.09767	95.271133	PASIGHAT	MIDDLE SIAWALK	PAS	22	PAS-23	164	136968	1.1	13.2310	1.2	1.8347	4.0	0.1761	3.8	0.95	1045.4	36.4	1058.0	26.1	1084.0	24.5	1084.0	24.5	1084.0	24.5	96
28.09767	95.271133	PASIGHAT	MIDDLE SIAWALK	PAS	23	PAS-24	215	180311	3.4	12.6086	0.6	2.1169	1.4	0.1036	1.3	0.89	1140.7	13.2	1154.3	9.8	1179.9	12.7	1179.9	12.7	1179.9	12.7	97
28.09767	95.271133	PASIGHAT	MIDDLE SIAWALK	PAS	24	PAS-25	125	77289	1.0	15.9487	2.1	1.0030	2.8	0.1160	1.8	0.65	707.6	12.1	705.3	14.2	698.1	45.3	707.6	12.1	101	101	101
28.09767	95.271133	PASIGHAT	MIDDLE SIAWALK	PAS	25	PAS-26	104	70780	0.8	10.1606	0.7	3.7743	2.9	0.2781	2.8	0.97	1582.0	39.6	1587.3	23.3	1594.4	12.6	1594.4	12.6	1594.4	12.6	99
28.09767	95.271133	PASIGHAT	MIDDLE SIAWALK	PAS	26	PAS-27	98	70283	1.6	12.4539	1.2	2.2153	4.0	0.2001	3.8	0.96	1175.8	41.2	1185.9	28.0	1204.2	22.9	1204.2	22.9	1204.2	22.9	98
28.09767	95.271133	PASIGHAT	MIDDLE SIAWALK	PAS	27	PAS-28	101	6650	1.1	22.4696	33.6	0.0678	34.0	0.0111	5.3	0.16	42.9	3.8	66.6	21.9	51.7	843.4	70.9	3.8	NA	NA	NA
28.09767	95.271133	PASIGHAT	MIDDLE SIAWALK	PAS	28	PAS-29	115	2908	0.9	21.2562	22.5	0.0837	23.1	0.0129	4.9	0.21	82.6	4.0	81.6	18.1	81.5	544.0	82.6	4.0	NA	NA	NA
28.09767	95.271133	PASIGHAT	MIDDLE SIAWALK	PAS	29	PAS-30	133	5443	1.5	19.0835	33.3	0.0673	33.4	0.0093	3.1	0.09	59.7	1.8	65.1	31.1	21.4	303.0	59.7	1.8	NA	NA	NA
28.09767	95.271133	PASIGHAT	MIDDLE SIAWALK	PAS	30	PAS-31	354	559863	9.1	8.4124	0.3	4.2548	3.4	0.2596	3.3	0.99	1487.8	44.4	1684.7	27.7	1939.3	6.2	1939.3	6.2	1939.3	6.2	77
28.09767	95.271133	PASIGHAT	MIDDLE SIAWALK	PAS	31	PAS-34	140	10671	1.9	20.0255	15.1	0.1178	15.7	0.0171	4.6	0.29	109.4	4.9	113.1	16.9	192.1	352.3	109.4	4.9	NA	NA	NA
28.09767	95.271133	PASIGHAT	MIDDLE SIAWALK	PAS	32	PAS-35	369	13614	1.7	21.1325	64.3	0.0205	64.4	0.0031	3.3	0.05	20.2	0.7	20.6	13.1	65.4	1708.8	20.2	0.7	NA	NA	NA
28.09767	95.271133	PASIGHAT	MIDDLE SIAWALK	PAS	33	PAS-36	34	36280	0.5	18.1389	12.3	0.6090	12.7	0.0801	3.0	0.24	496.9	14.6	483.0	48.7	417.5	275.6	496.9	14.6	119	119	119
28.09767	95.271133	PASIGHAT	MIDDLE SIAWALK	PAS	34	PAS-37	105	103408	1.3	14.3701	1.3	1.4502	3.3	0.1551	3.2	0.93	907.4	27.3	910.0	20.9	916.3	26.8	907.4	27.3	99	99	99
28.09767	95.271133	PASIGHAT	MIDDLE SIAWALK	PAS	35	PAS-38	462	370757	4.2	10.9519	4.6	2.7104	7.5	0.2153	6.0	0.80	1256.9	68.4	1331.3	55.9	1450.0	86.7	1450.0	86.7	1450.0	86.7	87
28.09767	95.271133	PASIGHAT	MIDDLE SIAWALK	PAS	36	PAS-39	654	7375	0.5	21.1267	8.2	0.0432	9.0	0.0066	3.8	0.42	42.5	1.6	42.9	3.8	42.9	3.8	42.9	3.8	42.9	3.8	98
28.09767	95.271133	PASIGHAT	MIDDLE SIAWALK	PAS	37	PAS-40	173	26420	1.2	20.3800	3.0	0.2531	3.7	0.0374	2.3	0.61	236.8	5.3	229.1	7.7	151.1	69.4	236.8	5.3	NA	NA	NA
28.09767	95.271133	PASIGHAT	MIDDLE SIAWALK	PAS	38	PAS-41	183	128142	6.1	13.4886	0.8	1.6300															

27.742817	94.715333	LIKABALI	UPPER SIWALIK	LG3	17	18	197	6692	2.1	17.5931	1.6	0.6191	2.7	0.0790	2.1	0.80	490.1	10.1	489.3	10.3	485.3	35.1	490.1	10.1	101	
27.742817	94.715333	LIKABALI	UPPER SIWALIK	LG3	18	18	4163	1162	2.2	20.3128	36.1	0.0966	36.4	0.0142	4.5	0.12	91.1	4.0	93.6	32.5	158.8	869.7	91.1	4.0	NA	
27.742817	94.715333	LIKABALI	UPPER SIWALIK	LG3	19	19	376	495130	5.6	8.6956	0.2	5.2965	0.7	0.3340	0.7	0.95	1857.9	11.2	1868.3	6.3	1879.9	41.1	1879.9	41.1	99	
27.742817	94.715333	LIKABALI	UPPER SIWALIK	LG3	20	20	4	191927	0.6	12.3521	2.3	1.2352	3.0	0.065	2.0	0.65	1122.1	20.4	1129.6	20.5	1129.6	44.7	1129.6	44.7	48	
27.742817	94.715333	LIKABALI	UPPER SIWALIK	LG3	21	21	498	153726	1.7	17.4210	1.0	0.6193	1.7	0.0782	1.4	0.82	485.6	6.4	489.4	6.5	507.0	21.0	485.6	6.4	96	
27.742817	94.715333	LIKABALI	UPPER SIWALIK	LG3	22	22	36	103439	0.6	9.0615	0.5	4.3591	1.5	0.5	2.865	3.4	0.99	1623.9	49.1	1704.6	28.6	1805.3	9.1	1805.3	9.1	90
27.742817	94.715333	LIKABALI	UPPER SIWALIK	LG3	23	23	326	249680	2.0	13.4061	0.5	1.7972	1.5	0.95	1038.2	14.1	1044.4	10.1	1057.6	9.8	1057.6	9.8	98	98	98	
27.742817	94.715333	LIKABALI	UPPER SIWALIK	LG3	24	24	833	407160	2.3	16.5358	5.3	0.6066	8.4	0.0728	6.5	0.77	452.7	28.3	481.4	32.1	620.6	114.7	452.7	28.3	73	
27.742817	94.715333	LIKABALI	UPPER SIWALIK	LG3	25	25	76	70662	1.5	29.5922	24.3	0.0666	25.4	0.0143	7.5	0.29	91.4	65.4	80.3	698.3	91.4	65.4	80.3	698.3	91.4	65.4
27.742817	94.715333	LIKABALI	UPPER SIWALIK	LG3	26	26	176	75071	1.8	17.4107	1.6	0.6364	1.7	0.0804	1.5	0.67	498.3	7.1	500.1	8.7	508.3	35.7	500.1	8.7	98	
27.742817	94.715333	LIKABALI	UPPER SIWALIK	LG3	27	27	124	2968	1.6	16.9094	3.9	0.6471	7.6	0.0794	6.6	0.86	492.3	31.2	506.7	30.5	572.2	84.7	492.3	31.2	86	
27.742817	94.715333	LIKABALI	UPPER SIWALIK	LG3	28	28	15	1703	3.1	12.8226	61.4	0.2213	63.1	0.0206	14.5	0.23	133.3	18.9	203.0	116.6	1146.6	1363.5	131.3	18.9	NA	
27.742817	94.715333	LIKABALI	UPPER SIWALIK	LG3	29	29	146	429638	2.5	4.9385	0.1	15.2002	1.0	0.5444	1.0	0.99	2802.0	23.0	2827.9	9.8	2846.4	2.4	2846.4	2.4	98	
27.742817	94.715333	LIKABALI	UPPER SIWALIK	LG3	30	30	124	7756	0.7	21.8200	15.0	0.0878	15.5	0.0139	4.0	0.26	89.0	3.5	85.5	12.7	-11.3	363.6	89.0	3.5	NA	
27.742817	94.715333	LIKABALI	UPPER SIWALIK	LG3	31	31	19	11175	0.9	15.8606	10.8	0.9841	11.2	0.1132	3.0	0.26	691.3	19.4	695.7	56.6	709.9	232.9	691.3	19.4	97	
27.742817	94.715333	LIKABALI	UPPER SIWALIK	LG3	32	32	43	2217	1.1	18.8616	140.2	0.1108	140.5	0.0152	8.6	0.06	97.0	8.3	106.7	143.3	329.6	113.2	97.0	8.3	NA	
27.742817	94.715333	LIKABALI	UPPER SIWALIK	LG3	33	33	63	5102	1.2	23.0403	38.4	0.0811	38.7	0.0135	4.3	0.11	86.7	3.7	79.1	29.4	-144.5	983.7	86.7	3.7	NA	
27.742817	94.715333	LIKABALI	UPPER SIWALIK	LG3	34	34	94	67527	2.2	4.8792	0.2	14.9900	0.6	0.5305	0.6	0.93	2743.4	12.7	2814.6	5.8	2866.0	3.6	2866.0	3.6	96	
27.742817	94.715333	LIKABALI	UPPER SIWALIK	LG3	35	35	261	109203	1.7	17.5469	2.3	0.6255	2.5	0.0796	1.0	0.41	493.7	4.9	493.3	9.7	491.1	49.8	493.7	4.9	101	
27.742817	94.715333	LIKABALI	UPPER SIWALIK	LG3	36	36	835	243207	25.8	15.1829	0.3	1.1265	2.3	0.1240	2.3	0.99	753.8	16.5	766.1	12.6	802.0	6.4	753.8	16.5	94	
27.742817	94.715333	LIKABALI	UPPER SIWALIK	LG3	37	37	490	185647	2.6	20.2349	0.3	1.2296	0.3	0.1333	0.8	0.92	806.8	5.7	814.2	4.6	834.3	6.8	806.8	5.7	97	
27.742817	94.715333	LIKABALI	UPPER SIWALIK	LG3	38	38	74	3268	0.7	20.2349	39.9	0.0954	40.1	0.0140	3.9	0.10	89.6	3.5	92.5	35.5	167.8	968.0	89.6	3.5	NA	
27.742817	94.715333	LIKABALI	UPPER SIWALIK	LG3	39	39	27	1578	0.9	10.4890	132.8	0.1600	134.1	0.0122	18.2	0.14	78.0	14.1	150.7	190.0	1534.7	145.3	78.0	14.1	NA	
27.742817	94.715333	LIKABALI	UPPER SIWALIK	LG3	40	40	34	1954	1.8	51.2174	103.1	0.0406	103.5	0.0151	8.9	0.09	96.5	8.5	40.4	4.0	49.0	NA	96.5	8.5	NA	
27.742817	94.715333	LIKABALI	UPPER SIWALIK	LG3	41	41	72	214008	1.1	6.0107	0.4	10.9967	0.8	0.4794	0.7	0.88	2524.6	14.5	2522.9	7.4	2521.4	6.4	2521.4	6.4	100	
27.742817	94.715333	LIKABALI	UPPER SIWALIK	LG3	42	42	221	122337	1.4	14.9755	1.1	1.2122	2.1	0.1317	1.7	0.84	797.3	12.9	806.2	11.4	830.8	23.4	797.3	12.9	96	
27.742817	94.715333	LIKABALI	UPPER SIWALIK	LG3	43	43	124	114139	2.3	11.7739	1.7	1.2748	3.1	0.1366	2.6	0.84	825.4	19.8	834.6	17.4	859.0	34.7	825.4	19.8	96	
27.742817	94.715333	LIKABALI	UPPER SIWALIK	LG3	44	44	125	105926	1.3	17.4817	0.6	4.5507	0.7	0.0698	0.4	0.38	445.2	44.2	445.2	44.2	445.2	44.2	445.2	44.2	102	
27.742817	94.715333	LIKABALI	UPPER SIWALIK	LG3	45	45	212	115875	1.0	16.7918	1.4	0.7816	2.1	0.0952	1.6	0.75	586.2	8.7	587.3	29.7	586.2	8.7	586.2	8.7	100	
27.742817	94.715333	LIKABALI	UPPER SIWALIK	LG3	46	46	179	26260	1.4	16.6029	6.7	0.6380	7.7	0.0768	3.8	0.49	477.1	17.4	501.1	30.3	611.8	144.4	477.1	17.4	78	
27.742817	94.715333	LIKABALI	UPPER SIWALIK	LG3	47	47	115	47634	2.0	14.9461	1.7	1.2306	2.0	0.75	20.0	0.75	807.2	15.1	814.6	14.6	834.9	36.8	807.2	15.1	97	
27.742817	94.715333	LIKABALI	UPPER SIWALIK	LG3	48	48	257	153282	2.4	17.3736	1.1	0.6339	2.1	0.0799	1.7	0.83	495.4	8.2	498.5	8.1	513.0	25.1	495.4	8.2	97	
27.742817	94.715333	LIKABALI	UPPER SIWALIK	LG3	49	49	284	85508	1.2	17.3732	1.3	0.5262	1.8	0.0789	1.3	0.72	489.6	6.1	493.8	7.0	513.2	27.6	489.6	6.1	95	
27.742817	94.715333	LIKABALI	UPPER SIWALIK	LG3	50	50	272	119857	1.7	17.1994	0.8	0.6479	1.4	0.0808	1.2	0.83	501.0	5.8	507.2	5.7	535.1	17.6	501.0	5.8	94	
27.742817	94.715333	LIKABALI	UPPER SIWALIK	LG3	51	51	126	317446	0.9	6.9398	0.6	8.2681	2.8	0.3834	2.7	0.98	2092.2	48.8	2260.8	25.3	2417.1	10.0	2417.1	10.0	87	
27.742817	94.715333	LIKABALI	UPPER SIWALIK	LG3	52	52	151	130678	1.2	13.3339	1.2	1.8706	3.0	0.1809	2.8	0.92	1071.9	27.2	1070.8	19.9	1068.4	24.3	1068.4	24.3	100	
27.742817	94.715333	LIKABALI	UPPER SIWALIK	LG3	53	53	136	7444	1.7	22.2383	52.7	0.0382	53.3	0.0062	8.1	0.15	39.8	3.2	39.1	39.1	67.3	1374.6	39.8	3.2	NA	
27.742817	94.715333	LIKABALI	UPPER SIWALIK	LG3	54	54	317	290563	1.6	14.9710	0.4	1.2654	3.0	0.1374	3.0	0.99	829.9	23.3	830.3	17.1	831.4	7.7	829.9	23.3	100	
27.742817	94.715333	LIKABALI	UPPER SIWALIK	LG3	55	55	101	3475	1.1	24.0794	31.6	0.0457	32.7	0.0080	8.3	0.25	51.2	4.2	45.4	34.5	254.0	25.6	51.2	4.2	NA	
27.742817	94.715333	LIKABALI	UPPER SIWALIK	LG3	56	56	552	355186	2.3	15.9389	0.5	0.8401	2.7	0.0971	2.7	0.98	597.5	15.3	610.2	12.7	699.4	11.1	597.5	15.3	85	
27.742817	94.715333	LIKABALI	UPPER SIWALIK	LG3	57	57	1405	587142	1.0	17.3582	0.2	0.6403	1.2	0.0806	1.2	0.98	499.8	5.7	502.5	4.8	514.9	4.9	499.8	5.7	97	
27.742817	94.715333	LIKABALI	UPPER SIWALIK	LG3	58	58	307	15193	2.2	6.3622	0.6	7.8800	3.3	0.3616	3.2	0.98	1989.5	55.1	2217.4	29.5	2435.1	9.8	2435.1	9.8	82	
27.742817	94.715333	LIKABALI	UPPER SIWALIK	LG3	59	59	35	2484	1.2	35.6320	77.4	0.0765	78.1	0.0198	10.1	0.13	126.2	12.7	74.8	26.4	-1368.7	1008.5	126.2	12.7	NA	
27.742817	94.715333	LIKABALI	UPPER SIWALIK	LG3	60	60	262	180055	54.9	17.5818	2.3	0.4840	4.8	0.0617	4.2	0.88	386.0	15.9	400.8	15.9	486.8	50.0	386.0	15.9	NA	
27.742817	94.715333	LIKABALI	UPPER SIWALIK	LG3	61	61	17600	17600	0.4	17.6252	9.4	0.5360	9.4	0.0813	1.4	0.15	503.9	7.0	499.8	36.9	481.3	204.6	503.9	7.0	105	
27.742817	94.715333	LIKABALI	UPPER SIWALIK	LG3	62	62	43	3286	1.4	31.1957	34.1	0.0611	35.2	0.0138	8.7	0.25	88.5	7.6	60.2	20.6	959.8	1026.5	88.5	7.6	NA	
27.742817	94.715333	LIKABALI	UPPER SIWALIK	LG3	63	63	63	10892	1.9	14.5707	7.6	1.3051	8.9	0.1379	4.5	0.51	832.9	34.9	848.0	50.9	887.7	158.1	832.9	34.9	94	
27.742817	94.715333	LIKABALI	UPPER SIWALIK	LG3	64	64	2758	320294	0.8	17.3181	0.3	0.6317	4.6	0.0793	4.6	1.00	492.2	21.8	497.2	18.1	520.0	7.0	492.2	21.8	95	
27.742817	94.715333	LIKABALI	UPPER SIWALIK	LG3	65	65	66	16604	1.8	17.1447	1.7	0.6604	2.2	0.0821	1.4	0.64	508.7	7.0	514.9	8.9	542.1	67.1	508.7	7.0	94	
27.742817	94.715333	LIKABALI	UPPER SIWALIK	LG3	66	66	15	6105	1.2	7.4837	244.1	0.3842	244.4	0.0209												

27.721233	94.706617	LIKABALI	MIDDLE SIAWALK	LG2.5	9	LG2.5-9	372	66655	0.9	13.1403	1.3	2.0285	7.7	0.1933	7.6	0.98	1139.3	78.9	1125.1	52.2	1097.8	26.7	1097.8	26.7	1014
27.721233	94.706617	LIKABALI	MIDDLE SIAWALK	LG2.5	10	LG2.5-10	178	18140	0.9	9.2429	0.5	3.7003	6.2	0.2480	6.1	1.00	1428.4	78.7	1571.4	49.3	1769.2	8.5	1769.2	8.5	81
27.721233	94.706617	LIKABALI	MIDDLE SIAWALK	LG2.5	11	LG2.5-11	330	25708	6.7	15.0066	0.8	1.2413	2.7	0.1351	2.6	0.95	816.9	20.0	819.5	15.4	826.4	17.5	816.9	20.0	99
27.721233	94.706617	LIKABALI	MIDDLE SIAWALK	LG2.5	12	LG2.5-12	457	15749	6.7	17.4619	1.1	1.0462	1.3	0.1629	1.1	0.97	492.6	22.1	491.1	18.7	490.1	22.1	491.1	22.1	86
27.721233	94.706617	LIKABALI	MIDDLE SIAWALK	LG2.5	13	LG2.5-13	303	33136	2.0	10.4447	0.9	2.1179	3.7	0.1182	3.6	0.97	720.0	24.8	766.7	20.1	805.6	17.6	720.0	24.8	80
27.721233	94.706617	LIKABALI	MIDDLE SIAWALK	LG2.5	14	LG2.5-14	510	294126	1.8	11.9179	0.2	2.3855	2.2	0.2062	2.2	1.00	1208.5	23.9	1238.3	15.6	1290.4	4.2	1290.4	4.2	94
27.721233	94.706617	LIKABALI	MIDDLE SIAWALK	LG2.5	15	LG2.5-15	820	555272	1.6	14.9449	0.2	1.3001	3.1	0.1409	3.1	1.00	849.8	24.5	845.8	17.7	845.8	3.8	849.8	24.5	102
27.721233	94.706617	LIKABALI	MIDDLE SIAWALK	LG2.5	16	LG2.5-16	247	142943	1.1	11.2577	1.0	0.6629	2.3	0.0830	2.0	0.89	513.8	10.0	516.4	9.2	527.7	22.8	513.8	10.0	97
27.721233	94.706617	LIKABALI	MIDDLE SIAWALK	LG2.5	17	LG2.5-17	193	79207	1.9	17.2539	3.9	0.6147	3.9	0.0759	3.3	0.84	471.7	15.1	486.5	15.2	528.2	46.8	477.7	15.1	90
27.721233	94.706617	LIKABALI	MIDDLE SIAWALK	LG2.5	18	LG2.5-18	954	605621	6.7	13.1464	2.1	1.6532	6.2	0.1576	6.2	1.00	943.6	54.8	990.8	39.5	1096.8	4.4	1096.8	4.4	86
27.721233	94.706617	LIKABALI	MIDDLE SIAWALK	LG2.5	19	LG2.5-19	316	114020	1.6	17.4740	1.7	0.6451	2.9	0.0818	2.3	0.79	506.6	11.1	505.5	11.4	500.3	38.3	506.6	11.1	101
27.721233	94.706617	LIKABALI	MIDDLE SIAWALK	LG2.5	20	LG2.5-20	280	85935	1.1	18.1043	1.6	0.5173	2.3	0.0679	1.7	0.72	423.7	6.8	423.4	8.0	421.7	35.9	423.7	6.8	100
27.721233	94.706617	LIKABALI	MIDDLE SIAWALK	LG2.5	21	LG2.5-21	29	6258	0.4	12.7507	4.0	1.7339	4.8	0.1603	2.5	0.53	958.7	22.5	1021.2	30.8	1157.7	80.3	1157.7	80.3	83
27.721233	94.706617	LIKABALI	MIDDLE SIAWALK	LG2.5	22	LG2.5-22	163	43377	0.5	17.4821	2.3	0.6598	4.6	0.0837	4.0	0.86	517.9	19.9	514.5	19.7	499.3	51.6	517.9	19.9	104
27.721233	94.706617	LIKABALI	MIDDLE SIAWALK	LG2.5	23	LG2.5-23	262	13942	1.8	21.4723	10.0	0.1020	10.4	0.0159	3.1	0.29	101.6	3.1	98.6	9.8	27.3	239.8	101.6	3.1	NA
27.721233	94.706617	LIKABALI	MIDDLE SIAWALK	LG2.5	24	LG2.5-24	103	152880	1.2	9.1159	0.4	4.5698	3.2	0.3023	3.2	0.99	1702.5	47.5	1743.8	8.0	1793.6	8.0	1793.6	8.0	95
27.721233	94.706617	LIKABALI	MIDDLE SIAWALK	LG2.5	25	LG2.5-25	2977	208919	64.8	20.0428	0.3	0.3715	3.9	0.0540	3.9	1.00	339.0	12.8	320.7	10.7	190.0	6.9	339.0	12.8	NA
27.721233	94.706617	LIKABALI	MIDDLE SIAWALK	LG2.5	26	LG2.5-26	1307	68074	0.6	20.9070	3.8	0.0321	4.8	0.0047	2.9	0.61	30.5	0.9	32.0	1.5	149.8	88.7	30.5	0.9	NA
27.721233	94.706617	LIKABALI	MIDDLE SIAWALK	LG2.5	27	LG2.5-27	441	137686	3.3	16.1645	0.5	0.9550	1.9	0.1120	1.8	0.96	684.1	11.7	680.7	9.4	669.4	11.4	684.1	11.7	102
27.721233	94.706617	LIKABALI	MIDDLE SIAWALK	LG2.5	28	LG2.5-28	186	25284	1.1	11.0523	0.8	2.5679	5.1	0.2058	5.1	0.99	1206.6	55.7	1291.6	37.5	1435.6	15.3	1435.6	15.3	84
27.721233	94.706617	LIKABALI	MIDDLE SIAWALK	LG2.5	29	LG2.5-29	175	8955	1.2	16.9325	3.5	0.6721	4.3	0.0825	2.5	0.58	511.2	12.3	522.0	17.5	569.3	76.2	511.2	12.3	90
27.721233	94.706617	LIKABALI	MIDDLE SIAWALK	LG2.5	30	LG2.5-30	257	219991	1.5	10.6858	1.7	2.9311	55.0	0.2272	55.0	1.00	1319.6	658.8	1390.0	442.8	1499.7	31.3	1499.7	31.3	88
27.721233	94.706617	LIKABALI	MIDDLE SIAWALK	LG2.5	31	LG2.5-31	753	12355	2.4	22.0139	7.2	0.0281	7.9	0.0045	3.3	4.41	28.9	0.9	28.1	2.2	-32.7	174.4	28.9	0.9	NA
27.721233	94.706617	LIKABALI	MIDDLE SIAWALK	LG2.5	32	LG2.5-32	375	36220	1.1	21.2845	7.6	0.0639	12.4	0.0099	9.7	0.79	63.3	6.1	62.9	7.5	48.4	182.8	63.3	6.1	NA
27.721233	94.706617	LIKABALI	MIDDLE SIAWALK	LG2.5	33	LG2.5-33	74	5848	1.2	20.2209	20.1	0.1262	20.6	0.0185	4.2	0.21	118.2	5.0	120.7	23.4	169.4	474.0	118.2	5.0	NA
27.721233	94.706617	LIKABALI	MIDDLE SIAWALK	LG2.5	34	LG2.5-34	288	53925	1.3	21.4157	0.3	2.4157	0.6	0.2168	4.5	1.00	1165.1	52.3	1247.3	32.8	1216.6	6.2	1216.6	6.2	104
27.721233	94.706617	LIKABALI	MIDDLE SIAWALK	LG2.5	35	LG2.5-35	427	18603	1.1	13.7289	1.1	1.5668	1.1	0.1563	3.2	0.94	956.3	28.0	958.3	21.1	1009.3	22.8	936.3	28.0	93
27.721233	94.706617	LIKABALI	MIDDLE SIAWALK	LG2.5	36	LG2.5-36	414	49355	4.1	49.355	4.1	1.1	1.1	0.0802	6.3	0.98	540.2	48.0	540.2	48.0	540.2	54.1	540.2	48.0	92
27.721233	94.706617	LIKABALI	MIDDLE SIAWALK	LG2.5	37	LG2.5-37	1721	390058	1.9	17.3078	0.3	0.6412	5.8	0.0805	5.8	1.00	499.0	27.8	503.0	23.0	521.3	7.3	499.0	27.8	96
27.721233	94.706617	LIKABALI	MIDDLE SIAWALK	LG2.5	38	LG2.5-38	2986	22197	2.0	20.0765	2.5	0.1514	19.0	0.0220	18.8	0.99	140.6	26.2	143.2	25.3	186.1	57.6	140.6	26.2	NA
27.721233	94.706617	LIKABALI	MIDDLE SIAWALK	LG2.5	39	LG2.5-39	427	191753	1.9	17.5278	1.0	0.4335	5.9	0.0551	5.8	0.98	140.6	19.5	143.6	18.3	191.6	27.6	140.6	19.5	NA
27.721233	94.706617	LIKABALI	MIDDLE SIAWALK	LG2.5	40	LG2.5-40	439	656677	1.6	12.5957	0.2	2.2367	2.4	0.2043	2.4	0.99	1198.5	25.9	1192.6	16.7	1182.0	4.8	1182.0	4.8	101
27.721233	94.706617	LIKABALI	MIDDLE SIAWALK	LG2.5	41	LG2.5-41	147	8210	2.5	25.4559	39.6	0.0299	41.0	0.0055	10.8	0.26	35.5	3.8	30.0	12.1	398.2	106.7	35.5	3.8	NA
27.721233	94.706617	LIKABALI	MIDDLE SIAWALK	LG2.5	42	LG2.5-42	533	186332	2.1	12.8078	20.9	1.9410	38.0	0.1803	31.8	0.84	1068.6	313.2	1095.3	260.5	1148.9	419.5	1148.9	419.5	93
27.721233	94.706617	LIKABALI	MIDDLE SIAWALK	LG2.5	43	LG2.5-43	358	35265	0.7	20.8249	12.5	0.0844	12.9	0.0127	3.3	0.25	81.6	2.6	82.3	10.2	100.2	296.7	81.6	2.6	NA
27.721233	94.706617	LIKABALI	MIDDLE SIAWALK	LG2.5	44	LG2.5-44	1141	856509	1.9	17.4862	0.5	0.6424	3.3	0.0213	3.2	0.99	504.9	15.7	503.8	13.0	498.8	10.2	504.9	15.7	101
27.721233	94.706617	LIKABALI	MIDDLE SIAWALK	LG2.5	45	LG2.5-45	962	92173	0.8	16.6224	10.7	0.0838	10.7	1.00	518.6	53.4	516.1	45.3	505.3	18.0	518.6	53.4	103		
27.721233	94.706617	LIKABALI	MIDDLE SIAWALK	LG2.5	46	LG2.5-46	365	128422	2.3	17.4257	0.6	0.6224	6.5	0.0796	6.4	0.98	493.5	30.3	491.4	25.3	481.6	26.5	493.5	30.3	102
27.721233	94.706617	LIKABALI	MIDDLE SIAWALK	LG2.5	47	LG2.5-47	1032	628884	1.2	17.3759	0.4	0.6385	2.5	0.0809	2.5	0.99	499.9	12.3	501.4	12.3	501.4	12.3	501.4	12.3	97
27.721233	94.706617	LIKABALI	MIDDLE SIAWALK	LG2.5	48	LG2.5-48	223	189753	4.7	13.8843	1.6	1.6513	4.8	0.1663	4.5	0.94	991.6	41.3	990.0	30.1	986.6	31.8	991.6	41.3	101
27.721233	94.706617	LIKABALI	MIDDLE SIAWALK	LG2.5	49	LG2.5-49	160	214826	0.6	9.4669	0.5	0.3133	3.3	0.0299	3.2	0.99	1742.6	49.5	1742.6	27.2	1725.3	9.4	1725.3	9.4	102
27.721233	94.706617	LIKABALI	MIDDLE SIAWALK	LG2.5	50	LG2.5-50	195	167193	0.9	12.5672	0.6	2.3189	4.1	0.2114	4.1	0.99	1236.1	46.2	1218.1	29.4	1186.4	11.0	1186.4	11.0	104
27.707233	94.675233	LIKABALI	MIDDLE SIAWALK	LG2	1	LG2-1	538	455420	10.0	6.5597	0.5	8.3925	1.3	0.3993	1.2	0.93	2165.7	22.6	2274.4	11.9	2373.5	8.1	2373.5	8.1	91
27.707233	94.675233	LIKABALI	MIDDLE SIAWALK	LG2	2	LG2-2	359	340153	1.4	0.9941	0.4	3.8318	5.4	0.2777	6.4	1.00	1580.0	89.9	1599.4	51.8	1625.2	6.7	1625.2	6.7	97
27.707233	94.675233	LIKABALI	MIDDLE SIAWALK	LG2	3	LG2-3	147	10809	2.2	20.7360	17.9	0.0528	18.6	0.0079	4.9	0.27	50.9	2.5	52.2	9.5	110.3	426.1	50.9	2.5	NA
27.707233	94.675233	LIKABALI	MIDDLE SIAWALK	LG2	4	LG2-4	83	2430	2.0	21.3306	118.3	0.0493	118.7	0.0076	10.3	0.09	48.9	5.0	48.8	56.7	43.2	1167.3	48.9	5.0	NA
27.707233	94.675233	LIKABALI	MIDDLE SIAWALK	LG2	5	LG2-5	715	441519	6.5	16.6774	0.3	0.7792	1.0	0.0094	0.9	0.96	580.6	5.2	585.0	4.4	602.2	5.7	580.6	5.2	96
27.707233	94.675233	LIKABALI	MIDDLE SIAWALK	LG2	6	LG2-6	38	1590	1.1	10.2957	226.1	0.1632	226.2	0.0122	6.2	0.03	78.1	4.8	153.5	333.7	1569.7	590.7	78.1	4.8	NA
27.707233	94.675233	LIKABALI	MIDDLE SIAWALK	LG2	7	LG2-7	163	216031	1.6	6.2574	0.2	9.8228													

27.7589	94.71505	LIKABALI	LOWER SIWALIK	LG4.5	39	MS16-43	137	876	1.9	14.6402	38.1	0.0867	38.7	0.0092	6.9	0.18	59.1	4.0	84.4	31.4	877.8	81.9	59.1	4.0	NA
27.7589	94.71505	LIKABALI	LOWER SIWALIK	LG4.5	40	MS16-44	634	454347	17.8	17.4433	1.0	0.6325	1.7	0.0800	1.4	0.83	496.2	6.9	6.8	504.2	210.0	210.0	496.2	6.9	98
27.7589	94.71505	LIKABALI	LOWER SIWALIK	LG4.5	41	MS16-45	218	94538	1.5	14.9463	0.8	1.2701	1.7	0.1377	1.5	0.87	831.5	11.8	83.24	9.8	834.8	17.7	831.5	11.8	100
27.7589	94.71505	LIKABALI	LOWER SIWALIK	LG4.5	42	MS16-46	258	341118	4.2	12.6242	0.7	2.0861	1.2	0.088	1.2	0.98	1123.1	11.2	1143.9	9.2	1143.9	11.2	1143.9	11.2	96
27.7589	94.71505	LIKABALI	LOWER SIWALIK	LG4.5	43	MS16-47	434	578336	1.7	12.6210	0.5	2.1483	1.3	0.1966	1.2	0.93	1157.3	12.6	1164.5	8.9	1178.0	9.5	1178.0	9.5	98
27.7589	94.71505	LIKABALI	LOWER SIWALIK	LG4.5	44	MS16-48	165	147695	2.0	12.1704	1.2	2.2403	1.0	0.65	1.0	0.65	1163.2	11.0	1193.8	11.1	1249.5	23.6	1249.5	23.6	93
27.7589	94.71505	LIKABALI	LOWER SIWALIK	LG4.5	45	MS16-49	114	232547	2.8	9.2282	0.4	4.6698	1.9	0.3125	1.9	0.98	1752.2	29.1	1761.9	16.2	1772.1	7.1	1772.1	7.1	99
27.7589	94.71505	LIKABALI	LOWER SIWALIK	LG4.5	46	MS16-53	161	17896	1.1	10.1139	1.6	3.5831	5.7	0.2628	5.5	0.96	1504.3	73.7	1545.8	45.3	1603.0	29.0	1603.0	29.0	94
27.7589	94.71505	LIKABALI	LOWER SIWALIK	LG4.5	47	MS16-54	952	15996	4.0	15.7207	1.8	1.3066	4.1	0.0350	3.6	0.89	221.5	77.9	271.5	9.7	271.5	9.7	271.5	9.7	94
27.7589	94.71505	LIKABALI	LOWER SIWALIK	LG4.5	48	MS16-55	124	14174	0.8	14.0669	1.7	1.3378	3.8	0.1365	3.5	0.90	824.7	26.8	862.3	22.3	862.3	34.1	862.3	34.1	86
27.7589	94.71505	LIKABALI	LOWER SIWALIK	LG4.5	49	MS16-56	128	140815	1.2	13.9811	1.4	1.5848	1.9	0.1607	1.3	0.67	960.7	11.5	964.3	11.9	972.4	28.8	960.7	11.5	99
27.7589	94.71505	LIKABALI	LOWER SIWALIK	LG4.5	50	MS16-57	124	8435	1.1	21.9049	24.0	0.0819	24.3	0.0130	3.4	0.14	83.4	2.8	79.9	18.7	-20.7	589.2	8.4	2.8	NA
27.7589	94.71505	LIKABALI	LOWER SIWALIK	LG4.5	51	MS16-59	79	106776	0.3	12.7392	2.1	2.2306	2.9	0.2061	2.1	0.72	1208.0	23.3	1190.7	20.7	1159.0	40.7	1159.0	40.7	104
27.7589	94.71505	LIKABALI	LOWER SIWALIK	LG4.5	52	MS16-60	231	107788	1.8	16.9919	1.2	0.7496	2.3	0.0924	2.0	0.86	569.6	10.7	568.0	9.9	561.6	25.2	568.0	10.7	101
27.7589	94.71505	LIKABALI	LOWER SIWALIK	LG4.5	53	MS16-61	873	454067	1.2	17.3962	0.5	0.6834	2.4	0.0862	2.3	0.98	533.2	11.8	532.8	8.7	510.1	10.8	533.2	11.8	105
27.7589	94.71505	LIKABALI	LOWER SIWALIK	LG4.5	54	MS16-63	64	110725	0.7	10.2825	1.4	3.4435	3.1	0.2568	2.7	0.89	1473.5	36.1	1514.4	24.4	1572.1	26.9	1572.1	26.9	94
27.7589	94.71505	LIKABALI	LOWER SIWALIK	LG4.5	55	MS16-64	135	328031	2.3	4.2200	0.9	18.2437	5.3	0.5584	5.2	0.99	2859.9	119.8	3002.7	50.6	3099.7	13.6	3099.7	13.6	92
27.7589	94.71505	LIKABALI	LOWER SIWALIK	LG4.5	56	MS16-65	226	252982	2.0	13.4833	0.7	1.7415	3.3	0.1703	3.2	0.98	1013.7	30.2	1024.0	21.2	1046.0	13.2	1046.0	13.2	97
27.7589	94.71505	LIKABALI	LOWER SIWALIK	LG4.5	57	MS16-66	992	7865	8.0	17.8479	1.1	0.2724	5.1	0.5353	5.5	0.98	223.4	12.0	244.6	12.1	453.5	25.4	224.4	12.0	NA
27.7589	94.71505	LIKABALI	LOWER SIWALIK	LG4.5	58	MS16-67	525	21500	0.8	22.2896	5.4	0.0586	5.6	0.0095	1.5	0.27	60.7	0.9	57.8	3.1	-63.0	131.1	60.7	0.9	NA
27.7589	94.71505	LIKABALI	LOWER SIWALIK	LG4.5	59	MS16-68	92	57439	0.6	12.8068	1.4	1.9019	2.7	0.1767	2.5	0.86	1048.7	22.5	1081.8	18.0	1149.0	27.2	1149.0	27.2	91
27.7589	94.71505	LIKABALI	LOWER SIWALIK	LG4.5	60	MS16-69	39	96363	1.2	12.4621	2.8	2.3083	3.8	0.2086	2.5	0.69	1221.5	29.4	1214.8	27.1	1203.0	54.4	1203.0	54.4	102
27.7589	94.71505	LIKABALI	LOWER SIWALIK	LG4.5	61	MS16-71	2137	683055	1.6	17.3765	0.3	0.6039	9.0	0.0761	9.0	1.00	472.8	40.8	479.7	34.3	512.6	7.3	472.8	40.8	92
27.7589	94.71505	LIKABALI	LOWER SIWALIK	LG4.5	62	MS16-72	239	31675	3.9	20.4229	4.6	0.0563	5.3	0.0083	5.7	0.51	53.6	1.4	55.6	2.9	146.2	107.3	57.6	1.4	NA
27.7589	94.71505	LIKABALI	LOWER SIWALIK	LG4.5	63	MS16-73	56	1675	1.2	20.3343	77.6	0.0562	87.3	0.0083	39.9	0.48	53.2	21.1	55.5	47.1	156.3	2195.5	53.2	21.1	NA
27.7589	94.71505	LIKABALI	LOWER SIWALIK	LG4.5	64	MS16-74	663	289373	6.7	17.3484	0.7	0.6605	3.9	0.0831	3.8	0.98	514.6	18.9	514.9	15.7	516.2	15.7	514.6	18.9	100
27.7589	94.71505	LIKABALI	LOWER SIWALIK	LG4.5	65	MS16-75	891	173079	1.0	17.3722	0.4	0.6466	2.2	0.0815	2.1	0.98	569.9	9.9	569.9	9.9	569.9	9.9	569.9	9.9	98
27.7589	94.71505	LIKABALI	LOWER SIWALIK	LG4.5	66	MS16-76	195	22103	1.0	17.2674	1.5	0.6521	2.4	0.0817	1.9	0.87	506.1	9.4	509.8	9.7	525.5	32.1	506.1	9.4	96
27.7589	94.71505	LIKABALI	LOWER SIWALIK	LG4.5	67	MS16-77	199	366408	1.1	9.9091	0.5	4.1416	3.3	0.2976	3.3	0.99	1679.6	48.3	1662.5	27.0	1641.0	8.5	1641.0	8.5	102
27.7589	94.71505	LIKABALI	LOWER SIWALIK	LG4.5	68	MS16-78	116	3200	1.1	19.2591	31.3	0.0576	31.8	0.0080	5.7	1.18	51.6	2.9	56.8	17.6	28.1	73.4	51.6	2.9	NA
27.7589	94.71505	LIKABALI	LOWER SIWALIK	LG4.5	69	MS16-80	109	99430	2.2	12.3529	1.4	2.2321	2.1	0.1992	1.6	0.76	1170.9	17.0	1188.3	14.7	1220.3	17.0	1220.3	17.0	96
27.7589	94.71505	LIKABALI	LOWER SIWALIK	LG4.5	70	MS16-81	156	197685	1.9	9.1827	1.3	4.7629	1.3	0.1172	1.2	0.96	1776.1	19.1	1778.4	10.7	1781.1	6.1	1781.1	6.1	100
27.7589	94.71505	LIKABALI	LOWER SIWALIK	LG4.5	71	MS16-82	303	145836	0.9	15.9343	0.5	2.3293	2.5	0.2016	2.4	0.97	1184.0	25.9	1221.3	17.4	1287.7	10.6	1287.7	10.6	92
27.7589	94.71505	LIKABALI	LOWER SIWALIK	LG4.5	72	MS16-83	805	360632	1.4	15.0399	0.6	1.1053	4.3	0.1206	4.2	0.99	733.9	29.4	735.9	22.8	821.9	12.3	733.9	29.4	89
27.7589	94.71505	LIKABALI	LOWER SIWALIK	LG4.5	73	MS16-84	247	50058	1.5	17.1498	1.3	0.6789	2.3	0.0844	1.9	0.83	522.6	9.7	526.1	9.5	541.4	28.2	522.6	9.7	97
27.7589	94.71505	LIKABALI	LOWER SIWALIK	LG4.5	74	MS16-86	914	25013	0.3	21.0976	2.3	0.0706	2.4	0.0844	1.9	0.83	522.6	9.7	526.1	9.5	541.4	28.2	522.6	9.7	97
27.7589	94.71505	LIKABALI	LOWER SIWALIK	LG4.5	75	MS16-87	285	9656	1.2	22.5935	13.5	0.0599	14.6	0.0098	5.3	0.37	62.9	3.3	59.0	8.4	-96.2	333.9	62.9	3.3	NA
27.7589	94.71505	LIKABALI	LOWER SIWALIK	LG4.5	76	MS16-88	558	30378	2.9	19.3122	1.9	0.2069	2.8	0.0290	2.0	0.71	184.2	3.5	190.9	4.8	275.7	44.5	184.2	3.5	NA
27.7589	94.71505	LIKABALI	LOWER SIWALIK	LG4.5	77	MS16-89	364	20994	0.7	12.4455	1.2	0.6270	1.8	0.0793	1.3	0.75	492.1	6.3	492.1	6.3	492.1	6.3	492.1	6.3	98
27.7589	94.71505	LIKABALI	LOWER SIWALIK	LG4.5	78	MS16-90	423	145820	0.2	17.5010	0.6	0.6345	1.1	0.0805	0.9	0.85	499.4	4.6	498.9	4.4	496.9	13.0	499.4	4.6	100
27.7589	94.71505	LIKABALI	LOWER SIWALIK	LG4.5	79	MS16-91	225	50181	1.4	19.8510	3.4	0.2611	3.8	0.0376	1.7	0.45	237.9	4.1	235.6	8.1	212.3	79.3	237.9	4.1	NA
27.7589	94.71505	LIKABALI	LOWER SIWALIK	LG4.5	80	MS16-92	428	260166	3.0	14.9702	0.6	1.2467	1.7	0.1354	1.6	0.94	818.4	12.0	821.9	9.4	831.5	11.8	818.4	12.0	98
27.7589	94.71505	LIKABALI	LOWER SIWALIK	LG4.5	81	MS16-93	147	16265	0.8	10.1686	0.6	3.3776	2.2	0.2491	2.2	0.97	1433.8	27.6	1499.2	17.4	1592.9	10.5	1592.9	10.5	90
27.7589	94.71505	LIKABALI	LOWER SIWALIK	LG4.5	82	MS16-94	59	26349	1.0	15.5092	3.4	1.0589	3.8	0.1191	1.5	0.40	725.4	10.3	733.3	19.6	757.3	72.6	725.4	10.3	96
27.7589	94.71505	LIKABALI	LOWER SIWALIK	LG4.5	83	MS16-95	244	19467	1.9	15.2182	4.5	1.7396	5.3	0.1667	2.7	0.51	939.8	24.7	1023.0	34.0	1095.9	91.2	1095.9	91.2	92
27.7589	94.71505	LIKABALI	LOWER SIWALIK	LG4.5	84	MS16-96	94	4469	1.5	20.4066	18.9	0.0609	21.4	0.0090	10.0	0.47	57.8	5.8	60.0	12.5	148.0	46.6	60.0	12.5	NA
27.7589	94.71505	LIKABALI	LOWER SIWALIK	LG4.5	85	MS16-97	291	154877	1.9	14.3156	0.8	1.5045	1.9	0.1562	1.8	0.90	935.6	15.3	932.2	11.8	924.1	17.0	935.6	15.3	101
27.7589	94.71505	LIKABALI	LOWER SIWALIK	LG4.5	86	MS16-98	3199	309994	4.7	17.3597	0.1	0.7685	4.6	0.0968	4.6	1.00	595.4	26.3	578.9	20.4	514.7	2.8	595.4	26.3	116
27.7589	94.71505	LIKABALI	LOWER SIWALIK	LG4.5	87	MS16-100	339	265451	1.8	14.7088	0.6	1.3515	1.6	0.1442	1.5	0.94	868.3	12.5	868.2	9.5	868.1	11.5	868.3	12.5	100
27.347517	93.974467	KIMIN	MIDDLE SIWAL																						

27.316217	93.966607	KIMIN	MIDDLE SIAWALK	KZ1.5	42	KZ1.5-51	1713	91185	3.5	17.3157	0.8	0.6104	5.4	0.0767	5.3	0.099	476.1	24.5	483.8	20.8	520.3	17.7	476.1	24.5	92
27.316217	93.966607	KIMIN	MIDDLE SIAWALK	KZ1.5	43	KZ1.5-52	84	162521	1.4	10.0750	0.9	3.8992	2.0	0.2849	1.7	0.89	1616.1	24.9	150.9	15.9	1610.2	17.1	1610.2	17.1	100
27.316217	93.966607	KIMIN	MIDDLE SIAWALK	KZ1.5	44	KZ1.5-55	35	70626	1.4	10.9104	1.9	3.2215	3.0	0.2549	2.3	0.77	1463.8	29.7	1462.4	22.9	1460.3	36.1	1460.3	36.1	100
27.316217	93.966607	KIMIN	MIDDLE SIAWALK	KZ1.5	45	KZ1.5-56	26	782	1.0	11.1510	28.2	0.3597	3.0	0.0210	1.6	0.87	134.0	14.2	234.5	52.2	141.6	13.0	134.0	14.2	100
27.316217	93.966607	KIMIN	MIDDLE SIAWALK	KZ1.5	46	KZ1.5-57	410	373424	31.7	11.4704	0.3	2.6080	1.8	0.2170	1.8	0.99	1265.8	21.0	1302.9	13.6	1364.5	5.5	1364.5	5.5	93
27.316217	93.966607	KIMIN	MIDDLE SIAWALK	KZ1.5	47	KZ1.5-58	96	95215	1.0	13.9863	2.1	1.6036	3.8	0.1627	3.2	0.83	971.5	29.0	971.6	24.1	971.7	43.3	971.5	29.0	100
27.316217	93.966607	KIMIN	MIDDLE SIAWALK	KZ1.5	48	KZ1.5-59	71	47315	0.9	12.7810	0.9	2.1556	2.0	0.1998	1.8	0.88	1174.9	19.1	1166.9	14.0	1153.0	18.8	1166.9	18.8	102
27.316217	93.966607	KIMIN	MIDDLE SIAWALK	KZ1.5	49	KZ1.5-60	137	5823	2.1	23.204	19.8	0.0611	20.0	0.0099	2.8	0.14	63.4	1.8	60.9	6.7	-66.4	486.8	63.4	1.8	NA
27.316217	93.966607	KIMIN	MIDDLE SIAWALK	KZ1.5	50	KZ1.5-61	579	9126	0.8	24.0615	17.5	0.0337	18.3	0.0059	5.3	0.29	37.8	2.0	33.7	11.1	251.3	445.8	37.8	2.0	NA
27.316217	93.966607	KIMIN	MIDDLE SIAWALK	KZ1.5	51	KZ1.5-62	1159	58770	6.3	20.9971	3.8	0.0613	4.3	0.0093	1.9	0.45	59.9	1.1	60.4	2.5	80.7	91.3	59.9	1.1	NA
27.316217	93.966607	KIMIN	MIDDLE SIAWALK	KZ1.5	52	KZ1.5-63	497	4398	0.5	22.2304	16.9	0.0253	17.5	0.0041	4.3	0.25	26.3	1.1	25.4	4.4	-56.5	415.2	26.3	1.1	NA
27.316217	93.966607	KIMIN	MIDDLE SIAWALK	KZ1.5	53	KZ1.5-64	453	371510	2.2	16.3684	0.8	0.8848	1.9	0.1050	1.7	0.90	643.9	10.2	643.6	8.8	642.5	17.7	643.9	10.2	100
27.316217	93.966607	KIMIN	MIDDLE SIAWALK	KZ1.5	54	KZ1.5-66	192	107616	1.7	14.9870	0.7	1.2447	1.5	0.1353	1.3	0.89	818.0	10.2	821.0	8.4	829.2	14.4	818.0	10.2	99
27.316217	93.966607	KIMIN	MIDDLE SIAWALK	KZ1.5	55	KZ1.5-67	149	79823	0.6	12.4162	0.6	2.2713	1.7	0.2045	1.6	0.94	1199.6	17.0	1210.3	11.7	1210.3	11.4	1210.3	11.4	99
27.316217	93.966607	KIMIN	MIDDLE SIAWALK	KZ1.5	56	KZ1.5-68	79	6079	0.7	12.0847	36.2	0.0847	36.7	0.0135	5.6	0.15	86.4	4.8	82.6	29.1	-28.2	904.0	86.4	4.8	NA
27.316217	93.966607	KIMIN	MIDDLE SIAWALK	KZ1.5	57	KZ1.5-69	146	111966	1.8	11.9666	1.0	0.6876	3.1	0.0858	2.2	0.73	530.6	11.4	531.3	12.7	534.5	46.4	530.6	11.4	99
27.316217	93.966607	KIMIN	MIDDLE SIAWALK	KZ1.5	58	KZ1.5-70	88	43571	0.3	16.4232	3.3	3.7790	4.9	0.0928	3.6	0.74	572.0	19.8	584.9	21.7	635.3	70.2	572.0	19.8	90
27.316217	93.966607	KIMIN	MIDDLE SIAWALK	KZ1.5	59	KZ1.5-71	804	745529	5.9	13.7535	0.2	1.6244	1.3	0.1620	1.3	0.99	968.1	11.3	979.7	8.0	1005.8	3.5	968.1	11.3	96
27.316217	93.966607	KIMIN	MIDDLE SIAWALK	KZ1.5	60	KZ1.5-72	73	8369	1.3	24.1084	27.0	0.0831	27.4	0.0210	4.4	0.16	93.0	4.1	81.1	21.3	-258.0	695.8	93.0	4.1	NA
27.316217	93.966607	KIMIN	MIDDLE SIAWALK	KZ1.5	61	KZ1.5-73	29	17662	0.6	16.7781	8.5	0.6654	9.8	0.0810	4.9	0.50	501.9	23.5	517.9	39.6	589.1	183.9	501.9	23.5	85
27.316217	93.966607	KIMIN	MIDDLE SIAWALK	KZ1.5	62	KZ1.5-75	173	92738	2.2	15.0724	0.9	0.9289	2.1	0.1015	1.9	0.91	623.5	11.4	667.1	10.4	817.3	18.4	623.5	11.4	76
27.316217	93.966607	KIMIN	MIDDLE SIAWALK	KZ1.5	63	KZ1.5-76	102	64113	1.3	17.1070	5.0	0.6654	5.2	0.0826	1.3	0.25	511.4	6.4	517.9	21.1	546.9	110.0	511.4	6.4	94
27.316217	93.966607	KIMIN	MIDDLE SIAWALK	KZ1.5	64	KZ1.5-77	249	269481	0.8	13.6696	0.3	1.6904	2.7	0.1676	2.7	0.99	998.8	25.0	1004.9	17.4	1018.2	7.0	1018.2	7.0	98
27.316217	93.966607	KIMIN	MIDDLE SIAWALK	KZ1.5	65	KZ1.5-78	812	24277	25.4	20.9811	2.6	0.0569	3.8	0.0086	2.7	0.72	55.4	1.5	56.2	2.1	89.7	62.0	55.4	1.5	NA
27.316217	93.966607	KIMIN	MIDDLE SIAWALK	KZ1.5	66	KZ1.5-79	48	55838	1.0	10.1689	1.2	3.7849	3.5	0.2791	3.2	0.93	1587.0	45.3	1589.5	27.7	1592.8	23.2	1592.8	23.2	100
27.316217	93.966607	KIMIN	MIDDLE SIAWALK	KZ1.5	67	KZ1.5-80	80	64560	0.5	12.6654	1.5	2.0198	8.3	0.1855	8.2	0.98	1097.1	82.5	1122.2	56.6	1171.0	30.1	1171.0	30.1	94
27.316217	93.966607	KIMIN	MIDDLE SIAWALK	KZ1.5	68	KZ1.5-82	2872	197307	7.3	17.4668	0.2	0.6618	7.2	0.0838	7.2	1.00	518.8	35.7	515.7	29.0	502.0	4.7	518.8	35.7	103
27.316217	93.966607	KIMIN	MIDDLE SIAWALK	KZ1.5	69	KZ1.5-83	953	104706	30.6	15.0921	4.0	0.7052	4.0	0.0773	3.6	0.67	480.0	16.8	540.5	18.5	540.5	84.6	480.0	16.8	59
27.316217	93.966607	KIMIN	MIDDLE SIAWALK	KZ1.5	70	KZ1.5-84	140	217529	1.2	7.9926	0.2	6.1188	2.1	0.3547	2.1	0.99	1957.0	35.6	1992.9	28.5	2030.4	4.0	2030.4	4.0	96
27.316217	93.966607	KIMIN	MIDDLE SIAWALK	KZ1.5	71	KZ1.5-85	2271	48023	41.5	21.5900	2.4	0.0266	2.7	0.0042	1.2	0.46	26.8	0.3	26.7	0.7	14.2	56.7	26.8	0.3	NA
27.316217	93.966607	KIMIN	MIDDLE SIAWALK	KZ1.5	72	KZ1.5-87	538	378554	2.0	14.9791	0.2	1.2451	1.3	0.1353	1.3	0.98	817.9	10.0	821.2	7.4	830.3	4.9	817.9	10.0	99
27.316217	93.966607	KIMIN	MIDDLE SIAWALK	KZ1.5	73	KZ1.5-88	850	95652	1.1	20.6384	2.5	0.1218	2.8	0.0182	1.3	0.47	116.4	1.5	116.7	3.1	121.5	15.9	116.4	1.5	NA
27.316217	93.966607	KIMIN	MIDDLE SIAWALK	KZ1.5	74	KZ1.5-89	758	142664	3.0	13.7657	0.9	1.2596	4.1	0.1258	4.0	0.97	763.6	28.6	827.7	23.2	1004.0	19.3	763.6	28.6	76
27.316217	93.966607	KIMIN	MIDDLE SIAWALK	KZ1.5	75	KZ1.5-91	122	13794	0.9	26.6391	26.9	0.0724	27.1	0.0140	3.9	0.14	67.9	3.5	71.0	18.6	51.7	72.8	89.6	3.5	NA
27.316217	93.966607	KIMIN	MIDDLE SIAWALK	KZ1.5	76	KZ1.5-92	221	27748	1.0	17.0095	2.5	0.6671	2.9	0.0823	1.5	0.50	509.8	7.1	518.9	13.9	559.3	55.1	509.8	7.1	91
27.316217	93.966607	KIMIN	MIDDLE SIAWALK	KZ1.5	77	KZ1.5-93	150	234988	2.4	9.2632	0.3	4.7724	1.6	0.3206	1.6	0.98	1792.8	24.9	1795.2	6.8	1765.2	6.2	1765.2	6.2	102
27.316217	93.966607	KIMIN	MIDDLE SIAWALK	KZ1.5	78	KZ1.5-94	142	313916	1.5	17.4234	1.4	0.6395	4.4	0.0808	4.1	0.94	500.9	19.9	502.0	17.4	506.7	31.9	500.9	19.9	99
27.316217	93.966607	KIMIN	MIDDLE SIAWALK	KZ1.5	79	KZ1.5-95	169	206682	5.4	9.2765	0.3	4.6013	1.9	0.3096	1.8	0.99	1738.6	28.0	1749.5	15.5	1762.5	5.5	1762.5	5.5	99
27.316217	93.966607	KIMIN	MIDDLE SIAWALK	KZ1.5	80	KZ1.5-96	123	127659	0.8	12.6105	0.9	2.1530	2.8	0.1969	2.7	0.95	1158.7	28.4	1166.0	27.7	1176.6	17.2	1176.6	17.2	98
27.316217	93.966607	KIMIN	MIDDLE SIAWALK	KZ1.5	81	KZ1.5-97	893	732583	9.0	10.2546	4.0	0.6549	1.9	0.0824	1.9	0.98	510.6	9.2	511.5	7.7	515.4	8.0	510.6	9.2	99
27.316217	93.966607	KIMIN	MIDDLE SIAWALK	KZ1.5	82	KZ1.5-98	363	36744	0.6	20.2220	2.8	0.1453	3.7	0.0213	2.4	0.65	136.0	3.2	137.8	4.7	169.3	65.5	136.0	3.2	NA
27.316217	93.966607	KIMIN	MIDDLE SIAWALK	KZ1.5	83	KZ1.5-99	186	174605	0.7	12.7531	0.8	2.0965	1.4	0.1939	1.1	0.81	1143.5	11.8	1147.6	9.6	1157.3	16.3	1157.3	16.3	99
27.316217	93.966607	KIMIN	MIDDLE SIAWALK	KZ1.5	84	KZ1.5-100	315	117131	1.0	11.8297	0.3	2.6342	1.7	0.2260	1.7	0.98	1312.5	19.8	1310.2	12.5	1304.8	6.3	1304.8	6.3	101
27.316217	93.966607	KIMIN	MIDDLE SIAWALK	KZ1.5	85	KZ1.5-101	856	152704	2.2	17.2981	0.8	0.6348	3.0	0.0796	2.9	0.97	494.0	13.9	499.1	11.9	522.5	17.0	494.0	13.9	95
27.316217	93.966607	KIMIN	MIDDLE SIAWALK	KZ1.5	86	KZ1.5-102	75	5474	1.4	24.5473	25.2	0.0793	26.0	0.0141	6.5	0.25	90.4	5.8	77.5	19.4	304.0	65.9	90.4	5.8	NA
27.316217	93.966607	KIMIN	MIDDLE SIAWALK	KZ1.5	87	KZ1.5-103	397	71266	3.3	20.9948	4.9	0.1336	5.3	0.0203	1.9	0.36	129.8	2.4	127.3	6.3	80.9	117.5	129.8	2.4	NA
27.316217	93.966607	KIMIN	MIDDLE SIAWALK	KZ1.5	88	KZ1.5-104	226	134873	3.5	17.5406	1.7	0.6359	3.0	0.0809	2.4	0.82	501.5	11.7	497.7	11.7	492.0	31.5	501.5	11.7	102

TABLE A2. Details of detrital zircon (U-Th)/Pb analyses (1 sigma uncertainties reported). Analyses conducted by Apatite to Zircon, Inc.

NORTHING	EASTING	LOCATION	UNIT	SAMPLE ID	GRAIN	GRAIN ID	U (ppm)	Th (ppm)	U/Th	Isotope ratios										Ages from concordant scans (Ma)				
										206Pb*/207Pb*	± (%)	207Pb*/235U*	± (%)	206Pb*/238U	± (%)	error corr.	206Pb*/238U*	± (Ma)	207Pb*/235U	206Pb*/207Pb*	± (Ma)</			

27.718442	94.668658	LKABALI	UPPER SIVALIK	DTCS	42	P1408_007_Zm_A_1_RAD_41	309	135	2.30	14.0410	2.7	1.6736	2.7	0.1704	17.0	0.28	1014.5	16.3	998.6	17.0	963.7	54.2	1014.5	16.3	100	
27.718442	94.668658	LKABALI	UPPER SIVALIK	DTCS	43	P1408_007_Zm_A_1_RAD_42	165	47	3.54	10.0817	2.3	3.6918	2.6	0.2699	27.0	0.47	1540.5	26.6	1569.6	20.7	1609.0	43.1	1569.6	20.7	94	
27.718442	94.668658	LKABALI	UPPER SIVALIK	DTCS	44	P1408_007_Zm_A_1_RAD_43	739	331	2.24	17.9308	2.3	6.0103	2.3	0.0794	7.9	0.36	492.4	8.6	483.8	8.9	444.3	8.6	492.4	8.6	94	
27.718442	94.668658	LKABALI	UPPER SIVALIK	DTCS	45	P1408_007_Zm_A_1_RAD_44	517	23	2.71	20.0562	0.8	2.0562	0.8	0.112	0.8	0.12	53.2	1.6	55.9	1.6	55.9	1.6	55.9	1.6	94	
27.718442	94.668658	LKABALI	UPPER SIVALIK	DTCS	46	P1408_007_Zm_A_1_RAD_45	85	43	1.99	12.7730	3.9	1.8998	3.8	0.1760	17.6	0.27	1045.1	23.7	1081.0	25.5	1154.3	77.4	1045.1	23.7	94	
27.718442	94.668658	LKABALI	UPPER SIVALIK	DTCS	47	P1408_007_Zm_A_1_RAD_46	313	89	3.50	15.5207	3.5	1.0978	7.2	0.1236	12.4	0.87	751.1	49.7	752.3	38.3	755.7	74.8	752.3	38.3	74	
27.718442	94.668658	LKABALI	UPPER SIVALIK	DTCS	48	P1408_007_Zm_A_1_RAD_47	276	11	25.15	5.4327	4.5	3.3101	4.5	0.1304	13.0	0.29	790.3	21.1	1483.4	34.7	2689.9	74.1	1483.4	34.7	77	
27.718442	94.668658	LKABALI	UPPER SIVALIK	DTCS	49	P1408_007_Zm_A_1_RAD_48	199	83	2.42	13.5740	2.7	1.7644	2.8	0.1737	17.4	0.35	1032.4	18.1	1032.5	54.9	1032.5	54.9	1032.5	54.9	100	
27.718442	94.668658	LKABALI	UPPER SIVALIK	DTCS	50	P1408_007_Zm_A_1_RAD_49	85	33	2.23	10.1021	2.6	3.4921	2.6	0.0616	28.2	0.42	1601.8	21.0	1605.1	27.7	1601.8	21.0	1605.1	27.7	100	
27.718442	94.668658	LKABALI	UPPER SIVALIK	DTCS	51	P1408_007_Zm_A_1_RAD_50	185	55	3.38	14.1123	3.4	1.4787	3.4	0.1514	15.1	0.32	908.5	16.3	921.7	21.2	953.4	68.7	908.5	16.3	94	
27.718442	94.668658	LKABALI	UPPER SIVALIK	DTCS	52	P1408_007_Zm_A_1_RAD_51	745	56	13.35	18.0440	2.5	5.5365	2.6	0.0702	7.0	0.32	437.4	6.7	436.1	9.2	429.1	55.6	437.4	6.7	100	
27.718442	94.668658	LKABALI	UPPER SIVALIK	DTCS	53	P1408_007_Zm_A_1_RAD_52	163	11	14.65	18.9717	23.0	0.0352	22.9	0.0048	0.5	0.06	31.1	1.4	35.1	7.9	316.5	384.9	31.1	1.4	61	
27.718442	94.668658	LKABALI	UPPER SIVALIK	DTCS	54	P1408_007_Zm_A_1_RAD_53	454	221	2.05	19.0295	7.5	0.0551	7.4	0.0076	0.8	0.11	48.8	1.2	54.4	3.9	309.6	170.9	48.8	1.2	65	
27.718442	94.668658	LKABALI	UPPER SIVALIK	DTCS	55	P1408_007_Zm_A_1_RAD_54	85	48	1.77	13.3032	2.9	2.0772	3.0	0.2004	20.0	0.29	1177.6	17.8	1141.3	20.9	1073.0	59.2	1177.6	17.8	94	
27.718442	94.668658	LKABALI	UPPER SIVALIK	DTCS	56	P1408_007_Zm_A_1_RAD_55	452	94	4.80	17.8476	2.6	6.6013	2.6	0.0778	7.8	0.29	483.2	7.4	478.0	10.0	453.5	57.1	483.2	7.4	100	
27.718442	94.668658	LKABALI	UPPER SIVALIK	DTCS	57	P1408_007_Zm_A_1_RAD_56	367	114	3.21	18.3824	3.3	0.6130	3.2	0.0817	8.2	0.17	506.4	8.8	485.4	12.4	387.6	74.6	506.4	8.8	90	
27.718442	94.668658	LKABALI	UPPER SIVALIK	DTCS	58	P1408_007_Zm_A_1_RAD_57	142	32	4.46	17.4246	9.8	0.0702	9.5	0.0089	0.9	0.06	56.9	1.8	68.9	6.3	50.7	216.3	56.9	1.8	87	
27.718442	94.668658	LKABALI	UPPER SIVALIK	DTCS	59	P1408_007_Zm_A_1_RAD_58	514	131	3.93	10.4570	2.2	3.2364	2.8	0.2455	24.6	0.65	1415.0	31.7	1465.9	22.1	1540.6	41.4	1465.9	22.1	55	
27.718442	94.668658	LKABALI	UPPER SIVALIK	DTCS	60	P1408_007_Zm_A_1_RAD_59	339	121	2.87	17.8667	2.4	0.6427	2.6	0.0833	8.3	0.42	515.7	8.9	504.0	10.4	451.0	53.5	515.7	8.9	100	
27.718442	94.668658	LKABALI	UPPER SIVALIK	DTCS	61	P1408_007_Zm_A_1_RAD_60	719	318	2.26	17.6678	2.5	0.6121	2.7	0.0784	7.8	0.48	486.8	9.7	484.9	10.3	476.1	54.9	484.9	10.3	100	
27.718442	94.668658	LKABALI	UPPER SIVALIK	DTCS	62	P1408_007_Zm_A_1_RAD_62	233	93	2.96	17.3100	3.6	0.6467	3.8	0.0812	8.1	0.38	503.2	10.7	508.4	15.0	521.1	79.8	503.2	10.7	97	
27.718442	94.668658	LKABALI	UPPER SIVALIK	DTCS	63	P1408_007_Zm_A_1_RAD_63	859	160	5.37	17.9598	2.4	0.6101	2.6	0.0795	7.9	0.45	493.0	8.6	483.6	10.0	439.7	52.5	493.0	8.6	94	
27.718442	94.668658	LKABALI	UPPER SIVALIK	DTCS	64	P1408_007_Zm_A_1_RAD_64	100	47	2.12	13.3120	2.7	1.7180	2.7	0.1659	16.6	0.36	989.3	19.2	1015.3	17.6	1017.8	54.4	1015.3	17.6	94	
27.718442	94.668658	LKABALI	UPPER SIVALIK	DTCS	65	P1408_007_Zm_A_1_RAD_65	67	25	2.71	19.8649	13.3	0.1955	13.3	0.0282	2.8	0.11	179.1	5.5	181.3	22.1	210.6	248.7	179.1	5.5	90	
27.718442	94.668658	LKABALI	UPPER SIVALIK	DTCS	66	P1408_007_Zm_A_1_RAD_66	478	31	22.17	20.8855	6.8	0.0579	6.4	0.0088	0.9	0.11	56.3	1.8	57.2	3.6	93.4	123.2	56.3	1.8	74	
27.718442	94.668658	LKABALI	UPPER SIVALIK	DTCS	67	P1408_007_Zm_A_1_RAD_67	670	65	7.27	17.8253	3.3	0.5793	3.3	0.0749	7.5	0.23	465.6	8.4	464.0	12.1	456.4	72.9	465.6	8.4	97	
27.718442	94.668658	LKABALI	UPPER SIVALIK	DTCS	68	P1408_007_Zm_A_1_RAD_68	283	24	20.11	17.6991	5.3	0.2095	5.2	0.0269	2.7	0.25	171.1	5.6	193.1	9.1	47.1	211.3	171.1	5.6	23	
27.718442	94.668658	LKABALI	UPPER SIVALIK	DTCS	69	P1408_007_Zm_A_1_RAD_69	465	16	17.07	10.8050	2.7	2.7433	3.1	0.2150	21.5	0.56	1255.2	30.4	1340.3	22.9	1478.8	50.3	1340.3	22.9	100	
27.690301	94.673102	LKABALI	MIDDLE SIVALIK	75b	1	P1408_001_Zm_A_1_RAD_0	650	470	1.38	15.1452	2.2	1.2011	2.7	0.1319	13.2	0.59	798.9	15.3	801.1	14.9	807.2	46.1	801.1	14.9	100	
27.690301	94.673102	LKABALI	MIDDLE SIVALIK	75b	1a	P1408_001_Zm_A_1a_RAD_0	604	438	1.30	15.3368	2.5	1.1692	3.0	0.1301	13.0	0.59	788.2	15.3	786.3	16.3	780.9	52.8	786.3	16.3	94	
27.690301	94.673102	LKABALI	MIDDLE SIVALIK	75b	weighted	-	-	-	15.2286	1.7	1.1867	2.0	0.1310	9.3	0.9	794.8	12.0	794.3	11.0	795.8	34.7	794.3	11.0	97		
27.690301	94.673102	LKABALI	MIDDLE SIVALIK	75b	2	P1408_001_Zm_A_1_RAD_1	93	93	1.01	16.3289	15.6	0.5889	15.7	0.0815	8.2	0.17	505.5	20.4	532.1	65.3	647.8	339.6	505.5	20.4	71	
27.690301	94.673102	LKABALI	MIDDLE SIVALIK	75b	2b	P1408_001_Zm_A_1b_RAD_1	79	93	0.85	16.4395	21.6	0.7362	22.0	0.0878	8.8	0.22	542.4	37.4	560.2	95.0	633.2	477.5	542.4	37.4	55	
27.690301	94.673102	LKABALI	MIDDLE SIVALIK	75b	weighted	-	-	-	16.3662	12.6	0.7049	12.8	0.0844	6.0	-	514.0	17.9	541.1	53.8	642.9	276.8	514.0	17.9	63		
27.690301	94.673102	LKABALI	MIDDLE SIVALIK	75b	3	P1408_001_Zm_A_1_RAD_2	1439	876	1.64	15.4396	2.7	1.1322	3.0	0.1268	12.7	0.47	769.5	16.8	768.8	15.9	766.8	57.3	768.8	15.9	87	
27.690301	94.673102	LKABALI	MIDDLE SIVALIK	75b	4	P1408_001_Zm_A_1_RAD_3	184	185	0.99	19.2616	18.1	0.1036	18.0	0.0145	1.4	0.08	92.6	4.1	100.1	17.1	281.7	325.6	92.6	4.1	77	
27.690301	94.673102	LKABALI	MIDDLE SIVALIK	75b	4a	P1408_001_Zm_A_1a_RAD_3	123	83	1.48	11.4741	49.1	0.1658	48.2	0.0138	1.4	0.02	88.3	9.6	155.7	69.6	136.9	1048.7	88.3	9.6	52	
27.690301	94.673102	LKABALI	MIDDLE SIVALIK	75b	weighted	-	-	-	18.3259	17.0	0.3112	16.8	0.0141	1.0	0.02	92.0	3.8	100.3	20.6	376.9	319.9	92.0	3.8	65		
27.690301	94.673102	LKABALI	MIDDLE SIVALIK	75b	5	P1408_001_Zm_A_1_RAD_4	1307	100	13.07	15.4600	2.3	5.1314	2.8	0.1136	11.4	0.60	693.8	13.3	710.6	14.3	764.0	47.6	693.8	13.3	71	
27.690301	94.673102	LKABALI	MIDDLE SIVALIK	75b	6	P1408_001_Zm_A_1_RAD_5	798	340	2.35	15.1504	2.3	1.2301	2.5	0.1352	13.5	0.46	817.3	13.0	814.4	14.1	806.5	47.4	817.3	13.0	100	
27.690301	94.673102	LKABALI	MIDDLE SIVALIK	75b	6a	P1408_001_Zm_A_1a_RAD_5	422	152	2.78	14.9596	3.2	1.2626	3.6	0.1370	13.7	0.46	827.6	16.7	829.1	20.2	833.0	66.4	827.6	16.7	100	
27.690301	94.673102	LKABALI	MIDDLE SIVALIK	75b	weighted	-	-	-	15.0864	1.8	1.2409	2.1	0.1361	9.6	-	821.1	10.2	815.5	38.6	812.1	11.2	815.5	38.6	821.1	10.2	100
27.690301	94.673102	LKABALI	MIDDLE SIVALIK	75b	7	P1408_001_Zm_A_1_RAD_6	2098	305	6.58	12.8043	1.9	2.0460	2.1	0.1900	19.0	0.53	1121.4	20.0	1131.0	14.0	1149.4	37.1	1131.0	14.0	100	
27.690301	94.673102	LKABALI	MIDDLE SIVALIK	75b	7a	P1408_001_Zm_A_1a_RAD_6	2007	377	7.56	12.4827	2.4	2.0964	2.9	0.1888	18.9	0.54	1120.3	23.1	1147.6	19.6	1199.7	48.2	1147.6	19.6	100	
27.690301	94.673102	LKABALI	MIDDLE SIVALIK	75b	weighted	-	-	-	12.6854	1.5	2.0632	1.7	0.1899	13.4	-	1120.9	15.1	1136.6	14.4	1168.2	29.4	1168.6	-	11.4	100	
27.690301	94.673102	LKABALI	MIDDLE SIVALIK	75b	8	P1408_001_Zm_A_1_RAD_7	168	217	0.77	11.3688	3.6	2.5185	3.8	0.2077	20.8	0.49	1216.3	37.5	1277.4	27.4	1381.6	68.9	1277.4	27.4	94	
27.690301	94.673102	LKABALI	MIDDLE SIVALIK	75b	8a	P1408_001_Zm_A_1a_RAD_7	162	196	0.82	11.6143	4.5	2.4955	5.6	0.2102	21.0	0.59	1229.9	41.5	1270.7	40.6	1340.4	87.3	1270.7	40.6	87	
27.690301	94.673102	LKABALI	MIDDLE SIVALIK	75b	8b	P1408_001_Zm_A_1b_RAD_7	205	226	0.91	11.1631	3.2	2.6983	3.8	0.2185	21.9											

27.690301	94.673102	LKABALI	MIDDLE SIWALKI	75b	32a	P1408_001_Zm_A_1a_RAD_31	359	24	15.10	8.9920	1.9	4.9417	2.3	0.3223	32.2	0.59	1800.9	28.9	1809.4	19.6	1819.3	34.3	1809.4	19.6	97
27.690301	94.673102	LKABALI	MIDDLE SIWALKI	75b	weighted	-	-	-	-	8.9930	1.8	4.9815	2.2	0.3234	22.9	-	1802.0	27.9	1815.9	18.5	1832.4	32.3	1815.9	18.5	94
27.690301	94.673102	LKABALI	MIDDLE SIWALKI	75b	33	P1408_001_Zm_A_1a_RAD_32	317	399	0.90	17.6057	18.9	0.0542	18.6	0.0069	0.7	0.03	44.5	1.7	53.6	6.7	483.8	426.3	44.5	1.7	52
27.690301	94.673102	LKABALI	MIDDLE SIWALKI	75b	33a	P1408_001_Zm_A_1a_RAD_32	319	354	0.90	20.3410	22.4	0.0542	18.6	0.0069	0.7	0.04	42.8	1.7	53.6	6.7	483.8	426.3	44.5	1.7	52
27.690301	94.673102	LKABALI	MIDDLE SIWALKI	75b	weighted	-	-	-	-	17.7422	14.4	0.0544	14.2	0.0068	0.5	-	43.8	1.3	49.2	6.9	266.6	248.0	43.8	1.3	60
27.690301	94.673102	LKABALI	MIDDLE SIWALKI	75b	34	P1408_001_Zm_A_1a_RAD_33	833	561	1.28	21.3150	3.3	0.0603	8.2	0.0093	0.9	0.08	59.8	1.3	59.4	4.7	44.9	116.3	59.8	1.3	71
27.690301	94.673102	LKABALI	MIDDLE SIWALKI	75b	34a	P1408_001_Zm_A_1a_RAD_33	883	168	2.48	18.9132	17.6	0.0644	17.5	0.0088	0.9	0.10	56.7	2.3	63.4	10.8	323.4	340.1	56.7	2.3	52
27.690301	94.673102	LKABALI	MIDDLE SIWALKI	75b	weighted	-	-	-	-	20.3762	7.5	0.0610	7.4	0.0091	0.6	-	59.0	1.2	60.1	4.3	74.1	110.0	59.0	1.2	61
27.690301	94.673102	LKABALI	MIDDLE SIWALKI	75b	35	P1408_001_Zm_A_1a_RAD_34	318	189	2.11	19.0306	9.0	0.1098	9.1	0.0139	1.4	0.22	89.1	2.8	97.5	8.5	309.0	204.9	89.1	2.8	55
27.690301	94.673102	LKABALI	MIDDLE SIWALKI	75b	35a	P1408_001_Zm_A_1a_RAD_34	394	174	1.80	19.5205	13.7	0.0950	13.7	0.0135	1.3	0.07	86.2	2.6	92.2	12.0	251.1	269.9	86.2	2.6	84
27.690301	94.673102	LKABALI	MIDDLE SIWALKI	75b	weighted	-	-	-	-	19.1783	7.5	0.0990	7.6	0.0137	1.0	-	87.5	1.9	95.8	6.9	287.8	163.2	87.5	1.9	69
27.690301	94.673102	LKABALI	MIDDLE SIWALKI	75b	36	P1408_001_Zm_A_1a_RAD_35	1059	752	1.41	13.9127	2.0	0.1610	2.5	0.0131	16.3	0.57	973.8	16.5	976.4	16.5	982.5	41.2	976.4	16.5	94
27.690301	94.673102	LKABALI	MIDDLE SIWALKI	75b	37	P1408_001_Zm_A_1a_RAD_36	365	93	3.93	12.2495	3.6	0.1791	8.0	0.1527	15.3	0.90	916.2	65.2	1015.7	51.6	1236.8	70.2	1015.7	51.6	45
27.690301	94.673102	LKABALI	MIDDLE SIWALKI	75b	38	P1408_001_Zm_A_1a_RAD_37	490	282	1.74	17.9453	3.7	0.0576	4.0	0.0778	7.8	0.41	482.9	11.4	475.7	15.0	441.4	81.8	482.9	11.4	74
27.690301	94.673102	LKABALI	MIDDLE SIWALKI	75b	39	P1408_001_Zm_A_1a_RAD_38	1458	836	1.74	15.1398	4.5	0.1789	5.4	0.1294	13.0	0.65	784.7	39.6	790.8	29.7	806.0	94.0	790.8	29.7	71
27.690301	94.673102	LKABALI	MIDDLE SIWALKI	75b	40	P1408_001_Zm_A_1a_RAD_39	2296	415	5.53	17.4840	2.2	0.0375	2.7	0.0888	8.1	0.61	501.7	11.5	500.8	10.7	499.1	48.9	500.8	10.7	94
27.690301	94.673102	LKABALI	MIDDLE SIWALKI	75b	41	P1408_001_Zm_A_1a_RAD_40	481	88	5.44	13.7957	2.5	0.1506	2.7	0.1561	15.6	0.47	933.3	19.1	954.7	16.7	999.6	50.6	954.7	16.7	90
27.690301	94.673102	LKABALI	MIDDLE SIWALKI	75b	42	P1408_001_Zm_A_1a_RAD_41	2654	1426	1.86	10.2263	2.1	0.3683	2.2	0.2498	25.0	0.39	1437.6	20.7	1497.1	17.5	1582.3	39.1	1497.1	17.5	100
27.690301	94.673102	LKABALI	MIDDLE SIWALKI	75b	42a	P1408_001_Zm_A_1a_RAD_41	2592	1307	1.98	10.3981	2.2	0.3612	2.6	0.2535	25.4	0.54	1456.4	20.1	1495.4	20.3	1551.1	41.0	1495.4	20.3	74
27.690301	94.673102	LKABALI	MIDDLE SIWALKI	75b	weighted	-	-	-	-	10.3084	1.5	0.3653	1.7	0.2516	17.8	-	1445.2	16.0	1496.4	13.3	1567.5	28.3	1496.4	13.3	87
27.690301	94.673102	LKABALI	MIDDLE SIWALKI	75b	43	P1408_001_Zm_A_1a_RAD_42	749	244	3.07	9.6173	2.2	0.4282	2.6	0.2680	28.8	0.55	1631.6	26.3	1660.1	21.2	1696.3	40.2	1660.1	21.2	97
27.690301	94.673102	LKABALI	MIDDLE SIWALKI	75b	44	P1408_001_Zm_A_1a_RAD_43	350	588	0.59	12.4919	2.3	0.1081	3.0	0.1910	19.1	0.65	1126.7	26.7	1151.5	20.5	1198.3	45.8	1151.5	20.5	84
27.690301	94.673102	LKABALI	MIDDLE SIWALKI	75b	44a	P1408_001_Zm_A_1a_RAD_43	304	184	1.66	12.2639	3.1	0.1691	3.4	0.1929	19.3	0.45	1137.2	22.6	1171.2	24.0	1234.5	60.6	1171.2	22.6	94
27.690301	94.673102	LKABALI	MIDDLE SIWALKI	75b	weighted	-	-	-	-	12.4096	1.9	0.2342	2.3	0.1920	13.6	-	1132.9	17.2	1159.8	15.6	1211.4	36.5	1145.0	15.2	89
27.690301	94.673102	LKABALI	MIDDLE SIWALKI	75b	45	P1408_001_Zm_A_1a_RAD_44	174	64	2.72	16.6582	5.5	0.5926	5.7	0.0716	7.2	0.37	445.8	16.5	472.5	21.7	604.7	120.2	445.8	16.5	68
27.690301	94.673102	LKABALI	MIDDLE SIWALKI	75b	45a	P1408_001_Zm_A_1a_RAD_44	760	35	21.59	18.4229	9.0	0.1204	9.2	0.0161	1.6	0.22	102.9	3.1	115.4	10.1	382.7	203.8	102.9	3.1	68
27.690301	94.673102	LKABALI	MIDDLE SIWALKI	75b	weighted	-	-	-	-	17.1420	4.7	0.4610	4.9	0.0188	1.6	0.37	114.6	3.0	178.8	9.1	547.4	103.5	114.6	3.0	68
27.690301	94.673102	LKABALI	MIDDLE SIWALKI	75b	46	P1408_001_Zm_A_1a_RAD_45	620	588	1.23	20.4076	16.3	0.0498	15.9	0.0073	0.7	0.06	40.0	0.49	49.3	7.5	25.5	2.0	49.3	7.5	68
27.690301	94.673102	LKABALI	MIDDLE SIWALKI	75b	46a	P1408_001_Zm_A_1a_RAD_45	732	485	1.30	19.1442	24.1	0.0525	24.1	0.0073	0.7	0.07	46.8	2.4	52.0	12.2	295.7	386.2	46.8	2.4	68
27.690301	94.673102	LKABALI	MIDDLE SIWALKI	75b	weighted	-	-	-	-	20.0572	13.5	0.0506	13.3	0.0073	0.5	-	47.2	1.5	50.1	6.5	185.1	204.6	47.2	1.5	68
27.690301	94.673102	LKABALI	MIDDLE SIWALKI	75b	47	P1408_001_Zm_A_1a_RAD_46	1069	501	2.14	20.4087	14.5	0.0268	14.3	0.0040	0.4	0.06	25.5	0.8	26.8	3.8	147.8	228.0	25.5	0.8	77
27.690301	94.673102	LKABALI	MIDDLE SIWALKI	75b	47a	P1408_001_Zm_A_1a_RAD_46	169	83	2.04	12.6461	8.6	1.1005	11.1	0.1009	10.1	0.63	619.9	46.1	753.6	59.0	1174.0	170.9	619.9	46.1	58
27.690301	94.673102	LKABALI	MIDDLE SIWALKI	75b	weighted	-	-	-	-	14.6720	7.4	0.6991	8.8	0.0041	0.4	-	25.7	0.8	29.8	3.8	804.8	136.8	25.7	0.8	68
27.690301	94.673102	LKABALI	MIDDLE SIWALKI	75b	48	P1408_001_Zm_A_1a_RAD_47	244	539	2.31	15.0458	2.4	1.1451	2.4	0.1250	12.5	0.37	759.0	14.8	774.9	13.2	821.0	50.8	774.9	13.2	100
27.690301	94.673102	LKABALI	MIDDLE SIWALKI	75b	48a	P1408_001_Zm_A_1a_RAD_47	1392	624	2.23	15.1418	2.4	1.1547	2.6	0.1268	12.7	0.43	769.6	13.4	779.5	14.1	807.7	49.8	769.6	13.4	94
27.690301	94.673102	LKABALI	MIDDLE SIWALKI	75b	48b	P1408_001_Zm_A_1b_RAD_47	1204	563	2.14	14.8701	3.1	1.1649	3.1	0.1256	12.6	0.34	762.9	14.6	784.3	17.4	845.6	64.4	762.9	14.6	90
27.690301	94.673102	LKABALI	MIDDLE SIWALKI	75b	weighted	-	-	-	-	15.0248	1.5	1.1532	1.6	0.1258	7.3	-	764.2	8.2	778.7	8.4	821.5	31.1	769.5	7.9	95
27.690301	94.673102	LKABALI	MIDDLE SIWALKI	75b	49	P1408_001_Zm_A_1a_RAD_48	459	87	5.29	16.8218	3.9	0.6886	4.0	0.0838	8.4	0.28	518.6	10.3	530.8	16.5	583.5	84.5	518.6	10.3	100
27.690301	94.673102	LKABALI	MIDDLE SIWALKI	75b	50	P1408_001_Zm_A_1a_RAD_49	1153	493	2.34	19.7311	10.8	0.0277	10.6	0.0040	0.4	0.11	25.5	0.9	27.7	3.9	226.4	22.8	25.5	0.9	87
27.690301	94.673102	LKABALI	MIDDLE SIWALKI	75b	51	P1408_001_Zm_A_1a_RAD_50	1196	189	6.32	17.2446	2.8	0.5930	3.2	0.0742	7.4	0.50	461.2	9.5	472.8	12.1	529.4	61.1	461.2	9.5	94
27.690301	94.673102	LKABALI	MIDDLE SIWALKI	75b	51a	P1408_001_Zm_A_1a_RAD_50	577	237	2.44	16.8389	3.8	0.6261	4.2	0.0765	7.6	0.42	475.0	11.6	493.7	16.2	581.3	87.9	475.0	11.6	87
27.690301	94.673102	LKABALI	MIDDLE SIWALKI	75b	51b	P1408_001_Zm_A_1b_RAD_50	950	301	3.16	18.2017	3.0	0.5712	3.3	0.0754	7.5	0.41	468.6	10.2	458.8	12.1	409.8	68.1	468.6	10.2	100
27.690301	94.673102	LKABALI	MIDDLE SIWALKI	75b	weighted	-	-	-	-	17.4917	1.8	0.5926	2.0	0.0753	4.4	-	467.4	5.9	471.8	7.6	500.4	39.9	467.4	5.9	94
27.690301	94.673102	LKABALI	MIDDLE SIWALKI	75b	52	P1408_001_Zm_A_1a_RAD_51	265	38	7.03	6.1807	4.7	8.9994	6.7	0.4034	40.4	0.72	2184.8	111.5	2337.9	61.3	2474.5	79.7	2337.9	61.3	100
27.690301	94.673102	LKABALI	MIDDLE SIWALKI	75b	52a	P1408_001_Zm_A_2_RAD_2	402	193	1.79	12.1925	3.1	2.0435	3.5	0.1807	18.1	0.48	1070.8	24.1	1130.1	24.2	1245.9	50.7	1130.1	24.2	77
27.690301	94.673102	LKABALI	MIDDLE SIWALKI	75b	weighted	-	-	-	-	12.3991	2.0	2.0396	2.0	0.1829	12.9	0.59	1085.3	15.4	1128.8	15.3	1213.3	38.9	1128.8	15.3	85
27.690301	94.673102	LKABALI	MIDDLE SIWALKI	75b	56	P1408_001_Zm_A_2_RAD_3	379	141	2.68	20.4570	23.9	0.0632	23.6	0.0094	0.9	0.04	60.1	2.8	62.2	14.3	142.2	311.7	60.1	2.8	68
27.690301	94.673102	LKABALI	MIDDLE SIWALKI	75b	57	P1408_001_Zm_A_2_RAD_4	705	199	3.55	16.9631	3.2	0.6175	3.6	0.0760	7.6	0.48	472.0	11.1	488.3	13.8	565.3	68.7	472.0	11.1	84
27.690301	94.673102	LKABALI	M																						

27.685349	94.678618	LKABALI	MIDDLE SIWALKI	50b	18	P1408_003_Zm_A_1_RAD_17	662	147	4.50	17.5234	3.0	0.4970	3.0	0.0632	6.3	0.26	394.8	8.8	409.6	10.1	494.1	66.2	394.8	8.8	87
27.685349	94.678618	LKABALI	MIDDLE SIWALKI	50b	19	P1408_003_Zm_A_1_RAD_18	177	223	0.79	17.3637	4.0	0.6901	4.0	0.0869	8.7	0.30	537.2	8.6	532.8	16.6	514.2	87.5	537.2	8.6	97
27.685349	94.678618	LKABALI	MIDDLE SIWALKI	50b	20	P1408_003_Zm_A_1_RAD_19	1563	53	29.44	18.1508	7.2	0.4486	2.5	0.0591	5.9	0.51	369.9	7.1	376.3	7.8	416.0	49.4	369.9	7.1	100
27.685349	94.678618	LKABALI	MIDDLE SIWALKI	50b	21	P1408_003_Zm_A_1_RAD_20	348	149	2.34	17.2333	14.6	0.0554	14.6	0.0773	14.7	0.07	41.7	31.3	57.2	0.7	57.2	66.9	57.2	1.3	58
27.685349	94.678618	LKABALI	MIDDLE SIWALKI	50b	22	P1408_003_Zm_A_1_RAD_21	53	32	1.65	15.9354	26.9	0.0703	26.4	0.0089	0.9	0.01	57.4	3.1	75.6	19.2	69.9	594.0	57.4	3.1	61
27.685349	94.678618	LKABALI	MIDDLE SIWALKI	50b	23	P1408_003_Zm_A_1_RAD_22	87	21	4.11	22.9341	32.3	0.0615	32.2	0.0102	1.0	0.03	65.6	2.4	60.6	18.9	0.0	258.6	65.6	2.4	77
27.685349	94.678618	LKABALI	MIDDLE SIWALKI	50b	24	P1408_003_Zm_A_1_RAD_23	1019	309	3.30	12.9619	1.7	1.8973	1.7	0.1784	1.7	0.27	1058.0	12.4	1080.1	11.1	1125.1	33.7	1080.1	11.1	90
27.685349	94.678618	LKABALI	MIDDLE SIWALKI	50b	25	P1408_003_Zm_A_1_RAD_24	24	55	2.18	9.4201	2.0	4.6837	2.0	0.3200	32.0	0.43	1789.7	24.1	1734.4	36.2	1734.4	36.2	1734.4	17.9	87
27.685349	94.678618	LKABALI	MIDDLE SIWALKI	50b	26	P1408_003_Zm_A_1_RAD_25	495	125	3.95	16.8062	2.9	0.6788	3.0	0.0621	8.2	0.31	508.8	7.7	523.0	12.1	585.5	62.1	508.8	7.7	100
27.685349	94.678618	LKABALI	MIDDLE SIWALKI	50b	27	P1408_003_Zm_A_1_RAD_26	361	58	6.18	11.2333	13.3	0.0677	13.3	0.0104	1.0	0.09	65.9	2.0	66.6	8.6	54.1	172.5	66.9	2.0	52
27.685349	94.678618	LKABALI	MIDDLE SIWALKI	50b	28	P1408_003_Zm_A_1_RAD_27	58	33	1.75	12.9828	4.8	1.7612	4.9	0.1658	16.6	0.22	989.1	17.9	1031.3	31.8	1121.8	96.8	989.1	17.9	81
27.685349	94.678618	LKABALI	MIDDLE SIWALKI	50b	29	P1408_003_Zm_A_1_RAD_28	1806	199	9.09	17.9058	1.6	0.6314	1.7	0.0820	8.2	0.41	508.0	6.2	497.0	6.7	446.3	34.9	508.0	6.2	94
27.685349	94.678618	LKABALI	MIDDLE SIWALKI	50b	30	P1408_003_Zm_A_1_RAD_29	67	11	6.11	18.5827	25.2	0.0892	24.9	0.0120	1.2	0.03	77.0	3.2	86.7	20.7	363.3	424.3	77.0	3.2	68
27.685349	94.678618	LKABALI	MIDDLE SIWALKI	50b	31	P1408_003_Zm_A_1_RAD_30	526	84	6.24	16.7796	2.2	0.7594	2.3	0.0924	9.2	0.31	569.8	7.3	573.7	10.0	588.9	47.9	569.8	7.3	100
27.685349	94.678618	LKABALI	MIDDLE SIWALKI	50b	32	P1408_003_Zm_A_1_RAD_31	1102	306	3.60	15.3115	1.6	1.1989	1.6	0.1351	13.3	0.30	865.7	9.6	800.1	8.8	784.4	33.3	800.1	8.8	100
27.685349	94.678618	LKABALI	MIDDLE SIWALKI	50b	33	P1408_003_Zm_A_1_RAD_32	384	189	2.03	12.8199	1.6	2.0130	1.7	0.1872	18.7	0.42	1106.0	13.1	1119.9	11.7	1147.0	31.7	1119.9	11.7	71
27.685349	94.678618	LKABALI	MIDDLE SIWALKI	50b	34	P1408_003_Zm_A_1_RAD_33	19	21	0.94	13.7082	7.5	1.4315	7.7	0.1423	14.2	0.26	857.8	25.4	902.2	46.1	1012.5	152.7	857.8	25.4	77
27.685349	94.678618	LKABALI	MIDDLE SIWALKI	50b	35	P1408_003_Zm_A_1_RAD_34	478	34	1.52	11.1348	7.3	2.4565	6.6	0.1984	19.8	0.10	1166.6	39.8	1259.3	48.0	1421.5	139.0	1166.6	39.8	100
27.685349	94.678618	LKABALI	MIDDLE SIWALKI	50b	36	P1408_003_Zm_A_1_RAD_35	273	94	2.91	12.5667	2.1	2.2741	2.3	0.2073	20.7	0.36	1214.2	35.8	1186.5	45.9	1186.5	42.1	1214.2	35.8	100
27.685349	94.678618	LKABALI	MIDDLE SIWALKI	50b	37	P1408_003_Zm_A_1_RAD_36	655	220	2.98	17.4496	2.2	0.6381	2.3	0.0808	8.1	0.35	500.7	8.4	501.2	8.9	503.4	49.5	500.7	8.4	100
27.685349	94.678618	LKABALI	MIDDLE SIWALKI	50b	38	P1408_003_Zm_A_1_RAD_37	197	53	3.70	18.9343	15.2	0.0667	15.3	0.0092	0.9	0.12	56.7	1.9	65.5	9.7	320.8	317.3	56.7	1.9	84
27.685349	94.678618	LKABALI	MIDDLE SIWALKI	50b	39	P1408_003_Zm_A_1_RAD_38	522	26	20.10	11.8382	2.0	2.4201	2.0	0.2078	20.8	0.28	1217.0	14.8	1248.6	38.6	1248.6	38.6	1248.6	14.4	100
27.685349	94.678618	LKABALI	MIDDLE SIWALKI	50b	40	P1408_003_Zm_A_1_RAD_39	12	2	5.07	15.2387	14.7	0.8043	14.7	0.0889	8.9	0.12	549.0	20.3	599.3	66.6	794.4	312.8	549.0	20.3	84
27.685349	94.678618	LKABALI	MIDDLE SIWALKI	50b	41	P1408_003_Zm_A_1_RAD_40	296	57	5.18	19.8435	7.4	0.0972	7.2	0.0140	1.4	0.07	89.6	2.1	94.2	6.5	213.2	171.3	89.6	2.1	77
27.685349	94.678618	LKABALI	MIDDLE SIWALKI	50b	42	P1408_003_Zm_A_1_RAD_41	622	135	4.60	15.5190	1.6	1.1926	2.5	0.1342	13.4	0.77	812.0	17.1	797.2	14.0	756.0	34.0	797.2	14.0	97
27.685349	94.678618	LKABALI	MIDDLE SIWALKI	50b	43	P1408_003_Zm_A_1_RAD_42	493	164	3.01	19.2492	10.6	0.0484	10.8	0.0068	0.7	0.20	43.4	1.4	48.0	5.1	283.2	245.3	43.4	1.4	65
27.685349	94.678618	LKABALI	MIDDLE SIWALKI	50b	44	P1408_003_Zm_A_1_RAD_43	320	79	4.04	10.1915	2.1	3.6412	2.0	0.2691	26.9	0.31	1536.4	23.5	1588.7	16.2	1588.7	16.2	1588.7	16.2	90
27.685349	94.678618	LKABALI	MIDDLE SIWALKI	50b	45	P1408_003_Zm_A_1_RAD_44	405	46	3.78	18.4248	6.8	2.1215	9.4	0.0024	0.2	0.07	180.5	2.6	195.6	16.8	214.1	180.5	16.8	2.6	84
27.685349	94.678618	LKABALI	MIDDLE SIWALKI	50b	46	P1408_003_Zm_A_1_RAD_45	740	156	4.76	19.7000	5.0	0.0661	4.9	0.0094	0.9	0.11	60.6	1.1	65.0	3.1	230.0	116.1	65.0	3.1	90
27.685349	94.678618	LKABALI	MIDDLE SIWALKI	50b	47	P1408_003_Zm_A_1_RAD_46	99	32	3.10	19.4466	21.3	0.0587	21.1	0.0083	0.8	0.03	53.2	2.0	57.9	11.9	259.8	343.6	53.2	2.0	94
27.685349	94.678618	LKABALI	MIDDLE SIWALKI	50b	48	P1408_003_Zm_A_1_RAD_47	358	87	4.13	17.0960	2.4	0.6166	2.5	0.0764	7.6	0.33	474.9	7.8	487.7	9.6	548.3	53.1	474.9	7.8	90
27.685349	94.678618	LKABALI	MIDDLE SIWALKI	50b	49	P1408_003_Zm_A_1_RAD_48	2330	1243	1.87	14.8324	1.7	1.2779	1.9	0.1375	13.7	0.52	830.3	11.9	835.9	10.9	850.8	34.5	835.9	10.9	100
27.685349	94.678618	LKABALI	MIDDLE SIWALKI	50b	50	P1408_003_Zm_A_1_RAD_49	191	71	2.69	12.5258	2.5	1.8820	2.7	0.1769	17.1	0.41	1017.3	14.4	1074.8	18.2	1193.2	49.6	1017.3	14.4	100
27.685349	94.678618	LKABALI	MIDDLE SIWALKI	50b	51	P1408_003_Zm_A_1_RAD_50	674	281	2.40	17.6799	2.4	0.6532	2.3	0.0838	8.4	0.26	518.5	7.7	510.5	9.3	474.5	52.0	518.5	7.7	100
27.685349	94.678618	LKABALI	MIDDLE SIWALKI	50b	52	P1408_003_Zm_A_1_RAD_51	172	45	3.81	14.5502	3.5	1.2801	3.4	0.1351	13.5	0.21	816.8	14.3	836.9	19.4	890.6	71.6	816.8	14.3	100
27.685349	94.678618	LKABALI	MIDDLE SIWALKI	50b	53	P1408_003_Zm_A_1_RAD_52	320	90	3.54	14.8583	2.8	1.2426	2.7	0.1339	13.4	0.33	810.1	17.8	820.0	15.0	847.1	59.1	820.0	15.0	100
27.685349	94.678618	LKABALI	MIDDLE SIWALKI	50b	54	P1408_003_Zm_A_1_RAD_53	790	129	7.51	19.8549	6.5	0.0466	6.3	0.0067	0.7	0.10	43.1	1.1	46.3	2.9	211.9	151.7	43.1	1.1	61
27.685349	94.678618	LKABALI	MIDDLE SIWALKI	50b	55	P1408_003_Zm_A_1_RAD_54	153	47	3.24	12.5792	3.0	1.9748	3.1	0.1802	18.0	0.38	1067.9	21.5	1107.0	20.7	1184.5	58.8	1107.0	20.7	74
27.685349	94.678618	LKABALI	MIDDLE SIWALKI	50b	56	P1408_003_Zm_A_1_RAD_55	22	33	1.31	23.6685	34.4	0.0810	33.9	0.0101	1.1	0.02	89.0	5.7	79.1	25.8	80.0	245.8	80.0	25.8	84
27.685349	94.678618	LKABALI	MIDDLE SIWALKI	50b	57	P1408_003_Zm_A_1_RAD_56	510	129	3.94	14.7139	3.3	1.0712	3.2	0.1143	11.4	0.11	697.8	11.0	739.4	16.8	867.4	69.5	697.8	11.0	55
27.685349	94.678618	LKABALI	MIDDLE SIWALKI	50b	58	P1408_003_Zm_A_1_RAD_57	59	25	2.39	20.5599	26.2	0.1201	25.9	0.0192	1.9	0.03	122.9	5.7	123.2	30.1	130.4	302.0	122.9	5.7	65
27.685349	94.678618	LKABALI	MIDDLE SIWALKI	50b	59	P1408_003_Zm_A_1_RAD_58	51	10	4.96	21.0688	25.9	0.1269	25.7	0.0194	1.9	0.03	124.0	4.9	121.3	29.4	68.3	295.2	124.0	4.9	77
27.685349	94.678618	LKABALI	MIDDLE SIWALKI	50b	60	P1408_003_Zm_A_1_RAD_59	174	22	7.85	20.6019	24.1	0.0349	23.9	0.0052	0.5	0.03	33.5	1.1	34.8	8.2	125.6	305.6	33.5	1.1	77
27.685349	94.678618	LKABALI	MIDDLE SIWALKI	50b	61	P1408_003_Zm_A_1_RAD_60	1738	774	2.25	19.8780	8.4	0.0364	8.5	0.0053	0.5	0.13	33.8	0.6	36.3	3.0	209.2	195.4	33.8	0.6	61
27.685349	94.678618	LKABALI	MIDDLE SIWALKI	50b	62	P1408_003_Zm_A_1_RAD_61	467	97	4.84	17.2714	3.7	0.6070	3.5	0.0750	7.6	0.62	472.4	11.1	481.6	13.2	525.9	59.8	472.4	11.1	100
27.685349	94.678618	LKABALI	MIDDLE SIWALKI	50b	63	P1408_003_Zm_A_1_RAD_62	98	48	2.04	18.7701	15.2	0.0621	15.2	0.0084	0.8	0.07	54.2	1.1	61.1	9.0	340.6	326.4	54.2	1.1	100
27.685349	94.678618	LKABALI	MIDDLE SIWALKI	50b	64	P1408_003_Zm_A_1_RAD_64	177	41	4.28	15.3387	2.5	1.2371	2.8	0.1376	13.8	0.42	831.2	13.7	817.6	15.5	780.6	53.5	831.2	13.7	94
27.685349	94.6																								

27.678317	94.682618	LKABALI	MIDDLE SIVALIK	25c	41	P1408_004_Zm_A_1_RAD_0	449	47	9.51	17.7617	5.6	0.6481	5.0	0.0835	8.4	0.17	516.9	18.8	507.3	19.9	464.3	125.3	516.9	18.8	97
27.678317	94.682618	LKABALI	MIDDLE SIVALIK	25c	42	P1408_004_Zm_A_1_RAD_1	351	107	3.21	17.1637	3.4	0.6682	3.4	0.0832	8.3	0.32	515.1	11.1	519.6	13.9	539.6	74.1	515.1	11.1	97
27.678317	94.682618	LKABALI	MIDDLE SIVALIK	25c	43	P1408_004_Zm_A_1_RAD_2	1530	381	4.01	21.9295	8.1	0.0369	8.1	0.0059	0.6	0.24	37.8	1.5	36.8	0.0	81.2	37.8	1.5	35	0.0
27.678317	94.682618	LKABALI	MIDDLE SIVALIK	25c	44	P1408_004_Zm_A_1_RAD_3	76	15	3.21	17.1637	3.4	0.6682	3.4	0.0832	8.3	0.32	515.1	11.1	519.6	13.9	539.6	74.1	515.1	11.1	97
27.678317	94.682618	LKABALI	MIDDLE SIVALIK	25c	45	P1408_004_Zm_A_1_RAD_4	1360	551	2.47	17.3155	2.1	0.6127	2.2	0.0769	7.7	0.37	477.8	8.2	485.2	8.5	520.4	46.6	477.8	8.2	100
27.678317	94.682618	LKABALI	MIDDLE SIVALIK	25c	46	P1408_004_Zm_A_1_RAD_5	503	173	2.90	17.7012	2.7	0.6070	2.9	0.0779	7.8	0.39	483.7	8.7	481.6	11.1	471.8	59.4	483.7	8.7	97
27.678317	94.682618	LKABALI	MIDDLE SIVALIK	25c	47	P1408_004_Zm_A_1_RAD_6	408	93	4.41	13.0623	2.2	1.7993	2.4	0.1705	17.1	0.45	1014.7	18.6	1045.2	15.5	1109.5	44.0	1045.2	15.5	94
27.678317	94.682618	LKABALI	MIDDLE SIVALIK	25c	48	P1408_004_Zm_A_1_RAD_7	182	111	1.64	13.6656	2.8	1.8180	3.0	0.1802	18.0	0.45	1068.0	20.4	1092.0	19.9	1018.8	56.3	1052.0	19.9	97
27.678317	94.682618	LKABALI	MIDDLE SIVALIK	25c	49	P1408_004_Zm_A_1_RAD_8	97	59	1.64	12.6722	3.0	2.1662	2.8	0.1802	18.0	0.24	1170.4	22.8	1192.0	19.7	1070.0	58.5	1170.3	19.7	100
27.678317	94.682618	LKABALI	MIDDLE SIVALIK	25c	50	P1408_004_Zm_A_1_RAD_9	390	95	4.10	19.1133	10.8	0.0556	10.7	0.0077	0.8	0.06	49.5	1.2	55.0	5.7	279.4	248.4	1.2	81	0.0
27.678317	94.682618	LKABALI	MIDDLE SIVALIK	25c	51	P1408_004_Zm_A_1_RAD_50	148	32	4.56	21.2467	13.3	0.0945	13.0	0.0146	1.5	0.03	93.2	3.1	91.7	11.4	52.6	171.6	93.2	3.1	81
27.678317	94.682618	LKABALI	MIDDLE SIVALIK	25c	52	P1408_004_Zm_A_1_RAD_51	359	148	2.42	15.2199	4.8	1.1907	4.1	0.1314	13.1	0.18	796.0	26.6	796.3	22.7	796.9	101.3	796.3	22.7	97
27.678317	94.682618	LKABALI	MIDDLE SIVALIK	25c	53	P1408_004_Zm_A_1_RAD_52	214	50	4.31	16.7200	4.2	0.6797	4.1	0.0824	8.2	0.24	510.6	13.1	526.6	16.7	596.7	91.6	510.6	13.1	100
27.678317	94.682618	LKABALI	MIDDLE SIVALIK	25c	54	P1408_004_Zm_A_1_RAD_53	102	50	2.07	17.6429	5.4	0.6548	5.3	0.0838	8.4	0.12	518.7	11.1	511.4	21.2	479.1	119.2	518.7	11.1	100
27.678317	94.682618	LKABALI	MIDDLE SIVALIK	25c	55	P1408_004_Zm_A_1_RAD_54	106	58	1.83	19.0106	17.9	0.0562	17.7	0.0078	0.8	0.05	49.8	1.9	55.5	9.5	311.7	337.0	49.8	1.9	84
27.678317	94.682618	LKABALI	MIDDLE SIVALIK	25c	56	P1408_004_Zm_A_1_RAD_55	1088	211	4.92	20.7586	7.7	0.0414	7.8	0.0062	0.6	0.21	40.1	1.3	41.2	3.1	107.8	140.2	40.1	1.3	42
27.678317	94.682618	LKABALI	MIDDLE SIVALIK	25c	57	P1408_004_Zm_A_1_RAD_56	110	29	3.81	19.9738	25.7	0.0626	25.2	0.0091	0.9	0.03	58.2	3.3	61.7	15.1	198.0	353.0	58.2	3.3	58
27.678317	94.682618	LKABALI	MIDDLE SIVALIK	25c	58	P1408_004_Zm_A_1_RAD_57	1289	215	5.99	17.6049	2.2	0.6116	2.3	0.0781	7.8	0.40	484.7	9.2	484.6	8.8	483.9	48.8	484.6	8.8	100
27.678317	94.682618	LKABALI	MIDDLE SIVALIK	25c	59	P1408_004_Zm_A_1_RAD_58	50	10	4.98	17.5416	6.8	0.6986	6.9	0.0889	8.9	0.19	549.8	13.4	538.0	18.0	491.8	151.0	549.8	13.4	81
27.678317	94.682618	LKABALI	MIDDLE SIVALIK	25c	60	P1408_004_Zm_A_1_RAD_59	726	78	9.29	15.1664	2.3	1.2462	2.5	0.1371	13.7	0.35	828.1	12.5	821.7	13.9	804.3	48.9	828.1	12.5	100
27.678317	94.682618	LKABALI	MIDDLE SIVALIK	25c	61	P1408_004_Zm_A_1_RAD_60	168	37	4.52	11.5086	2.6	2.7375	2.4	0.2285	22.9	0.36	1326.6	24.8	1338.7	18.0	1338.7	18.0	1338.7	18.0	100
27.678317	94.682618	LKABALI	MIDDLE SIVALIK	25c	62	P1408_004_Zm_A_1_RAD_61	56	19	2.92	18.0533	25.6	0.1120	25.2	0.0147	1.5	0.04	93.9	5.3	107.8	25.8	428.1	458.2	93.9	5.3	65
27.678317	94.682618	LKABALI	MIDDLE SIVALIK	25c	63	P1408_004_Zm_A_1_RAD_62	565	103	5.47	15.4914	2.3	1.1113	2.2	0.1249	12.5	0.26	758.4	11.7	758.8	12.0	759.8	47.6	758.4	11.7	100
27.678317	94.682618	LKABALI	MIDDLE SIVALIK	25c	64	P1408_004_Zm_A_1_RAD_63	151	45	3.38	18.2674	4.5	0.6184	4.5	0.0819	8.2	0.19	507.6	9.2	488.8	17.4	401.7	100.0	507.6	9.2	84
27.678317	94.682618	LKABALI	MIDDLE SIVALIK	25c	65	P1408_004_Zm_A_1_RAD_64	107	38	2.51	11.0823	2.4	3.1111	2.9	0.2501	25.0	0.54	1438.8	27.7	1435.4	22.1	1430.5	46.7	1435.4	22.1	100
27.678317	94.682618	LKABALI	MIDDLE SIVALIK	25c	66	P1408_004_Zm_A_1_RAD_65	173	69	2.83	17.3519	4.4	0.6527	4.5	0.0821	8.2	0.30	508.9	13.4	510.1	18.0	515.7	97.4	508.9	13.4	87
27.678317	94.682618	LKABALI	MIDDLE SIVALIK	25c	67	P1408_004_Zm_A_1_RAD_66	485	160	3.04	18.5874	9.8	0.0476	9.6	0.0064	0.6	0.08	41.2	1.3	41.2	4.4	362.7	222.1	362.7	4.4	45
27.678317	94.682618	LKABALI	MIDDLE SIVALIK	25c	68	P1408_004_Zm_A_1_RAD_67	101	27	4.12	17.8625	4.0	1.7112	4.0	0.1211	12.6	0.06	100.7	20.8	102.7	26.7	89.7	1045.7	20.8	26.7	89.7
27.678317	94.682618	LKABALI	MIDDLE SIVALIK	25c	69	P1408_004_Zm_A_1_RAD_68	354	74	4.80	18.0290	2.4	0.6494	2.6	0.0849	8.5	0.39	525.4	9.2	508.1	14.1	431.1	54.1	525.4	9.2	77
27.678317	94.682618	LKABALI	MIDDLE SIVALIK	25c	70	P1408_004_Zm_A_1_RAD_69	873	251	3.47	18.3511	2.6	0.6117	2.9	0.0814	8.1	0.52	504.6	11.3	484.6	11.4	391.5	57.4	504.6	11.3	100
27.678317	94.682618	LKABALI	MIDDLE SIVALIK	25c	71	P1408_004_Zm_A_1_RAD_70	226	91	2.47	22.1486	34.2	0.0522	34.1	0.0084	0.8	0.02	53.8	1.9	51.7	17.2	0.0	312.6	53.8	1.9	42
27.678317	94.682618	LKABALI	MIDDLE SIVALIK	25c	72	P1408_002_Zm_A_1_RAD_1	106	39	2.72	18.7671	10.4	0.0986	10.0	0.0136	1.4	0.03	87.1	2.8	86.6	3.3	338.5	238.3	87.1	2.8	67
27.678317	94.682618	LKABALI	MIDDLE SIVALIK	25c	73	P1408_002_Zm_A_1_RAD_2	107	34	3.18	17.2156	4.4	0.7051	4.5	0.0880	8.8	0.22	544.0	10.0	541.9	18.0	533.0	97.3	544.0	10.0	100
27.678317	94.682618	LKABALI	MIDDLE SIVALIK	25c	74	P1408_002_Zm_A_1_RAD_3	371	52	7.11	18.7840	6.8	0.0903	6.7	0.0123	1.2	0.11	78.8	1.9	87.7	5.6	338.9	154.7	78.8	1.9	100
27.678317	94.682618	LKABALI	MIDDLE SIVALIK	25c	5	P1408_002_Zm_A_1_RAD_4	131	25	5.23	16.4798	10.4	0.1253	10.1	0.0150	1.5	0.06	95.8	3.0	119.9	10.4	627.9	225.2	95.8	3.0	52
27.678317	94.682618	LKABALI	MIDDLE SIVALIK	25c	6	P1408_002_Zm_A_1_RAD_5	114	50	2.21	18.1952	10.9	0.1066	11.0	0.0141	1.4	0.10	90.1	2.2	102.9	10.8	410.6	246.0	90.1	2.2	74
27.678317	94.682618	LKABALI	MIDDLE SIVALIK	25c	7	P1408_002_Zm_A_1_RAD_7	1838	530	3.47	20.3247	4.0	0.0512	4.0	0.0076	0.8	0.33	48.5	1.3	50.7	2.0	157.4	93.8	48.5	1.3	42
27.678317	94.682618	LKABALI	MIDDLE SIVALIK	25c	8	P1408_002_Zm_A_1_RAD_8	420	146	2.80	19.4562	8.6	0.0483	8.4	0.0068	0.7	0.22	45.8	2.0	47.9	3.9	258.7	299.2	47.9	3.9	77
27.678317	94.682618	LKABALI	MIDDLE SIVALIK	25c	9	P1408_002_Zm_A_1_RAD_9	78	25	3.08	21.8491	21.6	0.0805	21.5	0.0142	1.4	0.03	90.8	2.8	87.0	17.9	0.0	219.3	90.8	2.8	87
27.678317	94.682618	LKABALI	MIDDLE SIVALIK	25c	10	P1408_002_Zm_A_1_RAD_10	60	38	1.58	13.7562	3.5	1.8004	3.9	0.1796	18.0	0.44	1064.9	23.8	1045.6	18.0	1005.4	171.6	1064.9	23.8	68
27.678317	94.682618	LKABALI	MIDDLE SIVALIK	25c	11	P1408_002_Zm_A_1_RAD_11	397	181	2.20	20.3840	6.4	0.0731	6.5	0.0108	1.1	0.27	69.3	2.1	71.7	4.5	150.6	147.0	69.3	2.1	68
27.678317	94.682618	LKABALI	MIDDLE SIVALIK	25c	12	P1408_002_Zm_A_1_RAD_12	379	88	4.30	13.3424	2.3	1.6347	2.5	0.1582	15.8	0.37	946.7	13.7	983.7	15.7	1067.1	47.1	946.7	13.7	81
27.678317	94.682618	LKABALI	MIDDLE SIVALIK	25c	13	P1408_002_Zm_A_1_RAD_13	148	36	4.10	18.5754	13.8	0.0951	13.3	0.0128	1.3	0.05	82.0	3.6	92.2	11.6	364.1	315.6	82.0	3.6	74
27.678317	94.682618	LKABALI	MIDDLE SIVALIK	25c	14	P1408_002_Zm_A_1_RAD_14	103	32	3.23	21.7207	14.4	0.0894	14.0	0.0141	1.4	0.03	90.1	3.4	85.9	11.7	9.1	157.6	90.1	3.4	65
27.678317	94.682618	LKABALI	MIDDLE SIVALIK	25c	15	P1408_002_Zm_A_1_RAD_15	153	21	7.16	17.8714	6.9	0.2182	6.9	0.0283	2.8	0.19	179.7	4.4	200.4	12.6	450.6	153.1	179.7	4.4	90
27.678317	94.682618	LKABALI	MIDDLE SIVALIK	25c	16	P1408_002_Zm_A_1_RAD_16	233	58	4.00	19.1347	5.8	0.1011	5.4	0.0140	1.4	0.15	89.8	2.8	97.8	5.1	296.9	133.5	89.8	2.8	61
27.678317	94.682618	LKABALI	MIDDLE SIVALIK	25c	17	P1408_002_Zm_A_1_RAD_17	79	26	3.04	17.8269	21.0	0.0671	20.7	0.0087	0.9	0.02	55.7	2.4	66.0	13.2	456.1	432.5	55.7	2.4	61
27.678317	94.682618	LKABALI	MIDDLE SIVALIK	25c	18	P1408_002_Zm_A_1_RAD_18	497	86	5.76	19.7322	4														

27.670815	94.683994	LIKABALI	MIDDLE SIWALIK	5b	63	P1408_002_Zrn_A_1_RAD_63	181	69	2.60	20.7615	10.5	0.0730	10.5	0.0110	1.1	0.09	70.5	1.5	71.6	7.2	107.4	169.2	70.5	1.5	77
27.670815	94.683994	LIKABALI	MIDDLE SIWALIK	5b	64	P1408_002_Zrn_A_1_RAD_64	363	131	2.77	21.4973	9.7	0.0505	9.5	0.0079	0.8	0.13	50.5	1.7	50.0	4.7	24.5	121.0	50.5	1.7	81
27.670815	94.683994	LIKABALI	MIDDLE SIWALIK	5b	65	P1408_002_Zrn_A_1_RAD_65	188	67	2.80	17.2646	15.8	0.0683	15.4	0.0085	0.9	0.08	54.9	2.8	67.1	10.0	526.8	352.5	54.9	2.8	77
27.670815	94.683994	LIKABALI	MIDDLE SIWALIK	5b	66	P1408_002_Zrn_A_1_RAD_66	256	139	1.84	19.8499	9.5	0.0574	9.2	0.0083	0.8	0.07	53.1	1.8	62.1	5.1	212.5	209.8	53.1	1.8	71
27.670815	94.683994	LIKABALI	MIDDLE SIWALIK	5b	67	P1408_002_Zrn_A_1_RAD_67	263	123	2.14	12.6695	2.0	2.0987	1.9	0.1928	19.3	0.23	1136.8	14.7	1148.4	12.9	1170.4	39.2	1148.4	12.9	97
27.670815	94.683994	LIKABALI	MIDDLE SIWALIK	5b	68	P1408_002_Zrn_A_1_RAD_68	850	326	2.60	18.4278	7.9	0.0602	7.8	0.0080	0.8	0.10	51.7	1.1	59.4	4.5	382.1	178.1	51.7	1.1	71
27.670815	94.683994	LIKABALI	MIDDLE SIWALIK	5b	69	P1408_002_Zrn_A_1_RAD_69	134	54	2.48	19.9261	14.6	0.1102	14.5	0.0159	1.6	0.07	101.9	3.2	106.2	14.6	203.6	255.5	101.9	3.2	52

2.10.2 Compilation of bedrock geochronology

BEDROCK	EASTERN HIM/NBM	21.1	Aikman et al., 2012	BEDROCK	EASTERN HIM/NBM	278	Webb et al., 2012
BEDROCK	EASTERN HIM/NBM	21.3	Aikman et al., 2012	BEDROCK	EASTERN HIM/NBM	199	Webb et al., 2012
BEDROCK	EASTERN HIM/NBM	22	Aikman et al., 2012				
BEDROCK	EASTERN HIM/NBM	23.9	Aikman et al., 2012				
BEDROCK	EASTERN HIM/NBM	25.4	Aikman et al., 2012				
BEDROCK	EASTERN HIM/NBM	25.5	Aikman et al., 2012				
BEDROCK	EASTERN HIM/NBM	18.9	Aikman et al., 2012				
BEDROCK	EASTERN HIM/NBM	19.4	Aikman et al., 2012				
BEDROCK	EASTERN HIM/NBM	19.5	Aikman et al., 2012				
BEDROCK	EASTERN HIM/NBM	19.5	Aikman et al., 2012				
BEDROCK	EASTERN HIM/NBM	19.5	Aikman et al., 2012				
BEDROCK	EASTERN HIM/NBM	19.8	Aikman et al., 2012				
BEDROCK	EASTERN HIM/NBM	19.8	Aikman et al., 2012				
BEDROCK	EASTERN HIM/NBM	20	Aikman et al., 2012				
BEDROCK	EASTERN HIM/NBM	20.1	Aikman et al., 2012				
BEDROCK	EASTERN HIM/NBM	20.1	Aikman et al., 2012				
BEDROCK	EASTERN HIM/NBM	20.3	Aikman et al., 2012				
BEDROCK	EASTERN HIM/NBM	20.3	Aikman et al., 2012				
BEDROCK	EASTERN HIM/NBM	20.4	Aikman et al., 2012				
BEDROCK	EASTERN HIM/NBM	20.5	Aikman et al., 2012				
BEDROCK	EASTERN HIM/NBM	20.5	Aikman et al., 2012				
BEDROCK	EASTERN HIM/NBM	20.6	Aikman et al., 2012				
BEDROCK	EASTERN HIM/NBM	20.7	Aikman et al., 2012				
BEDROCK	EASTERN HIM/NBM	20.7	Aikman et al., 2012				
BEDROCK	EASTERN HIM/NBM	20.8	Aikman et al., 2012				
BEDROCK	EASTERN HIM/NBM	20.8	Aikman et al., 2012				
BEDROCK	EASTERN HIM/NBM	20.9	Aikman et al., 2012				
BEDROCK	EASTERN HIM/NBM	21	Aikman et al., 2012				
BEDROCK	EASTERN HIM/NBM	21.2	Aikman et al., 2012				
BEDROCK	EASTERN HIM/NBM	21.6	Aikman et al., 2012				
BEDROCK	EASTERN HIM/NBM	21.6	Aikman et al., 2012				
BEDROCK	EASTERN HIM/NBM	21.8	Aikman et al., 2012				
BEDROCK	EASTERN HIM/NBM	21.9	Aikman et al., 2012				
BEDROCK	EASTERN HIM/NBM	22.4	Aikman et al., 2012				
BEDROCK	EASTERN HIM/NBM	23.8	Aikman et al., 2012				
BEDROCK	EASTERN HIM/NBM	220	Webb et al., 2012				
BEDROCK	EASTERN HIM/NBM	223	Webb et al., 2012				
BEDROCK	EASTERN HIM/NBM	243	Webb et al., 2012				
BEDROCK	EASTERN HIM/NBM	251	Webb et al., 2012				
BEDROCK	EASTERN HIM/NBM	252	Webb et al., 2012				
BEDROCK	EASTERN HIM/NBM	253	Webb et al., 2012				
BEDROCK	EASTERN HIM/NBM	275	Webb et al., 2012				

2.10.3 Compilation of detrital geochronology

MODERN ALLUVIUM	S3	SIANG RIVER (KAPU)	613.6	16.33	Lang et al., 2013	MODERN ALLUVIUM	S3	SIANG RIVER (KAPU)	1172.9	16.43	Lang et al., 2013
MODERN ALLUVIUM	S3	SIANG RIVER (KAPU)	1033.5	10.27	Lang et al., 2013	MODERN ALLUVIUM	S3	SIANG RIVER (KAPU)	69.1	4.72	Lang et al., 2013
MODERN ALLUVIUM	S3	SIANG RIVER (KAPU)	1673.7	5.38	Lang et al., 2013	MODERN ALLUVIUM	S3	SIANG RIVER (KAPU)	500.6	10.41	Lang et al., 2013
MODERN ALLUVIUM	S3	SIANG RIVER (KAPU)	199.2	7.83	Lang et al., 2013	MODERN ALLUVIUM	S3	SIANG RIVER (KAPU)	2603.7	54.76	Lang et al., 2013
MODERN ALLUVIUM	S3	SIANG RIVER (KAPU)	125.7	5.28	Lang et al., 2013	MODERN ALLUVIUM	S3	SIANG RIVER (KAPU)	27.0	0.67	Lang et al., 2013
MODERN ALLUVIUM	S3	SIANG RIVER (KAPU)	805.4	10.79	Lang et al., 2013	MODERN ALLUVIUM	S2	SIANG RIVER (TUTING)	1172.9	11.02	Lang et al., 2013
MODERN ALLUVIUM	S3	SIANG RIVER (KAPU)	47.6	1.9	Lang et al., 2013	MODERN ALLUVIUM	S2	SIANG RIVER (TUTING)	209.2	4.85	Lang et al., 2013
MODERN ALLUVIUM	S3	SIANG RIVER (KAPU)	507.5	19.33	Lang et al., 2013	MODERN ALLUVIUM	S2	SIANG RIVER (TUTING)	61.7	3.68	Lang et al., 2013
MODERN ALLUVIUM	S3	SIANG RIVER (KAPU)	111.9	7.85	Lang et al., 2013	MODERN ALLUVIUM	S2	SIANG RIVER (TUTING)	504.5	12.15	Lang et al., 2013
MODERN ALLUVIUM	S3	SIANG RIVER (KAPU)	525.0	16.38	Lang et al., 2013	MODERN ALLUVIUM	S2	SIANG RIVER (TUTING)	793.6	11.29	Lang et al., 2013
MODERN ALLUVIUM	S3	SIANG RIVER (KAPU)	124.9	2.46	Lang et al., 2013	MODERN ALLUVIUM	S2	SIANG RIVER (TUTING)	60.4	2.72	Lang et al., 2013
MODERN ALLUVIUM	S3	SIANG RIVER (KAPU)	19.8	1.11	Lang et al., 2013	MODERN ALLUVIUM	S2	SIANG RIVER (TUTING)	53.7	2.98	Lang et al., 2013
MODERN ALLUVIUM	S3	SIANG RIVER (KAPU)	467.6	9.64	Lang et al., 2013	MODERN ALLUVIUM	S2	SIANG RIVER (TUTING)	28.2	1.06	Lang et al., 2013
MODERN ALLUVIUM	S3	SIANG RIVER (KAPU)	850.1	76.01	Lang et al., 2013	MODERN ALLUVIUM	S2	SIANG RIVER (TUTING)	619.1	9.23	Lang et al., 2013
MODERN ALLUVIUM	S3	SIANG RIVER (KAPU)	1308.4	7.76	Lang et al., 2013	MODERN ALLUVIUM	S2	SIANG RIVER (TUTING)	191.5	4.73	Lang et al., 2013
MODERN ALLUVIUM	S3	SIANG RIVER (KAPU)	465.9	16.38	Lang et al., 2013	MODERN ALLUVIUM	S2	SIANG RIVER (TUTING)	1048.5	120.49	Lang et al., 2013
MODERN ALLUVIUM	S3	SIANG RIVER (KAPU)	80.0	3.89	Lang et al., 2013	MODERN ALLUVIUM	S2	SIANG RIVER (TUTING)	209.2	27.81	Lang et al., 2013
MODERN ALLUVIUM	S3	SIANG RIVER (KAPU)	1379.6	49.39	Lang et al., 2013	MODERN ALLUVIUM	S2	SIANG RIVER (TUTING)	1321.7	17.04	Lang et al., 2013
MODERN ALLUVIUM	S3	SIANG RIVER (KAPU)	824.1	14.35	Lang et al., 2013	MODERN ALLUVIUM	S2	SIANG RIVER (TUTING)	476.9	4.86	Lang et al., 2013
MODERN ALLUVIUM	S3	SIANG RIVER (KAPU)	422.3	9.78	Lang et al., 2013	MODERN ALLUVIUM	S2	SIANG RIVER (TUTING)	69.3	3.99	Lang et al., 2013
MODERN ALLUVIUM	S3	SIANG RIVER (KAPU)	503.2	6.55	Lang et al., 2013	MODERN ALLUVIUM	S2	SIANG RIVER (TUTING)	1151.9	13.02	Lang et al., 2013
MODERN ALLUVIUM	S3	SIANG RIVER (KAPU)	107.4	1.95	Lang et al., 2013	MODERN ALLUVIUM	S2	SIANG RIVER (TUTING)	46.9	1.14	Lang et al., 2013
MODERN ALLUVIUM	S3	SIANG RIVER (KAPU)	233.5	21.76	Lang et al., 2013	MODERN ALLUVIUM	S2	SIANG RIVER (TUTING)	115.3	1.41	Lang et al., 2013
MODERN ALLUVIUM	S3	SIANG RIVER (KAPU)	44.2	1.46	Lang et al., 2013	MODERN ALLUVIUM	S2	SIANG RIVER (TUTING)	39.8	4.01	Lang et al., 2013
MODERN ALLUVIUM	S3	SIANG RIVER (KAPU)	374.2	23.05	Lang et al., 2013	MODERN ALLUVIUM	S2	SIANG RIVER (TUTING)	791.7	31.64	Lang et al., 2013
MODERN ALLUVIUM	S3	SIANG RIVER (KAPU)	121.5	15.45	Lang et al., 2013	MODERN ALLUVIUM	S2	SIANG RIVER (TUTING)	63.6	4.03	Lang et al., 2013
MODERN ALLUVIUM	S3	SIANG RIVER (KAPU)	121.0	2.39	Lang et al., 2013	MODERN ALLUVIUM	S2	SIANG RIVER (TUTING)	581.9	6.58	Lang et al., 2013
MODERN ALLUVIUM	S3	SIANG RIVER (KAPU)	74.4	2.53	Lang et al., 2013	MODERN ALLUVIUM	S2	SIANG RIVER (TUTING)	44.9	1.63	Lang et al., 2013
MODERN ALLUVIUM	S3	SIANG RIVER (KAPU)	1171.8	16.63	Lang et al., 2013	MODERN ALLUVIUM	S2	SIANG RIVER (TUTING)	1641.8	12.41	Lang et al., 2013
MODERN ALLUVIUM	S3	SIANG RIVER (KAPU)	46.3	3.29	Lang et al., 2013	MODERN ALLUVIUM	S2	SIANG RIVER (TUTING)	1179.1	33.2	Lang et al., 2013
MODERN ALLUVIUM	S3	SIANG RIVER (KAPU)	2171.4	6.53	Lang et al., 2013	MODERN ALLUVIUM	S2	SIANG RIVER (TUTING)	116.6	5.81	Lang et al., 2013
MODERN ALLUVIUM	S3	SIANG RIVER (KAPU)	321.9	17.07	Lang et al., 2013	MODERN ALLUVIUM	S2	SIANG RIVER (TUTING)	65.7	4.58	Lang et al., 2013
MODERN ALLUVIUM	S3	SIANG RIVER (KAPU)	49.4	3.99	Lang et al., 2013	MODERN ALLUVIUM	S2	SIANG RIVER (TUTING)	116.7	1.26	Lang et al., 2013
MODERN ALLUVIUM	S3	SIANG RIVER (KAPU)	38.0	1.43	Lang et al., 2013	MODERN ALLUVIUM	S2	SIANG RIVER (TUTING)	964.3	12.24	Lang et al., 2013
MODERN ALLUVIUM	S3	SIANG RIVER (KAPU)	1102.4	24	Lang et al., 2013	MODERN ALLUVIUM	S2	SIANG RIVER (TUTING)	473.7	2.76	Lang et al., 2013
MODERN ALLUVIUM	S3	SIANG RIVER (KAPU)	49.1	2.74	Lang et al., 2013	MODERN ALLUVIUM	S2	SIANG RIVER (TUTING)	22.1	5.01	Lang et al., 2013
MODERN ALLUVIUM	S3	SIANG RIVER (KAPU)	1396.7	57.07	Lang et al., 2013	MODERN ALLUVIUM	S2	SIANG RIVER (TUTING)	539.0	6.26	Lang et al., 2013
MODERN ALLUVIUM	S3	SIANG RIVER (KAPU)	1586.8	14.41	Lang et al., 2013	MODERN ALLUVIUM	S2	SIANG RIVER (TUTING)	111.9	2.6	Lang et al., 2013
MODERN ALLUVIUM	S3	SIANG RIVER (KAPU)	52.4	5.09	Lang et al., 2013	MODERN ALLUVIUM	S2	SIANG RIVER (TUTING)	1685.8	4.91	Lang et al., 2013
MODERN ALLUVIUM	S3	SIANG RIVER (KAPU)	473.9	20.28	Lang et al., 2013	MODERN ALLUVIUM	S2	SIANG RIVER (TUTING)	39.0	1.3	Lang et al., 2013
MODERN ALLUVIUM	S3	SIANG RIVER (KAPU)	471.1	2.58	Lang et al., 2013	MODERN ALLUVIUM	S2	SIANG RIVER (TUTING)	1550.8	4.35	Lang et al., 2013
MODERN ALLUVIUM	S3	SIANG RIVER (KAPU)	1148.6	29.02	Lang et al., 2013	MODERN ALLUVIUM	S2	SIANG RIVER (TUTING)	432.6	36.08	Lang et al., 2013
MODERN ALLUVIUM	S3	SIANG RIVER (KAPU)	1169.0	5.12	Lang et al., 2013	MODERN ALLUVIUM	S2	SIANG RIVER (TUTING)	479.0	14.85	Lang et al., 2013
MODERN ALLUVIUM	S3	SIANG RIVER (KAPU)	56.0	2.16	Lang et al., 2013	MODERN ALLUVIUM	S2	SIANG RIVER (TUTING)	39.1	3.13	Lang et al., 2013
MODERN ALLUVIUM	S3	SIANG RIVER (KAPU)	418.8	19.08	Lang et al., 2013	MODERN ALLUVIUM	S2	SIANG RIVER (TUTING)	21.2	5.31	Lang et al., 2013
MODERN ALLUVIUM	S3	SIANG RIVER (KAPU)	57.2	3.43	Lang et al., 2013	MODERN ALLUVIUM	S2	SIANG RIVER (TUTING)	1677.7	92.48	Lang et al., 2013
MODERN ALLUVIUM	S3	SIANG RIVER (KAPU)	61.6	4.12	Lang et al., 2013	MODERN ALLUVIUM	S2	SIANG RIVER (TUTING)	25.0	2.92	Lang et al., 2013
MODERN ALLUVIUM	S3	SIANG RIVER (KAPU)	109.6	3.09	Lang et al., 2013	MODERN ALLUVIUM	S2	SIANG RIVER (TUTING)	1536.2	11.98	Lang et al., 2013
MODERN ALLUVIUM	S3	SIANG RIVER (KAPU)	63.8	4.79	Lang et al., 2013	MODERN ALLUVIUM	S2	SIANG RIVER (TUTING)	312.7	4.84	Lang et al., 2013
MODERN ALLUVIUM	S3	SIANG RIVER (KAPU)	1186.9	13.17	Lang et al., 2013	MODERN ALLUVIUM	S2	SIANG RIVER (TUTING)	775.0	73.91	Lang et al., 2013
MODERN ALLUVIUM	S3	SIANG RIVER (KAPU)	45.8	2.21	Lang et al., 2013	MODERN ALLUVIUM	S2	SIANG RIVER (TUTING)	1066.9	28.05	Lang et al., 2013
MODERN ALLUVIUM	S3	SIANG RIVER (KAPU)	48.6	1	Lang et al., 2013	MODERN ALLUVIUM	S2	SIANG RIVER (TUTING)	1701.8	5.42	Lang et al., 2013
MODERN ALLUVIUM	S3	SIANG RIVER (KAPU)	507.5	10.56	Lang et al., 2013	MODERN ALLUVIUM	S2	SIANG RIVER (TUTING)	275.2	10.77	Lang et al., 2013
MODERN ALLUVIUM	S3	SIANG RIVER (KAPU)	118.7	7.15	Lang et al., 2013	MODERN ALLUVIUM	S2	SIANG RIVER (TUTING)	745.7	30.24	Lang et al., 2013
MODERN ALLUVIUM	S3	SIANG RIVER (KAPU)	1756.2	9.11	Lang et al., 2013	MODERN ALLUVIUM	S2	SIANG RIVER (TUTING)	502.1	16.1	Lang et al., 2013
MODERN ALLUVIUM	S3	SIANG RIVER (KAPU)	1456.3	108.63	Lang et al., 2013	MODERN ALLUVIUM	S2	SIANG RIVER (TUTING)	59.1	1.2	Lang et al., 2013
MODERN ALLUVIUM	S3	SIANG RIVER (KAPU)	44.2	1.34	Lang et al., 2013	MODERN ALLUVIUM	S2	SIANG RIVER (TUTING)	1561.5	24.09	Lang et al., 2013
MODERN ALLUVIUM	S3	SIANG RIVER (KAPU)	65.6	1.9	Lang et al., 2013	MODERN ALLUVIUM	S2	SIANG RIVER (TUTING)	70.8	1.78	Lang et al., 2013

MODERN ALLUVIUM	S2	SIANG RIVER (TUTING)	115.0	1.57	Lang et al., 2013
MODERN ALLUVIUM	S2	SIANG RIVER (TUTING)	24.1	0.7	Lang et al., 2013
MODERN ALLUVIUM	S2	SIANG RIVER (TUTING)	382.2	27.63	Lang et al., 2013
MODERN ALLUVIUM	S2	SIANG RIVER (TUTING)	460.1	6.96	Lang et al., 2013
MODERN ALLUVIUM	S2	SIANG RIVER (TUTING)	742.2	11.63	Lang et al., 2013

2.11 Appendix

2.11.1 Analytical details

For analyses conducted at the University of Arizona LaserChron center:

U, Pb, and Th isotopes were measured simultaneously. Measurement error for $^{206}\text{Pb}/^{238}\text{U}$, $^{206}\text{Pb}/^{204}\text{Pb}$, $^{206}\text{Pb}/^{207}\text{Pb}$ isotopic ratios are typically $\sim 1\text{-}2\%$ (two sigma level) except for youngest grains with low ^{207}Pb signals. ^{204}Hg interference is accounted for by direct ^{202}Hg measurement during each analysis and subtraction of ^{204}Hg according to the natural ratio: $^{202}\text{Hg}/^{204}\text{Hg} = 4.35$. Common Pb correction assumes an initial Pb composition from Stacy and Kramers (1975), with uncertainties of 1.5 for $^{206}\text{Pb}/^{204}\text{Pb}$ and 0.3 for $^{207}\text{Pb}/^{204}\text{Pb}$. Isotopic fractionation is corrected from mid-run analyses of multiple (Sri Lankan and R33 zircon) standards. Analytical data was post-processed using NUPMagecalc and ISOPLOT (Ludwig, 2008) with the following standard age filters:

1. 10% error cutoff for $^{206}\text{Pb}/^{238}\text{U}$ and $^{206}\text{Pb}/^{207}\text{Pb}$ ratios
2. 30% maximum discordance and 5% maximum reverse discordance
3. $^{206}\text{Pb}/^{238}\text{U}$ ages preferred over $^{206}\text{Pb}/^{207}\text{Pb}$ ages under 1000 Ma.
4. 500 cps cutoff for excess ^{204}Pb .

Individual grain analyses were inspected to determine the preferred age, occasionally allowing slightly larger $^{206}\text{Pb}/^{238}\text{U}$ error for young ages and higher ^{204}Pb for grains with very high U concentrations (not to exceed 1000 cps).

For analyses conducted by Apatite to Zircon, Inc.:

During analytical scans, the fractionation of individual isotopes was modeled by twice fitting a sum of 10 Gaussian equations to the raw signal data, before and after

outlier elimination. Common Pb correction similarly assumes an initial Pb composition from Stacy and Kramers (1975). Isotopic fractionation is corrected from prior and mid-run analyses of multiple (Duluth Anorthosite, Fish Canyon Tuff, Tardee, Tioga Bed, Mount Dromedary, Temora, Nancy, Mud Tank Carbonatite) standards, this includes correction over multiple scans and for alpha-ejection damage (Donelick et al. 2010). Only concordant analytical scans (defined as overlapping $^{206}\text{Pb}/^{207}\text{Pb}$, $^{206}\text{Pb}/^{238}\text{U}$, $^{207}\text{Pb}/^{235}\text{U}$ ages within two sigma) were selected to calculate grain ages. The preferred age was selected based on minimizing the relative error of each age. Several analyses within sample 75b contained multiple analyses per pit (denoted with an 'a' or 'b' in the Grain ID). A simple weighted mean age was calculated for these grains.

Additional references:

Donelick, R.A., O'Sullivan, P.B., and Donelick, M.B., 2010, A Discordia-Based Method of Zircon U-Pb Dating from LA-ICP-MS Analysis of Single Spots. *Smart Science for Exploration and Mining*, v. 1 and 2, p. 276-278.

Ludwig, K., 2008, *Isoplot 3.6: Berkeley Geochronology Center Special Publication 4*, 77 p.

Stacey, J.S., and Kramers, J.D., 1975, Approximation of terrestrial lead isotope evolution by a two stage model: *Earth and Planetary Science Letters*, v. 26, p. 207-221.

CHAPTER 3. Erosion of the Tsangpo Gorge by megafloods, eastern Himalaya

Coauthor: Katharine W. Huntington

3.0 Abstract

At the southeastern margin of the Tibetan Plateau, the Yarlung-Tsangpo River plunges through the Himalaya to drop >2 km through the Tsangpo Gorge. Upstream, relict glacial dams and impounded lake terraces suggest that Quaternary lakes as large as 800 km³ catastrophically drained through the gorge as megafloods. We report on new megaflood deposits downstream of the gorge and use detrital zircon U-Pb provenance data to demonstrate that these high-magnitude events originated in Tibet, and more effectively focused erosion in the gorge than both the extremely erosive modern peak flows and one of the largest landslide-dam outburst floods ever documented. Our findings support the proposition that in this steep, narrow gorge, where hillslope angles are near the threshold angle of bedrock failure, megafloods provide a mechanism to rapidly evacuate hillslope material and focus erosion on channel adjacent hillslopes. Although megaflood frequency remains unconstrained, we demonstrate the capability of these events to contribute substantially to rapid exhumation in this region.

3.1 Introduction

Where the Yarlung-Tsangpo River (southeastern Tibetan Plateau) descends through the easternmost Himalaya, it carves the Tsangpo Gorge, a <200-m-wide, 200-km-long bedrock knickzone descending more than 2 km between two peaks with elevations >7 km (Figure 1A). Within the gorge, high stream power and high topographic

relief (Finnegan et al., 2008) drive contemporary erosion rates of >5 mm/yr (Larsen and Montgomery, 2012) and possibly as high as 10 mm/yr (Stewart et al., 2008) (Figure 1C). On a longer time scale, focused erosion has exhumed the Namche Barwa massif, an active crustal-scale antiform (Burg and Podladchikov, 1999), at an average rate of 3–5 km/m.y. since 5–10 Ma (Booth et al., 2004, 2009), and at a rate as high as 10 km/m.y. since 3–5 Ma (Burg et al., 1998; Seward and Burg, 2008; Enkelmann et al., 2011). This co-occurrence of focused surface erosion and active rock uplift led previous researchers to hypothesize a self-sustaining relationship between the two, localized to the gorge region since at least 3–5 Ma (Zeitler et al., 2001).

During the Quaternary (after 2.6 Ma), glacial ice and debris from Tibetan tributaries impounded massive lakes on the Yarlung-Tsangpo River in the immediate headwaters of the Tsangpo Gorge, with volumes estimated to be as much as ~ 800 km³ (Montgomery et al., 2004; Korup and Montgomery, 2008). Glacial ice and debris dams of main stem valleys by tributary glaciers often fail by overtopping or ice-marginal breaching, producing some of the largest freshwater floods on Earth (O'Connor et al., 2013). These megafloods may generate extreme discharges of water ($>10^6$ m³ s⁻¹) capable of focused downstream erosion (O'Connor et al., 2013) and sparse slackwater deposition in hydraulically sheltered areas (Atwater, 1984). Glacial moraines crosscut by the river at the entrance to the Tsangpo Gorge, and immediately downstream of multiple lake terrace levels extending throughout the upstream drainage network (Montgomery et al., 2004; Chen et al., 2008), provide evidence for lake impoundment and the possibility that megaflooding recurred. Here we present new evidence that megaflooding through the Tsangpo Gorge preferentially eroded the Namche Barwa massif where it is exposed in

the gorge.

3.2 Methods

3.2.1 Sampling

All samples collected for the new analyses included in this work were collected as random “grab” samples from active channel bars and banks or freshly exposed faces of flood deposits. Modern sediment samples were collected during low-flow periods in 2004, 2005, 2008, and 2011. When sampling active channel bedload, care was taken to avoid contamination from 2000 flood overbank deposits or recent landslides.

3.2.2 U-Pb and petrographic analyses

Samples were wet sieved into multiple size fractions. Standard magnetic and density separations were used to isolate dense minerals from the 63-250 μm size fraction; the remaining light mineral fraction was mounted on petrographic slides, etched and stained to distinguish feldspars. Over 300 grains were manually counted on polished grain mounts using the line traverse method following the Gazzi-Dickinson classification scheme with an Olympus BX50 polarizing microscope. Zircons were further separated to near 100% purity, and poured onto grain mounts, polished and imaged by high resolution backscattered electron and cathodoluminescence imaging on an Hitachi 3400N SEM at the University of Arizona. Zircons cores were randomly analyzed for U-Th-Pb by laser-ablation multi-collector inductively coupled mass spectrometry (LA-MC-ICPMS) using a 30 μm spot diameter at the Arizona LaserChron Center (Gehrels, 2011).

3.2.3 Synthetic CDF mixture modeling

We iteratively compared modeled cumulative probability density functions of zircon U-Pb crystallization ages <1000 Ma (older ages in this region are not diagnostic of a specific source area) to the observed sample CDFs for all combinations of four upstream sources (numbers correspond to numbered locations in Figure 1B): 1. Yarlung Tsangpo river at Pai; 2. the Layue Qu tributary; a mean CDF from two statistically indistinguishable grain-age populations from the Yigong (3.) and Parlung (4.) tributaries; and 5. a small tributary draining the western flank of the Namche Barwa Massif (proxy for the Tsangpo Gorge). Best fit synthetic CDFs were determined using two fit metrics, both reported in Figure 3B. The first uses a two sample Kolmogorov-Smirnov test, the second is the total absolute difference between the model and observation. Importantly, this modeling approach assumes an efficient fluvial system with little sediment storage in the Tsangpo Gorge itself, an assumption that is consistent with our observations and those of Stewart et al. (2008) and Finnegan et al. (2008). Furthermore this approach assumes there is no significant variability in source rock zircon concentration. Several datasets indicate this assumption is reasonable; as noted by Stewart et al. (2008) and Booth et al. (2004), zirconium concentration is broadly uniform across the region, and Garzanti et al. (2004), as well as our own observations of estimated zircon percentage by weight, confirm that there is no significant variation in zircon concentration in detrital sediments sampled from this region.

3.2.4 Estimating bed shear stress during peak discharges

To quantify the amount of erosion across the spectrum of discharges presented in this paper, we modeled the bed shear stress as a function of flow depth and hillslope angle for a trapezoidal river valley. Then, using estimated values of peak discharge for annual flows, the 2000 flood event and two megaflood magnitudes, we solved for the bed shear stress in a simple trapezoidal valley and the intermediate axis length of a median block size that could just be moved by that flow. See appendix for specific discharge and variable values used in calculations.

Our calculations followed the approach of Lamb and Fonstad (2010) where

$$Q = 8.1A \left(\frac{\tau_b}{\rho} \right)^{\frac{1}{2}} \left(\frac{h}{k_s} \right)^{\frac{1}{6}} \quad (1)$$

h is the flow depth and A is the cross sectional area of the flow, which we modeled as a trapezoidal valley

$$A = \left(\frac{h^2}{\tan \phi} \right) + wh \quad (2)$$

w is the flat bottom width. Bed shear stress τ_b is

$$\tau_b = \rho g h_r S \quad (3)$$

h_r is the hydraulic radius, closely approximated by mean depth \bar{h}

$$h_r = \frac{A \sin \phi}{2h + w} \cong \bar{h} \quad (4)$$

Using τ_b we solve for the intermediate axis length of a median block size \bar{D}_2 using the relation

$$\tau_{*c} = 0.15S^{0.25} \quad (5)$$

for the critical stress for incipient motion from Lamb et al. (2008) and citations therein

$$\bar{D}_2 = \frac{\tau_b}{\tau_{*c} g (\rho_s - \rho)} \quad (6)$$

for the bed shear stress for suspension

$$\tau_b = \rho(0.8w_s)^2 \quad (5)$$

using the settling velocity w_s approximated from Ferguson and Church (2004)

$$w_s = \frac{RgD^2}{C_1v+(0.75C_2RgD^3)^{0.5}} \quad (8)$$

where

$$R = \frac{\rho_s - \rho}{\rho} \quad (9)$$

3.3 Discussion

3.3.1 Slackwater deposits

We identified slackwater deposits in hydraulically sheltered areas along the main stem of the Yarlung Tsangpo (locally named Siang) River and at local tributary mouths downstream of the Tsangpo Gorge at elevations as much as 150 m above the modern channel. These deposits drape existing topography, in many cases unconformably overlying bedrock or unworked landslide deposits. Four identified deposits, as much as 30 m above the modern channel, originated from an A.D. 2000 flood (Evans and Delaney, 2011) resulting from the temporary impoundment of the Yigong River by a massive landslide 40 km upstream of the Tsangpo Gorge (Figure 1B). The 2000 flood deposits are generally very fine to medium-grained sand with millimeter-scale coarse-grained laminations and occasional scour features within fining-upward and massive sequences, indicating deposition from suspension. The deposits are tabular and laterally extensive, with vegetated surfaces occasionally capped by landslide debris. Four additional deposits span higher elevations as much as 120 m above the 2000 flood deposits; these higher deposits are also very fine to medium sands, with occasional scour features and isolated

pebbles. Unlike the 2000 flood deposits, the higher deposits show moderate soil development and destruction of primary depositional features by bioturbation; they are commonly overlain by poorly sorted, angular to subangular landslide deposits. Based on their similarity to the 2000 flood deposits, we interpret these older, higher deposits to have originated from megaflood events. In contrast to the megaflood deposits, alluvial terraces in the valley are characterized by discontinuous lenses of coarser grained sand that exhibit fluvial bedforms (e.g., cross-bedding) and are overlain by subrounded, imbricated gravel consistent with fluvial bedload transport.

Petrographic and detrital zircon U-Pb data indicate that the 2000 flood and megaflood sediments reflect a mixed Tibetan and Himalayan provenance (Figure 2), indicating that these floods originated in Tibet and entrained some amount of Himalayan input prior to deposition. In this region, detrital zircon U-Pb crystallization ages younger than 1000 Ma are characteristic of two primary sources: Tibetan zircons are younger than 300 Ma (Cina et al., 2009; Zhang et al., 2012), whereas Himalayan zircons are typically older than 300 Ma with a peak probability density ca. 500 Ma (Stewart et al., 2008; Cina et al., 2009; Amidon et al., 2005), except anatectic zircons younger than 30 Ma observed only in the Namche Barwa massif (Booth et al., 2009). These anatectic zircons are further distinguishable by high U/Th ratios of >10 (Booth et al., 2004; Zhang et al., 2012; see Hoskin and Schaltegger, 2003, for discussion; Figure 2). The U-Pb ages from Yarlung-Tsangpo River sediment upstream from the Tsangpo Gorge are dominantly Tibetan, and because zircon is an effective sediment tracer in this system (Stewart et al., 2008; Enkelmann et al., 2011), the downstream change in detrital Himalayan zircons is a proxy for the contribution of sediment flux originating within the gorge (Stewart et al., 2008)

(Figure 2A).

3.3.2 Tsangpo Gorge erosion

To constrain the contribution of sediment flux originating within the Tsangpo Gorge from each of three different events (the 2000 flood event, megaflood events, and the modern river discharge), we fit cumulative probability density functions (CDFs) from observed U-Pb ages to modeled CDFs representing variable contributions from upstream source areas and the Tsangpo Gorge (Figure 3A). Our modeling confirms previous work (Stewart et al., 2008; Singh and France-Lanord, 2002; Garzanti et al., 2004) showing that the Tsangpo Gorge is the source of ~40%–50% of zircons in modern river sediment downstream, an impressive contribution from just ~2% of the Yarlung-Tsangpo drainage area (Figure 3B).

The best-fit models of the A.D. 2000 flood deposits require a smaller contribution of sediment from the Tsangpo Gorge and a large contribution specifically from the Yigong River, where the 2000 flood was sourced. This difference in provenance suggests that preferential erosion immediately downstream of the Yigong landslide dam and along the path to the Tsangpo Gorge diluted the gorge sediment contribution typical of modern river discharge. This interpretation is consistent with accounts of extreme erosion downstream of the breached dam by channel incision and landsliding (Evans and Delaney, 2011).

While megaflood samples contain both Tibetan and Himalayan age components, they are significantly enriched in both ca. 500 Ma Himalayan zircons and anatectic zircons younger than 30 Ma relative to modern river samples. Our modeling indicates

that this enrichment is best explained by a nearly twofold increase in the contribution of zircons from the Namche Barwa massif rocks exposed in the Tsangpo Gorge. We interpret this increase to indicate preferential erosion of the gorge during megafloods that originated in Tibet, possibly by processes similar to those observed after the 2000 flood.

3.3.3 The role of megafloods

Larsen and Montgomery (2012) observed that the A.D. 2000 flood triggered landsliding along the channel immediately downstream of the failed dam, by eroding the base of channel adjacent hillslopes. Hillslope angles within the Tsangpo Gorge region are high (mode angles of 37° – 39°) and decoupled from long-term (>105 yr) averaged erosion rates, suggesting that hillslope in this region are persistently near the threshold of slope failure (Larsen and Montgomery, 2012). In such a region characterized by threshold angle hillslopes, we expect large floods to act as an efficient mechanism to contemporaneously trigger landsliding and transport fine-grained soil and landslide debris downstream.

The combined influence of steep hillslopes and narrow river valleys maximizes flood depth and therefore bed shear stress. Calculations of bed shear stress for valley widths and hillslope angles similar to those observed in the Tsangpo Gorge indicate that peak megaflood discharges on the order of $10^6 \text{ m}^3 \text{ s}^{-1}$ (Montgomery et al., 2004) are capable of moving landslide debris up to ~ 8 – 18 m in diameter (Figure 4), and fully suspending 1 m blocks (for calculation details, see the appendix). Given long-term exhumation rates of 5 – 10 km/m.y., a single event capable of removing this much material would be equivalent to ~ 1 – 4 k.y. worth of erosion.

Our results demonstrate the capability of Quaternary megafloods to preferentially erode the Tsangpo Gorge. While the number and recurrence intervals of such events are currently unknown, their impressive erosive potential raises the possibility that megafloods contributed substantially to the long-term exhumation of the gorge.

3.4 Acknowledgements

We acknowledge funding from the Quaternary Research Center at the University of Washington, National Science Foundation (NSF) grant EAR-0955309 to Huntington, and NSF grant EAR-1032156 to the Arizona LaserChron Center. We thank I. Larsen, N. Finnegan, and A. Henck for sharing samples; K. Sumner, K. Atakturk, N. Giesler, and M. Pecha for laboratory assistance; M. Turzewski for field assistance; and Oken Tayeng for logistical assistance in the field. The manuscript benefited from careful reviews by M. Lamb, E. Garzanti, and an anonymous reviewer.

3.5 References

- Amidon, W., Burbank, D.W., and Gehrels, G.E., 2005, U-Pb zircon ages as a sediment mixing tracer in the Nepal Himalaya: *Earth and Planetary Science Letters*, v. 235, p. 244–260, doi:10.1016/j.epsl.2005.03.019.
- Atwater, B.F., 1984, Periodic floods from glacial Lake Missoula into the Sanpoil arm of glacial Lake Columbia, northeastern Washington: *Geology*, v. 12, p. 464–467, doi:10.1130/0091-7613(1984)12<464:PFFGLM>2.0.CO;2.
- Booth, A.L., Zeitler, P.K., Kidd, W.S.F., Wooden, J., Liu, Y., Idleman, B., Hren, M., and Chamberlain, C.P., 2004, U-Pb zircon constraints on the tectonic evolution of

- southeastern Tibet, Namche Barwa Area: *American Journal of Science*, v. 304, p. 889–929, doi:10.2475/ajs.304.10.889.
- Booth, A.L., Chamberlain, C.P., Kidd, W.S.F., and Zeitler, P.K., 2009, Constraints on the metamorphic evolution of the eastern Himalayan syntaxis from geochronologic and petrologic studies of Namche Barwa: *Geological Society of America Bulletin*, v. 121, p. 385–407, doi:10.1130/B26041.1.
- Burg, J.P., and Podladchikov, Y., 1999, Lithospheric scale folding: Numerical modeling and application to the Himalayan syntaxes: *International Journal of Earth Sciences*, v. 88, p. 190–200, doi:10.1007/s005310050259.
- Burg, J.P., Nievergelt, P., Oberli, F., Seward, D., Davy, P., Maurin, J.-C., Diao, Z., and Meier, M., 1998, The Namche Barwa syntaxis: Evidence for exhumation related to compressional crustal folding: *Journal of Asian Earth Sciences*, v. 16, p. 239–252, doi:10.1016/S0743-9547(98)00002-6.
- Chen, Y., Huang, S., Lin, Y., Liu, J., Chung, L., Lai, K., Zhao, S., Yin, G., and Cao, Z., 2008, Holocene megafloods? Stories of the lacustrine strata along the Nyang River, Tibet: *American Geophysical Union Fall Meeting 2008*, abs. PP21A-1404.
- Cina, S.E., Yin, A., Grove, M., Dubey, C.S., Shukla, D.P., Lovera, O.M., Kelty, T.K., Gehrels, G.E., and Foster, D.A., 2009, Gangdese arc detritus within the eastern Himalayan Neogene foreland basin: Implications for the Neogene evolution of the Yalu-Brahmaputra River system: *Earth and Planetary Science Letters*, v. 285, p. 150–162, doi:10.1016/j.epsl.2009.06.005.
- Enkelmann, E., Ehlers, T.A., Zeitler, P.K., and Hallet, B., 2011, Denudation of the Namche Barwa antiform, eastern Himalaya: *Earth and Planetary Science Letters*,

- v. 307, p. 323–333, doi:10.1016/j.epsl.2011.05.004.
- Evans, S., and Delaney, K., 2011, Characterization of the 2000 Yigong Zangbo River (Tibet) landslide dam and impoundment by remote sensing, *in* Evans, S.G., et al., eds., *Natural and artificial rockslide dams*: Berlin, Springer-Verlag, p. 543–559.
- Finnegan, N.J., Hallet, B., Montgomery, D.R., Zeitler, P.K., Stone, J.O., Anders, A.M., and Liu, Y., 2008, Coupling of rock uplift and river incision in the Namche-Barwa-Gyala Peri massif, Tibet: *Geological Society of America Bulletin*, v. 120, p. 142–155, doi:10.1130/B26224.1.
- Garzanti, E., Vezzoli, G., Andò, S., France-Lanord, C., Singh, S.K., and Foster, G., 2004, Sand petrology and focused erosion in collision orogens: The Brahmaputra case: *Earth and Planetary Science Letters*, v. 220, p. 157–174, doi:10.1016/S0012-821X(04)00035-4.
- Hoskin, P., and Schaltegger, U., 2003, The composition of zircon and igneous and metamorphic petrogenesis: *Reviews of Mineralogy and Geochemistry*, v. 53, p. 27–62, doi:10.2113/0530027.
- Korup, O., and Montgomery, D.R., 2008, Tibetan plateau river incision inhibited by glacial stabilization of the Tsangpo gorge: *Nature*, v. 455, p. 786–789, doi:10.1038/nature07322.
- Larsen, I.J., and Montgomery, D.R., 2012, Landslide erosion coupled to tectonics and river incision: *Nature*, v. 5, p. 468–473.
- Montgomery, D.R., Hallet, B., Yuping, L., Finnegan, N., Anders, A., Gillespie, A., and Greenberg, H.M., 2004, Evidence for Holocene megafloods down the Tsangpo River gorge, southeastern Tibet: *Quaternary Research*, v. 62, p. 201–207, doi:10.1016/j.yqres.2004.06.008.

- O'Connor, J., Clague, J.J., Walder, J.S., Manville, V., and Beebee, R.A., 2013, Outburst floods, *in* Shroder, J., ed., *Treatise on geomorphology*: San Diego, California, Academic Press, p. 475–510.
- Seward, D., and Burg, J., 2008, Growth of the Namche Barwa Syntaxis and associated evolution of the Tsangpo Gorge: Constraints from structural and thermochronological data: *Tectonophysics*, v. 451, p. 282–289, doi:10.1016/j.tecto.2007.11.057.
- Singh, S., and France-Lanord, C., 2002, Tracing the distribution of erosion in the Brahmaputra water shed from isotopic compositions of stream sediments: *Earth and Planetary Science Letters*, v. 202, p. 645–662, doi:10.1016/S0012-821X(02)00822-1.
- Stewart, R., Hallet, B., Zeitler, P.K., Malloy, M.A., Allen, C.M., and Trippett, D., 2008, Brahmaputra sediment flux dominated by highly localized rapid erosion from the easternmost Himalaya: *Geology*, v. 36, p. 711–714, doi:10.1130/G24890A.1.
- Zeitler, P.K., Meltzer, A.S., Koons, P.O., Craw, C., Hallet, B., Chamberlain, C.P., Kidd, W.S.F., Park, S.K., Seeber, L., Bishop, M., and Shroder, J., 2001, Erosion, Himalayan geodynamics, and the geomorphology of metamorphism: *GSA Today*, v. 11, p. 4–9, doi:10.1130/1052-5173(2001)011<0004:EHGATG>2.0.CO;2.
- Zhang, J.Y., Yin, A., Liu, W.C., Wu, F.Y., Lin, D., and Grove, M., 2012, Coupled U-Pb dating and Hf isotopic analysis of detrital zircon of modern river sand from the Yalu River (Yarlung Tsangpo) drainage system in southern Tibet: Constraints on the transport processes and evolution of Himalayan rivers: *Geological Society of America Bulletin*, v. 124, p. 1449–1473, doi:10.1130/B30592.1.

3.6 Figures

Figure 3.6.1 Location map and river profile

A: Location of Yarlung-Tsangpo River (Tibetan Plateau). Where the river turns southward and plunges from the Tibetan Plateau through the Tsangpo Gorge, it begins to erode Himalayan source rocks of the Namche Barwa massif (NB) (Booth et al., 2009; Zhang et al., 2012). B: Relict glacial dams upstream of Tsangpo Gorge record impoundment of massive Quaternary lakes (Montgomery et al., 2004; Chen et al., 2008; Korup and Montgomery, 2008), which catastrophically drained through the gorge. An A.D. 2000 landslide impounded the Yigong River, a tributary to the gorge; failure of the landslide dam released an analogous smaller-magnitude flood through the gorge. C: We sampled megaflood and 2000 flood slackwater deposits downstream of the gorge (adapted from Montgomery et al., 2004; Finnegan et al., 2008; Larsen and Montgomery, 2012), and modern river sediment samples (locations 3, 5–8) throughout the watershed where previously published data (locations 1, 2, 4, 12 from Stewart et al., 2008; Cina et al., 2009; Zhang et al., 2012) did not exist. Sample 5 is from a small cirque draining the western Namche Barwa massif; a.s.l.—above sea level.

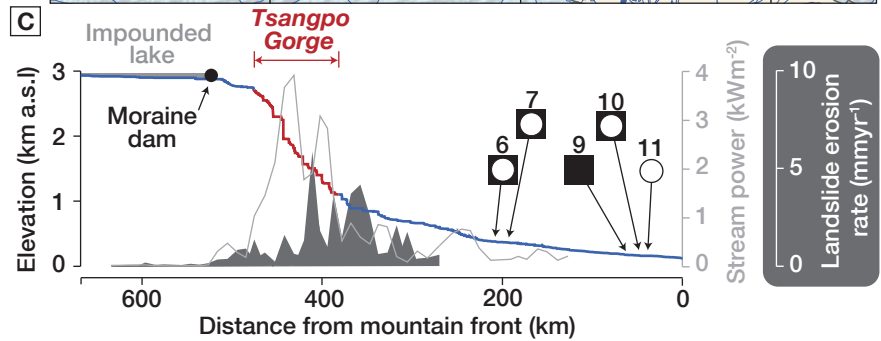
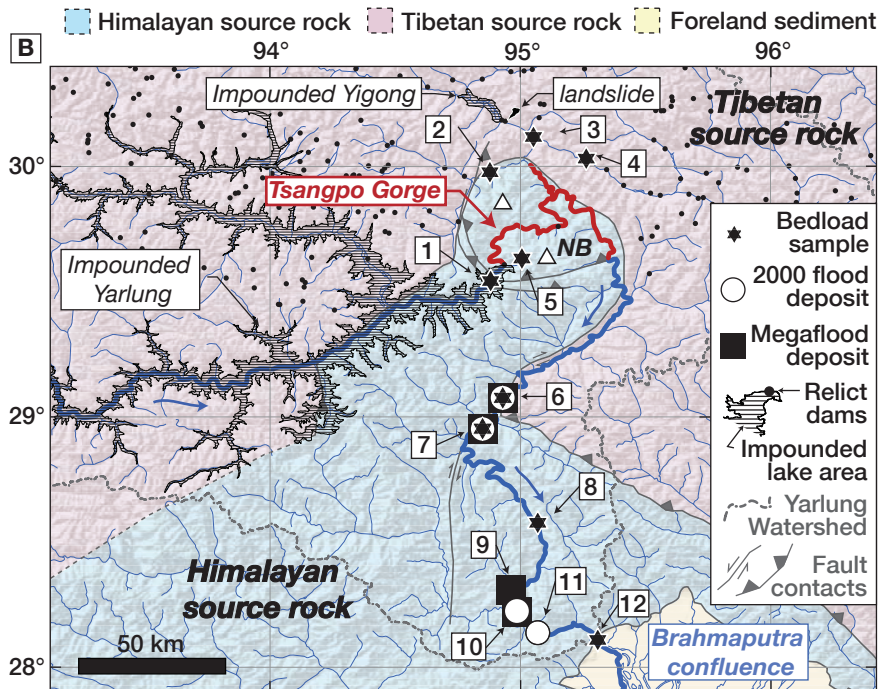
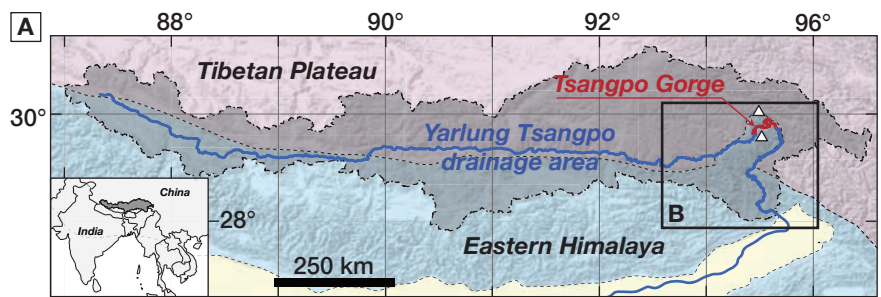


Figure 3.6.2 Detrital analyses

A: Detrital zircon U-Pb crystallization age probability density functions (black lines) and kernel density estimates (gray) characterize two primary sources: Tibetan zircons are younger than 250 Ma, shown in the Tibetan tributaries flowing into Tsangpo Gorge (compiled from this study and Zhang et al., 2012); and gorge-derived Himalayan zircons are typically ca. 500 Ma, with small component of <30 Ma anatectic grains from the western side of Namche Barwa massif (Booth et al., 2004), shown in both a detrital sample from a small west-draining cirque and compiled bedrock ages from Namche Barwa massif (gray histogram from Booth et al., 2004; Zhang et al., 2012; $n = 325$). Inset bar shows proportion of young (<30 Ma) anatectic zircons sourced only from Namche Barwa (black) with U/Th of >10, and young igneous zircons (white) with U/Th of <10. Himalayan-age zircons in modern sediment downstream of Tsangpo Gorge (compiled from this study; Stewart et al., 2008; Cina et al., 2009) demonstrate the addition of zircons eroded from the gorge, including a few young anatectic grains. A.D. 2000 flood deposits show a similar proportion of gorge derived zircons, with slightly fewer anatectic grains. Megaflood deposits contain a much higher proportion of Himalayan zircons and anatectic grains sourced only from Namche Barwa, indicating extreme focusing of erosion in the gorge by megafloods. Sample numbers refer to locations in Figure 1. B: Petrographic analyses of flood sediments rule out local sources for the deposits and confirm a mixed provenance between Himalayan and Tibetan sources (Himalayan and Tibetan source data from Zhang et al., 2012; Garzanti et al., 2004). Q—quartz; F—feldspar; L—lithics.

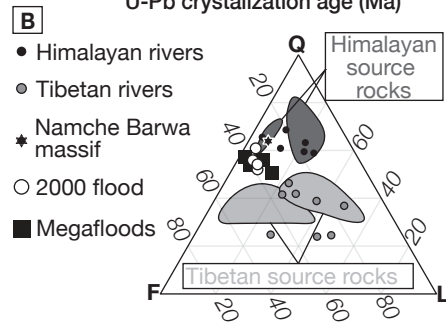
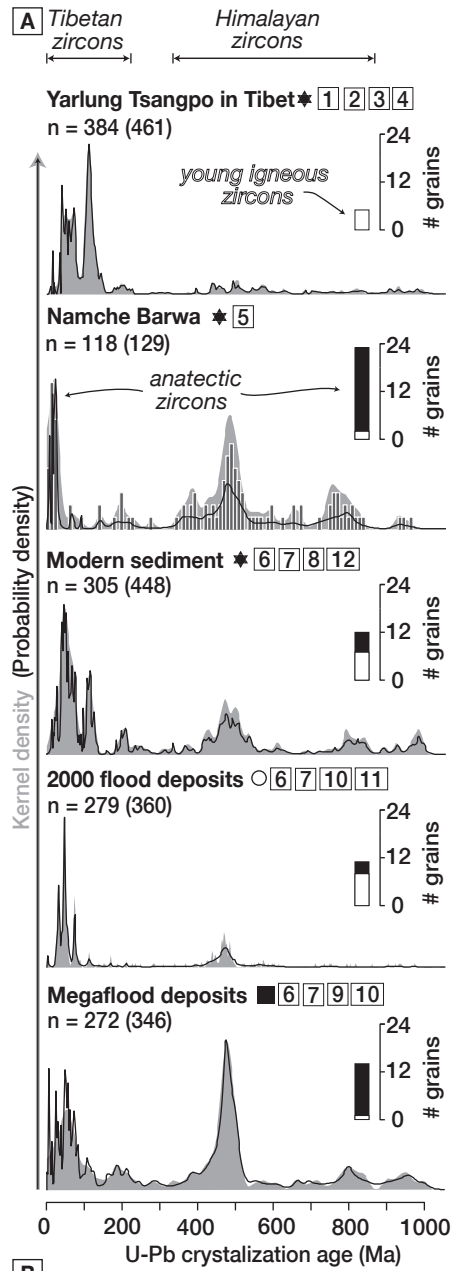


Figure 3.6.3 Mixture modeling

A: Cumulative probability density functions (CDFs) for mixtures of four source-area samples and fit of modeled CDF to observed CDFs of modern river sediment samples, an A.D. 2000 flood, and megaflood deposits. Sample numbers refer to locations in Figure 1. Models were fit using both the two-sample Kolmogorov-Smirnov (KS) test and the total difference (diff.) between the modeled and observed CDF. B: Best fit model results are insensitive to fit calculation, demonstrating a twofold increase in the contribution from the Tsangpo Gorge to megaflood deposits, relative to modern sediment. Modeling also demonstrates a significant contribution to the A.D. 2000 flood deposits from their source area in the Yigong River.

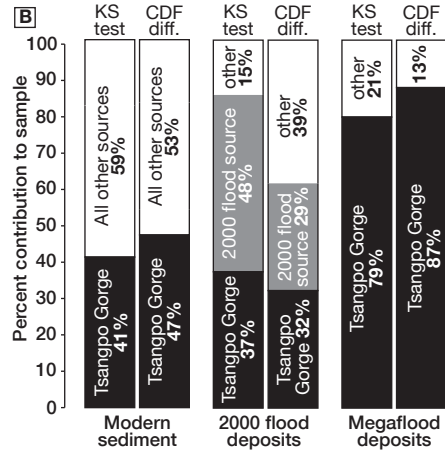
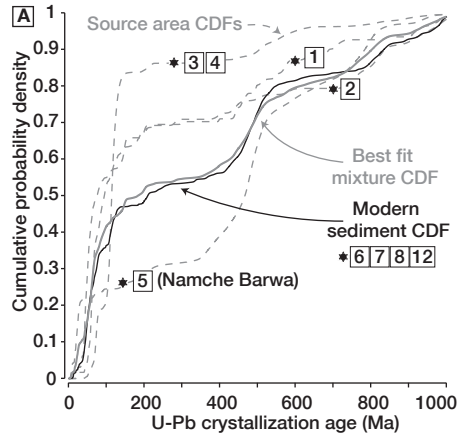
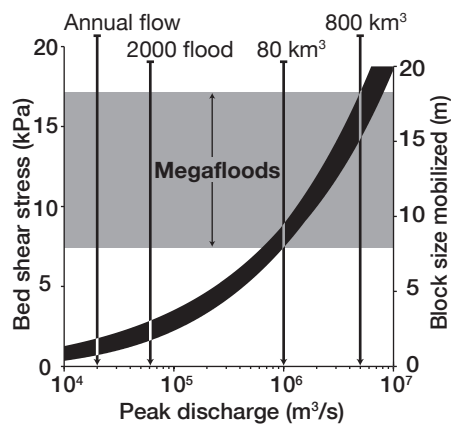


Figure 3.6.4. Shear stress calculations

Calculation of bed shear stress and maximum intermediate axis diameter (block size) of mobilized blocks as a function of peak discharge through a 200-m-wide gorge. Narrow range of solutions (thickness of black line) shows that this relationship is insensitive to hillslope angle and valley width for values similar to those observed.



3.7 Tables

3.7.1 Detrital zircon U-Pb data

TABLE DR1. NEW U-PB CRYSTALLIZATION AGES (2000 flood @ 7)

Grain	U (ppm)	206Pb 204Pb	U/Th	Isotope ratios							error corr.	Apparent ages (Ma)						Best age (Ma)	± (Ma)	Conc (Ma)	
				206Pb*	±	207Pb*	±	206Pb*	±	207Pb*		±	206Pb*	±	207Pb*	±	206Pb*				±
				207Pb*	(%)	235U*	(%)	238U	(%)	238U*		(Ma)	235U	(Ma)	207Pb*	(Ma)	207Pb*				(Ma)
08KH05-1	443	1656	38.7	11.1403	83.6	0.0143	89.4	0.0012	31.5	0.35	7.4	2.3	14.4	12.8	1420.5	2117.7	7.4	2.3	NA		
08KH05-2	108	42145	2	9.6009	1.4	4.3482	2.6	0.3028	2.3	0.86	1705	33.9	1702.5	21.8	1699.5	25.1	1699.5	25.1	100.3		
08KH05-3	776	16045	1.7	23.1694	10.6	0.0385	10.9	0.0065	2.4	0.22	41.5	1	38.3	4.1	-158.3	264.9	41.5	1	NA		
08KH05-4	656	21379	0.4	20.7173	7.4	0.0767	7.6	0.0115	1.8	0.23	73.8	1.3	75	5.5	112.5	175.2	73.8	1.3	NA		
08KH05-5	866	17768	0.7	21.2172	5.6	0.0759	5.7	0.0117	1	0.18	74.9	0.8	74.3	4.1	55.9	134.4	74.9	0.8	NA		
08KH05-6	1530	3255	5.4	16.9103	33.6	0.0056	35.7	0.0007	11.9	0.33	4.4	0.5	5.6	2	572.1	751.9	4.4	0.5	NA		
08KH05-8	82	59812	2.3	13.7195	2.4	1.6951	3.1	0.1687	2	0.64	1004.8	18.5	1006.7	19.7	1010.8	48	1010.8	48	99.4		
08KH05-9	423	150692	2.3	13.8718	0.6	1.5023	2.8	0.1511	2.7	0.97	907.4	22.8	931.3	16.9	988.5	12.7	907.4	22.8	91.8		
08KH05-10	1980	12176	9.9	12.3808	1	0.7081	3.9	0.0636	3.8	0.97	397.4	14.7	543.6	16.5	1215.9	18.8	397.4	14.7	NA		
08KH05-11	1101	28471	4.1	21.2315	5.1	0.0564	6.7	0.0087	4.3	0.65	55.7	2.4	55.7	3.6	54.3	121.7	55.7	2.4	NA		
08KH05-12	166	102938	1.5	11.719	0.9	2.6174	1.9	0.2225	1.6	0.88	1294.9	19.2	1305.5	13.7	1323.1	17.5	1323.1	17.5	97.9		
08KH05-13	3119	110665	2.3	21.3342	1.5	0.0542	2.9	0.0084	2.4	0.86	53.8	1.3	53.6	1.5	42.8	35.5	53.8	1.3	NA		
08KH05-14	672	362024	5.4	14.1851	1.2	1.2947	6.4	0.1332	6.3	0.98	806.1	47.8	843.4	36.8	942.8	24.1	806.1	47.8	85.5		
08KH05-15	601	7407	0.7	22.4142	19	0.0302	19.2	0.0049	3	0.15	31.6	0.9	30.2	5.7	-76.6	467.2	31.6	0.9	NA		
08KH05-16	245	8873	0.8	22.8003	8.7	0.1089	9.5	0.018	4	0.42	115.1	4.5	105	9.5	-118.6	213.9	115.1	4.5	NA		
08KH05-18	135	43002	4	15.3315	3.2	1.0883	3.8	0.121	2	0.54	736.4	14.1	747.7	20	781.6	67.1	736.4	14.1	94.2		
08KH05-19	570	56904	2	11.9423	1	2.3251	2	0.2014	1.7	0.87	1182.7	18.6	1220	14	1286.4	18.9	1286.4	18.9	91.9		
08KH05-20	1191	243003	1.9	17.4289	0.6	0.5544	2.6	0.0701	2.5	0.97	436.6	10.5	447.9	9.3	506	13.7	436.6	10.5	86.3		
08KH05-21	836	135217	1.7	17.4328	0.9	0.6127	4.6	0.0775	4.5	0.98	481	20.7	485.3	17.6	505.5	20.1	481	20.7	95.1		
08KH05-22	86	3776	0.6	12.5372	9.2	1.9824	15	0.1803	11.8	0.79	1068.4	116.6	1109.6	101.5	1191.1	181.7	1191.1	181.7	89.7		
08KH05-23	79	4605	0.6	22.6507	40.6	0.073	41.2	0.012	6.9	0.17	76.8	5.3	71.5	28.5	-102.4	1035.7	76.8	5.3	NA		
08KH05-24	77	54384	0.9	12.3121	2.1	2.3569	2.9	0.2105	1.9	0.66	1231.3	21.1	1229.6	20.3	1226.8	42.1	1226.8	42.1	100.4		
08KH05-25	577	224149	2.8	7.6177	0.2	6.269	4.3	0.3464	4.3	1	1917.2	71.6	2014.1	37.9	2115.1	2.8	2115.1	2.8	90.6		
08KH05-26	238	52656	2	17.3025	4.7	0.5027	5.1	0.0631	2	0.39	394.4	7.8	413.5	17.5	522	103.9	394.4	7.8	NA		
08KH05-27	407	376442	201.6	12.5162	0.5	2.2635	1.2	0.2055	1	0.89	1204.6	11.4	1201	8.2	1194.5	10.5	1194.5	10.5	100.9		

TABLE DR1. NEW U-PB CRYSTALLIZATION AGES (2000 flood @ 7)

Grain	U (ppm)	206Pb 204Pb	U/Th	Isotope ratios							error corr.	Apparent ages (Ma)						Best age (Ma)	± (Ma)	Conc (Ma)	
				206Pb*	±	207Pb*	±	206Pb*	±	207Pb*		±	206Pb*	±	207Pb*	±	206Pb*				±
				235U*	(%)	238U	(%)	238U*	(Ma)	235U		(Ma)	207Pb*	(Ma)							
08KH05-28	1117	35599	1.4	21.4001	1.8	0.0747	3.4	0.0116	2.9	0.84	74.3	2.1	73.1	2.4	35.4	43.7	74.3	2.1	NA		
08KH05-29	250	253560	1.5	6.1156	0.2	10.4513	1.7	0.4636	1.7	0.99	2455.3	34.2	2475.6	15.7	2492.3	3.7	2492.3	3.7	98.5		
08KH05-30	310	12376	1.2	21.7715	13.1	0.1094	13.6	0.0173	3.4	0.25	110.4	3.8	105.4	13.6	-6	318.1	110.4	3.8	NA		
08KH05-31	137	123859	1.8	10.1853	0.8	3.8165	2.8	0.2819	2.6	0.96	1601.1	37.5	1596.2	22.3	1589.8	15.2	1589.8	15.2	100.7		
08KH05-33	5008	67545	0.6	20.6338	0.8	0.079	44.2	0.0118	44.2	1	75.8	33.3	77.2	32.9	122	18.2	75.8	33.3	NA		
08KH05-35	33	4679	1	17.6368	11.8	0.6575	12.6	0.0841	4.6	0.36	520.6	23	513.1	51	479.8	261.1	520.6	23	108.5		
08KH05-36	714	135839	4.3	10.4846	0.5	2.6293	3.2	0.1999	3.2	0.99	1175	34.1	1308.9	23.6	1535.5	9.1	1535.5	9.1	76.5		
08KH05-37	391	12295	2.6	21.8625	16.3	0.0535	16.6	0.0085	3	0.18	54.5	1.6	53	8.6	-16	396.5	54.5	1.6	NA		
08KH05-38	85	31099	1.3	17.7859	9	0.6586	9.6	0.085	3.3	0.35	525.6	16.9	513.7	38.9	461.2	200.9	525.6	16.9	114		
08KH05-39	2356	17189	1.1	17.123	2.4	0.6332	9.2	0.0786	8.8	0.96	488	41.6	498.1	36.1	544.8	53.5	488	41.6	89.6		
08KH05-41	524	26081	0.7	21.7819	9.8	0.0809	10.1	0.0128	2.3	0.23	81.9	1.9	79	7.7	-7.1	237.6	81.9	1.9	NA		
08KH05-42	166	193969	0.5	9.5767	0.8	4.2781	3	0.2971	2.9	0.96	1677.1	42.8	1689.2	24.8	1704.1	15.5	1704.1	15.5	98.4		
08KH05-43	503	51026	4.1	19.4262	3.3	0.2366	3.8	0.0333	2	0.52	211.4	4.1	215.6	7.4	262.2	75.3	211.4	4.1	NA		
08KH05-44	735	31073	24.4	20.0014	3.2	0.0861	15.1	0.0125	14.8	0.98	80	11.8	83.9	12.2	194.8	75	80	11.8	NA		
08KH05-45	570	31693	9.2	11.6834	1.1	1.129	5.9	0.0957	5.8	0.98	589	32.5	767.3	31.7	1329	22.1	589	32.5	44.3		
08KH05-47	854	9610	50	19.4755	13.5	0.0288	14.6	0.0041	5.5	0.38	26.2	1.4	28.9	4.1	256.4	311.7	26.2	1.4	NA		
08KH05-48	509	26464	1.4	19.0522	5.4	0.0875	5.7	0.0121	1.8	0.32	77.5	1.4	85.2	4.6	306.7	122.4	77.5	1.4	NA		
08KH05-49	534	587	0.6	17.4724	22.6	0.0894	22.8	0.0113	3.5	0.15	72.6	2.5	86.9	19	500.6	502.9	72.6	2.5	NA		
08KH05-50	3835	5655	9.5	13.7755	0.6	0.2994	2.6	0.0299	2.6	0.97	190	4.8	265.9	6.2	1002.6	12.5	190	4.8	NA		

TABLE DR1. NEW U-PB CRYSTALLIZATION AGES (Megaflood @ 6)

Grain	U (ppm)	206Pb 204Pb	U/Th	Isotope ratios							Apparent ages (Ma)						Best (Ma)	age ± (Ma)	Conc (Ma)
				206Pb*	±	207Pb*	±	206Pb*	±	error corr.	206Pb*	±	207Pb*	±	206Pb*	±			
				207Pb*	(%)	235U*	(%)	238U	(%)		238U*	(Ma)	235U	(Ma)	207Pb*	(Ma)			
08KH15-1	138	2619	1.1	18.3573	18.5	0.1337	19.4	0.0178	6	0.31	113.8	6.8	127.4	23.3	390.7	418.4	113.8	6.8	NA
08KH15-2	177	42883	0.6	17.2183	2.7	0.6522	3	0.0814	1.4	0.45	504.7	6.7	509.8	12.1	532.7	59.1	504.7	6.7	94.8
08KH15-3	5621	59917	0.8	20.6131	0.6	0.1458	24.4	0.0218	24.4	1	139	33.5	138.2	31.5	124.3	13.5	139	33.5	NA
08KH15-4	506	113126	1.4	17.2813	1.9	0.5415	4.2	0.0679	3.7	0.89	423.3	15.3	439.4	14.9	524.7	41	423.3	15.3	80.7
08KH15-5	852	128424	6.8	12.5244	5.6	0.1777	49.1	0.0161	48.8	0.99	103.2	49.9	166.1	75.3	1193.2	110.8	103.2	49.9	NA
08KH15-6	322	325094	1.3	10.4074	0.5	3.4839	1.4	0.263	1.3	0.93	1505	18	1523.6	11.4	1549.4	9.8	1549.4	9.8	97.1
08KH15-8	557	46159	2.1	12.4518	0.6	2.1467	4	0.1939	3.9	0.99	1142.3	41.1	1164	27.5	1204.6	11.7	1204.6	11.7	94.8
08KH15-9	4826	68824	5.2	20.7637	0.9	0.059	3.2	0.0089	3	0.95	57	1.7	58.2	1.8	107.2	22.3	57	1.7	NA
08KH15-11	361	173029	1.9	13.9802	1.4	1.3712	4.4	0.139	4.2	0.94	839.2	32.8	876.7	25.9	972.6	29.5	839.2	32.8	86.3
08KH15-12	2321	107137	2.3	17.3393	1.1	0.4666	4.7	0.0587	4.6	0.97	367.6	16.5	388.8	15.3	517.3	23.2	367.6	16.5	NA
08KH15-13	95	53621	0.9	12.5342	1.5	2.1246	2.3	0.1931	1.7	0.76	1138.3	18.2	1156.8	15.9	1191.6	29.8	1191.6	29.8	95.5
08KH15-14	98	28500	1.1	14.7939	1.2	1.2123	2.6	0.1301	2.3	0.89	788.3	16.9	806.2	14.3	856.2	24.6	788.3	16.9	92.1
08KH15-15	214	10697	1.8	23.566	28	0.0583	28.2	0.01	3.9	0.14	63.9	2.5	57.5	15.8	-200.7	712.8	63.9	2.5	NA
08KH15-17	340	57847	5.5	13.2133	5.7	0.6523	11.5	0.0625	10	0.87	390.9	38	509.9	46.2	1086.7	113.8	390.9	38	NA
08KH15-18	1956	88138	1.5	20.5751	2.5	0.0758	4	0.0113	3.1	0.77	72.5	2.2	74.2	2.9	128.7	59.7	72.5	2.2	NA
08KH15-20	290	16068	5.7	15.7745	3.1	0.3839	7.7	0.0439	7	0.91	277.1	19	329.9	21.6	721.4	65.8	277.1	19	NA
08KH15-21	1690	1960	5	17.3645	7.4	0.0567	17.4	0.0071	15.7	0.91	45.9	7.2	56	9.5	514.1	162	45.9	7.2	NA
08KH15-22	670	47372	0.8	20.6761	5	0.0778	5.5	0.0117	2.3	0.43	74.8	1.7	76.1	4	117.2	117.2	74.8	1.7	NA
08KH15-23	543	2014	1.2	17.8974	15.5	0.0934	15.7	0.0121	2.1	0.14	77.7	1.6	90.7	13.6	447.3	346.7	77.7	1.6	NA
08KH15-24	395	252962	1.1	13.0601	1.2	1.9306	8.4	0.1829	8.3	0.99	1082.6	82.8	1091.7	56.3	1110	24.7	1110	24.7	97.5
08KH15-25	273	130085	2.2	15.1623	1.2	1.2052	1.5	0.1325	0.9	0.63	802.3	7.1	803	8.4	804.9	24.6	802.3	7.1	99.7
08KH15-26	350	166636	1.5	12.671	0.4	2.1256	2.4	0.1953	2.3	0.99	1150.2	24.6	1157.2	16.3	1170.1	7.5	1170.1	7.5	98.3
08KH15-27	769	24691	1.1	22.1216	4.3	0.0736	5.4	0.0118	3.2	0.59	75.7	2.4	72.1	3.7	-44.6	105	75.7	2.4	NA

TABLE DR1. NEW U-PB CRYSTALLIZATION AGES (Megaflood @ 6)

Grain	U (ppm)	206Pb 204Pb	U/Th	Isotope ratios							error corr.	Apparent ages (Ma)						Best (Ma)	age ± (Ma)	Conc (Ma)	
				206Pb*	±	207Pb*	±	206Pb*	±	207Pb*		±	206Pb*	±	207Pb*	±	206Pb*				±
				207Pb*	(%)	235U*	(%)	238U	(%)	238U*		(Ma)	235U	(Ma)	207Pb*	(Ma)					
08KH15-28	2086	4457	31.6	14.0252	0.8	0.38	2.5	0.0387	2.4	0.95	244.5	5.7	327.1	7	966.1	15.6	244.5	5.7	NA		
08KH15-29	982	25622	1.7	21.6659	8.6	0.0557	9.4	0.0088	3.6	0.39	56.2	2	55	5	5.7	207.6	56.2	2	NA		
08KH15-30	455	49756	1.8	13.8476	0.9	1.5369	1.7	0.1544	1.5	0.87	925.3	12.9	945.3	10.6	992	17.4	925.3	12.9	93.3		
08KH15-31	416	24844	0.8	22.5964	19.5	0.0725	20.6	0.0119	6.6	0.32	76.2	5	71.1	14.1	-96.5	482.5	76.2	5	NA		
08KH15-32	197	45799	2.2	14.0477	1.4	1.4767	2.5	0.1504	2	0.82	903.5	17.1	920.9	15	962.8	29.3	903.5	17.1	93.8		
08KH15-33	565	25575	1.6	15.9578	1.4	0.9378	1.8	0.1085	1.2	0.65	664.2	7.4	671.7	8.9	696.9	29.6	664.2	7.4	95.3		
08KH15-34	637	28286	1.3	21.1854	9.9	0.0973	11.2	0.0149	5.2	0.47	95.6	5	94.3	10.1	59.5	235.5	95.6	5	NA		
08KH15-35	1116	494126	5	8.847	0.4	4.2682	4.5	0.2739	4.4	1	1560.4	61.4	1687.3	36.6	1848.7	8	1848.7	8	84.4		
08KH15-36	541	339766	2	12.6914	0.6	2.0744	1.2	0.1909	1	0.88	1126.5	10.5	1140.4	7.9	1166.9	11	1166.9	11	96.5		
08KH15-37	394	19404	1.8	17.3158	2.7	0.5229	8.7	0.0657	8.3	0.95	410	32.8	427.1	30.3	520.3	58.2	410	32.8	78.8		
08KH15-38	220	20973	1.2	20.0752	10.5	0.1748	10.9	0.0255	2.8	0.26	162	4.5	163.6	16.5	186.2	246.1	162	4.5	NA		
08KH15-39	439	20697	2.7	20.3283	7.4	0.1235	8	0.0182	3	0.37	116.4	3.5	118.3	8.9	157	174	116.4	3.5	NA		
08KH15-40	529	146123	1.6	13.2605	0.7	1.7737	2.2	0.1706	2	0.94	1015.3	19.1	1035.9	14	1079.5	14.5	1079.5	14.5	94.1		
08KH15-41	2750	31340	5.4	19.647	3.8	0.0567	5	0.0081	3.2	0.64	51.9	1.6	56	2.7	236.2	88.3	51.9	1.6	NA		
08KH15-42	68	32322	1	12.6696	2.4	2.0969	3.7	0.1927	2.9	0.77	1135.9	29.9	1147.8	25.6	1170.3	46.7	1170.3	46.7	97.1		
08KH15-43	179	114303	1.1	11.3139	0.9	2.8266	1.6	0.2319	1.3	0.83	1344.7	15.7	1362.6	11.7	1390.9	16.5	1390.9	16.5	96.7		
08KH15-44	552	264634	1.7	11.9198	0.3	2.3508	1.2	0.2032	1.1	0.96	1192.6	12.5	1227.8	8.5	1290.1	6.3	1290.1	6.3	92.4		
08KH15-45	1070	22055	1.8	21.7124	6.7	0.0388	7	0.0061	2.1	0.31	39.3	0.8	38.7	2.7	0.6	160.7	39.3	0.8	NA		
08KH15-47	540	19321	1.2	20.8584	8.1	0.0747	8.3	0.0113	2.1	0.25	72.4	1.5	73.1	5.9	96.4	190.9	72.4	1.5	NA		
08KH15-48	1198	10288	2.5	10.4006	0.4	1.1067	7	0.0835	6.9	1	516.9	34.5	756.6	37.1	1550.7	7.5	1550.7	7.5	33.3		
08KH15-49	278	301106	4.2	9.2117	0.5	4.538	1.2	0.3032	1.1	0.9	1707.1	16	1738	9.8	1775.3	9.3	1775.3	9.3	96.2		
08KH15-50	106	12316	1.2	16.4562	7.6	0.6081	8.5	0.0726	3.8	0.44	451.7	16.5	482.4	32.7	631	164.7	451.7	16.5	71.6		

TABLE DR1. NEW U-PB CRYSTALLIZATION AGES (Megaflood @ 6)

Grain	U (ppm)	206Pb 204Pb	U/Th	Isotope ratios							error corr.	Apparent ages (Ma)						Best (Ma)	age ± (Ma)	Conc (Ma)	
				206Pb*	±	207Pb*	±	206Pb*	±	238U		±	206Pb*	±	207Pb*	±	206Pb*				±
				207Pb*	(%)	235U*	(%)	238U	(%)	238U*		(Ma)	235U	(Ma)	207Pb*	(Ma)					
08KH15-53	764	64950	2.1	10.8344	0.6	2.6737	2.2	0.2101	2.1	0.97	1229.3	24	1321.2	16.4	1473.5	11	1473.5	11	83.4		
08KH15-54	65	19582	3.2	14.4103	4.2	1.3506	5.1	0.1412	2.8	0.55	851.2	22.4	867.8	29.7	910.5	87.5	851.2	22.4	93.5		
08KH15-55	224	232619	1.2	11.1745	1.1	3.065	4	0.2484	3.8	0.96	1430.2	49.1	1424	30.4	1414.6	20.1	1414.6	20.1	101.1		
08KH15-56	372	97401	1.1	13.8048	0.9	1.5847	3.7	0.1587	3.6	0.97	949.4	32	964.2	23.2	998.3	18.3	949.4	32	95.1		
08KH15-57	103	34063	1.3	12.7737	1.7	1.975	2.1	0.183	1.2	0.59	1083.2	12.3	1107	14.2	1154.1	33.7	1154.1	33.7	93.9		
08KH15-58	221	102689	2.4	13.1461	1.3	1.3768	3.1	0.1313	2.8	0.9	795.1	20.6	879.1	18	1096.8	26.9	795.1	20.6	72.5		
08KH15-59	1382	21337	3.2	12.199	1	0.6865	9.1	0.0607	9.1	0.99	380.1	33.5	530.7	37.8	1244.9	20.5	380.1	33.5	NA		
08KH15-60	67	58865	1.5	12.5584	2.8	1.944	3.5	0.1771	2.2	0.62	1050.9	21.2	1096.4	23.7	1187.8	54.7	1187.8	54.7	88.5		
08KH15-61	169	51221	2	15.7777	3.5	0.9609	3.9	0.11	1.7	0.45	672.5	11.1	683.7	19.4	721	73.9	672.5	11.1	93.3		
08KH15-63	75	30581	1.2	12.7038	2.5	2.0698	3.3	0.1907	2.1	0.64	1125.2	21.6	1138.9	22.4	1165	50	1165	50	96.6		
08KH15-64	144	54307	1.6	13.9001	2.6	1.6603	2.9	0.1674	1.3	0.43	997.7	11.6	993.5	18.2	984.3	52.8	997.7	11.6	101.4		
08KH15-65	653	11948	1.6	21.4316	11.3	0.0726	11.7	0.0113	3	0.26	72.3	2.2	71.2	8.1	31.9	272	72.3	2.2	NA		

TABLE DR1. NEW U-PB CRYSTALLIZATION AGES (2000 flood @6)

Grain	U (ppm)	206Pb 204Pb	U/Th	Isotope ratios							error corr.	Apparent ages (Ma)						Best (Ma)	age ± (Ma)	Conc (Ma)	
				206Pb*	±	207Pb*	±	206Pb*	±	207Pb*		±	206Pb*	±	207Pb*	±	206Pb*				±
				207Pb*	(%)	235U*	(%)	238U	(%)	238U*		(Ma)	235U	(Ma)	207Pb*	(Ma)					
08KH10-1	548	3146	44.1	18.6701	45.4	0.0404	45.5	0.0055	3.5	0.08	35.1	1.2	40.2	17.9	352.6	1077.2	35.1	1.2	NA		
08KH10-2	288	4736	2.6	16.2694	253	0.0469	253.5	0.0055	6.1	0.02	35.6	2.2	46.6	115.9	655.6	0	35.6	2.2	NA		
08KH10-3	222	37072	0.9	17.4954	2.7	0.5971	3	0.0758	1.4	0.46	470.8	6.3	475.4	11.5	497.6	59.2	470.8	6.3	94.6		
08KH10-4	1303	19042	4.5	21.8306	7.2	0.0476	7.7	0.0075	2.8	0.37	48.4	1.4	47.2	3.6	-12.5	173.4	48.4	1.4	NA		
08KH10-5	2590	59771	5.2	21.4726	3.4	0.0469	4.7	0.0073	3.3	0.7	46.9	1.5	46.6	2.1	27.3	80.7	46.9	1.5	NA		
08KH10-6	1671	9606	1	17.5221	1.5	0.353	17.4	0.0449	17.4	1	282.8	48.1	306.9	46.2	494.3	33.8	282.8	48.1	NA		
08KH10-7	1022	17897	1.1	21.6566	12.2	0.0474	12.6	0.0074	3.3	0.26	47.8	1.6	47	5.8	6.8	294.6	47.8	1.6	NA		
08KH10-8	196	21227	0.6	17.7488	5.2	0.5881	5.6	0.0757	1.9	0.34	470.4	8.5	469.6	20.9	465.9	115.8	470.4	8.5	101		
08KH10-9	482	7502	1.3	22.6831	22.9	0.0462	23.9	0.0076	7.1	0.3	48.8	3.5	45.8	10.7	-105.9	568.7	48.8	3.5	NA		
08KH10-10	1514	23384	10.8	23.7129	8.5	0.0384	8.7	0.0066	1.9	0.22	42.4	0.8	38.3	3.3	-216.3	212.9	42.4	0.8	NA		
08KH10-11	125	17836	1.7	15.8551	8.8	0.3985	9.9	0.0458	4.6	0.46	288.8	13	340.5	28.7	710.6	187.3	288.8	13	NA		
08KH10-12	542	23688	0.4	16.9514	4.6	0.609	7.4	0.0749	5.8	0.79	465.4	26.2	482.9	28.5	566.8	100.2	465.4	26.2	82.1		
08KH10-13	433	7841	2	27.1886	33.4	0.0378	33.7	0.0074	4.1	0.12	47.8	2	37.7	12.5	-572.6	924.8	47.8	2	NA		
08KH10-14	401	15593	1	19.9951	11.8	0.1228	12.2	0.0178	3	0.24	113.8	3.4	117.6	13.5	195.6	274.9	113.8	3.4	NA		
08KH10-16	632	4800	1.2	21.4789	14.2	0.0486	14.4	0.0076	2.5	0.17	48.6	1.2	48.1	6.8	26.6	342.7	48.6	1.2	NA		
08KH10-17	176	5777	1.8	22.4997	16.1	0.1507	19.2	0.0246	10.6	0.55	156.6	16.3	142.6	25.6	-86	395.9	156.6	16.3	NA		
08KH10-18	1031	13774	2.9	20.5221	7.9	0.0504	8.1	0.0075	1.7	0.21	48.2	0.8	49.9	3.9	134.7	185.2	48.2	0.8	NA		
08KH10-19	1483	16892	2	21.4694	5.6	0.047	6.6	0.0073	3.5	0.53	47	1.6	46.6	3	27.7	135.2	47	1.6	NA		
08KH10-20	515	2476	2	16.7643	16.1	0.0583	16.8	0.0071	5	0.3	45.5	2.3	57.5	9.4	590.9	350.6	45.5	2.3	NA		
08KH10-21	1220	23525	7.9	21.2267	6.5	0.043	7	0.0066	2.7	0.39	42.6	1.2	42.8	2.9	54.8	154.8	42.6	1.2	NA		
08KH10-22	917	13678	1.6	20.8374	13.8	0.0481	14.1	0.0073	3	0.21	46.7	1.4	47.7	6.6	98.8	328.5	46.7	1.4	NA		
08KH10-23	236	149271	3.9	10.0897	0.9	3.2502	3.1	0.2378	2.9	0.95	1375.5	36.5	1469.2	24	1607.4	17.4	1607.4	17.4	85.6		
08KH10-24	272	223756	3.8	12.1911	3.4	1.9793	11.2	0.175	10.6	0.95	1039.6	102	1108.5	75.4	1246.2	66.9	1246.2	66.9	83.4		

TABLE DR1. NEW U-PB CRYSTALLIZATION AGES (2000 flood @6)

Grain	U (ppm)	206Pb 204Pb	U/Th	Isotope ratios							error corr.	Apparent ages (Ma)						Best (Ma)	age ± (Ma)	Conc (Ma)	
				206Pb*	±	207Pb*	±	206Pb*	±	207Pb*		±	206Pb*	±	207Pb*	±	206Pb*				±
				207Pb*	(%)	235U*	(%)	238U	(%)	238U*		(Ma)	235U	(Ma)	207Pb*	(Ma)					
08KH10-25	445	6737	2	26.5035	28.9	0.0474	29.5	0.0091	6	0.2	58.5	3.5	47	13.6	-504.1	783.6	58.5	3.5	NA		
08KH10-26	305	3806	1.1	14.412	17.6	0.071	20.7	0.0074	10.8	0.52	47.7	5.1	69.7	13.9	910.2	365.7	47.7	5.1	NA		
08KH10-27	551	10478	1.5	22.7632	20.3	0.0461	20.4	0.0076	2.3	0.11	48.9	1.1	45.8	9.1	-114.6	504.8	48.9	1.1	NA		
08KH10-28	220	31341	1.1	17.4079	4	0.6036	4.4	0.0762	1.9	0.42	473.5	8.5	479.5	17	508.7	88.7	473.5	8.5	93.1		
08KH10-29	838	15097	3	23.0894	16.2	0.0444	16.8	0.0074	4.1	0.24	47.8	1.9	44.1	7.2	-149.7	405.4	47.8	1.9	NA		
08KH10-30	606	60732	2.2	17.6402	1.5	0.567	2.5	0.0725	2	0.79	451.5	8.5	456.1	9.1	479.4	33.7	451.5	8.5	94.2		
08KH10-31	400	42837	1.1	18.018	1.2	0.5807	1.8	0.0759	1.4	0.76	471.5	6.4	464.9	6.9	432.4	26.5	471.5	6.4	109		
08KH10-32	2607	46984	1.1	21.0087	4.5	0.0492	6.6	0.0075	4.8	0.73	48.1	2.3	48.7	3.1	79.4	107.2	48.1	2.3	NA		
08KH10-34	177	33715	1.7	12.7552	1.6	2.0754	2.8	0.192	2.3	0.82	1132.2	24	1140.7	19.4	1157	32.4	1157	32.4	97.9		
08KH10-35	381	50832	1	17.6873	2.5	0.6111	4.3	0.0784	3.4	0.81	486.5	16.2	484.2	16.4	473.5	55.4	486.5	16.2	102.7		
08KH10-36	89	20786	1	18.2329	12.6	0.5669	12.8	0.075	2.1	0.17	466	9.6	456	47.1	405.9	283.7	466	9.6	114.8		
08KH10-37	1367	6043	6.3	18.6324	18.6	0.0394	19.4	0.0053	5.4	0.28	34.3	1.8	39.3	7.5	357.2	424	34.3	1.8	NA		
08KH10-38	1072	6113	2.6	19.2662	6.9	0.06	8	0.0084	4.1	0.51	53.8	2.2	59.2	4.6	281.2	157.9	53.8	2.2	NA		
08KH10-39	150	38281	1.7	14.2512	3.8	1.2735	5.9	0.1316	4.5	0.76	797.2	33.5	834	33.4	933.3	78	797.2	33.5	85.4		
08KH10-40	206	39200	1.3	18.333	3.6	0.578	4.8	0.0769	3.2	0.66	477.3	14.6	463.2	17.9	393.7	81.4	477.3	14.6	121.3		
08KH10-41	232	6140	1.8	19.9867	36.5	0.0591	37.7	0.0086	9.6	0.25	55	5.2	58.3	21.4	196.6	874	55	5.2	NA		
08KH10-42	1712	187567	1.2	17.6556	0.6	0.5149	18.7	0.0659	18.7	1	411.6	74.5	421.7	64.6	477.5	13.9	411.6	74.5	86.2		
08KH10-43	933	106961	1.7	17.6794	1.2	0.5823	2.4	0.0747	2.1	0.87	464.2	9.3	465.9	8.8	474.5	25.5	464.2	9.3	97.8		
08KH10-44	291	1712	0.8	11.9975	87.6	0.0663	93.4	0.0058	32.5	0.35	37.1	12	65.1	59	1277.4	43.3	37.1	12	NA		
08KH10-45	265	2984	1.9	20.0399	16.2	0.0507	17.7	0.0074	7.1	0.4	47.3	3.4	50.2	8.7	190.4	378.7	47.3	3.4	NA		
08KH10-46	651	112604	1.3	17.6569	1.5	0.6011	2.1	0.077	1.4	0.7	478.1	6.7	477.9	7.9	477.3	32.6	478.1	6.7	100.2		
08KH10-48	590	19880	1.1	17.6934	1.8	0.5849	5.5	0.0751	5.2	0.95	466.6	23.6	467.6	20.7	472.8	39.2	466.6	23.6	98.7		

TABLE DR1. NEW U-PB CRYSTALLIZATION AGES (2000 flood @6)

Grain	U (ppm)	206Pb 204Pb	U/Th	Isotope ratios							error corr.	Apparent ages (Ma)						Best (Ma)	age ± (Ma)	Conc (Ma)	
				206Pb*	±	207Pb*	±	206Pb*	±	207Pb*		±	206Pb*	±	207Pb*	±	206Pb*				±
				207Pb*	(%)	235U*	(%)	238U	(%)	238U*		(Ma)	235U	(Ma)	207Pb*	(Ma)					
08KH10-49	216	35644	0.7	16.7984	2.6	0.7718	4.5	0.094	3.7	0.82	579.4	20.4	580.8	20	586.5	56.9	579.4	20.4	98.8		
08KH10-50	62	25729	0.4	12.4181	4.6	2.1589	10.4	0.1944	9.3	0.9	1145.4	97.8	1167.9	72.3	1210	90.9	1210	90.9	94.7		
08KH10-51	3803	30570	0.7	20.8048	3.2	0.0336	4	0.0051	2.4	0.6	32.6	0.8	33.5	1.3	102.5	75.7	32.6	0.8	NA		
08KH10-52	262	4424	1.5	24.6552	42.8	0.0412	43.2	0.0074	5.9	0.14	47.3	2.8	41	17.4	-315.2	1143.3	47.3	2.8	NA		
08KH10-53	537	9102	0.9	21.3736	14.7	0.0472	15	0.0073	2.8	0.19	47	1.3	46.8	6.9	38.3	354	47	1.3	NA		
08KH10-54	554	9099	0.7	22.9316	14.6	0.0455	15	0.0076	3.2	0.21	48.6	1.5	45.2	6.6	-132.8	363.1	48.6	1.5	NA		
08KH10-55	2204	29874	4.8	21.6443	4.8	0.0483	5.7	0.0076	3.1	0.54	48.7	1.5	47.9	2.7	8.1	116	48.7	1.5	NA		
08KH10-56	224	88	2.5	6.0053	82.7	0.1696	91.2	0.0074	38.5	0.42	47.4	18.2	159.1	135.1	2522.9	725	47.4	18.2	NA		
08KH10-57	432	8107	1.6	24.3148	19.3	0.0425	19.9	0.0075	4.7	0.24	48.1	2.3	42.2	8.2	-279.7	494.9	48.1	2.3	NA		
08KH10-58	351	45158	1.5	17.3942	1.6	0.5949	3.2	0.075	2.8	0.86	466.5	12.5	474	12.2	510.4	35.6	466.5	12.5	91.4		
08KH10-59	192	41049	1.4	17.3085	4.2	0.6063	4.5	0.0761	1.5	0.34	472.9	6.9	481.2	17.3	521.2	93.2	472.9	6.9	90.7		
08KH10-60	471	8561	1.2	23.0212	24.9	0.0454	25.3	0.0076	4	0.16	48.6	2	45	11.1	-142.4	625.9	48.6	2	NA		
08KH10-61	1414	33150	1.7	21.6662	11.1	0.049	11.5	0.0077	2.9	0.25	49.5	1.4	48.6	5.4	5.7	268.1	49.5	1.4	NA		
08KH10-62	477	7780	0.9	17.6238	1.6	0.5599	3	0.0716	2.5	0.84	445.6	10.8	451.5	10.9	481.5	35.9	445.6	10.8	92.5		
08KH10-63	400	37981	1	17.7497	2.3	0.5778	2.9	0.0744	1.9	0.63	462.5	8.3	463	10.9	465.8	50.2	462.5	8.3	99.3		
08KH10-64	503	17083	1.8	19.9776	11.2	0.0528	11.8	0.0076	3.6	0.3	49.1	1.7	52.2	6	197.6	261.6	49.1	1.7	NA		
08KH10-65	233	24174	1.3	16.9529	4.7	0.6217	7.4	0.0764	5.7	0.77	474.8	26	490.9	28.6	566.6	102	474.8	26	83.8		
08KH10-66	220	2922	0.8	3.8886	637	0.177	637	0.005	13.2	0.02	32.1	4.2	165.5	1951	3229.4	358.3	32.1	4.2	NA		
08KH10-67	422	45490	1	17.5555	2.3	0.5838	4.4	0.0743	3.7	0.85	462.2	16.7	466.9	16.4	490.1	50.4	462.2	16.7	94.3		
08KH10-68	518	73875	2.8	17.485	2.4	0.537	5.4	0.0681	4.8	0.89	424.7	19.7	436.5	19	498.9	52.8	424.7	19.7	85.1		
08KH10-69	966	58925	2.2	17.6072	1.3	0.5524	3.9	0.0705	3.6	0.94	439.4	15.4	446.5	14	483.6	29.3	439.4	15.4	90.9		
08KH10-70	362	88022	1.1	17.4369	2.1	0.622	5	0.0787	4.5	0.91	488.1	21.2	491.1	19.4	505	46.5	488.1	21.2	96.7		

TABLE DR1. NEW U-PB CRYSTALLIZATION AGES (2000 flood @6)

Grain	U (ppm)	206Pb 204Pb	U/Th	Isotope ratios							error corr.	Apparent ages (Ma)						Best (Ma)	age ± (Ma)	Conc (Ma)	
				206Pb*	±	207Pb*	±	206Pb*	±	207Pb*		±	206Pb*	±	207Pb*	±	206Pb*				±
				207Pb*	(%)	235U*	(%)	238U	(%)	238U*		(Ma)	235U	(Ma)	207Pb*	(Ma)					
08KH10-71	577	10649	1.4	21.1283	19.1	0.0494	20	0.0076	5.8	0.29	48.6	2.8	48.9	9.6	65.9	459.2	48.6	2.8	NA		
08KH10-72	206	1748	1.6	13.4172	24.6	0.0765	26.5	0.0074	9.9	0.37	47.8	4.7	74.9	19.1	1055.9	502.8	47.8	4.7	NA		
08KH10-73	1045	34393	1.4	23.7246	18.1	0.0339	18.4	0.0058	3.1	0.17	37.4	1.1	33.8	6.1	-217.5	458.9	37.4	1.1	NA		
08KH10-74	119	4023	0.5	15.9736	11.7	0.6476	12.1	0.075	2.9	0.24	466.4	13.1	507	48.2	694.8	250.5	466.4	13.1	67.1		
08KH10-75	187	52671	0.9	16.9753	4.4	0.6191	5	0.0762	2.2	0.45	473.5	10.2	489.3	19.3	563.7	96.6	473.5	10.2	84		
08KH10-76	85	1410	1.6	8.8452	161	0.1138	162.9	0.0073	26.4	0.16	46.9	12.3	109.4	170.5	1849.1	73.3	46.9	12.3	NA		
08KH10-77	1075	18054	2.2	20.9193	9.8	0.0485	10.4	0.0074	3.7	0.35	47.3	1.7	48.1	4.9	89.5	232.2	47.3	1.7	NA		
08KH10-78	419	626	0.6	13.5418	41	0.0457	43.5	0.0045	14.5	0.33	28.9	4.2	45.4	19.3	1037.2	864.9	28.9	4.2	NA		
08KH10-79	741	8651	2.4	19.5639	22.8	0.0433	23	0.0061	3.2	0.14	39.5	1.2	43	9.7	246	530.5	39.5	1.2	NA		
08KH10-80	417	17392	4.7	22.9453	19.3	0.0553	19.7	0.0092	3.5	0.18	59.1	2.1	54.7	10.5	-134.2	482.3	59.1	2.1	NA		
08KH10-81	1328	10022	20	23.5178	11.9	0.0277	13.9	0.0047	7.2	0.51	30.4	2.2	27.8	3.8	-195.6	299.1	30.4	2.2	NA		
08KH10-82	227	25892	1.2	17.4713	3.9	0.5227	5.7	0.0662	4.1	0.72	413.4	16.3	426.9	19.7	500.7	86.2	413.4	16.3	82.6		
08KH10-83	269	89370	1.1	17.6949	3.2	0.6193	5.8	0.0795	4.8	0.83	493	22.7	489.4	22.5	472.6	71.8	493	22.7	104.3		
08KH10-84	1482	112683	1.7	17.631	0.6	0.5665	3.2	0.0724	3.2	0.98	450.8	13.8	455.7	11.8	480.6	12.7	450.8	13.8	93.8		
08KH10-85	424	39271	0.8	17.641	1.8	0.6131	4.1	0.0784	3.6	0.89	486.8	17	485.5	15.7	479.3	40.3	486.8	17	101.6		
08KH10-86	172	21257	0.7	17.1011	7.4	0.5975	7.6	0.0741	1.6	0.21	460.8	7.1	475.6	28.8	547.6	162.3	460.8	7.1	84.2		
08KH10-87	4632	41507	13.6	20.5531	3.3	0.0321	4.5	0.0048	3	0.68	30.8	0.9	32.1	1.4	131.2	77.5	30.8	0.9	NA		
08KH10-88	699	6868	1	23.9757	18.3	0.0278	19.5	0.0048	6.9	0.36	31.1	2.2	27.9	5.4	-244.1	464.5	31.1	2.2	NA		
08KH10-90	492	3740	0.7	22.6861	35.8	0.0289	36.4	0.0048	6.7	0.18	30.6	2	28.9	10.4	-106.2	906.3	30.6	2	NA		
08KH10-91	240	3934	0.6	3.1851	846	0.2047	845.6	0.0047	11.1	0.01	30.4	3.4	189.1	#####	3540.5	428.8	30.4	3.4	NA		
08KH10-92	778	60682	1.2	17.5247	1.4	0.6088	2.4	0.0774	2	0.83	480.5	9.3	482.8	9.3	493.9	29.8	480.5	9.3	97.3		
08KH10-93	137	2104	1.4	9.538	262	0.1081	262.1	0.0075	17.1	0.07	48	8.2	104.2	265.4	1711.6	632	48	8.2	NA		

TABLE DR1. NEW U-PB CRYSTALLIZATION AGES (2000 flood @6)

Grain	U (ppm)	206Pb 204Pb	U/Th	Isotope ratios							error corr.	Apparent ages (Ma)						Best (Ma)	age ± (Ma)	Conc (Ma)	
				206Pb*	±	207Pb*	±	206Pb*	±	207Pb*		±	206Pb*	±	207Pb*	±	206Pb*				±
				207Pb*	(%)	235U*	(%)	238U	(%)	238U*		(Ma)	235U	(Ma)	207Pb*	(Ma)					
08KH10-94	692	5158	1.5	21.9269	19.1	0.0491	19.2	0.0078	2.4	0.12	50.2	1.2	48.7	9.1	-23.1	465.6	50.2	1.2	NA		
08KH10-95	313	45184	1	17.5131	3.4	0.5972	5.3	0.0758	4.1	0.77	471.3	18.6	475.4	20.2	495.4	75.2	471.3	18.6	95.1		
08KH10-97	581	5304	2.4	20.491	38	0.035	38.2	0.0052	3.9	0.1	33.5	1.3	35	13.1	138.3	922.5	33.5	1.3	NA		
08KH10-99	124	3284	0.8	17.0435	8	0.5736	8.7	0.0709	3.4	0.39	441.6	14.7	460.3	32.2	555	174.5	441.6	14.7	79.6		
08KH10-100	826	19539	2.1	20.6826	9.6	0.0503	10.7	0.0076	4.8	0.45	48.5	2.3	49.9	5.2	116.4	225.7	48.5	2.3	NA		
08KH10-101	527	4836	0.8	25.0925	16.8	0.0317	18	0.0058	6.3	0.35	37.1	2.3	31.7	5.6	-360.5	437.6	37.1	2.3	NA		
08KH10-102	379	726	2.4	22.237	74.4	0.0384	74.7	0.0062	6.4	0.09	39.8	2.5	38.2	28.1	-57.3	2133.3	39.8	2.5	NA		
08KH10-103	794	13255	1	22.2388	17.1	0.0335	17.7	0.0054	4.6	0.26	34.7	1.6	33.4	5.8	-57.5	420.2	34.7	1.6	NA		
08KH10-104	230	15886	0.9	17.9657	6.5	0.5674	14	0.0739	12.4	0.89	459.8	55	456.3	51.5	438.9	145.2	459.8	55	104.8		
08KH10-105	866	8336	0.4	24.6856	27.9	0.0308	28.2	0.0055	3.8	0.13	35.4	1.3	30.8	8.5	-318.4	728.6	35.4	1.3	NA		
08KH10-106	354	3810	2.2	17.1611	45	0.0513	51.5	0.0064	24.9	0.48	41	10.2	50.8	25.5	540	1035.3	41	10.2	NA		
08KH10-107	165	4865	1.7	22.9298	78.1	0.0472	78.6	0.0079	8.3	0.11	50.4	4.2	46.9	36	-132.6	2327.4	50.4	4.2	NA		
08KH10-108	1281	32021	3.6	21.6218	6.6	0.0479	6.9	0.0075	2.1	0.3	48.3	1	47.5	3.2	10.7	159.3	48.3	1	NA		
08KH10-109	295	68314	1.1	17.2406	2.7	0.63	3.9	0.0788	2.9	0.73	488.8	13.4	496.1	15.4	529.9	58.7	488.8	13.4	92.3		
08KH10-110	861	6190	0.9	18.7244	9.3	0.0353	10.4	0.0048	4.7	0.46	30.8	1.5	35.2	3.6	346.1	209.8	30.8	1.5	NA		
08KH10-111	760	18684	1	21.3595	12.5	0.0465	13.4	0.0072	4.7	0.35	46.2	2.1	46.1	6	40	300.4	46.2	2.1	NA		
08KH10-112	154	82103	2.2	10.0778	1.4	3.6827	2.4	0.2692	2	0.83	1536.6	27.6	1567.6	19.5	1609.6	25.8	1609.6	25.8	95.5		
08KH10-113	278	67645	1	17.8729	4.6	0.5443	5.8	0.0705	3.6	0.62	439.5	15.3	441.2	20.8	450.4	101.6	439.5	15.3	97.6		
08KH10-114	172	1927	1.2	16.1506	11.4	0.6235	11.7	0.073	2.7	0.23	454.4	11.9	492	45.8	671.2	245	454.4	11.9	67.7		
08KH10-115	433	119718	1.4	17.632	2	0.5867	3.6	0.075	2.9	0.83	466.4	13.2	468.8	13.3	480.4	44.2	466.4	13.2	97.1		
08KH10-117	289	5424	1.4	22.1419	29.2	0.0477	30.1	0.0077	7.1	0.24	49.2	3.5	47.3	13.9	-46.8	724	49.2	3.5	NA		
08KH10-118	703	6140	0.7	20.8435	27.1	0.0326	28	0.0049	7.2	0.26	31.7	2.3	32.6	9	98.1	651.3	31.7	2.3	NA		

TABLE DR1. NEW U-PB CRYSTALLIZATION AGES (2000 flood @6)

Grain	U (ppm)	206Pb 204Pb	U/Th	Isotope ratios							error corr.	Apparent ages (Ma)						Best (Ma)	age ± (Ma)	Conc (Ma)	
				206Pb*	±	207Pb*	±	206Pb*	±	207Pb*		±	206Pb*	±	207Pb*	±	206Pb*				±
				207Pb*	(%)	235U*	(%)	238U	(%)	238U*		(Ma)	235U	(Ma)	207Pb*	(Ma)					
08KH10-119	810	12301	2	24.1464	10.9	0.0425	11.2	0.0074	2.2	0.2	47.8	1.1	42.3	4.6	-262	277.9	47.8	1.1	NA		
08KH10-120	1983	16047	37.7	19.4111	2.6	0.066	8.4	0.0093	8	0.95	59.6	4.8	64.9	5.3	264	58.8	59.6	4.8	NA		
08KH10-1 b	575	1984	0.8	16.3987	24.2	0.068	24.5	0.0081	4.2	0.17	51.9	2.2	66.8	15.9	638.6	526.8	51.9	2.2	NA		
08KH10-2 b	951	15584	59.1	20.9132	23.4	0.0321	23.6	0.0049	2.7	0.12	31.3	0.9	32.1	7.4	90.2	561.1	31.3	0.9	NA		
08KH10-3 b	698	22910	4.1	20.7877	3.7	0.0945	13.8	0.0142	13.3	0.96	91.2	12.1	91.7	12.1	104.4	87.5	91.2	12.1	NA		
08KH10-4 b	697	31776	1.2	21.6429	8.4	0.0494	9.2	0.0078	3.8	0.41	49.8	1.9	49	4.4	8.3	201.6	49.8	1.9	NA		
08KH10-5 b	1566	70087	11.2	21.9148	5	0.0446	5.1	0.0071	1.2	0.23	45.5	0.5	44.3	2.2	-21.8	120.8	45.5	0.5	NA		
08KH10-6 b	478	12849	1.5	20.3653	13.1	0.0513	13.5	0.0076	3	0.22	48.7	1.5	50.8	6.7	152.8	309	48.7	1.5	NA		
08KH10-7 b	4167	16794	0.7	17.3172	2.5	0.1904	84	0.0239	84	1	152.3	126.4	177	137.3	520.1	55.5	152.3	126.4	NA		
08KH10-8 b	120	28631	0.6	17.622	8.1	0.601	8.6	0.0768	2.8	0.32	477.1	12.8	477.9	32.8	481.7	180.1	477.1	12.8	99		
08KH10-9 b	1626	18090	1.2	20.7488	5.6	0.0603	7.5	0.0091	5	0.67	58.3	2.9	59.5	4.3	108.9	131.8	58.3	2.9	NA		
08KH10-10 b	148	123245	3.1	11.6035	1.4	2.4566	3	0.2067	2.6	0.88	1211.4	28.8	1259.4	21.4	1342.2	27.5	1342.2	27.5	90.3		
08KH10-11 b	352	9309	2.5	25.2012	16.8	0.0466	17.2	0.0085	3.9	0.23	54.7	2.1	46.3	7.8	-371.7	436.9	54.7	2.1	NA		
08KH10-12 b	905	10329	25.5	22.9889	14.2	0.0299	15	0.005	4.9	0.32	32.1	1.6	29.9	4.4	-138.9	352.7	32.1	1.6	NA		
08KH10-14 b	196	4056	0.9	19.6078	36.2	0.0528	37	0.0075	7.4	0.2	48.2	3.6	52.3	18.8	240.8	861.2	48.2	3.6	NA		
08KH10-15 b	1283	40159	1.6	22.1238	5.8	0.0467	6.2	0.0075	2.4	0.38	48.1	1.1	46.3	2.8	-44.8	140.5	48.1	1.1	NA		
08KH10-16 b	1204	27928	1	20.1534	4.3	0.0521	4.5	0.0076	1.2	0.26	48.9	0.6	51.5	2.2	177.2	100.6	48.9	0.6	NA		
08KH10-17 b	538	103222	0.9	17.5156	1.5	0.6094	2.1	0.0774	1.4	0.7	480.7	6.7	483.2	8	495.1	33	480.7	6.7	97.1		
08KH10-18 b	1038	47360	0.6	17.4398	0.8	0.5408	17.2	0.0684	17.2	1	426.6	71.1	439	61.5	504.7	17.7	426.6	71.1	84.5		
08KH10-19 b	438	101851	1.5	17.5523	2	0.5457	2.6	0.0695	1.7	0.65	433	7.2	442.2	9.4	490.5	44.1	433	7.2	88.3		
08KH10-20 b	447	4968	6.5	25.0398	27.8	0.0423	27.9	0.0077	2.5	0.09	49.3	1.2	42	11.5	-355	730.9	49.3	1.2	NA		
08KH10-21 b	2225	41499	20.8	22.2156	6.8	0.0329	6.9	0.0053	1.4	0.2	34	0.5	32.8	2.2	-54.9	164.7	34	0.5	NA		
08KH10-22 b	5190	17080	18.9	21.1911	2	0.0445	16.8	0.0068	16.7	0.99	43.9	7.3	44.2	7.3	58.9	46.6	43.9	7.3	NA		

TABLE DR1. NEW U-PB CRYSTALLIZATION AGES (2000 flood @6)

Grain	U (ppm)	206Pb 204Pb	U/Th	Isotope ratios							error corr.	Apparent ages (Ma)						Best (Ma)	age ± (Ma)	Conc (Ma)	
				206Pb*	±	207Pb*	±	206Pb*	±	207Pb*		±	206Pb*	±	207Pb*	±	206Pb*				±
				207Pb*	(%)	235U*	(%)	238U	(%)	238U*		(Ma)	235U	(Ma)	207Pb*	(Ma)					
08KH10-23 b	869	15359	1.6	21.492	12.4	0.0471	12.5	0.0073	1.7	0.14	47.2	0.8	46.8	5.7	25.1	298.1	47.2	0.8	NA		
08KH10-24 b	1445	43562	3.2	23.2495	7.6	0.0328	9.5	0.0055	5.6	0.59	35.6	2	32.8	3.1	-166.9	190.2	35.6	2	NA		
08KH10-25 b	1778	59214	14.6	21.0055	3.2	0.0466	4	0.0071	2.4	0.59	45.6	1.1	46.3	1.8	79.7	76.6	45.6	1.1	NA		
08KH10-26 b	2385	1037323	16.6	15.1012	0.3	1.1345	3.4	0.1243	3.3	0.99	755	23.8	769.9	18.1	813.4	7.1	755	23.8	92.8		
08KH10-27 b	347	45654	2.4	20.4266	6.2	0.1814	6.5	0.0269	1.7	0.27	170.9	2.9	169.2	10.1	145.7	146.5	170.9	2.9	NA		
08KH10-28 b	775	11596	3.1	23.3508	20.8	0.0288	21	0.0049	2.6	0.12	31.4	0.8	28.9	6	-177.7	523.5	31.4	0.8	NA		
08KH10-29 b	88	39505	1.8	10.4111	1.4	2.9811	2.7	0.2251	2.4	0.86	1308.7	27.9	1402.8	20.8	1548.8	26.1	1548.8	26.1	84.5		
08KH10-30 b	266	2538	1.3	25.2827	48.4	0.0269	49.7	0.0049	11.2	0.23	31.8	3.6	27	13.2	-380.1	1325.7	31.8	3.6	NA		
08KH10-31 b	296	1726	1.9	21.7366	26.9	0.0474	27.4	0.0075	5.6	0.2	48	2.7	47	12.6	-2.1	658.1	48	2.7	NA		
08KH10-32 b	531	177779	1.1	17.5352	0.8	0.5961	1.8	0.0758	1.7	0.91	471.1	7.6	474.8	7	492.6	16.8	471.1	7.6	95.6		
08KH10-33 b	368	83506	1.3	17.5186	1.8	0.5953	2.2	0.0756	1.2	0.55	470	5.6	474.3	8.4	494.7	40.6	470	5.6	95		
08KH10-34 b	885	11253	0.3	21.7459	14.7	0.0306	15.2	0.0048	3.8	0.25	31	1.2	30.6	4.6	-3.1	356.9	31	1.2	NA		
08KH10-35 b	190	2651	0.5	16.5808	171	0.0395	171.4	0.0047	11.9	0.07	30.5	3.6	39.3	66.2	614.7	1095.8	30.5	3.6	NA		
08KH10-36 b	307	6800	2.7	31.0666	40.6	0.0314	40.9	0.0071	5	0.12	45.4	2.3	31.4	12.6	-947.6	1229.1	45.4	2.3	NA		
08KH10-37 b	116	20991	0.6	18.1714	5.5	0.5779	5.8	0.0762	1.9	0.32	473.2	8.5	463.1	21.5	413.5	122.5	473.2	8.5	114.4		
08KH10-38 b	2477	46605	2.5	21.2151	4.1	0.0322	4.4	0.005	1.6	0.36	31.8	0.5	32.2	1.4	56.2	98.7	31.8	0.5	NA		
08KH10-39 b	350	9281	1.5	19.0908	14.2	0.0534	15.1	0.0074	5.2	0.34	47.5	2.4	52.8	7.8	302.1	325.9	47.5	2.4	NA		
08KH10-40 b	2177	119914	3.5	17.5429	0.3	0.5541	3.1	0.0705	3.1	0.99	439.2	13.2	447.7	11.3	491.7	7.2	439.2	13.2	89.3		
08KH10-41 b	1072	13712	7.8	22.1848	10.6	0.0309	10.9	0.005	2.1	0.19	31.9	0.7	30.9	3.3	-51.5	259.8	31.9	0.7	NA		
08KH10-42 b	517	10832	2.7	23.9665	11.7	0.0425	11.8	0.0074	1.9	0.16	47.5	0.9	42.3	4.9	-243.1	296.1	47.5	0.9	NA		
08KH10-44 b	1280	34932	3.3	21.442	10.6	0.0352	10.7	0.0055	1.5	0.14	35.2	0.5	35.1	3.7	30.7	254	35.2	0.5	NA		
08KH10-45 b	625	111314	6.7	14.8901	0.8	0.5031	5.8	0.0543	5.7	0.99	341.1	18.9	413.8	19.6	842.7	17.3	341.1	18.9	NA		

TABLE DR1. NEW U-PB CRYSTALLIZATION AGES (2000 flood @6)

Grain	U (ppm)	206Pb	U/Th	Isotope ratios							Apparent ages (Ma)						Best (Ma)	age ± (Ma)	Conc (Ma)
				206Pb*	±	207Pb*	±	206Pb*	±	error corr.	206Pb*	±	207Pb*	±	206Pb*	±			
				207Pb*	(%)	235U*	(%)	238U	(%)		238U*	(Ma)	235U	(Ma)	207Pb*	(Ma)			
08KH10-46 b	175	4691	1.2	20.7205	46.1	0.057	47.5	0.0086	11.2	0.24	55	6.1	56.3	26	112.1	1144.9	55	6.1	NA
08KH10-47 b	1599	166101	0.7	17.4795	0.7	0.5598	2.1	0.071	2	0.94	442	8.4	451.4	7.6	499.6	15.2	442	8.4	88.5
08KH10-48 b	3003	47909	2.2	20.7631	2.3	0.0511	2.5	0.0077	1	0.39	49.4	0.5	50.6	1.2	107.3	53.6	49.4	0.5	NA
08KH10-49 b	1549	21674	6.9	20.6236	6.8	0.0317	7.4	0.0047	2.9	0.39	30.5	0.9	31.7	2.3	123.1	160.6	30.5	0.9	NA
08KH10-50 b	2757	37310	0.5	20.6213	3.8	0.0341	4.2	0.0051	1.8	0.44	32.8	0.6	34.1	1.4	123.4	89.1	32.8	0.6	NA

TABLE DR1. NEW U-PB CRYSTALLIZATION AGES (2000 flood @ 10)

Grain	U (ppm)	206Pb 204Pb	U/Th	Isotope ratios							error corr.	Apparent ages (Ma)						Best (Ma)	age ± (Ma)	Conc (Ma)	
				206Pb*	±	207Pb*	±	206Pb*	±	207Pb*		±	206Pb*	±	207Pb*	±	206Pb*				±
				207Pb*	(%)	235U*	(%)	238U	(%)	238U*		(Ma)	235U	(Ma)	207Pb*	(Ma)					
08KH31-1	102	11869	1.8	10.6682	2.5	2.4035	4.3	0.186	3.5	0.82	1099.5	35.3	1243.7	30.7	1502.8	46.8	1502.8	46.8	73.2		
08KH31-2	169	31006	0.8	17.2612	5.8	0.6449	7.8	0.0807	5.1	0.66	500.5	24.7	505.3	31	527.3	128.1	500.5	24.7	94.9		
08KH31-3	1263	325029	1.7	17.5685	0.7	0.6078	2	0.0774	1.8	0.94	480.9	8.5	482.2	7.5	488.4	15.2	480.9	8.5	98.5		
08KH31-4	167	32999	0.9	17.6713	4.7	0.6099	5.2	0.0782	2.2	0.41	485.2	10.1	483.5	20	475.5	104.8	485.2	10.1	102		
08KH31-5	628	190715	8	14.5372	0.8	1.1702	2.2	0.1234	2	0.94	750	14.4	786.7	11.9	892.4	15.8	750	14.4	84		
08KH31-6	210	115088	0.9	12.7604	1.3	2.0441	1.8	0.1892	1.2	0.67	1116.9	12.1	1130.3	12.1	1156.2	26.3	1156.2	26.3	96.6		
08KH31-7	121	30162	0.8	12.6804	2.7	2.1469	3.2	0.1974	1.6	0.51	1161.6	17.1	1164	22	1168.6	54.1	1168.6	54.1	99.4		
08KH31-8	106	28461	0.4	12.7884	2.1	2.0197	2.5	0.1873	1.3	0.51	1106.9	12.8	1122.2	16.8	1151.8	42.3	1151.8	42.3	96.1		
08KH31-9	338	8257	1.7	23.3822	21.7	0.0652	22.9	0.0111	7.5	0.33	70.9	5.3	64.1	14.2	-181.1	546.2	70.9	5.3	NA		
08KH31-10	613	133889	1.9	10.5705	0.5	2.5999	4.6	0.1993	4.5	0.99	1171.6	48.6	1300.6	33.5	1520.2	10	1520.2	10	77.1		
08KH31-11	157	16583	1.2	17.2135	5.3	0.6303	5.5	0.0787	1.5	0.27	488.3	6.9	496.3	21.6	533.3	116.5	488.3	6.9	91.6		
08KH31-12	389	55011	0.7	17.6917	2.1	0.5971	2.9	0.0766	2	0.69	475.9	9	475.4	10.9	473	46.1	475.9	9	100.6		
08KH31-13	153	65132	4.6	12.7164	1.6	2.1299	1.8	0.1964	0.9	0.51	1156.1	9.9	1158.6	12.7	1163	31.4	1163	31.4	99.4		
08KH31-14	421	79598	6.1	17.41	1.8	0.6176	2.4	0.078	1.6	0.67	484	7.6	488.3	9.4	508.4	39.6	484	7.6	95.2		
08KH31-15	62	67249	0.5	10.2761	3.5	3.1669	13.2	0.236	12.7	0.96	1366	156.3	1449.1	101.9	1573.2	65.3	1573.2	65.3	86.8		
08KH31-16	404	27261	2.4	13.2328	0.8	1.6198	1.2	0.1555	0.9	0.75	931.5	7.8	977.9	7.6	1083.7	16	1083.7	16	86		
08KH31-17	240	9752	1.1	21.3147	19.3	0.173	19.4	0.0267	1.7	0.09	170.1	2.9	162	29.1	44.9	465.5	170.1	2.9	NA		
08KH31-18	422	85429	4.6	12.6487	1	1.9724	1.7	0.1809	1.4	0.8	1072.1	13.6	1106.1	11.6	1173.6	20.6	1173.6	20.6	91.4		
08KH31-19	466	23489	1.2	14.519	1.5	1.1139	12.6	0.1173	12.5	0.99	715	84.8	760	67.6	895	31.1	715	84.8	79.9		
08KH31-20	52	5319	1	14.0668	4.7	1.529	6	0.156	3.6	0.61	934.5	31.4	942.1	36.5	960	96.7	934.5	31.4	97.3		
08KH31-21	285	7197	0.6	27.1593	32.3	0.0581	32.6	0.0115	4.1	0.13	73.4	3	57.4	18.2	-569.7	891.8	73.4	3	NA		
08KH31-22	211	108828	1.8	9.8819	1.9	3.2464	4.2	0.2327	3.8	0.89	1348.5	46.1	1468.3	32.9	1646.1	35.4	1646.1	35.4	81.9		
08KH31-23	429	9085	1.3	22.6268	25.5	0.0701	25.7	0.0115	3.3	0.13	73.7	2.4	68.8	17.1	-99.8	635.2	73.7	2.4	NA		
08KH31-24	187	4100	1.3	22.9822	49.5	0.0433	50.4	0.0072	9.6	0.19	46.3	4.4	43	21.2	-138.2	1297.8	46.3	4.4	NA		
08KH31-25	2558	63802	0.8	21.2261	2.5	0.077	3.1	0.0119	1.7	0.56	76	1.3	75.3	2.2	54.9	60.8	76	1.3	NA		
08KH31-26	279	48545	1.3	17.6359	1.9	0.5922	4.4	0.0757	4	0.9	470.7	18.2	472.3	16.8	480	42.3	470.7	18.2	98.1		

TABLE DR1. NEW U-PB CRYSTALLIZATION AGES (2000 flood @ 10)

Grain	U (ppm)	206Pb 204Pb	U/Th	Isotope ratios							error corr.	Apparent ages (Ma)						Best (Ma)	age ± (Ma)	Conc (Ma)	
				206Pb*	±	207Pb*	±	206Pb*	±	207Pb*		±	206Pb*	±	207Pb*	±	206Pb*				±
				207Pb*	(%)	235U*	(%)	238U	(%)	238U*		(Ma)	235U	(Ma)	207Pb*	(Ma)					
08KH31-27	497	15297	0.9	22.1659	12.7	0.0726	12.8	0.0117	1.7	0.13	74.8	1.2	71.2	8.8	-49.5	309	74.8	1.2	NA		
08KH31-28	140	63113	1.6	13.5824	2	1.735	2.3	0.1709	1.2	0.51	1017.1	11.1	1021.6	15	1031.2	40.6	1031.2	40.6	98.6		
08KH31-29	275	19695	1.3	17.0189	5.6	0.5841	21.2	0.0721	20.5	0.96	448.8	88.8	467.1	79.7	558.2	122.6	448.8	88.8	80.4		
08KH31-30	315	47027	1	13.6668	1.3	1.5819	4.7	0.1568	4.6	0.96	939	39.9	963.1	29.5	1018.6	26.3	939	39.9	92.2		
08KH31-31	224	125478	2.3	13.634	1.6	1.6539	2.1	0.1635	1.3	0.64	976.4	12	991	13.2	1023.5	32.5	976.4	12	95.4		
08KH31-32	2063	87047	2.4	21.1027	4.5	0.0742	5.2	0.0114	2.6	0.5	72.8	1.9	72.6	3.6	68.8	106.4	72.8	1.9	NA		
08KH31-33	40	23546	1.6	10.2273	3.1	3.6059	3.9	0.2675	2.3	0.58	1527.9	30.9	1550.8	30.8	1582.2	58.9	1582.2	58.9	96.6		
08KH31-34	466	13527	0.9	19.0583	11.2	0.0865	11.6	0.012	2.9	0.25	76.6	2.2	84.2	9.4	306	256.9	76.6	2.2	NA		
08KH31-35	263	8826	3.4	22.1956	17.6	0.0869	27.2	0.014	20.7	0.76	89.6	18.4	84.6	22.1	-52.7	432.4	89.6	18.4	NA		
08KH31-36	94	17046	1.9	16.1478	7.7	0.8557	10.2	0.1002	6.8	0.66	615.7	39.9	627.8	48	671.6	164	615.7	39.9	91.7		
08KH31-37	116	60735	0.9	12.322	1.2	2.3355	3.9	0.2087	3.7	0.95	1222	41.4	1223.2	27.8	1225.2	23.7	1225.2	23.7	99.7		
08KH31-38	168	81305	1.8	13.0199	1.5	1.9583	2.2	0.1849	1.6	0.72	1093.8	15.6	1101.3	14.6	1116.2	30.2	1116.2	30.2	98		
08KH31-39	775	18181	1.4	21.4372	6.1	0.0748	6.6	0.0116	2.4	0.37	74.5	1.8	73.2	4.6	31.2	146	74.5	1.8	NA		
08KH31-40	299	7604	1.2	22.8271	16.8	0.1064	17.1	0.0176	3.3	0.19	112.5	3.7	102.6	16.7	-121.5	416.6	112.5	3.7	NA		
08KH31-41	511	13443	1	20.3223	11.8	0.0785	12.1	0.0116	2.4	0.2	74.1	1.8	76.7	8.9	157.7	277.6	74.1	1.8	NA		
08KH31-42	791	23855	1.3	20.1355	4.8	0.1227	5.2	0.0179	2	0.38	114.5	2.3	117.5	5.8	179.2	112.7	114.5	2.3	NA		
08KH31-43	795	20509	1.9	18.0798	5.7	0.0989	9.6	0.013	7.8	0.8	83.1	6.4	95.8	8.8	424.8	127.9	83.1	6.4	NA		
08KH31-44	395	8611	5.4	51.187	91.7	0.0178	91.9	0.0066	5.4	0.06	42.5	2.3	17.9	16.3	NA	NA	42.5	2.3	NA		
08KH31-45	3591	74674	4.6	21.473	4	0.0489	4.3	0.0076	1.7	0.39	48.9	0.8	48.5	2.1	27.3	95.9	48.9	0.8	NA		
08KH31-46	539	201134	3.3	16.9615	1.4	0.7406	2.3	0.0911	1.8	0.8	562.1	9.9	562.8	9.8	565.5	29.6	562.1	9.9	99.4		
08KH31-46	78	16659	0.5	12.822	2.5	2.0427	6.3	0.19	5.8	0.92	1121.1	59.6	1129.9	43.2	1146.6	50.6	1146.6	50.6	97.8		
08KH31-47	283	188458	1.4	9.8851	0.6	3.7651	2.5	0.2699	2.4	0.96	1540.5	32.5	1585.3	19.8	1645.5	12	1645.5	12	93.6		
08KH31-49	416	170259	1.5	13.4758	1.1	1.7082	1.6	0.1669	1.2	0.75	995.3	11.1	1011.6	10.2	1047.1	21.2	1047.1	21.2	95		
08KH31-50	433	72632	1.2	12.6286	1.2	2.0641	4.7	0.1891	4.5	0.97	1116.3	46.5	1137	32.1	1176.8	23.8	1176.8	23.8	94.9		
08KH31-51	141	87504	1.2	10.2844	1	3.7139	1.8	0.277	1.5	0.83	1576.3	20.4	1574.4	14.1	1571.7	18.7	1571.7	18.7	100.3		
08KH31-52	344	142172	0.8	12.6472	0.6	2.1051	1.7	0.1931	1.6	0.93	1138.1	16.8	1150.5	11.9	1173.9	12.3	1173.9	12.3	97		

TABLE DR1. NEW U-PB CRYSTALLIZATION AGES (2000 flood @ 10)

Grain	U (ppm)	206Pb 204Pb	U/Th	Isotope ratios							error corr.	Apparent ages (Ma)						Best (Ma)	age ± (Ma)	Conc (Ma)	
				206Pb*	±	207Pb*	±	206Pb*	±	207Pb*		±	206Pb*	±	207Pb*	±	206Pb*				±
				207Pb*	(%)	235U*	(%)	238U	(%)	238U*		(Ma)	235U	(Ma)	207Pb*	(Ma)					
08KH31-53	377	5572	1.2	22.3083	47.6	0.0519	47.8	0.0084	4.2	0.09	53.9	2.3	51.4	23.9	-65.1	1224	53.9	2.3	NA		
08KH31-54	143	4730	1.2	29.1469	34.4	0.0922	35	0.0195	6.3	0.18	124.5	7.7	89.6	30	-764.4	992.1	124.5	7.7	NA		
08KH31-55	55	1110	0.7	17.2579	103	0.1059	104	0.0133	16.7	0.16	84.9	14	102.2	101.4	527.7	654.2	84.9	14	NA		
08KH31-56	121	15969	2.2	17.3355	10.9	0.7015	14.2	0.0882	9.1	0.64	544.9	47.6	539.7	59.7	517.8	241	544.9	47.6	105.2		
08KH31-57	264	156917	2.2	14.2271	1.8	1.3879	3.5	0.1432	3	0.86	862.8	24.1	883.8	20.6	936.8	36.8	862.8	24.1	92.1		
08KH31-59	328	50764	1.5	17.7977	2.4	0.5935	2.9	0.0766	1.6	0.55	475.8	7.2	473.1	10.8	459.8	53.1	475.8	7.2	103.5		
08KH31-60	576	12517	2.8	11.0513	1.5	2.888	3.3	0.2315	3	0.89	1342.3	35.8	1378.8	25.1	1435.8	29.3	1435.8	29.3	93.5		
08KH31-61	2274	36253	26.7	23.3232	12.9	0.023	13.5	0.0039	3.8	0.28	25	0.9	23.1	3.1	-174.8	323.3	25	0.9	NA		
08KH31-62	186	50793	1.2	12.6995	0.9	2.1368	1.9	0.1968	1.6	0.88	1158.2	17.3	1160.8	12.9	1165.7	17.6	1165.7	17.6	99.4		
08KH31-63	420	115355	0.9	17.462	2.1	0.7233	2.7	0.0916	1.7	0.62	565	9	552.6	11.5	501.8	46.8	565	9	112.6		
08KH31-64	57	3122	1.1	-7.7601	267	-0.2058	267.7	0.0116	21.2	0.08	74.2	15.6	-233.9	-868	NA	NA	74.2	15.6	NA		
08KH31-65	247	13682	1.4	12.6345	1.6	2.1102	3.3	0.1934	2.8	0.87	1139.6	29.6	1152.2	22.5	1175.9	32.3	1175.9	32.3	96.9		
08KH31-66	43	17427	1	12.5066	8.2	2.2588	13.2	0.2049	10.3	0.78	1201.5	113.4	1199.5	93.2	1195.9	161.9	1195.9	161.9	100.5		
08KH31-67	268	8424	1.3	21.444	13.1	0.0762	14	0.0118	4.9	0.35	75.9	3.7	74.6	10.1	30.5	315.6	75.9	3.7	NA		
08KH31-68	354	5717	3.3	22.8718	26.2	0.0474	27.3	0.0079	7.8	0.28	50.5	3.9	47	12.6	-126.3	656.9	50.5	3.9	NA		
08KH31-69	130	41466	1.5	9.8733	1.2	4.0359	1.7	0.289	1.2	0.69	1636.6	16.8	1641.5	13.6	1647.7	22.4	1647.7	22.4	99.3		
08KH31-70	195	60685	1.1	10.3773	0.8	3.4204	3.9	0.2574	3.8	0.98	1476.7	49.8	1509.1	30.3	1554.9	15	1554.9	15	95		
08KH31-71	38	8582	1.3	16.1853	21.4	0.7947	22.3	0.0933	6.1	0.27	575	33.5	593.8	100.5	666.6	463.9	575	33.5	86.2		
08KH31-73	1248	40572	1.3	20.476	3.5	0.0814	9.3	0.0121	8.6	0.92	77.5	6.6	79.5	7.1	140.1	83.4	77.5	6.6	NA		
08KH31-74	242	88675	1.5	17.6802	4.8	0.6211	5.7	0.0796	3	0.53	494	14.4	490.5	22.1	474.4	106.2	494	14.4	104.1		
08KH31-75	240	46893	1.5	17.7609	2.2	0.6013	2.7	0.0775	1.6	0.59	480.9	7.5	478.1	10.4	464.4	48.8	480.9	7.5	103.6		
08KH31-76	190	97078	0.9	9.8791	0.6	3.9793	4.8	0.2851	4.8	0.99	1617.1	68.3	1630	39	1646.7	10.2	1646.7	10.2	98.2		
08KH31-77	147	44100	0.6	13.461	1.5	1.8956	2.8	0.1851	2.3	0.84	1094.6	23.6	1079.6	18.5	1049.3	30.2	1049.3	30.2	104.3		
08KH31-78	426	5300	5.2	13.1864	4.3	1.4186	17.1	0.1357	16.6	0.97	820.1	127.7	896.8	102.3	1090.7	86.3	820.1	127.7	75.2		
08KH31-79	815	2489	0.8	17.2514	4.2	0.5517	10.9	0.069	10	0.92	430.3	41.8	446.1	39.2	528.5	91.4	430.3	41.8	81.4		
08KH31-81	111	2309	0.9	8.8421	158	0.1081	157.8	0.0069	7.1	0.05	44.5	3.2	104.3	157.6	1849.7	58.3	44.5	3.2	NA		

TABLE DR1. NEW U-PB CRYSTALLIZATION AGES (2000 flood @ 10)

Grain	U (ppm)	206Pb 204Pb	U/Th	Isotope ratios							error corr.	Apparent ages (Ma)						Best (Ma)	age ± (Ma)	Conc (Ma)	
				206Pb*	±	207Pb*	±	206Pb*	±	207Pb*		±	206Pb*	±	207Pb*	±	206Pb*				±
				207Pb*	(%)	235U*	(%)	238U	(%)	238U*		(Ma)	235U	(Ma)	207Pb*	(Ma)					
08KH31-82	413	7232	1.3	23.1421	15.1	0.071	15.6	0.0119	4.1	0.26	76.4	3.1	69.7	10.5	-155.4	376.6	76.4	3.1	NA		
08KH31-83	379	5854	6.2	27.8829	30	0.0403	30.4	0.0082	4.5	0.15	52.4	2.3	40.2	12	-641.2	838.9	52.4	2.3	NA		
08KH31-84	509	17686	10.6	16.7279	5.6	0.2957	10.8	0.0359	9.3	0.86	227.2	20.8	263	25.1	595.6	120.4	227.2	20.8	NA		
08KH31-85	93	50438	1.4	10.2307	1.3	3.7986	2.8	0.2819	2.5	0.88	1600.7	35.4	1592.5	22.7	1581.5	24.6	1581.5	24.6	101.2		
08KH31-86	74	42694	1.3	11.3433	3.5	2.932	4.8	0.2412	3.3	0.69	1393	40.9	1390.2	36	1385.9	66.3	1385.9	66.3	100.5		
08KH31-88	775	8064	2.5	12.3229	1.8	2.2139	2.5	0.1979	1.7	0.68	1163.8	17.9	1185.4	17.4	1225.1	36.1	1225.1	36.1	95		
08KH31-89	537	105368	1.2	10.4372	0.4	2.5771	2.8	0.1951	2.8	0.99	1148.8	29.1	1294.2	20.4	1544.1	7	1544.1	7	74.4		
08KH31-90	538	26090	7.8	15.5874	3.8	0.524	9.7	0.0592	8.9	0.92	371	32.2	427.8	33.9	746.7	79.9	371	32.2	NA		
08KH31-92	902	13530	2.7	11.9801	1.1	2.1951	2.6	0.1907	2.4	0.9	1125.3	24.6	1179.5	18.4	1280.3	22.1	1280.3	22.1	87.9		
08KH31-93	1003	9999	8.1	19.6888	2.2	0.2335	2.6	0.0333	1.2	0.48	211.4	2.6	213.1	4.9	231.3	51.9	211.4	2.6	NA		
08KH31-95	223	57858	1.4	13.6285	1.2	1.7818	2.1	0.1761	1.7	0.81	1045.7	16.1	1038.8	13.5	1024.3	24.9	1024.3	24.9	102.1		
08KH31-96	212	6163	0.8	23.8858	37.3	0.0509	37.5	0.0088	3.6	0.1	56.6	2.1	50.4	18.4	-234.6	969.7	56.6	2.1	NA		
08KH31-97	371	201229	2.3	8.2413	0.3	4.7113	3	0.2816	3	0.99	1599.4	42.9	1769.2	25.5	1976	5.6	1976	5.6	80.9		
08KH31-98	240	44196	2.1	16.0332	2.5	0.6181	6	0.0719	5.4	0.91	447.4	23.5	488.7	23.3	686.9	54.2	447.4	23.5	65.1		
08KH31-99	2192	711168	39.3	9.9281	0.1	3.6955	1.5	0.2661	1.5	1	1520.9	19.9	1570.4	11.8	1637.5	1.2	1637.5	1.2	92.9		
08KH31-100	582	13851	0.9	19.311	15.9	0.0835	16.2	0.0117	2.9	0.18	75	2.2	81.4	12.7	275.9	367.3	75	2.2	NA		
08KH31-101	202	28608	6.6	16.0373	5	0.6458	6	0.0751	3.3	0.56	466.9	15	505.9	23.9	686.3	106.5	466.9	15	68		
08KH31-102	271	35091	0.8	17.7538	3.6	0.5876	4.6	0.0757	2.9	0.62	470.2	13	469.3	17.4	465.2	80.4	470.2	13	101.1		
08KH31-104	1120	10970	1.2	20.2761	9.8	0.0574	13.8	0.0084	9.7	0.71	54.1	5.3	56.6	7.6	163	229.1	54.1	5.3	NA		
08KH31-105	322	63288	5.5	16.9448	2.3	0.7568	4	0.093	3.2	0.8	573.3	17.4	572.2	17.3	567.7	51.1	573.3	17.4	101		
08KH31-106	63	123548	1.6	4.9022	0.6	15.334	1.6	0.5452	1.5	0.93	2805.1	34.8	2836.2	15.7	2858.4	9.8	2858.4	9.8	98.1		
08KH31-107	1301	75126	30.7	20.2654	3.1	0.1511	5.6	0.0222	4.7	0.84	141.6	6.6	142.9	7.5	164.2	71.7	141.6	6.6	NA		
08KH31-108	682	22103	4.3	14.4538	1.1	0.9302	6.7	0.0975	6.6	0.99	599.8	37.9	667.8	32.8	904.3	23.3	599.8	37.9	66.3		
08KH31-109	485	412094	6	12.0914	1	2.2125	8.7	0.194	8.7	0.99	1143.1	90.7	1185	61	1262.2	18.9	1262.2	18.9	90.6		

TABLE DR1. NEW U-PB CRYSTALLIZATION AGES (2000 flood @ 10)

Grain	U (ppm)	206Pb 204Pb	U/Th	Isotope ratios							error corr.	Apparent ages (Ma)						Best (Ma)	age ± (Ma)	Conc (Ma)	
				206Pb*	±	207Pb*	±	206Pb*	±	207Pb*		±	206Pb*	±	207Pb*	±	206Pb*				±
				207Pb*	(%)	235U*	(%)	238U	(%)	238U*		(Ma)	235U	(Ma)	207Pb*	(Ma)					
08KH31-110	1720	12401	2.9	21.0117	6.6	0.0504	6.9	0.0077	2.1	0.3	49.4	1	50	3.4	79	157.2	49.4	1	NA		
08KH31-111	592	8104	3.8	21.9072	28.8	0.0537	29	0.0085	3.6	0.12	54.7	2	53.1	15	-21	708.8	54.7	2	NA		
08KH31-112	861	394647	1.4	10.436	1	2.9649	1.6	0.2244	1.3	0.8	1305.1	15.6	1398.7	12.5	1544.3	18.5	1544.3	18.5	84.5		
08KH31-113	127	3581	1.5	3.5429	645	0.3402	645.1	0.0087	11.3	0.02	56.1	6.3	297.3	#####	3375.4	246.5	56.1	6.3	NA		
08KH31-114	188	18572	0.3	24.361	28.2	0.0629	28.5	0.0111	4.4	0.15	71.3	3.1	62	17.2	-284.5	730.6	71.3	3.1	NA		
08KH31-115	523	134207	4.1	12.8797	0.5	1.9294	2.5	0.1802	2.4	0.98	1068.2	24.1	1091.3	16.7	1137.7	9.6	1137.7	9.6	93.9		
08KH31-116	135	2186	1.4	22.4814	50.5	0.0521	51.7	0.0085	11.3	0.22	54.5	6.1	51.5	26	-84	1312.6	54.5	6.1	NA		
08KH31-117	577	46496	25.8	18.0744	17.5	0.0707	19.2	0.0093	8	0.42	59.5	4.7	69.4	12.9	425.4	392.3	59.5	4.7	NA		
08KH31-118	112	77408	1.7	8.179	0.7	6.4235	3.4	0.381	3.3	0.98	2081.1	59.5	2035.5	30.1	1989.5	13	1989.5	13	104.6		
08KH31-119	987	4998	13.1	12.7932	1.1	0.963	5.1	0.0894	5	0.98	551.7	26.3	684.9	25.3	1151.1	21	551.7	26.3	47.9		
08KH31-120	145	151636	0.3	9.243	1	4.7935	17.5	0.3213	17.4	1	1796.3	273.6	1783.8	147.8	1769.1	18.4	1769.1	18.4	101.5		

TABLE DR1. NEW U-PB CRYSTALLIZATION AGES (Megaflood @ 9)

Grain	U (ppm)	206Pb 204Pb	U/Th	Isotope ratios							error corr.	Apparent ages (Ma)						Best (Ma)	age ± (Ma)	Conc (Ma)	
				206Pb*	±	207Pb*	±	206Pb*	±	207Pb*		±	206Pb*	±	207Pb*	±	206Pb*				±
				207Pb*	(%)	235U*	(%)	238U	(%)	238U*		(Ma)	235U	(Ma)	207Pb*	(Ma)					
08KH28-1	97	16692	0.6	17.5661	6.7	0.6103	6.8	0.0777	1.5	0.22	482.7	6.9	483.7	26.3	488.7	147.4	482.7	6.9	98.8		
08KH28-2	3208	78414	4.4	20.7747	1.8	0.0589	2.5	0.0089	1.8	0.7	56.9	1	58.1	1.4	105.9	42.5	56.9	1	NA		
08KH28-3	1132	13397	123.1	21.0487	11.4	0.0316	11.6	0.0048	2	0.17	31	0.6	31.6	3.6	74.9	271.9	31	0.6	NA		
08KH28-4	623	553850	9.9	9.8588	0.3	3.3929	1.9	0.2426	1.8	0.99	1400.2	23	1502.8	14.5	1650.5	5.6	1650.5	5.6	84.8		
08KH28-5	758	21949	2	20.9625	5.8	0.0633	6	0.0096	1.7	0.28	61.8	1.1	62.3	3.7	84.6	137.5	61.8	1.1	NA		
08KH28-6	1853	162002	1.1	17.4616	0.9	0.5986	3.7	0.0758	3.5	0.97	471	16.1	476.3	13.9	501.9	20.5	471	16.1	93.9		
08KH28-7	891	15401	2.1	23.2503	13.3	0.0316	13.4	0.0053	2.2	0.16	34.2	0.7	31.6	4.2	-167	331.4	34.2	0.7	NA		
08KH28-8	346	461015	1.6	9.9364	0.2	3.773	1.9	0.2719	1.9	0.99	1550.4	25.8	1587	15.1	1635.9	3.7	1635.9	3.7	94.8		
08KH28-9	1301	9603	22	22.2488	18.5	0.0133	18.9	0.0021	4.3	0.23	13.8	0.6	13.4	2.5	-58.5	453	13.8	0.6	NA		
08KH28-10	127	9837	0.9	23.8827	19.6	0.1111	20	0.0192	4.3	0.21	122.8	5.2	106.9	20.3	-234.2	498.1	122.8	5.2	NA		
08KH28-11	171	85384	0.9	14.875	1.8	1.3019	3.9	0.1405	3.5	0.88	847.2	27.7	846.6	22.7	844.8	38.3	847.2	27.7	100.3		
08KH28-12	397	12934	1.2	25.6535	36	0.047	36.1	0.0087	2.6	0.07	56.1	1.5	46.6	16.4	-418	967.5	56.1	1.5	NA		
08KH28-13	919	251620	10.1	15.4663	1.5	0.9589	2.7	0.1076	2.2	0.83	658.6	13.9	682.7	13.3	763.2	31.5	658.6	13.9	86.3		
08KH28-14	1331	189480	9.7	16.8304	0.3	0.7377	1.8	0.0901	1.8	0.99	555.8	9.5	561.1	7.8	582.4	6.1	555.8	9.5	95.4		
08KH28-15	2383	32896	1.5	20.9485	3.7	0.039	4	0.0059	1.6	0.39	38.1	0.6	38.8	1.5	86.2	86.6	38.1	0.6	NA		
08KH28-16	615	7423	1.2	17.7558	6.3	0.064	8	0.0082	4.9	0.61	52.9	2.6	63	4.9	465	139.4	52.9	2.6	NA		
08KH28-17	474	60756	1.9	17.301	2.8	0.5894	6.9	0.074	6.3	0.91	460	27.9	470.5	25.9	522.2	62	460	27.9	88.1		
08KH28-19	1932	6938	0.6	19.1327	9	0.028	9.3	0.0039	2.2	0.23	25	0.5	28	2.6	297.1	206.7	25	0.5	NA		
08KH28-20	1549	4354	12.7	16.9427	2.8	0.1857	9.5	0.0228	9	0.95	145.5	13	173	15.1	567.9	62	145.5	13	NA		
08KH28-21	183	87285	1.4	10.2054	1	2.9174	6.8	0.2159	6.7	0.99	1260.4	76.9	1386.4	51.5	1586.2	19.4	1586.2	19.4	79.5		
08KH28-22	610	121882	11.4	15.7216	0.6	0.8728	2.2	0.0995	2.1	0.96	611.6	12.3	637.1	10.4	728.6	13.6	611.6	12.3	83.9		
08KH28-23	70	17836	1.2	13.5717	3.7	1.766	24.4	0.1738	24.1	0.99	1033.2	229.9	1033.1	159.2	1032.8	75.3	1032.8	75.3	100		
08KH28-25	67	3806	1.2	24.6165	24.6	0.1579	25.5	0.0282	6.8	0.27	179.2	12.1	148.9	35.3	-311.2	637.5	179.2	12.1	NA		
08KH28-26	133	51661	1.5	14.0994	1.4	1.5639	2.2	0.1599	1.6	0.76	956.4	14.5	956	13.3	955.2	28.7	956.4	14.5	100.1		
08KH28-27	627	123834	4.5	17.3281	1	0.6302	2.4	0.0792	2.1	0.91	491.3	10.2	496.2	9.2	518.7	20.9	491.3	10.2	94.7		
08KH28-28	2772	44100	23	20.9943	7.4	0.0175	7.6	0.0027	1.7	0.23	17.2	0.3	17.7	1.3	81	175.4	17.2	0.3	NA		

TABLE DR1. NEW U-PB CRYSTALLIZATION AGES (Megaflood @ 9)

Grain	U (ppm)	206Pb 204Pb	U/Th	Isotope ratios							error corr.	Apparent ages (Ma)						Best (Ma)	age ± (Ma)	Conc (Ma)	
				206Pb*	±	207Pb*	±	206Pb*	±	207Pb*		±	206Pb*	±	207Pb*	±	206Pb*				±
				207Pb*	(%)	235U*	(%)	238U	(%)	238U*		(Ma)	235U	(Ma)	207Pb*	(Ma)					
08KH28-29	936	125426	5.7	13.6283	0.8	0.679	10.1	0.0671	10	1	418.7	40.7	526.1	41.4	1024.4	17	418.7	40.7	40.9		
08KH28-30	272	12611	0.5	19.7368	7.7	0.138	8.1	0.0198	2.4	0.3	126.1	3	131.3	10	225.7	178.8	126.1	3	NA		
08KH28-31	473	11282	0.9	21.8387	15.4	0.0487	15.8	0.0077	3.6	0.23	49.6	1.8	48.3	7.5	-13.4	373.3	49.6	1.8	NA		
08KH28-32	729	25042	0.7	20.8679	3.8	0.0655	4.1	0.0099	1.6	0.38	63.6	1	64.4	2.5	95.4	89.3	63.6	1	NA		
08KH28-33	451	14896	2.2	24.795	13	0.0587	13.8	0.0106	4.6	0.33	67.7	3.1	57.9	7.8	-329.7	335.1	67.7	3.1	NA		
08KH28-34	343	17318	3	16.8055	11.3	0.25	13.5	0.0305	7.3	0.54	193.5	14	226.5	27.4	585.6	246.2	193.5	14	NA		
08KH28-36	820	67934	0.9	20.848	4.1	0.1111	4.5	0.0168	1.9	0.42	107.4	2	107	4.5	97.6	96.2	107.4	2	NA		
08KH28-37	361	18096	1.5	18.8013	9.4	0.111	12	0.0151	7.5	0.63	96.9	7.3	106.9	12.2	336.8	212.2	96.9	7.3	NA		
08KH28-38	860	244153	1.1	17.3821	1	0.6406	2.8	0.0808	2.7	0.94	500.7	12.8	502.7	11.2	511.9	20.9	500.7	12.8	97.8		
08KH28-39	411	192926	3.8	14.6386	0.5	1.2731	1.9	0.1352	1.8	0.97	817.3	13.8	833.8	10.6	878	9.4	817.3	13.8	93.1		
08KH28-40	83	5966	1.9	19.7981	14.1	0.1933	15.5	0.0278	6.4	0.41	176.5	11.1	179.4	25.4	218.5	327.6	176.5	11.1	NA		
08KH28-41	406	105968	1.2	12.5725	0.4	2.167	1.5	0.1976	1.4	0.97	1162.4	15	1170.5	10.1	1185.6	7	1185.6	7	98		
08KH28-42	1407	12736	5.4	17.3892	1	0.2841	3.2	0.0358	3	0.95	227	6.8	253.9	7.2	511	22.1	227	6.8	NA		
08KH28-43	313	214628	5	11.4335	0.6	2.7384	3.6	0.2271	3.6	0.99	1319.2	42.4	1338.9	26.7	1370.7	10.8	1370.7	10.8	96.2		
08KH28-44	530	7442	1	25.7205	37.4	0.0267	37.8	0.005	5.2	0.14	32.1	1.7	26.8	10	-424.9	1011	32.1	1.7	NA		
08KH28-46	280	7143	0.7	24.9118	21.4	0.0437	22.5	0.0079	6.8	0.3	50.7	3.5	43.4	9.6	-341.8	556.7	50.7	3.5	NA		
08KH28-47	260	30542	2.8	17.8905	3.9	0.2393	9.9	0.0311	9.1	0.92	197.1	17.7	217.9	19.4	448.2	85.7	197.1	17.7	NA		
08KH28-48	350	33270	2.2	17.3065	2.2	0.3819	6	0.0479	5.5	0.93	301.8	16.3	328.4	16.8	521.5	49	301.8	16.3	NA		
08KH28-49	811	13412	1.1	22.7189	6.7	0.0655	7	0.0108	2	0.29	69.2	1.4	64.4	4.4	-109.8	164.4	69.2	1.4	NA		
08KH28-50	267	9933	1.4	23.9835	16.8	0.0746	17.1	0.013	3	0.18	83.1	2.5	73	12.1	-244.9	428.3	83.1	2.5	NA		
08KH28-101	675	68569	3.1	19.7069	3.4	0.2341	4.2	0.0335	2.4	0.57	212.2	5	213.6	8	229.2	78.9	212.2	5	NA		
08KH28-102	746	33539	4.7	19.7135	3.2	0.1831	5.2	0.0262	4.1	0.79	166.6	6.7	170.8	8.1	228.5	73.9	166.6	6.7	NA		
08KH28-104	1296	1311685	4.2	10.4126	1	3.0376	3.3	0.2294	3.1	0.95	1331.3	37.9	1417.1	25.2	1548.5	18.5	1548.5	18.5	86		
08KH28-105	1291	363327	21.7	15.2026	1.1	0.8822	3.2	0.0973	3	0.94	598.4	16.9	642.2	15	799.3	23.4	598.4	16.9	74.9		
08KH28-109	2022	796347	142.8	13.5867	10.5	0.9474	13.5	0.0934	8.4	0.63	575.4	46.5	676.8	66.8	1030.5	213.6	575.4	46.5	55.8		

TABLE DR1. NEW U-PB CRYSTALLIZATION AGES (Megaflood @ 9)

Grain	U (ppm)	206Pb 204Pb	U/Th	Isotope ratios							error corr.	Apparent ages (Ma)						Best (Ma)	age ± (Ma)	Conc (Ma)	
				206Pb*	±	207Pb*	±	206Pb*	±	207Pb*		±	206Pb*	±	207Pb*	±	206Pb*				±
				207Pb*	(%)	235U*	(%)	238U	(%)	238U*		(Ma)	235U	(Ma)	207Pb*	(Ma)					
08KH28-110	346	112433	1.8	15.0378	1.3	1.2214	2.6	0.1332	2.3	0.87	806.2	17.3	810.4	14.6	822.1	26.7	806.2	17.3	98.1		
08KH28-111	648	151087	2.7	15.0654	0.4	1.073	3.1	0.1172	3	0.99	714.6	20.5	740.2	16.1	818.3	8.4	714.6	20.5	87.3		
08KH28-112	722	75823	9.3	17.3604	1.3	0.266	8.2	0.0335	8.1	0.99	212.4	17	239.5	17.6	514.7	28.3	212.4	17	NA		
08KH28-113	606	32887	1.4	17.4878	4.7	0.2275	11.7	0.0289	10.7	0.91	183.4	19.3	208.1	22	498.6	103.8	183.4	19.3	NA		
08KH28-114	522	5897	2.7	21.8353	11.9	0.0467	12.7	0.0074	4.4	0.35	47.5	2.1	46.4	5.7	-13	287.7	47.5	2.1	NA		
08KH28-115	794	83468	20.8	13.4539	4.4	0.5371	10	0.0524	8.9	0.9	329.3	28.7	436.5	35.5	1050.4	89.6	329.3	28.7	NA		
08KH28-116	38	38832	0.7	11.5651	4.5	2.7186	5.5	0.228	3.1	0.57	1324.2	37.5	1333.6	40.6	1348.6	86.5	1348.6	86.5	98.2		
08KH28-118	772	191033	1.2	16.8034	9	0.6082	10.9	0.0741	6.3	0.57	460.9	27.9	482.4	42	585.9	194.9	460.9	27.9	78.7		
08KH28-119	564	149231	2.8	15.0929	1.1	1.0545	2.5	0.1154	2.2	0.9	704.2	14.9	731.1	12.9	814.5	23.1	704.2	14.9	86.5		
08KH28-121	869	77417	3.6	17.6226	0.5	0.5943	4.7	0.076	4.7	0.99	472	21.2	473.6	17.7	481.6	10.8	472	21.2	98		
08KH28-122	495	152264	4.8	12.7291	2.2	1.7561	2.7	0.1621	1.6	0.58	968.6	14.1	1029.4	17.5	1161.1	43.5	1161.1	43.5	83.4		
08KH28-123	513	172264	5.9	12.5551	0.4	1.8107	2.4	0.1649	2.4	0.98	983.8	21.8	1049.3	15.9	1188.3	8.7	1188.3	8.7	82.8		
08KH28-124	140	89614	1.9	10.9664	1.1	3.3017	7.3	0.2626	7.2	0.99	1503.2	96.3	1481.5	56.7	1450.5	21	1450.5	21	103.6		
08KH28-125	362	33023	1	12.5356	1.6	2.066	2.1	0.1878	1.4	0.67	1109.6	14.7	1137.6	14.7	1191.4	31.3	1191.4	31.3	93.1		
08KH28-126	345	53905	3.5	16.0894	2.7	0.6284	7.4	0.0733	6.9	0.93	456.2	30.6	495.1	29.2	679.3	57.4	456.2	30.6	67.1		
08KH28-127	433	141934	5.1	17.7325	2.3	0.6159	3.2	0.0792	2.2	0.7	491.4	10.6	487.2	12.4	467.9	50.8	491.4	10.6	105		
08KH28-128	1171	145535	27.1	15.834	2.2	0.6596	13.9	0.0757	13.8	0.99	470.7	62.5	514.4	56.3	713.5	46.4	470.7	62.5	66		
08KH28-129	781	277591	77.4	15.2505	0.5	0.9846	8.3	0.1089	8.3	1	666.4	52.6	696	42	792.7	9.7	666.4	52.6	84.1		
08KH28-131	785	487477	2.4	15.0495	0.8	1.2639	7.1	0.138	7	0.99	833.1	55	829.7	40.1	820.5	16	833.1	55	101.5		
08KH28-132	269	44808	1.5	17.4941	2.9	0.61	7.1	0.0774	6.5	0.91	480.6	30	483.6	27.2	497.8	63.3	480.6	30	96.5		
08KH28-133	97	121387	1.6	4.954	0.8	15.7769	5.1	0.5669	5	0.99	2894.9	117.7	2863.4	48.9	2841.3	13.4	2841.3	13.4	101.9		
08KH28-134	242	14473	1.6	19.557	9	0.2146	10.7	0.0304	5.7	0.53	193.3	10.8	197.4	19.2	246.8	208.5	193.3	10.8	NA		

TABLE DR1. NEW U-PB CRYSTALLIZATION AGES (Megaflood @ 9)

Grain	U (ppm)	206Pb 204Pb	U/Th	Isotope ratios							error corr.	Apparent ages (Ma)						Best (Ma)	age ± (Ma)	Conc (Ma)	
				206Pb*	±	207Pb*	±	206Pb*	±	207Pb*		±	206Pb*	±	207Pb*	±	206Pb*				±
				207Pb*	(%)	235U*	(%)	238U	(%)	238U*		(Ma)	235U	(Ma)	207Pb*	(Ma)					
08KH28-135	944	20916	3.2	19.5169	3.6	0.234	4.5	0.0331	2.7	0.6	210.1	5.5	213.5	8.6	251.6	82.2	210.1	5.5	NA		
08KH28-136	321	117037	1.2	11.9503	0.7	2.4805	1.9	0.215	1.8	0.94	1255.3	20	1266.4	13.6	1285.1	12.9	1285.1	12.9	97.7		
08KH28-137	96	60452	0.4	12.4661	1.5	2.0797	3.3	0.188	2.9	0.89	1110.7	30	1142.1	22.6	1202.3	29.4	1202.3	29.4	92.4		
08KH28-138	1308	4706	0.8	20.0873	15.2	0.0525	16.1	0.0076	5.3	0.33	49.1	2.6	51.9	8.2	184.8	356.6	49.1	2.6	NA		
08KH28-139	769	539299	8.3	15.2439	1.1	1.0781	4	0.1192	3.8	0.96	725.9	26.4	742.7	21.1	793.6	23.1	725.9	26.4	91.5		
08KH28-140	327	93328	1.8	13.2477	0.7	1.8459	2.3	0.1774	2.2	0.96	1052.5	21.6	1062	15.3	1081.4	13.5	1081.4	13.5	97.3		
08KH28-141	779	26375	3.3	20.2621	7.3	0.0891	7.5	0.0131	1.8	0.24	83.8	1.5	86.6	6.2	164.6	170.2	83.8	1.5	NA		
08KH28-142	333	3699	1.7	22.6842	31.7	0.0306	33.9	0.005	11.8	0.35	32.4	3.8	30.6	10.2	-106	798	32.4	3.8	NA		
08KH28-143	467	87609	1.4	17.3442	1.6	0.6364	3.4	0.0801	3	0.88	496.4	14.4	500.1	13.5	516.7	35.9	496.4	14.4	96.1		
08KH28-144	1323	16943	1.1	20.6399	5.2	0.0542	6.4	0.0081	3.7	0.57	52.1	1.9	53.6	3.3	121.3	123.1	52.1	1.9	NA		
08KH28-145	321	7691	1.2	24.9313	17.2	0.0959	17.4	0.0173	2.9	0.17	110.8	3.2	93	15.5	-343.8	445.9	110.8	3.2	NA		
08KH28-147	67	5081	1.6	25.6083	30.6	0.1573	30.9	0.0292	4.5	0.14	185.6	8.2	148.3	42.7	-413.4	815.9	185.6	8.2	NA		
08KH28-148	522	24277	13.1	10.8414	0.9	1.0466	4.5	0.0823	4.4	0.98	509.8	21.5	727.2	23.2	1472.3	16.2	509.8	21.5	34.6		
08KH28-149	168	104217	1.2	10.5561	0.9	3.2196	5.3	0.2465	5.3	0.99	1420.4	67	1461.9	41.3	1522.7	16.2	1522.7	16.2	93.3		
08KH28-150	820	26869	37.4	6.0522	8.3	0.3992	10.8	0.0175	6.9	0.64	112	7.7	341.1	31.2	2509.9	139.1	112	7.7	NA		
08KH28-152	211	29768	2.3	17.7644	2.8	0.554	4.1	0.0714	3	0.73	444.4	12.7	447.6	14.8	463.9	62.1	444.4	12.7	95.8		
08KH28-154	381	8061	1.8	28.8266	27.7	0.0385	28.2	0.0081	5	0.18	51.7	2.6	38.4	10.6	-733.4	787.7	51.7	2.6	NA		
08KH28-155	249	73199	2.6	17.5507	2.4	0.6476	4.7	0.0824	4	0.86	510.6	19.7	507	18.8	490.7	53.7	510.6	19.7	104.1		
08KH28-157	263	43272	1.5	17.1906	2.7	0.6544	10.6	0.0816	10.2	0.97	505.6	49.6	511.2	42.5	536.2	60	505.6	49.6	94.3		
08KH28-159	884	2438	21.2	20.6622	7.6	0.0631	8.1	0.0095	2.9	0.35	60.7	1.7	62.1	4.9	118.7	179.5	60.7	1.7	NA		
08KH28-160	287	80847	1.8	17.6705	2.6	0.6069	4.5	0.0778	3.7	0.82	482.8	17.3	481.6	17.4	475.6	56.8	482.8	17.3	101.5		
08KH28-161	187	138199	2.2	9.9786	0.8	3.8436	3.3	0.2782	3.2	0.97	1582.1	45.2	1601.9	26.7	1628.1	13.9	1628.1	13.9	97.2		

TABLE DR1. NEW U-PB CRYSTALLIZATION AGES (Megaflood @ 9)

Grain	U (ppm)	206Pb 204Pb	U/Th	Isotope ratios							error corr.	Apparent ages (Ma)						Best (Ma)	age ± (Ma)	Conc (Ma)	
				206Pb*	±	207Pb*	±	206Pb*	±	207Pb*		±	206Pb*	±	207Pb*	±	206Pb*				±
				207Pb*	(%)	235U*	(%)	238U	(%)	238U*		(Ma)	235U	(Ma)	207Pb*	(Ma)					
08KH28-162	1049	221836	50.2	14.8826	1.7	0.8602	5.2	0.0928	4.9	0.95	572.4	26.9	630.2	24.4	843.7	35.3	572.4	26.9	67.8		
08KH28-163	240	55839	1.4	13.8663	0.9	1.6675	3.2	0.1677	3.1	0.96	999.4	28.5	996.2	20.3	989.2	17.8	999.4	28.5	101		
08KH28-164	291	140201	3.3	8.8065	0.5	5.2138	7	0.333	7	1	1852.9	112.7	1854.9	59.9	1857	9.7	1857	9.7	99.8		
08KH28-165	68	1088	2	25.6928	58.1	0.0455	60.6	0.0085	17	0.28	54.4	9.2	45.2	26.8	-422	1650.1	54.4	9.2	NA		
08KH28-166	519	44590	10.7	17.7393	2.6	0.2336	6.1	0.0301	5.5	0.9	190.9	10.3	213.2	11.7	467.1	57.9	190.9	10.3	NA		
08KH28-167	617	246379	1.4	15.1512	0.7	1.227	6.4	0.1348	6.4	0.99	815.4	49	813	36	806.4	14.1	815.4	49	101.1		
08KH28-168	303	242105	2.6	12.6301	0.8	2.112	1.2	0.1935	1	0.78	1140.1	10.1	1152.7	8.5	1176.6	15.3	1176.6	15.3	96.9		
08KH28-170	303	162912	2.3	9.8511	0.5	4.0339	2	0.2882	2	0.97	1632.6	28.2	1641.1	16.3	1651.9	8.4	1651.9	8.4	98.8		
08KH28-171	1990	820950	5	10.1477	0.1	3.1628	1.8	0.2328	1.8	1	1349.1	22	1448.1	14	1596.7	1.9	1596.7	1.9	84.5		
08KH28-173	2086	20199	124.2	22.0359	8.9	0.024	9.8	0.0038	4.1	0.42	24.6	1	24.1	2.3	-35.2	215.5	24.6	1	NA		
08KH28-174	1111	21336	4.9	19.158	5.6	0.2126	6.1	0.0295	2.4	0.39	187.6	4.4	195.7	10.8	294	127.2	187.6	4.4	NA		
08KH28-174	395	168200	12.6	11.4559	2	2.3183	3.9	0.1926	3.4	0.86	1135.5	35.3	1217.9	27.9	1366.9	38.3	1366.9	38.3	83.1		
08KH28-176	858	113891	89.4	17.0183	0.8	0.7213	2.8	0.089	2.7	0.96	549.8	14.2	551.4	12	558.2	17.6	549.8	14.2	98.5		
08KH28-177	641	117515	3	17.3407	1	0.6277	3.6	0.0789	3.5	0.96	489.8	16.3	494.6	14.1	517.1	22.1	489.8	16.3	94.7		
08KH28-178	189	158551	1.2	10.0421	0.6	3.9758	0.9	0.2896	0.7	0.76	1639.4	10.1	1629.3	7.5	1616.2	11.1	1616.2	11.1	101.4		
08KH28-179	726	37354	21.3	17.5406	4.7	0.091	9.1	0.0116	7.8	0.85	74.2	5.8	88.4	7.7	492	104.8	74.2	5.8	NA		
08KH28-180	1095	3302	1.5	14.9331	27.1	0.069	27.4	0.0075	4	0.15	48	1.9	67.7	17.9	836.7	574	48	1.9	NA		
08KH28-181	592	893	2.3	18.8836	16.4	0.0723	17.3	0.0099	5.4	0.31	63.6	3.4	70.9	11.8	326.9	374.3	63.6	3.4	NA		
08KH28-182	387	71080	2.6	17.523	2	0.5744	3.2	0.073	2.5	0.79	454.2	11.1	460.8	11.9	494.1	43.3	454.2	11.1	91.9		
08KH28-182	808	30613	71.4	23.8516	26.2	0.0242	26.5	0.0042	4.2	0.16	26.9	1.1	24.3	6.4	-231	669.4	26.9	1.1	NA		

TABLE DR1. NEW U-PB CRYSTALLIZATION AGES (2000 @ 11)

Grain	U (ppm)	206Pb 204Pb	U/Th	Isotope ratios							Apparent ages (Ma)							Best (Ma)	age ± (Ma)	Conc (Ma)
				206Pb*	±	207Pb*	±	206Pb*	±	error corr.	206Pb*	±	207Pb*	±	206Pb*	±				
				207Pb*	(%)	235U*	(%)	238U	(%)		238U*	(Ma)	235U	(Ma)	207Pb*	(Ma)				
08KH34-1	522	797611	0.9	9.9136	0.2	4.0153	2.2	0.2887	2.2	1	1635	31.7	1637.3	17.9	1640.2	3.2	1640.2	3.2	99.7	
08KH34-2	2172	37242	33.8	21.0747	3	0.0643	3.6	0.0098	2	0.56	63	1.3	63.2	2.2	71.9	70.2	63	1.3	NA	
08KH34-3	832	17437	1.3	9.6243	0.3	3.1049	10.1	0.2167	10.1	1	1264.5	115.8	1433.9	77.7	1695	6	1695	6	74.6	
08KH34-4	207	258470	1.6	10.1394	0.8	3.5939	3	0.2643	2.9	0.96	1511.7	38.8	1548.2	23.8	1598.3	15.3	1598.3	15.3	94.6	
08KH34-5	1316	84121	1	20.9964	3.3	0.0763	4.5	0.0116	3	0.67	74.5	2.2	74.7	3.2	80.8	79.5	74.5	2.2	NA	
08KH34-6	326	4531	1.3	12.314	2	1.5044	3.4	0.1344	2.8	0.82	812.7	21.2	932.2	20.7	1226.5	38.5	1226.5	38.5	66.3	
08KH34-7	549	8573	4.4	19.969	9.9	0.0462	14.6	0.0067	10.7	0.73	43	4.6	45.8	6.6	198.6	231.1	43	4.6	NA	
08KH34-8	479	16495	0.8	12.4842	2.4	1.7939	5	0.1624	4.4	0.88	970.2	40	1043.2	32.8	1199.5	46.7	1199.5	46.7	80.9	
08KH34-10	233	16770	1	13.6315	1.3	1.7872	4.1	0.1767	3.8	0.94	1048.9	37.1	1040.8	26.4	1023.9	27	1023.9	27	102.4	
08KH34-11	715	20561	0.9	20.5332	8.1	0.0785	8.3	0.0117	1.9	0.22	75	1.4	76.8	6.1	133.5	190.2	75	1.4	NA	
08KH34-12	467	545112	3	8.7877	0.3	4.6223	8	0.2946	8	1	1664.5	117.6	1753.3	67.1	1860.9	5.2	1860.9	5.2	89.4	
08KH34-13	992	24909	2.5	22.2525	6.5	0.0392	6.9	0.0063	2.3	0.33	40.7	0.9	39	2.6	-58.9	158.4	40.7	0.9	NA	
08KH34-14	4125	790222	2.6	17.482	0.1	0.5536	11.7	0.0702	11.7	1	437.3	49.4	447.3	42.3	499.3	1.9	499.3	1.9	87.6	
08KH34-15	1606	70298	1.4	20.7537	2	0.0796	3.3	0.012	2.6	0.79	76.8	2	77.8	2.4	108.3	46.8	76.8	2	NA	
08KH34-16	2160	20482	17.7	19.9711	4	0.0639	4.4	0.0093	2	0.45	59.4	1.2	62.9	2.7	198.3	92.1	59.4	1.2	NA	
08KH34-17	307	19444	1.5	12.4569	0.8	1.6662	4.1	0.1505	4.1	0.98	903.9	34.2	995.7	26.2	1203.8	16.2	1203.8	16.2	75.1	
08KH34-18	358	420489	2.7	14.3009	0.9	1.4577	1.6	0.1512	1.3	0.83	907.7	11	913.1	9.4	926.1	17.9	926.1	17.9	98	
08KH34-19	553	2482	0.3	18.7108	15.1	0.093	15.6	0.0126	3.7	0.24	80.8	2.9	90.3	13.4	347.7	343.8	80.8	2.9	NA	
08KH34-20	245	148616	1.1	11.1097	0.7	2.8651	3.5	0.2309	3.4	0.98	1339	41.1	1372.8	26.2	1425.8	13.9	1425.8	13.9	93.9	
08KH34-21	297	22837	1.5	19.4327	3.2	0.2669	6.8	0.0376	6	0.88	238.1	14	240.2	14.6	261.4	73.5	238.1	14	NA	
08KH34-22	188	146591	1.2	9.8578	0.4	3.9627	1.4	0.2833	1.3	0.95	1608	18.6	1626.6	11.1	1650.7	7.9	1650.7	7.9	97.4	
08KH34-23	163	85999	0.4	12.7322	1.3	2.0597	2.7	0.1902	2.4	0.88	1122.5	24.4	1135.5	18.5	1160.6	25.6	1160.6	25.6	96.7	
08KH34-24	86	49346	1.1	13.7321	2.6	1.6849	3.3	0.1678	2.1	0.62	1000	19.2	1002.8	21.2	1009	52.9	1009	52.9	99.1	
08KH34-25	1100	28981	0.6	21.8837	6.5	0.046	9.4	0.0073	6.7	0.72	46.9	3.1	45.7	4.2	-18.4	158.2	46.9	3.1	NA	
08KH34-26	5114	19855	0.5	20.8012	0.8	0.1775	20.2	0.0268	20.1	1	170.3	33.8	165.9	30.8	102.9	18.2	170.3	33.8	NA	
08KH34-27	295	25687	1.3	12.7516	1	1.4591	4.7	0.1349	4.6	0.98	816	35.4	913.6	28.5	1157.6	20.6	1157.6	20.6	70.5	

TABLE DR1. NEW U-PB CRYSTALLIZATION AGES (2000 @ 11)

Grain	U (ppm)	206Pb 204Pb	U/Th	Isotope ratios							Apparent ages (Ma)						Best (Ma)	age ± (Ma)	Conc (Ma)
				206Pb*	±	207Pb*	±	206Pb*	±	error corr.	206Pb*	±	207Pb*	±	206Pb*	±			
				207Pb*	(%)	235U*	(%)	238U	(%)		238U*	(Ma)	235U	(Ma)	207Pb*	(Ma)			
08KH34-28	809	1274	0.9	19.3719	8.1	0.0808	8.1	0.0113	1.2	0.15	72.7	0.9	78.9	6.2	268.6	185	72.7	0.9	NA
08KH34-29	169	193862	2.1	10.8125	1.4	2.9527	2.9	0.2315	2.6	0.88	1342.6	31.4	1395.5	22.2	1477.4	26	1477.4	26	90.9
08KH34-30	2739	427893	6.1	17.5796	0.3	0.3866	4.6	0.0493	4.6	1	310.1	13.9	331.9	13	487.1	6.3	310.1	13.9	NA
08KH34-33	243	325224	0.9	9.8733	0.5	3.8278	1.5	0.2741	1.4	0.94	1561.6	20	1598.6	12.4	1647.8	9.7	1647.8	9.7	94.8
08KH34-34	1219	85628	0.5	21.2404	5.8	0.0764	6.8	0.0118	3.5	0.52	75.4	2.7	74.7	4.9	53.3	137.6	75.4	2.7	NA
08KH34-35	945	27391	3.9	16.6608	0.9	0.6753	3.4	0.0816	3.3	0.97	505.7	15.8	523.9	13.8	604.3	18.7	604.3	18.7	83.7
08KH34-36	798	146796	19.9	10.725	0.6	0.5114	19.6	0.0398	19.6	1	251.5	48.2	419.4	67.3	1492.7	11.1	251.5	48.2	NA
08KH34-38	123	28105	1.7	12.8362	1.5	1.7982	6.2	0.1674	6	0.97	997.8	55.5	1044.8	40.4	1144.4	29	1144.4	29	87.2
08KH34-39	400	18752	0.7	7.3542	0.4	6.1026	9.6	0.3255	9.6	1	1816.5	151.4	1990.6	83.7	2176.6	7.8	2176.6	7.8	83.5
08KH34-40	107	52886	0.8	12.5987	1.4	1.9636	2.3	0.1794	1.8	0.8	1063.8	17.9	1103.1	15.3	1181.5	26.7	1181.5	26.7	90
08KH34-42	168	166336	1.2	12.795	1.3	2.0442	2.1	0.1897	1.7	0.8	1119.7	17.5	1130.4	14.5	1150.8	25	1150.8	25	97.3
08KH34-45	126	142632	1.5	4.8839	0.3	15.7647	2.4	0.5584	2.4	0.99	2860	54.7	2862.6	22.7	2864.5	4.3	2864.5	4.3	99.8
08KH34-46	468	31654	1.6	20.0104	8.7	0.1299	10.1	0.0188	5.2	0.51	120.4	6.2	124	11.8	193.8	202.3	120.4	6.2	NA
08KH34-47	105	3061	0.9	12.6584	95.9	0.0699	96.8	0.0064	12.9	0.13	41.2	5.3	68.6	64.3	1172.1	#VALUE!	41.2	5.3	NA
08KH34-48	414	13304	1.7	21.7007	18.7	0.0559	20.7	0.0088	8.8	0.43	56.5	5	55.2	11.1	1.9	455.1	56.5	5	NA
08KH34-50	1008	147814	1.1	17.5615	0.9	0.6107	3.8	0.0778	3.7	0.97	482.8	17	484	14.5	489.3	20.1	489.3	20.1	98.7

TABLE DR1. NEW U-PB CRYSTALLIZATION AGES (Megaflood @ 7)

Grain	U (ppm)	206Pb 204Pb	U/Th	Isotope ratios							error corr.	Apparent ages (Ma)						Best (Ma)	age ± (Ma)	Conc (Ma)	
				206Pb*	±	207Pb*	±	206Pb*	±	207Pb*		±	206Pb*	±	207Pb*	±	206Pb*				±
				207Pb*	(%)	235U*	(%)	238U	(%)	238U*		(Ma)	235U	(Ma)	207Pb*	(Ma)					
08KH24-1	765	281514	2.3	17.4342	0.9	0.5939	1.9	0.0751	1.6	0.87	466.8	7.4	473.3	7.1	505.3	20.6	466.8	7.4	92.4		
08KH24-2	178	29263	1.9	17.638	5.6	0.4384	18.8	0.0561	17.9	0.95	351.8	61.4	369.1	58.2	479.7	124	351.8	61.4	NA		
08KH24-3	181	33299	1	17.1169	3.2	0.6458	4.7	0.0802	3.4	0.72	497.1	16.1	505.9	18.6	545.6	70.9	497.1	16.1	91.1		
08KH24-5	344	140209	1.5	17.0465	2	0.6458	5.6	0.0798	5.2	0.93	495.2	24.8	505.9	22.2	554.6	43.7	495.2	24.8	89.3		
08KH24-7	326	86203	1.2	17.2506	2.4	0.6584	2.9	0.0824	1.7	0.57	510.3	8.1	513.6	11.7	528.6	52	510.3	8.1	96.5		
08KH24-8	669	298670	1.3	14.9767	0.6	1.2763	2.3	0.1386	2.3	0.97	837	17.7	835.2	13.3	830.6	12	837	17.7	100.8		
08KH24-9	351	201394	7.2	15.0913	1.2	1.079	3.8	0.1181	3.6	0.95	719.6	24.6	743.1	20	814.7	25	719.6	24.6	88.3		
08KH24-10	134	26185	0.9	17.7631	8	0.6052	8.3	0.078	2	0.24	484	9.2	480.5	31.7	464.1	178.4	484	9.2	104.3		
08KH24-11	67	28202	1.5	14.0424	2.7	1.5262	5.1	0.1554	4.3	0.84	931.4	37.3	941	31.3	963.5	56	931.4	37.3	96.7		
08KH24-12	186	336851	1.8	11.3428	0.8	2.888	2.8	0.2376	2.7	0.96	1374.1	33.6	1378.8	21.3	1386	14.7	1386	14.7	99.1		
08KH24-14	145	114826	3.7	9.8284	0.7	3.8907	2.6	0.2773	2.5	0.97	1577.9	34.6	1611.8	20.7	1656.2	12.3	1656.2	12.3	95.3		
08KH24-15	256	1651	53.3	1.9181	798	0.1075	798.4	0.0015	24.4	0.03	9.6	2.3	103.7	1048	NA	NA	9.6	2.3	NA		
08KH24-17	1650	47870	1	17.3024	1.1	0.6176	2.1	0.0775	1.8	0.87	481.2	8.5	488.4	8.2	522	23.3	481.2	8.5	92.2		
08KH24-18	220	24535	1	16.3448	7	0.6679	7.4	0.0792	2.2	0.3	491.2	10.3	519.5	30	645.6	151.5	491.2	10.3	76.1		
08KH24-19	47	30823	1.7	14.0305	5.6	1.6606	5.7	0.169	1.2	0.21	1006.5	11.1	993.6	36.3	965.3	114.6	1006.5	11.1	104.3		
08KH24-20	3508	657586	4.1	17.2244	0.2	0.604	2.2	0.0755	2.2	0.99	468.9	9.9	479.8	8.4	531.9	5.4	468.9	9.9	88.2		
08KH24-21	327	27374	1.8	17.4883	1.6	0.6004	2.6	0.0762	2	0.79	473.2	9.3	477.5	9.8	498.5	34.9	473.2	9.3	94.9		
08KH24-22	247	93343	1.5	13.7993	0.8	1.7252	1.6	0.1727	1.4	0.89	1026.7	13.7	1017.9	10.5	999.1	15.3	999.1	15.3	102.8		
08KH24-23	2275	522928	2.2	17.2165	0.4	0.6332	1.6	0.0791	1.6	0.98	490.6	7.6	498.1	6.5	532.9	7.8	490.6	7.6	92		
08KH24-24	294	86397	1.9	17.2727	1.6	0.6547	3.7	0.082	3.4	0.91	508.2	16.5	511.4	15	525.8	34.5	508.2	16.5	96.7		
08KH24-25	188	63147	1.5	17.7293	3.5	0.5873	3.8	0.0755	1.5	0.39	469.3	6.7	469.2	14.3	468.3	77.4	469.3	6.7	100.2		
08KH24-26	1045	25201	27.6	20.8634	6.6	0.0262	21.5	0.004	20.5	0.95	25.5	5.2	26.3	5.6	95.8	156.9	25.5	5.2	NA		
08KH24-27	703	8223	28.2	26.8759	42.9	0.02	43	0.0039	2.6	0.06	25.1	0.6	20.1	8.6	-541.4	1199.3	25.1	0.6	NA		
08KH24-28	687	259520	1.6	14.9045	0.3	1.2429	1.9	0.1344	1.9	0.98	812.7	14.3	820.2	10.7	840.7	6.9	812.7	14.3	96.7		
08KH24-29	323	155376	2.4	17.3073	1.7	0.6293	3.9	0.079	3.5	0.9	490.1	16.5	495.7	15.3	521.4	37.1	490.1	16.5	94		
08KH24-30	376	84854	2.4	17.2617	2.1	0.6082	3.6	0.0761	3	0.82	473	13.5	482.4	14	527.2	46	473	13.5	89.7		

TABLE DR1. NEW U-PB CRYSTALLIZATION AGES (Megaflood @ 7)

Grain	U (ppm)	206Pb 204Pb	U/Th	Isotope ratios							error corr.	Apparent ages (Ma)						Best (Ma)	age ± (Ma)	Conc (Ma)	
				206Pb*	±	207Pb*	±	206Pb*	±	207Pb*		±	206Pb*	±	207Pb*	±	206Pb*				±
				207Pb*	(%)	235U*	(%)	238U	(%)	238U*		(Ma)	235U	(Ma)	207Pb*	(Ma)					
08KH24-31	270	35149	1.7	17.6737	1.7	0.6015	2.2	0.0771	1.5	0.66	478.8	6.8	478.2	8.5	475.3	37.3	478.8	6.8	100.7		
08KH24-32	540	116576	1.7	17.5348	1.5	0.4932	3	0.0627	2.5	0.85	392.1	9.6	407.1	9.9	492.6	34.1	392.1	9.6	NA		
08KH24-34	60	810	1.4	6.7071	178	0.137	179.4	0.0067	23.1	0.13	42.8	9.8	130.3	223	2335.6	178	42.8	9.8	NA		
08KH24-35	1911	302900	2.5	17.3333	0.4	0.6408	1.6	0.0806	1.6	0.97	499.4	7.6	502.8	6.5	518.1	9.4	499.4	7.6	96.4		
08KH24-36	1487	422976	6.9	17.415	0.7	0.6245	1.9	0.0789	1.8	0.93	489.4	8.3	492.6	7.4	507.8	15.9	489.4	8.3	96.4		
08KH24-38	5309	383184	4.7	17.3941	0.3	0.6461	5.8	0.0815	5.8	1	505.1	28.1	506.1	23.1	510.4	7.4	505.1	28.1	99		
08KH24-39	330	81060	2.6	17.4436	1.8	0.6017	4.2	0.0761	3.8	0.9	473	17.4	478.3	16.1	504.1	39.5	473	17.4	93.8		
08KH24-40	2241	39110	257.7	20.2116	6.5	0.0245	16.5	0.0036	15.2	0.92	23.2	3.5	24.6	4	170.5	151.4	23.2	3.5	NA		
08KH24-41	380	209322	1.4	13.755	0.5	1.6738	3.8	0.167	3.8	0.99	995.5	34.9	998.6	24.3	1005.6	10	1005.6	10	99		
08KH24-43	177	9092	1.2	23.1166	19.4	0.0782	19.8	0.0131	3.8	0.19	83.9	3.2	76.4	14.6	-152.7	486.3	83.9	3.2	NA		
08KH24-44	80	57137	2.3	13.9073	2.8	1.6183	3.1	0.1632	1.5	0.46	974.7	13.2	977.3	19.7	983.3	56.6	974.7	13.2	99.1		
08KH24-45	427	266564	2.5	10.9793	0.4	2.9455	3.3	0.2346	3.3	0.99	1358.3	40.4	1393.7	25.2	1448.3	7.1	1448.3	7.1	93.8		
08KH24-46	276	14631	0.7	16.9645	2	0.6066	2.8	0.0746	2	0.71	464	9.1	481.4	10.9	565.1	43.2	464	9.1	82.1		
08KH24-47	176	23699	1.3	17.3365	4	0.5701	5.8	0.0717	4.2	0.72	446.3	18.1	458.1	21.4	517.7	87.8	446.3	18.1	86.2		
08KH24-48	439	160653	1.5	17.3112	1	0.5522	2.9	0.0693	2.7	0.94	432.1	11.4	446.4	10.4	520.9	21.4	432.1	11.4	83		
08KH24-49	250	68191	4.3	14.9965	2	1.1832	9.9	0.1287	9.7	0.98	780.4	71.1	792.8	54.4	827.9	41.1	780.4	71.1	94.3		
08KH24-50	532	231338	1.8	10.7719	0.7	3.2001	3.4	0.25	3.3	0.98	1438.5	43.1	1457.2	26.5	1484.5	13.8	1484.5	13.8	96.9		
08KH24-51	674	15153	99.3	24.8361	27.7	0.0237	28.4	0.0043	6	0.21	27.5	1.6	23.8	6.7	-334	725.3	27.5	1.6	NA		
08KH24-52	2448	297988	11.8	17.4211	0.4	0.5782	4.8	0.0731	4.7	1	454.5	20.8	463.3	17.7	507	9.6	454.5	20.8	89.7		
08KH24-53	175	54792	1.2	9.9333	1.4	3.2857	3.4	0.2367	3.1	0.92	1369.6	38.8	1477.7	26.6	1636.5	25.1	1636.5	25.1	83.7		
08KH24-54	105	109450	1.3	9.8207	0.9	3.9323	1.8	0.2801	1.5	0.87	1591.8	21.7	1620.4	14.4	1657.6	16.5	1657.6	16.5	96		
08KH24-55	150	86759	1.6	13.7596	1.6	1.5905	2.1	0.1587	1.3	0.63	949.7	11.6	966.5	13	1004.9	32.8	949.7	11.6	94.5		
08KH24-56	56	34732	1	12.6078	3.8	2.0976	4	0.1918	1.4	0.36	1131.1	15	1148	27.7	1180	74.2	1180	74.2	95.9		
08KH24-57	275	78306	4.7	14.0466	1.8	0.6838	5	0.0697	4.6	0.93	434.1	19.5	529.1	20.6	962.9	37.7	434.1	19.5	45.1		
08KH24-58	864	3160	109.5	14.0638	119	0.0137	120.1	0.0014	15.3	0.13	9	1.4	13.8	16.5	960.4	461.8	9	1.4	NA		
08KH24-59	974	193134	97.4	17.1933	0.7	0.6618	1.7	0.0825	1.6	0.92	511.2	7.6	515.7	6.8	535.9	14.8	511.2	7.6	95.4		

TABLE DR1. NEW U-PB CRYSTALLIZATION AGES (Megaflood @ 7)

Grain	U (ppm)	206Pb	U/Th	Isotope ratios							error corr.	Apparent ages (Ma)						Best (Ma)	age ± (Ma)	Conc (Ma)	
				206Pb*	±	207Pb*	±	206Pb*	±	207Pb*		±	206Pb*	±	207Pb*	±	206Pb*				±
				207Pb*	(%)	235U*	(%)	238U	(%)	238U*		(Ma)	235U	(Ma)	207Pb*	(Ma)					
08KH24-60	99	34691	0.9	17.065	6.1	0.6143	6.4	0.076	1.6	0.26	472.4	7.4	486.2	24.6	552.3	134.3	472.4	7.4	85.5		
08KH24-61	288	229661	1.7	11.047	0.5	2.7184	2.3	0.2178	2.3	0.98	1270.2	26.1	1333.5	17.3	1436.6	9.7	1436.6	9.7	88.4		
08KH24-63	255	41840	2	17.5132	2.1	0.6022	2.5	0.0765	1.4	0.55	475.2	6.3	478.6	9.6	495.4	46.2	475.2	6.3	95.9		
08KH24-64	2139	1128313	1.5	14.9917	0.9	1.1609	3.2	0.1262	3.1	0.96	766.3	22.3	782.4	17.5	828.5	18.5	766.3	22.3	92.5		
08KH24-65	1214	451065	10	13.0392	0.3	1.8794	1	0.1777	0.9	0.94	1054.6	8.9	1073.9	6.4	1113.2	6.4	1113.2	6.4	94.7		
08KH24-66	369	107928	1.8	13.7772	0.5	1.5916	1.6	0.159	1.6	0.96	951.4	13.9	966.9	10.2	1002.3	9.5	951.4	13.9	94.9		
08KH24-67	301	69208	6	16.3387	3.3	0.5051	7.6	0.0599	6.8	0.9	374.8	24.9	415.2	25.9	646.4	71.9	374.8	24.9	NA		
08KH24-68	232	39686	1.5	13.1679	1.1	1.8229	1.5	0.1741	1	0.67	1034.6	9.5	1053.7	9.7	1093.6	21.9	1093.6	21.9	94.6		
08KH24-69	1055	30188	1.3	17.3649	2.5	0.5982	5.2	0.0753	4.5	0.88	468.3	20.5	476.1	19.6	514.1	54	468.3	20.5	91.1		
08KH24-71	128	23959	1.5	17.5739	5.4	0.6	6	0.0765	2.4	0.4	475	11	477.2	22.7	487.7	120.3	475	11	97.4		
08KH24-72	597	94135	29.8	16.8588	2.5	0.5594	6.4	0.0684	5.8	0.92	426.5	24.1	451.1	23.1	578.7	54.2	426.5	24.1	73.7		
08KH24-73	243	86348	1.3	17.0113	3.8	0.5745	5.3	0.0709	3.7	0.7	441.4	15.9	460.9	19.6	559.1	82.1	441.4	15.9	78.9		
08KH24-74	294	73551	1	17.5304	2.5	0.629	3.8	0.08	2.9	0.77	495.9	14	495.4	15	493.2	54.2	495.9	14	100.6		
08KH24-75	124	60226	2.1	13.667	1.9	1.7101	2.3	0.1695	1.2	0.53	1009.4	11.2	1012.3	14.5	1018.6	38.7	1018.6	38.7	99.1		
08KH24-76	448	2165	112.2	7.9087	167	0.0225	168.8	0.0013	24.2	0.14	8.3	2	22.5	37.7	2049.1	33.4	8.3	2	NA		
08KH24-77	192	80905	1.6	15.0012	1.5	1.2051	1.8	0.1311	1.1	0.6	794.2	8.3	802.9	10.3	827.2	30.8	794.2	8.3	96		
08KH24-79	717	96633	2.1	17.5121	1.2	0.6327	2.3	0.0804	2	0.85	498.3	9.4	497.8	9	495.5	26.5	498.3	9.4	100.6		
08KH24-80	557	102668	2.7	17.2927	1.2	0.6158	3.1	0.0772	2.8	0.92	479.6	12.9	487.2	11.8	523.2	26.9	479.6	12.9	91.7		
08KH24-81	910	231651	4	17.3231	0.9	0.6118	1.4	0.0769	1.2	0.8	477.4	5.3	484.7	5.6	519.4	19	477.4	5.3	91.9		
08KH24-83	513	141059	2.9	14.9364	0.5	1.1896	2	0.1289	1.9	0.97	781.4	13.9	795.8	10.8	836.2	9.7	781.4	13.9	93.4		
08KH24-84	256	89914	2.2	15.0281	0.8	1.2193	1.9	0.1329	1.7	0.91	804.4	12.9	809.5	10.5	823.5	16.6	804.4	12.9	97.7		
08KH24-85	1020	25611	2.1	17.4116	1.3	0.529	6.3	0.0668	6.2	0.98	416.9	24.9	431.2	22.1	508.2	28	416.9	24.9	82		
08KH24-86	401	134027	1.9	17.6141	2.4	0.4798	3	0.0613	1.8	0.59	383.5	6.6	397.9	9.9	482.7	53.7	383.5	6.6	NA		
08KH24-87	128	48693	2.2	13.7564	1.1	1.524	4.6	0.1521	4.5	0.97	912.4	38	940.1	28.3	1005.4	23.3	912.4	38	90.8		
08KH24-88	1512	402977	8.7	17.3268	0.2	0.6312	2.1	0.0793	2.1	0.99	492.1	10.1	496.8	8.4	518.9	5.4	492.1	10.1	94.8		
08KH24-89	599	12206	6.1	22.6706	19.1	0.038	19.3	0.0063	2.8	0.15	40.2	1.1	37.9	7.2	-104.5	473.9	40.2	1.1	NA		

TABLE DR1. NEW U-PB CRYSTALLIZATION AGES (Megaflood @ 7)

Grain	U (ppm)	206Pb 204Pb	U/Th	Isotope ratios							error corr.	Apparent ages (Ma)						Best (Ma)	age ± (Ma)	Conc (Ma)	
				206Pb*	±	207Pb*	±	206Pb*	±	207Pb*		±	206Pb*	±	207Pb*	±	206Pb*				±
				207Pb*	(%)	235U*	(%)	238U	(%)	238U*		(Ma)	235U	(Ma)	207Pb*	(Ma)					
08KH24-90	933	768072	21.3	15.1214	0.4	1.1233	1.9	0.1232	1.9	0.98	748.9	13.3	764.6	10.4	810.5	8.8	748.9	13.3	92.4		
08KH24-91	242	61554	1.2	17.5738	3.5	0.5881	4.2	0.075	2.3	0.54	465.9	10.2	469.6	15.8	487.8	78.2	465.9	10.2	95.5		
08KH24-92	595	114579	3.8	17.4327	0.8	0.6052	2.6	0.0765	2.5	0.95	475.3	11.4	480.6	9.9	505.5	17.1	475.3	11.4	94		
08KH24-93	275	48125	1	17.6718	2.3	0.5873	3.8	0.0753	3.1	0.81	467.8	14	469.1	14.4	475.5	49.8	467.8	14	98.4		
08KH24-94	404	81590	2.3	17.4705	1.3	0.5625	4.7	0.0713	4.5	0.96	443.8	19.4	453.1	17.2	500.8	27.8	443.8	19.4	88.6		
08KH24-95	214	40670	1	17.6809	2.9	0.5939	3.1	0.0762	1	0.32	473.2	4.6	473.4	11.8	474.4	65.1	473.2	4.6	99.7		
08KH24-96	245	8797	32.2	17.4406	33.8	0.0343	37.2	0.0043	15.5	0.42	27.9	4.3	34.3	12.5	504.5	763.4	27.9	4.3	NA		
08KH24-97	493	288847	2.2	13.5962	0.6	1.6735	5.2	0.165	5.2	0.99	984.6	47.1	998.5	33.1	1029.1	13.1	1029.1	13.1	95.7		
08KH24-98	247	64372	2.1	15.1488	1.6	1.1996	2	0.1318	1.2	0.6	798.1	9	800.4	11	806.7	33.4	798.1	9	98.9		
08KH24-99	881	110234	1.4	17.6094	0.8	0.5947	1.1	0.076	0.8	0.72	471.9	3.5	473.9	4.1	483.3	16.7	471.9	3.5	97.6		
08KH24-100	665	199009	4.1	15.6684	0.8	0.6873	32.3	0.0781	32.2	1	484.8	150.6	531.2	134.2	735.8	16.2	484.8	150.6	65.9		

TABLE DR1. NEW U-PB CRYSTALLIZATION AGES (Megaflood @ 10)

Grain	U (ppm)	206Pb 204Pb	U/Th	Isotope ratios							error corr.	Apparent ages (Ma)						Best (Ma)	age ± (Ma)	Conc (Ma)	
				206Pb*	±	207Pb*	±	206Pb*	±	207Pb*		±	206Pb*	±	207Pb*	±	206Pb*				±
				207Pb*	(%)	235U*	(%)	238U	(%)	238U*		(Ma)	235U	(Ma)	207Pb*	(Ma)					
PFS-1	138	39971	0.8	17.307	4.4	0.6163	5	0.0774	2.3	0.47	480.4	10.8	487.6	19.2	521.4	96	480.4	10.8	92.1		
PFS-2	200	64045	1.5	13.7131	0.7	1.5093	3.7	0.1501	3.7	0.98	901.6	30.9	934.2	22.9	1011.8	14.5	901.6	30.9	89.1		
PFS-3	999	224194	4.1	17.4037	0.8	0.5997	2.2	0.0757	2.1	0.93	470.4	9.5	477	8.5	509.2	18.1	470.4	9.5	92.4		
PFS-4	240	16541	1.5	13.7648	3.3	1.3583	7.9	0.1356	7.2	0.91	819.7	55	871.1	46.1	1004.2	66.9	819.7	55	81.6		
PFS-5	330	83099	1	17.6791	1.8	0.5894	2.7	0.0756	2	0.74	469.6	8.9	470.5	10	474.6	39.8	469.6	8.9	98.9		
PFS-6	306	316897	2.5	12.9431	0.6	1.8235	1.8	0.1712	1.7	0.95	1018.6	16	1053.9	11.7	1128	11.2	1128	11.2	90.3		
PFS-7	787	602876	2.3	17.4554	0.6	0.6415	1.4	0.0812	1.2	0.91	503.3	6	503.2	5.4	502.7	12.2	503.3	6	100.1		
PFS-8	361	165028	2.1	9.694	0.6	3.9841	2.8	0.2801	2.7	0.98	1591.9	38.2	1631	22.5	1681.7	10.9	1681.7	10.9	94.7		
PFS-9	496	47174	30	17.3538	2.3	0.1252	6.5	0.0158	6.1	0.94	100.8	6.1	119.7	7.3	515.5	50.2	100.8	6.1	NA		
PFS-10	184	4557	1.5	25.2745	34.3	0.0477	34.6	0.0087	4.8	0.14	56.1	2.7	47.3	16	-379.2	913.5	56.1	2.7	NA		
PFS-11	139	72402	1.4	13.6745	2.1	1.6999	3.6	0.1686	2.9	0.82	1004.3	27.4	1008.5	23.1	1017.5	42.3	1017.5	42.3	98.7		
PFS-12	69	81178	0.9	11.9834	2.7	2.5144	3.2	0.2185	1.8	0.56	1274.1	21.1	1276.2	23.6	1279.7	52.4	1279.7	52.4	99.6		
PFS-13	1109	5871	1	17.2167	1.5	0.5385	6.7	0.0672	6.5	0.97	419.5	26.3	437.4	23.7	532.9	33.1	419.5	26.3	78.7		
PFS-14	295	22722	1.2	17.7194	3.2	0.359	4.7	0.0461	3.4	0.73	290.8	9.8	311.5	12.6	469.5	71.2	290.8	9.8	NA		
PFS-15	114	32265	1.1	17.9895	9.3	0.5581	11.1	0.0728	5.9	0.54	453.1	26	450.3	40.2	435.9	208.1	453.1	26	103.9		
PFS-16	194	20909	1.7	20.4884	10	0.2305	10.5	0.0342	2.9	0.28	217.1	6.3	210.6	19.9	138.6	236.3	217.1	6.3	NA		
PFS-18	76	177643	0.9	9.8661	1.3	3.8714	2.6	0.277	2.3	0.87	1576.3	32.1	1607.7	21.4	1649.1	24.6	1649.1	24.6	95.6		
PFS-19	387	30389	1.7	13.7358	1	1.6239	1.5	0.1618	1.1	0.73	966.6	9.9	979.5	9.5	1008.4	21	966.6	9.9	95.9		
PFS-21	5033	17488	54.1	21.999	15.1	0.0067	15.6	0.0011	3.8	0.25	6.9	0.3	6.8	1.1	-31.1	368.7	6.9	0.3	NA		
PFS-22	468	90578	1.9	17.3793	0.6	0.6376	1.1	0.0804	0.9	0.82	498.3	4.4	500.8	4.4	512.3	14	498.3	4.4	97.3		
PFS-23	991	244413	1.8	10.4092	0.1	3.3539	2.5	0.2532	2.5	1	1455	31.9	1493.7	19.2	1549.1	1.9	1549.1	1.9	93.9		
PFS-25	454	34049	1.7	17.4908	1.9	0.5018	3.5	0.0637	3	0.85	397.8	11.5	412.9	11.9	498.2	41.1	397.8	11.5	NA		
PFS-26	154	11889	1.2	9.7753	1.6	3.8663	2.4	0.2741	1.9	0.77	1561.6	26	1606.7	19.7	1666.2	29.1	1666.2	29.1	93.7		
PFS-27	271	50977	0.6	18.0645	3.2	0.5892	4.6	0.0772	3.3	0.72	479.3	15.1	470.3	17.1	426.7	70.6	479.3	15.1	112.3		
PFS-28	175	56216	1.6	13.699	1.3	1.5123	2.4	0.1503	2	0.83	902.4	16.7	935.4	14.6	1013.9	26.7	902.4	16.7	89		
PFS-29	477	145253	1	17.4945	1.2	0.6062	3.8	0.0769	3.7	0.95	477.7	16.8	481.2	14.7	497.7	26	477.7	16.8	96		

TABLE DR1. NEW U-PB CRYSTALLIZATION AGES (Megaflood @ 10)

Grain	U (ppm)	206Pb 204Pb	U/Th	Isotope ratios							error corr.	Apparent ages (Ma)						Best (Ma)	age ± (Ma)	Conc (Ma)	
				206Pb*	±	207Pb*	±	206Pb*	±	207Pb*		±	206Pb*	±	207Pb*	±	206Pb*				±
				207Pb*	(%)	235U*	(%)	238U	(%)	238U*		(Ma)	235U	(Ma)	207Pb*	(Ma)					
PFS-30	48	21576	0.6	12.8792	3.8	2.101	4.1	0.1963	1.6	0.39	1155.1	17.1	1149.1	28.3	1137.8	75.1	1137.8	75.1	101.5		
PFS-31	76	25389	1.7	13.957	3.4	1.5918	3.9	0.1611	2	0.5	963.1	17.5	967	24.3	976	68.6	963.1	17.5	98.7		
PFS-32	377	52746	0.8	11.2016	0.6	2.4981	5.9	0.2029	5.9	1	1191.1	64.2	1271.5	43	1410	11.2	1410	11.2	84.5		
PFS-33	721	61213	1	16.9779	5.1	0.5877	5.6	0.0724	2.5	0.44	450.4	10.7	469.4	21.2	563.4	110.5	450.4	10.7	79.9		
PFS-34	336	81579	1.1	17.7072	1.7	0.6141	3.3	0.0789	2.8	0.85	489.3	13	486.1	12.6	471.1	38.4	489.3	13	103.9		
PFS-35	700	54662	24.4	16.7558	1.5	0.6371	2.2	0.0774	1.6	0.73	480.7	7.5	500.5	8.8	592	33.1	480.7	7.5	81.2		
PFS-36	68	2059	1.3	20.3229	54.2	0.0844	54.8	0.0124	8.2	0.15	79.7	6.5	82.3	43.3	157.6	1363.7	79.7	6.5	NA		
PFS-37	928	104714	2.5	16.8378	5.2	0.4413	17.6	0.0539	16.9	0.96	338.4	55.6	371.2	54.9	581.4	112.1	338.4	55.6	NA		
PFS-38	725	97305	1.5	17.4633	1.4	0.599	2.5	0.0759	2.1	0.84	471.4	9.5	476.6	9.5	501.7	30.2	471.4	9.5	94		
PFS-39	740	234446	1.4	17.2749	0.8	0.6173	3.8	0.0773	3.7	0.98	480.2	16.9	488.1	14.5	525.5	18	480.2	16.9	91.4		
PFS-40	276	70512	1.1	17.3388	2.2	0.6032	4	0.0759	3.3	0.83	471.3	14.9	479.3	15.1	517.4	48.6	471.3	14.9	91.1		
PFS-41	683	91840	1.3	17.5353	1.2	0.6029	1.8	0.0767	1.4	0.77	476.3	6.4	479.1	6.9	492.6	25.6	476.3	6.4	96.7		
PFS-42	821	617929	0.7	9.9547	0.2	3.7564	1.1	0.2712	1.1	0.98	1546.9	15.4	1583.5	9.2	1632.5	4.3	1632.5	4.3	94.8		
PFS-44	111	56411	1.7	13.6753	1.7	1.58	2.4	0.1567	1.7	0.72	938.5	14.9	962.4	14.8	1017.4	33.7	938.5	14.9	92.2		
PFS-45	240	96194	1.4	15.143	1.4	0.906	9.2	0.0995	9.1	0.99	611.5	52.9	654.9	44.3	807.5	29.9	611.5	52.9	75.7		
PFS-46	220	52486	0.9	17.5425	2.8	0.586	3.6	0.0746	2.3	0.63	463.5	10.2	468.3	13.5	491.7	61.5	463.5	10.2	94.3		
PFS-47	83	36764	0.9	10.2545	1.3	3.38	3.8	0.2514	3.6	0.94	1445.6	46.1	1499.8	29.7	1577.2	24.6	1577.2	24.6	91.7		
PFS-48	108	18329	0.9	17.8176	4.9	0.5887	5.8	0.0761	3.1	0.54	472.6	14.1	470	21.7	457.3	107.9	472.6	14.1	103.4		
PFS-49	824	138921	2.2	17.4811	1.2	0.6043	1.6	0.0766	1.1	0.68	475.9	5	480	6.1	499.4	26	475.9	5	95.3		
PFS-50	573	117081	1.9	15.9994	4.7	0.8078	5.4	0.0937	2.6	0.49	577.6	14.5	601.2	24.5	691.3	100.5	577.6	14.5	83.5		
PFS-51	3315	104749	2.9	17.4673	0.4	0.423	29.1	0.0536	29.1	1	336.5	95.3	358.2	87.9	501.2	7.8	336.5	95.3	NA		
PFS-52	48	1786	1.1	13.9137	51.4	0.0891	54.8	0.009	18.9	0.34	57.7	10.8	86.6	45.5	982.3	1124.5	57.7	10.8	NA		
PFS-54	506	163249	3.6	15.206	0.6	1.0287	1.2	0.1135	1.1	0.88	692.8	7.2	718.3	6.4	798.8	12.5	692.8	7.2	86.7		
PFS-57	306	47949	1.2	17.825	1.2	0.612	2.4	0.0791	2	0.86	490.9	9.5	484.8	9.1	456.4	27.1	490.9	9.5	107.6		
PFS-59	141	84276	1	10.0209	0.8	3.8503	3.1	0.2798	3	0.96	1590.5	41.7	1603.3	24.7	1620.2	15.1	1620.2	15.1	98.2		
PFS-60	409	492	11	3.3948	118	0.0212	121.6	0.0005	28.9	0.24	3.4	1	21.3	25.6	3441.9	1082.2	3.4	1	NA		

TABLE DR1. NEW U-PB CRYSTALLIZATION AGES (Megaflood @ 10)

Grain	U (ppm)	206Pb 204Pb	U/Th	Isotope ratios							error corr.	Apparent ages (Ma)						Best (Ma)	age ± (Ma)	Conc (Ma)
				206Pb*	±	207Pb*	±	206Pb*	±	error corr.		206Pb*	±	207Pb*	±	206Pb*	±			
				207Pb*	(%)	235U*	(%)	238U	(%)	238U*		(Ma)	235U	(Ma)	207Pb*	(Ma)				
PFS-61	586	80279	2.6	17.5116	1.8	0.3481	3.6	0.0442	3.2	0.88	278.9	8.7	303.3	9.5	495.6	38.6	278.9	8.7	NA	
PFS-62	387	180570	1.4	17.5678	2.7	0.5986	6.8	0.0763	6.3	0.92	473.9	28.6	476.4	26	488.5	60.5	473.9	28.6	97	
PFS-63	62	53043	1.7	9.9482	2.1	3.2549	8.6	0.2348	8.3	0.97	1359.8	101.8	1470.3	66.6	1633.7	39.2	1633.7	39.2	83.2	
PFS-64	2191	69472	1.9	17.3594	1.8	0.3036	7	0.0382	6.8	0.97	241.8	16.1	269.2	16.6	514.8	39.5	241.8	16.1	NA	
PFS-65	156	25765	1.6	17.0901	4.3	0.6132	4.7	0.076	1.9	0.41	472.2	8.7	485.6	18.2	549.1	94.4	472.2	8.7	86	
PFS-66	126	25128	0.9	18.2063	4.8	0.5902	5	0.0779	1.6	0.32	483.7	7.4	471	18.9	409.2	106.4	483.7	7.4	118.2	
PFS-67	221	5292	535.8	27.009	32.5	0.0524	32.9	0.0103	5.1	0.16	65.8	3.4	51.8	16.6	-554.7	894	65.8	3.4	NA	
PFS-72	482	83093	1.4	13.8103	0.7	1.3867	2.3	0.1389	2.2	0.96	838.4	17	883.3	13.4	997.5	13.2	838.4	17	84.1	
PFS-74	289	20432	1.6	17.2478	2.7	0.5592	4.2	0.0699	3.2	0.77	435.8	13.6	451	15.3	529	58.6	435.8	13.6	82.4	
PFS-75	64	4345	1.3	11.8761	4.4	2.2672	9.9	0.1953	8.9	0.9	1149.9	93.3	1202.1	69.8	1297.2	85.8	1297.2	85.8	88.6	
PFS-76	65	1124	2	15.4552	20.4	0.5543	21.4	0.0621	6.5	0.3	388.6	24.4	447.8	77.5	764.7	433.3	388.6	24.4	NA	
PFS-77	553	19110	2.8	20.3861	13.8	0.0497	14.1	0.0073	3.2	0.22	47.2	1.5	49.2	6.8	150.3	323.9	47.2	1.5	NA	
PFS-79	1135	10743	11.7	12.7884	17.1	0.0743	21.3	0.0069	12.7	0.6	44.2	5.6	72.7	15	1151.8	342.1	44.2	5.6	NA	
PFS-80	1135	538501	1.1	17.4589	0.7	0.6317	1.8	0.08	1.7	0.92	496.1	8	497.2	7.1	502.2	15.9	496.1	8	98.8	
PFS-81	2637	192031	9.4	17.8572	1	0.2746	26.2	0.0356	26.2	1	225.3	58	246.4	57.4	452.3	21.5	225.3	58	NA	
PFS-82	425	44884	2.5	17.3298	1.4	0.5459	5.3	0.0686	5.2	0.97	427.8	21.3	442.3	19.1	518.5	30.6	427.8	21.3	82.5	
PFS-83	2954	174485	1.3	17.397	0.3	0.6118	1.5	0.0772	1.5	0.98	479.4	6.8	484.7	5.8	510.1	6.6	479.4	6.8	94	
PFS-84	1082	877563	2.4	9.468	0.2	4.1745	1.5	0.2867	1.5	0.99	1624.8	21.8	1669	12.6	1725.1	4.4	1725.1	4.4	94.2	
PFS-85	350	8912	2.4	21.2133	13.2	0.0507	13.3	0.0078	2.2	0.16	50.1	1.1	50.2	6.5	56.3	314.8	50.1	1.1	NA	
PFS-86	148	15219	1.3	13.419	3	1.6151	6.2	0.1572	5.5	0.88	941.1	47.8	976.1	39	1055.6	60	941.1	47.8	89.2	
PFS-87	1531	94218	2.3	13.8522	0.2	1.2771	1.8	0.1283	1.8	1	778.2	13.5	835.6	10.5	991.3	3.6	778.2	13.5	78.5	
PFS-88	527	319357	1.4	11.9114	0.3	2.395	2.8	0.2069	2.8	1	1212.3	31.1	1241.1	20.2	1291.4	5.2	1291.4	5.2	93.9	
PFS-89	389	358436	2.6	10.5237	1.5	2.4489	11.4	0.1869	11.3	0.99	1104.7	115.2	1257.1	82.6	1528.5	27.6	1528.5	27.6	72.3	
PFS-90	839	78144	1	17.5368	0.8	0.6045	1.9	0.0769	1.7	0.9	477.5	8	480.1	7.4	492.4	18.5	477.5	8	97	
PFS-91	109	14867	2	17.0489	9.4	0.6308	10.8	0.078	5.4	0.5	484.2	25.1	496.6	42.5	554.3	204.9	484.2	25.1	87.3	
PFS-92	736	34434	9.1	15.9097	2.2	0.7167	3.9	0.0827	3.2	0.82	512.2	15.5	548.7	16.3	703.3	47.3	512.2	15.5	72.8	

TABLE DR1. NEW U-PB CRYSTALLIZATION AGES (Megaflood @ 10)

Grain	U (ppm)	206Pb 204Pb	U/Th	Isotope ratios							error corr.	Apparent ages (Ma)						Best (Ma)	age ± (Ma)	Conc (Ma)	
				206Pb*	±	207Pb*	±	206Pb*	±	207Pb*		±	206Pb*	±	207Pb*	±	206Pb*				±
				207Pb*	(%)	235U*	(%)	238U	(%)	238U*		(Ma)	235U	(Ma)	207Pb*	(Ma)					
PFS-93	3034	4368	6.1	17.7049	2.3	0.1821	40.2	0.0234	40.2	1	149	59.1	169.8	63	471.3	49.9	149	59.1	NA		
PFS-94	128	30617	0.7	18.0377	5.4	0.604	5.6	0.079	1.6	0.29	490.3	7.7	479.8	21.5	430	119.7	490.3	7.7	114		
PFS-95	110	111383	1.6	5.0112	0.4	12.9393	4.8	0.4703	4.8	1	2484.8	98.8	2675.2	45.4	2822.5	7	2822.5	7	88		
PFS-96	121	39510	1	17.5287	5.7	0.6042	5.9	0.0768	1.3	0.22	477.1	6.1	479.9	22.6	493.4	126.8	477.1	6.1	96.7		
PFS-97	170	39438	1.3	17.2316	2.6	0.6191	3.3	0.0774	2.1	0.63	480.4	9.7	489.3	12.9	531	56.2	480.4	9.7	90.5		
PFS-98	761	165937	1.7	14.5546	1	0.7542	8.6	0.0796	8.5	0.99	493.8	40.4	570.7	37.4	889.9	21	493.8	40.4	55.5		
PFS-100	1653	499929	2	17.3872	0.4	0.633	2.6	0.0798	2.6	0.99	495.1	12.4	498	10.4	511.3	8.9	495.1	12.4	96.8		

TABLE DR1. NEW U-PB CRYSTALLIZATION AGES (Namche Barwa Cirque @ 5)

Grain	U (ppm)	206Pb 204Pb	U/Th	Isotope ratios							error corr.	Apparent ages (Ma)						Best (Ma)	age ± (Ma)	Conc (Ma)	
				206Pb*	±	207Pb*	±	206Pb*	±	207Pb*		±	206Pb*	±	207Pb*	±	206Pb*				±
				207Pb*	(%)	235U*	(%)	238U	(%)	238U*		(Ma)	235U	(Ma)	207Pb*	(Ma)					
NBO904-1	335	177234	8.3	14.4756	0.7	0.9228	3.1	0.0969	3	0.97	596.1	16.9	663.8	14.9	901.2	14.9	596.1	16.9	66.2		
NBO904-2	491	103314	0.8	17.4319	1.3	0.4542	2.7	0.0574	2.3	0.87	359.9	8.1	380.2	8.4	505.6	28.4	359.9	8.1	NA		
NBO904-3	414	6320	12.5	23.1959	33.7	0.0197	34	0.0033	4.7	0.14	21.3	1	19.8	6.7	-161.2	859	21.3	1	NA		
NBO904-4	257	73279	1.6	17.209	3.4	0.4996	14.5	0.0624	14.1	0.97	389.9	53.3	411.4	49.1	533.9	74.1	389.9	53.3	NA		
NBO904-5	1659	336316	14.6	15.5376	0.8	0.2784	14.6	0.0314	14.6	1	199.1	28.7	249.4	32.4	753.5	15.9	199.1	28.7	NA		
NBO904-7	682	5983	29	15.5489	25.9	0.0131	27.5	0.0015	9.3	0.34	9.5	0.9	13.2	3.6	751.9	555.3	9.5	0.9	NA		
NBO904-8	2881	40377	28.1	21.6689	3.6	0.0159	4.7	0.0025	3	0.64	16.1	0.5	16	0.7	5.4	86.9	16.1	0.5	NA		
NBO904-9	391	219411	3.7	15.1146	1.2	0.9685	2.3	0.1062	2	0.85	650.4	12.2	687.7	11.5	811.5	25	650.4	12.2	80.2		
NBO904-10	171	100046	1.8	17.4519	1.9	0.6438	3	0.0815	2.3	0.78	505	11.4	504.7	11.9	503.1	40.8	505	11.4	100.4		
NBO904-11	598	11451	76.3	20.3802	14.2	0.0309	14.6	0.0046	3.5	0.24	29.4	1	30.9	4.5	151.1	333.3	29.4	1	NA		
NBO904-12	91	46668	1.2	17.9326	4.5	0.6087	7.3	0.0792	5.8	0.79	491.2	27.2	482.8	28.1	443	100.9	491.2	27.2	110.9		
NBO904-13	661	15741	276.8	20.4861	8.9	0.027	26.7	0.004	25.2	0.94	25.8	6.5	27.1	7.1	138.9	209.3	25.8	6.5	NA		
NBO904-14	124	171570	3.2	9.1361	0.4	4.6986	4.4	0.3113	4.3	1	1747.3	66.3	1767	36.4	1790.4	7.5	1790.4	7.5	97.6		
NBO904-15	471	249194	6.8	11.4401	0.4	2.2259	2.6	0.1847	2.5	0.99	1092.5	25.5	1189.2	18	1369.6	8	1369.6	8	79.8		
NBO904-16	767	346792	14.2	14.6482	1.6	0.8324	4.1	0.0884	3.8	0.92	546.2	20	614.9	19.1	876.7	32.8	546.2	20	62.3		
NBO904-17	176	115462	2.5	17.4745	2.7	0.6298	12	0.0798	11.7	0.97	495	55.7	496	47.1	500.3	58.9	495	55.7	98.9		
NBO904-18	246	3015	16	29.531	41.1	0.0137	41.6	0.0029	6.6	0.16	18.9	1.3	13.9	5.7	-801.4	1207.5	18.9	1.3	NA		
NBO904-19	824	26052	8.4	19.3264	4.2	0.0339	16.7	0.0047	16.1	0.97	30.5	4.9	33.8	5.6	274	96.7	30.5	4.9	NA		
NBO904-20	318	635582	3.7	10.6429	1.1	2.515	4.9	0.1941	4.8	0.98	1143.7	50.2	1276.4	35.7	1507.3	20.2	1507.3	20.2	75.9		
NBO904-21	369	335290	0.7	14.9877	0.8	1.2384	2.3	0.1346	2.1	0.94	814.1	16.4	818.1	12.8	829.1	15.9	814.1	16.4	98.2		
NBO904-22	201	2499	5.3	32.0894	105	0.0118	105.9	0.0027	11.7	0.11	17.6	2.1	11.9	12.5	-1043.5	0	17.6	2.1	NA		
NBO904-23	386	176261	2.6	15.1559	0.8	0.7103	4	0.0781	3.9	0.98	484.6	18.1	544.9	16.7	805.7	15.9	484.6	18.1	60.1		
NBO904-25	199	66658	2.1	17.5935	1.6	0.6138	3.2	0.0783	2.7	0.86	486.1	12.8	486	12.2	485.3	35.2	486.1	12.8	100.2		
NBO904-26	297	192044	1.3	15.0049	0.6	1.1794	1.8	0.1284	1.7	0.94	778.5	12.7	791.1	10.1	826.7	13	778.5	12.7	94.2		
NBO904-27	342	420759	1.1	14.1049	0.6	1.5186	1.8	0.1553	1.7	0.95	930.9	14.4	937.9	10.8	954.4	11.7	930.9	14.4	97.5		
NBO904-28	115	40704	1.2	17.4091	2.7	0.4976	5.8	0.0628	5.2	0.89	392.8	19.8	410.1	19.7	508.5	58.6	392.8	19.8	NA		

TABLE DR1. NEW U-PB CRYSTALLIZATION AGES (Namche Barwa Cirque @ 5)

Grain	U (ppm)	206Pb 204Pb	U/Th	Isotope ratios							error corr.	Apparent ages (Ma)						Best (Ma)	age ± (Ma)	Conc (Ma)	
				206Pb*	±	207Pb*	±	206Pb*	±	207Pb*		±	206Pb*	±	207Pb*	±	206Pb*				±
				207Pb*	(%)	235U*	(%)	238U	(%)	238U*		(Ma)	235U	(Ma)	207Pb*	(Ma)					
NBO904-29	169	41471	1.9	17.66	2.8	0.6307	4.1	0.0808	3	0.74	500.8	14.6	496.5	16.1	476.9	61.3	500.8	14.6	105		
NBO904-30	452	3281	15.5	18.4595	33.1	0.0113	33.4	0.0015	4.8	0.14	9.7	0.5	11.4	3.8	378.2	762.5	9.7	0.5	NA		
NBO904-31	367	313770	0.5	12.2863	0.3	2.2528	1.5	0.2007	1.5	0.98	1179.3	15.8	1197.7	10.5	1230.9	5.9	1230.9	5.9	95.8		
NBO904-32	89	33953	2.2	15.1537	3.6	1.1509	6.8	0.1265	5.8	0.85	767.8	42.3	777.7	37.2	806.1	74.7	767.8	42.3	95.3		
NBO904-33	67	32565	1.7	14.8623	1.3	1.2304	1.9	0.1326	1.4	0.72	802.8	10.4	814.5	10.7	846.6	27.5	802.8	10.4	94.8		
NBO904-34	713	263521	3	17.3644	0.9	0.4796	3.1	0.0604	3	0.96	378.1	10.9	397.8	10.2	514.2	19.1	378.1	10.9	NA		
NBO904-35	312	122241	1	17.4474	0.8	0.6436	3.4	0.0814	3.3	0.97	504.7	15.9	504.5	13.5	503.7	18.4	504.7	15.9	100.2		
NBO904-36	365	105737	2.2	17.3981	1	0.5948	3	0.0751	2.8	0.94	466.5	12.5	473.9	11.2	509.9	22.5	466.5	12.5	91.5		
NBO904-37	467	377673	2.5	14.9875	0.3	1.1456	3.2	0.1245	3.2	0.99	756.5	23	775.1	17.5	829.1	7.1	756.5	23	91.3		
NBO904-38	374	236727	1	17.3669	1	0.6106	2	0.0769	1.8	0.86	477.6	8.1	483.9	7.9	513.8	22.7	477.6	8.1	93		
NBO904-39	659	604876	10	17.4678	0.8	0.6015	1.5	0.0762	1.3	0.86	473.4	5.8	478.2	5.7	501.1	17	473.4	5.8	94.5		
NBO904-40	928	21512	73.8	22.5905	9.5	0.0245	10.6	0.004	4.9	0.46	25.8	1.3	24.6	2.6	-95.8	233.1	25.8	1.3	NA		
NBO904-41	901	256263	3.5	15.0077	0.3	0.6878	3	0.0749	3	1	465.4	13.3	531.5	12.3	826.3	6	465.4	13.3	56.3		
NBO904-42	280	31449	1.5	19.8375	11.5	0.0998	11.8	0.0144	2.5	0.21	91.9	2.3	96.6	10.9	213.9	267.2	91.9	2.3	NA		
NBO904-43	2899	50288	0.6	17.4409	0.5	0.2937	29.8	0.0371	29.8	1	235.1	68.7	261.4	68.7	504.5	10	235.1	68.7	NA		
NBO904-45	268	135256	1.7	14.8515	1	1.2735	4.4	0.1372	4.2	0.97	828.6	33	833.9	24.9	848.1	21.4	828.6	33	97.7		
NBO904-47	376	175365	2.9	15.099	0.5	0.9743	6.2	0.1067	6.2	1	653.5	38.6	690.7	31.3	813.7	11.4	653.5	38.6	80.3		
NBO904-48	490	154979	4.7	17.4745	0.9	0.5301	4.4	0.0672	4.3	0.98	419.1	17.4	431.9	15.4	500.3	19.5	419.1	17.4	83.8		
NBO904-49	943	194205	79.7	18.0565	1.6	0.085	5.6	0.0111	5.4	0.96	71.3	3.8	82.8	4.5	427.6	35.9	71.3	3.8	NA		
NBO904-50	301	303357	1.4	13.6375	0.6	1.626	2.3	0.1608	2.2	0.96	961.4	19.9	980.3	14.6	1023	13.1	961.4	19.9	94		
NBO904-52	2070	511932	2.3	15.0308	0.2	1.0004	8.3	0.1091	8.3	1	667.2	52.6	704	42.2	823.1	4.5	667.2	52.6	81.1		
NBO904-53	303	53532	4	15.475	1.8	0.2781	13.3	0.0312	13.2	0.99	198.1	25.8	249.1	29.5	762	37.1	198.1	25.8	NA		
NBO904-54	153	33629	1	17.2104	1.7	0.49	5.8	0.0612	5.6	0.96	382.7	20.8	404.9	19.5	533.7	36.6	382.7	20.8	NA		
NBO904-55	372	235456	0.8	12.0732	0.5	2.0947	3	0.1834	3	0.99	1085.6	29.6	1147.1	20.6	1265.1	9.1	1265.1	9.1	85.8		
NBO904-56	492	303163	5.7	17.3455	0.6	0.6126	3.4	0.0771	3.4	0.98	478.6	15.5	485.2	13.2	516.5	13	478.6	15.5	92.6		
NBO904-57	181	74654	1.5	17.5428	1.1	0.6527	3.2	0.083	3	0.94	514.2	14.8	510.1	12.8	491.7	24.2	514.2	14.8	104.6		

TABLE DR1. NEW U-PB CRYSTALLIZATION AGES (Namche Barwa Cirque @ 5)

Grain	U (ppm)	206Pb 204Pb	U/Th	Isotope ratios							error corr.	Apparent ages (Ma)						Best (Ma)	age ± (Ma)	Conc (Ma)	
				206Pb*	±	207Pb*	±	206Pb*	±	207Pb*		±	206Pb*	±	207Pb*	±	206Pb*				±
				207Pb*	(%)	235U*	(%)	238U	(%)	238U*		(Ma)	235U	(Ma)	207Pb*	(Ma)					
NBO904-58	58	109753	1	11.0804	1.1	2.9293	4.6	0.2354	4.5	0.97	1362.8	55.4	1389.5	35.1	1430.8	20.7	1430.8	20.7	95.2		
NBO904-59	235	127530	6.1	15.1303	0.7	0.8805	4.4	0.0966	4.3	0.99	594.6	24.4	641.2	20.7	809.3	14.9	594.6	24.4	73.5		
NBO904-60	238	123078	1.9	14.9846	1	1.1326	4.5	0.1231	4.3	0.97	748.3	30.7	769	24.1	829.5	21.3	748.3	30.7	90.2		
NBO904-61	97	298	38.2	2.842	200	0.0439	204.5	0.0009	42.6	0.21	5.8	2.5	43.7	87.6	3715.1	957.6	5.8	2.5	NA		
NBO904-62	1294	549993	0.8	17.3518	0.2	0.5866	3.6	0.0738	3.6	1	459.2	15.8	468.7	13.4	515.7	5.1	459.2	15.8	89		
NBO904-63	147	112141	1.7	14.9466	1.2	1.1315	2.7	0.1227	2.4	0.89	745.9	17.1	768.5	14.7	834.8	26	745.9	17.1	89.3		
NBO904-64	308	334807	1.1	9.5846	0.5	3.851	2.8	0.2677	2.7	0.98	1529.1	37.1	1603.5	22.3	1702.6	9.3	1702.6	9.3	89.8		
NBO904-65	175	82409	1.6	17.3883	1.9	0.5563	4.5	0.0702	4.1	0.91	437.1	17.2	449.1	16.3	511.1	42	437.1	17.2	85.5		
NBO904-67	727	374545	1.9	17.4013	0.6	0.6152	1.6	0.0776	1.5	0.94	482	7	486.8	6.2	509.5	12.3	482	7	94.6		
NBO904-68	220	86352	1.3	17.2333	2.4	0.4905	4.2	0.0613	3.4	0.82	383.6	12.7	405.3	14	530.8	53.1	383.6	12.7	NA		
NBO904-69	2898	225109	8.1	17.3137	0.1	0.7551	5.5	0.0948	5.5	1	583.9	30.9	571.2	24.2	520.6	3.1	583.9	30.9	112.2		
NBO904-70	349	10215	15.5	18.7254	25.7	0.0191	26.9	0.0026	7.8	0.29	16.7	1.3	19.2	5.1	346	590.5	16.7	1.3	NA		
NBO904-72	1665	251794	3.7	17.4166	0.6	0.4549	3.2	0.0575	3.1	0.98	360.1	10.9	380.7	10.1	507.5	12.6	360.1	10.9	NA		
NBO904-73	283	497776	2.6	12.4353	0.5	1.6475	7	0.1486	6.9	1	893.1	58	988.6	44.1	1207.2	10.5	1207.2	10.5	74		
NBO904-74	1576	75403	40.8	16.6894	0.4	0.4554	5.7	0.0551	5.7	1	345.9	19.2	381	18.2	600.6	9.6	345.9	19.2	NA		
NBO904-75	1000	20858	18.9	21.5008	12.8	0.0252	13.3	0.0039	3.7	0.28	25.3	0.9	25.3	3.3	24.1	307.4	25.3	0.9	NA		
NBO904-76	65	48529	2.6	17.4031	4.4	0.6667	4.9	0.0842	2.2	0.45	520.9	11.1	518.7	20	509.3	96.9	520.9	11.1	102.3		
NBO904-77	288	41002	5.8	17.8192	2.9	0.2668	5.6	0.0345	4.8	0.86	218.6	10.4	240.2	12.1	457.1	64.8	218.6	10.4	NA		
NBO904-78	239	179237	1.6	14.9322	0.7	1.2208	1.7	0.1322	1.5	0.9	800.4	11.6	810.1	9.5	836.8	15.1	800.4	11.6	95.7		
NBO904-79	388	714626	11.4	10.0911	1.4	3.1538	5.7	0.2308	5.5	0.97	1338.8	66.4	1445.9	43.7	1607.2	26	1607.2	26	83.3		
NBO904-81	332	3869	69.1	25.6698	26.3	0.021	26.9	0.0039	5.4	0.2	25.2	1.4	21.1	5.6	-419.7	699.1	25.2	1.4	NA		
NBO904-82	436	300951	3.6	10.7709	3.3	2.8391	6.2	0.2218	5.3	0.85	1291.3	61.7	1365.9	46.6	1484.7	61.7	1484.7	61.7	87		
NBO904-83	628	298024	0.9	14.9134	0.4	1.0182	3.2	0.1101	3.2	0.99	673.5	20.5	713	16.5	839.4	7.6	673.5	20.5	80.2		
NBO904-84	960	482054	1.4	17.4515	0.6	0.6177	2.2	0.0782	2.2	0.97	485.3	10.1	488.4	8.6	503.2	12.3	485.3	10.1	96.4		
NBO904-85	106	41687	1.7	17.4957	4.2	0.606	5.1	0.0769	2.9	0.57	477.6	13.4	481.1	19.5	497.6	92.1	477.6	13.4	96		
NBO904-86	2564	37082	38.2	21.189	3.9	0.021	4.7	0.0032	2.6	0.56	20.8	0.5	21.1	1	59.1	93.5	20.8	0.5	NA		

TABLE DR1. NEW U-PB CRYSTALLIZATION AGES (Namche Barwa Cirque @ 5)

Grain	U (ppm)	206Pb 204Pb	U/Th	Isotope ratios							error corr.	Apparent ages (Ma)						Best (Ma)	age ± (Ma)	Conc (Ma)	
				206Pb*	±	207Pb*	±	206Pb*	±	207Pb*		±	206Pb*	±	207Pb*	±	206Pb*				±
				207Pb*	(%)	235U*	(%)	238U	(%)	238U*		(Ma)	235U	(Ma)	207Pb*	(Ma)					
NBO904-87	302	111439	2.8	17.2586	1.4	0.6211	4.7	0.0777	4.5	0.95	482.7	20.9	490.6	18.3	527.6	31	482.7	20.9	91.5		
NBO904-88	359	179692	0.7	17.4008	0.9	0.582	4.4	0.0735	4.3	0.98	456.9	19.1	465.8	16.6	509.6	20.7	456.9	19.1	89.7		
NBO904-89	31	30416	0.7	13.8522	3.9	1.5595	4.5	0.1567	2.2	0.49	938.3	19.4	954.3	28	991.3	80.1	938.3	19.4	94.6		
NBO904-90	745	616885	3.8	11.7225	0.5	2.0629	2.7	0.1754	2.7	0.98	1041.7	25.7	1136.6	18.6	1322.5	9.6	1322.5	9.6	78.8		
NBO904-91	2832	467238	28.6	17.1475	3.3	0.2336	6.6	0.0291	5.7	0.87	184.6	10.4	213.2	12.7	541.7	72.3	184.6	10.4	NA		
NBO904-92	791	296867	12	15.2519	2.5	0.7536	3.7	0.0834	2.8	0.74	516.1	13.7	570.3	16.3	792.5	52.8	516.1	13.7	65.1		
NBO904-93	131	59407	1.1	14.4236	2.8	0.6586	4.7	0.0689	3.8	0.81	429.5	15.9	513.8	19.1	908.6	57.2	429.5	15.9	47.3		
NBO904-94	287	67818	1.6	14.9961	0.8	0.9342	5	0.1016	5	0.99	623.8	29.6	669.9	24.8	827.9	17.5	623.8	29.6	75.3		
NBO904-95	502	90281	20.4	16.4435	2.1	0.1869	4.5	0.0223	4	0.89	142.1	5.7	174	7.3	632.7	44.6	142.1	5.7	NA		
NBO904-96	1077	20997	29.2	23.4818	11.8	0.0177	11.9	0.003	1.4	0.12	19.4	0.3	17.8	2.1	-191.7	295.9	19.4	0.3	NA		
NBO904-97	607	152828	4.4	17.3513	1.1	0.5079	3.4	0.0639	3.2	0.95	399.4	12.5	417	11.6	515.8	23.3	399.4	12.5	NA		
NBO904-98	127	51119	2.1	15.6402	3.2	0.707	5.5	0.0802	4.4	0.81	497.3	21.3	543	23	739.6	67	497.3	21.3	67.2		
NBO904-99	557	203526	1.5	17.4213	0.5	0.6412	4.3	0.081	4.2	0.99	502.2	20.5	503.1	16.9	507	11	502.2	20.5	99.1		
NBO904-100	801	2912	57	19.8135	54.5	0.0064	55.1	0.0009	8	0.15	6	0.5	6.5	3.6	216.7	1360.8	6	0.5	NA		
NBO904-101	649	472325	3.9	17.4188	0.9	0.5557	4.3	0.0702	4.2	0.98	437.4	17.9	448.7	15.7	507.3	20.8	437.4	17.9	86.2		
NBO904-102	292	96273	1.6	17.4677	1	0.6424	2.3	0.0814	2.1	0.89	504.4	10	503.8	9.2	501.1	22.8	504.4	10	100.6		
NBO904-103	760	387832	56.3	15.0268	0.4	0.8409	7.2	0.0916	7.2	1	565.2	39.1	619.6	33.6	823.7	7.7	565.2	39.1	68.6		
NBO904-104	306	91106	1.3	14.9363	0.7	1.2078	1.4	0.1308	1.2	0.85	792.6	8.8	804.2	7.8	836.3	15.5	792.6	8.8	94.8		
NBO904-106	794	441658	15.4	17.4276	0.4	0.5723	2.5	0.0723	2.5	0.99	450.2	10.7	459.5	9.2	506.2	9	450.2	10.7	88.9		
NBO904-107	2907	47167	39.6	21.1003	3.2	0.0273	3.6	0.0042	1.7	0.46	26.9	0.4	27.4	1	69.1	76.6	26.9	0.4	NA		
NBO904-108	627	11208	12.4	22.9395	13.9	0.0244	15.3	0.0041	6.4	0.42	26.2	1.7	24.5	3.7	-133.6	344	26.2	1.7	NA		
NBO904-109	326	301917	1.3	14.0305	0.5	1.2709	3.8	0.1293	3.8	0.99	784	28.2	832.8	21.9	965.3	9.8	784	28.2	81.2		
NBO904-110	412	72345	4.9	17.448	0.9	0.5019	5.7	0.0635	5.6	0.99	396.9	21.5	413	19.2	503.6	20.8	396.9	21.5	NA		
NBO904-111	321	12377	3.2	15.6313	4	0.6603	6	0.0749	4.5	0.75	465.4	20.4	514.8	24.4	740.8	84.6	465.4	20.4	62.8		

TABLE DR1. NEW U-PB CRYSTALLIZATION AGES (Namche Barwa Cirque @ 5)

Grain	U (ppm)	206Pb 204Pb	U/Th	Isotope ratios							error corr.	Apparent ages (Ma)						Best (Ma)	age ± (Ma)	Conc (Ma)	
				206Pb*	±	207Pb*	±	206Pb*	±	207Pb*		±	206Pb*	±	207Pb*	±	206Pb*				±
				207Pb*	(%)	235U*	(%)	238U	(%)	238U*		(Ma)	235U	(Ma)	207Pb*	(Ma)					
NBO904-112	2904	95425	44.7	21.461	2.4	0.0226	3.3	0.0035	2.2	0.67	22.6	0.5	22.7	0.7	28.6	57.7	22.6	0.5	NA		
NBO904-113	351	570862	5.4	14.5644	0.7	1.171	9.3	0.1237	9.3	1	751.8	66	787.1	51.1	888.6	14.8	751.8	66	84.6		
NBO904-114	170	82898	1.3	15.1157	1.3	1.1334	4.5	0.1243	4.3	0.96	755	30.7	769.4	24.3	811.4	27.7	755	30.7	93.1		
NBO904-115	456	183222	1.2	17.4381	0.9	0.6171	2.3	0.078	2.1	0.92	484.5	9.7	488	8.7	504.8	18.8	484.5	9.7	96		
NBO904-116	317	248317	1.7	13.8046	1.7	1.2946	6.9	0.1296	6.7	0.97	785.7	49.3	843.3	39.4	998.3	33.9	785.7	49.3	78.7		
NBO904-117	811	118168	12.4	17.572	2	0.1812	8.2	0.0231	7.9	0.97	147.1	11.6	169.1	12.8	488	44.5	147.1	11.6	NA		
NBO904-118	823	758446	3	15.0344	0.2	1.1626	2.4	0.1268	2.4	1	769.4	17.2	783.2	13	822.6	3.9	769.4	17.2	93.5		
NBO904-119	326	60504	3.4	17.2955	2	0.3536	18.1	0.0444	18	0.99	279.8	49.3	307.4	48.1	522.9	43	279.8	49.3	NA		
NBO904-120	209	132246	1.7	17.2213	1.4	0.6556	4.5	0.0819	4.3	0.95	507.3	21	511.9	18.2	532.3	30.4	507.3	21	95.3		
NBO904-121	300	419193	1.8	14.9955	0.6	1.1528	3.3	0.1254	3.3	0.98	761.5	23.5	778.6	18.1	828	12.1	761.5	23.5	92		
NBO904-122	2889	52060	65.5	21.5277	2.2	0.0245	3.5	0.0038	2.7	0.78	24.6	0.7	24.5	0.8	21.1	52.8	24.6	0.7	NA		
NBO904-123	467	10964	14.1	21.2666	21.2	0.0218	21.6	0.0034	4.6	0.21	21.6	1	21.9	4.7	50.3	509.9	21.6	1	NA		
NBO904-124	352	4334	83.5	22.1725	21.3	0.0235	26.4	0.0038	15.5	0.59	24.3	3.8	23.6	6.2	-50.2	524.1	24.3	3.8	NA		
NBO904-125	36	289	54.5	4.5629	34.9	0.1528	46.6	0.0051	30.9	0.66	32.5	10	144.4	62.8	2974.5	582.8	32.5	10	NA		
NBO904-126	177	59146	1.6	17.4958	1.6	0.6303	7.4	0.08	7.3	0.98	496	34.7	496.3	29.2	497.6	36	496	34.7	99.7		
NBO904-127	564	4758	46	26.0702	45	0.007	45.8	0.0013	8.7	0.19	8.5	0.7	7.1	3.2	-460.4	1241.9	8.5	0.7	NA		
NBO904-128	170	9672	1.9	14.8043	1.9	1.0996	2.8	0.1181	2.1	0.74	719.4	14.3	753.1	15	854.7	39.2	719.4	14.3	84.2		
NBO904-129	1312	535899	20.7	15.4628	0.6	0.8068	11	0.0905	11	1	558.4	58.9	600.7	50	763.6	11.7	558.4	58.9	73.1		
NBO904-130	212	52010	1.3	17.392	1.1	0.627	2.5	0.0791	2.2	0.89	490.7	10.5	494.2	9.7	510.7	24.6	490.7	10.5	96.1		
NBO904-132	1145	193062	15.2	17.4909	0.9	0.246	8.2	0.0312	8.2	0.99	198.1	15.9	223.3	16.5	498.2	18.9	198.1	15.9	NA		
NBO904-133	329	197285	1.2	14.9877	0.5	1.2555	3.6	0.1365	3.6	0.99	824.7	27.6	825.9	20.3	829.1	11.1	824.7	27.6	99.5		
NBO904-134	2153	260115	6.1	17.4074	0.3	0.607	4.3	0.0766	4.2	1	476	19.5	481.7	16.3	508.7	5.6	476	19.5	93.6		

TABLE DR1. NEW U-PB CRYSTALLIZATION AGES (Namche Barwa Cirque @ 5)

Grain	U (ppm)	206Pb 204Pb	U/Th	Isotope ratios							error corr.	Apparent ages (Ma)						Best (Ma)	age ± (Ma)	Conc (Ma)	
				206Pb*	±	207Pb*	±	206Pb*	±	207Pb*		±	206Pb*	±	207Pb*	±	206Pb*				±
				207Pb*	(%)	235U*	(%)	238U	(%)	238U*		(Ma)	235U	(Ma)	207Pb*	(Ma)					
NBO904-135	721	14059	43.3	19.4123	12.3	0.0179	12.6	0.0025	2.6	0.2	16.2	0.4	18	2.2	263.9	283.2	16.2	0.4	NA		
NBO904-136	718	42102	2.4	17.7662	2.9	0.08	5.1	0.0103	4.1	0.82	66.1	2.7	78.1	3.8	463.7	64.5	66.1	2.7	NA		
NBO904-137	205	74763	0.5	17.1555	1.2	0.6934	5.4	0.0863	5.3	0.98	533.5	27.2	534.9	22.6	540.7	26	533.5	27.2	98.7		
NBO904-139	720	236044	10.5	17.35	0.5	0.5425	2.1	0.0683	2.1	0.97	425.7	8.6	440.1	7.6	516	10.6	425.7	8.6	82.5		
NBO904-140	257	77983	1.2	17.2191	1.1	0.6279	4.1	0.0784	4	0.96	486.6	18.6	494.8	16.2	532.6	25.1	486.6	18.6	91.4		

TABLE DR1. NEW U-PB CRYSTALLIZATION AGES (Downstream sample @ 8)

Grain	U (ppm)	206Pb 204Pb	U/Th	Isotope ratios							error corr.	Apparent ages (Ma)						Best (Ma)	age ± (Ma)	Conc (Ma)	
				206Pb*	±	207Pb*	±	206Pb*	±	207Pb*		±	206Pb*	±	207Pb*	±	206Pb*				±
				207Pb*	(%)	235U*	(%)	238U	(%)	238U*		(Ma)	235U	(Ma)	207Pb*	(Ma)					
03250816-1	218	574506	1.8	10.0555	0.6	2.9525	4	0.2153	4	0.99	1257.1	45.2	1395.5	30.3	1613.8	10.4	1613.8	10.4	77.9		
03250816-2	730	1275720	1.4	12.8667	0.3	1.6141	2.7	0.1506	2.7	0.99	904.5	22.5	975.7	16.8	1139.7	5.7	1139.7	5.7	79.4		
03250816-3	98	569	1.5	22.753	27.8	0.0557	29	0.0092	8.3	0.29	59	4.9	55	15.5	-113.5	696	59	4.9	NA		
03250816-5	113	4629	3.3	23.7888	55.2	0.0327	56.5	0.0056	12	0.21	36.3	4.4	32.7	18.2	-224.3	1495.3	36.3	4.4	NA		
03250816-6	326	181370	3.8	16.1327	1	0.9513	2.2	0.1113	2	0.91	680.3	13.1	678.8	11.1	673.6	20.4	680.3	13.1	101		
03250816-7	355	905	1.4	19.7726	8.7	0.0576	11.7	0.0083	7.7	0.66	53.1	4.1	56.9	6.5	221.5	202.4	53.1	4.1	NA		
03250816-8	273	12759	0.6	19.7626	16.9	0.0521	18.3	0.0075	6.9	0.38	47.9	3.3	51.5	9.2	222.7	394.4	47.9	3.3	NA		
03250816-9	393	28842	3.1	12.0944	3.1	1.9853	5.4	0.1741	4.5	0.82	1034.9	42.9	1110.5	36.7	1261.7	60.1	1261.7	60.1	82		
03250816-10	612	247566	3	12.1104	0.5	2.0891	2.8	0.1835	2.8	0.99	1086	28.1	1145.2	19.6	1259.2	9.3	1259.2	9.3	86.2		
03250816-11	220	7349	1	20.6756	9.8	0.0703	10.4	0.0105	3.7	0.36	67.6	2.5	68.9	7	117.2	230.5	67.6	2.5	NA		
03250816-12	157	10816	1.3	19.7589	15.1	0.0811	15.4	0.0116	3.3	0.22	74.5	2.5	79.2	11.7	223.1	350	74.5	2.5	NA		
03250816-13	3152	1434162	1.9	20.4257	0.6	0.1707	2.3	0.0253	2.3	0.97	161	3.6	160	3.5	145.8	13.2	161	3.6	NA		
03250816-15	359	22418	8	21.0758	10.9	0.0471	11.8	0.0072	4.5	0.38	46.2	2.1	46.7	5.4	71.8	259.5	46.2	2.1	NA		
03250816-16	130	5527	1.2	20.6348	37.3	0.0409	39.6	0.0061	13.3	0.33	39.3	5.2	40.7	15.8	121.9	908.3	39.3	5.2	NA		
03250816-17	175	53963	0.8	17.4971	1.4	0.6084	2	0.0772	1.5	0.74	479.4	6.8	482.6	7.7	497.4	29.9	479.4	6.8	96.4		
03250816-18	114	30040	1.5	11.0268	5.2	3.1262	10.7	0.25	9.4	0.87	1438.5	121	1439.2	82.8	1440	100	1440	100	99.9		
03250816-19	146	297965	2.8	10.2788	0.4	3.3273	3.4	0.248	3.4	0.99	1428.4	43.4	1487.5	26.6	1572.8	7.6	1572.8	7.6	90.8		
03250816-20	234	95360	0.5	17.3844	1.7	0.6068	2.4	0.0765	1.7	0.7	475.3	7.6	481.6	9.1	511.7	37.1	475.3	7.6	92.9		
03250816-21	31	21014	0.8	18.5314	10.4	0.5693	10.6	0.0765	2.1	0.19	475.3	9.4	457.5	39.1	369.5	234.8	475.3	9.4	128.6		
03250816-22	73	72186	1	12.8859	1.4	2.0663	3.4	0.1931	3.1	0.91	1138.2	32.5	1137.7	23.5	1136.8	28.6	1136.8	28.6	100.1		
03250816-23	274	58101	1.5	17.3881	2.1	0.5932	3.1	0.0748	2.2	0.72	465.1	9.8	472.9	11.6	511.2	47	465.1	9.8	91		
03250816-24	370	31156	3.2	21.1432	12.1	0.0587	14.6	0.009	8.2	0.56	57.8	4.7	57.9	8.2	64.2	287.9	57.8	4.7	NA		
03250816-25	895	19781	6	20.5111	8.3	0.0457	10.5	0.0068	6.4	0.61	43.7	2.8	45.4	4.6	136	196	43.7	2.8	NA		

TABLE DR1. NEW U-PB CRYSTALLIZATION AGES (Downstream sample @ 8)

Grain	U (ppm)	206Pb 204Pb	U/Th	Isotope ratios							error corr.	Apparent ages (Ma)						Best (Ma)	age ± (Ma)	Conc (Ma)	
				206Pb*	±	207Pb*	±	206Pb*	±	207Pb*		±	206Pb*	±	207Pb*	±	206Pb*				±
				207Pb*	(%)	235U*	(%)	238U	(%)	238U*		(Ma)	235U	(Ma)	207Pb*	(Ma)					
03250816-26	53	67676	1	9.8118	1.2	3.8637	1.8	0.275	1.3	0.75	1565.9	18.4	1606.1	14.2	1659.3	21.4	1659.3	21.4	94.4		
03250816-27	77	132831	1.5	10.0396	0.9	3.719	1.8	0.2708	1.6	0.87	1544.9	21.9	1575.5	14.7	1616.7	16.9	1616.7	16.9	95.6		
03250816-28	70	97651	1.7	10.0996	1.4	3.6573	2.2	0.2679	1.7	0.78	1530.1	23.6	1562.1	17.7	1605.6	25.9	1605.6	25.9	95.3		
03250816-29	73	28610	1.3	15.2305	3.8	0.9008	5.4	0.0995	3.8	0.71	611.5	22.3	652.1	26	795.5	80.3	611.5	22.3	76.9		
03250816-31	232	22787	0.3	22.7436	15.2	0.0708	15.5	0.0117	3.1	0.2	74.9	2.3	69.5	10.4	-112.4	376.1	74.9	2.3	NA		
03250816-33	216	211011	0.5	17.4178	1.9	0.5977	3.1	0.0755	2.5	0.79	469.2	11.2	475.8	11.9	507.4	42.8	469.2	11.2	92.5		
03250816-34	175	38539	1.8	14.961	1.7	1.2022	4.1	0.1304	3.7	0.91	790.4	27.6	801.6	22.7	832.8	36	790.4	27.6	94.9		
03250816-36	334	22156	2.4	24.3202	14.3	0.0507	14.5	0.0089	2.3	0.16	57.4	1.3	50.2	7.1	-280.3	365.7	57.4	1.3	NA		
03250816-37	78	23163	0.7	18.2806	5.7	0.5674	5.9	0.0752	1.6	0.28	467.6	7.4	456.4	21.7	400.1	127.5	467.6	7.4	116.9		
03250816-38	67	38200	1.5	13.7576	2.8	1.6329	3.5	0.1629	2.1	0.59	973	18.8	983	22.2	1005.2	57.8	973	18.8	96.8		
03250816-40	643	29832	0.7	21.7904	7.7	0.054	7.9	0.0085	1.5	0.18	54.7	0.8	53.4	4.1	-8	187.1	54.7	0.8	NA		
03250816-41	290	29786	0.5	20.9003	5.2	0.1275	7.1	0.0193	4.8	0.67	123.4	5.8	121.8	8.1	91.7	123.6	123.4	5.8	NA		
03250816-42	73	42996	0.9	17.8222	4	0.6224	6.4	0.0805	5	0.78	498.8	24	491.4	24.9	456.7	87.8	498.8	24	109.2		
03250816-43	1341	82295	0.4	17.2807	0.9	0.3872	7.8	0.0485	7.8	0.99	305.5	23.2	332.4	22.2	524.8	19.3	305.5	23.2	NA		
03250816-44	106	72731	2.1	12.9508	1.8	1.5132	5.1	0.1421	4.8	0.93	856.7	38.5	935.7	31.4	1126.7	36.8	856.7	38.5	76		
03250816-46	1975	26040	2.9	21.1555	8.2	0.0138	8.6	0.0021	2.9	0.33	13.6	0.4	13.9	1.2	62.8	194.6	13.6	0.4	NA		
03250816-47	963	912313	3.4	10.3712	0.1	3.5417	3.4	0.2664	3.4	1	1522.5	46.3	1536.6	27.1	1556	2.8	1556	2.8	97.9		
03250816-48	342	95271	1.9	17.5979	0.9	0.5462	4.3	0.0697	4.2	0.98	434.5	17.8	442.5	15.5	484.8	20.3	434.5	17.8	89.6		
03250816-49	209	78182	1	17.2454	1.3	0.634	2	0.0793	1.5	0.74	491.9	6.9	498.6	7.8	529.3	29.1	491.9	6.9	92.9		
03250816-50	130	6496	0.4	20.9012	24.3	0.079	24.8	0.012	5.3	0.21	76.8	4	77.2	18.5	91.5	582.1	76.8	4	NA		
03250816-51	196	110531	0.6	12.708	0.6	2.1627	4	0.1993	4	0.99	1171.7	42.3	1169.1	27.7	1164.3	11.3	1164.3	11.3	100.6		
03250816-53	980	30968	1.5	17.564	0.9	0.3119	4.8	0.0397	4.7	0.98	251.1	11.6	275.6	11.6	489	19.6	251.1	11.6	NA		

TABLE DR1. NEW U-PB CRYSTALLIZATION AGES (Downstream sample @ 8)

Grain	U (ppm)	206Pb 204Pb	U/Th	Isotope ratios							error corr.	Apparent ages (Ma)						Best (Ma)	age ± (Ma)	Conc (Ma)	
				206Pb*	±	207Pb*	±	206Pb*	±	207Pb*		±	206Pb*	±	207Pb*	±	206Pb*				±
				207Pb*	(%)	235U*	(%)	238U	(%)	238U*		(Ma)	235U	(Ma)	207Pb*	(Ma)					
3250816-54	200	15936	0.5	23.3838	12.6	0.0604	13.3	0.0102	4.1	0.31	65.7	2.7	59.6	7.7	-181.3	316.3	65.7	2.7	NA		
3250816-56	83	75726	0.5	12.727	1.4	1.9758	2	0.1824	1.5	0.72	1080	14.6	1107.3	13.8	1161.4	28.2	1161.4	28.2	93		
3250816-57	656	5714	1	21.275	10.8	0.0566	11	0.0087	2.1	0.19	56.1	1.2	55.9	6	49.4	259.5	56.1	1.2	NA		
3250816-58	499	1077569	0.6	9.907	0.2	3.8771	1.7	0.2786	1.7	0.99	1584.2	23.3	1608.9	13.5	1641.4	3.3	1641.4	3.3	96.5		
3250816-59	162	73266	1.3	13.2043	0.8	1.7882	2.2	0.1712	2	0.93	1019	18.9	1041.2	14.1	1088	16.3	1088	16.3	93.7		
3250816-60	100	134799	0.9	10.1826	0.9	3.7323	3	0.2756	2.8	0.95	1569.4	39.4	1578.3	23.8	1590.3	16.7	1590.3	16.7	98.7		
3250816-61	57	1876	0.8	20.6085	44.5	0.0509	47.2	0.0076	15.8	0.33	48.8	7.7	50.4	23.2	124.9	1096.7	48.8	7.7	NA		
3250816-63	79	3976	1	23.259	50.3	0.0506	51.2	0.0085	9.3	0.18	54.8	5.1	50.1	25.1	-167.9	1329.4	54.8	5.1	NA		
3250816-64	302	366461	14	16.3043	0.5	0.876	2	0.1036	1.9	0.97	635.4	11.4	638.8	9.2	651	10.5	635.4	11.4	97.6		
3250816-65	256	9562	1.5	22.7491	19.5	0.0501	20.3	0.0083	5.9	0.29	53.1	3.1	49.7	9.8	-113	482.9	53.1	3.1	NA		
3250816-66	347	134219	1.5	17.4088	1	0.605	1.4	0.0764	1	0.69	474.5	4.4	480.4	5.4	508.5	22.3	474.5	4.4	93.3		
3250816-67	179	15472	1.5	21.0541	13.9	0.1177	14.1	0.018	2.6	0.18	114.8	3	113	15.1	74.3	331.8	114.8	3	NA		
3250816-68	647	449091	0.7	10.081	0.2	3.88	1.3	0.2837	1.3	0.99	1609.9	18.2	1609.5	10.4	1609	2.9	1609	2.9	100.1		
3250816-69	70	50310	1.2	13.8599	2.1	1.5545	2.6	0.1563	1.5	0.58	935.9	12.9	952.3	15.9	990.2	42.6	935.9	12.9	94.5		
3250816-70	531	41313	0.5	20.9896	5.9	0.0762	6.7	0.0116	3.1	0.46	74.3	2.3	74.5	4.8	81.5	140.3	74.3	2.3	NA		
3250816-71	155	25082	1.8	19.0985	8.3	0.3034	8.5	0.042	1.9	0.22	265.3	4.9	269	20.1	301.2	188.8	265.3	4.9	NA		
3250816-72	1700	41825	2.6	21.1042	4.4	0.0415	5.7	0.0064	3.5	0.63	40.8	1.4	41.3	2.3	68.6	104.9	40.8	1.4	NA		
3250816-73	68	29482	0.9	12.9045	1.2	1.6678	4.2	0.1561	4.1	0.96	935	35.4	996.4	26.9	1133.9	23.9	1133.9	23.9	82.5		
3250816-74	46	37483	1.5	13.7204	2.4	1.6631	2.9	0.1655	1.7	0.58	987.2	15.3	994.6	18.4	1010.7	48	987.2	15.3	97.7		
3250816-75	222	193230	3.4	13.7612	0.8	1.6432	1.9	0.164	1.7	0.91	979	15.5	986.9	11.8	1004.7	15.8	979	15.5	97.4		
3250816-76	627	28435	0.8	21.3769	7.8	0.0783	12.4	0.0121	9.7	0.78	77.8	7.5	76.6	9.2	38	186.8	77.8	7.5	NA		
3250816-78	605	1110646	2.7	10.7436	0.2	3.1629	1.8	0.2465	1.8	0.99	1420.2	23.4	1448.2	14.2	1489.5	3.6	1489.5	3.6	95.3		
3250816-79	253	18206	1	20.1483	10.7	0.1052	10.9	0.0154	2.1	0.19	98.3	2	101.5	10.5	177.8	250.5	98.3	2	NA		
3250816-80	941	250896	12.6	17.274	0.5	0.5479	2.3	0.0686	2.2	0.97	428	9.2	443.6	8.3	525.6	11.9	428	9.2	81.4		
3250816-81	2385	30859	0.6	21.2251	3.1	0.031	8	0.0048	7.4	0.92	30.7	2.3	31	2.5	55	73.2	30.7	2.3	NA		
3250816-82	206	114755	2.9	13.7786	1	1.4991	2.4	0.1498	2.2	0.91	899.9	18.8	930	14.9	1002.1	20.1	899.9	18.8	89.8		

TABLE DR1. NEW U-PB CRYSTALLIZATION AGES (Downstream sample @ 8)

Grain	U (ppm)	206Pb 204Pb	U/Th	Isotope ratios							error corr.	Apparent ages (Ma)						Best (Ma)	age ± (Ma)	Conc (Ma)	
				206Pb*	±	207Pb*	±	206Pb*	±	207Pb*		±	206Pb*	±	207Pb*	±	206Pb*				±
				207Pb*	(%)	235U*	(%)	238U	(%)	238U*		(Ma)	235U	(Ma)	207Pb*	(Ma)					
3250816-83	438	35216	0.4	21.0428	4.9	0.1106	5.2	0.0169	1.7	0.33	107.9	1.8	106.5	5.2	75.5	115.8	107.9	1.8	NA		
3250816-84	738	248968	3.2	19.5493	1.5	0.2414	4	0.0342	3.7	0.93	217	7.9	219.6	7.9	247.7	33.5	217	7.9	NA		
3250816-85	90	5062	0.7	16.8523	8.9	0.5729	9.3	0.07	2.6	0.28	436.3	11.1	459.9	34.3	579.6	193.6	436.3	11.1	75.3		
3250816-86	370	8919	1	21.7805	13.4	0.0401	13.8	0.0063	3.5	0.25	40.7	1.4	39.9	5.4	-7	324	40.7	1.4	NA		
3250816-87	1241	23008	1.7	22.6303	5.3	0.0375	5.5	0.0062	1.2	0.22	39.6	0.5	37.4	2	-100.2	130.9	39.6	0.5	NA		
3250816-88	313	16086	32	17.298	17.8	0.0174	58.8	0.0022	56	0.95	14.1	7.9	17.6	10.2	522.6	392.5	14.1	7.9	NA		
3250816-89	86	69635	1.1	9.935	0.7	3.8649	2.2	0.2785	2.1	0.95	1583.8	29	1606.4	17.6	1636.2	12.9	1636.2	12.9	96.8		
3250816-90	342	385858	1.1	12.6607	0.4	2.2102	3.3	0.2029	3.3	0.99	1191.1	35.7	1184.3	23.1	1171.8	7.9	1171.8	7.9	101.7		
3250816-91	232	33127	0.5	21.4787	7.9	0.1109	8.2	0.0173	2.1	0.26	110.4	2.3	106.8	8.3	26.6	189.7	110.4	2.3	NA		
3250816-92	488	36970	1	21.2993	3	0.0776	3.7	0.012	2.2	0.58	76.8	1.7	75.9	2.7	46.7	72.5	76.8	1.7	NA		
3250816-94	382	3186	0.3	20.6808	33.5	0.0248	34.2	0.0037	6.6	0.19	24	1.6	24.9	8.4	116.6	811.2	24	1.6	NA		
3250816-95	102	121298	1	10.2962	0.7	3.5785	3.3	0.2672	3.2	0.98	1526.7	43.2	1544.8	25.8	1569.6	13	1569.6	13	97.3		
3250816-96	408	14767	1.5	20.7588	7.6	0.0801	8.2	0.0121	2.9	0.36	77.3	2.3	78.2	6.1	107.8	179.8	77.3	2.3	NA		

TABLE DR1. NEW U-PB CRYSTALLIZATION AGES (Downstream sample @ 8)

Grain	U (ppm)	206Pb 204Pb	U/Th	Isotope ratios							error corr.	Apparent ages (Ma)						Best (Ma)	age ± (Ma)	Conc (Ma)			
				206Pb*	±	207Pb*	±	206Pb*	±	238U		±	206Pb*	±	207Pb*	±	206Pb*				±	207Pb*	±
					(%)	235U*	(%)	238U	(%)	238U*		(Ma)	235U	(Ma)	207Pb*	(Ma)	207Pb*				(Ma)		
3250816-97	79	2968	1	15.2288	27	0.078	27.5	0.0086	5.1	0.18	55.3	2.8	76.3	20.2	795.7	576.6	55.3	2.8	NA				
3250816-98	47	29969	0.9	12.587	2.6	2.118	3	0.1934	1.5	0.5	1139.5	15.7	1154.7	20.7	1183.3	51.2	1183.3	51.2	96.3				
3250816-99	583	826014	1.3	9.9156	0.1	3.9896	1.9	0.2869	1.9	1	1626.1	27.3	1632.1	15.5	1639.8	1.3	1639.8	1.3	99.2				
3250816-100	129	360258	1.4	10.1249	0.7	3.7492	1.1	0.2753	0.8	0.76	1567.7	11.1	1581.9	8.4	1600.9	12.8	1600.9	12.8	97.9				

TABLE DR1. NEW U-PB CRYSTALLIZATION AGES (Yigong river @ 3)

Grain	U (ppm)	206Pb 204Pb	U/Th	Isotope ratios							error corr.	Apparent ages (Ma)						Best (Ma)	age ± (Ma)	Conc (Ma)	
				206Pb*	±	207Pb*	±	206Pb*	±	207Pb*		±	206Pb*	±	207Pb*	±	206Pb*				±
				207Pb*	(%)	235U*	(%)	238U	(%)	238U*		(Ma)	235U	(Ma)	207Pb*	(Ma)					
NB0404-1	821	172023	0.7	20.6603	5.4	0.1112	5.8	0.0167	2.1	0.37	106.5	2.3	107	5.9	118.9	127.1	106.5	2.3	NA		
NB0404-2	532	5168	0.6	21.5401	15.1	0.072	17	0.0112	7.9	0.47	72.1	5.7	70.6	11.6	19.8	364	72.1	5.7	NA		
NB0404-3	944	59695	1.5	20.2216	3	0.1196	3.3	0.0175	1.5	0.45	112.1	1.7	114.7	3.6	169.3	69.8	112.1	1.7	NA		
NB0404-4	902	19258	3.9	20.0582	6.3	0.0552	7.2	0.008	3.6	0.5	51.5	1.8	54.5	3.8	188.2	146	51.5	1.8	NA		
NB0404-5	72	144662	2	9.5334	1.2	4.2528	3.9	0.2941	3.7	0.95	1661.7	54	1684.3	32	1712.4	22.8	1712.4	22.8	97		
NB0404-6	363	174021	3.4	13.9639	1.2	1.5381	5.7	0.1558	5.6	0.98	933.2	48.7	945.7	35.3	975	24	933.2	48.7	95.7		
NB0404-7	2011	22310	2.6	20.3278	2.4	0.1265	5.5	0.0186	5	0.9	119.1	5.8	120.9	6.3	157.1	55.2	119.1	5.8	NA		
NB0404-8	175	14541	1.6	24.7945	36.6	0.0615	37.1	0.0111	6	0.16	70.9	4.2	60.6	21.9	-329.7	969.4	70.9	4.2	NA		
NB0404-9	501	23561	1.4	22.5711	14.6	0.0692	15.1	0.0113	3.5	0.23	72.6	2.6	68	9.9	-93.7	361.1	72.6	2.6	NA		
NB0404-10	893	1297	0.8	19.9899	13.8	0.0476	14.9	0.0069	5.5	0.37	44.3	2.4	47.2	6.8	196.2	321.8	44.3	2.4	NA		
NB0404-12	1870	40433	1.4	20.3612	2.7	0.1182	2.9	0.0175	1.1	0.36	111.5	1.2	113.4	3.2	153.2	64.3	111.5	1.2	NA		
NB0404-13	736	20549	2.2	21.4342	14.7	0.0537	14.9	0.0083	2.2	0.15	53.5	1.2	53.1	7.7	31.6	354.7	53.5	1.2	NA		
NB0404-14	317	4915	0.7	26.4101	19.6	0.0608	20.1	0.0116	4.6	0.23	74.6	3.4	59.9	11.7	-494.7	524.2	74.6	3.4	NA		
NB0404-15	1411	148567	1.5	21.0292	2.5	0.1073	3.5	0.0164	2.3	0.68	104.7	2.4	103.5	3.4	77.1	60.4	104.7	2.4	NA		
NB0404-16	333	7820	0.6	18.6174	16.2	0.0794	16.7	0.0107	4.1	0.25	68.8	2.8	77.6	12.5	359	367.9	68.8	2.8	NA		
NB0404-17	893	21835	2.1	20.3033	9.1	0.0743	9.4	0.0109	2.6	0.28	70.1	1.8	72.7	6.6	159.9	212.4	70.1	1.8	NA		
NB0404-18	361	14518	1.8	19.5019	11.4	0.12	12	0.017	3.8	0.31	108.5	4.1	115.1	13.1	253.3	263.1	108.5	4.1	NA		
NB0404-19	469	19034	1.3	19.6583	8.3	0.1265	9	0.018	3.4	0.38	115.2	3.9	121	10.3	234.9	192.7	115.2	3.9	NA		
NB0404-20	774	23367	1.6	20.7441	6.3	0.1182	6.9	0.0178	2.9	0.43	113.7	3.3	113.5	7.4	109.4	147.7	113.7	3.3	NA		
NB0404-21	417	12481	2.1	23.0164	14.7	0.101	15	0.0169	3	0.2	107.8	3.2	97.7	14	-141.9	365.1	107.8	3.2	NA		
NB0404-22	313	11748	2.3	21.3347	11.9	0.1194	12.1	0.0185	2.2	0.19	118	2.6	114.5	13.1	42.7	284.7	118	2.6	NA		
NB0404-23	367	15529	0.7	21.6495	15.8	0.1053	16	0.0165	2.6	0.16	105.7	2.7	101.6	15.4	7.6	381.3	105.7	2.7	NA		
NB0404-24	578	31277	1	21.1312	5.3	0.1162	5.6	0.0178	1.8	0.33	113.8	2.1	111.6	5.9	65.6	125.3	113.8	2.1	NA		
NB0404-25	1345	79306	2.6	20.5721	2.6	0.1118	4.7	0.0167	4	0.84	106.6	4.2	107.6	4.8	129.1	60.7	106.6	4.2	NA		
NB0404-26	644	98720	1.4	12.7888	2.8	0.6505	15	0.0603	14.8	0.98	377.7	54.2	508.8	60.2	1151.8	56.2	377.7	54.2	NA		
NB0404-28	427	12542	0.8	20.0711	7.2	0.1241	7.6	0.0181	2.4	0.32	115.4	2.8	118.8	8.5	186.7	167.9	115.4	2.8	NA		

TABLE DR1. NEW U-PB CRYSTALLIZATION AGES (Yigong river @ 3)

Grain	U (ppm)	206Pb 204Pb	U/Th	Isotope ratios							error corr.	Apparent ages (Ma)						Best (Ma)	age ± (Ma)	Conc (Ma)	
				206Pb*	±	207Pb*	±	206Pb*	±	207Pb*		±	206Pb*	±	207Pb*	±	206Pb*				±
				207Pb*	(%)	235U*	(%)	238U	(%)	238U*		(Ma)	235U	(Ma)	207Pb*	(Ma)					
NB0404-29	110	2986	1	13.6413	25.1	0.1664	27.4	0.0165	10.8	0.4	105.3	11.3	156.3	39.6	1022.4	516.2	105.3	11.3	NA		
NB0404-30	524	20979	1.2	21.074	4.5	0.1191	5.6	0.0182	3.3	0.6	116.3	3.8	114.2	6	72	106.8	116.3	3.8	NA		
NB0404-31	613	20395	1.9	20.7236	3.5	0.1134	3.7	0.017	1	0.28	108.9	1.1	109	3.8	111.7	83.2	108.9	1.1	NA		
NB0404-32	638	16887	1	20.3809	9.6	0.0785	10	0.0116	2.8	0.28	74.4	2.1	76.7	7.4	151	225.4	74.4	2.1	NA		
NB0404-33	419	19686	2.3	20.2797	9.6	0.1322	10	0.0194	2.9	0.29	124.1	3.5	126.1	11.9	162.6	225.2	124.1	3.5	NA		
NB0404-34	380	33864	1.9	17.2434	2	0.6468	4.9	0.0809	4.5	0.91	501.4	21.5	506.5	19.5	529.5	44.3	501.4	21.5	94.7		
NB0404-35	818	110107	3.5	19.5855	3	0.2364	5.2	0.0336	4.2	0.82	213	8.9	215.5	10.1	243.5	69	213	8.9	NA		
NB0404-36	432	108278	0.8	17.3834	0.6	0.6402	2.1	0.0807	2	0.95	500.4	9.6	502.4	8.3	511.8	14	500.4	9.6	97.8		
NB0404-37	182	61239	2.1	13.9231	1.8	1.2735	5.9	0.1286	5.7	0.96	779.9	41.7	834	33.9	980.9	35.8	779.9	41.7	79.5		
NB0404-38	514	3654	1.1	19.8693	9.2	0.122	9.6	0.0176	2.8	0.29	112.4	3.1	116.9	10.6	210.2	212.6	112.4	3.1	NA		
NB0404-39	337	9605	1.1	20.2053	10.7	0.1184	11.3	0.0174	3.4	0.3	110.9	3.7	113.6	12.1	171.2	251.1	110.9	3.7	NA		
NB0404-40	611	5454	0.9	20.3894	11.6	0.078	11.9	0.0115	2.9	0.24	73.9	2.1	76.3	8.8	150	271.5	73.9	2.1	NA		
NB0404-41	89	191	3.7	15.2686	84.8	0.0857	85.8	0.0095	12.9	0.15	60.9	7.8	83.5	68.9	790.2	2349.1	60.9	7.8	NA		
NB0404-42	315	195714	1.8	10.7153	2.5	2.7979	4.4	0.2174	3.6	0.82	1268.3	41.4	1355	32.9	1494.5	47.8	1494.5	47.8	84.9		
NB0404-43	1207	20208	1	21.614	2.3	0.0758	4.7	0.0119	4.1	0.87	76.1	3.1	74.2	3.4	11.5	56.2	76.1	3.1	NA		
NB0404-44	990	48813	1.8	20.9218	3.4	0.1186	5.2	0.018	3.9	0.76	114.9	4.5	113.8	5.6	89.3	80.4	114.9	4.5	NA		
NB0404-45	779	269645	4.7	13.7766	2.1	0.8478	14.8	0.0847	14.7	0.99	524.2	73.8	623.4	69.1	1002.4	43.1	524.2	73.8	52.3		
NB0404-46	1118	31541	1.1	20.0271	3.6	0.1134	4.4	0.0165	2.5	0.57	105.3	2.6	109.1	4.5	191.9	83.5	105.3	2.6	NA		
NB0404-47	2022	101928	1.1	20.5698	4.3	0.0778	5.1	0.0116	2.7	0.53	74.3	2	76	3.7	129.3	100.7	74.3	2	NA		
NB0404-48	735	12421	1.4	20.8027	7.7	0.1155	8.1	0.0174	2.7	0.33	111.3	3	111	8.5	102.8	181.5	111.3	3	NA		
NB0404-49	790	21284	2.3	20.3993	5.5	0.0771	6.9	0.0114	4.2	0.6	73.1	3	75.4	5	148.9	130.1	73.1	3	NA		
NB0404-50	422	14684	1.4	20.9375	14.4	0.119	14.8	0.0181	3.6	0.24	115.4	4.1	114.2	16	87.5	342.5	115.4	4.1	NA		
NB0404-51	829	25162	0.8	20.8901	6.4	0.0778	7.6	0.0118	4.2	0.55	75.6	3.1	76.1	5.6	92.8	151.4	75.6	3.1	NA		
NB0404-52	403	14702	0.6	21.8639	21.8	0.0719	21.9	0.0114	2.9	0.13	73.1	2.1	70.5	14.9	-16.2	531.3	73.1	2.1	NA		
NB0404-53	477	5161	0.7	19.4261	20.3	0.0805	23.7	0.0113	12.3	0.52	72.7	8.9	78.6	18	262.2	470.1	72.7	8.9	NA		
NB0404-54	713	26773	0.7	21.8584	6.6	0.1051	7	0.0167	2.4	0.35	106.5	2.6	101.5	6.8	-15.6	159	106.5	2.6	NA		

TABLE DR1. NEW U-PB CRYSTALLIZATION AGES (Yigong river @ 3)

Grain	U (ppm)	206Pb 204Pb	U/Th	Isotope ratios							error corr.	Apparent ages (Ma)						Best (Ma)	age ± (Ma)	Conc (Ma)	
				206Pb*	±	207Pb*	±	206Pb*	±	207Pb*		±	206Pb*	±	207Pb*	±	206Pb*				±
				207Pb*	(%)	235U*	(%)	238U	(%)	238U*		(Ma)	235U	(Ma)	207Pb*	(Ma)					
NB0404-55	684	179444	2.1	11.3348	0.6	2.6172	5.6	0.2152	5.6	0.99	1256.2	63.6	1305.5	41.2	1387.3	11.2	1387.3	11.2	90.5		
NB0404-56	805	31189	1.2	20.4833	4.3	0.1196	5.3	0.0178	3.1	0.59	113.5	3.5	114.7	5.7	139.2	100.6	113.5	3.5	NA		
NB0404-57	98	5311	1.2	19.1254	34.7	0.1356	35.8	0.0188	8.8	0.25	120.1	10.5	129.1	43.4	297.9	814	120.1	10.5	NA		
NB0404-58	81	103250	0.5	6.9537	0.7	7.9591	3.9	0.4014	3.9	0.99	2175.5	71.8	2226.4	35.6	2273.6	11.6	2273.6	11.6	95.7		
NB0404-60	867	21646	1.2	22.2389	8.6	0.0712	8.9	0.0115	2	0.22	73.6	1.4	69.9	6	-57.5	210.7	73.6	1.4	NA		
NB0404-61	189	6765	0.8	22.8847	16.7	0.1059	18.2	0.0176	7.2	0.4	112.3	8.1	102.2	17.7	-127.7	415.2	112.3	8.1	NA		
NB0404-62	463	19737	1.4	20.7789	7.2	0.1259	8	0.019	3.7	0.46	121.2	4.4	120.4	9.1	105.4	169.2	121.2	4.4	NA		
NB0404-63	125	64464	1.4	10.4664	1.3	3.1925	3	0.2423	2.7	0.91	1398.9	34.1	1455.3	23.1	1538.8	23.5	1538.8	23.5	90.9		
NB0404-64	449	25711	2.4	20.9847	5.9	0.1514	12.3	0.023	10.7	0.88	146.8	15.6	143.1	16.4	82.1	140.6	146.8	15.6	NA		
NB0404-65	764	20388	1.3	22.7473	10.7	0.0492	11.1	0.0081	3.1	0.28	52.1	1.6	48.7	5.3	-112.8	263.7	52.1	1.6	NA		
NB0404-66	451	1934	0.8	17.7826	23.7	0.0881	24.2	0.0114	4.7	0.19	72.9	3.4	85.8	19.9	461.6	532.5	72.9	3.4	NA		
NB0404-67	359	18676	1.6	20.8717	12.3	0.1147	12.6	0.0174	2.4	0.19	110.9	2.6	110.2	13.1	94.9	292.8	110.9	2.6	NA		
NB0404-68	454	19386	1.2	20.7573	7.6	0.1124	8.1	0.0169	2.6	0.33	108.2	2.8	108.2	8.3	107.9	180.4	108.2	2.8	NA		
NB0404-69	653	21194	2.5	20.8146	6.9	0.1123	7.9	0.017	3.9	0.49	108.4	4.2	108.1	8.1	101.4	163.2	108.4	4.2	NA		
NB0404-70	471	14636	26.3	21.4792	19	0.0701	19.3	0.0109	3.1	0.16	70	2.1	68.8	12.8	26.5	460	70	2.1	NA		
NB0404-71	276	5675	1.4	17.8182	18.7	0.0748	19	0.0097	3.7	0.19	62	2.3	73.2	13.5	457.2	417.8	62	2.3	NA		
NB0404-72	546	32365	1.8	19.8197	4.8	0.1343	5.3	0.0193	2.1	0.39	123.2	2.5	127.9	6.3	216	112.2	123.2	2.5	NA		
NB0404-73	1238	30957	5.8	20.7683	2.4	0.1195	3	0.018	1.8	0.62	115	2.1	114.6	3.2	106.7	55.6	115	2.1	NA		
NB0404-74	80	20901	1.3	14.5873	4.6	1.2224	5.7	0.1293	3.5	0.6	784	25.5	810.9	32.1	885.3	94.9	784	25.5	88.6		
NB0404-75	978	26261	0.8	21.1789	2.3	0.1204	3.1	0.0185	2.1	0.68	118.1	2.5	115.4	3.4	60.2	53.7	118.1	2.5	NA		
NB0404-76	625	19937	1.1	20.2807	3.5	0.1215	4.5	0.0179	2.9	0.65	114.2	3.3	116.4	5	162.5	81.1	114.2	3.3	NA		
NB0404-77	1039	33465	1.8	21.0481	4	0.1178	4.3	0.018	1.6	0.37	114.9	1.8	113.1	4.6	75	95.9	114.9	1.8	NA		
NB0404-78	223	13648	1.6	19.204	16	0.1397	16.9	0.0195	5.2	0.31	124.3	6.5	132.8	21	288.6	368.8	124.3	6.5	NA		
NB0404-79	2307	173825	2.8	19.7638	0.9	0.2274	2.5	0.0326	2.3	0.93	206.8	4.7	208.1	4.6	222.5	20.3	206.8	4.7	NA		
NB0404-80	773	38739	1.2	21.1136	5.9	0.1125	6.3	0.0172	2.1	0.34	110.1	2.3	108.3	6.4	67.6	140.3	110.1	2.3	NA		
NB0404-81	284	9100	2	22.7698	11.2	0.1174	12	0.0194	4.4	0.37	123.7	5.4	112.7	12.8	-115.3	277	123.7	5.4	NA		

TABLE DR1. NEW U-PB CRYSTALLIZATION AGES (Yigong river @ 3)

Grain	U (ppm)	206Pb 204Pb	U/Th	Isotope ratios							error corr.	Apparent ages (Ma)						Best (Ma)	age ± (Ma)	Conc (Ma)	
				206Pb*	±	207Pb*	±	206Pb*	±	207Pb*		±	206Pb*	±	207Pb*	±	206Pb*				±
				207Pb*	(%)	235U*	(%)	238U	(%)	238U*		(Ma)	235U	(Ma)	207Pb*	(Ma)					
NB0404-82	85	59825	0.8	8.5706	1.1	5.4123	4.5	0.3364	4.4	0.97	1869.5	71.1	1886.8	38.7	1905.9	19.8	1905.9	19.8	98.1		
NB0404-83	1403	1245421	1.9	5.1121	0.7	14.1799	3.1	0.5257	3	0.97	2723.5	66	2761.8	28.9	2789.9	11.2	2789.9	11.2	97.6		
NB0404-84	611	9433	1.1	20.4173	13.2	0.0821	27.4	0.0122	24.1	0.88	77.9	18.6	80.1	21.1	146.8	310.8	77.9	18.6	NA		
NB0404-85	321	7176	1.3	20.3823	10	0.1176	10.6	0.0174	3.6	0.34	111.1	3.9	112.9	11.3	150.8	234.3	111.1	3.9	NA		
NB0404-86	451	5467	1.3	15.5549	21.3	0.1508	21.5	0.017	2.8	0.13	108.8	3	142.7	28.6	751.1	454.2	108.8	3	NA		
NB0404-87	608	54721	8.4	19.0191	3.5	0.1376	19.5	0.019	19.2	0.98	121.2	23	130.9	24	310.7	79.6	121.2	23	NA		
NB0404-88	238	254698	1.3	10.3807	0.9	3.293	4.2	0.2479	4.1	0.98	1427.8	52.9	1479.4	33	1554.3	17	1554.3	17	91.9		
NB0404-89	2692	75493	4.7	20.4888	1.8	0.1131	5.1	0.0168	4.8	0.93	107.4	5.1	108.8	5.3	138.6	43.4	107.4	5.1	NA		
NB0404-90	488	37859	1.5	19.1561	7.8	0.1275	8	0.0177	1.9	0.23	113.2	2.1	121.9	9.2	294.3	177.2	113.2	2.1	NA		
NB0404-91	377	10041	1.1	23.2195	22.9	0.0702	23.4	0.0118	4.6	0.2	75.7	3.5	68.9	15.6	-163.7	576.9	75.7	3.5	NA		
NB0404-92	534	7775	0.7	20.0874	14	0.0755	14.6	0.011	4.1	0.28	70.5	2.9	73.9	10.4	184.8	328.6	70.5	2.9	NA		
NB0404-93	2001	51630	1.6	20.4872	2.7	0.0644	3.4	0.0096	2.1	0.61	61.4	1.3	63.4	2.1	138.7	62.4	61.4	1.3	NA		
NB0404-94	840	1582	2	19.3736	11.4	0.1224	11.5	0.0172	1.8	0.16	109.9	2	117.2	12.7	268.4	261.3	109.9	2	NA		
NB0404-95	432	8411	0.8	21.7217	14.9	0.0727	15.2	0.0114	3	0.2	73.4	2.2	71.2	10.4	-0.4	360.2	73.4	2.2	NA		
NB0404-96	386	3590	0.7	18.2054	14.6	0.1251	16.4	0.0165	7.6	0.46	105.6	8	119.7	18.5	409.3	327	105.6	8	NA		
NB0404-97	809	27357	1.8	20.2987	4.7	0.1181	5.3	0.0174	2.3	0.44	111.1	2.6	113.3	5.6	160.5	110.3	111.1	2.6	NA		
NB0404-98	1543	968	1.3	19.5145	9.2	0.1133	10	0.016	4	0.4	102.6	4.1	109	10.4	251.8	211.5	102.6	4.1	NA		
NB0404-99	327	46918	1.4	16.6586	1.5	0.7646	4	0.0924	3.7	0.93	569.6	20.3	576.7	17.6	604.6	31.4	569.6	20.3	94.2		
NB0404-100	517	253086	0.7	14.7561	0.8	1.2704	1.9	0.136	1.7	0.91	821.8	13.4	832.6	10.8	861.5	16	821.8	13.4	95.4		
NB0404-101	2725	76895	4.1	20.869	2.3	0.1153	3.4	0.0174	2.5	0.73	111.5	2.7	110.8	3.6	95.2	55.1	111.5	2.7	NA		
NB0404-102	464	64455	2.2	17.3601	0.9	0.6476	4.2	0.0815	4.1	0.98	505.3	20.2	507	16.9	514.7	19.1	505.3	20.2	98.2		
NB0404-103	626	30771	0.4	20.6164	9.1	0.0794	11.1	0.0119	6.4	0.57	76.1	4.8	77.6	8.3	123.9	213.5	76.1	4.8	NA		
NB0404-104	890	82785	1.2	21.4705	4	0.1165	4.3	0.0181	1.6	0.37	115.9	1.8	111.9	4.6	27.5	95.8	115.9	1.8	NA		
NB0404-105	1063	655477	36.3	9.9925	0.1	3.8602	1.8	0.2798	1.8	1	1590.1	24.9	1605.4	14.3	1625.5	2.7	1625.5	2.7	97.8		
NB0404-106	133	83866	1.1	6.222	0.8	7.0533	5.4	0.3183	5.4	0.99	1781.4	83.3	2118.2	48.1	2463.2	13.1	2463.2	13.1	72.3		

TABLE DR1. NEW U-PB CRYSTALLIZATION AGES (Yigong river @ 3)

Grain	U (ppm)	206Pb 204Pb	U/Th	Isotope ratios							error corr.	Apparent ages (Ma)						Best (Ma)	age ± (Ma)	Conc (Ma)	
				206Pb*	±	207Pb*	±	206Pb*	±	207Pb*		±	206Pb*	±	207Pb*	±	206Pb*				±
				207Pb*	(%)	235U*	(%)	238U	(%)	238U*		(Ma)	235U	(Ma)	207Pb*	(Ma)					
NB0404-107	1795	129804	100	19.4414	0.7	0.2471	1.3	0.0348	1	0.81	220.8	2.2	224.2	2.5	260.5	17	220.8	2.2	NA		
NB0404-108	178	123691	2.5	14.2738	1.4	1.507	3.3	0.156	2.9	0.91	934.6	25.6	933.2	19.9	930	28.4	934.6	25.6	100.5		
NB0404-109	422	322497	2.6	14.007	0.8	1.4109	6.9	0.1433	6.9	0.99	863.5	55.8	893.5	41.3	968.7	15.8	863.5	55.8	89.1		
NB0404-111	1104	116314	2.3	20.998	7.6	0.0763	8.5	0.0116	3.8	0.45	74.5	2.8	74.7	6.1	80.6	180.3	74.5	2.8	NA		
NB0404-112	677	94071	8.1	20.1139	1.9	0.2294	2.8	0.0335	2.1	0.74	212.2	4.3	209.7	5.3	181.8	43.5	212.2	4.3	NA		
NB0404-113	572	30893	1.3	20.114	6.4	0.1285	7.4	0.0187	3.7	0.5	119.8	4.4	122.8	8.6	181.7	149.5	119.8	4.4	NA		
NB0404-114	504	24278	1.5	21.1069	7.1	0.1162	7.8	0.0178	3.3	0.43	113.7	3.7	111.6	8.2	68.3	168	113.7	3.7	NA		
NB0404-115	1226	53594	10.9	20.8829	2.5	0.1099	3.4	0.0167	2.3	0.68	106.5	2.4	105.9	3.4	93.7	58.5	106.5	2.4	NA		
NB0404-116	527	13159	1.2	20.4491	8.8	0.1316	9.3	0.0195	3.1	0.33	124.6	3.8	125.5	11	143.1	207.3	124.6	3.8	NA		
NB0404-117	1148	4103	1.7	18.3508	13.7	0.1429	15.2	0.019	6.6	0.43	121.4	7.9	135.6	19.3	391.5	309	121.4	7.9	NA		
NB0404-118	1790	138315	5.9	20.5988	1.7	0.115	2.5	0.0172	1.8	0.73	109.8	2	110.5	2.6	126	39.3	109.8	2	NA		
NB0404-119	398	6096	1.6	19.0826	8.4	0.1314	9	0.0182	3.3	0.36	116.2	3.8	125.3	10.6	303.1	190.8	116.2	3.8	NA		
NB0404-120	424	3640	2.3	21.2463	9.8	0.137	14.6	0.0211	10.8	0.74	134.7	14.4	130.4	17.9	52.6	235	134.7	14.4	NA		

TABLE DR1. NEW U-PB CRYSTALLIZATION AGES (Downstream sample @ 6)

Grain	U (ppm)	206Pb 204Pb	U/Th	Isotope ratios							error corr.	Apparent ages (Ma)						Best (Ma)	age ± (Ma)	Conc (Ma)	
				206Pb*	±	207Pb*	±	206Pb*	±	207Pb*		±	206Pb*	±	207Pb*	±	206Pb*				±
				207Pb*	(%)	235U*	(%)	238U	(%)	238U*		(Ma)	235U	(Ma)	207Pb*	(Ma)					
03280836-1	373	267955	0.7	14.5867	0.8	1.3296	1.7	0.1407	1.6	0.89	848.4	12.4	858.7	10.1	885.4	16.3	848.4	12.4	95.8		
03280836-2	432	12472	0.3	25.3453	18.6	0.0314	19.3	0.0058	5.2	0.27	37.1	1.9	31.4	6	-386.5	487.3	37.1	1.9	NA		
03280836-4	956	29189	4.3	21.869	5.2	0.0673	6	0.0107	3	0.5	68.4	2	66.1	3.8	-16.7	125	68.4	2	NA		
03280836-5	634	1639	0.7	20.4353	29.4	0.0516	29.9	0.0076	5.4	0.18	49.1	2.6	51	14.9	144.7	703.2	49.1	2.6	NA		
03280836-6	4627	1687322	3.7	17.4088	0.1	0.6257	1.7	0.079	1.7	1	490.2	7.9	493.4	6.6	508.5	3	490.2	7.9	96.4		
03280836-7	1256	131446	6.4	19.9765	0.9	0.2306	1.5	0.0334	1.2	0.79	211.8	2.5	210.7	2.9	197.7	21.6	211.8	2.5	NA		
03280836-9	74	3484	1.7	12.5738	3.4	2.0392	4.8	0.186	3.3	0.7	1099.5	33.6	1128.7	32.5	1185.4	67.6	1185.4	67.6	92.8		
03280836-10	77	3864	0.8	19.8794	18.3	0.1208	18.5	0.0174	3.3	0.18	111.3	3.6	115.8	20.3	209	426.3	111.3	3.6	NA		
03280836-11	308	71974	2.1	12.8985	2	1.0263	5	0.096	4.5	0.91	591	25.6	717.1	25.6	1134.8	40.1	591	25.6	52.1		
03280836-12	488	96254	2.9	15.0637	1.7	0.7109	7.3	0.0777	7.1	0.97	482.2	32.9	545.3	30.7	818.6	35.1	482.2	32.9	58.9		
03280836-13	1692	281331	21.9	16.1216	0.5	0.854	2.8	0.0999	2.8	0.98	613.6	16.3	626.9	13.3	675.1	10.7	613.6	16.3	90.9		
03280836-14	589	171982	11.2	13.5666	0.5	1.7384	2.3	0.171	2.2	0.97	1017.9	20.9	1022.9	14.7	1033.5	10.3	1033.5	10.3	98.5		
03280836-15	319	156178	0.8	9.7358	0.3	3.855	2.4	0.2722	2.4	0.99	1552	32.6	1604.3	19.2	1673.7	5.4	1673.7	5.4	92.7		
03280836-16	410	23883	23.1	17.5909	5.2	0.246	6.5	0.0314	4	0.61	199.2	7.8	223.3	13.1	485.6	114.3	199.2	7.8	NA		
03280836-17	429	81102	0.9	21.3918	5.7	0.1269	7.1	0.0197	4.2	0.6	125.7	5.3	121.3	8.1	36.3	137	125.7	5.3	NA		
03280836-18	232	61604	106	15.0375	0.7	1.2201	1.6	0.1331	1.4	0.89	805.3	10.8	809.8	8.9	822.2	15.2	805.3	10.8	98		
03280836-19	936	20652	2.2	21.0842	7.2	0.0484	8.3	0.0074	4	0.49	47.6	1.9	48	3.9	70.9	172	47.6	1.9	NA		
03280836-20	116	39336	1.8	17.656	5.1	0.6397	6.5	0.0819	4	0.61	507.5	19.3	502.1	25.7	477.4	113.8	507.5	19.3	106.3		
03280836-21	332	24259	1.3	17.7077	8	0.1364	10.7	0.0175	7.1	0.66	111.9	7.8	129.8	13	471	177.2	111.9	7.8	NA		
03280836-22	468	84522	2	15.7135	1	0.7445	3.4	0.0848	3.2	0.95	525	16.4	565	14.8	729.7	21.9	525	16.4	71.9		
03280836-23	508	59979	1.9	20.166	5	0.1338	5.4	0.0196	2	0.37	124.9	2.5	127.5	6.4	175.7	116.2	124.9	2.5	NA		
03280836-24	1134	9019	51.3	23.3223	15.5	0.0181	16.5	0.0031	5.6	0.34	19.7	1.1	18.3	3	-174.7	389.2	19.7	1.1	NA		
03280836-25	2161	456660	6	17.5777	0.3	0.5901	2.2	0.0752	2.1	0.99	467.6	9.6	470.9	8.1	487.3	6.1	467.6	9.6	96		

TABLE DR1. NEW U-PB CRYSTALLIZATION AGES (Downstream sample @ 6)

Grain	U (ppm)	206Pb 204Pb	U/Th	Isotope ratios							error corr.	Apparent ages (Ma)						Best (Ma)	age ± (Ma)	Conc (Ma)	
				206Pb*	±	207Pb*	±	206Pb*	±	207Pb*		±	206Pb*	±	207Pb*	±	206Pb*				±
				207Pb*	(%)	235U*	(%)	238U	(%)	238U*		(Ma)	235U	(Ma)	207Pb*	(Ma)					
03280836-26	496	10001	1.1	13.2416	1.6	1.4678	9.7	0.141	9.5	0.99	850.1	76	917.2	58.5	1082.4	32.5	850.1	76	78.5		
03280836-27	565	450006	1.6	11.808	0.4	2.4626	1	0.2109	0.9	0.92	1233.6	10.3	1261.1	7.2	1308.4	7.8	1308.4	7.8	94.3		
03280836-28	72	15213	0.9	17.9629	6.5	0.5752	7.4	0.0749	3.6	0.49	465.9	16.4	461.4	27.6	439.2	144.3	465.9	16.4	106.1		
03280836-29	285	11897	0.8	23.7403	15.6	0.0726	16.3	0.0125	4.9	0.3	80	3.9	71.1	11.2	-219.2	393.8	80	3.9	NA		
03280836-30	886	965960	2	11.3806	2.6	2.4553	6.7	0.2027	6.2	0.92	1189.6	67.2	1259	48.4	1379.6	49.4	1379.6	49.4	86.2		
03280836-32	186	63652	4.9	14.0352	1.5	1.3397	2.4	0.1364	1.9	0.77	824.1	14.3	863.1	14	964.6	31.1	824.1	14.3	85.4		
03280836-33	391	113324	0.9	17.5052	1.4	0.5332	2.8	0.0677	2.4	0.86	422.3	9.8	433.9	9.8	496.4	30.6	422.3	9.8	85.1		
03280836-34	1143	226013	1.5	17.5383	0.6	0.6383	1.5	0.0812	1.4	0.91	503.2	6.5	501.2	5.9	492.3	13.7	503.2	6.5	102.2		
03280836-35	1147	58883	4.7	20.6707	2.8	0.1121	3.4	0.0168	1.8	0.55	107.4	1.9	107.9	3.4	117.8	66.2	107.4	1.9	NA		
03280836-37	1510	231746	6.6	18.4604	2.6	0.2755	9.8	0.0369	9.5	0.96	233.5	21.8	247.1	21.6	378.1	58.2	233.5	21.8	NA		
03280836-38	440	10696	1.2	22.4014	13.8	0.0424	14.1	0.0069	3.3	0.23	44.2	1.5	42.1	5.8	-75.2	337.7	44.2	1.5	NA		
03280836-39	387	130718	3.1	13.5754	1.5	0.6069	6.5	0.0598	6.3	0.97	374.2	23.1	481.6	25	1032.2	31.3	374.2	23.1	NA		
03280836-41	147	8749	1	19.3606	11.3	0.1355	17.1	0.019	12.8	0.75	121.5	15.5	129	20.7	270	259	121.5	15.5	NA		
03280836-42	724	42070	1.5	20.43	3.9	0.1279	4.3	0.0189	2	0.46	121	2.4	122.2	5	145.3	90.7	121	2.4	NA		
03280836-43	265	56290	0.7	19.8186	14.1	0.0807	14.5	0.0116	3.4	0.23	74.4	2.5	78.8	11	216.1	328.8	74.4	2.5	NA		
03280836-44	217	185526	0.7	12.6605	0.8	2.0967	1.6	0.1925	1.3	0.85	1135	13.8	1147.7	10.8	1171.8	16.6	1171.8	16.6	96.9		
03280836-45	403	9639	2.2	21.917	34.5	0.0454	35.2	0.0072	7.1	0.2	46.3	3.3	45	15.5	-22	856.2	46.3	3.3	NA		
03280836-46	283	251638	1.2	7.3762	0.4	6.6159	5.3	0.3539	5.3	1	1953.3	89.2	2061.5	46.9	2171.4	6.5	2171.4	6.5	90		
03280836-47	255	37044	1.1	17.8789	3	0.3948	6.2	0.0512	5.4	0.88	321.9	17.1	337.9	17.8	449.6	66.2	321.9	17.1	NA		
03280836-48	166	6158	1.8	23.3614	37.4	0.0454	38.3	0.0077	8.1	0.21	49.4	4	45.1	16.9	-178.9	962.5	49.4	4	NA		
03280836-49	1576	40022	2.7	21.7608	6.7	0.0375	7.7	0.0059	3.8	0.49	38	1.4	37.3	2.8	-4.8	162.1	38	1.4	NA		
03280836-50	196	159236	1.8	13.1102	1.2	1.9431	2.6	0.1848	2.3	0.88	1092.9	22.7	1096.1	17.1	1102.4	24	1102.4	24	99.1		

TABLE DR1. NEW U-PB CRYSTALLIZATION AGES (Downstream sample @ 6)

Grain	U (ppm)	206Pb 204Pb	U/Th	Isotope ratios							error corr.	Apparent ages (Ma)						Best (Ma)	age ± (Ma)	Conc (Ma)	
				206Pb*	±	207Pb*	±	206Pb*	±	207Pb*		±	206Pb*	±	207Pb*	±	206Pb*				±
				207Pb*	(%)	235U*	(%)	238U	(%)	238U*		(Ma)	235U	(Ma)	207Pb*	(Ma)					
03280836-51	424	528	1.7	14.7482	37.5	0.0715	37.9	0.0076	5.6	0.15	49.1	2.7	70.1	25.7	862.6	806	49.1	2.7	NA		
03280836-53	632	344572	2.8	11.2798	3	2.4534	11.1	0.2007	10.7	0.96	1179.1	115.8	1258.4	80.6	1396.7	57.1	1396.7	57.1	84.4		
03280836-54	119	51037	1.6	10.2017	0.8	3.4716	2.3	0.2569	2.1	0.94	1473.8	28.3	1520.8	18	1586.8	14.4	1586.8	14.4	92.9		
03280836-55	142	3125	1.5	11.361	297	0.0991	296.6	0.0082	9.7	0.03	52.4	5.1	95.9	278.2	1382.9	1100.8	52.4	5.1	NA		
03280836-56	88	29771	1.2	16.197	4.2	0.6494	6.1	0.0763	4.4	0.73	473.9	20.3	508.1	24.3	665.1	89	473.9	20.3	71.3		
03280836-57	206	6168	1	16.6679	32.2	0.0607	32.7	0.0073	5.5	0.17	47.1	2.6	59.8	19	603.4	713.7	47.1	2.6	NA		
03280836-58	176	47235	3.6	12.8095	1.5	1.6761	1.9	0.1557	1.3	0.66	932.9	11.1	999.5	12.3	1148.6	29	1148.6	29	81.2		
03280836-59	924	477353	9.6	12.6784	0.3	2.0036	2.1	0.1842	2.1	0.99	1090.1	20.6	1116.7	14.1	1169	5.1	1169	5.1	93.3		
03280836-61	650	14273	1.5	20.7852	8.6	0.0579	9.5	0.0087	3.9	0.41	56	2.2	57.1	5.3	104.7	204.5	56	2.2	NA		
03280836-63	1864	350707	16.6	13.3492	0.4	0.6932	4.7	0.0671	4.7	1	418.8	19.1	534.7	19.6	1066.1	7.2	418.8	19.1	39.3		
03280836-64	323	5948	1.8	21.72	28.7	0.0566	29.3	0.0089	6	0.21	57.2	3.4	55.9	15.9	-0.2	703.3	57.2	3.4	NA		
03280836-65	225	8932	3	24.4841	29.5	0.054	30.3	0.0096	6.7	0.22	61.6	4.1	53.4	15.7	-297.4	767.5	61.6	4.1	NA		
03280836-66	465	21693	1.7	21.4653	4.6	0.1102	5.4	0.0171	2.8	0.52	109.6	3.1	106.1	5.5	28.1	111	109.6	3.1	NA		
03280836-67	158	3308	0.7	14.9234	39	0.0918	39.7	0.0099	7.6	0.19	63.8	4.8	89.2	33.9	838	843.8	63.8	4.8	NA		
03280836-69	239	108283	1.3	12.5643	0.7	2.1136	7.7	0.1926	7.7	1	1135.5	79.8	1153.3	53.1	1186.9	13.2	1186.9	13.2	95.7		
03280836-70	326	11901	4.9	23.6721	39.8	0.0415	40.1	0.0071	4.8	0.12	45.7	2.2	41.3	16.2	-212	1035.6	45.7	2.2	NA		
03280836-71	2109	29113	1.6	20.3113	2.8	0.0513	3.5	0.0076	2.1	0.59	48.6	1	50.8	1.7	159	66.4	48.6	1	NA		
03280836-72	109	17723	1.1	17.4245	5.1	0.6481	5.5	0.0819	2.2	0.39	507.5	10.6	507.3	22.1	506.6	112.3	507.5	10.6	100.2		
03280836-73	157	6654	0.5	25.8488	25.6	0.0991	26.3	0.0186	6.1	0.23	118.7	7.1	96	24.1	-437.9	681.1	118.7	7.1	NA		
03280836-74	197	144926	1.8	9.3089	0.5	4.467	1.4	0.3016	1.3	0.94	1699.2	19.9	1724.9	11.8	1756.2	9.1	1756.2	9.1	96.8		
03280836-75	70	81948	2.1	10.933	5.7	2.5386	8.7	0.2013	6.5	0.75	1182.3	70.7	1283.2	63.3	1456.3	108.6	1456.3	108.6	81.2		
03280836-76	1575	5264	0.6	20.8176	5.7	0.0455	6.5	0.0069	3	0.47	44.2	1.3	45.2	2.9	101.1	135.8	44.2	1.3	NA		

TABLE DR1. NEW U-PB CRYSTALLIZATION AGES (Downstream sample @ 6)

Grain	U (ppm)	206Pb 204Pb	U/Th	Isotope ratios							error corr.	Apparent ages (Ma)						Best (Ma)	age ± (Ma)	Conc (Ma)	
				206Pb*	±	207Pb*	±	206Pb*	±	207Pb*		±	206Pb*	±	207Pb*	±	206Pb*				±
				207Pb*	(%)	235U*	(%)	238U	(%)	238U*		(Ma)	235U	(Ma)	207Pb*	(Ma)					
03280836-77	3235	3367	13.8	15.8112	4.2	0.0892	5.1	0.0102	2.9	0.57	65.6	1.9	86.8	4.2	716.5	89	65.6	1.9	NA		
03280836-78	267	183403	2.9	12.6533	0.8	2.1206	3.7	0.1946	3.6	0.98	1146.3	38.2	1155.5	25.8	1172.9	16.4	1172.9	16.4	97.7		
03280836-79	931	34451	26.1	21.7668	3.1	0.0683	7.5	0.0108	6.9	0.91	69.1	4.7	67.1	4.9	-5.4	73.6	69.1	4.7	NA		
03280836-80	963	407807	3.1	17.4401	0.9	0.6383	2.4	0.0807	2.2	0.92	500.6	10.4	501.3	9.3	504.6	20.8	500.6	10.4	99.2		
03280836-81	64	179890	0.8	5.7223	3.3	10.5489	5	0.4378	3.7	0.75	2340.8	73.6	2484.2	46.3	2603.7	54.8	2603.7	54.8	89.9		
03280836-82	938	9907	1.1	23.5088	17	0.0246	17.2	0.0042	2.5	0.15	26.9	0.7	24.6	4.2	-194.6	427.9	26.9	0.7	NA		

TABLE DR1. NEW U-PB CRYSTALLIZATION AGES (Downstream sample @ 7)

Grain	U (ppm)	206Pb 204Pb	U/Th	Isotope ratios							error corr.	Apparent ages (Ma)						Best (Ma)	age ± (Ma)	Conc (Ma)	
				206Pb*	±	207Pb*	±	206Pb*	±	207Pb*		±	206Pb*	±	207Pb*	±	206Pb*				±
				207Pb*	(%)	235U*	(%)	238U	(%)	238U*		(Ma)	235U	(Ma)	207Pb*	(Ma)					
TUTING-1	327	152891	0.8	12.6534	0.6	2.0081	1.2	0.1843	1	0.88	1090.4	10.3	1118.3	7.9	1172.9	11	1172.9	11	93		
TUTING-2	138	62087	2	20.567	8.8	0.2211	9.1	0.033	2.4	0.26	209.2	4.8	202.8	16.7	129.6	206.4	209.2	4.8	NA		
TUTING-3	611	1574	1.1	19.0965	14.3	0.0694	15.5	0.0096	6	0.39	61.6	3.7	68.1	10.2	301.4	327.1	61.6	3.7	NA		
TUTING-5	40	15309	0.4	17.0738	6.2	0.6574	6.7	0.0814	2.5	0.37	504.5	12.2	513	27	551.1	135.6	504.5	12.2	91.5		
TUTING-7	424	469421	1.2	14.9834	0.4	1.2055	1.6	0.131	1.5	0.96	793.6	11.3	803.1	8.8	829.7	9.3	793.6	11.3	95.6		
TUTING-8	489	30797	1.7	20.8581	7.8	0.0622	9	0.0094	4.5	0.5	60.4	2.7	61.3	5.3	96.5	183.7	60.4	2.7	NA		
TUTING-9	118	3195	1.2	20.6708	33.3	0.0558	33.8	0.0084	5.6	0.17	53.7	3	55.1	18.1	117.8	805.5	53.7	3	NA		
TUTING-10	447	11009	1.3	25.4455	30.9	0.0237	31.1	0.0044	3.8	0.12	28.2	1.1	23.8	7.3	-396.8	821.3	28.2	1.1	NA		
TUTING-11	84	43854	1.3	16.034	3.6	0.8668	3.9	0.1008	1.6	0.4	619.1	9.2	633.8	18.4	686.7	76.2	619.1	9.2	90.1		
TUTING-13	561	61594	8.8	19.8449	3.2	0.2095	4.1	0.0302	2.5	0.61	191.5	4.7	193.1	7.2	213	74.7	191.5	4.7	NA		
TUTING-14	16	8446	0.9	13.4667	6	1.8214	7.7	0.1779	4.8	0.63	1055.5	46.9	1053.2	50.3	1048.5	120.5	1048.5	120.5	100.7		
TUTING-15	3073	16739	0.4	20.273	1.6	0.2243	13.6	0.033	13.5	0.99	209.2	27.8	205.5	25.3	163.4	37.8	209.2	27.8	NA		
TUTING-16	407	220207	1.7	11.7275	0.9	2.6217	2.3	0.223	2.1	0.92	1297.6	24.8	1306.7	16.8	1321.7	17	1321.7	17	98.2		
TUTING-17	1119	217364	0.9	17.3788	0.6	0.6092	1.2	0.0768	1.1	0.88	476.9	4.9	483	4.6	512.3	12.5	476.9	4.9	93.1		
TUTING-18	154	6672	2.7	21.4007	25.9	0.0696	26.5	0.0108	5.8	0.22	69.3	4	68.3	17.5	35.3	628.6	69.3	4	NA		
TUTING-19	166	102446	1.6	12.7881	0.7	1.9805	4.6	0.1837	4.6	0.99	1087.1	45.7	1108.9	31.1	1151.9	13	1151.9	13	94.4		
TUTING-20	725	24428	0.8	20.8525	8.6	0.0483	8.9	0.0073	2.4	0.27	46.9	1.1	47.9	4.2	97.1	203.4	46.9	1.1	NA		
TUTING-21	1498	73950	0.8	20.3768	2.7	0.1221	3	0.018	1.2	0.41	115.3	1.4	116.9	3.3	151.4	63.9	115.3	1.4	NA		
TUTING-22	85	3766	0.6	4.1503	505	0.2059	505.5	0.0062	10.1	0.02	39.8	4	190.1	1326	3126.2	181.9	39.8	4	NA		
TUTING-23	68	36988	1.1	14.3648	2.8	1.2543	5.1	0.1307	4.2	0.83	791.7	31.6	825.3	28.8	917	58.1	791.7	31.6	86.3		
TUTING-24	2489	4123	2.6	20.544	4.7	0.0665	7.9	0.0099	6.4	0.81	63.6	4	65.4	5	132.3	109.4	63.6	4	NA		
TUTING-26	187	83870	0.4	16.6078	1.2	0.7842	1.7	0.0945	1.2	0.69	581.9	6.6	587.9	7.7	611.2	27	581.9	6.6	95.2		
TUTING-27	405	19471	2	22.3178	13.9	0.0431	14.3	0.007	3.6	0.25	44.9	1.6	42.9	6	-66.1	339.9	44.9	1.6	NA		

TABLE DR1. NEW U-PB CRYSTALLIZATION AGES (Downstream sample @ 7)

Grain	U (ppm)	206Pb 204Pb	U/Th	Isotope ratios							error corr.	Apparent ages (Ma)						Best (Ma)	age ± (Ma)	Conc (Ma)	
				206Pb*	±	207Pb*	±	206Pb*	±	207Pb*		±	206Pb*	±	207Pb*	±	206Pb*				±
				207Pb*	(%)	235U*	(%)	238U	(%)	238U*		(Ma)	235U	(Ma)	207Pb*	(Ma)					
TUTING-28	104	63899	1.1	9.9051	0.7	4.0652	2.9	0.292	2.9	0.97	1651.7	41.7	1647.4	23.9	1641.8	12.4	1641.8	12.4	100.6		
TUTING-30	52	40759	0.6	12.6137	1.7	2.1867	2.4	0.2	1.7	0.7	1175.6	17.8	1176.8	16.4	1179.1	33.2	1179.1	33.2	99.7		
TUTING-31	66	9271	0.8	21.2761	20.7	0.1182	21.3	0.0182	5	0.24	116.6	5.8	113.5	22.9	49.3	499.9	116.6	5.8	NA		
TUTING-32	91	4313	1.9	23.5851	48.1	0.0599	48.6	0.0102	7	0.14	65.7	4.6	59.1	27.9	-202.7	1271.9	65.7	4.6	NA		
TUTING-33	232	19809	1	20.5073	8.7	0.1228	8.8	0.0183	1.1	0.12	116.7	1.3	117.6	9.7	136.4	204.5	116.7	1.3	NA		
TUTING-34	353	302933	5.1	14.0289	0.6	1.5858	1.5	0.1614	1.4	0.92	964.3	12.2	964.7	9.2	965.5	11.5	964.3	12.2	99.9		
TUTING-36	276	79951	3.7	17.5492	1.7	0.5991	1.8	0.0762	0.6	0.34	473.7	2.8	476.6	6.8	490.8	36.8	473.7	2.8	96.5		
TUTING-37	461	10713	8.4	18.8054	16.7	0.0252	28.2	0.0034	22.7	0.81	22.1	5	25.3	7	336.3	381.1	22.1	5	NA		
TUTING-39	766	141871	72.5	16.8237	0.5	0.7147	1.3	0.0872	1.2	0.91	539	6.3	547.5	5.6	583.2	11.6	539	6.3	92.4		
TUTING-40	194	20582	0.8	21.5905	7.5	0.1118	7.9	0.0175	2.3	0.3	111.9	2.6	107.6	8.1	14.1	181.1	111.9	2.6	NA		
TUTING-40_2	145	192302	1.1	9.6721	0.3	4.2284	0.9	0.2966	0.9	0.96	1674.5	12.7	1679.5	7.4	1685.8	4.9	1685.8	4.9	99.3		
TUTING-41	319	11937	6.8	20.8345	12.9	0.0401	13.3	0.0061	3.3	0.25	39	1.3	40	5.2	99.1	306.6	39	1.3	NA		
TUTING-42	617	16053	1.1	10.3996	0.2	2.0891	3.3	0.1576	3.3	1	943.3	29	1145.2	22.7	1550.8	4.4	1550.8	4.4	60.8		
TUTING-44	403	114147	10.8	15.0198	0.5	0.6372	8.6	0.0694	8.6	1	432.6	36.1	500.6	34.1	824.6	10.3	432.6	36.1	52.5		
TUTING-47	816	184230	0.8	17.4633	0.4	0.6091	3.2	0.0771	3.2	0.99	479	14.8	483	12.5	501.7	9.2	479	14.8	95.5		
TUTING-48	179	4445	1.9	23.2598	38.4	0.0361	39.2	0.0061	8	0.2	39.1	3.1	36	13.9	-168	986.9	39.1	3.1	NA		
TUTING-49	378	450	0.7	15.0438	38.2	0.0301	45.7	0.0033	25.1	0.55	21.2	5.3	30.2	13.6	821.3	827	21.2	5.3	NA		
TUTING-51	65	50142	1	9.7148	5	3.6992	20	0.2606	19.4	0.97	1493.1	258.6	1571.2	161.4	1677.7	92.5	1677.7	92.5	89		
TUTING-53	474	2342	2.8	21.3673	22.4	0.0251	25.3	0.0039	11.7	0.46	25	2.9	25.1	6.3	39.1	542.8	25	2.9	NA		
TUTING-54	378	103935	1.4	10.481	0.6	3.3623	4	0.2556	4	0.99	1467.2	52.5	1495.7	31.7	1536.2	12	1536.2	12	95.5		
TUTING-55	430	67616	1.1	17.4873	1.9	0.3919	2.5	0.0497	1.6	0.65	312.7	4.8	335.8	7	498.6	41.3	312.7	4.8	NA		
TUTING-56	226	57207	1	14.7568	1.3	1.1936	10.2	0.1277	10.1	0.99	775	73.9	797.6	56.5	861.4	27.5	775	73.9	90		
TUTING-57	171	21596	1.4	13.3442	1.4	1.6526	2.8	0.1599	2.5	0.87	956.5	22	990.6	18	1066.9	28.1	1066.9	28.1	89.7		
TUTING-58	336	28444	2.2	9.5889	0.3	3.6513	3.3	0.2539	3.3	1	1458.7	43.2	1560.8	26.5	1701.8	5.4	1701.8	5.4	85.7		
TUTING-59	611	283733	1.9	19.3706	1.3	0.3104	4.2	0.0436	4	0.95	275.2	10.8	274.5	10.1	268.8	29.1	275.2	10.8	NA		
TUTING-60	493	209688	8.6	13.9509	0.7	1.2121	4.4	0.1226	4.3	0.99	745.7	30.2	806.1	24.2	976.9	14.5	745.7	30.2	76.3		

TABLE DR1. NEW U-PB CRYSTALLIZATION AGES (Downstream sample @ 7)

Grain	U (ppm)	206Pb 204Pb	U/Th	Isotope ratios							error corr.	Apparent ages (Ma)						Best (Ma)	age ± (Ma)	Conc (Ma)	
				206Pb*	±	207Pb*	±	206Pb*	±	207Pb*		±	206Pb*	±	207Pb*	±	206Pb*				±
				207Pb*	(%)	235U*	(%)	238U	(%)	238U*		(Ma)	235U	(Ma)	207Pb*	(Ma)					
TUTING-61	54	15463	1.1	17.7668	5.6	0.6285	6.5	0.081	3.3	0.51	502	16.1	495.2	25.4	463.6	123.5	502	16.1	108.3		
TUTING-62	1756	5631	3.2	20.4605	4.3	0.0621	4.8	0.0092	2	0.43	59.1	1.2	61.2	2.8	141.8	101.6	59.1	1.2	NA		
TUTING-63	174.7	250019	1.165	10.3407	1.28	3.089	5.69	0.2317	5.6	0.97	1343.3	67.3	1430	43.7	1561.5	24.1	1561.5	24.1	86		
TUTING-64	198	11117	1.6	22.6677	6.4	0.0671	6.9	0.011	2.5	0.37	70.8	1.8	66	4.4	-104.2	156.8	70.8	1.8	NA		
TUTING-65	495	43221	1.4	20.6388	3.8	0.1203	4.1	0.018	1.4	0.34	115	1.6	115.3	4.5	121.4	90.6	115	1.6	NA		
TUTING-66	422	12908	1.4	22.9548	10.2	0.0225	10.6	0.0037	2.9	0.27	24.1	0.7	22.6	2.4	-135.3	253.6	24.1	0.7	NA		
TUTING-68	419	118383	1.1	17.4335	1.4	0.4831	7.6	0.0611	7.4	0.98	382.2	27.6	400.2	25.1	505.4	31.8	382.2	27.6	NA		
TUTING-69	106	10241	0.6	17.7234	3.8	0.5755	4.1	0.074	1.6	0.38	460.1	7	461.6	15.4	469	85.1	460.1	7	98.1		
TUTING-70	84	85787	1.7	15.0167	2.5	1.1203	3	0.122	1.7	0.55	742.2	11.6	763.1	16.1	825	52.3	742.2	11.6	90		

New U-Pb age data for flood deposits at locations 6,7,9,10,11; and downstream samples from locations 3,5,6,7,8. Other U-Pb data used in modeling analysis are previously published by Amidon et al., 2005; Stewart et al., 2008; Zhang et al., 2012.

3.7.2 Sample locations and new petrographic data

Sample location data for all new samples (U-Pb and petrographic data) as well as new quartz, feldspar, lithics (QFL) petrographic data for flood deposits and select modern sediment samples. Other QFL data used in Figure 2 are from Garzanti et al., 2004; Zhang et al., 2012.

TABLE DR2. SAMPLE LOCATION AND NEW PETROGRAPHIC DATA

Downstream sample (# corresponds with Fig. 1B)	Latitude (N)	Longitude (E)	Elev. (m)	Quartz (%)	Feldspar (%)	Lithic (%)
Namche Barwa Cirque at #5	29.60642	94.93687	2884	64	29	7
Yigong river at #3	30.0967	95.0647	2154	39	35	26
Downstream sample at #6	29.04847	94.91079	449	66	22	12
Downstream sample at #7	28.99628	94.90344	425	-	-	-
Downstream sample at #8	28.57666	95.0702	264	66	15	19
2000 flood at #6	29.04868	94.9108	475	58	41	2
2000 flood at #7	28.96083	94.86507	466	56	38	6
2000 flood at #10	28.23504	94.99652	230	55	38	8
2000 flood at #11	28.17352	95.03054	199	61	35	4
Mega-flood at #6	29.05137	94.90618	502	56	38	6
Mega-flood at #7	28.96552	94.84708	553	55	41	5
Mega-flood at #9	28.31759	94.95328	353	50	34	15
Mega-flood at #10	28.23392	94.98344	270	56	35	9

3.8 Appendices

3.8.1 U-Pb analytical details

U-Pb age data was reduced using NUPMagecalc and ISOPLOT with the following standard age filters:

1. 10% error cutoff for $^{206}\text{Pb}/^{238}\text{U}$ and $^{206}\text{Pb}/^{207}\text{Pb}$ ratios (individually, higher $^{206}\text{Pb}/^{238}\text{U}$ error was allowed for extremely young ages)
2. 30% maximum discordance, 5% maximum reverse discordance
3. $^{206}\text{Pb}/^{238}\text{Pb}$ ages used under 1000 Ma, otherwise $^{206}\text{Pb}/^{207}\text{Pb}$ ages used

Ages were individually assessed for excess ^{204}Pb , with a typical cutoff of 500 cps.

3.8.2 Variables used in shear stress calculations

Discharge Q values:

Annual peak discharge = $\sim 2 \times 10^4 \text{ m}^3/\text{s}$ (from Goswami, 1985)

2000 flood peak discharge = $\sim 6.1 \times 10^4 \text{ m}^3/\text{s}$ (from Evans and Delaney, 2010)

Peak discharge from a megaflood emptying an 80 km^3 lake = $\sim 1.0 \times 10^6 \text{ m}^3/\text{s}$ (from Montgomery et al., 2004)

Peak discharge from a megaflood emptying an 800 km^3 lake = $\sim 5.0 \times 10^6 \text{ m}^3/\text{s}$ (from Montgomery et al., 2004)

Variables:

bed roughness length scale $k_s = 0.1$ to 1 m

hillslope angle $\phi = 37$ to 39 degrees (modal values for outer and inner gorge, respectively, from Larsen and Montgomery, 2012)

mean bed slope $S = 0.02$ (from Finnegan et al., 2008)

average rock density $\rho_s = 2700 \text{ kg/m}^3$

water density $\rho = 1000 \text{ kg/m}^3$

kinematic viscosity at 20 C $\nu = 1 \times 10^{-6} \text{ m}^2/\text{s}$

empirical constants for block shape and roughness $C_1 = 20$, $C_2 = 1.1$ (from Ferguson and Church, 2004)

CHAPTER 4: Rapid exhumation of the eastern Himalayan syntaxis since the Late Miocene

Coauthor: Katharine W. Huntington, Russ F. Burmester, Bernard A. Housen

4.0 Abstract

The peripheral Himalayan foreland basin preserves a rich archive of Himalayan landscape dynamics. In particular, analysis of sedimentary detritus provides a detailed record of landscape response to changes in tectonic and geomorphic conditions. Despite a wealth of bedrock analyses that demonstrate some of the most dynamic crustal processes on Earth, localized feedbacks between surface erosion and tectonic uplift within the Himalayan syntaxes obscure the distinction between an initial change in conditions and the subsequent landscape response. We refocus interpretation on the exhumation history on detrital analyses from Neogene sedimentary units proximal to the eastern syntaxis where active tectonic uplift and fluvial incision are inextricably linked. Combining magnetostratigraphy, detrital muscovite $^{40}\text{Ar}/^{39}\text{Ar}$ thermochronology, and coupled zircon U-Pb and fission track geo-thermochronology from a new 4.6 km section, we present a record of syntaxial exhumation since the Late Miocene. Our results indicate an increase in rock exhumation rates occurred within the eastern syntaxis between 5-7 Ma, and rapid exhumation rates (5-10 km/Ma) have been persistent since 5 Ma. We attribute this rate increase to enhanced erosion along an antecedent Yarlung-Siang-Brahmaputra River following tectonic uplift of Himalayan units. The persistence of rapid exhumation rates since 5 Ma may indicate the subsequent emergence of thermo-mechanical feedbacks between tectonic uplift and surface erosion at the intersection of the antecedent river and

the active structure. Comparison to similar work from across the Himalayan front further illustrates how the emergence of such localized thermo-mechanical feedbacks may be uniquely attributed to the particular geomorphic and tectonic conditions present in the Himalayan syntaxes, in particular the antecedent drainage or large rivers.

4.1 Introduction

The evolution of mountain landscapes reflects complex feedbacks between tectonic processes transferring mass within the Earth's interior and erosional processes redistributing mass at the Earth's surface (e.g., Davis et al., 1983; Beaumont et al., 1992; Avouac and Burov, 1996). Numerical (e.g., Willet, 1999; Beaumont et al., 2000), analog (e.g., Mugnier, et al., 1997; Marques et al., 2002; Hoth et al., 2006), and analytical (e.g., Whipple and Meade, 2004; Simpson, 2006) experiments document the dynamic influence of erosion and deposition on crustal deformation from local to orogenic scales. Erosion may influence crustal deformation patterns by reducing the influence of gravity (Simpson, 2004; 2006), focusing regional patterns of crustal strain by locally promoting crustal-scale folding (Burg and Podladchikov, 2000) and thrust faulting (Burg and Schmalholz, 2008). The resulting rock uplift steepens river channels (Whipple and Tucker, 1999), sustaining elevated erosion rates to rapidly exhume crustal material (Ring et al., 2001). The persistence of rapid rock exhumation will sufficiently increase the shallow geothermal gradient (Koons et al., 2002) to initiate a thermo-mechanical feedback sustaining steep topography on top of hot, actively deforming crust (Zeitler et al., 2001; Koons et al. 2013).

A concomitance of steep topography (Burbank, et al., 1996; Larsen and

Montgomery, 2012), steep geothermal gradients (Winslow et al., 1994; Craw et al., 2005) and active crustal-scale structures (Burg et al., 1998; Schneider et al., 1999) is observed at both ends of the Himalayan orogen. In these regions, margin-normal motion of the Indian-Eurasian plate collision transitions to strike-slip motion, warping Himalayan terrains southward into broad syntaxes (Wadia, 1931; Gansser, 1966; Treloar and Coward, 1991). Longitudinal rivers draining southern Tibet abruptly cross the Himalaya through the syntaxes, dramatically steepening (Finlayson et al., 2002) as they bisect rapidly exhumed metamorphic massifs (Zeitler et al., 1982; Burg et al., 1998). Bedrock thermochronology from both regions indicate rapid cooling of these massifs during the Late Pliocene and Pleistocene (e.g., Zeitler et al., 1993; Winslow et al., 1996; Burg et al., 1998; Malloy, 2004; Enkelmann et al., 2011) and geochronology further suggests that localized anatexis related to massif decompression has been ongoing since the Late Miocene (e.g., Schneider et al., 1999b; Booth et al., 2004). However, detailed exhumation histories of these regions are difficult to obtain from rapidly exhumed bedrock samples alone. Detrital cooling ages from foreland basin units proximal to the western syntaxis have proven useful for interpreting a Neogene record of rapid exhumation (e.g., Cervený et al., 1988; also see Bernet and Garver, 2005; Ruiz and Seward, 2006), but similar constraints on the onset and duration of rapid exhumation are lacking for the eastern syntaxis.

Existing detrital cooling ages from the eastern Himalayan foreland basin units lack clear evidence for rapid exhumation rates prior to the Quaternary (Chirouze et al., 2013). Instead, detrital samples collected over 300 km downstream of the Brahmaputra confluence indicate constant exhumation rates between 1-2 km/Ma from 7 to 3 Ma.

However, young cooling ages indicating rapid syntaxial exhumation may have been rapidly diluted by older ages from local Himalayan sources (Zhang et al., 2012). For example, detrital zircons are rapidly diluted within the upper Brahmaputra River to less than 10% of detrital age populations (Cina et al., 2009), indicating that an early signal of rapid exhumation may have been unobserved in a ~50 grain zircon sample (Vermeesch, 2004).

We build on the early work of Chirouze et al. (2012, 2013) by sampling foreland basin units proximal to the eastern syntaxis. Specifically, we present new magnetostratigraphy, detrital zircon fission track and muscovite $^{40}\text{Ar}/^{39}\text{Ar}$ thermochronology from a stratigraphic section upstream of the transverse Subansiri and Kameng river drainages in Arunachal Pradesh, India. Coupling fission track and U-Pb analyses on detrital zircons permit source-specific analysis of low temperature mineral cooling, and complimentary muscovite analyses bolster out interpretation with independent data from a different target mineral. We use a one-dimensional thermal model to constrain the timing and magnitude of an exhumation rate increase within the eastern syntaxis, and interpret this increase as the potential consequence of regional river drainage reorganization, localized tectonic uplift or global climate change.

4.2 Background

4.2.1 Tectonic and geomorphic setting of the eastern Himalayan syntaxis

Following subduction of the Tethys ocean basin by the Early Eocene, collision between the Indian and Eurasian tectonic plates has deformed and uplifted the northern margin of the Indian plate to form the Himalayan orogen (e.g., Gansser, 1964; Searle et

al., 1987). Portions of the subducted oceanic lithosphere demarcate the formal suture zone (called the Indus-Yarlung Suture Zone) between Transhimalayan intrusive units within Eurasian Plate terranes from orogenic units in the Himalaya. The Himalayan orogeny is defined along-strike by major thrust faults that subdivide a sequence of tectono-stratigraphic units. Primarily, the Main Central Thrust places deeply exhumed crystalline rocks of the Greater Himalaya above lower grade metamorphic rocks of the Lesser Himalaya, the Main Boundary Thrust places Lesser Himalayan rocks above sedimentary rocks of the Sub-Himalaya and where it is exposed, the Main Frontal Thrust places Sub-Himalayan rocks over modern foreland basin alluvium. The Greater Himalaya are separated from folded and faulted sedimentary rocks of the Tethyan margin by the South Tibetan Detachment fault (e.g., LeFort, 1975; Yin and Harrison, 2000).

At the eastern margin of the plate collision, transition from margin-normal convergence to dextral strike-slip movement warps the suture zone, Himalayan and Transhimalayan units southward to form the eastern Himalayan syntaxis (Figure 1A; e.g., Peltzer and Tapponnier, 1988; Holt, et al., 1991; Koons, 1995). Within the syntaxis, lithospheric strain is manifest in surface topography (Hallet and Molnar, 2001), exhibiting a clockwise motion that demonstrates transmission of strain from the crust to the upper mantle (Sol et al., 2007). The peculiar tectonic position of the syntaxis focuses deformation around the Indian plate indenter (Tapponnier et al., 1990) such that relatively small stress changes produced locally may result in proportionately larger changes in lithospheric strain (Enlow and Koons, 1998) – essentially priming the region for the dynamic modification by surface processes (Simpson et al., 2006).

Within the eastern syntaxis, an active crustal-scale antiform (Burg et al., 1998) or

pop-up structure (Ding et al., 2001) called the Namche Barwa metamorphic massif is deeply incised by a rapidly eroding reach of the Yarlung River. Along this reach, the Yarlung River abruptly drops over 2 km through a narrow bedrock gorge, often called the “Tsangpo Gorge,” after flowing >1000 km along the Indus-Tsangpo Suture zone in southeastern Tibet (Montgomery, 2004). Within the gorge, erosion rates increase (Stewart et al., 2008; Enkelmann et al., 2011) along with proxies for fluvial incision (Finlayson et al., 2002; Finnegan et al., 2008) and local topographic relief (Larsen and Montgomery, 2012).

Extensive bedrock thermochronology documents rapid Plio-Quaternary cooling rates (5-10 km/Ma) focused around the Namche Barwa massif (Burg et al., 1998; Zeitler et al., 2001, Malloy, 2004; Enkelmann et al., 2011; Zeitler et al., 2014). Zircon fission track data, which reflect cooling from shallow crustal temperatures of $\sim 230^{\circ}$ C (Brandon and Vance, 1992) during rock exhumation, are younger than 3.5 Ma within the massif, and locally younger than 1 Ma along the Tsangpo Gorge (Figure 1B; Burg, 1998; Seward and Burg, 2008; Enkelman et al., 2011; Zeitler et al., 2014). Biotite $^{40}\text{Ar}/^{39}\text{Ar}$ cooling ages, which are sensitive to higher temperatures of over 300° C (McDougall and Harrison, 1999) for such rapid cooling rates (e.g., Dodson, 1973), are also younger than 1 Ma in samples collected along the Tsangpo Gorge and rapidly increase in age with distance from the core of the massif (Figure 1B data from Ding et al., 2001; Malloy, 2004; Geng et al., 2006; Zeitler et al., 2014). Zircon U-Pb geochronology from bedrock samples within the gorge further indicates that local anatexis was associated with rapid rock exhumation in the Plio-Quaternary, and potentially even earlier in the Late Miocene (Ding et al., 2001; Booth et al., 2004; 2009). While modeling of bedrock data aid a

reconstruction of exhumation history from spatial patterns of mineral cooling, a detailed exhumation history may be better preserved in the proximal sedimentary record.

Erosion of the massif enriches downstream river sediment in rapidly cooled minerals from Namche Barwa bedrock. Up to 45% of detrital mineral entering the Himalayan foreland basin have young cooling ages consistent with derivation from the Namche Barwa massif, adding a characteristic young cooling age component to the older detrital ages sourced upstream of the gorge (e.g., Pik et al., 2005; Stewart et al., 2008; Enklemann et al., 2011). Antecedent drainage through the syntaxis would have carried a similarly young age components to the foreland once rapid exhumation within the syntaxis had begun, so we predict that the presence of young cooling ages (relative to depositional age) in proximal foreland basin units should constrain the onset of rapid exhumation in the region. To reconstruct this exhumation history, we focus on detailed observations from a 4.6 km stratigraphic section along the Siji River near the village of Likabali in the easternmost portion of the Himalayan foreland basin (Figure 1B).

4.2.2 The easternmost Himalayan foreland basin

The Himalayan foreland basin is peripheral to the mountain front and nearly continuous along the Himalayan arc (Beaumont, 1981; Najman, 2006). At its eastern limit, the basin is less than 100 km wide, narrowly constrained between active thrust faults: the Main Frontal Thrust to the northwest, Mishmi Thrust to the northeast and Naga Thrust to the southeast. Estimates for the total thickness of Cenozoic sedimentary units within the basin range up to 7 km (Mathur and Evans, 1964; Karunakaran and Rangarao, 1976), thickening to the west with proximity to the Himalayan mountain front (Figure

1B; Verma and Mukhopadhyay, 1977). Neogene units are uplifted by the Tipi Thrust and Main Frontal Thrust to form steep foothills along the mountain front. These units are often offset by smaller cross-cutting faults (e.g., Agarwal, 1991; Yin et al., 2010; Burgess et al., 2013) but remain traceable along strike of the mountain front from the eastern syntaxis westward into Bhutan (Rangarao, 1983; Kumar, 1997).

Sedimentary rocks exposed in these foothills are traditionally divided into three lithologically distinct units (e.g., Karunakaran and Rangarao, 1976; Bhareli and Ratnam, 1978; Yin, 2006) and litho-correlated to the more extensively studied Siwalik Group in the central and western Himalaya (e.g., Kumar, 1997; Chirouze et al., 2012). Although these units are locally called the Kimin, Subansiri and Dafla formations (Kumar, 1997), we adopt the corresponding Upper, Middle and Lower Siwalik nomenclature for consistency with the well-established, broader Himalayan literature (e.g., Pilgrim, 1913).

Regionally, these Siwalik units comprise an upward coarsening clastic sedimentary sequence representing terrestrial deposition unconformable on Permian metasedimentary units of the Gondwana formation (Rangarao, 1983; Kumar, 1997). The Lower Siwalik is characterized by compact interbedded sandstone and shale, the Middle Siwalik is a softer and coarser micaceous, concretionary sandstone, and the Upper Siwalik is defined by interbedded conglomerate, sandstone and mudstone (e.g., Rangarao, 1983; Kumar, 1997; Chirouze et al., 2012). A gradational contact between the Upper and Middle Siwaliks is often preserved in Siwalik sections (e.g., Jain et al., 1974; Chirouze et al., 2012), whereas the Lower Siwalik is more commonly thrust over these units on the Tipi Thrust (e.g., Agarwal, 1991; Yin et al., 2010; Burgess et al., 2013).

4.2.2.1 Constraints on depositional age

Depositional ages of eastern Siwalik units are poorly constrained. Biostratigraphic constraints from mammalian fossils consists of only a single specimen (*Bos* sp.) from a conglomeratic bed of the Upper Siwalik (Singh, 1975; 1976). This solitary observation corroborates an informal description of a similar fossil by Maclaren (1904) observed north of the Subansiri River to loosely indicate a Pleistocene depositional age for the Upper Siwalik. Arenaceous foraminifera (specifically *Trocommina* sp.; Ranagrao, 1983), megafloreal assemblages including *Zizyphus* sp. and *Sigigium* sp. (Singh and Prakash, 1980) and playnofossil suites (Dutta, 1980) observed in the Lower Siwalik suggest an Early or Middle Miocene depositional age for this unit (Singh and Tripathi, 1989; Singh, 1999).

The most robust depositional age constraints for these units come from a combination of detrital thermochronology and magnetostratigraphy (Chirouze et al., 2012; 2013). This work brackets the depositional ages for Upper and Middle Siwalik contact between 2 and 3 Ma and the Middle-Lower Siwalik contact between 11 and 13.5 Ma in a section along the Kameng River near Bhalukpong. The authors estimate the average sediment accumulation rate varies in this location between 420 and 440 m/Ma, higher than correlated sections from the central and western Himalaya (e.g., Johnson et al., 1985; Gautam and Fujiwara, 2000; Ojha et al., 2009).

4.2.2.2 Constraints on sedimentary provenance

Siwalik units are broadly interpreted across the Himalayan foreland to represent synorogenic deposition of Himalayan detritus eroded during periods of Late Cenozoic

thrusting (e.g., Heim and Gansser, 1939; DeCelles et al., 1998; Najman, 2006).

Paleocurrent indicators from easternmost exposures of Middle and Upper Siwaliks indicate that flow direction varied (Chirouze et al., 2013) but was dominantly to the south or southwest from a northern source region (e.g., Jain et al., 1974; Cina et al., 2009; Kesari, 2010; Chirouze et al., 2012) with no indication of flow reversal during deposition of the sequence.

Modal analyses are consistent with a northern source in both Himalayan and Tibetan terranes. Framework grains (e.g., Gogoi, 1989; Baruah, 2001) are characteristic of a recycled orogenic provenance, and heavy mineral suites indicate contributions from plutonic and metamorphic sources. Specifically, tourmaline, epidote, zircon, rutile and hornblende, garnet, staurolite, and kyanite metamorphic index minerals are found in all units, with andalusite and sillimanite appearing in the Upper Siwalik (Singh, 1976; Singh et al., 1982; Rangarao, 1983; Gogoi, 1989).

Detrital zircon U-Pb geochronology from five sections in eastern Siwalik units (Cina et al., 2009; Lang and Huntington, 2014) all indicate a mixed Tibetan and Himalayan provenance. Specifically, the presence of Gangdese-age zircons (Stewart et al., 2008; Cina et al., 2009; Zhang et al., 2012) in all Siwalik samples north of Bhalukpong (see Figure 1B) demonstrates a connection through the eastern syntaxis to source areas presently west of the Namche Barwa massif since at least the Middle or Early Miocene (Lang and Huntington, 2014). Moreover, bulk ϵ_{Nd} and ϵ_{Hf} isotopic analyses indicate that the absence of Gangdese-derived detritus in the Lower Siwalik near Bhalukpong may be explained by local deposition from a transverse Himalayan river like the Kameng River (Chirouze et al., 2013).

4.3 Methods

4.3.1 Mapping and stratigraphic surveying

To identify potential faulting and other complications for the interpretation of Siwalik stratigraphy, we conducted reconnaissance mapping of the Siji River area with a main focus on Upper and Middle Siwalik exposures. Accessibility in the area is severely restricted and exposure is limited to river channels at low-flow conditions, road cuts, and landslide scars. Because of inaccessibility, mapping and stratigraphic surveying focused on traverses along the Siji River and adjacent tributaries. Bedding measurements and unit contacts were plotted in the field on 1:12,000 satellite images and contacts away from the direct observations were extrapolated along strike of topographic dip-slopes measured in Google Earth.

Stratigraphic surveying of the Upper and Middle Siwaliks was completed using a 1.5 m Jacob's Staff and Abney level, progressing up-section along the Siji River from the mountain front near Likabali to the Tipi Thrust near Siji village. Surveying included regular observations of bed thickness, grain size and other characteristics, sedimentary structures, approximate mica and heavy mineral content, and clast lithology in channel lag deposits and conglomerate beds.

4.3.2 Magnetostratigraphy

We collected at least one oriented block sample for analysis of paleomagnetic polarity every 20 m in the lower 1.6 km of the Middle Siwalik. Every 100 m, we collected 3 to 6 samples for repeat analysis from single bedding horizons. Block samples

were cored, cut into specimens and analyzed in the magnetic field free room at the Pacific Northwest Paleomagnetism Laboratory at Western Washington University. To determine paleomagnetic polarity, we measured the remanent magnetization of 126 specimens from 79 sites spanning the lower 1.6 km of the Middle Siwalik. Measurements were conducted on a 2-G Enterprises 755 superconducting rock magnetometer with 0.001 mA/m sensitivity. Thermal demagnetization in an ASC Model TD48 oven began with a subset of specimens with closely spaced steps to determine optimal temperature steps. This was followed for the rest of the specimens by demagnetization in seven 70° C to 100° C temperature steps from approximately 180° C to 580° C. Magnetic susceptibility was measured on a Bartington MS2 susceptometer after monitoring changes in magnetic mineralogy. Standard analytical methods were used to identify, quantify and analyse remanent magnetization components and interpret original polarity.

4.3.3 Detrital thermochronology

To interpret changes in source exhumation rates, we compared detrital mineral cooling ages from multiple stratigraphic horizons to additional samples from the modern Siang River and adjoining Himalayan tributaries. We collected five samples from the Upper and Middle Siwaliks in the Tipi Thrust footwall for zircon fission track and muscovite $^{40}\text{Ar}/^{39}\text{Ar}$ thermochronology. Modern fission track analyses have been previously published in the Siang River and adjoining Himalayan tributaries (Enkelmann et al. 2011), and we collected an additional six samples of modern sediment from the same locations for muscovite $^{40}\text{Ar}/^{39}\text{Ar}$ analyses. Combining multiple thermochronological datasets from the same stratigraphic horizons permits a more robust

interpretation of exhumation rate changes that accounts for potential biases from mineral heterogeneity in the source region (e.g., Avdeev et al., 2012).

Sediment and sedimentary rock samples were manually disaggregated in a dilute (<3%) HCl solution and wet-sieved to isolate the 63 to 250 μm , 250 to 500 μm , and 500 to 1,000 μm grain size fractions. For both zircon and muscovite samples, we analyzed at least 50 grains per sample (and more when possible) to be at least 95% confident that our analyses did not miss an age component greater than 10% of the true age distribution (Vermeesch, 2004).

4.3.3.1 Muscovite $^{40}\text{Ar}/^{39}\text{Ar}$

Optically pure muscovite grains were randomly hand selected from the 500 to 1,000 μm grain size fraction (and also the 250 to 500 μm fraction for the Kapu sample to identify any potential size-age bias), cleaned in acetone, methanol and deionized water and packaged in aluminum foil packages for fast neutron irradiation. Irradiation was conducted in Cd-shielded packages for 0.5 and 6.1 hours in the 5C core and medium-flux positions at the McMaster University nuclear reactor in Hamilton, Ontario, Canada. Within the irradiation package, biotite age standard HD-B1 (24.18 Ma, Schwarz and Trieloff, 2007) were used to monitor the neutron flux gradient and Kalsilite and CaF_2 salts were used to determine interfering nuclear production ratios.

Single grain, total fusion $^{40}\text{Ar}/^{39}\text{Ar}$ analyses were conducted at the Arizona State University Noble Gas Geochronology and Geochemistry laboratory on a high sensitivity Nu Instruments Noblesse multi collector mass spectrometer with Nier-type source and zoom optics, coupled to a 60W IPG Photonics 970 nm diode laser with Photon Machine

optics linked to a Newport controller. Age standard and unknown single grain samples were at 120° C in an ultra-high vacuum chamber for one day, then turbo pumped for one day to remove adsorbed atmospheric argon from the samples and chamber walls.

Total grain fusion was accomplished by firing the laser at 15 W for 2 minutes with a 0.6 mm beam diameter; the beam was moved to completely fuse each grain. Gases released by laser heating were cleaned in SAES NP10 getter pumps at 400° C and room temperature to remove active gases. Ar isotopes were measured on one Faraday detector fitted with a 10¹¹ Ohm resistor and one ETP ion counting multiplier detector calibrated with air pipette shots. Automation of the analytical system was controlled by the Mass Spec software program (see Data Repository for blank and correction values).

Age calculations were performed from isotopic ratios using the *Isoplot* software plug-in following the decay constant, branching ratio and atmospheric Ar ratios from Steiger and Jäger (1977). Isotopic ratios, J values and calculated cooling ages for all analyses are reported with two sigma errors in the Data Repository, however only single grain analyses with at least 80% radiogenic ⁴⁰Ar were used in cooling age interpretations.

4.3.3.2 Zircon fission-track

Fission-track analyses were performed at Apatite to Zircon, Inc. using the laser ablation, inductively coupled plasma mass spectrometry (LA-ICP-MS) methods of Donelick et al. (2005) and Chew and Donelick (2012). Zircons were separated from the 63 to 250 µm grain size fraction with standard magnetic and density separation techniques. A random subsample of grains from each sample were mounted in Teflon, polished to expose internal grain surfaces and imaged with cathodoluminescence and high-

resolution electron backscattering prior to U-Pb analyses - see Lang and Huntington (2014) for details of U-Pb analyses and data reduction.

Fission-track analyses were subsequently performed on the same zircon grains. Grain mounts were etched in a NaOH-KOH eutectic melt at $\sim 230^{\circ}$ C for 24 to 72 hours and fission tracks were counted from within each ~ 30 μ m diameter ablation pit at 1562.5x dry magnification in unpolarized, transmitted and reflected light on a Nikon Optiphot 2 microscope. The LA-ICP-MS approach uses a modified zeta calibration (Hurford and Green, 1983; Hasabe et al., 2003) where zeta calibration standards from Fish Canyon Tuff were updated during each LA-ICP-MS session and smoothed using a load-specific running-median. U, Th and Sm abundances were determined by LA-ICP-MS using an Agilent 7700x quadrupole mass spectrometer coupled to a Resolnetics RESolution M-50 193 nm excimer laser.

4.4 Results

4.4.1 Stratigraphy of the Siji River region

We focused stratigraphic surveying and sampling across the gradational Upper and Middle Siwalik contact exposed in the footwall of the Tipi Thrust. Exposures of the Lower Siwalik were faulted out of stratigraphic section and internally deformed (Jain et al., 1974; Agarwal, 1991) restricting the interpretability of stratigraphic position without extensive additional magnetostratigraphy, which was impractical due to the severe inaccessibility of the unit. In contrast, the gradational Upper and Middle Siwalik contact is complete and well exposed in Siji River exposures. This contact marks a distinct, previously dated lithological boundary that aid correlation of our observations to other

Siwalik sections. This contact is gradational where coarse sandstones of the Middle Siwalik are interbedded with siltstone and conglomerate beds of the Upper Siwalik, so we defined the bottom of the Upper Siwalik where the frequency of siltstone beds first increases (Figure 3).

4.4.1.1 Middle Siwalik

The Middle Siwalik is at least 3.1 km thick in the Siji River region. Exposures support relatively high topography with steep slopes that commonly follow bedding planes. This unit is defined by thin to very thick beds of monotonous sandstone that coarsen upward from fine to very coarse sands with interbedded gravel and cobble conglomerate. The lower 1.7 km of the unit are distinguished by the reduced and eventual absence of quartzite, metamorphic and volcanic clasts in channel deposits as well as a reduction in grain size, bed thickness and mica concentration. This lower portion of the unit contains thin to thick beds of very fine to medium sandstone with rare beds of matrix-supported conglomerate. Sandstone beds exhibit parallel and cross stratification at centimeter to meter scales, including climbing ripples, planar bedding and trough cross bedding. Beds often exhibit truncated fining upward sequences. Sand grains are angular to subangular and range from poorly to well sorted. At the lowest horizons, interbedded matrix-supported conglomerate contain angular to subangular clasts of hard red or grey siltstone, mudstone and coal. Decimeter to meter scale round and tabular concretions are concentrated along bedding planes and surround coal fragments. Detrital coal fragments are ubiquitous and whole logs and stumps are observed throughout this portion of the unit.

The upper 1.4 km of the unit are distinguished by very thickly bedded coarse to very coarse sandstone, less common matrix and clast supported conglomerate and rare siltstone and mudstone beds. Sandstones coarsen upward from coarse to very coarse grained in the uppermost 500 m of the unit. Sandstones are generally massive or exhibit faint cross bedding at meter scales or larger; some contain pebble-gravel channel deposits. Grains are angular to subangular and poorly to moderately sorted. Sandstones are micaceous, with large micas observed in very coarse horizons. Channel deposits first appear as discontinuous stringers but progressively thicken up section into thick lenticular beds of matrix and clast supported conglomerate. These deposits contain variously colored quartzite, vein quartz, metamorphic and volcanic rock fragments similar to those observed in the Upper Siwalik. This part of the Middle Siwalik also contains centimeter to meter scale round and tabular concretions, commonly distributed along bedding planes. Coal logs, stumps and large coal fragments are observed throughout this portion of the section, as well as thick beds of laminated grey siltstone. Green-brown claystone are observed, but rarely.

4.4.1.2 Upper Siwalik

The Upper Siwalik is at least 1.5 km thick in the Siji River region. Relative to the Middle and Lower Siwaliks, the unit is recessive and forms subdued topography. The angular route of the Siji River apparently results from exploitation of easily erodible silt beds in the lower portion of the unit before the river crossed the Middle Siwalik to enter the Brahmapura braid plain. The lower 900 m of the Upper Siwalik are characterized by discontinuous sequences of thickly to very thickly interbedded conglomerate, sandstone

and siltstone. Gravel-cobble conglomerate is clast supported and typically massive or crudely cross bedded. Conglomerate clasts are moderately sorted, subangular to subrounded and contain similar lithologies as observed in channel deposits of the Middle Siwalik. Specifically, clasts include volcanic breccia, amygdular and vesicular basalt, orthogneiss and schist, quartzite in a variety of colors, vein quartz, siltstone and detrital coal. Siltstone clasts are commonly angular and appear to be scoured from silt beds within the unit, whereas the remaining clasts are remarkably similar to Lesser Himalayan units exposed in the Siang valley. In particular the observed volcanic rocks is particularly diagnostic of the Abor Volcanics only exposed along the Siang River (Figure 1B; Jain and Thakur, 1978; Ali et al., 2012). Sandstones are medium to very coarse grained and exhibit decimeter to meter scale cross bedding, parallel bedding or may be massive. Siltstone and very fine sandstone beds may exhibit parallel lamination, cross lamination, and occasional post-depositional dewatering and soft sediment deformation structures (e.g., dish structures, convolute lamination). Both sandstone and siltstone beds are micaceous, commonly containing large mica grains. Large stumps and logs are occasionally observed in this portion of the unit.

In the upper 600 m of the unit the frequency of conglomerate beds increases as medium and coarse sandstone and siltstone beds are reduced to discontinuous lenses within conglomerate beds. In this portion of the section clast-supported conglomerates are notably more oxidized, and loosely consolidated. Clasts are moderately to well sorted, subangular to subrounded, and subtly coarsen upward from cobble to boulder sizes. Beds are typically massive, but may be crudely cross bedded. Clasts are also crudely imbricated, exhibiting a dominantly south-southeastern flow direction (similar to

observations of Jain et al., 1974) or showing no preferential flow direction. Clasts are dominated by variously colored quartzite (red, green, white, grey) with some basalt, gneissic metamorphic rock fragments, dolomite and rare coal fragments. We note that the dip of the uppermost conglomerate beds decreases with proximity to the Tipi Thrust, indicating that these strata may have been deposited during tilting of underlying units (i.e., growth strata). Growth strata have also been observed in the uppermost Upper Siwalik near Bhalukpong (Burgess et al., 2013).

4.4.1.3 Interpretation of depositional environment

Our observations are consistent with previous interpretations of primarily alluvial deposition for Upper and Middle Siwaliks in this region (e.g., Karunakaran and Rangarao, 1972; Rangrao, 1983; Kumar, 1997; Chirouze et al., 2012). Specifically, the abundance of large-scale characteristic fluvial bedforms in the Middle Siwalik indicates deposition by a large, braided sand-bed river (e.g., Bristow and Best, 1993; Miall, 1996). Overlapping channel deposits with truncated fining upward sequences indicate a vertically stacked fluvial architecture (e.g., Walker and Cant, 1984) characteristic of axial deposition in a narrowly constrained basin similar to the present Brahmaputra River valley.

Considering this interpretation of the depositional environment, the up-section increase in grain size and characteristic bedform scale within the Middle Siwalik may indicate increasing flow velocity (e.g., Middleton and Southard, 1978; van Rijn, 1984), flow depth (e.g., Yalin, 1972) and sediment discharge (e.g., Gilbert, 1914; Karim and Kennedy, 1990), rather than increasing input of coarse sediment from transverse

Himalayan rivers at the axial river margin. Unfortunately, truncation of existing bedforms in this portion of the section complicates a detailed interpretation of paleocurrent direction in the field. Future work complimenting provenance analyses with detailed paleocurrent analyses (e.g., using the anisotropy of magnetic susceptibility from paleomagnetic specimens) at a single bed-scale might better evaluate this interpretation.

We interpret the increased frequency in gravel-cobble conglomerate and siltstone beds across the Upper-Middle Siwalik contact to represent a new contribution from transverse Himalayan rivers. This interpretation is consistent with the bulk isotopic measurements of Chirouze et al. (2013) that indicate a local Himalayan provenance in the Upper Siwalik near Bhalukpong. Moreover, movement of the Tipi Thrust since approximately 1 Ma (Chirouze et al., 2013) may explain the decreasing dip of depositional surfaces in the uppermost portion of the Upper Siwalik as growth strata deposited concurrently with tilting of underlying units. Importantly, the presence of growth strata demonstrates that sedimentary recycling of lower stratigraphic levels may have acted as an additional source of detrital cooling ages in the upper DTC3 sample, but not samples from lower stratigraphic levels.

The appearance of gravel and cobble conglomerate in the Upper Siwalik has been previously explained as a consequence of erosional unroofing of the Himalaya during the onset of glaciation in the Plio-Quaternary (Burbank, 1992). Although the eastern Himalayan foreland is more narrowly constrained than the central and western regions, we consider that this hypothesis may be equally valid to explain the abrupt change in grain size between the Middle and Upper Siwaliks. Moreover, glaciation of the Himalaya may have changed the characteristic grain size distribution of eroded Himalayan detritus

(Goldthwait, 1971), supplying both more silt and gravel to the foreland. The thick siltstone and fine sandstone beds interbedded with conglomerate in the lower portion of the Upper Siwalik is curious in a proximal alluvial environment, and we speculate that these beds may represent deposition of fine sediment along the mountain front from episodic glacial outburst floods (e.g., Montgomery et al., 2004; Lang et al., 2013) that may have began around the approximate age of the Upper-Middle Siwalik contact. Many finer beds cap fining upward sequences that include characteristic dewatering structures indicative of rapid deposition of hyperconcentrated floodwaters (Benvenuti and Martini, 2002), and appear sedimentologically similar to recent flood deposits observed along the Siang Valley (Lang et al., 2013). Future analyses of these specific bed sequences may provide insight into the longevity, periodicity, and erosional impact of such rare, yet geomorphically significant events.

4.4.2 Structure of the Siji River section

Our map of the study area (Figure 2) identifies the locations of and relationships between Siwalik unit contacts. Near the northern margin of the study area the Main Boundary Thrust places Paleozoic units including the Permian Gondwana formation over the Lower Siwalik forming distinctive topographic lineaments. The Lower Siwalik is internally deformed, with at least one antithetic reverse fault observed in outcrops along the Likabali-Garu road. This internal deformation combined with poor exposure prohibits an accurate assessment of Lower Siwalik thickness, although it has been previously estimated to be approximately 2 km thick in this location (Jain et al., 1974). The Tipi Thrust places the Lower Siwalik over the Upper Siwalik. This relationship is directly

observed in the Siji River near Siji village and may be traced in regional topography owing to the contrasting competence between the units. The Main Frontal Thrust places the Upper and Middle Siwaliks over Quaternary alluvium along the mountain front. This relationship is primarily inferred from the abrupt change in topographic relief, but bedding relationships vary along the Siji River near the town of Likabali where slivers of compact sandstone and mudstone are locally observed.

Several west-northwest to east-southeast striking faults locally displace the Upper-Middle Siwalik contact in a left lateral sense. These faults may also extend southeastward to the trace of the Main Frontal Thrust at the mountain front. As has been previously suggested by Misra and Srivastava (2009), young fluvial terraces near Likabali may indicate recent activity along these faults. The northwestern tips of the faults disappear within the Upper Siwalik and do not obviously cut the Tipi Thrust and may be buried by growth strata in the uppermost portion of the unit (e.g., Burgess et al., 2013). In this case, offset on these west-northwest to east-southeast striking faults must predate the < 1 Ma growth strata, indicating that young terraces along the mountain front may instead owe their origin to a change in climatic conditions.

Left lateral displacement on these west-southwest to east-southeast striking faults may be consistent with reverse sense movement, however without more detailed observations it is difficult to quantify the total amount of slip. Regardless, the continuity of Siwalik units suggest that these structures should not dramatically complicate our stratigraphic interpretations. However, there is some potential for duplication of the upper Middle Siwalik where the west-northwest to east-southeast striking faults intersect the section between our highest block sample and the Upper-Middle Siwalik contact.

4.4.3 Magnetostratigraphy

Characteristic remanent magnetizations were difficult to resolve from demagnetization paths. As has been previously observed in the region (Chirouze et al., 2012), in most specimens natural remanent magnetization became highly unstable at high temperatures, primarily resulting from a change in magnetic mineralogy consistent with growth of magnetite. Growth of magnetite was documented by a marked increase in magnetic susceptibility around 250°C in more than a third of the specimens analyzed. Instrument noise is not a significant confounding factor as it was at least an order of magnitude less than specimens' magnetic moments prior to the onset of erratic behavior. Only a few of the coarser grained specimens physically disintegrated before the onset of erratic behavior.

The inability to define characteristic magnetizations for most specimens invalidates use of declination and inclination, or the derivative virtual geomagnetic poles (VGPs) to define polarity zones. For most specimens, we were only able to fit lines to low and medium temperature parts of demagnetization paths, which generally did not trend toward the origin. Least squares free line fits to low and medium temperature measurements have a mean declination of 1.7° and inclination of 43.8° with a 3.3° 95% confidence interval. This direction is not statistically different from the present axial dipole field (0° declination and 43.6° inclination) which supports the interpretation that recent overprinting was removed. We therefore assume that demagnetization paths trend toward more stable original magnetizations and evaluated demagnetization paths on orthogonal and equal area plots.

We calculated the polarity tendency for each specimen from demagnetization paths. Polarity tendency is defined as the angle between a normal polarity reference direction (359.5° declination and 46.7° inclination) and directions from the lowest and highest temperature measurements used for the line fitting. A decrease in this angle indicates a tendency for demagnetization to resolve toward a normal direction, while an increase in this angle indicates a reverse direction. We estimated the precision of polarity tendency angles as the maximum angular deviation of a line fit (MAD, Krischvink, 1980) in place of circular standard deviation in the calculation of the 95% confidence interval based on the Fisher k statistic. Polarity tendency allowed us to qualitatively distinguish horizons of likely normal polarity from reversed polarity.

We graded the quality of data from each specimen and used only the first and second quality specimens in the interpretation of polarity zones. First quality data have distinct normal or reverse polarity tendency (i.e., demagnetization paths trend clearly toward normal or reverse reference directions, see examples in Figure 4B). Second quality data are more ambiguous, due to short or noisy demagnetization paths. Third quality data are most ambiguous and generally indicate that the higher stability component may be a post-tilting overprint (additional examples of characteristic samples are in the Data Repository).

4.4.3.1 New constraints on depositional age

Calculations of polarity tendency do not indicate any normal polarity intervals thicker than approximately 120 m preserved in the 1670 m sampled portion of the Middle Siwalik. At deposition rates consistent with the central and eastern Himalaya (Ojha et al.,

2009; Chirouze et al., 2012) the long C5n.2n normal chron between 9.984 and 11.056 Ma (Gradstein et al., 2012) would be between approximately 370 m and 485 m thick, and the absence of this long interval suggests that this portion of the Middle Siwalik is less than ~10 Ma. In fact, the absence of long normal polarity intervals is remarkably similar to polarity measurements between the C2An.3n chron at 3.032 Ma and C4n.1n chron at 7.528 Ma (Gradstein et al., 2012) made by Chirouze et al. (2012) in the Tipi Thrust footwall near Bhalukpong (Figure 8). Chirouze et al. (2012) further observe similar trends in grain size and bed thickness at the same stratigraphic horizons. Based on these similarities, we tentatively suggest a similar correlation to the geomagnetic polarity timescale.

This correlation establishes a minimum accumulation rate of 371 m/Ma for this portion of the section, which is consistent with regional accumulation rates between 340 and 440 m/Ma (Ojha et al., 2009; Chirouze et al., 2012). With no evidence for duplication of this portion of the section, we estimate the depositional ages of sampled horizons by linear interpolation from the top and bottom of the section assuming accumulation rates up to 440 m/Ma. The depositional age for the single Upper Siwalik sample (DTC3) is better constrained by detrital thermochronology. Zircon fission track ages are not diagenetically reset in the eastern Himalayan foreland (Bernet et al., 2006; Chirouze et al., 2013) so the depositional age of this horizon must be younger than the 1.8 Ma youngest detrital age component. Moreover, apatite fission track analyses from the correlative horizon near Bhalukpong have been thermally reset after deposition (apatite records cooling below temperatures as low as 90° C; Reiners et al., 2005), providing a 0.6 Ma minimum depositional age constraint (Chirouze et al., 2013). Deposition of sample

DTC3 between 0.6 Ma and 1.8 Ma is internally consistent with the stratigraphic position of the sample above the 2-3 Ma Upper-Middle Siwalik contact (Chirouze et al., 2012) and near the appearance of growth strata potentially correlating to an approximate 1 Ma exhumation of the Tipi Thrust (Chirouze et al., 2013).

4.4.4 Detrital thermochronology

4.4.4.1 New $^{40}\text{Ar}/^{39}\text{Ar}$ analyses of river sediment

4.4.4.1.1 Samples from Himalayan tributaries

Muscovite $^{40}\text{Ar}/^{39}\text{Ar}$ analyses from three sampled Himalayan tributaries produce older cooling ages with narrow age ranges recording early exhumation of tectono-stratigraphic units associated with the Himalayan orogeny (Figure 6). Specifically, the Yamne (sample Z) and Yang Sang rivers (sample Y) both drain ophiolitic assemblages along the Indus-Yarlung suture zone (Singh, 1993; Acharyya, 2007) and consequentially share a ~29 Ma component indicating Oligocene exhumation of this unit. The Yamne River also drains Transhimalayan intrusive units (Misra, 2009) north of the suture zone, which may explain the additional, smaller component of older ages around 43 Ma. The Siyom River (sample X) has a ~16 Ma cooling age peak consistent with Early Miocene exhumation of the Greater Himalaya along the Main Central Thrust (e.g., Yin et al., 2010; Uddin et al., 2010; Mathew et al., 2013; Warren et al., 2014).

4.4.4.1.2 Samples from the Siang River

Muscovite $^{40}\text{Ar}/^{39}\text{Ar}$ analysis of river sediment collected from three different

locations along the main channel of the Siang River (samples A, B, and C) consistently have a wider range of cooling ages than are observed in Himalayan tributaries. Cooling age distributions include older ages similar to those observed in Himalayan tributaries with additional younger ages clustering around ~9 Ma. Each sample also contains a minor component of extremely young ages (<5 Ma) with percentage radiogenic argon less than the 80% cut off. Gong et al. (2009) observed similarly low radiogenic argon analyses in river sediment immediately downstream of the Tsangpo Gorge, which may indicate the local influence of hydrothermal fluid circulation (Zeitler et al. 2014). Low radiogenic argon percentage may alternatively result from alteration of mineral grains by weathering, complicating the interpretation of these very young grains as necessarily reflecting rapid mineral cooling.

Like previous observations of young zircon fission track cooling ages (Stewart et al., 2008; Enkelmann et al., 2011), young cooling ages in Siang River samples indicates a contribution from the Namche Barwa Massif. No alternative sources of similarly young cooling ages are observed within the immediate drainage area. Bedrock $^{40}\text{Ar}/^{39}\text{Ar}$ ages of biotite from the Namche Barwa massif range between ~5 and <1 Ma (Malloy, 2004; Zeitler et al. 2014), and considering that muscovite has a slightly higher closure temperature (McDougall and Harrison, 1999) the same bedrock should produce slightly older muscovite cooling ages. Alternative sources of young muscovite in igneous bedrock surrounding the massif produces $^{40}\text{Ar}/^{39}\text{Ar}$ cooling ages older than 10 Ma (e.g., Maluski et al., 1982; Coulon et al., 1986; Copeland et al., 1987; Copeland and Harrison, 1990; Copeland et al., 1995; Harrison et al., 2000), potentially contributing to the older ages observed in Siang River samples but not also observed in Himalayan tributaries (e.g., ~23

Ma ages).

4.4.4.2 New analyses of Siwalik units

4.4.4.2.1 Coupled zircon fission track and U-Pb analyses

By coupling fission track analyses to U-Pb dated zircons, we can identify the provenance and cooling age of individual grains simultaneously. Detrital zircon U-Pb geochronology is a well-established provenance indicator in the eastern Himalaya (e.g., Stewart et al., 2008; Cina et al., 2009) as crystallization ages younger than 300 Ma are predominantly derived from Tibetan igneous units (Zhang et al., 2012; Lang and Huntington, 2014). Zircons from the Namche Barwa massif are typically older than 300 Ma, except for extremely young ages from anatectic units (Booth et al., 2004; Lang et al., 2013). To interpret exhumation of the massif specifically, we focus interpretation to fission track analyses of zircons with crystallization ages older than 300 Ma, still including zircons less than 30 Ma as the U/Th ratio indicates a metamorphic origin (U/Th >10, Hoskin and Schaltegger, 2003).

To interpret fission track data, we deconvolved cooling age populations into constituent age components, or “peaks” using the DensityPlotter application of Vermeesch (2012). Overlapping analytical error on single grain analyses reduces the interpretability of individual grain analyses, instead we focus interpretation on the minimum distinguishable age component. Results from analyses, including decomposed age components are presented in Figure 5 and detailed in the Data Repository.

The Upper Siwalik sample (DTC3) is dominated by young cooling ages with two discernable age components at 1.8 and 4.1 Ma. These young ages are reminiscent of

young cooling ages previously observed in samples from the Siang River. This previously published work attributes two young cooling age components at 0.9 and 3.5 Ma observed in Siang River samples to recent exhumation of the massif and slightly older age components at ~7 and ~11 Ma to incipient exhumation in the Late Miocene (Stewart et al., 2008; Enkleman et al., 2011). Similarly, we attribute the young cooling ages to samples DTC3 to a Namche Barwa source.

Middle Siwalik samples have a wider spread of older ages with a youngest age component that decreases up section. The lowest sample is curiously dominated by Tibetan zircons, with Himalayan zircons only defining a singular component at 16.7 Ma. Above this, sample 25c, 50b and 75b are defined by three components, the youngest of which systematically decreases from 11.4 Ma to 6.0 Ma to 4.3 Ma in each sample, respectively. For all samples, fission track analyses of zircons with Tibetan igneous U-Pb ages produce relatively old age components around 12 Ma and 26 Ma. Based on analyses from Tibetan and Himalayan tributaries, Enkleman et al. (2011) attributed age components older than ~18 Ma to either Transhimalayan or Lesser Himalayan units, so we anticipate that the younger age components in these sections may also reflect early exhumation of the Namche Barwa massif.

4.4.4.2.2 Muscovite $^{40}\text{Ar}/^{39}\text{Ar}$ analyses

$^{40}\text{Ar}/^{39}\text{Ar}$ analyses produce a wide range of cooling ages in Siwalik samples (Figure 7). The high analytical precision of $^{40}\text{Ar}/^{39}\text{Ar}$ analyses permits interpretation of single grain ages rather than age components, particularly as irregular age spectra may reflect mineral heterogeneity in source region bedrock (e.g., Clift et al., 2004) in addition to

source exhumation patterns. To avoid speculation on such complications, we focus interpretations to the presence of young $^{40}\text{Ar}/^{39}\text{Ar}$ cooling ages (as in provenance analyses; e.g., Lang and Huntington, 2014) in Siwalik samples.

Analysis of sample DTC3 primarily produce older cooling ages similar to analyses from Himalayan tributaries, but also produce a few younger (<5 Ma) ages originating from the Namche Barwa massif. The simplest interpretation for the predominance of Himalayan ages is the Upper Siwalik unit requires mixing of young, recently exhumed cooling ages from the massif with older ages from Himalayan tectono-stratigraphic units, potentially recycled from lower Siwalik levels. Uplift of Siwalik units is estimated to have begun by ~1 Ma (Chirouze et al., 2013) indicating that recycling of lower levels may have begun concurrent or prior to the deposition of this sample.

The youngest individual cooling ages in Middle Siwalik samples systematically decrease up section. The lowest sample, 5b, is dominated by older ages between 20 and 35 Ma. Such ages are very similar to observations from Himalayan tributaries draining the portions of the suture zone, and combined with the dearth of zircons with characteristic Himalayan ages these observations suggest that this lowest sample may record erosion of the suture zone prior to exhumation of the Namche Barwa massif. However, the presence of Himalayan zircons in samples above and below this sample (Lang and Huntington, 2014) alternatively suggest that this sample may instead represent an anomalous contribution from Tibetan units. The youngest individual ages from the remaining Middle Siwalik samples decrease up section from 12.9 Ma to 8.1 Ma to 6.9 Ma for samples 25c, 50b and 75b. The decrease in these young ages may represent increased exhumation in the Namche Barwa massif within the eastern syntaxial source region.

4.5 Discussion

4.5.1 Interpretation of thermochronologic lag time

Source region exhumation history may be interpreted from detrital thermochronology in foreland basin units by calculation of thermochronological lag time (Bernet and Garver, 2005). Thermochronological lag time is the difference between a minimum thermochronologic cooling age (or age component) and the depositional age of the sampled sedimentary unit (Garver and Brandon, 1994). When the duration of intermontane sediment storage is small relative to the timescale of mineral cooling (e.g., Garver et al., 1999; Bernet et al., 2004) and dynamic perturbations to the subsurface thermal field may be accounted for (usually with a thermal model, e.g., Braun et al., 2006) lag time is a useful proxy for exhumation rates in the source region. Moreover, systematic variations in lag time with depositional age may elucidate fundamental changes in the exhumation of source terranes. An upsection decrease in lag time (increase with depositional age) may indicate accelerating exhumation during tectonic uplift, or a constructive phase of orogenesis (Bernet and Garver, 2005). Constant lag time may further indicate attainment of a localized exhumational steady state (e.g., Willet and Brandon, 2002; Burbank, 2007).

For Siwalik samples, we calculated thermochronologic lag time for the youngest individual grain $^{40}\text{Ar}/^{39}\text{Ar}$ cooling ages and fission track age components (Figure 9). In both datasets, minimum lag times systematically decrease up-section reaching lag times similar to modern river sediment samples by approximately 5 Ma (at sample 50b), after which they remain consistently low. We interpret this pattern to indicate an increase in

exhumation rates within the syntaxial source area in the Late Miocene and constant, rapid rates of rock exhumation since ~5 Ma. Because lag time decreases to within the range of modern bedrock cooling ages uniquely attributed to the Namche Barwa massif, and no alternative sources of similarly rapid exhumation are observed within the syntaxis, we specifically attribute this exhumation rate increase to unroofing of the massif. This attribution is consistent with independent modeling of massif exhumation constrained by a compilation of bedrock cooling ages (Zeitler et al., 2014), suggesting that our proximal sedimentary section preserves a detailed history of syntaxial exhumation.

4.5.1.1 Thermal modeling with PECUBE

To quantify the timing and magnitude of exhumation rate change, we use a simplified one-dimensional version of PECUBE, a finite element numerical code (Braun, 2003) often used for interpreting thermochronological data (Braun et al., 2013). We use the code to predict a time series of cooling ages resulting from a step change in Late Miocene exhumation rate (Figure 10A). PECUBE incorporates the influence of heat advection as well as heat diffusion and production to interpret cooling in the source region - an important influence on mineral cooling at such extreme rates of rock exhumation (Braun et al., 2006). A one-dimensional model neglects the potential effects of lateral heat transfer or changes in topographic relief. However, both the crustal-scale folding (Burg et al., 1998) and pop-up structures (Ding et al., 2001) proposed as exhumation mechanisms for the Namche Barwa massif predict dominantly vertical heat advection such that lateral thermal gradients may be neglected (e.g., Zeitler et al., 2014), and previous modeling of detrital cooling populations indicate that even large changes in

topographic relief have only a secondary effect on the width of the detrital age distribution (Braun et al., 2006; Whipp et al., 2009) rather than the cooling age peaks (Ruhl and Hodges, 2005).

We predicted cooling ages from scenarios reflecting a 1-20 fold instantaneous change in exhumation rate occurring between 1-15 Ma. Over six sets of simulations, we varied the final exhumation rate between 5 km/Ma and 10 km/Ma, characteristic of Plio-Quaternary rates (Burg et al., 1998; Ding et al., 2001; Booth et al., 2009; Enkleman et al., 2011; Koons et al., 2013; Zeitler et al., 2014). We used a simple root-mean-squared misfit function to compare cooling age predictions with our observations. The composite misfit values from all sets of models are presented for both thermochronologic datasets in Figure 10B.

Thermal modeling consistently indicates that the upsection change in lag time is best explained by a ~5-10 fold increase in the exhumation rate between 5-7 Ma. Because our samples do not extend earlier into the Miocene, it is difficult to constrain the onset of this rate increase within the Late Miocene. Work by Zeitler et al. (2014) suggest that this onset is ~10 Ma, however we anticipate that further analyses of Siwalik units will constrain this time more precisely. Interestingly, thermal modeling suggests that exhumation rates may have been closer to 1-2 km/Ma in the eastern syntaxis, prior to the rate increase. Chirouze et al. (2013) propose that the eastern Himalayan front have been exhuming at a similar pace since 13 Ma. Considering this proposition, it may be that exhumation rates only increased in the syntaxis where an antecedent river system could maintain surface erosion rates commensurate with an increase in the rate of rock uplift.

4.5.2 A mechanism to initiate rapid exhumation

Integration of the Yarlung and Brahmaputra rivers by river capture has been proposed as a mechanism to initiate rapid exhumation of the Namche Barwa massif (Zeitler et al., 2001; Clark et al., 2004). However, provenance analyses from the same Siwalik units demonstrate that such an event must have occurred prior to deposition of the Lower Siwalik in the Middle or Early Miocene (Lang and Huntington, 2014). The lag of at least 6 Ma between these events strongly suggests that onset of rapid exhumation within the syntaxis was unrelated to integration of the rivers. Instead, erosion by an antecedent river may have amplified regional tectonic uplift of the eastern Himalaya, focusing strain to the syntaxis since the Late Miocene.

At a continental scale, focused crustal strain may be anticipated in a syntaxial setting where the 3D structure of a curved subduction boundary acts to stiffen the under ridding plate (Bendick and Ehlers, 2014). This effect may explain regional patterns of uplift within the eastern syntaxis, but not also deformation of Himalayan units on the under riding Indian Plate. Field observations, geochronology and thermochronology from the broader eastern Himalaya constrain two incidences of Late Miocene duplexing in the footwall of the Main Central Thrust (Yin et al. 2010). Out-of-sequence faulting above the northern duplex was ongoing by ~ 7 Ma (Adlakha et al., 2013; Warren et al., 2014), tectonically uplifting Greater Himalayan units. By either mechanism, tectonic uplift may have extended northeastward to concurrently initiate uplift of the Namche Barwa antiform by ~ 7 Ma.

As the eastern Himalaya uplifted, transverse rivers responded by eroding headward whereas the antecedent drainage of the ancestral Yarlung-Siang-Brahmaputra River

incised into the actively uplifting antiform (e.g., Friend et al., 1999). The correspondence of similarly rapid rates of surface erosion and rock uplift is a critical factor for the modification of tectonic uplift by surface processes (Simpson, 2006), and if focused erosion at the northeastern margin of this structure was commensurate with rates of rocks uplift we would predict the local development of a thermo-mechanical feedback (Koons et al., 2002; 2013). Feedback behavior may have developed between ~7-5 Ma and has since sustained rapid exhumation of the Namche Barwa massif while exhumation rates remained low across the broader eastern Himalaya.

4.5.3 Lag time across the Himalaya

Chirouze et al. (2013) interpret constant exhumation rates between 1-2 km/Ma sustained since 13 Ma in the broader eastern Himalaya. This constant, slower exhumation history may better reflect erosion by transverse rivers (e.g., the Kameng River) that have developed in response to, rather than despite orogenic uplift. In this case, we anticipate that evaluation of lag time from correlative foreland units across the Himalayan front should similarly record constant, slower rock exhumation and that an upsection decrease in lag time should only be observed proximal to antecedent river drainages.

Compilation of lag time studies from across the Himalaya (Figure 13) appears to validate this hypothesis. In addition to this study, an upsection decrease in lag time is only observed in Indus River deposits proximal to the western Himalayan syntaxis (Cervený et al., 1988 also in Bernet and Garver, 2005; Ruiz and Seward, 2006; Rahl et al., 2007). In contrast, all other sections along the main Himalayan front record constant or slightly decelerating exhumation histories (e.g., Bernet et al., 2006; Jain et al., 2009;

Chirouze et al., 2012b; Chirouze et al., 2013). While this dataset remains sparse (and difficult to obtain), the collective dataset suggests that erosion by large, antecedent rivers has fundamentally altered the exhumation history of the Himalayan syntaxes.

4.6 Summary and conclusions

This study investigates the exhumation history of the eastern Himalayan syntaxis by interpreting the eroded detritus from the region. We focus specifically on a proximal sequence of foreland basin deposits in a 4.6 km thick section of Upper and Middle Siwaliks exposed along the Siji River. We combine detailed stratigraphic surveying, magnetostratigraphy and analyses of two different detrital thermochronometric systems, muscovite $^{40}\text{Ar}/^{39}\text{Ar}$ thermochronology and coupled zircon fission track and U-Pb geothermochronology to measure thermochronologic lag time since the Late Miocene. Lag times from both thermochronologic systems decrease up section in the Middle Siwalik, consistent with a 5 to 10 fold increase in syntaxial exhumation rates prior to 5 Ma. Since 5 Ma rapid exhumation rates are similar to those presently observed from the Namche Barwa massif suggesting that steep topographic gradients and rapid surface erosion presently exhuming the massif may be a long lived feature of this landscape.

We conclude that the >6 Ma time lag between the integration of the Yarlung and Brahmaputra river systems and the onset of rapid exhumation indicates that integration of the river system was not a mechanism to initiate rapid exhumation of the Namche Barwa massif. Instead, we propose that antecedent drainage of the ancestral Yarlung-Siang-Brahmaputra River locally exhumed Himalayan units tectonically uplifted by Late Miocene structures extending into the eastern Himalaya. Localized exhumation may have

ultimately initiated a thermo-mechanical feedback between tectonic uplift and surface erosion that has sustained rapid exhumation rates to the present.

Similar observations of accelerating rock exhumation are observed in lag time studies of Siwalik units proximal to the western Himalayan syntaxis, but not also in studies from across the main Himalayan front. Considering our observations within the context of this broader pattern, we highlight the importance of antecedent river drainage in the development of localized thermo-mechanical feedbacks that may have long-sustained steep topography and high sedimentary discharges at the terminal Himalayan syntaxes.

4.7 Acknowledgements

The authors acknowledge funding from the National Science foundation (EAR 0955309 and EAR 1349279 to K.W.H.), the Geological Society of America (Graduate Student Research Grant to K.A.L.), and the Quaternary Research Center at the University of Washington. The authors thank M. Turzewski, G. Messe, K. Bage and O. Tayeng for field assistance; J. Wartho, K. Atakturk, K. Sumner and B. Novak for laboratory assistance. This paper greatly benefited from detailed reviews from informal reviews and comments from D. Montgomery and B. Hallet.

4.8 References

Acharyya, S.K., 2007. Evolution of the Himalayan Paleogene foreland basin, influence of its litho-packet on the formation of thrust-related domes and windows in the Eastern Himalayas – A Review. *J. Geol. Soc. India*. 31, 1-17.

- Adlakha, V., Lang, K.A., Patel, R.C., Lal, N., Huntington, K.W., 2013. Rapid long-term erosion in the rain shadow of the Shillong Plateau, eastern Himalaya. *Tectonophysics*. 582, 76-83.
- Agarwal, R.P., Srivastava, A.K. Maithani, A., 1991, Geology of the Eastern Himalayan Foothill Belt of Bhutan and Arunachal Pradesh: An Overview. *J. Him. Geol.* 2(2), 197-205.
- Ali, J.R., Aitchison, J.C., Chik, S.Y.S., Baxter, A.T., Bryan, S.E., 2012. Paleomagnetic data support Early Permian age for the Abor Volcanics in the lower Siang Valley, NE India: Significance for Gondwana-related break-up models. *J. Asian Earth Sci.* 50, 105-115.
- Armijo, R., Tapponnier, P., Han, T., 1989. Late Cenozoic right-lateral strike-slip faulting in southern Tibet. *J. Geophys. Res.* 94, 2787-2838.
- Avdeev, B., Niemi, N.A., Clark, M.K., 2011. Doing more with less: Bayesian estimation of erosion models with detrital thermochronometric data. *Earth and Planet. Sci. Lett.* 305, 3-4, 385-395.
- Avouac, J.P., Burov, E.B., 1996. Erosion as a driving mechanism of intracontinental mountain growth. *Journal of Geophys. Res.* 101, B8, 17,747-17,769.
- Baruah, J.M.B., Handique, G.K., Rath, S., Mallick, R.K., 1992. Exploration for Palaeocene-lower Eocene hydrocarbon prospects in the eastern parts of Upper Assam basin. *Indian J. Petrol. Geol.* 1, 117-129.
- Baruah, P.K., 2001. Sandstone composition and tectono-provenance of Dafla and Subansiri formations from Kimin-Zero road section of Arunachal Pradesh. *Himalayan. Geol.* 22, 41-54.

- Beaumont, C., 1981. Foreland basins. *Geophys. J. R. astr. Soc.* 65, 291-329.
- Beaumont, C., Fullsack, P., Hamilton, J., 1992, Erosional control of active compressional orogens, in K.R. McClay ed., *Thrust tectonics*, Chapman and Hall, London, 1-18.
- Beaumont, C., Kooi, H., and Willet, S., 2000, Coupled tectonic-surface process models with applications to rifted margins and collisional orogens, *in* Summerfield, M.A., ed., *Geomorphology and global tectonics*: Chichester, John Wiley and Sons, Ltd., p. 29-55.
- Bendick, R., Ehlers, T.A., 2014. Extreme localized exhumation at syntaxes initiated by subduction geometry. *Geophys. Res. Lett.* doi: 10.1002/2014GL061026
- Benvenuti, M., Martini, I.P., 2002. Analysis of terrestrial hyperconcentrated flows and their deposits. In Baker, V., Martini, I.P., Garzon, G., (Eds), *Floods and Megafloods Processes and Deposits*, International Association of Sedimentologists Special Publication, 32, 167-193.
- Bernet, M., Brandon, M.T., Garver, J.I., Molitor, B.R., 2004. Fundamentals of detrital zircon fission-track analysis for provenance and exhumation studies with examples from the European Alps. *Geol. Soc. Am. Spec. Papers.* 378, 25-36.
- Bernet, M., Garver, J.I., 2005. Fission-track analysis of detrital zircon, in Reiners, P.W., Ehlers, T.A., *Reviews in Mineralogy and Geochemistry, Low-Temperature Thermochronology: Techniques, Interpretations and Applications*, 58, 205-238.
- Bernet, M., van der Beek, P., Pik, R., Huyghe, P., Mugnier, J-L., Labrin, E., Szulc, A., 2006. Miocene to recent exhumation of the central Himalaya determined from combined detrital zircon fission-track and U/Pb analysis of Siwalik sediments, western Nepal. *Basin Res.* 18, 393-412.

- Bhareli, B., and C. Ratnam, 1978, Some contributions to the geology of northeastern India, *Himalayan Geology*, v. 8, i. 2, 757-768.
- Booth, A.L., Zeitler, P.K., Kidd, W.S.F., Wooden, J., Liu, Y., Idleman, B., Hren, M., Chamberlain, C.P., 2004. U-Pb zircon constraints on the tectonic evolution of southeastern Tibet, Namche Barwa Area. *Am. J. Sci.* 304, 10, 889-929.
- Booth, A.L., Chamberlain, C.P., Kidd, W.S.F., Zeitler, P.K., 2009, Constraints on the metamorphic evolution of the eastern Himalayan syntaxis from geochronologic and petrologic studies of Namche Barwa. *Geol. Soc. Am. Bull.* 121, 385-407.
- Bristow, C.S., Best, J.L., 1993. Braided rivers: perspectives and problems. Geological Society, London, Special Publications, 75, 1-11.
- Burbank, D.W., Leland, J., Fielding, E., Anderson, R.S., Brozovic, N., Reid, M.R., Duncan, C., 1996. Bedrock incision, rock uplift and threshold hillslopes in the northwestern himalayas. *Nature.* 379, 505-510.
- Burbank, D.W., Brewer, I.D., Sobel, E.R., Bullen, M.E., 2007. Single-crystal dating and the detrital record of orogenesis, in Nichols, G., Williams, E., Paola, C., eds. *Sedimentary Processes, Environments and Basins: A tribute to Peter Friend.* Blackwell Publishing, Malden, MA. 253-281.
- Burbank, D.W., 1992. Causes of recent Himalayan uplift deduced from deposited patterns in the Ganges basin. *Nature*, 357, 680-683.
- Burg, J.-P., Nievergelt, P., Oberli, F., Seward, D., Davy, P., Mairing, J.-C., Diao, Z., Meier, M., 1998. The Namche Barwa syntaxis: Evidence for exhumation related to compressional crustal folding. *J. Asian Earth Sci.* 16, 239-252.

- Burg, J.P., Podladchikov, Y., 2000. From buckling to asymmetric folding of the continental lithosphere: numerical modeling and application to the Himalayan syntaxes. *J. Geol. Soc. London Special Pub.* 170, 219-236.
- Burg, J.P., Schmalholz, S.M., 2008. Viscous heating allows thrusting to overcome crustal-scale buckling: Numerical investigation with application to the Himalayan syntaxes. *Earth and Planet. Sci. Lett.* 274, 189-203.
- Burgess, W.P., Yin, A., Dubey, C.S., Shen, Z.K., Kelty, T.K., 2013. Holocene shortening across the Main Frontal Thrust zone in the eastern Himalaya. *Earth Planet Sci. Lett.* 357-358, 152-167.
- Braun, J., 2003. Pecube: a finite-element code to solve the 3D heat transport equation including the effects of a time-varying, finite amplitude surface topography. *Computers and Geosciences.* 29, 787-794.
- Braun, J., van der Beek, P., Batt, G., 2006. *Quantitative Thermochronology.* Cambridge University Press, Cambridge. 270 p.
- Braun, J., van der Beek, P., Valla, P., Robert, X., Herman, F., Glotzbach, C., Pedersen, V., Perry, C., Simon-Labric, T., Prigent, C., 2012. Quantifying rates of landscape evolution and tectonics processes by thermochronology and numerical modeling of crustal heat transport using PECUBE. 524-525, 1-28.
- Cerveny, P.F., Naeser, N.D., Zeitler, P.K., Naeser, C.W., Johnson, N.M., 1988. History of uplift and relief of the Himalaya during the past 18 million years: Evidence from fission track ages of detrital zircons from sandstones of the Siwalik Group, in Kleinspehn, K.L., Paola, C. eds. *New perspectives in basin analysis*, Springer, New York. 43-61.

- Chew, D.M., Donelick, R.A., 2012. Combined apatite fission track and U-Pb dating by LA-ICP-MS and its application in apatite provenance analysis, in: Sylvester, P., Quantitative mineralogy and microanalysis of sediments and sedimentary rocks. Mineralogical association of Canada Short Course 42, St. John's, Newfoundland and Labrador, 219-247.
- Chirouze, F., Dupont-Nivet, G., Huyghe, P., van der Beek, P., Chakraborti, T., Bernet, M., Erens, V., 2012. Magnetostratigraphy of the Neogene Siwalik Group of far eastern Himalaya, Kameng section, Arunachal Pradesh, India. *J. Asian Earth Sci.* 44, 117-135.
- Chirouze, F., Bernet, M., Huyghe, P., Erens, V., Dupont-Nivet, G., Senebier, F., 2012b. Detrital thermochronology and sediment petrology of the middle Siwaliks along the Muksar Khola section in eastern Nepal. *J. Asian Earth Sci.* 44, 94-106.
- Chirouze, F., Huyghe, P., van der Beek, P., Chauvel, C., Chakraborty, T., Dupont-Nivet, G., Bernet, M., 2013. Tectonics, exhumation and drainage evolution of the eastern Himalaya since 13 Ma from detrital geochemistry and thermochronology, Kameng River section, Arunachal Pradesh. *Geol. Soc. Am. Bull.* 125, 523-538.
- Cina, S.E., Yin, A., Grove, M., Dubey, C.S., Shukla, D.P., Lovera, O.M., Kelty, T.K., Gehrels, G.E., Foster, D.A., 2009. Gangdese arc detritus within the eastern Himalayan Neogene foreland basin: Implications for the Neogene evolution of the Yalu-Brahmaputra River system. *Earth Planet. Sci. Lett.* 285, 150-162.
- Clark, M.K., Schoenbohm, L.M., Royden, L.H., Whipple, K.X., Burchfiel, B.C., Zhang, X., Tang, W., Wang, E., Chen, L., 2004. Surface uplift, tectonics and erosion of eastern Tibet from large-scale drainage patterns. *Tectonics*, 23, 1.

- Clift, P.D., Campbell, I.H., Pringle, M.S., Carter, A., Zhang, X., Hodges, K.V., Khan, A.A., Allen, C.M., 2004, Thermochronology of the modern Indus River bedload: new insight into the controls on the marine stratigraphic record. *Tectonics*. 23, 5.
- Copeland, P., Harrison, T.M., Kidd, W.S.F., Ronghua, X., Yuquan, Z., 1987. Rapid early Miocene acceleration of uplift in the Gangdese Belt, Xizang (southern Tibet), and its bearing on accommodation mechanisms of the India-Asia collision. *Earth and Planetary Science Letters*. 86, 2-4, 240-252.
- Copeland, P., Harrison, T.M., 1990. Episodic rapid uplift in the Himalaya revealed by $^{40}\text{Ar}/^{39}\text{Ar}$ analysis of detrital K-feldspar and muscovite, Bengal Fan. *Geology*. 18, 354-357.
- Copeland, P., Harrison, T.M., Yun, P., Kidd, W.S.F., Roden, M., Yuquan, Z., 1995. Thermal evolution of the Gangdese batholith, southern Tibet: A history of episodic unroofing. *Tectonics*. 14, 223-236.
- Coulon C., Maluski, H., Bollinger, C., Wang, S., 1986. Mesozoic and Cenozoic volcanic rocks from central and southern Tibet: $^{39}\text{Ar}/^{40}\text{Ar}$ dating petrological characteristics and geodynamical significance. *Earth and Planet. Sci. Lett.* 79, 281-302.
- Craw, D., Koons, P.O., Zeitler, P.K., Kidd, W.S.F., 2005. Fluid evolution and thermal structure in the rapidly exhuming gneiss complex of Namche Barwa-Gyala Peri, eastern Himalayan syntaxis. *J. Metamorphic Geol.* 23, 9, 829-845.
- Crittelli, S., Garzanti, E., 1994. Provenance of the Lower Tertiary Murree redbeds (Hazara-Kashmir Syntaxis, Pakistan) and initial rising of the Himalayas. *Sed. Geol.* 89, 265-284.

- Davis, D., Supper, J., Dahlen, F.A., 1983, Mechanics of fold –and-thrust belts and accretionary wedges. *Journal of Geophysical Research*, v. 89, p. 1153-1172.
- DeCelles, P.G., Gehrels, G.E., Quade, J., Ojha, T.P., Kapp, P.A., Upreti, B.N., 1998. Neogene foreland basin deposits, erosional unroofing, and the kinematic history of the Himalayan fold-thrust belt, western Nepal. *Geol. Soc. Am. Bull.* 110, 2-21.
- Ding, L., Zhong, D., Yin, A., Kapp, P., Harrison, T.M., 2001. Cenozoic structural and metamorphic evolution of the eastern Himalayan syntaxis (Namche Barwa). *Earth Planet. Sci. Lett.* 192, 423-438.
- Dodson, M.H., 1973. Closure temperature in cooling geochronological and petrological systems. *Contrib. Mineral. And Petrol.* 40, 359-274.
- Donelick, R.A., O’Sullivan, P.B., Ketcham, R.A., 2005. Apatite fission-track analysis. *Reviews in Mineralogy and Geochemistry*, Mineralogical Society of America, v. 58, 49-94.
- Dutta, S.K., 1980. Palynostratigraphy of the sedimentary formations of Arunachal Pradesh – 2. Palynology of the Siwalik equivalent rocks of Kameng District. *Geophytology* 10, 5–13.
- Duvall, A.R., Clark, M.K., Avdeev, B., Farley, K.A., Chen, Z., 2012. Widespread late Cenozoic increase in erosion rates across the interior of eastern Tibet constrained by detrital low-temperature thermochrometry. *Tectonics*. 31, doi: 10.1029/2011TC002969
- Enkelmann, E., Ehlers, T.A., Zeitler, P.K., Hallet, B., 2011. Denudation of the Namche Barwa antiform, eastern Himalaya. *Earth and Planet. Sci. Lett.* 307, 323-333.

- Enlow, R.L., Koons, P.O., 1998. Critical wedges in three dimensions: Analytical expressions from Mohr-Coulomb constrained perturbation analysis. *J. Geophys. Res. Solid Earth*, 103, B3, 4897-4914.
- Finlayson, D.P., Montgomery, D.R., Hallet, B., 2002. Spatial coincidence of rapid inferred erosion with young metamorphic massifs in the Himalayas. *Geology*. 30, 219-222.
- Finnegan, N.J., Hallet, B., Montgomery, D.R., Zeitler, P.K., Stone, J.O., Anders, A.M., Liu, Y., 2008. Coupling of rock uplift and river incision in the Namche Barwa–Gyala Peri massif, Tibet, China. *Geol. Soc. Am. Bull.* 120, 142–155.
- Friend, P.F., Jones, N.E., Vincent, S.J., 1999. Drainage evolution in active mountain belts: extrapolation backwards from present-day Himalayan river patterns. *Spec. Publs. Int. Ass. Sediment.* 28, 305-313.
- Gansser, A., 1966. *The Indian Ocean and the Himalayas: a geological interpretation.* Geologisches Institut der Eidg. Technischen Hochschule und der Universität Zurich.
- Garver, J.I., and Brandon, M. T., 1994, Erosional denudation of the British Columbia Coast Ranges as determined from fission-track ages of detrital zircon from the Tofino basin, Olympic Peninsula, Washington: *Geological Society of America Bulletin*, v. 106, p. 1398–1412.
- Garver, J.I., Brandon, M.T., Roden-Tice, M., Kamp, P.J.J., 1999. Exhumation history of orogenic highlands determined by detrital fission-track thermochronology. *Geol. Soc. London Spec. Pub.* 154, 283-304.
- Gautam, P., Fujiwara, Y., 2000. Magnetic polarity stratigraphy of Siwalik Group

- sediments of Karnali River section in western Nepal. *Geophysical Journal International*. 142, 812–824.
- Geng, Q., Guitang, P., Zheng, L., Chen, Z., Fisher, R.D., Sun, Z., Chunsheng, O., Dong, H., Wang, X., Li, Sheng, Lou, X., Fu, H., 2006. The eastern Himalayan syntaxis: major tectonic domains, ophiolitic melanges and geologic evolution. *J. Asian Earth Sci.* 27, 265-285.
- Gilbert, G.K., 1914. Transportation of débris by running water. United States Geological Survey Professional Paper 86, 263 p.
- Gong, J., Ji, J., Zhou, J., Chen, J., Qing, J., Sun, D., Han, B., Zhong, D., 2009. Cooling history constrained by detrital $^{40}\text{Ar}/^{39}\text{Ar}$ geochronology in eastern Himalaya syntaxis: Implications for climatic and tectonic records. *Acta Petrologica Sinica*, 25, 3, 621-635.
- Gogoi, K.D., Stratigraphy and sedimentation of the Siwaliks of Arunachal Himalaya, Northeast India, in: Proceedings of the international symposium on intermontane basins: Geology and resources, Chiang Mai, Thailand; Thanasuthipitak, T and Ouchanum, P, eds., 427-451.
- Goldthwait, R.P., 1971. Till: A symposium. Ohio State University Press, Wooster. 402 p.
- Gradstein, F.M., Ogg, J.G., Schmitz, M., Ogg, G., 2012. The Geologic time scale 2012. Elsevier publishing, Amsterdam. 85-111.
- Hallet, B., Molnar, P., 2001. Distorted drainage basins as markers of crustal strain east of the Himalaya. *J. Geophys. Res.* 106, 13,697–13,709.

- Harrison, T.M., Yin, A., Grove, M., Lovera, O.M., Ryerson, F.J., Zhou, X., 2000. The Zedong window: a record of superposed Tertiary convergence in southeastern Tibet. *J. Geophys. Res.* 105, B8, 19211-19230.
- Hasabe, N., Barbarand, J., Jarvis, K., Carter, A., Hurford, A.J., 2004. Apatite fission-track chronometry using laser ablation ICP-MS. *Chem. Geol.* 207, 135-145.
- Heim A., Gansser A., 1939. Central Himalaya: Geological observations from the Swiss expedition 1936. Debruder Fretz. Zurich. 246.
- Hoskin, P.W.O., Schaltegger, U., 2003. The composition of zircon and igneous and metamorphic petrogenesis: *Reviews of Mineralogy and Geochemistry*, 53, 27-62.
- Hoth, S., Adam, J., Kukowski, N., Oncken, O., 2006, Influence of erosion on the kinematics of bivergent orogens: Results from scaled sandbox simulations, in Willet, S.D., Hovius, N., Brandon, M.T., and Fisher, D., eds., *Tectonics, Climate and Landscape Evolution: Geological Society of America Special Paper 398*, p. 201-225.
- Holt, W.E., Ni, J.F., Wallace, T.C., Haines, A.J., 1991. The active tectonics of the eastern Himalayan syntaxis and surrounding regions. *J. Geophys. Res: Solid Earth.* 96, 14595-14632.
- Hurford, A.J., Green, P.F., 1983. The zeta age calibration of fission-track dating. *Isotope Geoscience*, 1.285-317.
- Jain, A.K., Thakur, V.C., Tandon, S.K., 1974. Stratigraphy and structure of the Siang District, Arunachal (NEFA) Himalaya. *Him. Geol.* 4, 28-60.
- Jain, A.K., Thakur, V.C., 1978. Abor volcanics of Arunachal Himalaya. *J. Geol. Soc. India.* 19, 8, 335-349.

- Johnson, N.M., Stix, J., Tauxe, L., Cervený, P.F., Tahirkheli, R.A.K., 1985. Paleomagnetic chronology, fluvial processes and tectonic implications of the Siwalik deposits near Chinji village, Pakistan. *Journal of Geology*. 93, 27-40.
- Karim, M.F., Kennedy, J.F., Menu of coupled velocity and sediment-discharge relations for rivers. *J. Hydraul. Eng.* 116, 8, 978-996.
- Karunakaran, C., Rangarao, A., 1976. Status of exploration for hydrocarbons in the Himalayan region-Contributions to stratigraphy and structure, *Misc. Publ. Geol. Surv. India*. 41, 1-66.
- Kesari, G.K., 2010. Geology and mineral resources of Arunachal Pradesh, *Misc. Publ. of the Geol. Soc. India*, v. 30, p. IV, vol. 1, 60 p.
- Kirschvink, J.L., 1980. The least-squares line and plane and the analysis of paleomagnetic data. *Geophysical Journal of the Royal Astronomical Society*, 62, 699-718.
- Koons, P. O., 1995. Modeling the topographic evolution of collisional belts, *Annu. Rev. Earth Planet. Sci.* 23, 375-408.
- Koons, P.O., Zeitler, P.K., Chamberlain, C.P., Craw, D., Meltzer, A.S., 2002. Mechanical links between erosion and metamorphism in Nanga Parbat, Pakistan Himalaya. *American Journal of Science*. 302, 749-773.
- Koons, P.O., Zeitler, P.K., Hallet, B., 2013. Tectonic aneurysms and mountain building, in: *Treatise on Geomorphology*. Owen, L.A., ed., 5, 32 pp.
- Kumar, D., 1997. Geology of Arunachal Pradesh. *Geol. Soc. India*. Bangalore. 217 pp.
- Lang, K.A., Huntington, K.W., Montgomery, D.R., 2013. Erosion of the Tsangpo Gorge by megafloods, eastern Himalaya. *Geology*. 41, 1003-1006.

- Lang, K.A., Huntington, K.W., 2014. Antecedence of the Yarlung-Siang-Brahmaputra River, eastern Himalaya. *Earth and Planet. Sci. Lett.* 397,145-158.
- Larsen, I.J., Montgomery, D.R., 2012. Landslide erosion coupled to tectonics and river incision. *Nature Geos.* 5, 468-473.
- LeFort, P., 1975. Himalayas: The collided range. Present knowledge of the continental arc. *Am. J. Sci.* 275A, 1-44.
- Maclaren, J.M., 1904. The geology of Upper Assam. *Rec. Geol. Surv. India.* 31, 179-209.
- Malloy, M., 2004. Rapid erosion at the Tsangpo knickpoint and exhumation of southeastern Tibet. [M.S. thesis] Bethlehem, Pennsylvania, Lehigh University, 67 p.
- Maluski, H., Proust, F., Xiao, X.C., 1982. $^{39}\text{Ar}/^{40}\text{Ar}$ dating of the trans-Himalayan calc-alkaline magmatism of southern Tibet. *Nature.* 298. 152-154.
- Marques, F.O., Cobbold, P.R., 2002. Topography as a major factor in the development of arcuate thrust belts: insights from sandbox experiments. *Tectonophysics.* 348, 247-268.
- Mathew, G., De Sarkar, S., Pande, K., Dutta, S., Ali, S., Rai, A., Netrawali, S., 2013. Thermal metamorphism of the Arunachal Himalaya, India: Raman thermometry and thermochronological constraints on the tectono-thermal evolution. *Int. J. Earth Sci.* 102, 191-1936.
- Mathur, L.P. and P. Evans, 1964, Oil in India, 2nd International Geological Congress, New Delhi, v. 85.
- McDougall, I., Harrison, T.M., 1999, Geochronology and thermochronology by the $^{40}\text{Ar}/^{39}\text{Ar}$ method. Oxford, New York. 269.

- Miall, A.D., 1996. The geology of fluvial deposits. Springer, Berlin. 582.
- Middleton, G.V., Southard, J.B., 1984. Mechanics of sediment movement. Lecture notes for Short Course No. 3, Providence, Rhode Island, Soc. Sed. Geol. Second Edition.
- Misra, D.K., 2009. Litho-tectonic sequence and their regional correlation along the Lohit and Dibang valleys, eastern Arunachal Pradesh. *J. Geol. Soc. India.* 73, 213-219.
- Misra, D.K., Srivastava, P., 2009. River response to continuing movements along the active faults in the Siang valley, north-eastern Himalaya, India. *Zeit. Für Geomorph.* 53, 4, 455-468.
- Montgomery, D. R., 2004. Observations on the role of lithology in strath terrace formation and bedrock channel width, *Am. J. Sci.* 304, 454-476.
- Montgomery, D.R., Hallet, B., Yuping, Liu, Finnegan, N., Anders, A., Gillespie, A., Greenberg, H.M., 2004. Evidence for Holocene megafloods down the Tsangpo River gorge, southeastern Tibet. *Quatern. Res.* 62, 2, 201-207.
- Mugnier, J.L., Baby, P., Colletta, B., Vinour, P., Bale, P., Leturmy, P., 1997. Thrust geometry controlled by erosion and sedimentation: a view from analogue models. *Geology.* 25, 427-430.
- Najman, Y., 2006, The detrital record of orogenesis: A review of approaches and techniques used in the Himalayan sedimentary basins. *Earth Sci. Rev.* v. 74, 1-72.
- Ojha, T.P., Butler, R.F., Quade, J., DeCelles, P.G., Richards, D., Upreti, B.N., 2000. Magnetic polarity stratigraphy of the Neogene Siwalik Group at Khutia Khola, far western Nepal. *Geol. Soc. Am. Bull.* 112, 424-434.

- Ojha, T.P., Butler, R.F., DeCellers, P.G., Quade, J., 2009. Magnetic polarity stratigraphy of the Neogen foreland basin deposits of Nepal. *Basin Research*. 21, 61-90.
- Pan, G., Ding, J., Yao, D., Wang, L., 2004. Geological map of Qinhai-Xizhang (Tibet) and adjacent areas. Chengdu Cartographic Publishing House, scale 1:1,500,000, 6 sheets.
- Pik, R., France-Lanord, C., Carignan, J., 2005. Extreme uplift and erosion rates in eastern Himalayas (Siang-Brahmaputra basin) revealed by detrital (U-Th)/He thermochronology. *Geophysical Research Abstracts*, 7. 09421.
- Pilgrim, G.E., 1913. The correlation of the Siwalik with the mammal horizon of Europe. *Rec. Geol. Surv. India*. 43, 264-325.
- Peltzer, G., Tapponier, P., 1988. Formation and evolution of strike-slip faults, rifts, and basins during the India-Asia collision: an experimental approach. *J. Geophys. Res.* v. 93, n. B12, p. 15085-15117.
- Rahl, J.M., Ehlers, T.A., van der Pluijm, B.A., 2007. Quantifying transient erosion of orogens with detrital thermochronology from syntectonic basin deposits. *Earth and Planet. Sci. Lett.* 256. 147-161.
- Rangarao, A., 1983. Geology and hydrocarbon potential of a part of Assam-Arakan basin and its adjacent region, in Bhandari, L.L., Venkatachala, B.S., Kumar, R., Swamy, S.N., Garga, P., Srivastava, D.C. (eds.) *Petroliferous Basins of India*. *Petrol. Asia J.* 6, 112-127.
- Reiners, P.W., Ehlers, T.A., Zeitler, P.K., 2005. Past, Present and Future of Thermochronology. In Reiners, P.W., Ehlers, T.A., (eds). *Reviews in Mineralogy*

- and Geochemistry, Low-Temperature Thermochronology: Techniques, Interpretations and Applications, 58, 1-18.
- Ring, W., Brandon, M.T., Willet, S.D., Lister, G.S., 1999. Exhumation processes. Geological Society of London Special Publications, 154, 1-27.
- Ruhl, K.W., Hodges, K.V., 2005, The use of detrital mineral cooling ages to evaluate steady state assumptions in active orogens: An examples from the central Nepalese Himalaya. *Tectonics*. 24, TC4015.
- Ruiz, G., Seward, D., 2006. The Punjab foreland basin of Pakistan: a reinterpretation of zircon fission-track data in the light of Miocene hinterland dynamics. *Terra Nova*, 18, 4, 248-256.
- Schneider, D.A., Edwards, M.A., Kidd, W.S.F., Asif Khan, M., Seeber, L., Zeitler, P.K., 1999. Tectonics of Nanga Parbat, western Himalaya: Synkinematic plutonism within the double vergent shear zones of a crustal scale pop-up structure. *Geology*, 2, 11, 999-1002.
- Schneider, D.A., Edwards, M.A., Kidd, W.S.F., Zeitler, P.K., Coath, C.D., 1999b. Early Miocene anatexis identified in the western syntaxis, Pakistan Himalaya. *Earth and Planetary Science Letters*, 167, 3-4, 121-129.
- Schwarz, W.H., Trieloff, M., 2007. Intercalibration of ^{40}Ar - ^{39}Ar age standards NL-25, HB3gr hornblende, GA1550, SB-3, HD-B1 biotite and BMus/2 muscovite. *Chemical Geology*, 242, 218-231.
- Searle, M.P., Windley, B.F., Coward, M.P., Cooper, D.J.W., Rex, A.J., Rex, D., Tingdong, L., Xuchang, X., Jan, M.Q., Thakur, V.C., Kumar, S., 1987. The

- closing of Tethys and the tectonics of the Himalaya. *Geol. Soc. Am. Bull.* 98, 6, 678-701.
- Seward, D., Burg, J.-P., 2008. Growth of the Namche Barwa Syntaxis and associated evolution of the Tsangpo Gorge: Constraints from structural and thermochronological data. *Tectonophys.* 451, 282–289.
- Simpson, G., 2004. Role of river incision in enhancing deformation. *Geol.* 32, 341-344.
- Simpson, G., 2006. Influence of erosion and deposition on deformation in fold belts, in Willet, S.D., Hovius, N., Brandon, M.T., and Fisher, D., eds., *Tectonics, Climate and Landscape Evolution: Geological Society of America Special Paper 398*, p. 267-281.
- Singh, G., 1975, First report of vertebrate fossil from Arunachal Pradesh, *Geological Survey of India News*, v. 6. i. 2.
- Singh, G., 1976, On the stratigraphic correlation of Upper Tertiary of Arunachal Pradesh, *Geological Survey of India Miscellaneous Publication* v. 43, p. 82-84.
- Singh, T., 1999, Paleontological Records from the Eastern Himalaya: A Synthesis. In: *Geological studies in the Eastern Himalayas*, ed. P.K. Verma, 129-163.
- Singh, T., Prakash, U., 1980. Leaf impressions from the Siwalik sediments of Arunachal Pradesh, India. *Geophytology*, 10, 104-107.
- Singh, T., Tripathi, S.K.M., 1989. Siwalik sediments of Arunachal Himalaya: Palynology, palaeocology and palaeogeography. *Paleobotanists*, 38, 325-332.
- Singh, S., 1993. Geology and Tectonics of the Eastern Syntaxial Bend, Arunachal Himalaya. *J. Him. Geol.* v. 4, i. 2, 149-163.

- Sol, S., Meltzer, A., Burgmann, R., van der Hilst, R.D., King, R., Chen, Z., Koons, P.O., Lev, E., Liu, Y.P., Zeitler, P.K., Zhang, X., Zhang, J., Zurek, B., 2007. Geodynamics of the southeastern Tibetan Plateau from seismic anisotropy and geodesy. *Geology*, 35, 563-566.
- Steiger, R.J. and Jäger, E., 1977. Subcommittee on geochronology : Convention on the use of decay constants in geo- and cosmochronology. *Earth and Planet. Sci. Lett.*, 36, 359-362.
- Stewart, R.J., Hallet, B., Zeitler, P.K., Malloy, M.A., Allen, C.M., Trippett, D., 2008. Brahmaputra sediment flux dominated by highly localized rapid erosion from the easternmost Himalaya. *Geology*. 36, 711-714.
- Tapponier, P, Lacassin, R., Leloup, P.H., Schärer, U., Dalai, Z., Haiwei, W., Xiaohan, L., Shaocheng, J., Lianshang, Z., Jiayou, Z., 1990. The Ailao Shan/Red River metamorphic belt: Tertiary left-lateral shear between Indochina and South China. 343, 431-437.
- Treloar, P.J., Coward, M.O., 1991. Indian plate motion and shape: constraints on the geometry of the Himalayan orogeny. *Tectonophysics*. 191, 189-198.
- Uddin, A., Hames, W.E., Zahid, K.M., 2010. Laser $^{40}\text{Ar}/^{39}\text{Ar}$ constraints on Miocene sequences from the Bengal basin: Implications for Middle Miocene denudation of the eastern Himalayas. *J. Geophys. Res. Solid Earth*. 115, B7.
- van Rijn, L.C., 1984. Sediment Transport, Part 1: Bed load transport. *J. Hydraul. Eng.* 110, 10, 1431-1456.
- Verma, R.K., Mukhopadhyay, M., 1977, An analysis of the gravity field in Northeastern India, *Tectonophysics*, 42, p. 283-317.

- Vermeesch, P., 2004. How many grains are needed for a provenance study. *Earth and Planet. Sci. Lett.* 224, 3-4, 441-451.
- Vermeesch, P., 2012. On the visualization of detrital age distributions. *Chem. Geol.* 312-313, 190-194.
- Wadia, D.N., 1931. The syntaxis of the northwest Himalaya: its rocks, tectonics and orogeny. *Rec. Geol. Surv. India.* 65, 189-220.
- Walker, R.G., Cant, D.J., 1984. Sandy fluvial systems, in Walker, R.G., ed. *Facies models*, *Geosci. Can.* 2nd ed. P. 71-89.
- Warren, C., Singh, A.K., Riberts, N.M.W., Regis, D., Halton, A.M., Singh, R.B., 2014. Timing and conditions of peak metamorphism and cooling across the Simithang Thrust, Arunachal Pradesh, India. *Lithos.* 200-201, 94-110.
- Whipp, D.M., Ehlers, T.A., Braun, J., Spath, C.D., 2009. Effects of exhumation kinematics and topographic evolution on detrital thermochronometer data. *J. Geophys. Res. Earth Surface.* 114, F4.
- Whipple, K.X., Tucker, G.E., 1999. Dynamics of the stream-power river incision model: Implications for height limits of mountain ranges, landscape response timescales, and research needs. *J. Geophys. Res.* 104, 17661-17674.
- Whipple, K.X., Meade, B.J., 2004. Controls on the strength of coupling among climate, erosion and deformation in two-sided, frictional orogenic wedges at steady state. *J. Geophys. Res. Earth Surface.* 109, F1.
- Willet, S., 1999. Orogeny and orography: the effects of erosion on the structure of mountain belts. *J. Geophys. Res. Solid Earth.* 104, B12.

- Willet, S., Brandon, M.T., 2001. On steady states in mountain belts. *Geology*. 30, 175-178.
- Winslow, D.M., Zeitler, P.K., Chamberlain, C.P., Williams, I.S., 1996. Geochronologic constraints on syntaxial development in the Nanga Parbat region, Pakistan. *Tectonics*. 15, 1292-1308.
- Yalin, M.S., 1972. *Mechanics of sediment transport*. New York, Pergamon Press.
- Yin, A., 2006; Cenozoic tectonic evolution of the Himalayan orogen as constrained by along-strike variation of structural geometry, exhumation history, and foreland sedimentation. *Earth Sci. Reviews*. V. 76, v. 1, p. 1-131.
- Yin, A., Harrison, T.M., 2000. Geologic evolution of the Himalayan-Tibetan orogen. *Ann. Rev. Earth and Planet. Sci.* 28, 211-280.
- Yin, A., Dubey, C.S., Kelty, T.K., Webb, A.A.G., Harrison, T.M., Chou, C.Y., Celerier, J., 2010. Geologic correlation of the Himalayan orogeny and Indian craton: Part 2. Structural geology, geochronology and tectonic evolution of the Eastern Himalaya. *Geol. Soc. Am. Bull.* 122, 360-395.
- Zeitler, P.K., Johnson, N.M., Naeser, C.W., Tahirkheli, R.A.K., 1982. Fission-track evidence for Quaternary uplift of the Nanga Parbat region, Pakistan. *Nature*, 298, 255-257.
- Zeitler, P.K., Chamberlain, C.P., Smith, H.A., 1993. Synchronous anatexis, metamorphism and rapid denudation at Nanga Parbat, Pakistan Himalaya. *Geology*. 21, 247-350.

- Zeitler, P.K., Meltzer, A.S., Koons, P.O., Craw, D., Hallet, B., Chamberlain, C.P., Kidd, W.S.F., Park, S.K., Seeber, L., Bishop, M., Shroder, J., 2001. Erosion, Himalayan geodynamics, and the geomorphology of metamorphism, *GSA Today*, 11(1), 4–9.
- Zeitler, P.K., Meltzer, A.S., Brown, L., Kidd, W.S.F., Lim, C., Enkelmann, E., 2014. Tectonics and topographic evolution of Namche Barwa and the easternmost Lhasa block, Tibet. *Geol. Soc. Am. Special Paper 507*, 23.
- Zhang, J.Y., Yin, A., Liu, W.C., Wu, F.Y., Lin, D., Grove, M., 2012. Coupled U-Pb dating and Hf isotopic analysis of detrital zircon of modern river sand from the Yalu River (Yarlung Tsangpo) drainage system in southern Tibet: Constraints on the transport processes and evolution of Himalayan rivers. *Geol. Soc. Am. Bull.* 124, 1449-1473.

4.9 Figures

Figure 4.9.1 Study area in the eastern syntaxis and foreland basin

A. Eastward transition from Himalayan convergence to dextral strike-slip motion in Burma warps tectonic units southward to form the eastern Himalayan syntaxis. The Yarlung River follows the Indus-Yarlung Suture Zone (dashed line) >1000 km along the southern margin of Tibet before abruptly turning southward around Namche Barwa (NB, 7,782 m peak elevation) to bisect the syntaxis to join the Brahmaputra River in the easternmost part of the Himalayan foreland basin (yellow area). B. Within the syntaxis, the Yarlung River drops >2 km through the Tsangpo Gorge (highlighted in red). Regional bedrock thermochronology constrains rapid Plio-Quaternary cooling of the Namche Barwa massif, making the region a unique source of anomalously young cooling ages (pink area encompasses zircon fission track ages <3 Ma, Burg et al., 1998; Seward and Burg, 2008; and biotite $^{40}\text{Ar}/^{39}\text{Ar}$ ages < 10 Ma, Zeitler et al., 2014). Young cooling ages are also observed in detrital samples collected downstream of the Tsangpo gorge including in samples A, B, C collected from the locally named “Siang” reach of the river (muscovite $^{40}\text{Ar}/^{39}\text{Ar}$ analyses in this study, zircon fission track from Enkelmann et al., 2011). Sediment leaving the mountains accumulates proximally in the easternmost portion of the Himalayan foreland basin, a narrowly constrained sedimentary basin that thickens toward thrust boundaries (Verma and Mukhopadhyay, 1977). Regional structures dividing tectono-morphic units: MCT = Main Central Thrust, MBT = Main Boundary Thrust, STD = South Tibetan Detachment, MFT = Main Frontal Thrust, TPT = Tipi Thust, MT = Mishmi Thrust, NT = Naga Thrust. Transhimalayan intrusive units in light grey. Regional geology compiled from Armijo et al., 1989; Agarwal et al., 1991;

Baruah et al., 1992; Pan et al., 2004; Acharyya et al., 2007; Misra, 2009; Yin et al., 2010;
Zeitler et al. 2014.

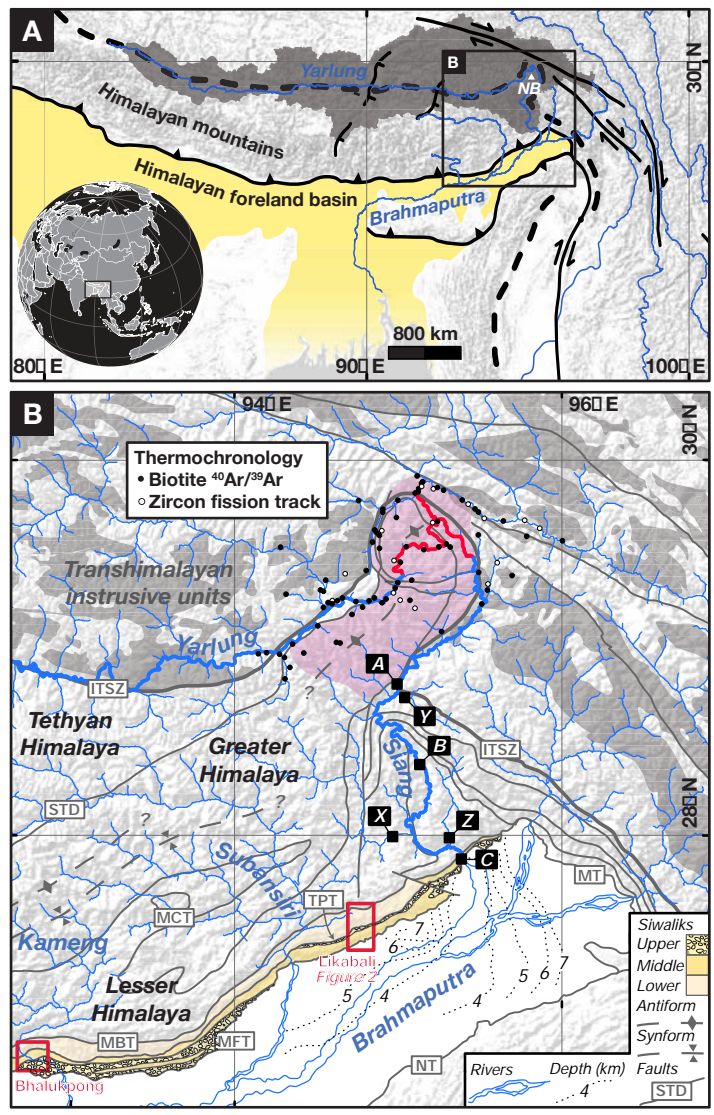


Figure 1.

Figure 4.9.2 Detailed geology of the Siji River area

1:100,000 scale geologic map of the Siji River area from reconnaissance mapping along the Siji River. Bedding measurements define main surveying transect through Upper and Middle Siwaliks for stratigraphy, magnetostratigraphy and detrital sampling. Sample locations from detrital zircon U-Pb samples published by Lang and Huntington (2014) as well as new detrital thermochronology presented in this study.

West-northwest to east-southeast striking faults do not obviously disrupt Siwalik stratigraphy, potentially complicating stratigraphic interpretations of the surveyed transect. Boulder print illustrates approximate extent of growth strata in the Upper Siwalik unit (see text for discussion).

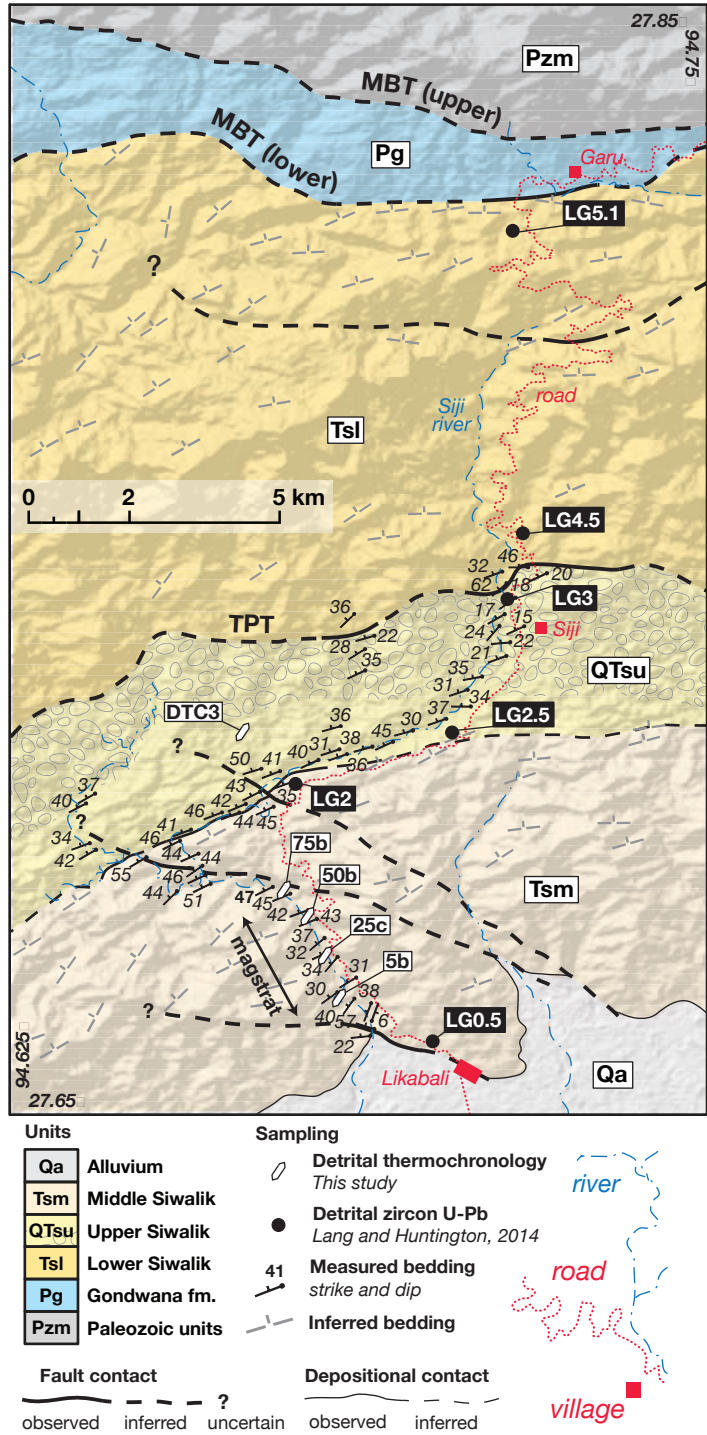


Figure 2.

Figure 4.9.3 Upper and Middle Siwalik stratigraphy in the study area

Stratigraphic section of the Tipi Thrust footwall measured along the Siji River (see Figures 1 and 2 for location). Upper and Middle Siwalik units are an upward coarsening sequence of siltstone, sandstone and conglomerates that we interpret to represent alluvial deposition in a narrowly constrained basin similar to the modern Brahmaputra River valley. The increase in conglomerate in the Upper Siwalik may represent contribution from transverse rivers draining Himalayan units as deposition became more proximal to the mountain front. Shallowing of depositional surfaces in highly oxidized upper conglomerates of the Upper Siwalik indicate deposition during uplift and tilting of underlying units (e.g., growth strata). The first appearance of quartzite, gneiss and basaltic clasts from Himalayan units best exposed along the Siang River valley are shown with the presence of cobble conglomerate beds and the stratigraphic position of samples from this study and Lang and Huntington (2014).

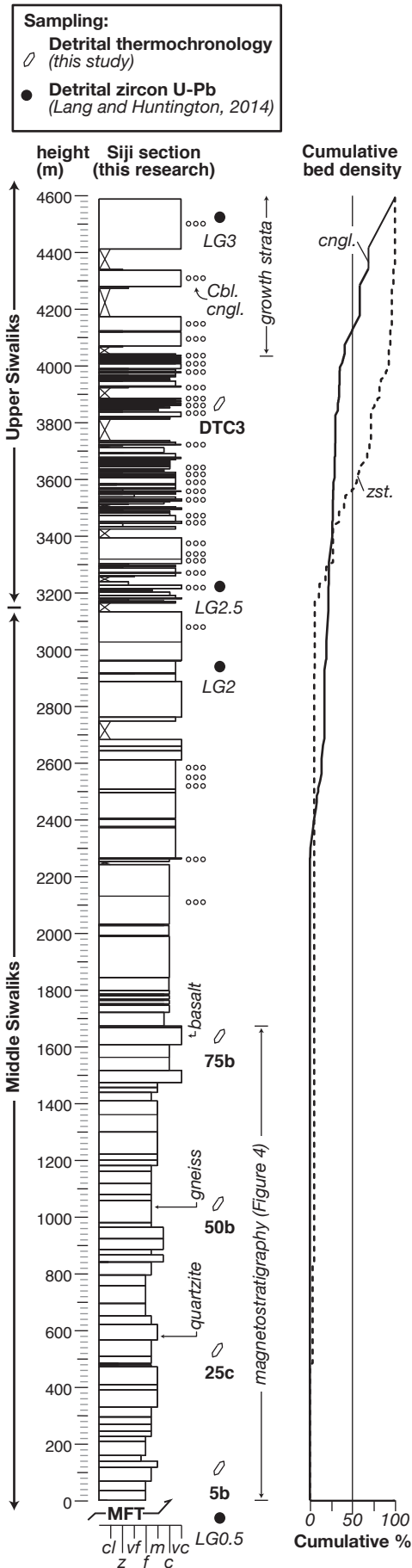


Figure 3.

Figure 4.9.4 Magnetostratigraphy of lower Middle Siwalik exposures

Magnetostratigraphy of the lowest portion of the Middle Siwalik. Stratigraphic position of block samples are shown. Each site has 1-5 specimens. For least squares line fits, N is the number of measurements and MAD is the maximum angular deviation (Kirschvink, 1980). For sites with multiple samples, averages for N and MAD are indicated with tick marks. We used the tendency for the direction to change during demagnetization toward a normal (259.5° declination, 46.7° inclination) or reverse direction in tilt-corrected coordinates as an indication of polarity. See text for discussion of data quality and precision. We did not observe evidence for any long normal polarity zones in this portion of the section (e.g., C5n.2n from 9.9-11.0 Ma). Orthogonal projections of characteristic demagnetization paths onto horizontal (map view) and south-north vertical plane (section view) for specimens with normal (54a1) and reverse (29a2) polarity. Individual measurements are labeled from the natural remnant magnetism (nrm) with temperature in $^\circ\text{C}$. The higher temperature segments are interpreted to be original magnetizations because their inclinations (dashed lines) are closer to that expected for the magnetic field in tilt-corrected coordinates (as shown) than before tilt correction.

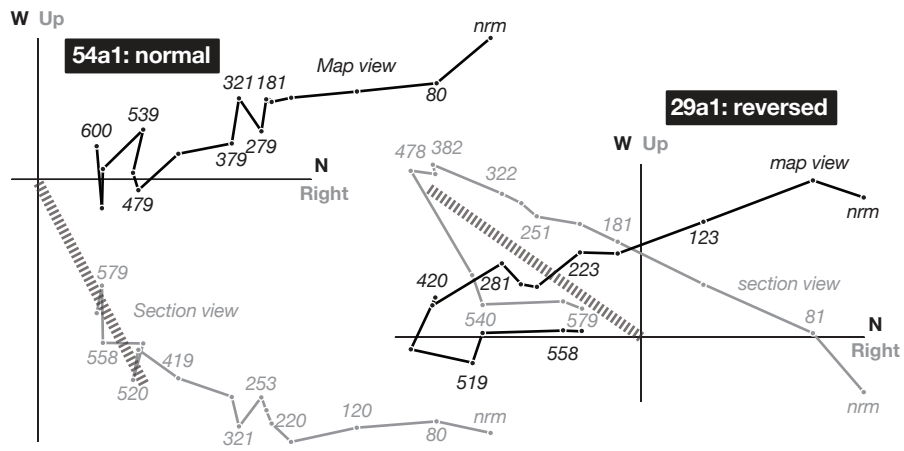
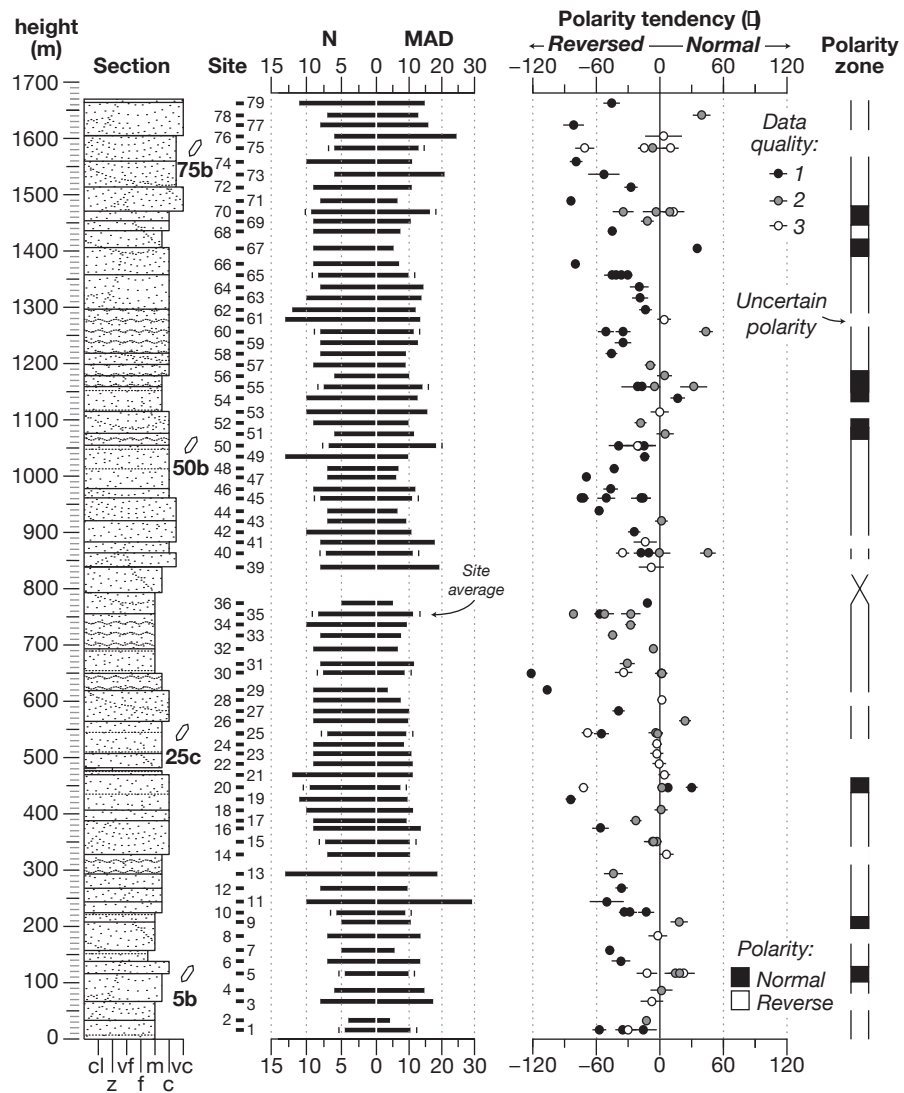


Figure 4.

Figure 4.9.5 Detrital muscovite $^{40}\text{Ar}/^{39}\text{Ar}$ thermochronology of river sediment

Detrital muscovite $^{40}\text{Ar}/^{39}\text{Ar}$ cooling ages from river sediment samples (see Figure 1 for sample locations). Cooling ages from Himalayan tributaries are older than 13 Ma with narrowly defined age populations at ~16, characteristic of Greater Himalayan exhumation on the Main Central Thrust; ~29 indicating Oligocene exhumation of units along the suture zone; and ~43 Ma, cooling of Transhimalayan intrusives north of the suture zone. Cooling ages from three Siang River samples span a wider range. We interpret the addition of younger (~9 Ma) ages to represent contribution from more rapidly cooled bedrock of the Namche Barwa massif. Extremely young ages with low radiogenic argon ($^{40}\text{Ar}^*$) may be derived from the Tsangpo Gorge specifically (Zeitler et al., 2014). Cooling ages older than 55 Ma are considered precursory to the Himalayan orogeny and not included in data plots. The total number of single grain analyses (n_{all}) and the number of analyses plotted (n_{plot}) are stated for each sample. Area normalized, summed probability density functions are plotted as thin black lines and kernel density estimates are plotted as thick grey lines. Kernel density estimation and cooling age peak discrimination was determined using the DensityPlotter application of Vermeesch (2012).

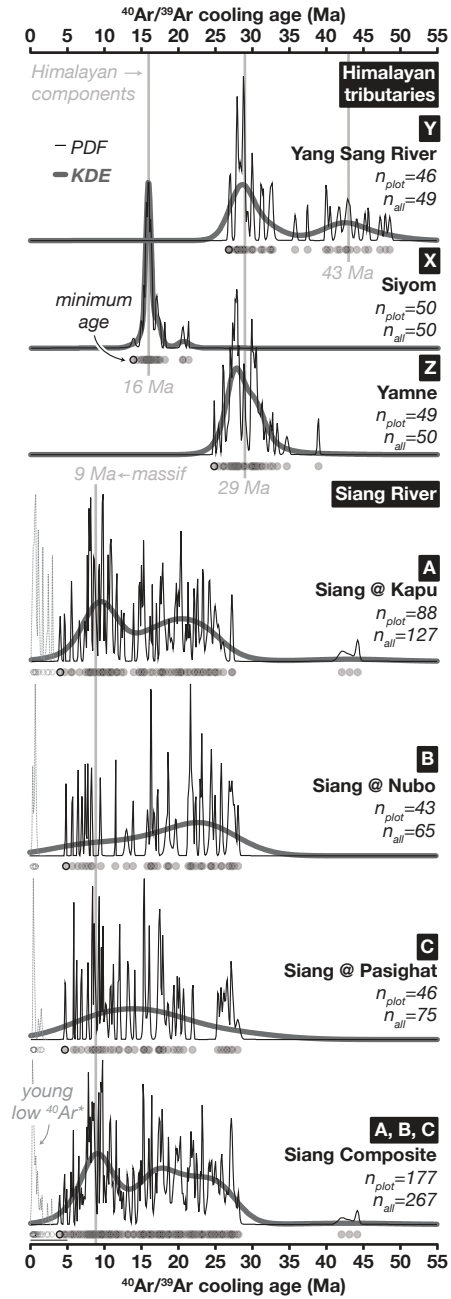


Figure 5.

Figure 4.9.6 Detrital muscovite $^{40}\text{Ar}/^{39}\text{Ar}$ thermochronology of Siwalik units

Detrital muscovite $^{40}\text{Ar}/^{39}\text{Ar}$ cooling ages from Upper and Middle Siwalik samples compared to modern samples from the Siang River. Cooling ages are plotted in the same fashion as in Figure 5. The Upper Siwalik sample is dominated by cooling ages characteristic of Himalayan units, but also includes a few younger ages characteristic of the Namche Barwa massif. We interpret the predominance of Himalayan ages to represent increased contribution from local Himalayan sources following removal of this depositional sequence from an axial basin depocenter or recycling of Siwalik units.

Detrital samples from lower stratigraphic levels contain younger age components, with the exception of sample 5b. Minimum single grain ages decrease up section from 13 to 6 Ma and grain age density is variable, potentially reflecting changes in source erosion patterns. The lowest sample 5b, contains much older ages similar to those observed in Himalayan tributaries draining the suture zone. These ages may reflect erosion of suture zone and northern plutonic source rocks potentially prior to exhumation of the Namche Barwa massif.

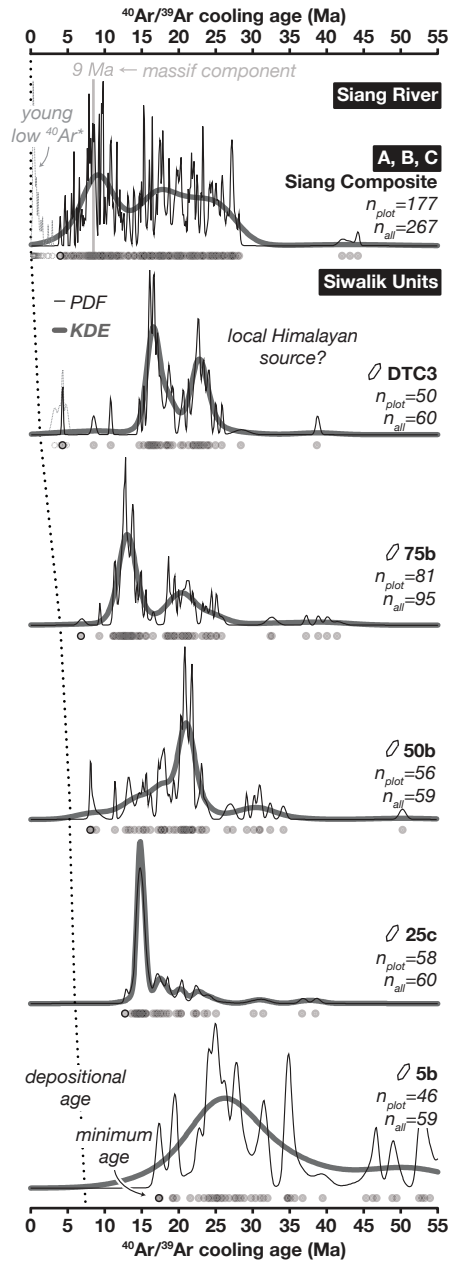


Figure 6.

Figure 4.9.7 Coupled detrital zircon fission-track and U-Pb analyses of Siwalik units

Fission track cooling ages of U-Pb dated detrital zircons from Upper and Middle Siwalik samples compared with ages from the Siang River (Enkelmann, 2012). Plots only show cooling ages from zircons with >300 Ma crystallization ages, filtering out ages from Transhimalayan sources in Tibet. Cooling ages are plotted in the same fashion as in Figure 5. Ages older than 55 Ma are considered pre-orogenic and not plotted. Fission track age components determined with the DensityPlotter application of Vermeesch (2012) are plotted as white boxes. The Upper Siwalik sample DTC3 is dominated by young cooling ages, similar to analyses from the Siang River. The youngest age component in Middle Siwalik samples decreases up section, and reach within ~3 Ma of the depositional age by sample 50b. Notably, the lowest sample 5b is dominated by zircons with a Transhimalayan intrusive source in Tibet, supporting the hypothesis that muscovite $^{40}\text{Ar}/^{39}\text{Ar}$ ages from this sample reflect contribution from erosion of the suture zone and northern Transhimalayan units prior to massif exhumation.

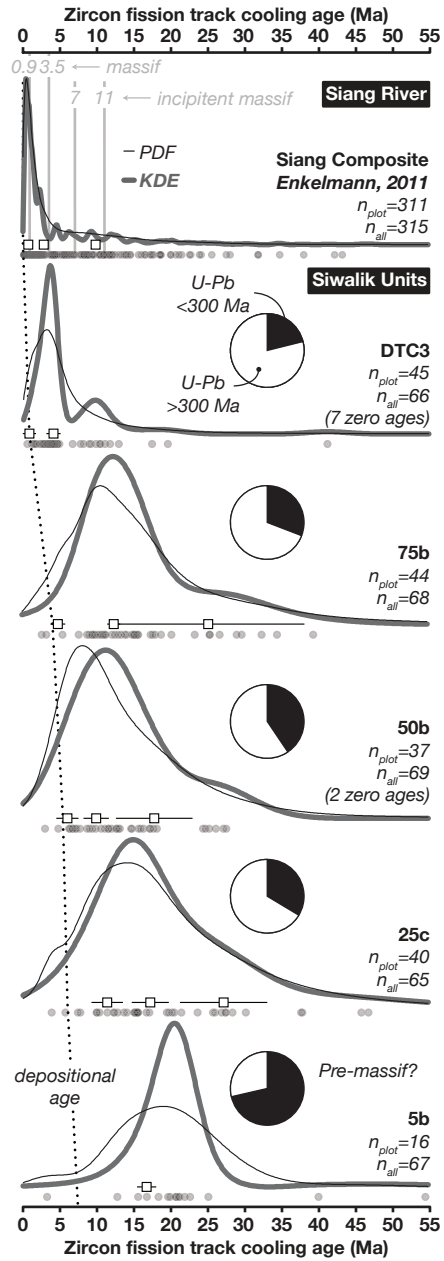


Figure 7.

Figure 4.9.8 Correlation of the Siji River and Bhalukpong sections

Correlation of stratigraphic sections between the Siji River and Kameng River (near Bhalukpong, Chirouze et al., 2012) sections. Within the approximately 4-8 Ma sequence from the Kameng River, we observe similar up section coarsening trends as Chirouze et al. (2012) and a similar absence of long normal polarity zones. Depositional ages are further constrained by the minimum detrital zircon fission track age components observed at both sections. We conservatively correlate the Upper-Middle Siwalik contact where the frequency of siltsone beds increase to the estimated 2-3 Ma age from Chirouze et al. (2012).

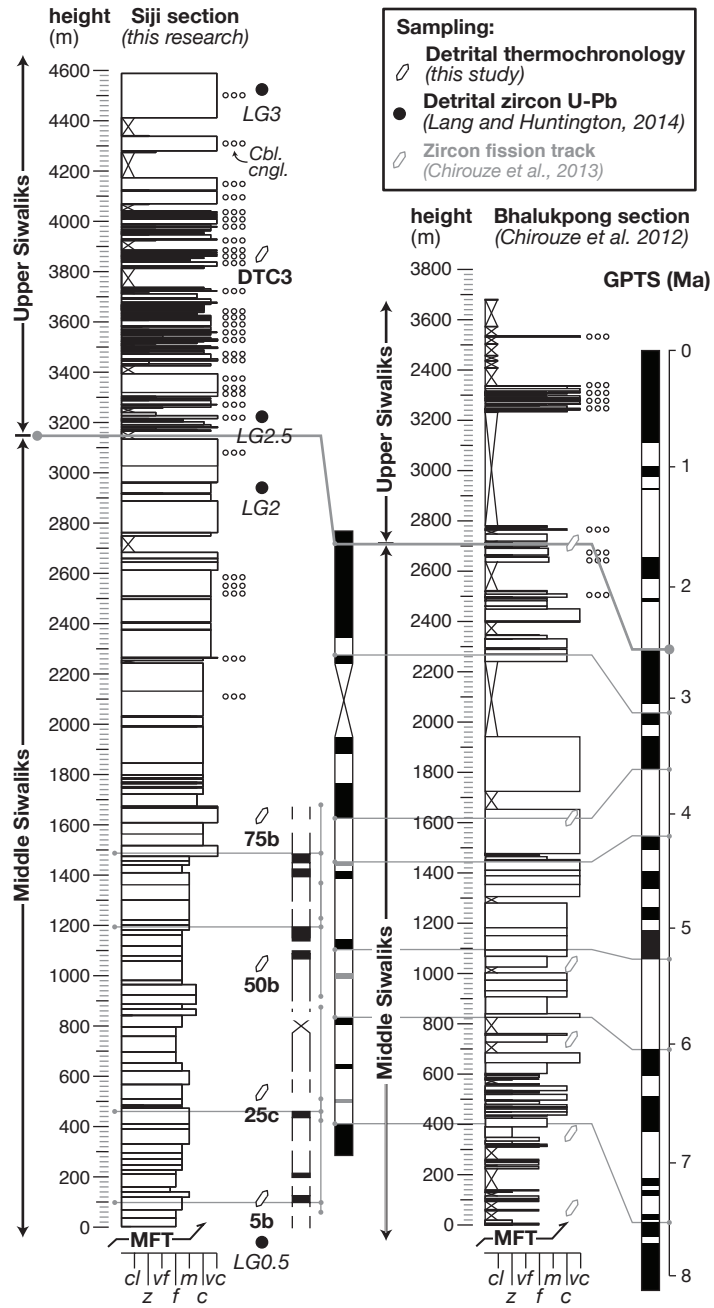


Figure 8.

Figure 4.9.9 Thermochronologic lag time in Siwalik samples

Thermochronologic lag time calculated from youngest cooling age components (fission track, white squares) and single grain ages ($^{40}\text{Ar}/^{39}\text{Ar}$, grey circles). New samples from the Siji River section are outlined in black (Siang River samples from Enklemann et al., 2011) while samples collected near Bhalukpong are light grey (Chirouze et al., 2013). In both new thermochronologic datasets, lag time decreases up section in the lowest three samples and then remains within or below the range of lag times presently observed in Siang River sediment. In contrast, lag time from Bhalukpong decreases between 6-7 Ma but remains older than samples observed in the Siji River section.

Figure 4.9.10 Quantitative constraints from thermal modeling

One dimensional thermal modeling of thermochronologic lag time. **A.** Model scenarios of a step-increase in exhumation rate of the source region varied the factor ($\times E$) and time (t) of exhumation rate increase. Final exhumation rate (E_f) was fixed between 5 and 10 km/Ma. **B.** Contoured plots of root-mean-squared (RMS) misfit between predicted and observed observed lag time. Both thermochronologic datasets are best explained by a ~5-10 fold increase in exhumation rate between 5-7 Ma. Each gridded point represents an individual model scenario. Misfit is summed over six sets of model output for final exhumation rates (E_f) between 5-10 km/Ma.

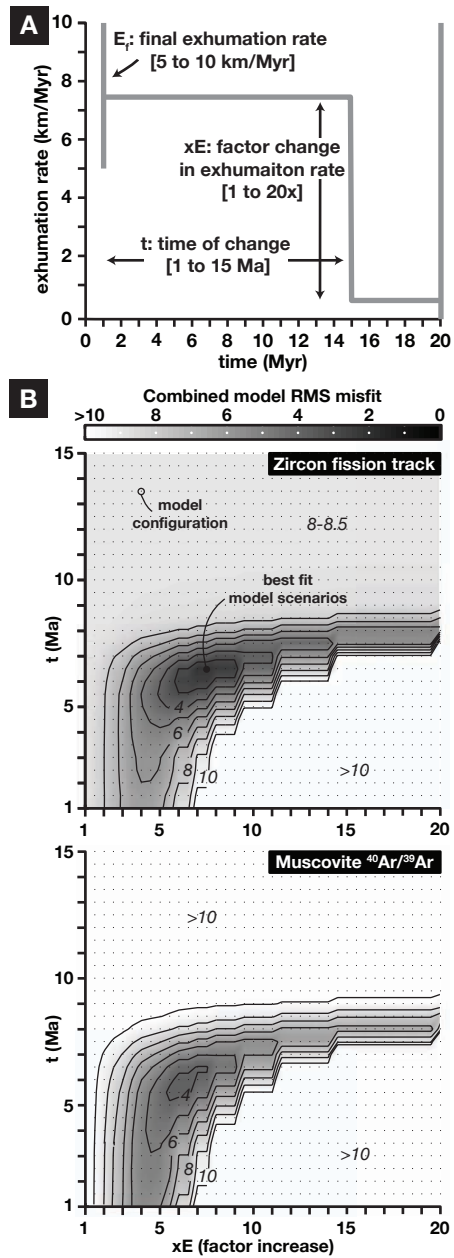


Figure 10.

Figure 4.9.11 Exhumation history of the Namche Barwa massif

Cartoon illustrating the proposed exhumation history of the Namche Barwa massif. Active structures are illustrated in black, unactive structures are light grey. Knickzone within zone of rapid exhumation highlighted in white. **A.** Late Miocene duplexing in the footwall of the Main Central Thrust folds and uplifts Greater Himalayan units in the MCT hangingwall across the eastern Himalaya (Yin et al., 2010). Transverse rivers erode headward and the antecedent course of the ancestral Yarlung-Siang-Brahmaputra begins to incise across the regional antiform. **B.** By 5 Ma, rapid exhumation by the antecedent river has initiated a thermo-mechanical feedback, focusing strain within the eastern syntaxis, exhuming the Namche Barwa massif and warping the Indus-Yarlung suture zone (IYSZ) northward. **C.** Northward migration of the massif captures and reverses flow in the Parlung River within the Quaternary, enhancing exhumation within the present Tsangpo Gorge region (Seward and Burg, 2008).

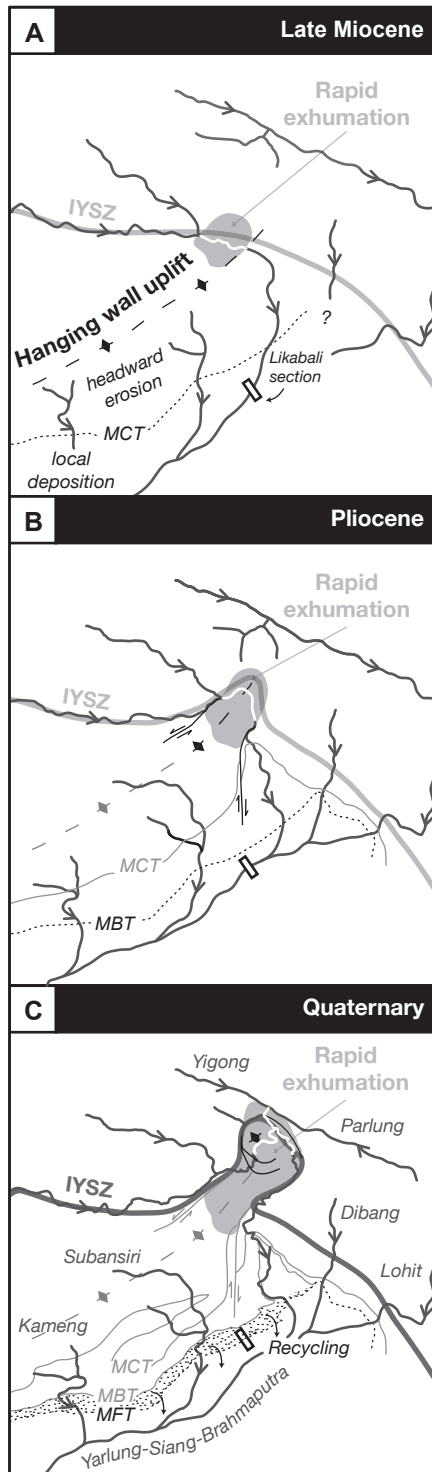


Figure 11.

Figure 4.9.12 Compilation of Himalayan lag time data

Compilation of lag time data from Siwalik units across the Himalaya. Location of sections are illustrated on simplified map of tectonic and foreland units (Crittelli and Garzanti, 1994). Lag time is calculated from minimum zircon fission track age components for all sections, linear fits are added to show general trend of data from each section individually. Lag time data from Siwalik sections proximal to the Himalayan syntaxes (CK = Chani Khel, CV = Chinji Village, Cervený et al., 1988; SR = Siji River, this study) indicate a decrease in lag time up section, whereas lag time data from sections along the Himalayan front do not decrease up section (KR = Karnali River, S = Surai Khola, T = Tinau Khola, Bernet et al., 2006; M = Muksar Khola, Chirouze et al., 2012b; K = Kameng River, Chirouze et al. 2013). We interpret the variation in exhumation history to reflect a local acceleration of exhumation where antecedent rivers cross through the Himalayan syntaxes.

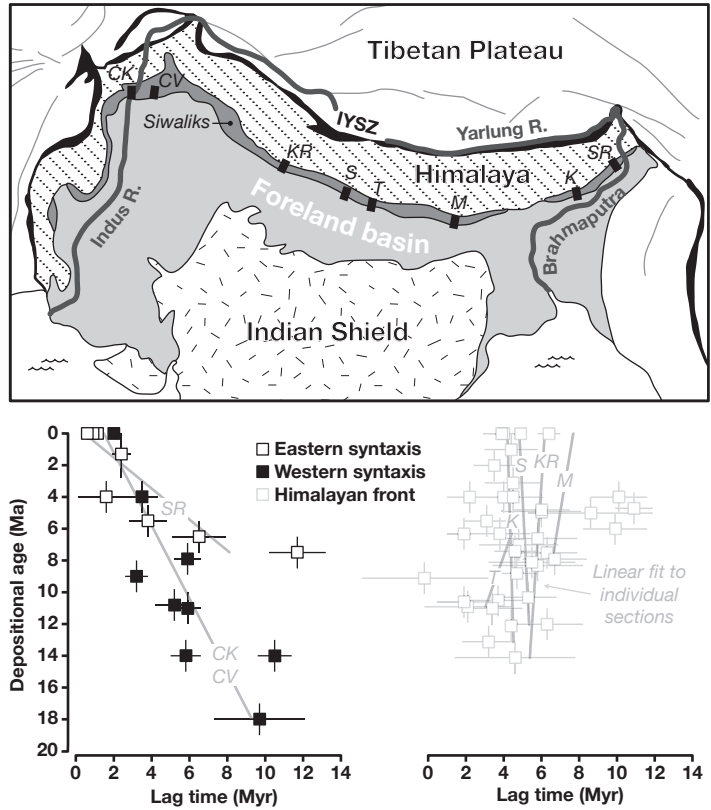


Figure 12.

4.10 Tables

4.10.1 Sample data

TABLE A1. SAMPLE DATA AND ZFT AGE CLUSTERING.

Sample ID	Latitude (Degrees N)	Longitude (Degrees E)	Siwalik Unit	Height above base (m)	Approximate depositional age (Ma)
Siwalik samples					
DTC3	27.718442	94.668658	Upper	3870	0.6 - 1.8
75b	27.690301	94.673102	Middle	1640	3.2-3.9
50b	27.685349	94.678618	Middle	1060	4.4-5.1
25c	27.678317	94.682618	Middle	540	5.6-6.3
5b	27.670815	94.683994	Middle	120	6.6-7.3
Siang River samples					
SIANG R. @ KAPU	29.048672	94.910801		modern	
SIANG R. @ NUBO	28.576655	95.070195		modern	
SIANG R. @ PASIGHAT	28.098664	95.293839		modern	
Himalayan tributary samples					
YANG SANG R.	28.977366	94.904728		modern	
YAMNE R.	28.186037	95.222736		modern	
SIYOM R.	28.219327	94.865888		modern	

4.10.2 Magnetostratigraphy

Table A1. Magnetostratigraphic data. Overprint references is 0 dec. 43.6 inc. N reference polarity is 359.5 dec. 46.7 inc.

Site information			Bedding		n	Maximum angular deviation	Angle from overprint (0 dec. 43.6 inc.)	Precision estimate	Beginning measurement				End measurement			
Site ID	Specimen ID	Height above base (m)	Strike	Dip					dec.	inc.	Angle from N reference	Angle from overprint	dec.	inc.	Angle from N reference	Angle from overprint
1	1a1b	15.8	243.8	46.5	3	7.0	23.5	a	358.5	-6.1	52.8	23.5	338.7	-39.3	88.0	59.4
1	1b1	15.8	243.8	46.5	5	8.4	24.3	6.5	340.1	-0.4	50.1	24.3	246.9	-2.8	107.4	95.9
1	1c1	15.8	243.8	46.5	5	16.4	14.4	12.7	333.1	-5.9	57.5	11	315.3	-26.2	73.3	53.0
1	1d2	15.8	243.8	46.5	5	10.3	21.6	8.0	334.9	-1.7	53.0	14.4	334.6	-6.1	83.1	27.1
2	2a	33	243.8	46.5	4	4.2	11.0	3.6	349.1	3.1	44.5	21.6	350.8	-26.2	57.3	46.9
3	3a1	66.8	243.8	46.5	8	17.5	24.7	10.7	347.8	-2.8	50.6	24.7	345.5	-10.2	58.3	28.2
4	4a1	86.3	243.8	46.5	6	14.8	19.1	10.4	351.4	4.4	42.9	19.1	334.5	11.0	41.5	16.2
5	5a1	116.3	243.8	46.5	4	16.6	20.8	14.3	358.0	4.4	42.3	20.8	19.9	29.1	23.7	30.4
5	5c1	116.3	243.8	46.5	5	8.4	12.0	6.5	329.5	-19.2	71.3	12	320.2	1.3	56.8	33.1
5	5d1	116.3	243.8	46.5	5	12.6	9.6	9.7	343.4	-1.8	50.5	9.6	335.9	-12.5	62.9	31.3
5	5b1	116.3	243.8	46.5	4	1.8	2.3	1.6	352.4	22.0	25.4	2.3	0.9	43.7	3.1	29.9
6	6a1b	138	250.3	53.8	7	13.5	24.8	8.8	356.9	8.2	38.6	24.8	289.4	1.3	75.5	61.9
7	7a1	157.5	250.3	53.8	5	5.6	10.8	4.3	351.8	10.8	36.5	10.8	281.9	-3.4	84.0	69.3
8	8a1	183	247.0	48.0	7	13.6	20.2	8.9	356.9	4.1	42.6	20.2	23.8	7.2	44.7	34.3
9	9a2	207.8	247.0	48.0	5	10.6	30.7	8.2	357.0	-4.3	51.1	30.7	15.9	16.6	33.0	30.7
10	10a1	224.3	247.0	48.0	6	9.7	8.6	6.8	333.2	10.3	42.7	8.6	299.7	-1.8	71.2	48.1
10	10b1	224.3	247.0	48.0	5	9.8	14.4	7.6	344.1	1.6	47.0	14.4	325.1	-5.1	60.1	30.5
10	10d1	224.3	247.0	48.0	6	7.2	20.7	5.1	343.3	1.1	47.7	20.7	290.7	-7.6	81.5	58.8
11	11a1	243.8	247.0	48.0	10	29.5	22.7	16.1	351.8	-15.2	62.3	22.7	268.0	-30.4	112.6	89.2
12	12a1	267.8	244.0	48.3	8	9.6	15.4	5.9	343.0	1.3	47.6	15.4	346.0	-36.4	83.9	59.0
13	13a1	293.3	244.0	48.3	13	18.8	34.8	9.0	5.2	18.5	28.6	34.8	281.5	12.7	72.6	65.2
14	14a1	327.8	250.0	45.3	7	10.4	17.1	6.8	348.6	3.6	44.2	17.1	350.9	9.3	38.1	7.3
15	15b1	350.3	250.0	45.3	8	12.5	11.2	7.6	20.6	37.7	17.9	11.2	24.8	66.9	24.1	56.1
15	15c1	350.3	250.0	45.3	6	11.7	17.2	8.3	358.1	-2.0	48.7	17.2	19.7	-6.1	55.7	38.1
15	15d2b	350.3	250.0	45.3	8	6.7	6.4	4.1	341.3	18.6	31.9	6.4	312.9	38.1	34.9	38.0
16	16a1	374.3	250.0	45.3	9	13.7	26.4	7.9	343.2	36.0	16.2	26.4	280.6	13.8	72.4	50.3
17	17a1	387.8	250.0	45.3	9	9.3	10.3	5.4	340.6	7.0	42.9	10.3	297.2	7.4	65.8	50.4
18	18a1	406.5	250.0	43.7	10	11.3	20.2	6.2	14.3	7.8	40.9	20.2	45.0	28.2	39.9	53.9
19	19a1b	426	250.0	43.7	11	9.6	11.8	5.0	352.1	12.8	34.5	11.8	207.8	9.0	118.8	132.0
20	20a1	447	250.0	43.7	10	3.6	17.7	2.0	349.2	13.5	34.3	17.7	319.5	48.8	26.7	35.2
20	20b1	447	250.0	43.7	12	11.2	23.8	5.6	259.5	1.1	96.0	23.8	297.1	7.1	66.1	47.4
20	20d1	447	250.0	43.7	9	8.1	19.8	4.7	353.4	23.9	23.3	19.8	308.1	-37.1	95.6	66.4
20	20c2	447	250.0	43.7	7	6.8	86.5	4.4	251.4	7.1	96.9	86.5	266.0	-3.7	95.1	80.3
21	21a1	469.5	250.0	43.7	12	11.2	21.7	5.6	9.0	5.3	42.2	21.7	24.1	14.6	38.1	38.3
22	22a1	489	250.0	43.7	9	11.2	19.5	6.5	11.3	-3.4	51.1	19.5	9.4	-4.4	51.8	16.7
23	23a1	507	246.7	45.3	9	10.8	6.2	6.2	345.5	19.2	29.8	6.2	4.4	14.2	32.8	14.0
24	24a1	523.5	246.7	45.3	9	8.5	8.4	4.9	351.0	14.4	33.1	8.4	334.7	17.0	36.1	15.4
25	25a1	542.3	247.0	50.4	9	8.4	13.6	4.8	155.5	64.1	67.6	13.6	105.5	41.9	69.8	100.7
25	25b1	542.3	247.0	50.4	6	10.0	47.2	7.1	2.5	-2.4	49.2	47.2	345.3	-57.1	104.5	69.1
25	25d1	543.8	247.0	50.4	8	11.2	11.4	6.8	29.3	40.6	22.3	11.4	36.9	43.2	26.4	51.6

25	25c1	543.8	247.0	50.4	5	7.1	55.3	5.5	59.6	72.4	37.2	55.3	136.7	16.8	105.7	136.9
26	26a1	565.5	245.5	45.2	9	9.8	7.4	5.6	352.3	14.0	33.2	7.4	347.6	42.1	9.6	30.2
27	27a1	582.8	250.0	43.0	9	10.1	7.1	5.8	344.1	19.0	30.5	7.1	278.6	19.7	69.6	73.0
28	28a1	602.3	250.0	43.0	9	7.5	16.4	4.3	8.8	3.9	43.6	16.4	54.6	35.9	41.9	61.4
29	29a1	620.3	253.7	42.3	9	3.5	5.7	2.0	324.8	-0.8	56.4	5.7	188.5	-31.2	163.0	155.8
30	30a1	651	253.7	42.3	8	13.6	2.6	8.3	350.9	4.6	42.7	2.6	0.4	-30.3	77.1	40.9
30	30b1	649.5	253.7	42.3	7	7.7	7.5	5.0	349.3	0.7	46.8	7.5	29.4	9.4	45.1	40.2
30	30c1	649.5	253.7	42.3	5	3.1	10.8	2.4	356.0	7.6	39.2	10.8	162.8	-32.3	160.8	156.0
30	30e1	649.5	253.7	42.3	9	8.9	12.8	5.1	256.4	-2.2	100.6	12.8	252.6	3.1	99.1	95.4
30	30f1	649.5	253.7	42.3	9	10.3	5.9	5.9	347.7	9.1	38.9	5.9	354.1	9.2	37.8	5.5
31	31a1	666.8	237.5	43.5	8	11.6	10.5	7.1	11.2	-19.3	66.9	10.5	37.1	-45.4	97.8	59.0
32	32a1	693	237.5	43.5	9	6.6	6.6	3.8	350.7	-1.1	48.4	6.6	356.9	-7.9	54.7	20.0
33	33a1	717	237.5	43.5	8	7.6	13.9	4.6	7.1	20.8	26.7	13.9	69.6	6.8	71.5	76.4
34	34a1	736.5	237.5	43.5	10	9.4	3.7	5.1	349.2	10.3	37.4	3.7	339.4	-15.9	65.2	29.7
35	35b1	755.3	241.2	43.2	8	15.1	5.3	9.2	265.8	71.7	47.4	5.3	172.4	58.2	75.0	111.2
35	35d1	755.3	241.2	43.2	8	5.6	7.7	3.4	8.2	3.6	43.8	7.7	139.6	-4.5	125.6	147.4
35	35a1b	755.3	241.2	43.2	8	8.7	2.1	5.3	326.0	-9.2	63.3	2.1	283.8	-55.4	120.2	86.9
35	35c1	755.3	241.2	43.2	9	15.7	6.7	9.0	312.5	-0.9	62.9	6.7	271.8	-38.1	115.3	89.0
36	36a2	774.8	241.2	43.2	5	5.1	7.9	3.9	14.7	24.4	25.3	7.9	41.5	28.5	37.3	49.5
37	37a	792.8	241.2	43.2	NaN	NaN	NaN	NaN	NaN	NaN	NaN	NaN	NaN	NaN	NaN	NaN
38	38a	811.5	241.2	43.2	NaN	NaN	NaN	NaN	NaN	NaN	NaN	NaN	NaN	NaN	NaN	NaN
39	39a1	838.5	241.0	48.0	8	19.4	4.9	11.9	358.5	14.0	32.7	4.9	349.0	6.8	40.9	6.6
40	40a1	863.3	241.0	48.0	6	7.4	22.0	5.2	8.5	28.8	19.2	22	321.7	36.4	29.8	46.2
40	40b1	863.3	241.0	48.0	7	15.9	18.4	10.4	324.8	23.3	36.3	18.4	303.3	49.3	36.9	64.7
40	40c1	863.3	241.0	48.0	5	8.9	7.5	6.9	46.9	6.3	57.3	7.5	75.5	7.1	75.3	84.0
40	40d1	863.3	241.0	48.0	9	12.8	4.9	7.4	325.2	8.1	48.4	4.9	2.9	49.0	3.2	50.5
40	40e1	863.3	241.0	48.0	9	10.9	34.3	6.3	9.9	24.2	24.0	34.3	355.8	-12.6	59.4	12.8
41	41a1	882.8	233.5	35.0	8	18.0	11.6	11.0	344.7	-9.9	58.2	11.6	321.3	-16.8	72.2	34.0
42	42a1	900.8	233.5	35.0	10	10.8	3.7	5.9	3.4	5.5	41.4	3.7	56.7	3.1	65.8	64.9
43	43a1	920.3	241.3	36.0	7	9.2	5.9	6.0	4.7	17.3	29.7	5.9	37.2	39.1	28.4	54.2
44	44a1	938.3	241.3	36.0	7	6.5	15.4	4.2	333.8	2.8	49.2	15.4	269.7	-23.4	106.7	84.2
45	45e1b	960.8	241.3	36.0	9	6.3	8.7	3.6	17.3	6.1	43.4	8.7	112.7	-16.6	117.8	120.8
45	45a1	960.8	241.3	36.0	8	13.9	5.4	8.5	16.9	13.1	36.6	5.4	94.9	8.6	87.4	102.5
45	45b1	960.8	241.3	36.0	6	13.3	13.6	9.4	344.7	41.6	11.8	13.6	5.1	76.4	29.8	72.9
45	45c1	960.8	241.3	36.0	7	8.0	6.8	5.2	301.0	13.1	59.1	6.8	204.7	-3.3	131.4	147.0
45	45d1	960.8	241.3	36.0	10	13.5	20.0	7.4	20.4	-27.1	76.2	20	248.4	15.9	92.2	101.7
46	46a2	977.3	241.0	35.7	9	12.0	5.0	6.9	327.8	14.0	42.1	5	242.1	25.1	88.7	104.6
47	47a1b	998.3	241.7	35.0	7	6.1	5.3	4.0	335.3	14.1	38.3	5.3	236.4	5.2	107.9	113.4
48	48a1	1014	241.7	35.0	7	6.8	9.4	4.4	346.6	7.8	40.4	9.4	297.7	-15.9	83.6	56.1
49	49a1	1035	230.0	56.5	13	9.8	61.9	4.7	40.4	-33.7	88.4	61.9	78.8	-27.4	102.9	90.6
50	50a2b	1054.5	231.3	40.7	9	23.2	16.4	13.4	34.5	-4.1	59.4	16.4	59.2	-12.3	79.5	65.1
50	50b1	1054.5	231.3	40.7	4	11.8	15.1	10.2	1.7	3.3	43.4	15.1	30.1	-11.9	64.7	37.3
50	50b2	1054.5	231.3	40.7	8	26.5	117.4	16.2	199.4	48.1	83.7	117.4	171.4	29.1	103.8	148.2
50	50c1	1054.5	231.3	40.7	6	13.3	10.7	9.4	325.2	40.8	25.2	10.7	258.5	46.1	64.3	93.0
50	50d1	1054.5	231.3	40.7	7	17.3	24.9	11.3	337.0	13.5	38.2	24.9	316.8	7.8	53.3	38.8
51	51a1	1075.5	235.0	34.3	6	11.6	12.1	8.2	359.1	18.7	28.0	12.1	9.1	24.8	23.2	26.0

52	52a1b	1095	247.0	36.7	9	9.9	10.9	5.7	337.8	33.0	21.5	10.9	299.8	46.8	39.9	64.8
53	53a1b	1114.5	247.0	36.7	10	15.7	32.6	8.6	353.4	-27.1	74.0	32.6	11.7	-26.8	74.3	33.5
54	54a1	1139.3	232.0	37.0	10	12.7	12.6	6.9	349.5	24.8	23.4	12.6	4.8	52.5	6.7	52.4
55	55a1	1158.8	232.0	37.0	9	6.2	7.1	3.6	72.8	71.4	41.2	7.1	68.9	25.1	58.2	78.7
55	55b1	1158.8	232.0	37.0	8	24.8	16.3	15.2	65.3	-1.6	74.9	16.3	94.7	-3.6	96.2	100.9
55	55d1	1158.8	232.0	37.0	8	9.1	13.2	5.6	284.1	70.2	42.0	13.2	312.8	18.7	47.2	46.2
55	55e2	1158.8	232.0	37.0	5	16.6	6.6	12.8	352.6	10.4	36.8	6.6	356.4	42.2	5.0	46.5
56	56a1	1178.3	234.7	35.3	6	10.1	6.2	7.1	348.2	13.7	34.3	6.2	324.6	32.4	30.1	41.7
57	57a1	1197.8	234.7	35.3	9	9.0	9.2	5.2	357.1	-7.6	54.3	9.2	342.8	-15.0	63.5	18.9
58	58a1b	1218	252.0	41.0	8	9.1	26.6	5.6	356.6	-22.8	69.5	26.6	296.0	-55.7	115.4	74.3
59	59a1	1237.5	215.5	33.8	8	12.8	18.0	7.8	347.0	12.4	35.9	18	268.5	27.6	70.9	85.6
60	60a1	1257	215.5	33.8	6	10.8	26.0	7.6	357.1	49.4	3.1	26	86.5	50.5	54.2	90.0
60	60b1	1257	215.5	33.8	9	11.3	8.4	6.5	286.5	21.2	63.2	8.4	342.5	31.8	19.8	32.1
60	60c1	1257	215.5	33.8	9	12.4	30.1	7.1	273.3	55.0	51.5	30.1	191.3	46.3	86.4	129.7
61	61a1c	1278.8	224.5	33.0	13	13.5	6.1	6.5	346.9	0.0	48.0	6.1	333.0	8.8	44.1	22.4
62	62a1	1296	228.0	34.7	12	12.1	13.8	6.0	2.3	-16.7	63.5	13.8	17.5	-28.7	77.2	37.7
63	63a1	1317	228.0	34.7	10	13.9	6.4	7.6	314.0	12.0	51.6	6.4	276.3	21.0	70.4	78.8
64	64a1	1336.5	180.0	34.7	8	14.5	6.7	8.9	15.1	2.0	46.7	6.7	47.2	-4.5	66.3	53.0
65	65c1	1357.5	228.0	33.7	9	13.3	24.9	7.7	73.6	-25.7	98.4	24.9	121.6	-54.8	143.6	110.5
65	65a1b	1357.5	228.0	33.7	8	7.5	10.8	4.6	347.7	15.4	32.9	10.8	259.6	46.5	63.4	93.2
65	65b1	1357.5	228.0	33.7	10	10.0	13.9	5.5	10.9	29.0	19.8	13.9	301.9	9.3	61.3	53.0
65	65d1	1357.5	228.0	33.7	6	8.8	26.6	6.2	354.4	-11.7	58.6	26.6	18.8	-46.9	95.1	51.6
66	66a1	1377.8	228.0	33.7	9	7.0	28.6	4.0	10.1	12.7	35.2	28.6	252.8	-19.2	115.2	100.9
67	67a1	1405.5	228.0	26.0	9	5.3	2.8	3.1	354.6	7.9	39.0	2.8	5.2	47.0	3.9	49.8
68	68a1	1435.5	228.0	26.0	9	7.4	5.4	4.3	24.9	34.3	22.8	5.4	102.5	42.4	67.9	105.7
69	69a1	1453.5	228.0	35.0	9	10.6	32.8	6.1	2.7	27.4	19.4	32.8	322.3	32.8	31.4	45.5
70	70b2	1470	214.5	35.0	7	15.7	14.3	10.3	2.8	6.1	40.7	14.3	356.0	18.8	28.0	20.9
70	70a1b	1470	214.5	35.0	9	21.9	15.2	12.6	33.6	11.1	45.8	15.2	54.4	23.2	49.5	64.4
70	70c1	1470	214.5	35.0	8	16.2	18.7	9.9	56.5	10.1	60.3	18.7	98.8	1.7	95.1	105.4
70	70d1	1470	214.5	35.0	13	12.0	6.6	5.8	8.0	2.1	45.2	6.6	18.1	14.2	36.0	29.3
71	71a2	1489.5	214.5	35.0	8	6.5	16.9	4.0	1.8	29.8	17.0	16.9	180.3	32.2	101.1	139.7
72	72a1	1513.5	235.5	25.0	9	10.9	31.0	6.3	7.3	22.0	25.5	31	277.6	47.6	52.9	82.0
73	73a2	1536.8	231.5	33.5	6	21.0	24.0	14.8	3.2	-3.6	50.4	24	2.1	-56.6	103.4	48.8
74	74a1	1559.3	235.5	32.5	10	11.0	39.7	6.0	339.9	15.7	35.0	39.7	64.6	-53.2	114.2	71.5
75	75a1	1583.3	235.5	32.5	5	9.9	6.7	7.7	343.3	16.5	33.0	6.7	345.4	26.6	23.0	27.3
75	75b1	1583.3	235.5	32.5	5	7.8	51.1	6.0	344.2	-11.4	59.7	51.1	5.0	-27.7	74.6	30.4
75	75c1	1583.3	235.5	32.5	7	13.8	18.9	9.0	353.8	27.2	20.0	18.9	265.8	2.0	91.1	86.6
75	75d1	1583.3	235.5	32.5	7	20.5	44.9	13.4	328.4	37.3	24.8	44.9	324.2	30.2	31.8	40.3
76	76a1	1604.3	235.5	32.5	6	24.7	20.3	17.4	337.6	11.6	39.7	20.3	338.0	15.0	36.4	20.5
77	77a1	1624.5	216.0	36.0	8	16.0	23.9	9.8	352.8	10.6	36.5	23.9	290.7	-56.5	118.1	75.0
78	78a1	1641.8	210.6	36.0	7	12.9	11.2	8.4	319.8	11.6	48.4	11.2	10.1	41.7	9.1	44.5
79	79a1	1663.2	210.6	36.0	11	14.9	18.1	7.8	349.5	6.2	41.4	18.1	19.9	-38.5	87.1	46.1

Polarity tendency (- = R, + = N)	Data Quality (per specimen)	Subjective interpretation of orthogonal plot	Polarity interpretation
-35.2	1	path upward; but directions north and up in strat	
-57.3	1	path upward and south; up in strat going away from N	
-15.8	1	path toward origin, but too shallow for total recent overprint	R
-30.1	3	path upward until 250; directions slightly shallow for post-folding N overprint	
-12.8	2	path upward, up in strat going away from N	R
-7.7	3	path toward origin, but too shallow for total recent overprint	?
1.4	2	path toward origin, but too shallow for total recent overprint	R
18.6	2	path aimed to bypass origin; may head south	
14.5	2	path toward origin, but too shallow for total recent overprint	N
-12.4	3	path aimed to bypass origin; may head south	
22.3	3	path aimed to bypass origin; may head south but last measurement near but west of pre-folding N	
-36.9	1	path aimed to bypass origin; heading south but all directions down	R
-47.5	1	path aimed to bypass origin; heading south	R
-2.1	3	path toward origin, but too shallow for total recent overprint	?
18.1	2	path aimed to bypass origin; may head south	N
-28.5	1	path aimed to bypass origin; heading south	
-13.1	1	path aimed to bypass origin; may head south	R
-33.8	1	path aimed to bypass origin; heading south	
-50.3	1	too noisy to call path but dominantly up, so may be r even though all to the north	R
-36.3	1	path aimed to bypass origin; may head south	R
-44.0	2	odd path but high T directions W	R
6.1	3	path toward origin, but too shallow for total recent overprint	?
-6.2	2	path sort of toward origin but higher T steeper, expected N in strat	
-7.0	3	odd path; no high T but not to origin and too shallow for overprint or N	R
-3.0	2	odd path toward origin to 250, then bypass, heading south	
-56.2	1	odd path toward origin to 250, then bypass, heading south	R
-22.9	2	path looks to be bypassing origin, but demag nearly complete	R
1.0	2	path aimed to bypass origin; heading south	R
-84.3	1	path sort of toward origin to 280 but higher T is south although erratic	R
7.6	1	path aimed to bypass origin; may head south but near expected N in strat at 540	
29.9	1	path sort of toward origin but higher T steeper, near expected N in strat	N
-72.3	3	path upward, high T up to SW in strat	
1.8	2	toward origin but shallow to west makes no sense	
4.1	3	path toward origin, but too shallow for total recent overprint or viable N	?
-0.7	3	path toward origin, but too shallow for total recent overprint or viable N	?
-3.0	3	path toward origin; expected in g, too shallow in s	?
-3.0	3	path toward origin; expected in g, too shallow in s	?
-2.2	2	path looks to be bypassing origin, heading south and up in strat	
-55.3	1	odd west and down direction removed but trend is south and almost up	R
-4.1	2	path toward origin; clockwise of expected in g, but too shallow in s	

-68.5	3	odd east and down direction removed but trend is south and up	
23.6	2	path toward origin; slightly clockwise of expected	R
-39.1	1	path looks to be bypassing origin, heading south but not up in strat	R
1.7	3	path toward origin to 280; possibly toward south after that ;possibly overprint before noise.	
-106.6	1	path past origin to 478, then back toward origin from S and Up direction, but end point closer to R n	R
-34.4	3	path toward origin before noise; expected in g, too shallow in s	
1.7	2	path to bypass origin before noise; expected but trending clockwise in g, too shallow in s	
-121.6	1	path past origin to 251, then back sort of toward it before onset of noise	R
1.5	3	path sort of toward origin; slightly too shallow for expected in geog but nonsensically shallow up to	
1.1	3	path kinked at 251-322, but mostly toward origin; near expected in g, too shallow in s	
-30.9	2	path upward from N; too shallow in g; up but still N in s	R
-6.3	2	path slightly upward from N; too shallow in g; up but still N and very shallow in s	R
-44.8	2	path up to SE not origin; looks to be heading to shallow up to the S in strat, steeper and closer to ex	R
-27.8	2	path might bypass origin but most to 420 are expected N in g, too shallow in s, with hint of circle aw	R
-27.6	2	path upward toward south; too shallow in g, up but still N in s	
-81.8	2	path might bypass origin but most to 420 are expected N in g, too shallow in s, with hint of circle aw	
-56.9	1	path up to SE past origin but looks like R expected in g, not s so could be post-folding remag?	R
-52.4	2	odd direction SW and down; demag going up to S but projected end point on GS too shallow in strat	
-12.0	1	S-shaped path away from expected N in g but not obviously toward S and Up in s.	R
NaN	NaN	-	-
NaN	NaN	-	-
-8.2	3	path toward origin before noise onset above 280; a bit shallow in g but way too shallow in s	?
-10.6	1	path past origin but not convincingly R, could be fake normal in strat as GS migration is shallow to st	
-0.6	2	path apparently past origin but like 40a1 could be migrating to normal in strat.	
-18.0	1	path up and to S but gets noisy above 251; still looks like shallow up to S might be destination.	R
45.2	2	path upward to S; but too shallow in s so possibly post-folding reverse overprint?	
-35.4	3	path might bypass origin but there is no clear GS going to south, so could be N post-folding overprin	
-14.0	3	nonsensical Z path, no part toward origin; might be noisy overprint -- too shallow in s for N so possil	?
-24.4	1	path not to origin, appears migrating to south but not up	R
1.3	2	path headed to bypass origin, possibly S; GS toward E but nowhere up	R
-57.5	1	path bypassed origin to S, up at 283 in strat but shallow at higher T	R
-74.4	1	path headed to bypass origin but stalled 279-419, then very noisy; GS toward S not not up	
-50.8	1	path headed up and south; GS ends up	
-18.0	1	path bypassed origin; GS very noisy after demag only overprint to 280	R
-72.3	1	path bypassed origin, GS south but not up in strat	
-16.0	1	path bypassed origin to S, but no up directions	
-46.6	1	path bypassed origin but stalled 220-325; GS to south but no up directions	R
-69.6	1	path bypassed origin but stalled 253-419; went up in g but not in strat; GS to south, just not up	R
-43.2	1	path bypassed origin with up in mid range; GS to south but shallow	R
-14.5	1	odd path to east and up from upward NRM; GS in strat to shallower directions.	R
-20.1	1	path aimed up and south; short GS segment all up in strat, heading S but still NE	
-21.3	3	path pretty much toward origin before jump in moment and early end of demag.	
-20.1	3	path from south, headed up. Odd direction suggests orientation error.	R
-39.1	1	path toward south and upward but still steeply down in strat before noise bloomed.	
-15.1	1	path southward might bypass origin; GS away from present field in geog, shallow and down in strat.	
4.8	2	path might bypass origin but no convincing GS. What was measured could all be overprint -- too sha	N

-18.4	2	path bypassed origin; GS headed S but last directions still down to northwest, so possibly original N	N
-0.3	3	path kinked ~421; no good GS; directions shallow down in g, shallow up in s	?
16.7	1	path bypassed origin but GS segment ended steeply down to N	N
-17.0	1	path aimed to bypass origin, kinked at 420 to go up from W; GS segment clearly aimed south and up	
-21.3	1	path kinked about 221, toward origin after that before onset of noise; however, direction odd being	R
-5.2	2	path looks to bypass origin but only gets to steeply down in strat	
31.8	2	path could be going to origin before noise onset but consensus may be N	
4.2	2	path looks to be going to bypass origin but can't say it isn't N	N
-9.2	2	path aimed to bypass origin but useful measurements all moderately down N in geog, nonsensically	R
-45.9	1	path aimed to miss origin heading up but SW; end GS segment steeply up but NW in strat so probab	R
-35.0	1	path bypassed origin; long GS segment got to very shallow W in strat so probably R	R
-51.1	1	path definitely not toward origin but up to SE; got to E and horizontal in strat	
43.4	2	path bypassed origin to S, but all directions down, maybe too steep for N in strat but still very far fr	R
-34.9	1	odd NRM moderately down to SW suggests orientation error; GS segment is toward S but ends mod	
3.9	3	path toward origin but very shallow in strat	?
-13.7	1	first part of path aimed to bypass origin, going up to SSE; GS segment up to N, heading S in strat	R
-18.8	1	ragged path with turn about 321; GS segment to shallow down to W in strat so a long way to go for	R
-19.6	1	path turn and stall 382-540, from removing downNNW to down and NE components. May end shall	R
-45.2	1	similar to 65a1b	
-30.5	1	path to 420 removes down NE component, erratic above that but possibly end of GS in strat is steep	R
-41.5	1	erratic path bypasses origin; GS segment ends down SW in strat, showing tendency toward R	
-36.5	1	screwy curved path to 383 then wild but heads upward; GS upper hemisphere toward	
-80.0	1	path stalls 321-479, sort of continues to SW and up in geog; GS segment might end SW end up in ge	R
35.1	1	path turns about 382-420, toward origin after that, last segment mid down and N in strat	N
-45.1	1	path bypasses origin going up to south but stalls with increasing noise after 479; GS segment progre	R
-12.0	2	path toward origin to onset of noise at 421; cluster of noisy directions to 600 is moderately down to	N
12.7	3	path aimed to bypass origin but noisy going nowhere 325-559 with clustered directions NNE and ste	
-3.7	2	path very noisy, might turn about 379; possible GS segment toward S but down to ENE so nonsense	N
-34.8	2	path may turn 280; with directions going from NE and shallow down to shallow up in geog or E and :	
9.2	2	path static 322-540, maybe with slight bend there; short GS segment trends SE but directions all mo	
-84.1	1	path to south but noisy above 382; definitely south but down in strat so better fit for post-folding o	R
-27.4	1	path aimed W and upward in geog, Very noisy at high T but directions mostly down	R
-53.0	1	path turns from removal of W and down to N and down components at about 281; directions get sh	R
-79.2	1	path from removal of W and down component goes shallow up to NE in geog, steeper up to NE in st	R
10.0	3	path kink about 220 from removal of a NW and down to a NNE and shallower component; higher T i	
-14.9	3	path from removal of W and down component, End of life at 258.	?
-71.1	3	path noisy to 379, impossible beyond that.	?
-7.0	2	path in geog from removal of steeply down component, very noisy but possibly up S directions in sti	
3.3	3	path might be toward origin after kink cluster 181-281; most directions at higher T down	?
-81.6	1	path noisy but seems to be going up; No GS but all high T directions are up, some even south in Stra	R
39.3	2	path passed origin, then again. GS segment to 470 to SSW and shallow in geog, moderately down in	R
-45.7	1	path somewhat erratic but to south and up in geog; GS to SE and shallow up, passing through R in st	R

4.10.3 Detrital zircon fission track analyses

TABLE A3. Coupled detrital zircon fission-track & U-Pb analyses

Sample ID	Spot ID	Spot Index	Unique Grain #	FT age (Ma)	Symmetric ±1s (Ma)	95% CI (-)	95% CI (+)	U-Pb age (Ma)	±2s (Ma)	Ns	Area (um ²)	U/Cation	±1s	[U] (ppm)	[Th] (ppm)	[Sm] (ppm)	Zeta	±1s	Rho	±1s	
Middle Siwalik																					
5b	P1408_002_Zm_A_1_RAD_0	1	1	23.90	7.63	11.26	21.27	0.00	0.00	14	5.3120E+02	0.0012	0.0002	95	157	2	1105018	16414.47	52.617	1.4837	
5b	P1408_002_Zm_A_1_RAD_1	2	2	43.87	15.84	22.52	46.11	87.06	5.60	10	5.3087E+02	0.0005	0.0001	36	48	0	1105018	16414.47	52.617	1.4837	
5b	P1408_002_Zm_A_1_RAD_2	3	3	83.88	24.16	36.60	64.60	543.95	20.01	19	5.2917E+02	0.0005	0.0001	31	33	1	1105018	16414.47	52.617	1.4837	
5b	P1408_002_Zm_A_1_RAD_3	4	4	13.63	4.60	6.69	13.11	78.79	3.75	12	5.3075E+02	0.0018	0.0003	120	66	0	1105018	16414.47	52.617	1.4837	
5b	P1408_002_Zm_A_1_RAD_4	5	5	11.83	6.26	7.73	22.23	95.84	6.03	4	5.2949E+02	0.0007	0.0001	64	51	0	1105018	16414.47	52.617	1.4837	
5b	P1408_002_Zm_A_1_RAD_5	6	6	26.10	9.82	13.79	29.16	90.09	4.41	9	5.2929E+02	0.0007	0.0001	63	90	0	1105018	16414.47	52.617	1.4837	
5b	P1408_002_Zm_A_1_RAD_7	8	7	26.97	5.96	9.62	14.93	48.51	2.61	55	5.3248E+02	0.0042	0.0007	391	472	0	1105018	16414.47	52.617	1.4837	
5b	P1408_002_Zm_A_1_RAD_8	9	8	28.58	6.09	9.90	15.13	43.77	3.94	69	5.2980E+02	0.0050	0.0009	241	307	1	1105018	16414.47	52.617	1.4837	
5b	P1408_002_Zm_A_1_RAD_9	10	9	19.71	11.89	13.81	45.91	0.00	0.00	3	5.3055E+02	0.0003	0.0001	27	30	0	1105018	16414.47	52.617	1.4837	
5b	P1408_002_Zm_A_1_RAD_10	11	10	567.99	120.15	190.34	280.16	1064.94	47.51	70	5.3040E+02	0.0002	0.0000	21	48	0	1105018	16414.47	52.617	1.4837	
5b	P1408_002_Zm_A_1_RAD_11	12	11	19.91	6.36	9.39	17.76	69.33	4.15	14	5.3047E+02	0.0015	0.0003	115	104	0	1105018	16414.47	52.617	1.4837	
5b	P1408_002_Zm_A_1_RAD_12	13	12	21.15	6.44	9.64	17.69	946.69	25.61	16	5.2977E+02	0.0016	0.0003	135	140	0	1105018	16414.47	52.617	1.4837	
5b	P1408_002_Zm_A_1_RAD_13	14	13	65.70	20.04	29.93	54.73	82.05	7.18	16	5.3057E+02	0.0005	0.0001	41	39	0	1105018	16414.47	52.617	1.4837	
5b	P1408_002_Zm_A_1_RAD_14	15	14	27.37	10.29	14.45	30.55	90.15	6.87	9	5.3022E+02	0.0007	0.0001	52	48	0	1105018	16414.47	52.617	1.4837	
5b	P1408_002_Zm_A_1_RAD_15	16	15	28.69	10.36	14.74	30.26	179.75	8.84	10	5.3021E+02	0.0007	0.0001	54	35	0	1105018	16414.47	52.617	1.4837	
5b	P1408_002_Zm_A_1_RAD_16	17	16	15.55	6.13	8.47	18.60	89.81	5.67	8	5.3057E+02	0.0011	0.0002	95	88	0	1105018	16414.47	52.617	1.4837	
5b	P1408_002_Zm_A_1_RAD_17	18	17	14.11	8.51	9.88	32.90	55.70	4.89	3	5.3164E+02	0.0004	0.0001	30	37	0	1105018	16414.47	52.617	1.4837	
5b	P1408_002_Zm_A_1_RAD_18	19	18	18.92	4.91	7.65	12.83	101.66	3.71	27	5.3257E+02	0.0030	0.0005	191	160	0	1105018	16414.47	52.617	1.4837	
5b	P1408_002_Zm_A_1_RAD_19	20	19	27.61	10.39	14.59	30.87	91.86	6.66	9	5.3106E+02	0.0007	0.0001	35	70	0	1105018	16414.47	52.617	1.4837	
5b	P1408_002_Zm_A_1_RAD_20	21	20	20.00	6.10	9.12	16.74	491.25	14.15	16	5.3280E+02	0.0017	0.0003	64	55	0	1105018	16414.47	52.617	1.4837	
5b	P1408_002_Zm_A_1_RAD_21	22	21	10.30	6.21	7.22	24.05	86.85	8.64	3	5.3215E+02	0.0006	0.0001	34	64	1	1105018	16414.47	52.617	1.4837	
5b	P1408_002_Zm_A_1_RAD_22	23	22	9.18	4.86	6.00	17.26	91.85	6.18	4	5.3171E+02	0.0009	0.0002	70	145	2	1105018	16414.47	52.617	1.4837	
5b	P1408_002_Zm_A_1_RAD_23	24	23	21.11	5.66	8.76	14.95	85.81	2.82	24	5.3209E+02	0.0024	0.0004	190	10	0	1105018	16414.47	52.617	1.4837	
5b	P1408_002_Zm_A_1_RAD_24	25	24	22.60	6.90	10.32	18.96	92.28	5.29	16	5.2975E+02	0.0015	0.0003	122	137	0	1105018	16414.47	52.617	1.4837	
5b	P1408_002_Zm_A_1_RAD_25	26	25	6.67	6.77	5.80	43.99	100.54	8.77	1	5.3050E+02	0.0003	0.0001	26	26	0	1105018	16414.47	52.617	1.4837	
5b	P1408_002_Zm_A_1_RAD_26	27	26	30.20	7.84	12.22	20.48	89.55	5.73	27	5.3049E+02	0.0019	0.0003	123	135	1	1105018	16414.47	52.617	1.4837	
5b	P1408_002_Zm_A_1_RAD_28	29	27	35.83	10.16	15.48	27.20	91.06	4.61	20	5.3243E+02	0.0012	0.0002	108	188	1	1105018	16414.47	52.617	1.4837	
5b	P1408_002_Zm_A_1_RAD_29	30	28	18.43	4.42	7.02	11.33	1161.84	29.19	37	5.3050E+02	0.0042	0.0007	247	347	2	1105018	16414.47	52.617	1.4837	
5b	P1408_002_Zm_A_1_RAD_30	31	29	20.80	7.83	10.99	23.26	1148.34	27.84	9	5.3040E+02	0.0009	0.0002	56	93	0	1105018	16414.47	52.617	1.4837	
5b	P1408_002_Zm_A_1_RAD_31	32	30	18.05	10.89	12.64	42.07	98.96	7.86	3	5.3254E+02	0.0003	0.0001	33	48	0	1105018	16414.47	52.617	1.4837	
5b	P1408_002_Zm_A_1_RAD_32	33	31	57.35	15.42	23.80	40.54	55.21	3.86	24	5.3036E+02	0.0009	0.0002	46	64	0	1105018	16414.47	52.617	1.4837	
5b	P1408_002_Zm_A_1_RAD_33	34	32	5.52	5.60	4.79	36.39	95.08	7.28	1	5.3098E+02	0.0004	0.0001	38	56	0	1105018	16414.47	52.617	1.4837	
5b	P1408_002_Zm_A_1_RAD_34	35	33	19.25	5.17	7.99	13.65	48.08	2.85	24	5.3067E+02	0.0026	0.0005	124	78	0	1105018	16414.47	52.617	1.4837	
5b	P1408_002_Zm_A_1_RAD_35	36	34	12.44	3.81	5.69	10.49	49.81	6.73	16	5.3178E+02	0.0027	0.0005	265	92	0	1105018	16414.47	52.617	1.4837	
5b	P1408_002_Zm_A_1_RAD_36	37	35	44.08	21.17	27.17	70.46	133.11	5.90	5	5.3045E+02	0.0002	0.0000	27	21	0	1105018	16414.47	52.617	1.4837	
5b	P1408_002_Zm_A_1_RAD_37	38	36	54.65	11.89	19.23	29.61	498.09	14.62	60	5.3063E+02	0.0023	0.0004	112	121	0	1105018	16414.47	52.617	1.4837	
5b	P1408_002_Zm_A_1_RAD_38	39	37	12.84	2.94	4.72	7.45	805.33	25.03	46	5.3048E+02	0.0075	0.0013	345	122	0	1105018	16414.47	52.617	1.4837	
5b	P1408_002_Zm_A_1_RAD_39	40	38	22.71	5.91	9.21	15.46	770.33	24.67	27	5.2975E+02	0.0025	0.0004	144	6	0	1105018	16414.47	52.617	1.4837	
5b	P1408_002_Zm_A_1_RAD_40	41	39	3.52	3.57	3.05	23.21	94.03	6.83	1	5.2969E+02	0.0006	0.0001	51	106	1	1105018	16414.47	52.617	1.4837	
5b	P1408_002_Zm_A_1_RAD_41	42	40	20.43	10.82	13.34	38.31	93.32	6.56	4	5.3071E+02	0.0004	0.0001	39	51	0	1105018	16414.47	52.617	1.4837	
5b	P1408_002_Zm_A_1_RAD_42	43	41	19.30	6.72	9.68	19.38	87.72	4.02	11	5.3045E+02	0.0012	0.0002	89	97	0	1105018	16414.47	52.617	1.4837	
5b	P1408_002_Zm_A_1_RAD_43	44	42	21.99	8.68	11.99	26.32	735.61	33.95	8	5.3052E+02	0.0008	0.0001	33	76	0	1105018	16414.47	52.617	1.4837	
5b	P1408_002_Zm_A_1_RAD_44	45	43	21.27	5.25	8.28	13.53	1067.34	28.62	33	5.3165E+02	0.0032	0.0006	175	30	0	1105018	16414.47	52.617	1.4837	
5b	P1408_002_Zm_A_1_RAD_45	46	44	3.30	3.35	2.87	21.79	1542.60	40.43	1	5.3040E+02	0.0006	0.0001	44	73	1	1105018	16414.47	52.617	1.4837	
5b	P1408_002_Zm_A_1_RAD_46	47	45	19.74	5.51	8.44	14.74	1170.32	25.51	21	5.3027E+02	0.0022	0.0004	229	355	1	1105018	16414.47	52.617	1.4837	
5b	P1408_002_Zm_A_1_RAD_47	48	46	25.19	6.04	9.58	15.45	1149.88	31.45	37	5.3042E+02	0.0031	0.0005	281	16	0	1105018	16414.47	52.617	1.4837	
5b	P1408_002_Zm_A_1_RAD_48	49	47	20.80	6.82	9.99	19.20	2052.33	38.02	13	5.3094E+02	0.0013	0.0002	128	39	1	1105018	16414.47	52.617	1.4837	
5b	P1408_002_Zm_A_1_RAD_49	50	48	24.00	11.52	14.80	38.49	88.04	7.22	5	5.3044E+02	0.0004	0.0001	38	53	1	1105018	16414.47	52.617	1.4837	
5b	P1408_002_Zm_A_1_RAD_50	51	49	46.97	22.59	28.98	75.21	84.54	12.47	5	5.3057E+02	0.0002	0.0000	22	21	1	1105018	16414.47	52.617	1.4837	
5b	P1408_002_Zm_A_1_RAD_51	52	50	15.63	4.58	6.92	12.42	2792.86	31.45	18	5.3048E+02	0.0024	0.0004	211	499	3	1105018	16414.47	52.617	1.4837	
5b	P1408_002_Zm_A_1_RAD																				

5b	P1408_002_Zm_A_1_RAD_65	66	63	46.88	12.34	19.15	32.30	54.88	5.66	26	5.3091E+02	0.0012	0.0002	72	116	1	1105018	16414.47	52.617	1.4837
5b	P1408_002_Zm_A_1_RAD_66	67	64	33.44	9.80	14.81	26.54	53.09	3.52	18	5.2886E+02	0.0011	0.0002	78	178	1	1105018	16414.47	52.617	1.4837
5b	P1408_002_Zm_A_1_RAD_67	68	65	16.83	5.02	7.56	13.70	1148.38	25.74	17	5.2952E+02	0.0021	0.0004	145	268	2	1105018	16414.47	52.617	1.4837
5b	P1408_002_Zm_A_1_RAD_68	69	66	24.07	6.03	9.47	15.60	51.68	2.14	31	5.3039E+02	0.0027	0.0005	193	248	1	1105018	16414.47	52.617	1.4837
5b	P1408_002_Zm_A_1_RAD_69	70	67	44.31	15.44	22.20	44.35	101.88	6.42	11	5.3051E+02	0.0005	0.0001	39	64	0	1105018	16414.47	52.617	1.4837
25c	P1408_004_Zm_A_1_RAD_0	1	1	26.11	6.85	10.65	17.96	505.47	15.71	26	5.3063E+02	0.0021	0.0004	239	297	1	1105018	16414.47	92.467	2.5467
25c	P1408_004_Zm_A_1_RAD_1	2	2	12.60	4.13	6.06	11.67	51.80	3.14	13	5.3183E+02	0.0021	0.0004	170	214	0	1105018	16414.47	92.467	2.5467
25c	P1408_004_Zm_A_1_RAD_2	3	3	43.53	15.16	21.80	43.53	56.29	3.37	11	5.3083E+02	0.0005	0.0001	57	129	1	1105018	16414.47	92.467	2.5467
25c	P1408_004_Zm_A_1_RAD_3	4	4	17.20	4.31	6.77	11.16	833.10	26.64	31	5.2908E+02	0.0038	0.0007	403	431	2	1105018	16414.47	92.467	2.5467
25c	P1408_004_Zm_A_1_RAD_5	6	5	46.89	14.29	21.36	39.11	1055.12	26.56	16	5.2964E+02	0.0007	0.0001	75	15	0	1105018	16414.47	92.467	2.5467
25c	P1408_004_Zm_A_1_RAD_6	7	6	53.17	14.10	21.83	36.93	54.18	6.61	25	5.3142E+02	0.0010	0.0002	111	178	1	1105018	16414.47	92.467	2.5467
25c	P1408_004_Zm_A_1_RAD_7	8	7	26.98	6.87	10.75	17.84	494.16	12.99	29	5.3203E+02	0.0022	0.0004	285	218	0	1105018	16414.47	92.467	2.5467
25c	P1408_004_Zm_A_1_RAD_8	9	8	12.94	2.93	4.71	7.40	38.73	2.03	48	5.3042E+02	0.0077	0.0013	683	224	0	1105018	16414.47	92.467	2.5467
25c	P1408_004_Zm_A_1_RAD_9	10	9	14.15	4.23	6.36	11.54	500.47	17.74	17	5.3059E+02	0.0025	0.0004	339	240	1	1105018	16414.47	92.467	2.5467
25c	P1408_004_Zm_A_1_RAD_10	11	10	12.98	4.88	6.86	14.53	96.36	4.21	9	5.2985E+02	0.0014	0.0003	195	404	1	1105018	16414.47	92.467	2.5467
25c	P1408_004_Zm_A_1_RAD_12	13	11	27.53	6.04	9.77	15.12	515.21	20.93	56	5.3047E+02	0.0042	0.0007	606	469	1	1105018	16414.47	92.467	2.5467
25c	P1408_004_Zm_A_1_RAD_13	14	12	15.58	6.92	9.16	22.20	519.67	12.97	6	5.3051E+02	0.0008	0.0001	118	103	0	1105018	16414.47	92.467	2.5467
25c	P1408_004_Zm_A_1_RAD_14	15	13	15.64	4.71	7.07	12.89	511.62	18.95	17	5.3062E+02	0.0023	0.0004	351	326	0	1105018	16414.47	92.467	2.5467
25c	P1408_004_Zm_A_1_RAD_16	17	14	7.83	2.34	3.52	6.39	418.27	10.97	17	5.3044E+02	0.0045	0.0008	670	74	0	1105018	16414.47	92.467	2.5467
25c	P1408_004_Zm_A_1_RAD_17	18	15	17.57	4.06	6.50	10.31	37.51	1.36	43	5.3033E+02	0.0051	0.0009	772	681	1	1105018	16414.47	92.467	2.5467
25c	P1408_004_Zm_A_1_RAD_18	19	16	20.29	4.93	7.80	12.66	528.06	21.27	35	5.3223E+02	0.0036	0.0006	512	319	0	1105018	16414.47	92.467	2.5467
25c	P1408_004_Zm_A_1_RAD_19	20	17	15.44	3.39	5.48	8.49	42.80	2.33	56	5.3061E+02	0.0075	0.0013	954	59	0	1105018	16414.47	92.467	2.5467
25c	P1408_004_Zm_A_1_RAD_20	21	18	10.00	2.53	3.97	6.57	485.04	20.49	30	5.3036E+02	0.0062	0.0011	1029	729	1	1105018	16414.47	92.467	2.5467
25c	P1408_004_Zm_A_1_RAD_21	22	19	16.07	3.59	5.79	9.05	41.24	3.03	51	5.2926E+02	0.0066	0.0012	956	626	0	1105018	16414.47	92.467	2.5467
25c	P1408_004_Zm_A_1_RAD_22	23	20	15.29	4.88	7.21	13.63	41.25	2.21	14	5.3128E+02	0.0019	0.0003	315	264	0	1105018	16414.47	92.467	2.5467
25c	P1408_004_Zm_A_1_RAD_23	24	21	15.73	8.33	10.27	29.52	97.80	6.34	4	5.3067E+02	0.0005	0.0001	77	72	1	1105018	16414.47	92.467	2.5467
25c	P1408_004_Zm_A_1_RAD_24	25	22	5.11	2.27	3.01	7.31	40.75	3.15	6	5.3036E+02	0.0024	0.0004	372	271	0	1105018	16414.47	92.467	2.5467
25c	P1408_004_Zm_A_1_RAD_25	26	23	37.75	8.47	13.63	21.30	501.82	15.51	50	5.3063E+02	0.0028	0.0005	311	209	0	1105018	16414.47	92.467	2.5467
25c	P1408_004_Zm_A_1_RAD_26	27	24	27.51	9.32	13.52	26.55	833.01	24.38	12	5.2997E+02	0.0009	0.0002	106	100	0	1105018	16414.47	92.467	2.5467
25c	P1408_004_Zm_A_1_RAD_27	28	25	10.32	3.29	4.87	9.20	39.53	2.20	14	5.3063E+02	0.0028	0.0005	317	61	0	1105018	16414.47	92.467	2.5467
25c	P1408_004_Zm_A_1_RAD_28	29	26	12.42	4.68	6.57	13.92	492.24	16.70	9	5.3050E+02	0.0015	0.0003	149	66	0	1105018	16414.47	92.467	2.5467
25c	P1408_004_Zm_A_1_RAD_29	30	27	25.82	6.01	9.60	15.26	339.89	10.83	42	5.3051E+02	0.0034	0.0006	678	23	0	1105018	16414.47	92.467	2.5467
25c	P1408_004_Zm_A_1_RAD_30	31	28	3.91	1.36	1.96	3.94	547.49	22.43	11	5.3101E+02	0.0058	0.0010	339	32	0	1105018	16414.47	92.467	2.5467
25c	P1408_004_Zm_A_1_RAD_31	32	29	15.57	5.86	8.23	17.44	537.33	20.58	9	5.3067E+02	0.0012	0.0002	134	345	2	1105018	16414.47	92.467	2.5467
25c	P1408_004_Zm_A_1_RAD_34	35	30	16.87	7.49	9.92	24.04	80.69	4.18	6	5.3000E+02	0.0007	0.0001	81	101	0	1105018	16414.47	92.467	2.5467
25c	P1408_004_Zm_A_1_RAD_35	36	31	15.12	3.60	5.73	9.22	511.22	19.24	38	5.2896E+02	0.0052	0.0009	573	77	1	1105018	16414.47	92.467	2.5467
25c	P1408_004_Zm_A_1_RAD_36	37	32	12.35	4.17	6.06	11.87	814.38	22.74	12	5.3033E+02	0.0020	0.0004	222	272	1	1105018	16414.47	92.467	2.5467
25c	P1408_004_Zm_A_1_RAD_37	38	33	23.71	5.59	8.90	14.24	694.36	31.87	40	5.3043E+02	0.0035	0.0006	344	174	0	1105018	16414.47	92.467	2.5467
25c	P1408_004_Zm_A_1_RAD_38	39	34	9.33	2.38	3.73	6.20	38.37	2.89	29	5.3133E+02	0.0065	0.0011	563	265	0	1105018	16414.47	92.467	2.5467
25c	P1408_004_Zm_A_1_RAD_39	40	35	20.57	5.00	7.91	12.84	1081.26	31.42	35	5.3057E+02	0.0035	0.0006	346	315	1	1105018	16414.47	92.467	2.5467
25c	P1408_004_Zm_A_1_RAD_40	41	36	12.91	3.94	5.90	10.85	516.92	37.68	16	5.3066E+02	0.0026	0.0005	228	93	0	1105018	16414.47	92.467	2.5467
25c	P1408_004_Zm_A_1_RAD_41	42	37	30.25	8.23	12.67	21.77	515.06	23.51	23	5.2996E+02	0.0016	0.0003	169	241	0	1105018	16414.47	92.467	2.5467
25c	P1408_004_Zm_A_1_RAD_42	43	38	16.56	3.67	5.93	9.24	0.00	0.00	54	5.3036E+02	0.0068	0.0012	768	776	1	1105018	16414.47	92.467	2.5467
25c	P1408_004_Zm_A_1_RAD_43	44	39	19.52	10.35	12.75	36.67	1158.86	50.34	4	5.3028E+02	0.0004	0.0001	37	75	0	1105018	16414.47	92.467	2.5467
25c	P1408_004_Zm_A_1_RAD_44	45	40	15.40	3.50	5.62	8.85	477.84	16.31	47	5.3044E+02	0.0063	0.0011	647	1072	2	1105018	16414.47	92.467	2.5467
25c	P1408_004_Zm_A_1_RAD_45	46	41	15.16	4.30	6.56	11.55	483.72	17.44	20	5.3056E+02	0.0027	0.0005	290	410	1	1105018	16414.47	92.467	2.5467
25c	P1408_004_Zm_A_1_RAD_46	47	42	37.92	9.76	15.23	25.41	1045.19	31.07	28	5.3069E+02	0.0015	0.0003	148	180	1	1105018	16414.47	92.467	2.5467
25c	P1408_004_Zm_A_1_RAD_47	48	43	10.09	4.85	6.23	16.24	1051.97	39.81	5	4.1485E+02	0.0013	0.0002	92	312	1	1105018	16414.47	92.467	2.5467
25c	P1408_004_Zm_A_1_RAD_48	49	44	73.45	21.55	32.51	58.05	1170.27	39.45	18	5.3066E+02	0.0005	0.0001	47	142	1	1105018	16414.47	92.467	2.5467
25c	P1408_004_Zm_A_1_RAD_49	50	45	19.33	6.17	9.11	17.23	49.52	2.46	14	5.3078E+02	0.0015	0.0003	155	194	0	1105018	16414.47	92.467	2.5467
25c	P1408_004_Zm_A_1_RAD_50	51	46	31.57	11.41	16.23	33.30	93.19	6.26	10	5.2895E+02	0.0007	0.0001	65	80	0	1105018	16414.47	92.467	2.5467
25c	P1408_004_Zm_A_1_RAD_51	52	47	19.84	5.33	8.24	14.09	796.28	45.32	24	5.3111E+02	0.0025	0.0004	196	388	0	1105018	16414.47	92.467	2.5467
25c	P1408_004_Zm_A_1_RAD_52	53	48	66.91	14.46	23.41	35.90	510.60	26.24	63	5.3040E+02	0.0020	0.0003	107	135	0	1105018	16414.47	92.467	2.5467
25c	P1408_004_Zm_A_1_RAD_53	54	49	7.49	5.45	5.75	24.60	518.69	22.16	2	5.3176E+02	0.0006	0.0001	51	146	0	1105018	16414.47	92.467	2.5467
25c	P1408_004_Zm_A_1_RAD_54	55	50	13.63	8.22	9.55	31.81	49.77	3.84	3	5.3096E+02	0.0005	0.0001	40	82	0	1105018	16414.47	92.467	2.5467
25c	P1408_004_Zm_A_1_RAD_55	56	51	15.79	3.87	6.11	9.97	40.06	2.57	34	5.3064E+02	0.0045	0.0008	422	323	0	1105018	16414.47	92.467	2.5467
25c	P1408_004_Zm_A_1_RAD_56	57	52	19.49	7.69															

25c	P1408_004_Zm_A_1_RAD_64	65	60	102.67	31.39	46.76	85.31	1435.45	44.25	16	3.8249E+02	0.0004	0.0001	37	100	1	1105018	16414.47	92.467	2.5467
25c	P1408_004_Zm_A_1_RAD_65	66	61	28.44	9.93	14.27	28.59	508.90	26.78	11	5.3046E+02	0.0008	0.0001	77	167	1	1105018	16414.47	92.467	2.5467
25c	P1408_004_Zm_A_1_RAD_66	67	62	9.99	3.19	4.71	8.91	41.23	2.59	14	5.2999E+02	0.0029	0.0005	244	305	0	1105018	16414.47	92.467	2.5467
25c	P1408_004_Zm_A_1_RAD_67	68	63	15.28	7.34	9.43	24.58	1045.69	41.60	5	5.3044E+02	0.0007	0.0001	58	144	0	1105018	16414.47	92.467	2.5467
25c	P1408_004_Zm_A_1_RAD_68	69	64	21.53	5.93	9.12	15.79	525.41	18.49	22	5.3041E+02	0.0021	0.0004	197	196	0	1105018	16414.47	92.467	2.5467
25c	P1408_004_Zm_A_1_RAD_69	70	65	11.48	3.89	5.65	11.10	504.58	22.51	12	4.0133E+02	0.0029	0.0005	295	335	0	1105018	16414.47	92.467	2.5467
50b	P1408_003_Zm_A_1_RAD_0	1	1	11.32	11.49	9.83	74.41	58.16	6.60	1	5.2872E+02	0.0002	0.0000	15	14	0	1105018	16414.47	77.147	2.4463
50b	P1408_003_Zm_A_1_RAD_1	2	2	520.18	104.00	166.85	241.12	1447.11	42.81	105	5.3033E+02	0.0004	0.0001	35	39	0	1105018	16414.47	77.147	2.4463
50b	P1408_003_Zm_A_1_RAD_2	3	3	46.40	15.65	22.72	44.37	59.99	5.05	12	5.3013E+02	0.0005	0.0001	44	46	1	1105018	16414.47	77.147	2.4463
50b	P1408_003_Zm_A_1_RAD_3	4	4	47.78	13.15	20.19	34.86	53.42	2.28	22	5.3026E+02	0.0010	0.0002	74	116	0	1105018	16414.47	77.147	2.4463
50b	P1408_003_Zm_A_1_RAD_4	5	5	18.21	5.09	7.79	13.59	1143.90	28.60	21	5.3056E+02	0.0024	0.0004	250	490	2	1105018	16414.47	77.147	2.4463
50b	P1408_003_Zm_A_1_RAD_5	6	6	25.29	9.51	13.36	28.25	944.48	23.41	9	5.3043E+02	0.0007	0.0001	73	149	1	1105018	16414.47	77.147	2.4463
50b	P1408_003_Zm_A_1_RAD_6	7	7	17.30	6.51	9.14	19.38	592.57	17.92	9	5.3051E+02	0.0011	0.0002	105	95	2	1105018	16414.47	77.147	2.4463
50b	P1408_003_Zm_A_1_RAD_7	8	8	8.73	2.44	3.73	6.52	504.36	11.38	21	5.2971E+02	0.0050	0.0009	455	299	0	1105018	16414.47	77.147	2.4463
50b	P1408_003_Zm_A_1_RAD_8	9	9	11.88	3.70	5.50	10.25	35.80	1.52	15	5.3092E+02	0.0026	0.0005	210	190	1	1105018	16414.47	77.147	2.4463
50b	P1408_003_Zm_A_1_RAD_9	10	10	27.61	8.03	23.98	179.83	912.01	55.24	1	5.2899E+02	0.0001	0.0000	9	22	2	1105018	16414.47	77.147	2.4463
50b	P1408_003_Zm_A_1_RAD_10	11	11	27.20	13.06	16.77	43.61	1106.89	35.86	5	5.3045E+02	0.0004	0.0001	43	151	1	1105018	16414.47	77.147	2.4463
50b	P1408_003_Zm_A_1_RAD_11	12	12	28.38	11.82	16.03	36.72	96.70	7.05	7	5.3158E+02	0.0005	0.0001	46	87	1	1105018	16414.47	77.147	2.4463
50b	P1408_003_Zm_A_1_RAD_12	13	13	24.81	25.19	21.55	161.88	1191.17	63.36	1	5.3138E+02	0.0001	0.0000	7	27	1	1105018	16414.47	77.147	2.4463
50b	P1408_003_Zm_A_1_RAD_13	14	14	10.65	3.25	4.86	8.94	814.24	25.56	16	5.3162E+02	0.0031	0.0005	247	106	0	1105018	16414.47	77.147	2.4463
50b	P1408_003_Zm_A_1_RAD_14	15	15	12.80	5.68	7.53	18.26	1156.76	35.85	6	5.3095E+02	0.0010	0.0002	121	168	0	1105018	16414.47	77.147	2.4463
50b	P1408_003_Zm_A_1_RAD_15	16	16	9.02	2.09	3.34	5.31	36.42	1.06	43	5.3063E+02	0.0099	0.0017	1122	11	0	1105018	16414.47	77.147	2.4463
50b	P1408_003_Zm_A_1_RAD_16	17	17	16.40	4.45	6.87	11.81	1257.33	25.03	23	5.2991E+02	0.0029	0.0005	226	95	0	1105018	16414.47	77.147	2.4463
50b	P1408_003_Zm_A_1_RAD_17	18	18	7.73	2.41	3.59	6.68	394.81	17.66	15	5.3227E+02	0.0040	0.0007	302	280	1	1105018	16414.47	77.147	2.4463
50b	P1408_003_Zm_A_1_RAD_18	19	19	15.71	7.54	9.69	25.24	537.19	17.29	5	5.3194E+02	0.0007	0.0001	58	347	2	1105018	16414.47	77.147	2.4463
50b	P1408_003_Zm_A_1_RAD_19	20	20	9.07	2.17	3.45	5.57	369.88	14.29	37	5.3069E+02	0.0085	0.0015	953	32	0	1105018	16414.47	77.147	2.4463
50b	P1408_003_Zm_A_1_RAD_20	21	21	14.00	4.46	6.60	12.47	47.74	2.56	14	3.7928E+02	0.0029	0.0005	327	356	1	1105018	16414.47	77.147	2.4463
50b	P1408_003_Zm_A_1_RAD_21	22	22	35.99	19.05	23.49	67.23	57.35	6.26	4	5.3069E+02	0.0002	0.0000	28	86	1	1105018	16414.47	77.147	2.4463
50b	P1408_003_Zm_A_1_RAD_22	23	23	0.00	0.00	0.00	16.88	0.00	0.00	0	5.3249E+02	0.0004	0.0001	29	37	0	1105018	16414.47	77.147	2.4463
50b	P1408_003_Zm_A_1_RAD_23	24	24	6.81	2.37	3.42	6.85	1080.14	22.17	11	5.3064E+02	0.0034	0.0006	308	491	1	1105018	16414.47	77.147	2.4463
50b	P1408_003_Zm_A_1_RAD_24	25	25	57.40	18.32	27.02	50.85	1764.33	35.73	14	5.3035E+02	0.0005	0.0001	64	112	0	1105018	16414.47	77.147	2.4463
50b	P1408_003_Zm_A_1_RAD_25	26	26	9.91	3.45	4.97	9.97	508.83	15.45	11	5.3037E+02	0.0023	0.0004	295	209	1	1105018	16414.47	77.147	2.4463
50b	P1408_003_Zm_A_1_RAD_26	27	27	25.60	6.25	9.88	16.08	66.90	3.92	34	5.3046E+02	0.0028	0.0005	211	102	0	1105018	16414.47	77.147	2.4463
50b	P1408_003_Zm_A_1_RAD_27	28	28	72.39	30.18	40.84	93.04	989.10	35.77	7	5.3060E+02	0.0002	0.0000	22	56	0	1105018	16414.47	77.147	2.4463
50b	P1408_003_Zm_A_1_RAD_28	29	29	6.28	1.56	2.46	4.04	508.01	12.40	32	5.3260E+02	0.0106	0.0018	1291	599	0	1105018	16414.47	77.147	2.4463
50b	P1408_003_Zm_A_1_RAD_29	30	30	12.94	9.42	9.92	42.41	76.99	6.49	2	5.3050E+02	0.0003	0.0001	39	27	0	1105018	16414.47	77.147	2.4463
50b	P1408_003_Zm_A_1_RAD_30	31	31	26.19	6.29	9.97	16.08	569.80	14.53	37	5.3005E+02	0.0029	0.0005	377	131	0	1105018	16414.47	77.147	2.4463
50b	P1408_003_Zm_A_1_RAD_31	32	32	9.47	2.73	4.15	7.37	800.06	17.51	19	5.2955E+02	0.0042	0.0007	543	570	1	1105018	16414.47	77.147	2.4463
50b	P1408_003_Zm_A_1_RAD_32	33	33	17.24	5.81	8.45	16.55	1119.91	23.39	12	5.3329E+02	0.0014	0.0002	201	342	1	1105018	16414.47	77.147	2.4463
50b	P1408_003_Zm_A_1_RAD_33	34	34	0.00	0.00	0.00	88.38	857.78	50.82	0	5.3074E+02	0.0001	0.0000	9	25	1	1105018	16414.47	77.147	2.4463
50b	P1408_003_Zm_A_1_RAD_34	35	35	6.42	2.53	3.50	7.70	1166.60	79.61	8	3.5713E+02	0.0039	0.0007	400	599	1	1105018	16414.47	77.147	2.4463
50b	P1408_003_Zm_A_1_RAD_35	36	36	24.46	7.46	11.16	20.48	1214.22	30.76	16	4.9161E+02	0.0015	0.0003	149	195	2	1105018	16414.47	77.147	2.4463
50b	P1408_003_Zm_A_1_RAD_36	37	37	7.32	2.75	3.87	8.20	500.66	16.81	9	5.3056E+02	0.0026	0.0004	337	548	2	1105018	16414.47	77.147	2.4463
50b	P1408_003_Zm_A_1_RAD_37	38	38	56.32	11.50	18.83	28.21	58.74	3.75	88	5.2952E+02	0.0032	0.0006	415	329	0	1105018	16414.47	77.147	2.4463
50b	P1408_003_Zm_A_1_RAD_38	39	39	6.74	2.99	3.97	9.63	1248.58	28.77	6	5.3060E+02	0.0019	0.0003	251	39	1	1105018	16414.47	77.147	2.4463
50b	P1408_003_Zm_A_1_RAD_39	40	40	236.66	105.21	138.33	324.65	548.98	40.51	6	5.3180E+02	0.0001	0.0000	7	5	0	1105018	16414.47	77.147	2.4463
50b	P1408_003_Zm_A_1_RAD_40	41	41	24.84	7.05	10.74	18.90	89.57	4.22	20	5.3053E+02	0.0017	0.0003	189	134	0	1105018	16414.47	77.147	2.4463
50b	P1408_003_Zm_A_1_RAD_41	42	42	3.04	1.83	2.13	7.11	797.17	28.02	3	3.9111E+02	0.0028	0.0005	386	240	0	1105018	16414.47	77.147	2.4463
50b	P1408_003_Zm_A_1_RAD_42	43	43	11.40	4.51	6.23	13.71	43.40	2.80	8	5.3093E+02	0.0015	0.0003	364	200	0	1105018	16414.47	77.147	2.4463
50b	P1408_003_Zm_A_1_RAD_43	44	44	11.64	3.71	5.49	10.37	1558.59	32.48	14	4.3033E+02	0.0031	0.0005	400	318	0	1105018	16414.47	77.147	2.4463
50b	P1408_003_Zm_A_1_RAD_44	45	45	10.56	5.07	6.52	16.99	180.48	7.28	5	3.8778E+02	0.0013	0.0002	136	127	0	1105018	16414.47	77.147	2.4463
50b	P1408_003_Zm_A_1_RAD_45	46	46	20.54	5.34	8.32	13.98	60.62	2.20	27	5.3072E+02	0.0027	0.0005	185	103	0	1105018	16414.47	77.147	2.4463
50b	P1408_003_Zm_A_1_RAD_46	47	47	9.74	7.09	7.47	31.98	53.17	3.95	2	5.3018E+02	0.0004	0.0001	52	51	0	1105018	16414.47	77.147	2.4463
50b	P1408_003_Zm_A_1_RAD_47	48	48	13.01	4.53	6.52	13.07	474.89	15.54	11	5.3049E+02	0.0018	0.0003	289	302	0	1105018	16414.47	77.147	2.4463
50b	P1408_003_Zm_A_1_RAD_48	49	49	11.16	2.44	3.94	6.10	835.92	21.75	58	5.2942E+02	0.0108	0.0019	1688	3909	3	1105018	16414.47	77.147	2.4463
50b	P1408_003_Zm_A_1_RAD_49	50	50	15.99	5.57	8.02	16.05	1017.32	28.87	11	5.3165E+02	0.0014	0.0002	230	326	0	1105018	16414.47	77.147	2.4463
50b	P1408_003_Zm_A_1_RAD_50	51	51	4.82	1.68	2.4														

50b	P1408_003_Zm_A_1_RAD_58	59	59	17.34	12.63	13.30	56.75	123.99	9.74	2	5.3047E+02	0.0002	0.0000	44	30	0	1105018	16414.47	77.147	2.4463
50b	P1408_003_Zm_A_1_RAD_59	60	60	20.43	7.38	10.50	21.57	33.49	2.28	10	5.3194E+02	0.0010	0.0002	146	73	0	1105018	16414.47	77.147	2.4463
50b	P1408_003_Zm_A_1_RAD_60	61	61	10.95	2.62	4.17	6.72	33.77	1.17	37	5.3058E+02	0.0070	0.0012	1301	2166	1	1105018	16414.47	77.147	2.4463
50b	P1408_003_Zm_A_1_RAD_61	62	62	7.15	2.49	3.59	7.20	472.39	22.24	11	5.3056E+02	0.0032	0.0006	490	443	0	1105018	16414.47	77.147	2.4463
50b	P1408_003_Zm_A_1_RAD_62	63	63	18.01	10.87	12.62	42.02	54.24	2.24	3	5.3059E+02	0.0003	0.0001	59	130	1	1105018	16414.47	77.147	2.4463
50b	P1408_003_Zm_A_1_RAD_64	65	64	17.76	7.40	10.03	23.02	831.23	27.32	7	4.2174E+02	0.0010	0.0002	140	146	0	1105018	16414.47	77.147	2.4463
50b	P1408_003_Zm_A_1_RAD_65	66	65	105.77	29.97	45.54	79.49	104.00	16.14	20	5.3091E+02	0.0004	0.0001	77	107	0	1105018	16414.47	77.147	2.4463
50b	P1408_003_Zm_A_1_RAD_66	67	66	13.20	5.21	7.20	15.81	512.63	17.56	8	5.3057E+02	0.0013	0.0002	248	288	2	1105018	16414.47	77.147	2.4463
50b	P1408_003_Zm_A_1_RAD_67	68	67	14.79	10.77	11.34	48.43	1467.00	41.57	2	5.3180E+02	0.0003	0.0000	53	77	1	1105018	16414.47	77.147	2.4463
50b	P1408_003_Zm_A_1_RAD_68	69	68	37.03	12.13	17.77	34.06	0.00	0.00	13	5.3068E+02	0.0007	0.0001	127	96	0	1105018	16414.47	77.147	2.4463
50b	P1408_003_Zm_A_1_RAD_69	70	69	21.45	5.90	9.07	15.70	49.55	2.08	22	3.1807E+02	0.0036	0.0006	711	317	0	1105018	16414.47	77.147	2.4463
75b	P1408_001_Zm_A_1_RAD_0	1	1	15.44	5.69	8.05	16.80	801.07	29.89	14	5.3100E+02	0.0036	0.0009	92	110	0	2132117	59574.77	234	7.98
75b	P1408_001_Zm_A_1a_RAD_0	1	1	13.12	4.84	6.84	14.28	786.28	32.60	14	5.3100E+02	0.0043	0.0011	131	188	0	2132117	59574.77	234	7.98
	w. avg.	1	1	14.09	3.69															
75b	P1408_001_Zm_A_1_RAD_1	2	2	377.23	103.37	156.36	261.69	505.52	40.75	96	5.3100E+02	0.0010	0.0003	18	33	0	2132117	59574.77	234	7.98
75b	P1408_001_Zm_A_1_RAD_2	3	3	10.26	3.34	4.91	9.42	768.80	31.84	24	5.3000E+02	0.0094	0.0024	196	104	0	2132117	59574.77	234	7.98
75b	P1408_001_Zm_A_1_RAD_3	4	4	32.14	13.49	18.22	41.94	92.65	8.24	9	5.3100E+02	0.0011	0.0003	28	47	0	2132117	59574.77	234	7.98
75b	P1408_001_Zm_A_1a_RAD_3	4	4	27.27	11.86	15.84	37.69	88.32	19.24	8	5.3100E+02	0.0012	0.0003	35	53	0	2132117	59574.77	234	7.98
75b	P1408_001_Zm_A_1b_RAD_3	4	4	33.44	15.23	19.97	49.40	0.00	0.00	7	5.3100E+02	0.0008	0.0002	41	26	0	2132117	59574.77	234	7.98
	w. avg.	4	4	30.00	7.69															
75b	P1408_001_Zm_A_1_RAD_4	5	5	8.70	2.82	4.14	7.89	693.79	26.53	25	5.3000E+02	0.0115	0.0029	216	13	0	2132117	59574.77	234	7.98
75b	P1408_001_Zm_A_1_RAD_5	6	6	13.42	5.05	7.09	15.02	817.26	25.92	13	5.3100E+02	0.0039	0.0010	91	67	0	2132117	59574.77	234	7.98
75b	P1408_001_Zm_A_1a_RAD_5	6	6	21.16	7.96	11.18	23.66	827.60	33.47	13	5.3100E+02	0.0025	0.0006	78	57	0	2132117	59574.77	234	7.98
	w. avg.	6	6	15.64	4.26															
75b	P1408_001_Zm_A_1_RAD_6	7	7	23.27	6.95	10.44	18.91	1130.97	28.00	41	5.3100E+02	0.0071	0.0018	228	65	0	2132117	59574.77	234	7.98
75b	P1408_001_Zm_A_1a_RAD_6	7	7	18.35	5.31	8.08	14.41	1147.64	39.27	51	5.3100E+02	0.0112	0.0028	435	122	0	2132117	59574.77	234	7.98
	w. avg.	7	7	20.16	4.22															
75b	P1408_001_Zm_A_1_RAD_7	8	8	51.40	22.41	29.86	70.88	1277.39	54.89	8	5.3100E+02	0.0006	0.0002	19	39	0	2132117	59574.77	234	7.98
75b	P1408_001_Zm_A_1a_RAD_7	8	8	53.84	20.77	28.88	62.00	1270.72	81.11	12	5.3100E+02	0.0009	0.0002	35	84	0	2132117	59574.77	234	7.98
75b	P1408_001_Zm_A_1b_RAD_7	8	8	20.01	9.63	12.35	32.22	1328.01	55.69	6	5.3100E+02	0.0012	0.0003	50	74	0	2132117	59574.77	234	7.98
	w. avg.	8	8	29.00	8.14															
75b	P1408_001_Zm_A_1_RAD_8	9	9	25.37	8.59	12.46	24.46	809.26	36.13	20	5.3000E+02	0.0032	0.0008	79	31	0	2132117	59574.77	234	7.98
75b	P1408_001_Zm_A_1_RAD_9	10	10	12.92	4.61	6.59	13.42	507.68	25.19	16	5.3100E+02	0.0050	0.0013	153	99	0	2132117	59574.77	234	7.98
75b	P1408_001_Zm_A_1_RAD_10	11	11	10.18	4.13	5.66	12.72	496.87	20.47	10	5.3100E+02	0.0039	0.0010	121	85	0	2132117	59574.77	234	7.98
75b	P1408_001_Zm_A_1a_RAD_10	11	11	11.18	3.79	5.50	10.81	480.52	24.82	20	5.3100E+02	0.0072	0.0018	319	446	0	2132117	59574.77	234	7.98
	w. avg.	11	11	10.72	2.79															
75b	P1408_001_Zm_A_1_RAD_12	13	12	40.37	12.78	18.91	35.47	51.28	4.84	28	5.3000E+02	0.0028	0.0007	91	90	0	2132117	59574.77	234	7.98
75b	P1408_001_Zm_A_1_RAD_13	14	13	29.89	9.29	13.79	25.56	85.49	5.21	32	5.3000E+02	0.0043	0.0011	132	255	0	2132117	59574.77	234	7.98
75b	P1408_001_Zm_A_1_RAD_15	16	14	17.23	5.50	8.12	15.34	497.32	38.31	27	5.3100E+02	0.0063	0.0016	162	33	0	2132117	59574.77	234	7.98
75b	P1408_001_Zm_A_1a_RAD_15	16	14	15.69	4.95	7.33	13.74	493.17	24.12	29	5.3100E+02	0.0074	0.0019	174	38	0	2132117	59574.77	234	7.98
75b	P1408_001_Zm_A_1b_RAD_15	16	14	14.07	5.03	7.18	14.65	479.20	42.88	16	5.3100E+02	0.0046	0.0012	161	54	0	2132117	59574.77	234	7.98
	w. avg.	14	14	15.57	2.97															
75b	P1408_001_Zm_A_1_RAD_16	17	15	31.64	10.97	15.80	31.50	516.03	23.90	18	5.3000E+02	0.0023	0.0006	69	76	0	2132117	59574.77	234	7.98
75b	P1408_001_Zm_A_1a_RAD_16	17	15	19.29	7.60	10.51	23.07	489.38	22.50	11	5.3000E+02	0.0023	0.0006	94	121	0	2132117	59574.77	234	7.98
	w. avg.	15	15	23.30	6.25															
75b	P1408_001_Zm_A_1_RAD_17	18	16	32.41	13.61	18.38	42.30	1777.40	54.63	9	5.3000E+02	0.0011	0.0003	29	23	0	2132117	59574.77	234	7.98
75b	P1408_001_Zm_A_1_RAD_18	19	17	9.01	3.56	4.92	10.82	511.51	19.57	11	5.3100E+02	0.0049	0.0012	133	28	0	2132117	59574.77	234	7.98
75b	P1408_001_Zm_A_1_RAD_19	20	18	18.76	6.92	9.78	20.41	449.60	21.58	14	5.3000E+02	0.0030	0.0008	93	126	0	2132117	59574.77	234	7.98
75b	P1408_001_Zm_A_1_RAD_20	21	19	57.91	18.25	26.98	50.32	842.40	33.29	29	5.3100E+02	0.0020	0.0005	66	46	0	2132117	59574.77	234	7.98
75b	P1408_001_Zm_A_1_RAD_21	22	20	27.05	13.91	17.37	48.35	61.85	7.11	5	5.3000E+02	0.0007	0.0002	25	13	0	2132117	59574.77	234	7.98
75b	P1408_001_Zm_A_1a_RAD_22	23	21	133.79	44.29	61.50	112.82	1091.02	47.53	32	5.3000E+02	0.0010	0.0002	37	121	0	2132117	59574.77	234	7.98
75b	P1408_001_Zm_A_1_RAD_22	23	21	144.89	41.51	65.87	119.65	1094.02	50.97	35	5.3000E+02	0.0010	0.0002	36	112	0	2132117	59574.77	234	7.98
	w. avg.	21	21	138.98	30.29															
75b	P1408_001_Zm_A_1_RAD_23	24	22	12.49	4.67	6.58	13.87	372.02	18.09	14	5.3000E+02	0.0045	0.0012	159	96	0	2132117	59574.77	234	7.98
75b	P1408_001_Zm_A_1_RAD_24	25	23	34.52	17.76	22.16	61.58	1104.03	52.86	5	5.3000E+02	0.0006	0.0001	20	17	0	2132117	59574.77	234	7.98
75b	P1408_001_Zm_A_1_RAD_25	26	24	60.75	19.36	28.59	53.78	86.47	9.98	27	5.2800E+02	0.0018	0.0005	59	95	0	2132117	59574.77	234	7.98
75b	P1408_001_Zm_A_1a_RAD_25	26	24	41.33	14.18	20.48	40.48	90.24	15.11	19	5.2800E+02	0.0019	0.0005	59	98	0	2132117	59574.77	234	7.98
	w. avg.	24	24	48.11	11.44															
75b	P1408_001_Zm_A_1_RAD_27	28	25	11.23	4.31	6.02	12.97	498.44	22.24	12	5.3000E+02	0.0043	0.0011	190	209	0	2132117	59574.77	234	7.98
75b	P1408_001_Zm_A_1_RAD_29	30	26	12.09	4.55	6.39	13.56	462.97	28.44	13	5.3000E+02	0.0043	0.0011	93	52	0	2132117	59574.77	234	7.98
75b	P1408_001_Zm_A_1_RAD_30	31	27	10.52	3.42	5.03	9.65	485.83	14.75	24	5.3000E+02	0.0092	0.0023	240	264	0	2132117	59574.77	234	7.98
75b	P1408_001_Zm_A_1a_RAD_30	31	27	9.07	2.85	4.23	7.94	473.91	20.23	29	5.3000E+02	0.0129	0.0033	380	212	0	2132117	59574.77	234	7.98
	w. avg.	27	27	9.66	2.19															

75b	P1408_001_Zm_A_1_RAD_32	33	29	52.09	17.10	25.03	48.01	44.47	3.44	23	5.3100E+02	0.0018	0.0004	71	150	0	2132117	59574.77	234	7.98
75b	P1408_001_Zm_A_1a_RAD_32	33	29	78.17	25.64	37.55	71.87	42.82	4.30	23	5.3100E+02	0.0012	0.0003	66	123	0	2132117	59574.77	234	7.98
	w. avg.		29	60.12	14.23															
75b	P1408_001_Zm_A_1_RAD_33	34	30	25.97	10.24	14.15	31.02	59.78	2.69	11	5.3000E+02	0.0017	0.0004	89	61	0	2132117	59574.77	234	7.98
75b	P1408_001_Zm_A_1a_RAD_33	34	30	6.77	4.27	4.85	17.10	56.73	4.67	3	5.3000E+02	0.0018	0.0005	93	67	0	2132117	59574.77	234	7.98
	w. avg.		30	9.61	3.94															
75b	P1408_001_Zm_A_1_RAD_34	35	31	35.32	11.61	16.99	32.64	89.11	5.68	23	5.3000E+02	0.0026	0.0007	95	75	0	2132117	59574.77	234	7.98
75b	P1408_001_Zm_A_1a_RAD_34	35	31	62.77	19.22	28.69	52.62	86.16	5.23	34	5.3000E+02	0.0022	0.0005	87	69	0	2132117	59574.77	234	7.98
	w. avg.		31	42.66	9.94															
75b	P1408_001_Zm_A_1_RAD_35	36	32	11.15	4.52	6.20	13.93	976.45	30.91	10	5.3100E+02	0.0036	0.0009	192	210	0	2132117	59574.77	234	7.98
75b	P1408_001_Zm_A_1_RAD_36	37	33	15.19	5.61	7.93	16.56	1015.68	103.19	14	5.3000E+02	0.0037	0.0009	118	20	0	2132117	59574.77	234	7.98
75b	P1408_001_Zm_A_1_RAD_37	38	34	17.61	5.70	8.38	15.96	482.86	22.84	25	5.3000E+02	0.0057	0.0014	209	134	0	2132117	59574.77	234	7.98
75b	P1408_001_Zm_A_1_RAD_39	40	35	13.33	4.26	6.30	11.91	500.75	21.39	27	5.3000E+02	0.0081	0.0021	295	111	0	2132117	59574.77	234	7.98
75b	P1408_001_Zm_A_1_RAD_41	42	36	6.27	1.95	2.90	5.40	1497.06	35.03	31	5.3100E+02	0.0199	0.0050	638	632	0	2132117	59574.77	234	7.98
75b	P1408_001_Zm_A_1a_RAD_41	42	36	4.87	1.55	2.30	4.34	1495.41	40.64	27	5.3100E+02	0.0223	0.0056	715	634	0	2132117	59574.77	234	7.98
	w. avg.		36	5.41	1.21															
75b	P1408_001_Zm_A_1_RAD_42	43	37	39.43	11.98	17.93	32.79	1660.10	42.37	36	5.3000E+02	0.0037	0.0009	182	118	0	2132117	59574.77	234	7.98
75b	P1408_001_Zm_A_1_RAD_43	44	38	2.19	2.26	1.91	15.06	1151.45	41.09	1	5.3100E+02	0.0018	0.0005	87	270	0	2132117	59574.77	234	7.98
75b	P1408_001_Zm_A_1a_RAD_43	44	38	7.28	4.59	5.22	18.40	1137.23	45.11	3	5.3100E+02	0.0017	0.0004	75	80	0	2132117	59574.77	234	7.98
	w. avg.		38	3.18	2.03															
75b	P1408_001_Zm_A_1_RAD_44	45	39	12.34	6.35	7.93	22.14	445.78	33.02	5	5.3100E+02	0.0016	0.0004	62	37	0	2132117	59574.77	234	7.98
75b	P1408_001_Zm_A_1a_RAD_44	45	39	6.36	3.27	4.09	11.43	102.87	6.21	5	5.3100E+02	0.0032	0.0008	183	18	0	2132117	59574.77	234	7.98
	w. avg.		39	7.61	2.91															
75b	P1408_001_Zm_A_1_RAD_45	46	40	36.59	10.61	16.08	28.63	47.46	3.95	51	5.3000E+02	0.0056	0.0014	190	285	0	2132117	59574.77	234	7.98
75b	P1408_001_Zm_A_1a_RAD_45	46	40	31.20	8.98	13.65	24.23	46.83	4.80	54	5.3000E+02	0.0069	0.0018	207	244	0	2132117	59574.77	234	7.98
	w. avg.		40	33.45	6.85															
75b	P1408_001_Zm_A_1_RAD_46	47	41	6.53	2.51	3.50	7.56	25.50	1.63	12	5.3100E+02	0.0074	0.0019	406	412	0	2132117	59574.77	234	7.98
75b	P1408_001_Zm_A_1_RAD_47	48	42	18.53	5.35	8.12	14.44	774.94	26.40	53	5.3100E+02	0.0115	0.0029	359	321	0	2132117	59574.77	234	7.98
75b	P1408_001_Zm_A_1a_RAD_47	48	42	13.18	3.88	5.87	10.56	769.63	26.79	45	5.3100E+02	0.0137	0.0035	431	315	0	2132117	59574.77	234	7.98
	w. avg.		42	15.02	3.14															
75b	P1408_001_Zm_A_1_RAD_48	49	43	2.58	1.94	2.01	9.01	518.58	20.62	2	5.3000E+02	0.0031	0.0008	144	46	0	2132117	59574.77	234	7.98
75b	P1408_001_Zm_A_1_RAD_49	50	44	19.18	5.92	8.82	16.30	25.51	1.86	33	5.3100E+02	0.0069	0.0018	291	219	0	2132117	59574.77	234	7.98
75b	P1408_001_Zm_A_1_RAD_50	51	45	16.23	4.83	7.26	13.11	461.24	18.91	43	5.3100E+02	0.0106	0.0027	367	116	0	2132117	59574.77	234	7.98
75b	P1408_001_Zm_A_1a_RAD_50	51	45	4.48	3.88	2.88	8.05	475.00	23.11	5	5.3100E+02	0.0045	0.0011	192	140	0	2132117	59574.77	234	7.98
75b	P1408_001_Zm_A_1b_RAD_50	51	45	6.02	2.53	3.42	7.89	468.60	20.44	9	5.3100E+02	0.0060	0.0015	319	184	0	2132117	59574.77	234	7.98
	w. avg.		45	9.46	1.94															
75b	P1408_001_Zm_A_1_RAD_51	52	46	9.87	5.53	6.65	20.38	2337.95	122.50	4	5.3000E+02	0.0016	0.0004	78	26	0	2132117	59574.77	234	7.98
75b	P1408_001_Zm_A_2_RAD_0	1	47	11.59	4.37	6.12	12.98	160.43	9.33	13	5.3100E+02	0.0045	0.0011	245	37	0	2132117	59574.77	234	7.98
75b	P1408_001_Zm_A_2_RAD_1	2	48	31.95	9.57	14.37	26.07	190.25	9.27	40	5.3000E+02	0.0050	0.0013	244	326	0	2132117	59574.77	234	7.98
75b	P1408_001_Zm_A_2_RAD_2	3	49	31.67	10.17	14.98	28.36	1127.97	39.68	26	5.3000E+02	0.0033	0.0008	137	151	0	2132117	59574.77	234	7.98
75b	P1408_001_Zm_A_2a_RAD_2	3	49	28.11	9.09	13.37	25.45	1130.13	48.39	25	5.3000E+02	0.0036	0.0009	148	136	0	2132117	59574.77	234	7.98
	w. avg.		49	29.69	6.78															
75b	P1408_001_Zm_A_2_RAD_3	4	50	21.19	7.56	10.79	21.96	60.14	5.52	16	5.3000E+02	0.0030	0.0008	115	118	0	2132117	59574.77	234	7.98
75b	P1408_001_Zm_A_2_RAD_4	5	51	20.60	6.45	9.57	17.85	472.02	22.14	30	5.3000E+02	0.0059	0.0015	175	115	0	2132117	59574.77	234	7.98
75b	P1408_001_Zm_A_2a_RAD_4	5	51	16.50	4.79	7.27	12.98	0.00	0.00	50	5.3000E+02	0.0122	0.0031	496	218	0	2132117	59574.77	234	7.98
	w. avg.		51	17.96	3.85															
75b	P1408_001_Zm_A_2_RAD_5	6	52	13.84	4.14	6.23	11.31	807.22	19.64	40	5.3100E+02	0.0116	0.0029	555	690	0	2132117	59574.77	234	7.98
75b	P1408_001_Zm_A_2_RAD_6	7	53	10.12	4.41	5.88	14.03	494.89	30.99	8	5.3100E+02	0.0032	0.0008	179	151	0	2132117	59574.77	234	7.98
75b	P1408_001_Zm_A_2a_RAD_6	7	53	8.96	3.30	4.68	9.76	466.45	17.78	14	5.3100E+02	0.0063	0.0016	311	256	0	2132117	59574.77	234	7.98
	w. avg.		53	9.38	2.64															
75b	P1408_001_Zm_A_2_RAD_7	8	54	26.72	8.79	12.86	24.75	1481.91	42.64	23	5.3000E+02	0.0035	0.0009	131	31	0	2132117	59574.77	234	7.98
75b	P1408_001_Zm_A_2_RAD_8	9	55	57.94	20.70	29.47	59.70	47.78	6.51	16	5.3100E+02	0.0011	0.0003	49	78	0	2132117	59574.77	234	7.98
75b	P1408_001_Zm_A_2_RAD_9	10	56	14.82	4.87	7.13	13.74	458.86	18.67	23	5.3000E+02	0.0062	0.0016	206	278	0	2132117	59574.77	234	7.98
75b	P1408_001_Zm_A_2_RAD_10	11	57	51.62	15.52	23.27	42.23	45.60	3.87	39	5.3100E+02	0.0030	0.0008	142	277	0	2132117	59574.77	234	7.98
75b	P1408_001_Zm_A_2_RAD_11	12	58	9.29	3.57	4.98	10.74	776.55	28.84	12	5.3100E+02	0.0052	0.0013	257	305	0	2132117	59574.77	234	7.98
75b	P1408_001_Zm_A_2a_RAD_11	12	58	15.74	6.05	8.44	18.19	792.87	26.66	12	5.3100E+02	0.0031	0.0008	175	90	0	2132117	59574.77	234	7.98
	w. avg.		58	10.96	3.07															
75b	P1408_001_Zm_A_2_RAD_12	13	59	40.59	17.03	23.01	52.92	83.24	8.29	9	5.3000E+02	0.0009	0.0002	43	73	0	2132117	59574.77	234	7.98
75b	P1408_001_Zm_A_3_RAD_0	1	60	7.62	2.89	4.05	8.64	0.00	0.00	15	5.3000E+02	0.0079	0.0022	82	19	0	2132117	59574.77	234	7.98
75b	P1408_001_Zm_A_3_RAD_1	2	61	17.21	5.53	8.15	15.47	0.00	0.00	27	5.3100E+02	0.0063	0.0016	102	106	0	2132117	59574.77	234	7.98
75b	P1408_001_Zm_A_3_RAD_2	3	62	17.35	17.90	15.14	118.04	827.61	50.70	1	5.3000E+02	0.0002	0.0001	10	11	0	2132117	59574.77	234	7.98
75b	P1408_001_Zm_A_3_RAD_3	4	63	15.07	9.51	10.80	37.99	468.45	23.00	3	5.3000E+02	0.0008	0.0002	33	131	0	2132117	59574.		

75b	P1408_001_Zm_A_3_RAD_6	7	65	32.87	10.62	15.63	29.71	28.96	2.13	25	5.3000E+02	0.0031	0.0008	101	27	0	2132117	59574.77	234	7.98
75b	P1408_001_Zm_A_3_RAD_7	8	66	25.35	8.58	12.45	24.41	496.25	28.07	20	5.3100E+02	0.0032	0.0008	119	164	0	2132117	59574.77	234	7.98
75b	P1408_001_Zm_A_3_RAD_8	9	67	56.46	19.78	28.42	56.98	1107.87	34.61	17	5.3000E+02	0.0012	0.0003	54	109	0	2132117	59574.77	234	7.98
75b	P1408_001_Zm_A_3_RAD_9	10	68	10.54	3.71	5.32	10.72	488.01	19.22	17	5.3000E+02	0.0065	0.0016	239	420	0	2132117	59574.77	234	7.98

*note: weighted averages are used for replicated spots on single grain analyses for 75b

Upper Siwalk

DTC3	P1408_007_Zm_A_1_RAD_0	1	1	2.10	1.11	1.37	3.96	114.37	5.22	4	5.3004E+02	0.0040	0.0007	533	17	0	1105018	16414.47	89.219	2.8218
DTC3	P1408_007_Zm_A_1_RAD_1	2	2	10.36	4.97	6.39	16.67	513.76	21.65	5	5.3060E+02	0.0010	0.0002	135	292	1	1105018	16414.47	89.219	2.8218
DTC3	P1408_007_Zm_A_1_RAD_2	3	3	2.41	4.20	2.21	26.15	302.12	114.16	2	5.3191E+02	0.0017	0.0027	267	478	1	1105018	16414.47	89.219	2.8218
DTC3	P1408_007_Zm_A_1_RAD_3	4	4	19.51	11.77	13.67	45.48	70.32	7.48	3	5.2898E+02	0.0003	0.0001	45	145	2	1105018	16414.47	89.219	2.8218
DTC3	P1408_007_Zm_A_1_RAD_4	5	5	0.00	0.00	0.00	7.22	1546.55	43.31	0	5.3089E+02	0.0009	0.0002	118	146	0	1105018	16414.47	89.219	2.8218
DTC3	P1408_007_Zm_A_1_RAD_5	6	6	3.32	1.12	1.63	3.21	451.45	22.13	12	5.3263E+02	0.0075	0.0013	897	518	0	1105018	16414.47	89.219	2.8218
DTC3	P1408_007_Zm_A_1_RAD_6	7	7	12.94	13.14	11.24	85.10	504.05	55.01	1	5.3002E+02	0.0002	0.0000	22	33	2	1105018	16414.47	89.219	2.8218
DTC3	P1408_007_Zm_A_1_RAD_7	8	8	3.94	2.09	2.58	7.44	1629.85	57.85	4	5.3044E+02	0.0021	0.0004	311	620	1	1105018	16414.47	89.219	2.8218
DTC3	P1408_007_Zm_A_1_RAD_8	9	9	0.00	0.00	0.00	11.09	1600.52	57.41	0	5.3179E+02	0.0006	0.0001	77	78	0	1105018	16414.47	89.219	2.8218
DTC3	P1408_007_Zm_A_1_RAD_9	10	10	4.08	2.46	2.86	9.56	383.57	23.13	3	5.2933E+02	0.0015	0.0003	146	97	0	1105018	16414.47	89.219	2.8218
DTC3	P1408_007_Zm_A_1_RAD_10	11	11	10.45	5.05	6.48	16.99	430.17	18.17	5	5.3039E+02	0.0010	0.0002	214	160	0	1105018	16414.47	89.219	2.8218
DTC3	P1408_007_Zm_A_1_RAD_11	12	12	2.60	2.64	2.26	17.22	1523.95	54.43	1	5.3046E+02	0.0008	0.0001	117	121	0	1105018	16414.47	89.219	2.8218
DTC3	P1408_007_Zm_A_1_RAD_12	13	13	3.77	1.28	1.85	3.64	479.98	18.24	12	5.3065E+02	0.0066	0.0012	1621	1251	1	1105018	16414.47	89.219	2.8218
DTC3	P1408_007_Zm_A_1_RAD_13	14	14	3.83	1.84	2.36	6.17	1600.04	54.03	5	5.3050E+02	0.0027	0.0005	206	324	1	1105018	16414.47	89.219	2.8218
DTC3	P1408_007_Zm_A_1_RAD_14	15	15	2.77	1.67	1.94	6.48	451.38	21.67	3	5.3054E+02	0.0023	0.0004	343	513	1	1105018	16414.47	89.219	2.8218
DTC3	P1408_007_Zm_A_1_RAD_15	16	16	4.23	3.08	3.24	13.91	482.17	19.97	2	5.3049E+02	0.0010	0.0002	148	196	0	1105018	16414.47	89.219	2.8218
DTC3	P1408_007_Zm_A_1_RAD_16	17	17	4.89	1.93	2.67	5.87	1076.03	39.60	8	5.3034E+02	0.0034	0.0006	455	583	1	1105018	16414.47	89.219	2.8218
DTC3	P1408_007_Zm_A_1_RAD_17	18	18	19.59	5.47	8.38	14.62	503.66	17.45	21	5.2990E+02	0.0022	0.0004	341	329	1	1105018	16414.47	89.219	2.8218
DTC3	P1408_007_Zm_A_1_RAD_18	19	19	4.59	1.81	2.50	5.51	1693.58	39.99	8	5.3066E+02	0.0036	0.0006	509	275	0	1105018	16414.47	89.219	2.8218
DTC3	P1408_007_Zm_A_1_RAD_20	21	20	1.79	1.30	1.38	5.91	1623.24	46.34	2	5.3033E+02	0.0023	0.0004	342	359	2	1105018	16414.47	89.219	2.8218
DTC3	P1408_007_Zm_A_1_RAD_21	22	21	3.97	1.50	2.10	4.46	1443.73	41.11	9	5.3189E+02	0.0047	0.0008	434	461	1	1105018	16414.47	89.219	2.8218
DTC3	P1408_007_Zm_A_1_RAD_22	23	22	0.00	0.00	0.00	3.44	1655.21	69.08	0	5.2947E+02	0.0018	0.0003	296	122	0	1105018	16414.47	89.219	2.8218
DTC3	P1408_007_Zm_A_1_RAD_23	24	23	3.19	1.93	2.24	7.47	1577.53	56.03	3	5.3216E+02	0.0020	0.0003	236	274	0	1105018	16414.47	89.219	2.8218
DTC3	P1408_007_Zm_A_1_RAD_24	25	24	1.18	0.57	0.73	1.90	1445.07	51.84	5	5.2965E+02	0.0089	0.0016	1740	5745	2	1105018	16414.47	89.219	2.8218
DTC3	P1408_007_Zm_A_1_RAD_25	26	25	6.70	2.33	3.36	6.75	373.68	13.83	11	5.3156E+02	0.0034	0.0006	573	130	0	1105018	16414.47	89.219	2.8218
DTC3	P1408_007_Zm_A_1_RAD_26	27	26	2.21	0.98	1.30	3.16	1269.98	48.43	6	5.3054E+02	0.0056	0.0010	563	135	0	1105018	16414.47	89.219	2.8218
DTC3	P1408_007_Zm_A_1_RAD_27	28	27	5.20	5.28	4.52	34.31	75.11	9.15	1	5.3051E+02	0.0004	0.0001	71	170	1	1105018	16414.47	89.219	2.8218
DTC3	P1408_007_Zm_A_1_RAD_28	29	28	3.85	1.23	1.82	3.44	479.18	16.76	14	5.3029E+02	0.0076	0.0013	1430	1414	1	1105018	16414.47	89.219	2.8218
DTC3	P1408_007_Zm_A_1_RAD_29	30	29	4.31	1.92	2.54	6.17	513.52	19.59	6	5.3161E+02	0.0029	0.0005	460	431	0	1105018	16414.47	89.219	2.8218
DTC3	P1408_007_Zm_A_1_RAD_30	31	30	5.30	1.79	2.61	5.12	40.23	2.29	12	5.2985E+02	0.0047	0.0008	821	2425	2	1105018	16414.47	89.219	2.8218
DTC3	P1408_007_Zm_A_1_RAD_31	32	31	2.61	1.38	1.71	4.92	86.95	3.60	4	5.2877E+02	0.0032	0.0006	712	1424	2	1105018	16414.47	89.219	2.8218
DTC3	P1408_007_Zm_A_1_RAD_32	33	32	11.08	5.87	7.23	20.82	486.47	20.06	4	5.3181E+02	0.0007	0.0001	130	208	1	1105018	16414.47	89.219	2.8218
DTC3	P1408_007_Zm_A_1_RAD_33	34	33	11.59	3.08	4.77	8.11	15.34	0.83	25	5.3090E+02	0.0045	0.0008	690	26	0	1105018	16414.47	89.219	2.8218
DTC3	P1408_007_Zm_A_1_RAD_34	35	34	17.48	12.73	13.41	57.24	1261.16	49.90	2	5.3056E+02	0.0002	0.0000	36	594	0	1105018	16414.47	89.219	2.8218
DTC3	P1408_007_Zm_A_1_RAD_35	36	35	0.00	0.00	0.00	11.99	1588.55	43.18	0	5.3059E+02	0.0005	0.0001	90	98	1	1105018	16414.47	89.219	2.8218
DTC3	P1408_007_Zm_A_1_RAD_36	37	36	0.00	0.00	0.00	2.10	481.22	21.33	0	5.3005E+02	0.0030	0.0005	504	623	1	1105018	16414.47	89.219	2.8218
DTC3	P1408_007_Zm_A_1_RAD_37	38	37	2.92	1.55	1.91	5.51	1142.76	55.72	4	5.2979E+02	0.0029	0.0005	1647	3511	2	1105018	16414.47	89.219	2.8218
DTC3	P1408_007_Zm_A_1_RAD_38	39	38	3.59	1.30	1.85	3.80	487.67	20.41	10	5.3075E+02	0.0058	0.0010	914	728	1	1105018	16414.47	89.219	2.8218
DTC3	P1408_007_Zm_A_1_RAD_39	40	39	1.50	1.09	1.15	4.95	475.71	18.59	2	5.3016E+02	0.0028	0.0005	439	533	1	1105018	16414.47	89.219	2.8218
DTC3	P1408_007_Zm_A_1_RAD_40	41	40	6.29	3.80	4.41	14.72	0.00	0.00	3	5.3070E+02	0.0010	0.0002	157	181	2	1105018	16414.47	89.219	2.8218
DTC3	P1408_007_Zm_A_1_RAD_41	42	41	1.40	1.42	1.21	9.23	1014.54	32.70	1	5.2903E+02	0.0015	0.0003	254	466	2	1105018	16414.47	89.219	2.8218
DTC3	P1408_007_Zm_A_1_RAD_42	43	42	4.62	3.37	3.54	15.18	1569.59	41.45	2	5.3064E+02	0.0009	0.0002	138	143	0	1105018	16414.47	89.219	2.8218
DTC3	P1408_007_Zm_A_1_RAD_43	44	43	0.53	0.54	0.46	3.49	492.35	17.20	1	5.3052E+02	0.0040	0.0007	507	625	1	1105018	16414.47	89.219	2.8218
DTC3	P1408_007_Zm_A_1_RAD_44	45	44	7.97	4.83	5.59	18.74	52.79	3.16	3	5.3033E+02	0.0008	0.0001	123	79	0	1105018	16414.47	89.219	2.8218
DTC3	P1408_007_Zm_A_1_RAD_45	46	45	0.00	0.00	0.00	7.17	1045.07	47.40	0	5.3055E+02	0.0009	0.0002	99	217	1	1105018	16414.47	89.219	2.8218
DTC3	P1408_007_Zm_A_1_RAD_46	47	46	11.78</																

DTC3	P1408_007_Zm_A_1_RAD_61	62	59	4.41	3.22	3.39	14.53	0.00	0.00	2	5.3052E+02	0.0009	0.0002	119	42	0	1105018	16414.47	89.219	2.8218
DTC3	P1408_007_Zm_A_1_RAD_62	63	60	4.18	2.52	2.93	9.78	503.21	25.36	3	5.3058E+02	0.0015	0.0003	212	297	1	1105018	16414.47	89.219	2.8218
DTC3	P1408_007_Zm_A_1_RAD_63	64	61	2.71	1.30	1.67	4.37	492.95	17.19	5	5.3130E+02	0.0038	0.0007	446	327	0	1105018	16414.47	89.219	2.8218
DTC3	P1408_007_Zm_A_1_RAD_64	65	62	9.15	4.85	5.97	17.20	1015.29	35.30	4	5.3007E+02	0.0009	0.0002	93	144	1	1105018	16414.47	89.219	2.8218
DTC3	P1408_007_Zm_A_1_RAD_65	66	63	70.43	23.12	33.81	64.69	179.08	10.97	13	5.3097E+02	0.0004	0.0001	52	63	0	1105018	16414.47	89.219	2.8218
DTC3	P1408_007_Zm_A_1_RAD_66	67	64	4.31	1.91	2.54	6.16	56.30	3.50	6	4.7268E+02	0.0033	0.0006	529	95	0	1105018	16414.47	89.219	2.8218
DTC3	P1408_007_Zm_A_1_RAD_67	68	65	1.67	1.22	1.28	5.49	465.56	16.70	2	5.2944E+02	0.0025	0.0004	342	162	0	1105018	16414.47	89.219	2.8218
DTC3	P1408_007_Zm_A_1_RAD_68	69	66	11.53	3.03	4.70	7.94	171.05	11.14	26	5.3047E+02	0.0047	0.0008	542	63	0	1105018	16414.47	89.219	2.8218

4.10.4 Zircon fission track peak decomposition

TABLE A4. Results of peak decomompostion for zircon fission-track cooling ages < 55 Ma with U-Pb ages > 300 Ma. Densityplotter application from Vermeesch et al., 2012, only components >5% used

Sample ID	n	PEAK (Ma)	SIGMA (Ma)	PEAK (Ma)	SIGMA (Ma)	PEAK (Ma)	SIGMA (Ma)
DTC3	45	1.8	1.0	4.1	1.0	-	-
75b	43	4.7	1.0	12.3	0.9	25.0	13.0
50b	37	6.0	1.5	9.9	1.7	17.7	5.2
25c	40	11.4	2.1	17.2	2.5	27.1	5.9
5b	16	16.7	1.3	-	-	-	-

4.10.5 Detrital muscovite $^{40}\text{Ar}/^{39}\text{Ar}$ analyses

TABLE A5. Detrital muscovite 40Ar/39Ar analytical data

Sample ID	Lab ID#	J	± 2s	⁴⁰ Ar*/ ³⁹ Ar	± 2s	⁴⁰ Ar/ ³⁹ Ar	± 2s	³⁶ Ar/ ³⁹ Ar	± 2s	³⁶ Ar/ ³⁹ Ar	± 2s	Cl/K	³⁹ Ar (moles)	% ⁴⁰ Ar*	Age (Ma)	± 2s
Middle Siwalik																
5b	688-01	4.5580E-04	6.7184E-06	461.341	1.625	463.109	3.246	0.0124	0.0011	0.0059	0.0010	0.002	1.09E-16	99.62	344.29	2.21
5b	688-02	4.5580E-04	6.7184E-06	39.279	0.216	40.448	0.330	0.0128	0.0010	0.0039	0.0010	0.002	9.49E-17	97.15	32.01	0.35
5b	688-03	4.5580E-04	6.7184E-06	35.392	0.446	37.372	0.482	0.0124	0.0024	0.0067	0.0026	0.002	3.25E-17	94.74	28.87	0.72
5b	688-04	4.5580E-04	6.7184E-06	57.568	0.221	59.070	0.395	0.0126	0.0009	0.0050	0.0007	0.002	1.32E-16	97.48	46.72	0.35
5b	688-05	4.5580E-04	6.7184E-06	34.004	0.243	35.245	0.355	0.0124	0.0012	0.0041	0.0012	0.002	7.78E-17	96.52	27.75	0.39
5b	688-06	4.5580E-04	6.7184E-06	69.802	0.440	70.274	0.734	0.0123	0.0017	0.0015	0.0017	0.002	5.36E-17	99.35	56.50	0.70
5b	688-07	4.5580E-04	6.7184E-06	69.950	0.331	71.155	0.597	0.0118	0.0011	0.0040	0.0010	0.002	9.41E-17	98.33	56.62	0.53
5b	688-08	4.5580E-04	6.7184E-06	34.837	0.353	36.760	0.454	0.0122	0.0018	0.0065	0.0019	0.002	4.47E-17	94.81	28.42	0.57
5b	688-09	4.5580E-04	6.7184E-06	65.665	0.203	66.493	0.387	0.0128	0.0006	0.0027	0.0004	0.002	2.16E-16	98.78	53.20	0.32
5b	688-10	4.5580E-04	6.7184E-06	29.361	0.170	31.123	0.225	0.0115	0.0009	0.0059	0.0009	0.002	1.03E-16	94.39	23.98	0.28
5b	688-11	4.5580E-04	6.7184E-06	75.747	0.314	78.331	0.591	0.0136	0.0008	0.0087	0.0009	0.002	1.27E-16	96.72	61.23	0.50
5b	688-12	4.5580E-04	6.7184E-06	32.206	0.212	32.842	0.266	0.0112	0.0011	0.0021	0.0011	0.002	7.62E-17	98.11	26.29	0.34
5b	688-13	4.5580E-04	6.7184E-06	64.757	0.209	66.386	0.388	0.0120	0.0007	0.0055	0.0006	0.002	1.61E-16	97.57	52.48	0.33
5b	688-14	4.5580E-04	6.7184E-06	68.080	0.391	68.987	0.625	0.0127	0.0015	0.0030	0.0016	0.002	5.34E-17	98.71	55.13	0.62
5b	688-15	4.5580E-04	6.7184E-06	34.417	0.210	37.523	0.296	0.0139	0.0011	0.0105	0.0011	0.002	9.13E-17	91.76	28.08	0.34
5b	688-16	4.5580E-04	6.7184E-06	28.698	0.383	29.145	0.320	0.0128	0.0021	0.0105	0.0024	0.002	4.00E-17	98.52	23.44	0.62
5b	688-17	4.5580E-04	6.7184E-06	70.523	0.854	71.470	1.256	0.0125	0.0032	0.0032	0.0040	0.002	2.23E-17	98.70	57.07	1.36
5b	688-18	4.5580E-04	6.7184E-06	540.490	3.224	542.894	6.439	0.0137	0.0020	0.0081	0.0023	0.002	3.71E-17	99.56	397.28	4.25
5b	688-19	4.5580E-04	6.7184E-06	21.208	0.210	22.376	0.216	0.0134	0.0014	0.0039	0.0012	0.002	6.84E-17	94.85	17.35	0.34
5b	688-20	4.5580E-04	6.7184E-06	81.062	0.800	83.003	1.227	0.0151	0.0033	0.0065	0.0036	0.002	2.42E-17	97.68	65.45	1.27
5b	688-21	4.5580E-04	6.7184E-06	31.728	0.413	33.135	0.395	0.0112	0.0021	0.0047	0.0025	0.002	3.67E-17	95.80	25.90	0.67
5b	688-22	4.5580E-04	6.7184E-06	27.801	0.235	28.343	0.273	0.0127	0.0014	0.0018	0.0013	0.002	6.55E-17	98.14	22.72	0.38
5b	688-23	4.5580E-04	6.7184E-06	30.829	0.480	31.623	0.508	0.0140	0.0027	0.0026	0.0028	0.002	2.82E-17	97.53	25.17	0.78
5b	688-24	4.5580E-04	6.7184E-06	43.097	0.263	44.135	0.424	0.0115	0.0011	0.0035	0.0011	0.002	7.47E-17	97.68	35.09	0.42
5b	688-25	4.5580E-04	6.7184E-06	29.606	0.250	31.830	0.292	0.0130	0.0014	0.0075	0.0014	0.002	6.51E-17	93.06	24.18	0.41
5b	688-26	4.5580E-04	6.7184E-06	29.918	0.552	30.943	0.489	0.0126	0.0030	0.0034	0.0034	0.002	2.79E-17	96.74	24.43	0.90
5b	688-27	4.5580E-04	6.7184E-06	136.847	0.534	137.459	1.047	0.0105	0.0010	0.0020	0.0008	0.002	1.15E-16	99.57	109.15	0.83
5b	688-28	4.5580E-04	6.7184E-06	24.072	0.178	25.073	0.213	0.0121	0.0011	0.0033	0.0010	0.002	8.92E-17	96.07	19.69	0.29
5b	688-29	4.5580E-04	6.7184E-06	38.111	0.331	39.933	0.437	0.0132	0.0017	0.0061	0.0017	0.002	4.76E-17	95.48	31.07	0.53
5b	688-30	4.5580E-04	6.7184E-06	42.657	0.287	44.294	0.408	0.0113	0.0015	0.0055	0.0014	0.002	6.34E-17	96.34	34.74	0.46
5b	688-31	4.5580E-04	6.7184E-06	48.489	0.658	50.514	0.832	0.0169	0.0035	0.0068	0.0035	0.003	2.41E-17	96.02	39.44	1.06
5b	688-32	4.5580E-04	6.7184E-06	42.625	0.236	43.427	0.369	0.0125	0.0012	0.0027	0.0010	0.002	8.45E-17	98.19	34.71	0.38
5b	688-33	4.5580E-04	6.7184E-06	60.254	0.286	61.671	0.503	0.0132	0.0010	0.0047	0.0010	0.002	9.03E-17	97.73	48.88	0.46
5b	688-34	4.5580E-04	6.7184E-06	21.338	0.369	26.061	0.325	0.0155	0.0022	0.0159	0.0023	0.002	4.10E-17	81.93	17.46	0.60
5b	688-35	4.5580E-04	6.7184E-06	201.467	1.351	203.987	2.654	0.0147	0.0019	0.0085	0.0022	0.002	4.31E-17	98.77	158.49	2.03
5b	688-36	4.5580E-04	6.7184E-06	31.073	0.350	35.870	0.374	0.0147	0.0018	0.0162	0.0021	0.002	5.46E-17	86.67	25.37	0.57
5b	688-37	4.5580E-04	6.7184E-06	43.819	0.474	44.752	0.591	0.0125	0.0024	0.0031	0.0025	0.002	3.54E-17	97.95	35.67	0.76
5b	688-38	4.5580E-04	6.7184E-06	32.851	0.280	33.483	0.357	0.0140	0.0015	0.0021	0.0015	0.002	5.85E-17	98.16	26.81	0.45
5b	688-39	4.5580E-04	6.7184E-06	31.512	0.706	32.699	0.609	0.0128	0.0036	0.0040	0.0043	0.002	1.99E-17	96.41	25.73	1.14
5b	688-40	4.5580E-04	6.7184E-06	55.842	1.212	59.254	1.393	0.0198	0.0058	0.0115	0.0069	0.003	1.32E-17	94.27	45.34	1.94
5b	688-41	4.5580E-04	6.7184E-06	30.675	0.201	31.872	0.266	0.0126	0.0010	0.0040	0.0010	0.002	8.29E-17	96.29	25.05	0.33
5b	688-42	4.5580E-04	6.7184E-06	26.425	0.594	28.211	0.491	0.0117	0.0032	0.0060	0.0037	0.002	2.27E-17	93.72	21.60	0.96
5b	688-43	4.5580E-04	6.7184E-06	75.363	0.578	77.034	0.938	0.0154	0.0023	0.0056	0.0024	0.002	3.47E-17	97.85	60.93	0.92
5b	688-44	4.5580E-04	6.7184E-06	37.263	0.534	37.858	0.572	0.0152	0.0030	0.0020	0.0031	0.002	2.70E-17	98.47	30.38	0.86
5b	688-45	4.5580E-04	6.7184E-06	66.573	0.274	67.088	0.492	0.0119	0.0010	0.0017	0.0008	0.002	1.10E-16	99.26	53.93	0.44
5b	688-46	4.5580E-04	6.7184E-06	38.606	0.206	40.143	0.289	0.0123	0.0012	0.0052	0.0010	0.002	8.69E-17	96.21	31.47	0.33
5b	688-47	4.5580E-04	6.7184E-06	42.674	0.301	42.669	0.432	0.0127	0.0017	-0.0001	0.0014	0.002	5.78E-17	100.00	34.75	0.49
5b	688-48	4.5580E-04	6.7184E-06	33.733	0.200	34.327	0.263	0.0114	0.0012	0.0020	0.0010	0.002	8.12E-17	98.31	27.53	0.32
5b	688-49	4.5580E-04	6.7184E-06	30.829	0.383	32.037	0.380	0.0110	0.0020	0.0040	0.0023	0.002	3.86E-17	96.27	25.17	0.62
5b	688-50	4.5580E-04	6.7184E-06	36.564	1.000	39.677	0.811	0.0091	0.0048	0.0105	0.0062	0.001	1.60E-17	92.19	29.82	1.62
5b	688-51	4.5580E-04	6.7184E-06	82.640	0.378	84.414	0.719	0.0125	0.0010	0.0060	0.0009	0.002	1.04E-16	97.92	66.70	0.60
5b	688-52	4.5580E-04	6.7184E-06	30.276	0.269	30.953	0.293	0.0108	0.0015	0.0022	0.0015	0.002	5.89E-17	97.86	24.72	0.44
5b	688-53	4.5580E-04	6.7184E-06	23.579	0.193	25.954	0.204	0.0130	0.0012	0.0080	0.0011	0.002	8.39E-17	90.91	19.28	0.31

5b	688-54	4.5580E-04	6.7184E-06	65.281	0.390	68.403	0.660	0.0140	0.0015	0.0105	0.0016	0.002	6.46E-17	95.46	52.89	0.62
5b	688-55	4.5580E-04	6.7184E-06	60.973	0.427	61.613	0.689	0.0113	0.0018	0.0021	0.0017	0.002	5.70E-17	98.99	49.45	0.68
5b	688-56	4.5580E-04	6.7184E-06	56.925	0.485	57.252	0.726	0.0108	0.0018	0.0011	0.0022	0.002	4.23E-17	99.45	46.21	0.78
5b	688-57	4.5580E-04	6.7184E-06	45.134	0.687	47.452	0.818	0.0070	0.0032	0.0078	0.0038	0.001	2.31E-17	95.15	36.73	1.11
5b	688-58	4.5580E-04	6.7184E-06	23.515	0.445	24.985	0.400	0.0086	0.0022	0.0049	0.0027	0.001	3.23E-17	94.17	19.23	0.72
5b	688-59	4.5580E-04	6.7184E-06	82.380	0.484	83.309	0.893	0.0109	0.0014	0.0031	0.0013	0.002	6.16E-17	98.90	66.50	0.77
25c	700-01	4.7280E-04	5.5740E-06	37.361	0.524	39.590	0.607	0.0086	0.0029	0.0075	0.0030	0.001	3.07E-17	94.41	31.59	0.88
25c	700-02	4.7280E-04	5.5740E-06	17.290	0.420	18.921	0.300	0.0130	0.0027	0.0055	0.0027	0.002	3.16E-17	91.45	14.69	0.71
25c	700-03	4.7280E-04	5.5740E-06	26.682	0.344	27.709	0.342	0.0082	0.0021	0.0034	0.0020	0.001	4.00E-17	96.35	22.62	0.58
25c	700-04	4.7280E-04	5.5740E-06	17.953	0.289	20.902	0.243	0.0131	0.0018	0.0099	0.0018	0.002	4.97E-17	85.95	15.25	0.49
25c	700-05	4.7280E-04	5.5740E-06	21.025	0.266	23.171	0.216	0.0139	0.0016	0.0072	0.0017	0.002	5.44E-17	90.80	17.85	0.45
25c	700-06	4.7280E-04	5.5740E-06	16.289	0.592	20.837	0.362	0.0164	0.0034	0.0153	0.0039	0.002	2.37E-17	78.23	13.84	1.00
25c	700-07	4.7280E-04	5.5740E-06	27.931	0.515	28.731	0.450	0.0122	0.0027	0.0027	0.0032	0.002	2.56E-17	97.27	23.67	0.87
25c	700-08	4.7280E-04	5.5740E-06	17.539	0.289	21.502	0.244	0.0167	0.0018	0.0134	0.0018	0.002	5.24E-17	81.63	14.90	0.49
25c	700-09	4.7280E-04	5.5740E-06	17.904	0.571	18.654	0.358	0.0157	0.0034	0.0025	0.0037	0.003	2.15E-17	96.06	15.21	0.97
25c	700-10	4.7280E-04	5.5740E-06	17.524	0.213	19.154	0.179	0.0162	0.0013	0.0055	0.0013	0.003	6.39E-17	91.57	14.89	0.36
25c	700-11	4.7280E-04	5.5740E-06	28.366	0.320	34.167	0.332	0.0167	0.0018	0.0196	0.0020	0.002	5.43E-17	83.06	24.04	0.54
25c	700-12	4.7280E-04	5.5740E-06	17.363	0.350	21.252	0.255	0.0141	0.0023	0.0131	0.0023	0.002	4.12E-17	81.76	14.75	0.59
25c	700-13	4.7280E-04	5.5740E-06	17.984	0.159	19.221	0.137	0.0138	0.0010	0.0041	0.0010	0.002	8.93E-17	93.64	15.27	0.27
25c	700-14	4.7280E-04	5.5740E-06	16.265	0.280	18.296	0.219	0.0132	0.0020	0.0068	0.0018	0.002	4.71E-17	88.98	13.82	0.47
25c	700-15	4.7280E-04	5.5740E-06	17.368	0.281	19.452	0.199	0.0124	0.0017	0.0070	0.0018	0.002	4.87E-17	89.35	14.75	0.48
25c	700-16	4.7280E-04	5.5740E-06	17.448	0.226	18.345	0.185	0.0120	0.0015	0.0030	0.0014	0.002	6.57E-17	95.20	14.82	0.38
25c	700-17	4.7280E-04	5.5740E-06	16.830	0.280	18.861	0.206	0.0117	0.0018	0.0068	0.0018	0.002	5.18E-17	89.31	14.30	0.47
25c	700-18	4.7280E-04	5.5740E-06	17.920	0.166	19.168	0.159	0.0120	0.0011	0.0042	0.0010	0.002	9.16E-17	93.57	15.22	0.28
25c	700-19	4.7280E-04	5.5740E-06	18.068	0.901	18.132	0.510	0.0101	0.0053	0.0002	0.0059	0.002	1.42E-17	99.73	15.35	1.52
25c	700-20	4.7280E-04	5.5740E-06	20.465	0.441	21.005	0.317	0.0115	0.0026	0.0018	0.0028	0.002	3.09E-17	97.50	17.37	0.75
25c	700-21	4.7280E-04	5.5740E-06	29.837	0.932	29.913	0.707	0.0127	0.0048	0.0002	0.0058	0.002	1.60E-17	99.80	25.27	1.57
25c	700-22	4.7280E-04	5.5740E-06	17.297	0.181	19.431	0.159	0.0149	0.0012	0.0072	0.0011	0.002	8.24E-17	89.09	14.69	0.31
25c	700-23	4.7280E-04	5.5740E-06	16.725	0.465	18.906	0.287	0.0139	0.0026	0.0073	0.0030	0.002	2.85E-17	88.54	14.21	0.79
25c	700-24	4.7280E-04	5.5740E-06	24.186	0.386	25.339	0.310	0.0127	0.0023	0.0039	0.0024	0.002	3.57E-17	95.51	20.51	0.65
25c	700-25	4.7280E-04	5.5740E-06	21.383	0.368	21.655	0.280	0.0105	0.0022	0.0009	0.0023	0.002	3.96E-17	98.82	18.15	0.62
25c	700-26	4.7280E-04	5.5740E-06	18.191	0.361	21.463	0.240	0.0143	0.0020	0.0110	0.0023	0.002	4.64E-17	84.82	15.45	0.61
25c	700-27	4.7280E-04	5.5740E-06	29.990	0.497	39.017	0.544	0.0171	0.0027	0.0305	0.0031	0.002	3.60E-17	76.89	25.40	0.84
25c	700-28	4.7280E-04	5.5740E-06	18.124	0.328	20.702	0.277	0.0133	0.0016	0.0087	0.0021	0.002	4.96E-17	87.61	15.39	0.55
25c	700-29	4.7280E-04	5.5740E-06	20.003	0.151	21.297	0.172	0.0126	0.0009	0.0043	0.0009	0.002	1.10E-16	94.00	16.98	0.26
25c	700-30	4.7280E-04	5.5740E-06	17.044	0.269	19.363	0.231	0.0135	0.0016	0.0078	0.0017	0.002	5.28E-17	88.10	14.48	0.46
25c	700-31	4.7280E-04	5.5740E-06	35.870	0.599	39.406	0.684	0.0114	0.0029	0.0119	0.0035	0.002	2.67E-17	91.06	30.34	1.01
25c	700-32	4.7280E-04	5.5740E-06	17.390	0.205	18.057	0.177	0.0114	0.0015	0.0022	0.0013	0.002	6.10E-17	96.39	14.77	0.35
25c	700-33	4.7280E-04	5.5740E-06	19.726	0.538	22.037	0.380	0.0131	0.0031	0.0078	0.0035	0.002	2.32E-17	89.58	16.75	0.91
25c	700-34	4.7280E-04	5.5740E-06	18.592	0.701	18.795	0.391	0.0065	0.0040	0.0006	0.0046	0.001	1.81E-17	99.00	15.79	1.19
25c	700-35	4.7280E-04	5.5740E-06	23.782	0.191	25.610	0.213	0.0137	0.0012	0.0061	0.0011	0.002	8.44E-17	92.92	20.17	0.32
25c	700-36	4.7280E-04	5.5740E-06	24.189	0.111	24.727	0.174	0.0120	0.0008	0.0018	0.0005	0.002	1.38E-16	97.89	20.52	0.19
25c	700-37	4.7280E-04	5.5740E-06	17.922	0.143	20.292	0.166	0.0129	0.0011	0.0080	0.0008	0.002	9.26E-17	88.39	15.22	0.24
25c	700-38	4.7280E-04	5.5740E-06	17.015	0.258	20.254	0.255	0.0130	0.0017	0.0109	0.0016	0.002	4.41E-17	84.08	14.46	0.44
25c	700-39	4.7280E-04	5.5740E-06	18.190	0.321	18.519	0.265	0.0091	0.0021	0.0011	0.0020	0.002	3.02E-17	98.31	15.45	0.54
25c	700-40	4.7280E-04	5.5740E-06	15.211	0.125	18.565	0.134	0.0139	0.0009	0.0113	0.0008	0.002	9.69E-17	82.00	12.93	0.21
25c	700-41	4.7280E-04	5.5740E-06	20.335	0.171	23.662	0.174	0.0151	0.0010	0.0112	0.0010	0.002	1.03E-16	86.00	17.26	0.29
25c	700-42	4.7280E-04	5.5740E-06	17.632	0.157	18.588	0.158	0.0132	0.0011	0.0032	0.0009	0.002	8.56E-17	94.94	14.98	0.27
25c	700-43	4.7280E-04	5.5740E-06	17.066	0.144	19.820	0.148	0.0136	0.0010	0.0093	0.0009	0.002	1.02E-16	86.18	14.50	0.24
25c	700-44	4.7280E-04	5.5740E-06	17.328	0.120	18.147	0.135	0.0120	0.0009	0.0027	0.0007	0.002	1.11E-16	95.56	14.72	0.20
25c	700-45	4.7280E-04	5.5740E-06	18.546	0.639	19.937	0.391	0.0112	0.0032	0.0047	0.0041	0.002	2.03E-17	93.09	15.75	1.08
25c	700-46	4.7280E-04	5.5740E-06	26.610	0.219	29.647	0.267	0.0133	0.0013	0.0102	0.0012	0.002	7.99E-17	89.80	22.56	0.37
25c	700-47	4.7280E-04	5.5740E-06	16.846	0.106	17.114	0.111	0.0120	0.0009	0.0009	0.0006	0.002	1.37E-16	98.52	14.31	0.18
25c	700-48	4.7280E-04	5.5740E-06	23.431	0.464	24.426	0.362	0.0115	0.0027	0.0033	0.0029	0.002	2.64E-17	95.99	19.88	0.78
25c	700-49	4.7280E-04	5.5740E-06	17.595	0.206	19.744	0.215	0.0115	0.0014	0.0072	0.0012	0.002	6.97E-17	89.19	14.95	0.35

25c	700-50	4.7280E-04	5.5740E-06	17.378	0.207	18.866	0.197	0.0130	0.0015	0.0050	0.0013	0.002	6.29E-17	92.19	14.76	0.35
25c	700-51	4.7280E-04	5.5740E-06	26.224	0.190	27.797	0.215	0.0129	0.0012	0.0053	0.0011	0.002	8.93E-17	94.39	22.23	0.32
25c	700-52	4.7280E-04	5.5740E-06	21.830	0.104	23.282	0.142	0.0126	0.0008	0.0049	0.0005	0.002	1.69E-16	93.82	18.52	0.18
25c	700-53	4.7280E-04	5.5740E-06	45.848	0.273	47.551	0.415	0.0126	0.0013	0.0057	0.0013	0.002	6.64E-17	96.45	38.69	0.46
25c	700-54	4.7280E-04	5.5740E-06	43.644	0.290	44.802	0.463	0.0118	0.0016	0.0039	0.0012	0.002	6.25E-17	97.45	36.85	0.48
25c	700-55	4.7280E-04	5.5740E-06	18.508	0.194	20.568	0.179	0.0136	0.0012	0.0069	0.0012	0.002	8.30E-17	90.05	15.72	0.33
25c	700-56	4.7280E-04	5.5740E-06	17.473	0.136	20.210	0.145	0.0141	0.0009	0.0092	0.0008	0.002	1.24E-16	86.52	14.84	0.23
25c	700-57	4.7280E-04	5.5740E-06	18.161	0.180	19.563	0.192	0.0129	0.0011	0.0047	0.0011	0.002	8.01E-17	92.91	15.42	0.30
25c	700-58	4.7280E-04	5.5740E-06	22.244	0.186	23.223	0.207	0.0128	0.0013	0.0033	0.0011	0.002	7.69E-17	95.85	18.87	0.31
25c	700-59	4.7280E-04	5.5740E-06	17.028	0.140	18.523	0.122	0.0117	0.0009	0.0050	0.0009	0.002	1.02E-16	92.01	14.47	0.24
25c	700-60	4.7280E-04	5.5740E-06	20.814	0.278	21.984	0.232	0.0130	0.0019	0.0039	0.0017	0.002	4.66E-17	94.75	17.67	0.47
50b	693-01	4.6580E-04	5.3798E-06	24.327	0.133	25.097	0.180	0.0123	0.0009	0.0026	0.0007	0.002	1.37E-16	96.99	20.33	0.22
50b	693-02	4.6580E-04	5.3798E-06	24.897	0.152	25.826	0.207	0.0132	0.0009	0.0031	0.0008	0.002	1.08E-16	96.46	20.80	0.25
50b	693-03	4.6580E-04	5.3798E-06	18.318	0.423	21.204	0.336	0.0139	0.0024	0.0097	0.0027	0.002	3.09E-17	86.45	15.33	0.71
50b	693-04	4.6580E-04	5.3798E-06	26.234	0.155	27.767	0.235	0.0125	0.0010	0.0051	0.0007	0.002	1.25E-16	94.53	21.91	0.26
50b	693-06	4.6580E-04	5.3798E-06	36.336	0.122	37.611	0.201	0.0119	0.0007	0.0043	0.0005	0.002	2.02E-16	96.65	30.28	0.20
50b	693-07	4.6580E-04	5.3798E-06	25.154	0.125	25.859	0.170	0.0125	0.0008	0.0023	0.0006	0.002	1.36E-16	97.33	21.01	0.21
50b	693-08	4.6580E-04	5.3798E-06	24.608	0.197	26.174	0.236	0.0125	0.0012	0.0053	0.0011	0.002	7.98E-17	94.07	20.56	0.33
50b	693-09	4.6580E-04	5.3798E-06	21.106	0.116	21.644	0.124	0.0106	0.0009	0.0018	0.0007	0.002	1.11E-16	97.58	17.65	0.19
50b	693-10	4.6580E-04	5.3798E-06	25.237	0.132	27.103	0.178	0.0131	0.0008	0.0063	0.0007	0.002	1.25E-16	93.17	21.08	0.22
50b	693-11	4.6580E-04	5.3798E-06	15.831	0.134	17.425	0.120	0.0129	0.0010	0.0053	0.0008	0.002	1.26E-16	90.93	13.25	0.22
50b	693-12	4.6580E-04	5.3798E-06	41.143	0.213	42.359	0.354	0.0128	0.0011	0.0041	0.0008	0.002	1.00E-16	97.16	34.25	0.35
50b	693-13	4.6580E-04	5.3798E-06	21.670	0.113	21.977	0.144	0.0115	0.0008	0.0010	0.0006	0.002	1.36E-16	98.67	18.12	0.19
50b	693-14	4.6580E-04	5.3798E-06	24.427	0.231	25.073	0.248	0.0135	0.0013	0.0021	0.0013	0.002	6.95E-17	97.49	20.41	0.38
50b	693-15	4.6580E-04	5.3798E-06	13.647	0.070	14.127	0.076	0.0119	0.0006	0.0016	0.0004	0.002	2.42E-16	96.71	11.43	0.12
50b	693-16	4.6580E-04	5.3798E-06	21.153	0.263	22.290	0.220	0.0120	0.0017	0.0038	0.0016	0.002	5.67E-17	94.97	17.69	0.44
50b	693-17	4.6580E-04	5.3798E-06	26.218	0.062	26.501	0.118	0.0119	0.0003	0.0009	0.0001	0.002	7.46E-16	98.99	21.90	0.10
50b	693-18	4.6580E-04	5.3798E-06	25.734	0.136	27.796	0.188	0.0134	0.0008	0.0069	0.0007	0.002	1.48E-16	92.63	21.50	0.23
50b	693-19	4.6580E-04	5.3798E-06	37.282	0.139	38.157	0.241	0.0120	0.0008	0.0029	0.0005	0.002	1.85E-16	97.75	31.06	0.23
50b	693-20	4.6580E-04	5.3798E-06	19.419	0.119	21.080	0.144	0.0133	0.0008	0.0056	0.0007	0.002	1.42E-16	92.19	16.24	0.20
50b	693-21	4.6580E-04	5.3798E-06	31.972	0.259	33.598	0.321	0.0115	0.0015	0.0055	0.0014	0.002	6.32E-17	95.20	26.67	0.43
50b	693-22	4.6580E-04	5.3798E-06	80.774	0.463	84.851	0.848	0.0143	0.0016	0.0137	0.0015	0.002	6.13E-17	95.21	66.63	0.75
50b	693-23	4.6580E-04	5.3798E-06	37.196	0.190	38.039	0.299	0.0110	0.0011	0.0028	0.0008	0.002	1.04E-16	97.82	30.99	0.31
50b	693-24	4.6580E-04	5.3798E-06	38.969	0.168	40.361	0.276	0.0139	0.0008	0.0047	0.0007	0.002	1.38E-16	96.59	32.45	0.28
50b	693-25	4.6580E-04	5.3798E-06	22.527	0.125	23.464	0.136	0.0129	0.0009	0.0031	0.0007	0.002	1.26E-16	96.07	18.83	0.21
50b	693-26	4.6580E-04	5.3798E-06	26.051	0.068	26.431	0.126	0.0125	0.0003	0.0012	0.0002	0.002	5.85E-16	98.62	21.76	0.11
50b	693-27	4.6580E-04	5.3798E-06	26.148	0.107	28.265	0.167	0.0134	0.0005	0.0071	0.0005	0.002	2.28E-16	92.56	21.84	0.18
50b	693-28	4.6580E-04	5.3798E-06	21.193	0.210	23.108	0.190	0.0136	0.0013	0.0064	0.0013	0.002	8.03E-17	91.78	17.72	0.35
50b	693-29	4.6580E-04	5.3798E-06	60.812	0.274	61.811	0.510	0.0141	0.0009	0.0033	0.0007	0.002	1.22E-16	98.41	50.39	0.45
50b	693-30	4.6580E-04	5.3798E-06	24.375	0.064	24.762	0.097	0.0123	0.0005	0.0013	0.0003	0.002	3.17E-16	98.50	20.37	0.11
50b	693-31	4.6580E-04	5.3798E-06	115.630	0.370	116.549	0.734	0.0122	0.0006	0.0031	0.0004	0.002	2.19E-16	99.22	94.64	0.59
50b	693-32	4.6580E-04	5.3798E-06	24.902	0.074	25.404	0.119	0.0122	0.0005	0.0016	0.0003	0.002	2.93E-16	98.09	20.81	0.12
50b	693-33	4.6580E-04	5.3798E-06	24.972	0.075	25.996	0.139	0.0128	0.0004	0.0034	0.0002	0.002	4.95E-16	96.12	20.86	0.12
50b	693-34	4.6580E-04	5.3798E-06	25.801	0.092	28.954	0.135	0.0137	0.0005	0.0106	0.0005	0.002	2.97E-16	89.16	21.55	0.15
50b	693-35	4.6580E-04	5.3798E-06	25.310	0.302	26.085	0.291	0.0127	0.0018	0.0026	0.0018	0.002	5.38E-17	97.09	21.14	0.50
50b	693-36	4.6580E-04	5.3798E-06	27.895	0.236	31.320	0.243	0.0124	0.0014	0.0115	0.0014	0.002	7.78E-17	89.11	23.29	0.39
50b	693-37	4.6580E-04	5.3798E-06	25.300	0.285	26.275	0.293	0.0134	0.0017	0.0033	0.0017	0.002	5.94E-17	96.35	21.14	0.47
50b	693-38	4.6580E-04	5.3798E-06	25.284	0.092	26.101	0.133	0.0125	0.0006	0.0027	0.0004	0.002	2.31E-16	96.93	21.12	0.15
50b	693-39	4.6580E-04	5.3798E-06	81.569	0.287	82.856	0.548	0.0133	0.0008	0.0043	0.0006	0.002	1.68E-16	98.46	67.27	0.46
50b	693-40	4.6580E-04	5.3798E-06	15.405	0.278	17.193	0.168	0.0116	0.0018	0.0060	0.0018	0.002	5.49E-17	89.69	12.90	0.46
50b	693-41	4.6580E-04	5.3798E-06	24.779	0.216	27.142	0.221	0.0121	0.0013	0.0079	0.0013	0.002	8.05E-17	91.35	20.70	0.36
50b	693-42	4.6580E-04	5.3798E-06	27.748	0.079	29.260	0.123	0.0125	0.0005	0.0051	0.0004	0.002	3.47E-16	94.89	23.17	0.13
50b	693-43	4.6580E-04	5.3798E-06	27.295	0.175	29.049	0.195	0.0125	0.0012	0.0059	0.0010	0.002	1.03E-16	94.01	22.79	0.29
50b	693-44	4.6580E-04	5.3798E-06	28.508	0.225	31.913	0.269	0.0140	0.0012	0.0115	0.0013	0.002	9.06E-17	89.38	23.80	0.37
50b	693-45	4.6580E-04	5.3798E-06	9.923	0.151	10.491	0.082	0.0129	0.0012	0.0019	0.0010	0.002	9.77E-17	94.73	8.32	0.25

50b	693-46	4.6580E-04	5.3798E-06	17.584	0.156	18.253	0.140	0.0121	0.0011	0.0022	0.0009	0.002	1.07E-16	96.42	14.72	0.26
50b	693-47	4.6580E-04	5.3798E-06	21.669	0.201	21.743	0.187	0.0137	0.0014	0.0002	0.0012	0.002	7.83E-17	99.73	18.12	0.34
50b	693-48	4.6580E-04	5.3798E-06	21.701	0.160	22.843	0.164	0.0124	0.0010	0.0038	0.0009	0.002	1.12E-16	95.06	18.14	0.27
50b	693-49	4.6580E-04	5.3798E-06	9.671	0.061	11.266	0.054	0.0134	0.0005	0.0054	0.0004	0.002	3.24E-16	85.95	8.11	0.10
50b	693-50	4.6580E-04	5.3798E-06	35.124	0.108	36.905	0.200	0.0139	0.0004	0.0060	0.0003	0.002	4.31E-16	95.22	29.28	0.18
50b	693-51	4.6580E-04	5.3798E-06	10.616	0.382	12.284	0.173	0.0135	0.0022	0.0056	0.0025	0.002	4.02E-17	86.53	8.90	0.64
50b	693-52	4.6580E-04	5.3798E-06	16.808	0.335	18.266	0.219	0.0139	0.0019	0.0049	0.0022	0.002	4.72E-17	92.10	14.07	0.56
50b	693-53	4.6580E-04	5.3798E-06	26.287	0.083	28.811	0.109	0.0133	0.0005	0.0085	0.0004	0.002	3.01E-16	91.29	21.96	0.14
50b	693-54	4.6580E-04	5.3798E-06	23.624	0.194	23.867	0.191	0.0126	0.0013	0.0008	0.0011	0.002	8.68E-17	99.05	19.74	0.32
50b	693-55	4.6580E-04	5.3798E-06	32.824	0.251	33.741	0.278	0.0134	0.0015	0.0031	0.0014	0.002	7.08E-17	97.33	27.37	0.42
50b	693-56	4.6580E-04	5.3798E-06	18.734	0.064	19.173	0.088	0.0123	0.0006	0.0014	0.0003	0.002	3.30E-16	97.79	15.67	0.11
50b	693-57	4.6580E-04	5.3798E-06	23.190	0.090	23.340	0.124	0.0120	0.0006	0.0005	0.0004	0.002	2.32E-16	99.43	19.38	0.15
50b	693-58	4.6580E-04	5.3798E-06	16.122	0.191	17.076	0.142	0.0131	0.0013	0.0032	0.0012	0.002	8.41E-17	94.50	13.50	0.32
50b	693-59	4.6580E-04	5.3798E-06	20.665	0.072	22.078	0.099	0.0126	0.0005	0.0047	0.0004	0.002	3.42E-16	93.67	17.28	0.12
50b	693-60	4.6580E-04	5.3798E-06	18.222	0.093	18.743	0.108	0.0120	0.0007	0.0017	0.0005	0.002	2.13E-16	97.30	15.25	0.16
75b	690-01	4.5600E-04	1.0250E-05	15.880	0.089	18.478	0.097	0.0132	0.0006	0.0087	0.0005	0.002	2.20E-16	86.01	13.02	0.14
75b	690-02	4.5600E-04	1.0250E-05	16.055	0.213	17.808	0.164	0.0127	0.0014	0.0059	0.0014	0.002	6.48E-17	90.23	13.16	0.35
75b	690-03	4.5600E-04	1.0250E-05	13.753	0.091	15.258	0.084	0.0139	0.0007	0.0050	0.0006	0.002	1.83E-16	90.23	11.28	0.15
75b	690-04	4.5600E-04	1.0250E-05	233.905	0.779	237.649	1.563	0.0132	0.0009	0.0126	0.0008	0.002	1.41E-16	98.43	182.83	1.16
75b	690-05	4.5600E-04	1.0250E-05	105.213	0.518	106.604	0.989	0.0119	0.0014	0.0047	0.0012	0.002	7.01E-17	98.71	84.54	0.81
75b	690-06	4.5600E-04	1.0250E-05	15.411	0.108	16.815	0.106	0.0125	0.0007	0.0047	0.0006	0.002	1.46E-16	91.74	12.63	0.18
75b	690-07	4.5600E-04	1.0250E-05	23.211	0.081	23.644	0.116	0.0116	0.0005	0.0014	0.0004	0.002	2.32E-16	98.23	18.99	0.13
75b	690-08	4.5600E-04	1.0250E-05	25.121	0.130	27.214	0.160	0.0128	0.0009	0.0070	0.0007	0.002	1.48E-16	92.36	20.55	0.21
75b	690-09	4.5600E-04	1.0250E-05	2490.706	5.390	2491.591	10.783	0.0117	0.0005	0.0029	0.0004	0.002	3.58E-16	99.97	1368.91	4.15
75b	690-10	4.5600E-04	1.0250E-05	16.685	0.143	18.482	0.140	0.0128	0.0010	0.0060	0.0009	0.002	1.07E-16	90.35	13.67	0.23
75b	690-11	4.5600E-04	1.0250E-05	26.204	0.246	27.161	0.275	0.0111	0.0014	0.0032	0.0014	0.002	6.14E-17	96.53	21.43	0.40
75b	690-12	4.5600E-04	1.0250E-05	15.544	0.242	17.922	0.199	0.0120	0.0017	0.0080	0.0015	0.002	5.66E-17	86.81	12.74	0.40
75b	690-13	4.5600E-04	1.0250E-05	26.250	0.085	26.919	0.126	0.0126	0.0006	0.0022	0.0004	0.002	2.47E-16	97.57	21.47	0.14
75b	690-14	4.5600E-04	1.0250E-05	14.847	0.224	17.421	0.172	0.0143	0.0015	0.0087	0.0014	0.002	6.41E-17	85.30	12.17	0.37
75b	690-15	4.5600E-04	1.0250E-05	15.583	0.047	16.355	0.062	0.0126	0.0004	0.0026	0.0002	0.002	3.92E-16	95.37	12.77	0.08
75b	690-16	4.5600E-04	1.0250E-05	13.771	0.122	14.528	0.112	0.0133	0.0010	0.0025	0.0007	0.002	1.17E-16	94.89	11.29	0.20
75b	690-17	4.5600E-04	1.0250E-05	16.449	0.347	17.065	0.245	0.0163	0.0022	0.0020	0.0022	0.003	3.98E-17	96.48	13.48	0.57
75b	690-18	4.5600E-04	1.0250E-05	17.666	0.240	22.138	0.230	0.0161	0.0016	0.0151	0.0015	0.002	6.75E-17	79.86	14.47	0.39
75b	690-19	4.5600E-04	1.0250E-05	16.725	0.080	19.999	0.086	0.0147	0.0006	0.0110	0.0005	0.002	2.62E-16	83.69	13.71	0.13
75b	690-20	4.5600E-04	1.0250E-05	23.734	0.066	25.437	0.098	0.0127	0.0005	0.0057	0.0003	0.002	3.19E-16	93.36	19.42	0.11
75b	690-21	4.5600E-04	1.0250E-05	15.421	0.110	18.607	0.121	0.0142	0.0009	0.0107	0.0007	0.002	1.66E-16	82.95	12.64	0.18
75b	690-22	4.5600E-04	1.0250E-05	16.844	0.118	17.674	0.127	0.0130	0.0009	0.0028	0.0007	0.002	1.15E-16	95.39	13.80	0.19
75b	690-23	4.5600E-04	1.0250E-05	31.651	0.202	32.224	0.267	0.0115	0.0013	0.0019	0.0010	0.002	8.63E-17	98.27	25.85	0.33
75b	690-24	4.5600E-04	1.0250E-05	15.820	0.179	16.691	0.166	0.0119	0.0014	0.0029	0.0011	0.002	7.61E-17	94.87	12.97	0.29
75b	690-25	4.5600E-04	1.0250E-05	23.832	0.089	24.602	0.140	0.0120	0.0006	0.0026	0.0004	0.002	2.03E-16	96.93	19.50	0.14
75b	690-26	4.5600E-04	1.0250E-05	25.727	0.222	25.841	0.247	0.0107	0.0014	0.0003	0.0013	0.002	6.51E-17	99.62	21.04	0.36
75b	690-27	4.5600E-04	1.0250E-05	15.699	0.096	17.913	0.106	0.0115	0.0007	0.0074	0.0006	0.002	1.90E-16	87.71	12.87	0.16
75b	690-28	4.5600E-04	1.0250E-05	20.288	0.128	21.960	0.147	0.0131	0.0008	0.0056	0.0007	0.002	1.42E-16	92.45	16.61	0.21
75b	690-29	4.5600E-04	1.0250E-05	1902.608	5.411	1903.650	10.827	0.0109	0.0008	0.0035	0.0006	0.002	1.87E-16	99.95	1126.86	4.77
75b	690-30	4.5600E-04	1.0250E-05	17.436	0.094	22.661	0.115	0.0150	0.0006	0.0176	0.0006	0.002	2.81E-16	77.00	14.29	0.15
75b	690-31	4.5600E-04	1.0250E-05	16.282	0.115	17.659	0.119	0.0138	0.0008	0.0046	0.0007	0.002	1.33E-16	92.29	13.34	0.19
75b	690-32	4.5600E-04	1.0250E-05	22.407	0.081	23.407	0.107	0.0125	0.0006	0.0033	0.0004	0.002	2.27E-16	95.79	18.34	0.13
75b	690-33	4.5600E-04	1.0250E-05	15.667	0.044	16.295	0.058	0.0123	0.0005	0.0021	0.0002	0.002	4.45E-16	96.24	12.84	0.07
75b	690-34	4.5600E-04	1.0250E-05	14.833	0.094	15.939	0.105	0.0129	0.0007	0.0037	0.0005	0.002	1.73E-16	93.15	12.16	0.15
75b	690-35	4.5600E-04	1.0250E-05	25.852	0.111	26.670	0.162	0.0125	0.0008	0.0027	0.0005	0.002	1.68E-16	96.99	21.14	0.18
75b	690-36	4.5600E-04	1.0250E-05	15.002	0.094	15.949	0.100	0.0127	0.0007	0.0032	0.0005	0.002	1.71E-16	94.15	12.30	0.15
75b	690-37	4.5600E-04	1.0250E-05	14.481	0.295	16.546	0.197	0.0133	0.0020	0.0069	0.0019	0.002	5.11E-17	87.60	11.87	0.48
75b	690-38	4.5600E-04	1.0250E-05	15.289	0.073	16.195	0.088	0.0128	0.0006	0.0030	0.0004	0.002	2.73E-16	94.50	12.53	0.12
75b	690-39	4.5600E-04	1.0250E-05	16.857	0.159	18.796	0.145	0.0134	0.0011	0.0065	0.0010	0.002	9.96E-17	89.76	13.81	0.26
75b	690-40	4.5600E-04	1.0250E-05	17.011	0.061	18.628	0.072	0.0137	0.0005	0.0054	0.0003	0.002	3.19E-16	91.39	13.94	0.10

75b	690-41	4.5600E-04	1.0250E-05	30.733	0.079	31.697	0.131	0.0121	0.0005	0.0032	0.0003	0.002	2.91E-16	97.01	25.11	0.13
75b	690-42	4.5600E-04	1.0250E-05	15.709	0.194	18.396	0.170	0.0143	0.0013	0.0090	0.0012	0.002	8.09E-17	85.47	12.88	0.32
75b	690-43	4.5600E-04	1.0250E-05	15.327	0.312	20.571	0.221	0.0164	0.0020	0.0177	0.0020	0.002	5.22E-17	74.56	12.56	0.51
75b	690-44	4.5600E-04	1.0250E-05	79.589	0.531	79.965	0.894	0.0149	0.0019	0.0012	0.0020	0.002	4.35E-17	99.55	64.31	0.84
75b	690-45	4.5600E-04	1.0250E-05	16.535	0.299	17.829	0.214	0.0107	0.0019	0.0043	0.0019	0.002	4.38E-17	92.83	13.55	0.49
75b	690-46	4.5600E-04	1.0250E-05	28.449	0.084	29.621	0.158	0.0126	0.0003	0.0039	0.0002	0.002	5.67E-16	96.09	23.25	0.14
75b	690-47	4.5600E-04	1.0250E-05	16.191	0.323	17.633	0.215	0.0127	0.0021	0.0048	0.0021	0.002	4.10E-17	91.90	13.27	0.53
75b	690-48	4.5600E-04	1.0250E-05	25.464	0.234	26.746	0.253	0.0122	0.0014	0.0043	0.0014	0.002	6.93E-17	95.26	20.83	0.38
75b	690-49	4.5600E-04	1.0250E-05	18.021	0.075	18.400	0.097	0.0134	0.0006	0.0012	0.0004	0.002	2.22E-16	98.02	14.76	0.12
75b	690-50	4.5600E-04	1.0250E-05	16.895	0.071	19.425	0.089	0.0135	0.0006	0.0085	0.0004	0.002	2.84E-16	87.04	13.84	0.12
75b	690-51	4.5600E-04	1.0250E-05	18.122	0.194	22.270	0.380	0.0142	0.0003	0.0140	0.0003	0.002	5.80E-16	81.43	14.85	0.32
75b	690-52	4.5600E-04	1.0250E-05	22.696	0.066	23.011	0.099	0.0107	0.0005	0.0010	0.0003	0.002	2.80E-16	98.70	18.57	0.11
75b	690-53	4.5600E-04	1.0250E-05	86.540	0.244	88.376	0.481	0.0127	0.0006	0.0062	0.0004	0.002	3.18E-16	97.94	69.82	0.39
75b	690-54	4.5600E-04	1.0250E-05	30.811	0.158	31.233	0.216	0.0110	0.0011	0.0014	0.0008	0.002	1.03E-16	98.70	25.17	0.26
75b	690-55	4.5600E-04	1.0250E-05	49.275	0.216	50.724	0.380	0.0120	0.0009	0.0049	0.0008	0.002	1.18E-16	97.17	40.09	0.35
75b	690-56	4.5600E-04	1.0250E-05	289.935	0.838	291.896	1.680	0.0122	0.0005	0.0066	0.0003	0.002	3.63E-16	99.33	224.00	1.22
75b	690-57	4.5600E-04	1.0250E-05	17.097	0.245	23.966	0.247	0.0165	0.0016	0.0232	0.0015	0.002	7.45E-17	71.38	14.01	0.40
75b	690-58	4.5600E-04	1.0250E-05	45.753	0.166	46.439	0.284	0.0126	0.0008	0.0023	0.0006	0.002	1.61E-16	98.56	37.25	0.27
75b	690-59	4.5600E-04	1.0250E-05	17.556	0.056	18.566	0.101	0.0123	0.0003	0.0034	0.0002	0.002	7.65E-16	94.64	14.38	0.09
75b	690-60	4.5600E-04	1.0250E-05	39.857	0.500	41.420	0.642	0.0111	0.0026	0.0052	0.0027	0.002	3.15E-17	96.26	32.49	0.81
75b	690-61	4.5600E-04	1.0250E-05	22.745	0.067	24.383	0.104	0.0134	0.0005	0.0055	0.0003	0.002	3.69E-16	93.34	18.61	0.11
75b	690-62	4.5600E-04	1.0250E-05	1563.574	5.759	1564.081	11.519	0.0122	0.0009	5.0017	0.0007	0.002	1.33E-16	99.97	970.98	5.53
75b	690-63	4.5600E-04	1.0250E-05	15.650	0.071	16.711	0.081	0.0122	0.0005	0.0035	0.0004	0.002	2.57E-16	93.74	12.83	0.12
75b	690-64	4.5600E-04	1.0250E-05	15.392	0.041	16.214	0.055	0.0127	0.0004	0.0027	0.0002	0.002	5.09E-16	95.02	12.62	0.07
75b	690-65	4.5600E-04	1.0250E-05	18.220	0.044	18.972	0.068	0.0126	0.0004	0.0025	0.0002	0.002	5.11E-16	96.12	14.93	0.07
75b	690-66	4.5600E-04	1.0250E-05	26.186	0.283	27.343	0.329	0.0143	0.0017	0.0039	0.0016	0.002	5.47E-17	95.82	21.41	0.46
75b	690-67	4.5600E-04	1.0250E-05	15.156	0.084	16.541	0.080	0.0139	0.0006	0.0046	0.0005	0.002	2.16E-16	91.71	12.42	0.14
75b	690-68	4.5600E-04	1.0250E-05	16.605	0.105	19.844	0.125	0.0141	0.0007	0.0109	0.0006	0.002	2.11E-16	83.74	13.61	0.17
75b	690-69	4.5600E-04	1.0250E-05	19.164	0.247	21.549	0.199	0.0152	0.0014	0.0080	0.0016	0.002	6.28E-17	89.00	15.70	0.40
75b	690-70	4.5600E-04	1.0250E-05	29.012	0.106	29.825	0.170	0.0129	0.0006	0.0027	0.0004	0.002	2.18E-16	97.33	23.71	0.17
75b	690-71	4.5600E-04	1.0250E-05	16.095	0.085	18.009	0.091	0.0132	0.0007	0.0064	0.0005	0.002	2.20E-16	89.45	13.19	0.14
75b	690-72	4.5600E-04	1.0250E-05	11.426	0.074	11.676	0.067	0.0123	0.0007	0.0008	0.0005	0.002	1.95E-16	97.99	9.37	0.12
75b	690-73	4.5600E-04	1.0250E-05	14.637	0.225	15.716	0.145	0.0127	0.0014	0.0036	0.0015	0.002	7.33E-17	93.23	12.00	0.37
75b	690-74	4.5600E-04	1.0250E-05	25.203	0.261	26.578	0.248	0.0139	0.0014	0.0046	0.0016	0.002	6.00E-17	94.88	20.61	0.42
75b	690-75	4.5600E-04	1.0250E-05	22.867	0.070	23.399	0.105	0.0127	0.0005	0.0017	0.0003	0.002	3.04E-16	97.79	18.71	0.11
75b	690-76	4.5600E-04	1.0250E-05	29.240	0.505	29.835	0.444	0.0134	0.0031	0.0020	0.0031	0.002	2.91E-17	98.06	23.89	0.82
75b	690-77	4.5600E-04	1.0250E-05	29.935	0.074	30.610	0.143	0.0120	0.0002	0.0022	0.0001	0.002	8.69E-16	97.84	24.46	0.12
75b	690-78	4.5600E-04	1.0250E-05	40.018	0.352	41.186	0.437	0.0125	0.0021	0.0039	0.0019	0.002	5.10E-17	97.20	32.62	0.57
75b	690-79	4.5600E-04	1.0250E-05	23.858	0.759	26.331	0.563	0.0132	0.0044	0.0083	0.0048	0.002	1.92E-17	90.66	19.52	1.24
75b	690-80	4.5600E-04	1.0250E-05	26.786	0.064	27.626	0.109	0.0125	0.0004	0.0028	0.0002	0.002	4.24E-16	97.02	21.90	0.10
75b	690-81	4.5600E-04	1.0250E-05	47.795	0.181	48.554	0.303	0.0114	0.0008	0.0025	0.0007	0.002	1.37E-16	98.47	38.89	0.29
75b	690-82	4.5600E-04	1.0250E-05	13.834	0.076	14.667	0.075	0.0116	0.0007	0.0028	0.0005	0.002	2.09E-16	94.42	11.34	0.12
75b	690-83	4.5600E-04	1.0250E-05	23.452	0.176	24.187	0.201	0.0124	0.0010	0.0024	0.0010	0.002	1.04E-16	97.02	19.19	0.29
75b	690-84	4.5600E-04	1.0250E-05	24.458	0.062	26.194	0.099	0.0127	0.0004	0.0058	0.0003	0.002	4.33E-16	93.43	20.01	0.10
75b	690-85	4.5600E-04	1.0250E-05	19.027	0.052	20.679	0.070	0.0130	0.0004	0.0055	0.0003	0.002	4.53E-16	92.08	15.58	0.09
75b	690-86	4.5600E-04	1.0250E-05	29.712	0.139	30.751	0.201	0.0116	0.0009	0.0035	0.0007	0.002	1.46E-16	96.67	24.28	0.23
75b	690-87	4.5600E-04	1.0250E-05	50.957	0.482	52.431	0.957	0.0134	0.0005	0.0049	0.0004	0.002	2.51E-16	97.22	41.44	0.77
75b	690-88	4.5600E-04	1.0250E-05	16.840	0.099	17.424	0.104	0.0115	0.0007	0.0019	0.0006	0.002	1.79E-16	96.73	13.80	0.16
75b	690-89	4.5600E-04	1.0250E-05	89.888	0.312	92.190	0.603	0.0135	0.0007	0.0077	0.0006	0.002	1.90E-16	97.52	72.47	0.49
75b	690-90	4.5600E-04	1.0250E-05	17.830	0.219	21.308	0.196	0.0142	0.0014	0.0117	0.0014	0.002	7.35E-17	83.74	14.61	0.36
75b	690-91	4.5600E-04	1.0250E-05	27.208	0.079	27.973	0.125	0.0123	0.0006	0.0025	0.0003	0.002	3.06E-16	97.32	22.24	0.13
75b	690-92	4.5600E-04	1.0250E-05	14.043	0.079	14.466	0.084	0.0122	0.0007	0.0014	0.0005	0.002	2.00E-16	97.18	11.51	0.13
75b	690-93	4.5600E-04	1.0250E-05	25.006	0.463	26.015	0.429	0.0109	0.0026	0.0034	0.0028	0.002	3.35E-17	96.18	20.45	0.75
75b	690-94	4.5600E-04	1.0250E-05	8.433	0.253	9.659	0.114	0.0127	0.0016	0.0041	0.0017	0.002	5.90E-17	87.45	6.92	0.42
75b	690-95	4.5600E-04	1.0250E-05	20.815	0.500	27.728	0.407	0.0167	0.0027	0.0234	0.0032	0.002	3.51E-17	75.11	17.04	0.81

Upper Siwalik

DTC3	695-01	4.7550E-04	1.0479E-05	20.625	0.142	23.444	0.149	0.0139	0.0009	0.0095	0.0008	0.002	1.50E-16	88.04	17.61	0.24
DTC3	695-02	4.7550E-04	1.0479E-05	17.892	0.057	18.548	0.075	0.0122	0.0005	0.0022	0.0003	0.002	4.00E-16	96.55	15.28	0.10
DTC3	695-03	4.7550E-04	1.0479E-05	17.187	0.073	17.725	0.089	0.0120	0.0006	0.0018	0.0004	0.002	2.66E-16	97.05	14.68	0.13
DTC3	695-04	4.7550E-04	1.0479E-05	19.494	0.058	20.050	0.083	0.0125	0.0004	0.0018	0.0003	0.002	4.19E-16	97.30	16.65	0.10
DTC3	695-05	4.7550E-04	1.0479E-05	18.612	0.113	20.398	0.114	0.0119	0.0007	0.0060	0.0007	0.002	1.88E-16	91.31	15.90	0.19
DTC3	695-06	4.7550E-04	1.0479E-05	45.713	0.155	46.263	0.259	0.0121	0.0008	0.0018	0.0006	0.002	1.88E-16	98.84	38.79	0.26
DTC3	695-07	4.7550E-04	1.0479E-05	22.532	0.071	22.843	0.097	0.0115	0.0006	0.0010	0.0004	0.002	3.19E-16	98.71	19.23	0.12
DTC3	695-08	4.7550E-04	1.0479E-05	26.513	0.082	27.524	0.119	0.0128	0.0005	0.0034	0.0004	0.002	3.07E-16	96.38	22.60	0.14
DTC3	695-09	4.7550E-04	1.0479E-05	28.362	0.086	29.074	0.132	0.0122	0.0005	0.0024	0.0004	0.002	3.11E-16	97.60	24.17	0.15
DTC3	695-10	4.7550E-04	1.0479E-05	33.418	0.586	35.466	0.525	0.0076	0.0027	0.0069	0.0036	0.001	3.09E-17	94.27	28.44	0.99
DTC3	695-11	4.7550E-04	1.0479E-05	30.356	0.095	32.789	0.130	0.0131	0.0006	0.0082	0.0005	0.002	2.92E-16	92.62	25.86	0.16
DTC3	695-12	4.7550E-04	1.0479E-05	28.178	0.112	29.722	0.166	0.0123	0.0006	0.0052	0.0005	0.002	2.40E-16	94.85	24.01	0.19
DTC3	695-13	4.7550E-04	1.0479E-05	18.810	0.061	19.628	0.079	0.0121	0.0005	0.0027	0.0003	0.002	3.62E-16	95.91	16.06	0.10
DTC3	695-14	4.7550E-04	1.0479E-05	3.741	0.198	5.665	0.066	0.0128	0.0012	0.0065	0.0013	0.002	8.70E-17	66.22	3.21	0.34
DTC3	695-15	4.7550E-04	1.0479E-05	3.723	0.230	8.669	0.085	0.0155	0.0013	0.0167	0.0016	0.002	7.77E-17	43.03	3.19	0.39
DTC3	695-16	4.7550E-04	1.0479E-05	5.311	0.206	8.137	0.070	0.0147	0.0011	0.0095	0.0014	0.002	8.50E-17	65.40	4.55	0.35
DTC3	695-17	4.7550E-04	1.0479E-05	19.401	0.162	21.311	0.156	0.0127	0.0011	0.0064	0.0010	0.002	1.17E-16	91.10	16.57	0.28
DTC3	695-18	4.7550E-04	1.0479E-05	25.833	0.146	26.281	0.174	0.0125	0.0009	0.0015	0.0008	0.002	1.38E-16	98.35	22.03	0.25
DTC3	695-19	4.7550E-04	1.0479E-05	9.924	0.149	11.576	0.098	0.0134	0.0011	0.0055	0.0010	0.002	1.14E-16	85.85	8.49	0.26
DTC3	695-20	4.7550E-04	1.0479E-05	26.670	0.074	27.040	0.130	0.0116	0.0005	0.0012	0.0002	0.002	4.34E-16	98.69	22.74	0.12
DTC3	695-21	4.7550E-04	1.0479E-05	19.690	0.258	20.103	0.214	0.0112	0.0015	0.0013	0.0016	0.002	6.79E-17	98.02	16.81	0.44
DTC3	695-22	4.7550E-04	1.0479E-05	26.396	0.100	27.456	0.146	0.0120	0.0007	0.0035	0.0005	0.002	2.25E-16	96.19	22.50	0.17
DTC3	695-23	4.7550E-04	1.0479E-05	18.594	0.093	19.805	0.108	0.0123	0.0007	0.0041	0.0005	0.002	2.05E-16	93.96	15.88	0.16
DTC3	695-24	4.7550E-04	1.0479E-05	192.252	0.500	193.455	0.993	0.0124	0.0006	0.0040	0.0005	0.002	2.47E-16	99.39	157.82	0.79
DTC3	695-25	4.7550E-04	1.0479E-05	237.138	0.955	239.582	1.903	0.0136	0.0011	0.0082	0.0010	0.002	1.25E-16	98.99	192.76	1.47
DTC3	695-26	4.7550E-04	1.0479E-05	27.531	0.113	29.746	0.157	0.0137	0.0007	0.0074	0.0006	0.002	2.14E-16	92.60	23.46	0.19
DTC3	695-27	4.7550E-04	1.0479E-05	25.788	0.256	27.245	0.251	0.0136	0.0015	0.0049	0.0015	0.002	7.39E-17	94.71	21.99	0.43
DTC3	695-28	4.7550E-04	1.0479E-05	20.453	0.093	22.720	0.102	0.0140	0.0006	0.0076	0.0005	0.002	2.52E-16	90.08	17.46	0.16
DTC3	695-29	4.7550E-04	1.0479E-05	19.540	0.070	21.389	0.092	0.0136	0.0005	0.0062	0.0004	0.002	3.74E-16	91.42	16.69	0.12
DTC3	695-30	4.7550E-04	1.0479E-05	21.794	0.080	23.974	0.107	0.0137	0.0006	0.0073	0.0004	0.002	3.29E-16	90.96	18.60	0.14
DTC3	695-31	4.7550E-04	1.0479E-05	24.192	0.080	24.436	0.112	0.0119	0.0005	0.0008	0.0004	0.002	3.02E-16	99.06	20.63	0.13
DTC3	695-32	4.7550E-04	1.0479E-05	26.074	0.112	27.405	0.153	0.0131	0.0007	0.0045	0.0006	0.002	2.13E-16	95.19	22.23	0.19
DTC3	695-33	4.7550E-04	1.0479E-05	28.008	0.110	29.955	0.149	0.0134	0.0007	0.0065	0.0006	0.002	2.30E-16	93.55	23.87	0.19
DTC3	695-34	4.7550E-04	1.0479E-05	26.759	0.175	29.599	0.194	0.0135	0.0010	0.0096	0.0010	0.002	1.34E-16	90.45	22.81	0.30
DTC3	695-35	4.7550E-04	1.0479E-05	5.637	0.149	10.572	0.076	0.0148	0.0010	0.0167	0.0010	0.002	1.40E-16	53.40	4.83	0.25
DTC3	695-36	4.7550E-04	1.0479E-05	19.338	0.075	20.552	0.100	0.0122	0.0005	0.0041	0.0004	0.002	3.55E-16	94.16	16.51	0.13
DTC3	695-37	4.7550E-04	1.0479E-05	12.623	0.074	13.224	0.061	0.0114	0.0006	0.0020	0.0005	0.002	2.67E-16	95.57	10.80	0.13
DTC3	695-38	4.7550E-04	1.0479E-05	4.577	0.124	5.850	0.043	0.0124	0.0008	0.0043	0.0008	0.002	1.48E-16	78.44	3.92	0.21
DTC3	695-39	4.7550E-04	1.0479E-05	26.930	0.259	27.741	0.255	0.0108	0.0014	0.0027	0.0015	0.002	7.80E-17	97.13	22.96	0.44
DTC3	695-40	4.7550E-04	1.0479E-05	19.980	0.099	21.152	0.115	0.0132	0.0007	0.0039	0.0006	0.002	2.32E-16	94.53	17.06	0.17
DTC3	695-41	4.7550E-04	1.0479E-05	25.733	0.421	26.993	0.372	0.0126	0.0021	0.0042	0.0026	0.002	4.33E-17	95.39	21.94	0.71
DTC3	695-42	4.7550E-04	1.0479E-05	19.075	0.133	20.447	0.134	0.0124	0.0008	0.0046	0.0008	0.002	1.63E-16	93.36	16.29	0.23
DTC3	695-43	4.7550E-04	1.0479E-05	19.991	0.096	25.157	0.127	0.0151	0.0006	0.0174	0.0006	0.002	2.99E-16	79.51	17.07	0.16
DTC3	695-44	4.7550E-04	1.0479E-05	27.355	0.107	28.361	0.155	0.0123	0.0006	0.0034	0.0005	0.002	2.52E-16	96.51	23.32	0.18
DTC3	695-45	4.7550E-04	1.0479E-05	18.903	0.103	21.281	0.116	0.0136	0.0007	0.0080	0.0006	0.002	2.31E-16	88.89	16.14	0.18
DTC3	695-46	4.7550E-04	1.0479E-05	21.618	0.270	24.998	0.236	0.0133	0.0015	0.0114	0.0017	0.002	6.87E-17	86.53	18.45	0.46
DTC3	695-47	4.7550E-04	1.0479E-05	21.592	0.227	25.352	0.221	0.0133	0.0013	0.0127	0.0014	0.002	8.92E-17	85.22	18.43	0.39
DTC3	695-48	4.7550E-04	1.0479E-05	19.175	0.157	20.073	0.145	0.0139	0.0010	0.0030	0.0010	0.002	1.21E-16	95.60	16.37	0.27
DTC3	695-49	4.7550E-04	1.0479E-05	19.754	0.150	20.874	0.148	0.0119	0.0010	0.0037	0.0009	0.002	1.38E-16	94.71	16.87	0.25
DTC3	695-50	4.7550E-04	1.0479E-05	22.125	0.090	26.622	0.115	0.0148	0.0006	0.0152	0.0005	0.002	3.24E-16	83.16	18.88	0.15
DTC3	695-51	4.7550E-04	1.0479E-05	21.440	0.346	23.398	0.269	0.0131	0.0017	0.0066	0.0022	0.002	5.72E-17	91.69	18.30	0.59
DTC3	695-52	4.7550E-04	1.0479E-05	25.014	0.057	25.429	0.107	0.0117	0.0003	0.0014	0.0001	0.002	1.03E-15	98.43	21.33	0.10
DTC3	695-53	4.7550E-04	1.0479E-05	23.805	0.126	24.181	0.147	0.0115	0.0008	0.0012	0.0007	0.002	1.74E-16	98.51	20.31	0.21
DTC3	695-54	4.7550E-04	1.0479E-05	27.167	0.153	27.987	0.210	0.0119	0.0008	0.0027	0.0008	0.002	1.47E-16	97.12	23.16	0.26
DTC3	695-55	4.7550E-04	1.0479E-05	18.797	0.095	19.814	0.113	0.0126	0.0007	0.0034	0.0005	0.002	2.20E-16	94.94	16.05	0.16

DTC3	695-56	4.7550E-04	1.0479E-05	4.970	0.055	5.796	0.029	0.0129	0.0005	0.0027	0.0004	0.002	3.32E-16	85.98	4.26	0.09
DTC3	695-57	4.7550E-04	1.0479E-05	29.360	0.088	30.310	0.160	0.0126	0.0004	0.0032	0.0003	0.002	4.48E-16	96.91	25.01	0.15
DTC3	695-58	4.7550E-04	1.0479E-05	78.904	0.248	79.485	0.485	0.0127	0.0005	0.0019	0.0004	0.002	2.70E-16	99.29	66.45	0.41
DTC3	695-59	4.7550E-04	1.0479E-05	20.044	0.063	20.954	0.090	0.0127	0.0006	0.0030	0.0003	0.002	4.17E-16	95.73	17.11	0.11
DTC3	695-60	4.7550E-04	1.0479E-05	18.886	0.218	24.721	0.220	0.0146	0.0012	0.0197	0.0014	0.002	1.03E-16	76.45	16.13	0.37

Himalayan tributaries

YAMNE	242-50	2.07E-04	1.23E-06	84.386	0.535	89.091	0.55	0.0162	0.0005	0.0158	0.0004	0.002	4.28E-16	94.7	31.22	0.2
YAMNE	242-51	2.07E-04	1.23E-06	76.437	0.323	77.396	0.314	0.0139	0.0005	0.0032	0.0003	0.002	3.83E-16	98.8	28.3	0.12
YAMNE	242-52	2.07E-04	1.23E-06	75.863	0.43	84.362	0.408	0.0178	0.0006	0.0287	0.0007	0.002	2.60E-16	90	28.09	0.16
YAMNE	242-53	2.07E-04	1.23E-06	73.532	0.31	79.089	0.307	0.0162	0.0004	0.0187	0.0004	0.002	5.15E-16	93	27.23	0.11
YAMNE	242-54	2.07E-04	1.23E-06	74.484	0.3	77.784	0.288	0.0146	0.0004	0.0111	0.0004	0.002	4.30E-16	95.8	27.58	0.11
YAMNE	242-55	2.07E-04	1.23E-06	75.451	0.253	88.181	0.252	0.0205	0.0003	0.043	0.0003	0.002	9.56E-16	85.6	27.94	0.09
YAMNE	242-56	2.07E-04	1.23E-06	68.609	0.341	76.45	0.319	0.0175	0.0005	0.0265	0.0006	0.002	4.06E-16	89.8	25.42	0.13
YAMNE	242-57	2.07E-04	1.23E-06	74.23	0.637	78.214	0.583	0.0147	0.001	0.0134	0.0011	0.002	1.17E-16	94.9	27.49	0.23
YAMNE	242-58	2.07E-04	1.23E-06	75.324	0.239	79.727	0.236	0.0155	0.0003	0.0148	0.0002	0.002	7.52E-16	94.5	27.89	0.09
YAMNE	242-59	2.07E-04	1.23E-06	73.129	0.268	74.208	0.264	0.0129	0.0003	0.0036	0.0002	0.002	5.38E-16	98.6	27.08	0.1
YAMNE	242-60	2.07E-04	1.23E-06	77.761	0.463	79.678	0.43	0.013	0.0006	0.0064	0.0006	0.002	2.10E-16	97.6	28.79	0.17
YAMNE	242-61	2.07E-04	1.23E-06	70.238	0.271	72.064	0.257	0.014	0.0005	0.0061	0.0003	0.002	4.05E-16	97.5	26.02	0.1
YAMNE	242-62	2.07E-04	1.23E-06	85.934	0.378	89.823	0.375	0.0175	0.0005	0.0131	0.0004	0.003	4.17E-16	95.7	31.79	0.14
YAMNE	242-63	2.07E-04	1.23E-06	70.687	0.333	73.468	0.321	0.0147	0.0005	0.0093	0.0004	0.002	3.04E-16	96.3	26.19	0.12
YAMNE	242-64	2.07E-04	1.23E-06	74.589	0.475	78.872	0.449	0.0149	0.0007	0.0144	0.0007	0.002	1.83E-16	94.6	27.62	0.17
YAMNE	242-65	2.07E-04	1.23E-06	73.885	0.231	75.498	0.222	0.0141	0.0004	0.0054	0.0002	0.002	5.40E-16	97.9	27.36	0.08
YAMNE	242-66	2.07E-04	1.23E-06	81.985	0.331	83.602	0.317	0.0133	0.0005	0.0054	0.0004	0.002	3.66E-16	98.1	30.34	0.12
YAMNE	242-67	2.07E-04	1.23E-06	90.262	0.317	92.827	0.307	0.0155	0.0004	0.0086	0.0003	0.002	5.03E-16	97.3	33.37	0.12
YAMNE	242-68	2.07E-04	1.23E-06	93.781	0.581	94.744	0.558	0.0174	0.0008	0.0032	0.0006	0.003	1.67E-16	99	34.66	0.21
YAMNE	242-69	2.07E-04	1.23E-06	88.53	0.258	90.374	0.249	0.0153	0.0003	0.0062	0.0003	0.002	7.45E-16	98	32.74	0.09
YAMNE	242-70	2.07E-04	1.23E-06	84.647	0.302	86.696	0.296	0.0146	0.0004	0.0069	0.0003	0.002	5.16E-16	97.7	31.31	0.11
YAMNE	242-71	2.07E-04	1.23E-06	82.585	0.256	89.121	0.254	0.0163	0.0003	0.022	0.0003	0.002	9.37E-16	92.7	30.56	0.09
YAMNE	242-72	2.07E-04	1.23E-06	78.843	0.447	83.104	0.421	0.0146	0.0007	0.0143	0.0006	0.002	2.13E-16	94.9	29.18	0.16
YAMNE	242-73	2.07E-04	1.23E-06	74.974	0.288	77.13	0.282	0.0137	0.0004	0.0072	0.0003	0.002	4.76E-16	97.2	27.76	0.11
YAMNE	242-74	2.07E-04	1.23E-06	74.668	0.287	75.528	0.28	0.0138	0.0003	0.0028	0.0002	0.002	4.98E-16	98.9	27.65	0.11
YAMNE	242-75	2.07E-04	1.23E-06	75.922	0.476	78.56	0.452	0.0139	0.0007	0.0088	0.0006	0.002	1.92E-16	96.7	28.11	0.17
YAMNE	242-76	2.07E-04	1.23E-06	75.517	0.227	78.599	0.225	0.0142	0.0003	0.0103	0.0002	0.002	1.04E-15	96.1	27.96	0.08
YAMNE	242-77	2.07E-04	1.23E-06	78.118	0.227	82.8	0.222	0.0152	0.0003	0.0158	0.0002	0.002	9.58E-16	94.4	28.92	0.08
YAMNE	242-78	2.07E-04	1.23E-06	81.173	0.623	89.494	0.57	0.0219	0.001	0.0281	0.0011	0.003	1.41E-16	90.7	30.04	0.23
YAMNE	242-79	2.07E-04	1.23E-06	83.694	0.395	88.268	0.385	0.0157	0.0005	0.0154	0.0005	0.002	3.19E-16	94.8	30.96	0.14
YAMNE	242-80	2.07E-04	1.23E-06	77.851	0.282	85.812	0.277	0.0177	0.0004	0.0269	0.0004	0.002	7.34E-16	90.8	28.82	0.1
YAMNE	242-81	2.07E-04	1.23E-06	105.472	0.277	108.291	0.277	0.0172	0.0002	0.0095	0.0002	0.003	1.31E-15	97.4	38.93	0.1
YAMNE	242-82	2.07E-04	1.23E-06	76.152	0.228	78.663	0.223	0.0142	0.0003	0.0084	0.0002	0.002	8.41E-16	96.8	28.2	0.08
YAMNE	242-83	2.07E-04	1.23E-06	71.956	0.357	75.175	0.332	0.0144	0.0006	0.0108	0.0005	0.002	2.68E-16	95.8	26.65	0.13
YAMNE	242-84	2.07E-04	1.23E-06	87.7	0.294	90.318	0.275	0.015	0.0004	0.0088	0.0004	0.002	5.57E-16	97.1	32.43	0.11
YAMNE	242-85	2.07E-04	1.23E-06	81.251	0.236	83.143	0.232	0.014	0.0003	0.0063	0.0002	0.002	7.70E-16	97.8	30.07	0.09
YAMNE	242-86	2.07E-04	1.23E-06	82.59	0.297	83.439	0.286	0.013	0.0003	0.0028	0.0003	0.002	5.86E-16	99	30.56	0.11
YAMNE	242-87	2.07E-04	1.23E-06	72.677	0.265	77.483	0.248	0.0155	0.0004	0.0162	0.0004	0.002	6.33E-16	93.8	26.92	0.1
YAMNE	242-88	2.07E-04	1.23E-06	73.958	0.192	76.684	0.19	0.0222	0.0002	0.0092	0.0002	0.003	1.33E-15	96.5	27.39	0.07
YAMNE	242-89	2.07E-04	1.23E-06	70.448	0.212	73.07	0.21	0.015	0.0003	0.0088	0.0002	0.002	1.03E-15	96.4	26.1	0.08
YAMNE	242-90	2.07E-04	1.23E-06	80.864	0.235	84.183	0.234	0.0145	0.0002	0.0112	0.0002	0.002	1.16E-15	96.1	29.93	0.09
YAMNE	242-91	2.07E-04	1.23E-06	74.857	0.232	75.45	0.23	0.0132	0.0002	0.0019	0.0001	0.002	1.18E-15	99.3	27.72	0.09
YAMNE	242-92	2.07E-04	1.23E-06	733.591	173.529	12969.87	2553.664	8.3248	1.6506	41.4092	8.1582	0.094	1.30E-18	5.7	254.86	56.22
YAMNE	242-93	2.07E-04	1.23E-06	80.754	0.246	83.791	0.243	0.0152	0.0003	0.0102	0.0002	0.002	1.21E-15	96.4	29.88	0.09
YAMNE	242-94	2.07E-04	1.23E-06	80.661	0.243	83.853	0.241	0.0145	0.0002	0.0107	0.0002	0.002	1.25E-15	96.2	29.85	0.09
YAMNE	242-95	2.07E-04	1.23E-06	82.999	0.398	85.43	0.386	0.0162	0.0005	0.0081	0.0004	0.002	3.42E-16	97.2	30.71	0.15
YAMNE	242-96	2.07E-04	1.23E-06	67.084	0.188	70.053	0.186	0.0157	0.0002	0.01	0.0001	0.002	2.18E-15	95.8	24.86	0.07
YAMNE	242-97	2.07E-04	1.23E-06	73.019	0.229	74.784	0.226	0.0138	0.0002	0.0059	0.0002	0.002	1.10E-15	97.7	27.04	0.08
YAMNE	242-98	2.07E-04	1.23E-06	82.096	0.297	85.989	0.291	0.0148	0.0004	0.0131	0.0003	0.002	6.12E-16	95.5	30.38	0.11

YAMNE	242-99	2.07E-04	1.23E-06	81.548	0.215	85.135	0.213	0.015	0.0002	0.0121	0.0001	0.002	1.77E-15	95.8	30.18	0.08
YANG SANG	232-01	2.04E-04	1.16E-06	74.307	0.228	77.663	0.222	0.0152	0.0003	0.0113	0.0002	0.002	9.43E-16	95.7	27.16	0.08
YANG SANG	232-02	2.04E-04	1.16E-06	76.265	0.235	77.821	0.23	0.014	0.0003	0.0052	0.0002	0.002	9.38E-16	98	27.87	0.09
YANG SANG	232-03	2.04E-04	1.16E-06	125.877	0.318	130.455	0.319	0.015	0.0002	0.0154	0.0002	0.002	1.79E-15	96.5	45.78	0.11
YANG SANG	232-04	2.04E-04	1.16E-06	124.53	0.39	128.281	0.389	0.0147	0.0003	0.0126	0.0003	0.002	7.49E-16	97.1	45.3	0.14
YANG SANG	232-05	2.04E-04	1.16E-06	79.018	0.229	96.156	0.227	0.0233	0.0003	0.0579	0.0003	0.002	1.56E-15	82.2	28.87	0.08
YANG SANG	232-06	2.04E-04	1.16E-06	85.509	0.267	88.589	0.262	0.0223	0.0004	0.0104	0.0003	0.003	6.91E-16	96.6	31.22	0.1
YANG SANG	232-07	2.04E-04	1.16E-06	110.324	0.305	118.744	0.305	0.0179	0.0003	0.0284	0.0003	0.002	1.25E-15	92.9	40.19	0.11
YANG SANG	232-08	2.04E-04	1.16E-06	76.701	0.269	82.361	0.264	0.0163	0.0003	0.0191	0.0003	0.002	7.58E-16	93.2	28.03	0.1
YANG SANG	232-09	2.04E-04	1.16E-06	85.839	0.347	88.292	0.332	0.014	0.0005	0.0082	0.0004	0.002	3.54E-16	97.3	31.34	0.13
YANG SANG	232-10	2.04E-04	1.16E-06	82.033	0.276	86.145	0.272	0.015	0.0003	0.0138	0.0003	0.002	7.38E-16	95.3	29.97	0.1
YANG SANG	232-11	2.04E-04	1.16E-06	102.97	0.264	107.561	0.265	0.015	0.0002	0.0155	0.0002	0.002	2.02E-15	95.8	37.53	0.1
YANG SANG	232-12	2.04E-04	1.16E-06	117.42	1.161	123.043	1.062	0.0155	0.0014	0.0189	0.0018	0.002	9.03E-17	95.5	42.74	0.42
YANG SANG	232-13	2.04E-04	1.16E-06	80.59	0.327	82.066	0.31	0.014	0.0004	0.0049	0.0004	0.002	5.91E-16	98.2	29.44	0.12
YANG SANG	232-14	2.04E-04	1.16E-06	78.203	0.337	78.798	0.315	0.0133	0.0004	0.0019	0.0004	0.002	4.64E-16	99.3	28.58	0.12
YANG SANG	232-16	2.04E-04	1.16E-06	114.976	0.43	115.257	0.422	0.0123	0.0004	0.0009	0.0003	0.002	6.36E-16	99.8	41.86	0.15
YANG SANG	232-17	2.04E-04	1.16E-06	76.523	0.339	81.845	0.323	0.0161	0.0005	0.0179	0.0005	0.002	4.10E-16	93.5	27.97	0.12
YANG SANG	232-18	2.04E-04	1.16E-06	118.039	0.483	125.881	0.481	0.0172	0.0004	0.0265	0.0005	0.002	5.07E-16	93.8	42.96	0.17
YANG SANG	232-19	2.04E-04	1.16E-06	79.558	0.297	90.074	0.288	0.0191	0.0004	0.0355	0.0004	0.002	8.62E-16	88.4	29.07	0.11
YANG SANG	232-20	2.04E-04	1.16E-06	77.848	0.41	83.36	0.39	0.0155	0.0006	0.0186	0.0006	0.002	2.86E-16	93.4	28.45	0.15
YANG SANG	232-21	2.04E-04	1.16E-06	117.5	0.937	126.861	0.923	0.0196	0.001	0.0316	0.0012	0.002	1.22E-16	92.6	42.77	0.34
YANG SANG	232-22	2.04E-04	1.16E-06	78.954	0.35	86.862	0.34	0.0172	0.0005	0.0267	0.0005	0.002	4.87E-16	90.9	28.85	0.13
YANG SANG	232-23	2.04E-04	1.16E-06	73.92	0.253	77.371	0.249	0.0148	0.0003	0.0116	0.0002	0.002	7.38E-16	95.6	27.02	0.09
YANG SANG	232-24	2.04E-04	1.16E-06	82.532	0.399	83.893	0.382	0.0122	0.0005	0.0045	0.0004	0.002	2.87E-16	98.4	30.15	0.14
YANG SANG	232-25	2.04E-04	1.16E-06	78.725	0.255	81.61	0.248	0.0146	0.0003	0.0097	0.0003	0.002	7.05E-16	96.5	28.77	0.09
YANG SANG	232-26	2.04E-04	1.16E-06	130.338	0.445	134.51	0.446	0.016	0.0004	0.014	0.0003	0.002	6.65E-16	96.9	47.38	0.16
YANG SANG	232-27	2.04E-04	1.16E-06	76.994	0.481	79.493	0.436	0.0145	0.0007	0.0084	0.0007	0.002	1.94E-16	96.9	28.14	0.17
YANG SANG	232-28	2.04E-04	1.16E-06	109.894	0.26	113.695	0.259	0.0149	0.0002	0.0128	0.0002	0.002	1.55E-15	96.7	40.03	0.09
YANG SANG	232-29	2.04E-04	1.16E-06	133.897	0.446	137.059	0.443	0.0146	0.0004	0.0106	0.0003	0.002	5.12E-16	97.7	48.66	0.16
YANG SANG	232-30	2.04E-04	1.16E-06	121.422	0.466	131.063	0.469	0.0188	0.0004	0.0325	0.0005	0.002	4.75E-16	92.7	44.18	0.17
YANG SANG	232-31	2.04E-04	1.16E-06	89.862	0.34	100.36	0.343	0.0187	0.0004	0.0354	0.0004	0.002	5.69E-16	89.6	32.8	0.12
YANG SANG	232-32	2.04E-04	1.16E-06	79.018	0.315	83.367	0.29	0.0156	0.0004	0.0146	0.0005	0.002	6.58E-16	94.8	28.87	0.11
YANG SANG	232-33	2.04E-04	1.16E-06	86.374	0.249	95.92	0.246	0.0189	0.0002	0.0322	0.0003	0.002	1.41E-15	90.1	31.54	0.09
YANG SANG	232-34	2.04E-04	1.16E-06	111.443	0.313	117.48	0.313	0.016	0.0002	0.0203	0.0002	0.002	1.24E-15	94.9	40.59	0.11
YANG SANG	232-35	2.04E-04	1.16E-06	132.256	0.377	142.731	0.381	0.0189	0.0003	0.0354	0.0003	0.002	1.22E-15	92.7	48.07	0.14
YANG SANG	232-36	2.04E-04	1.16E-06	114.186	0.532	120.923	0.531	0.0158	0.0005	0.0227	0.0005	0.002	3.08E-16	94.5	41.58	0.19
YANG SANG	232-37	2.04E-04	1.16E-06	762.524	3.538	763.57	3.54	0.0135	0.0005	0.0035	0.0004	0.002	2.36E-16	99.9	261.04	1.13
YANG SANG	232-38	2.04E-04	1.16E-06	76.746	0.322	78.115	0.313	0.0133	0.0004	0.0045	0.0003	0.002	3.43E-16	98.3	28.05	0.12
YANG SANG	232-39	2.04E-04	1.16E-06	76.885	0.468	82.204	0.453	0.0164	0.0007	0.0179	0.0006	0.002	1.94E-16	93.6	28.1	0.17
YANG SANG	232-40	2.04E-04	1.16E-06	79.25	0.258	89.303	0.252	0.0187	0.0003	0.0339	0.0004	0.002	1.02E-15	88.8	28.96	0.09
YANG SANG	232-41	2.04E-04	1.16E-06	41.685	1.273	73.991	0.936	0.0312	0.0028	0.1092	0.0041	0.002	3.48E-17	56.4	15.29	0.46
YANG SANG	232-42	2.04E-04	1.16E-06	73.497	0.288	77.224	0.272	0.0148	0.0004	0.0125	0.0004	0.002	4.91E-16	95.2	26.87	0.1
YANG SANG	232-43	2.04E-04	1.16E-06	88.949	0.469	98.592	0.457	0.0183	0.0007	0.0325	0.0007	0.002	2.45E-16	90.2	32.47	0.17
YANG SANG	232-44	2.04E-04	1.16E-06	89.13	0.518	95.836	0.492	0.0173	0.0006	0.0226	0.0008	0.002	2.09E-16	93	32.54	0.19
YANG SANG	232-45	2.04E-04	1.16E-06	77.679	0.332	86.741	0.313	0.0186	0.0005	0.0306	0.0006	0.002	3.59E-16	89.6	28.39	0.12
YANG SANG	232-46	2.04E-04	1.16E-06	98.324	0.417	104.91	0.413	0.0211	0.0005	0.0222	0.0005	0.003	3.75E-16	93.7	35.86	0.15
YANG SANG	232-47	2.04E-04	1.16E-06	89.454	0.896	91.784	0.803	0.0148	0.0013	0.0078	0.0015	0.002	7.87E-17	97.5	32.65	0.32
YANG SANG	232-48	2.04E-04	1.16E-06	119.036	0.452	122.017	0.415	0.0157	0.0006	0.01	0.0007	0.002	4.23E-16	97.6	43.32	0.16
YANG SANG	232-49	2.04E-04	1.16E-06	6655.987	171.694	6836.387	175.604	0.1947	0.0113	0.6105	0.0548	0.014	1.25E-17	97.4	1548.29	26.81
YANG SANG	232-50	2.04E-04	1.16E-06	82.26	0.274	87.626	0.272	0.0163	0.0003	0.0181	0.0003	0.002	6.59E-16	93.9	30.05	0.1
SIYOM	235-01	1.98E-04	1.21E-06	43.851	0.136	48.573	0.128	0.0156	0.0003	0.0159	0.0002	0.002	1.13E-15	90.3	15.57	0.05
SIYOM	235-02	1.98E-04	1.21E-06	43.471	0.255	44.045	0.207	0.0138	0.0007	0.0019	0.0005	0.002	1.94E-16	98.8	15.44	0.09
SIYOM	235-03	1.98E-04	1.21E-06	43.91	0.246	45.096	0.226	0.0133	0.0005	0.0039	0.0004	0.002	3.01E-16	97.4	15.59	0.09
SIYOM	235-04	1.98E-04	1.21E-06	45.504	1.268	47.36	0.694	0.0109	0.003	0.0062	0.0036	0.002	3.46E-17	96.1	16.16	0.45

SIYOM	235-05	1.98E-04	1.21E-06	45.311	0.177	45.858	0.162	0.0132	0.0004	0.0018	0.0002	0.002	4.63E-16	98.9	16.09	0.06
SIYOM	235-06	1.98E-04	1.21E-06	44.773	0.108	46.746	0.102	0.0153	0.0002	0.0066	0.0001	0.002	1.93E-15	95.8	15.9	0.04
SIYOM	235-07	1.98E-04	1.21E-06	44.768	0.145	48.445	0.134	0.0149	0.0003	0.0124	0.0002	0.002	8.18E-16	92.5	15.9	0.05
SIYOM	235-08	1.98E-04	1.21E-06	44.301	0.572	68.204	0.491	0.0284	0.0013	0.0808	0.0017	0.002	1.20E-16	65	15.73	0.2
SIYOM	235-09	1.98E-04	1.21E-06	45.202	0.219	47.987	0.184	0.0144	0.0004	0.0093	0.0004	0.002	4.06E-16	94.3	16.05	0.08
SIYOM	235-10	1.98E-04	1.21E-06	50.964	0.206	54.036	0.188	0.0155	0.0004	0.0103	0.0003	0.002	5.01E-16	94.4	18.09	0.07
SIYOM	235-11	1.98E-04	1.21E-06	43.877	0.302	45.011	0.265	0.0136	0.0006	0.0038	0.0005	0.002	2.29E-16	97.5	15.58	0.11
SIYOM	235-12	1.98E-04	1.21E-06	38.924	0.599	46.388	0.409	0.0151	0.0013	0.0252	0.0017	0.002	7.53E-17	84	13.83	0.21
SIYOM	235-13	1.98E-04	1.21E-06	44.511	0.208	46.941	0.181	0.0139	0.0004	0.0081	0.0004	0.002	4.51E-16	94.9	15.81	0.07
SIYOM	235-14	1.98E-04	1.21E-06	48.829	0.304	50.192	0.257	0.0133	0.0007	0.0045	0.0006	0.002	2.05E-16	97.3	17.33	0.11
SIYOM	235-15	1.98E-04	1.21E-06	45.899	0.341	49.694	0.273	0.0149	0.0008	0.0128	0.0008	0.002	1.73E-16	92.4	16.3	0.12
SIYOM	235-16	1.98E-04	1.21E-06	44.279	0.216	45.738	0.197	0.0137	0.0005	0.0049	0.0003	0.002	3.81E-16	96.9	15.72	0.08
SIYOM	235-17	1.98E-04	1.21E-06	49.222	0.312	57.087	0.271	0.0206	0.0007	0.0265	0.0007	0.003	3.16E-16	86.3	17.47	0.11
SIYOM	235-18	1.98E-04	1.21E-06	57.742	0.594	64.184	0.502	0.0177	0.0012	0.0217	0.0013	0.002	8.95E-17	90	20.48	0.21
SIYOM	235-19	1.98E-04	1.21E-06	40.401	4.004	46.949	1.652	0.0115	0.0095	0.0221	0.0017	0.001	9.18E-18	86.1	14.35	1.42
SIYOM	235-20	1.98E-04	1.21E-06	44.909	0.327	47.808	0.289	0.0138	0.0007	0.0097	0.0006	0.002	2.24E-16	94	15.95	0.12
SIYOM	235-21	1.98E-04	1.21E-06	44.623	0.496	49.457	0.347	0.0167	0.0013	0.0163	0.0013	0.002	9.24E-17	90.3	15.84	0.18
SIYOM	235-22	1.98E-04	1.21E-06	45.389	0.332	48.886	0.273	0.0146	0.0007	0.0117	0.0007	0.002	1.90E-16	92.9	16.12	0.12
SIYOM	235-23	1.98E-04	1.21E-06	44.198	0.271	54.419	0.238	0.0192	0.0005	0.0345	0.0006	0.002	3.17E-16	81.3	15.69	0.1
SIYOM	235-24	1.98E-04	1.21E-06	48.025	0.262	54.114	0.204	0.0203	0.0006	0.0205	0.0006	0.003	3.79E-16	88.8	17.05	0.09
SIYOM	235-25	1.98E-04	1.21E-06	45.91	0.132	52.444	0.123	0.0181	0.0002	0.022	0.0002	0.002	1.34E-15	87.6	16.3	0.05
SIYOM	235-26	1.98E-04	1.21E-06	44.686	0.131	50.431	0.122	0.0169	0.0002	0.0194	0.0002	0.002	1.38E-15	88.7	15.87	0.05
SIYOM	235-27	1.98E-04	1.21E-06	42.982	0.284	44.93	0.223	0.0137	0.0007	0.0065	0.0006	0.002	2.05E-16	95.7	15.26	0.1
SIYOM	235-28	1.98E-04	1.21E-06	44.606	0.238	46.594	0.215	0.0148	0.0006	0.0066	0.0004	0.002	3.17E-16	95.8	15.84	0.08
SIYOM	235-29	1.98E-04	1.21E-06	47.045	0.346	55.586	0.307	0.0199	0.0006	0.0288	0.0007	0.002	2.28E-16	84.7	16.7	0.12
SIYOM	235-30	1.98E-04	1.21E-06	41.879	0.282	42.621	0.23	0.0135	0.0007	0.0024	0.0006	0.002	2.00E-16	98.3	14.87	0.1
SIYOM	235-31	1.98E-04	1.21E-06	36.65	0.357	57.148	0.305	0.0271	0.0009	0.0693	0.0009	0.002	2.37E-16	64.2	13.02	0.13
SIYOM	235-32	1.98E-04	1.21E-06	48.33	0.337	54.936	0.274	0.0177	0.0007	0.0223	0.0008	0.002	2.27E-16	88	17.16	0.12
SIYOM	235-33	1.98E-04	1.21E-06	45.085	0.785	47.72	0.46	0.0159	0.002	0.0088	0.0022	0.002	5.08E-17	94.5	16.01	0.28
SIYOM	235-34	1.98E-04	1.21E-06	57.912	0.404	59.768	0.372	0.0138	0.0007	0.0062	0.0006	0.002	2.18E-16	96.9	20.54	0.14
SIYOM	235-35	1.98E-04	1.21E-06	47.95	0.353	50.65	0.313	0.015	0.0006	0.0091	0.0006	0.002	2.22E-16	94.7	17.02	0.12
SIYOM	235-36	1.98E-04	1.21E-06	42.195	0.372	43.754	0.288	0.013	0.0009	0.0052	0.0008	0.002	1.26E-16	96.5	14.99	0.13
SIYOM	235-37	1.98E-04	1.21E-06	42.996	0.151	47.169	0.135	0.0151	0.0003	0.014	0.0003	0.002	7.46E-16	91.2	15.27	0.05
SIYOM	235-38	1.98E-04	1.21E-06	45.136	0.338	52.667	0.292	0.0187	0.0007	0.0254	0.0007	0.002	2.26E-16	85.7	16.03	0.12
SIYOM	235-39	1.98E-04	1.21E-06	46.044	0.286	47.823	0.266	0.0137	0.0005	0.0059	0.0004	0.002	2.77E-16	96.3	16.35	0.1
SIYOM	235-40	1.98E-04	1.21E-06	44.124	0.231	45.256	0.208	0.0136	0.0005	0.0037	0.0004	0.002	3.29E-16	97.6	15.67	0.08
SIYOM	235-41	1.98E-04	1.21E-06	46.34	0.181	47.592	0.163	0.0145	0.0004	0.0042	0.0003	0.002	5.62E-16	97.4	16.45	0.06
SIYOM	235-42	1.98E-04	1.21E-06	43.637	0.164	44.589	0.153	0.0142	0.0004	0.0031	0.0002	0.002	5.02E-16	97.9	15.5	0.06
SIYOM	235-43	1.98E-04	1.21E-06	45.422	0.116	50.043	0.11	0.0155	0.0002	0.0156	0.0002	0.002	1.13E-15	90.8	16.13	0.04
SIYOM	235-44	1.98E-04	1.21E-06	45.788	0.142	47.244	0.133	0.0132	0.0003	0.0048	0.0002	0.002	6.67E-16	97	16.26	0.05
SIYOM	235-45	1.98E-04	1.21E-06	43.771	0.36	46.115	0.252	0.0147	0.0009	0.0078	0.0009	0.002	1.42E-16	95	15.54	0.13
SIYOM	235-46	1.98E-04	1.21E-06	44.151	0.386	48.182	0.288	0.016	0.0009	0.0136	0.0009	0.002	1.36E-16	91.7	15.68	0.14
SIYOM	235-47	1.98E-04	1.21E-06	44.864	0.294	46.078	0.237	0.0131	0.0007	0.004	0.0006	0.002	2.02E-16	97.4	15.93	0.1
SIYOM	235-48	1.98E-04	1.21E-06	47.661	0.176	50.464	0.145	0.0148	0.0004	0.0094	0.0004	0.002	7.09E-16	94.5	16.92	0.06
SIYOM	235-49	1.98E-04	1.21E-06	59.991	0.104	64.869	0.102	0.0163	0.0002	0.0164	0.0001	0.002	2.33E-15	92.5	21.27	0.04
SIYOM	235-50	1.98E-04	1.21E-06	44.506	0.069	48.398	0.064	0.0155	0.0002	0.0131	0.0001	0.002	3.28E-15	92	15.8	0.02

Siang River samples

KAPU (250-500 um)	230-01	1.95E-04	1.01E-06	27.656	0.187	29.841	0.132	0.0142	0.0005	0.0073	0.0005	0.002	2.69E-16	92.8	9.72	0.07
KAPU (250-500 um)	230-02	1.95E-04	1.01E-06	27.137	0.322	33.919	0.18	0.0157	0.0008	0.0229	0.001	0.002	2.40E-16	80.1	9.54	0.11
KAPU (250-500 um)	230-03	1.95E-04	1.01E-06	53.291	0.282	56.118	0.265	0.014	0.0005	0.0095	0.0004	0.002	3.14E-16	95	18.69	0.1
KAPU (250-500 um)	230-04	1.95E-04	1.01E-06	62.96	0.212	64.701	0.206	0.0132	0.0003	0.0058	0.0002	0.002	7.19E-16	97.4	22.06	0.07
KAPU (250-500 um)	230-05	1.95E-04	1.01E-06	18.644	0.273	22.713	0.145	0.0138	0.0009	0.0137	0.0008	0.002	1.38E-16	82.2	6.56	0.1
KAPU (250-500 um)	230-06	1.95E-04	1.01E-06	61.493	0.328	72.144	0.315	0.0202	0.0005	0.036	0.0006	0.002	3.97E-16	85.3	21.54	0.11
KAPU (250-500 um)	230-07	1.95E-04	1.01E-06	27.48	0.133	28.171	0.114	0.0133	0.0004	0.0023	0.0002	0.002	5.02E-16	97.6	9.66	0.05
KAPU (250-500 um)	230-08	1.95E-04	1.01E-06	26.238	0.123	26.683	0.107	0.0127	0.0004	0.0014	0.0002	0.002	4.89E-16	98.4	9.22	0.04

KAPU (250-500 um)	230-09	1.95E-04	1.01E-06	24.403	0.258	31.576	0.143	0.0174	0.0007	0.0242	0.0008	0.002	2.58E-16	77.4	8.58	0.09
KAPU (250-500 um)	230-10	1.95E-04	1.01E-06	43.645	0.223	46.481	0.193	0.014	0.0005	0.0095	0.0004	0.002	3.81E-16	94	15.32	0.08
KAPU (250-500 um)	230-11	1.95E-04	1.01E-06	43.962	0.447	47.456	0.32	0.014	0.001	0.0117	0.0011	0.002	1.14E-16	92.7	15.43	0.16
KAPU (250-500 um)	230-12	1.95E-04	1.01E-06	32.92	0.483	34.262	0.261	0.0155	0.0015	0.0045	0.0014	0.002	8.32E-17	96.2	11.57	0.17
KAPU (250-500 um)	230-13	1.95E-04	1.01E-06	54.373	0.502	59.237	0.392	0.0143	0.001	0.0164	0.0012	0.002	1.07E-16	91.8	19.06	0.18
KAPU (250-500 um)	230-14	1.95E-04	1.01E-06	31.184	0.214	32.588	0.14	0.0129	0.0006	0.0047	0.0006	0.002	2.21E-16	95.8	10.96	0.07
KAPU (250-500 um)	230-15	1.95E-04	1.01E-06	26.099	0.151	29.056	0.105	0.0144	0.0004	0.0099	0.0004	0.002	5.26E-16	89.9	9.18	0.05
KAPU (250-500 um)	230-16	1.95E-04	1.01E-06	1.108	0.523	20.961	0.129	0.029	0.0012	0.0671	0.0018	0.003	1.44E-16	5.3	0.39	0.18
KAPU (250-500 um)	230-17	1.95E-04	1.01E-06	27.248	0.433	30.27	0.237	0.0152	0.0012	0.0101	0.0013	0.002	9.60E-17	90.1	9.58	0.15
KAPU (250-500 um)	230-18	1.95E-04	1.01E-06	25.138	0.263	28.814	0.167	0.0158	0.0008	0.0124	0.0007	0.002	1.74E-16	87.3	8.84	0.09
KAPU (250-500 um)	230-19	1.95E-04	1.01E-06	402.371	1.782	404.265	1.784	0.0128	0.0005	0.0063	0.0005	0.002	3.07E-16	99.5	136.52	0.58
KAPU (250-500 um)	230-20	1.95E-04	1.01E-06	12.993	0.115	14.102	0.062	0.0134	0.0005	0.0037	0.0003	0.002	3.37E-16	92.3	4.57	0.04
KAPU (250-500 um)	230-21	1.95E-04	1.01E-06	14.603	0.318	18.816	0.104	0.0159	0.0008	0.0142	0.001	0.002	1.89E-16	77.7	5.14	0.11
KAPU (250-500 um)	230-22	1.95E-04	1.01E-06	15.456	0.081	16.516	0.065	0.0132	0.0003	0.0035	0.0002	0.002	7.66E-16	93.7	5.44	0.03
KAPU (250-500 um)	230-23	1.95E-04	1.01E-06	38.002	0.229	54.537	0.218	0.0254	0.0004	0.0559	0.0005	0.003	6.33E-16	69.7	13.34	0.08
KAPU (250-500 um)	230-24	1.95E-04	1.01E-06	0.873	0.429	6.411	0.073	0.0187	0.0015	0.0187	0.0014	0.003	9.33E-17	13.7	0.31	0.15
KAPU (250-500 um)	230-25	1.95E-04	1.01E-06	71.06	0.403	77.782	0.375	0.0171	0.0007	0.0227	0.0007	0.002	2.16E-16	91.4	24.87	0.14
KAPU (250-500 um)	230-26	1.95E-04	1.01E-06	19.498	0.248	30.466	0.141	0.0198	0.0007	0.037	0.0008	0.002	2.49E-16	64.1	6.86	0.09
KAPU (250-500 um)	230-27	1.95E-04	1.01E-06	24.473	0.278	25.788	0.131	0.0135	0.0008	0.0044	0.0008	0.002	2.60E-16	95	8.61	0.1
KAPU (250-500 um)	230-28	1.95E-04	1.01E-06	50.898	0.302	52.943	0.275	0.0156	0.0007	0.0068	0.0005	0.002	2.42E-16	96.2	17.85	0.11
KAPU (250-500 um)	230-29	1.95E-04	1.01E-06	16.764	0.874	35.639	0.328	0.0266	0.0022	0.0638	0.003	0.002	6.08E-17	47.1	5.9	0.31
KAPU (250-500 um)	230-30	1.95E-04	1.01E-06	23.001	0.169	24.607	0.109	0.0136	0.0006	0.0054	0.0005	0.002	2.54E-16	93.6	8.09	0.06
KAPU (250-500 um)	230-31	1.95E-04	1.01E-06	11.28	0.242	12.342	0.061	0.0137	0.0007	0.0035	0.0008	0.002	2.63E-16	91.6	3.97	0.09
KAPU (250-500 um)	230-32	1.95E-04	1.01E-06	22.623	0.395	23.773	0.164	0.0126	0.0012	0.0038	0.0012	0.002	1.02E-16	95.3	7.96	0.14
KAPU (250-500 um)	230-33	1.95E-04	1.01E-06	16.599	0.585	24.244	0.224	0.0181	0.0017	0.0258	0.0019	0.002	6.33E-17	68.5	5.84	0.21
KAPU (250-500 um)	230-34	1.95E-04	1.01E-06	39.525	0.206	40.833	0.181	0.0148	0.0005	0.0043	0.0004	0.002	3.24E-16	96.9	13.88	0.07
KAPU (250-500 um)	230-35	1.95E-04	1.01E-06	3.14	0.219	4.772	0.035	0.0055	0.0015	0.0055	0.0007	0.009	1.27E-16	66.2	1.11	0.08
KAPU (250-500 um)	230-36	1.95E-04	1.01E-06	6.829	0.083	8.935	0.035	0.018	0.0005	0.007	0.0003	0.003	4.58E-16	76.7	2.41	0.03
KAPU (250-500 um)	230-37	1.95E-04	1.01E-06	15.754	0.197	16.732	0.068	0.0144	0.0006	0.0032	0.0006	0.002	3.33E-16	94.3	5.54	0.07
KAPU (250-500 um)	230-38	1.95E-04	1.01E-06	65.699	0.5	67.435	0.428	0.013	0.0009	0.0058	0.0009	0.002	1.20E-16	97.5	23.01	0.17
KAPU (250-500 um)	230-39	1.95E-04	1.01E-06	71.266	0.994	73.42	0.805	0.0119	0.0019	0.0072	0.0021	0.002	4.87E-17	97.1	24.95	0.35
KAPU (250-500 um)	230-40	1.95E-04	1.01E-06	1.614	1.943	11.448	0.28	0.0185	0.0053	0.0332	0.0066	0.002	1.44E-17	14.1	0.57	0.68
KAPU (250-500 um)	230-41	1.95E-04	1.01E-06	72.68	0.406	82.796	0.363	0.0188	0.0007	0.0342	0.0008	0.002	2.32E-16	87.8	25.44	0.14
KAPU (250-500 um)	230-42	1.95E-04	1.01E-06	68.738	0.512	69.236	0.471	0.0127	0.0008	0.0016	0.0007	0.002	1.52E-16	99.3	24.07	0.18
KAPU (250-500 um)	230-43	1.95E-04	1.01E-06	46.01	0.258	47.481	0.234	0.0127	0.0005	0.0049	0.0004	0.002	3.10E-16	97	16.14	0.09
KAPU (250-500 um)	230-44	1.95E-04	1.01E-06	20.855	0.288	23.844	0.156	0.0146	0.0009	0.01	0.0009	0.002	1.28E-16	87.6	7.34	0.1
KAPU (250-500 um)	230-45	1.95E-04	1.01E-06	32.934	0.24	39.151	0.196	0.0176	0.0007	0.021	0.0006	0.002	2.42E-16	84.2	11.57	0.08
KAPU (250-500 um)	230-46	1.95E-04	1.01E-06	23.266	0.188	26.8	0.124	0.0153	0.0006	0.0119	0.0005	0.002	3.19E-16	86.9	8.18	0.07
KAPU (250-500 um)	230-47	1.95E-04	1.01E-06	210.916	1.506	218.067	1.51	0.0169	0.0012	0.0241	0.0012	0.002	1.11E-16	96.7	72.85	0.51
KAPU (250-500 um)	230-48	1.95E-04	1.01E-06	21.472	1.538	35.25	0.563	0.0187	0.0037	0.0465	0.0051	0.002	2.21E-17	61	7.55	0.54
KAPU (250-500 um)	230-49	1.95E-04	1.01E-06	1.937	0.09	3.141	0.015	0.0151	0.0004	0.004	0.0003	0.002	5.14E-16	62.2	0.68	0.03
KAPU (250-500 um)	230-50	1.95E-04	1.01E-06	22.977	0.527	42.452	0.323	0.0236	0.0013	0.0658	0.0017	0.002	9.86E-17	54.2	8.08	0.18
KAPU (500-1000 um)	228-01	1.94E-04	1.15E-06	33.478	0.094	34.346	0.089	0.0132	0.0003	0.0029	0.0001	0.002	1.02E-15	97.6	11.68	0.03
KAPU (500-1000 um)	228-02	1.94E-04	1.15E-06	34.938	0.204	49.042	0.176	0.0259	0.0005	0.0477	0.0005	0.003	4.99E-16	71.3	12.18	0.07
KAPU (500-1000 um)	228-03	1.94E-04	1.15E-06	24.808	0.11	29.354	0.096	0.0156	0.0003	0.0153	0.0002	0.002	7.65E-16	84.6	8.66	0.04
KAPU (500-1000 um)	228-04	1.94E-04	1.15E-06	28.099	0.098	31.07	0.087	0.0152	0.0002	0.01	0.0002	0.002	1.02E-15	90.5	9.81	0.03
KAPU (500-1000 um)	228-05	1.94E-04	1.15E-06	45.124	0.265	61.299	0.235	0.0244	0.0006	0.0547	0.0006	0.002	3.92E-16	73.6	15.72	0.09
KAPU (500-1000 um)	228-06	1.94E-04	1.15E-06	349.71	1.492	352.598	1.497	0.0137	0.0006	0.0097	0.0004	0.002	2.87E-16	99.2	118.4	0.49
KAPU (500-1000 um)	228-07	1.94E-04	1.15E-06	35.998	0.205	38.799	0.185	0.0163	0.0005	0.0094	0.0003	0.002	4.19E-16	92.8	12.55	0.07
KAPU (500-1000 um)	228-08	1.94E-04	1.15E-06	78.574	0.314	82.585	0.31	0.0151	0.0004	0.0135	0.0003	0.002	4.78E-16	95.2	27.29	0.11
KAPU (500-1000 um)	228-09	1.94E-04	1.15E-06	8.379	0.126	12.474	0.048	0.0163	0.0005	0.0138	0.0004	0.002	3.52E-16	67.3	2.93	0.04
KAPU (500-1000 um)	228-10	1.94E-04	1.15E-06	78.289	0.323	80.572	0.31	0.0139	0.0004	0.0076	0.0004	0.002	3.51E-16	97.2	27.19	0.11
KAPU (500-1000 um)	228-11	1.94E-04	1.15E-06	65.023	0.314	69.31	0.3	0.0155	0.0005	0.0144	0.0004	0.002	3.50E-16	93.9	22.61	0.11
KAPU (500-1000 um)	228-12	1.94E-04	1.15E-06	50.212	0.173	56.841	0.164	0.0173	0.0003	0.0224	0.0003	0.002	8.51E-16	88.4	17.49	0.06
KAPU (500-1000 um)	228-13	1.94E-04	1.15E-06	24.378	0.129	25.397	0.111	0.0137	0.0004	0.0034	0.0002	0.002	4.89E-16	96.1	8.51	0.05

KAPU (500-1000 um)	228-14	1.94E-04	1.15E-06	69.495	0.206	70.408	0.203	0.0132	0.0002	0.003	0.0001	0.002	9.60E-16	98.7	24.16	0.07
KAPU (500-1000 um)	228-15	1.94E-04	1.15E-06	12.127	0.09	16.974	0.06	0.0159	0.0003	0.0163	0.0002	0.002	8.34E-16	71.6	4.24	0.03
KAPU (500-1000 um)	228-16	1.94E-04	1.15E-06	67.061	0.268	69.601	0.255	0.0139	0.0005	0.0085	0.0003	0.002	4.19E-16	96.4	23.32	0.09
KAPU (500-1000 um)	228-17	1.94E-04	1.15E-06	22.974	0.15	26.067	0.123	0.0157	0.0004	0.0104	0.0003	0.002	4.41E-16	88.2	8.02	0.05
KAPU (500-1000 um)	228-18	1.94E-04	1.15E-06	21.836	0.118	26.521	0.091	0.0159	0.0003	0.0158	0.0003	0.002	7.78E-16	82.4	7.63	0.04
KAPU (500-1000 um)	228-19	1.94E-04	1.15E-06	47.219	0.158	48.285	0.15	0.0131	0.0003	0.0035	0.0002	0.002	7.50E-16	97.8	16.45	0.05
KAPU (500-1000 um)	228-20	1.94E-04	1.15E-06	56.498	0.141	61.167	0.139	0.0154	0.0002	0.0157	0.0001	0.002	2.17E-15	92.4	19.66	0.05
KAPU (500-1000 um)	228-21	1.94E-04	1.15E-06	64.858	0.215	67.853	0.211	0.0138	0.0003	0.0101	0.0002	0.002	8.29E-16	95.6	22.55	0.07
KAPU (500-1000 um)	228-22	1.94E-04	1.15E-06	4.675	0.065	6.665	0.019	0.0148	0.0003	0.0066	0.0002	0.002	7.33E-16	70.4	1.64	0.02
KAPU (500-1000 um)	228-23	1.94E-04	1.15E-06	42.851	0.14	45.839	0.133	0.0152	0.0003	0.01	0.0002	0.002	8.99E-16	93.5	14.93	0.05
KAPU (500-1000 um)	228-53	1.94E-04	1.15E-06	42.18	0.154	48.224	0.131	0.0175	0.0003	0.0204	0.0003	0.002	8.98E-16	87.5	14.7	0.05
KAPU (500-1000 um)	228-54	1.94E-04	1.15E-06	57.452	0.295	61.685	0.275	0.0152	0.0005	0.0142	0.0005	0.002	3.28E-16	93.2	19.99	0.1
KAPU (500-1000 um)	228-55	1.94E-04	1.15E-06	48.843	0.21	49.927	0.198	0.0131	0.0004	0.0036	0.0003	0.002	4.41E-16	97.9	17.01	0.07
KAPU (500-1000 um)	228-56	1.94E-04	1.15E-06	70.084	0.324	71.17	0.308	0.0131	0.0005	0.0036	0.0004	0.002	3.47E-16	98.5	24.36	0.11
KAPU (500-1000 um)	228-57	1.94E-04	1.15E-06	29.747	0.199	32.06	0.153	0.0168	0.0006	0.0077	0.0005	0.003	2.47E-16	92.9	10.38	0.07
KAPU (500-1000 um)	228-58	1.94E-04	1.15E-06	58.434	0.27	61.109	0.254	0.0145	0.0005	0.009	0.0004	0.002	3.74E-16	95.7	20.33	0.09
KAPU (500-1000 um)	228-59	1.94E-04	1.15E-06	66.998	0.206	70.473	0.201	0.014	0.0003	0.0117	0.0002	0.002	9.88E-16	95.1	23.29	0.07
KAPU (500-1000 um)	228-60	1.94E-04	1.15E-06	51.348	0.293	53.347	0.272	0.0159	0.0006	0.0067	0.0004	0.002	2.82E-16	96.3	17.88	0.1
KAPU (500-1000 um)	228-61	1.94E-04	1.15E-06	58.434	0.266	64.02	0.254	0.0164	0.0005	0.0188	0.0004	0.002	4.28E-16	91.3	20.33	0.09
KAPU (500-1000 um)	228-62	1.94E-04	1.15E-06	323.701	1.865	345.357	1.925	0.0694	0.0016	0.0732	0.0015	0.009	1.46E-16	93.7	109.86	0.61
KAPU (500-1000 um)	228-63	1.94E-04	1.15E-06	19.348	0.305	29.255	0.173	0.0185	0.0009	0.0334	0.001	0.002	1.59E-16	66.2	6.76	0.11
KAPU (500-1000 um)	228-64	1.94E-04	1.15E-06	30.96	0.295	40.514	0.231	0.0181	0.0008	0.0322	0.0008	0.002	2.08E-16	76.5	10.8	0.1
KAPU (500-1000 um)	228-65	1.94E-04	1.15E-06	43.822	0.206	46.424	0.188	0.0146	0.0004	0.0087	0.0003	0.002	3.94E-16	94.5	15.27	0.07
KAPU (500-1000 um)	228-66	1.94E-04	1.15E-06	68.592	0.764	69.548	0.635	0.0115	0.0015	0.0032	0.0015	0.002	6.59E-17	98.7	23.84	0.26
KAPU (500-1000 um)	228-67	1.94E-04	1.15E-06	31.076	0.197	31.891	0.173	0.0132	0.0005	0.0027	0.0003	0.002	3.93E-16	97.5	10.84	0.07
KAPU (500-1000 um)	228-68	1.94E-04	1.15E-06	58.172	0.488	61.561	0.407	0.0176	0.001	0.0114	0.001	0.003	1.25E-16	94.5	20.24	0.17
KAPU (500-1000 um)	228-69	1.94E-04	1.15E-06	6.441	0.467	26.6	0.208	0.0531	0.002	0.0682	0.0017	0.007	9.86E-17	24.2	2.25	0.16
KAPU (500-1000 um)	228-70	1.94E-04	1.15E-06	77.959	18.877	2303.625	94.458	1.419	0.0683	7.5318	0.3137	0.001	6.69E-18	3.4	27.08	6.51
KAPU (500-1000 um)	228-71	1.94E-04	1.15E-06	50.571	0.337	53.515	0.314	0.014	0.0007	0.0099	0.0005	0.002	2.41E-16	94.5	17.61	0.12
KAPU (500-1000 um)	228-72	1.94E-04	1.15E-06	194.737	0.762	196.542	0.761	0.0138	0.0004	0.006	0.0003	0.002	4.02E-16	99.1	66.89	0.26
KAPU (500-1000 um)	228-73	1.94E-04	1.15E-06	74.853	0.616	89.457	0.601	0.0222	0.001	0.0493	0.0011	0.002	1.29E-16	83.7	26.01	0.21
KAPU (500-1000 um)	228-74	1.94E-04	1.15E-06	56.034	0.228	57.899	0.216	0.0147	0.0004	0.0062	0.0003	0.002	4.76E-16	96.8	19.5	0.08
KAPU (500-1000 um)	228-75	1.94E-04	1.15E-06	0.988	0.354	6.868	0.05	0.0166	0.0011	0.0198	0.0012	0.002	1.04E-16	14.4	0.35	0.12
KAPU (500-1000 um)	228-76	1.94E-04	1.15E-06	30.35	0.465	34.61	0.293	0.0171	0.0014	0.0143	0.0013	0.002	8.24E-17	87.8	10.59	0.16
KAPU (500-1000 um)	228-77	1.94E-04	1.15E-06	60.291	0.32	67.332	0.314	0.0179	0.0005	0.0237	0.0005	0.002	3.75E-16	89.6	20.98	0.11
KAPU (500-1000 um)	228-78	1.94E-04	1.15E-06	72.165	0.425	83.991	0.421	0.0197	0.0006	0.0399	0.0007	0.002	3.02E-16	85.9	25.08	0.15
KAPU (500-1000 um)	228-79	1.94E-04	1.15E-06	51.147	0.771	58.93	0.572	0.0156	0.0018	0.0263	0.002	0.002	6.27E-17	86.8	17.81	0.27
KAPU (500-1000 um)	228-80	1.94E-04	1.15E-06	18.874	0.224	24.645	0.124	0.0161	0.0007	0.0194	0.0007	0.002	1.92E-16	76.7	6.59	0.08
KAPU (500-1000 um)	228-81	1.94E-04	1.15E-06	18.994	0.121	24.068	0.083	0.0159	0.0003	0.0171	0.0003	0.002	7.28E-16	79	6.63	0.04
KAPU (500-1000 um)	228-82	1.94E-04	1.15E-06	28.706	0.197	29.042	0.168	0.0131	0.0004	0.0011	0.0004	0.002	3.65E-16	98.9	10.02	0.07
KAPU (500-1000 um)	228-83	1.94E-04	1.15E-06	61.213	0.147	61.734	0.144	0.0128	0.0002	0.0017	0.0001	0.002	1.20E-15	99.2	21.29	0.05
KAPU (500-1000 um)	228-84	1.94E-04	1.15E-06	121.698	1.379	123.808	1.26	0.0138	0.0017	0.0071	0.002	0.002	4.37E-17	98.3	42.09	0.47
KAPU (500-1000 um)	228-85	1.94E-04	1.15E-06	67.751	0.704	85.114	0.626	0.024	0.0015	0.0587	0.0017	0.002	8.00E-17	79.6	23.55	0.24
KAPU (500-1000 um)	228-86	1.94E-04	1.15E-06	1.609	0.171	2.77	0.016	0.0159	0.0008	0.0039	0.0006	0.003	2.11E-16	58.7	0.56	0.06
KAPU (500-1000 um)	228-87	1.94E-04	1.15E-06	30.05	0.146	33.672	0.129	0.0158	0.0003	0.0122	0.0003	0.002	6.92E-16	89.3	10.49	0.05
KAPU (500-1000 um)	228-88	1.94E-04	1.15E-06	128.048	0.628	137.944	0.631	0.0191	0.0006	0.0334	0.0007	0.002	2.50E-16	92.8	44.26	0.21
KAPU (500-1000 um)	228-89	1.94E-04	1.15E-06	30.807	0.213	38.2	0.173	0.0183	0.0005	0.0249	0.0005	0.002	5.02E-16	80.7	10.75	0.07
KAPU (500-1000 um)	228-90	1.94E-04	1.15E-06	57.105	0.363	59.289	0.337	0.014	0.0007	0.0073	0.0005	0.002	2.58E-16	96.4	19.87	0.13
KAPU (500-1000 um)	228-91	1.94E-04	1.15E-06	35.189	0.225	39.453	0.202	0.0188	0.0004	0.0144	0.0004	0.003	3.70E-16	89.3	12.27	0.08
KAPU (500-1000 um)	228-92	1.94E-04	1.15E-06	21.585	0.574	48.161	0.353	0.0298	0.0014	0.0899	0.002	0.002	1.11E-16	44.8	7.54	0.2
KAPU (500-1000 um)	228-93	1.94E-04	1.15E-06	355.359	2.542	367.933	2.584	0.0205	0.0012	0.0425	0.0014	0.002	1.04E-16	96.6	120.25	0.83
KAPU (500-1000 um)	228-94	1.94E-04	1.15E-06	58.638	0.54	63.397	0.435	0.0172	0.0011	0.016	0.0012	0.002	1.09E-16	92.5	20.4	0.19
KAPU (500-1000 um)	228-95	1.94E-04	1.15E-06	124.977	1.868	125.097	1.469	0.0114	0.0031	0.0003	0.0039	0.002	4.17E-17	99.9	43.21	0.64
KAPU (500-1000 um)	228-96	1.94E-04	1.15E-06	31.396	0.394	38.118	0.268	0.0168	0.001	0.0227	0.0011	0.002	1.10E-16	82.4	10.95	0.14
KAPU (500-1000 um)	228-97	1.94E-04	1.15E-06	1.768	0.556	12.537	0.122	0.0212	0.0017	0.0364	0.0019	0.002	7.11E-17	14.1	0.62	0.19
KAPU (500-1000 um)	228-98	1.94E-04	1.15E-06	63.824	0.264	68.113	0.258	0.0158	0.0004	0.0144	0.0003	0.002	5.23E-16	93.7	22.2	0.09

KAPU (500-1000 um)	228-99	1.94E-04	1.15E-06	43.174	0.218	45.377	0.203	0.0148	0.0004	0.0074	0.0003	0.002	4.24E-16	95.2	15.05	0.08
KAPU (500-1000 um)	228-100	1.94E-04	1.15E-06	22.509	0.115	24.138	0.103	0.0139	0.0003	0.0054	0.0002	0.002	6.38E-16	93.4	7.86	0.04
KAPU (500-1000 um)	228-101	1.94E-04	1.15E-06	22.583	0.414	25.774	0.199	0.0163	0.0012	0.0107	0.0013	0.002	9.60E-17	87.7	7.89	0.14
KAPU (500-1000 um)	228-102	1.94E-04	1.15E-06	34.452	0.407	43.581	0.254	0.0196	0.001	0.0308	0.0012	0.002	1.48E-16	79.1	12.02	0.14
KAPU (500-1000 um)	228-103	1.94E-04	1.15E-06	2.699	0.076	9.013	0.021	0.0342	0.0004	0.0213	0.0003	0.005	9.89E-16	30	0.94	0.03
KAPU (500-1000 um)	228-104	1.94E-04	1.15E-06	17.889	0.297	24.178	0.154	0.015	0.0009	0.0212	0.0009	0.002	1.49E-16	74.1	6.25	0.1
KAPU (500-1000 um)	228-105	1.94E-04	1.15E-06	52.225	0.433	56.161	0.375	0.0169	0.0009	0.0132	0.0009	0.002	1.31E-16	93	18.18	0.15
KAPU (500-1000 um)	228-106	1.94E-04	1.15E-06	42.048	0.311	48.643	0.278	0.0171	0.0006	0.0222	0.0006	0.002	2.63E-16	86.5	14.65	0.11
NUBO	225-01	2.04E-04	1.04E-06	35.793	0.567	41.34	0.359	0.0163	0.0015	0.0187	0.0016	0.002	6.44E-17	86.64	13.11	0.21
NUBO	225-02	2.04E-04	1.04E-06	51.473	1.238	60.298	0.803	0.0172	0.0028	0.0298	0.0035	0.002	3.45E-17	85.4	18.82	0.45
NUBO	225-03	2.04E-04	1.04E-06	21.497	1.27	31.166	0.478	0.0173	0.0032	0.0326	0.0042	0.002	2.54E-17	69.04	7.88	0.46
NUBO	225-04	2.04E-04	1.04E-06	46.001	0.335	52.557	0.272	0.017	0.0007	0.0221	0.0008	0.002	1.71E-16	87.57	16.83	0.12
NUBO	225-05	2.04E-04	1.04E-06	48.105	0.626	74.336	0.483	0.0303	0.0013	0.0887	0.0019	0.002	1.13E-16	64.74	17.6	0.23
NUBO	225-06	2.04E-04	1.04E-06	68.639	0.262	69.58	0.253	0.0136	0.0003	0.0031	0.0003	0.002	5.72E-16	98.69	25.06	0.09
NUBO	225-07	2.04E-04	1.04E-06	47.248	0.158	48.222	0.155	0.0133	0.0002	0.0032	0.0001	0.002	1.11E-15	98.04	17.28	0.06
NUBO	225-08	2.04E-04	1.04E-06	38.187	0.268	41.932	0.231	0.0144	0.0005	0.0126	0.0005	0.002	2.95E-16	91.13	13.98	0.1
NUBO	225-09	2.04E-04	1.04E-06	1.103	0.113	3.018	0.014	0.0153	0.0005	0.0064	0.0004	0.002	3.54E-16	36.89	0.41	0.04
NUBO	225-10	2.04E-04	1.04E-06	70.989	0.258	73.874	0.249	0.0143	0.0004	0.0097	0.0003	0.002	5.41E-16	96.13	25.91	0.09
NUBO	225-11	2.04E-04	1.04E-06	434.336	1.254	447.873	1.274	0.0545	0.0006	0.0458	0.0004	0.008	8.92E-16	96.98	152.98	0.42
NUBO	225-12	2.04E-04	1.04E-06	20.485	0.201	31.236	0.127	0.0205	0.0005	0.0363	0.0006	0.002	5.01E-16	65.64	7.51	0.07
NUBO	225-13	2.04E-04	1.04E-06	1.494	0.263	2.248	0.087	0.0288	0.0008	0.0702	0.0009	0.003	2.84E-16	6.72	0.55	0.1
NUBO	225-14	2.04E-04	1.04E-06	59.353	0.234	61.996	0.227	0.0143	0.0004	0.0089	0.0003	0.002	4.93E-16	95.78	21.69	0.08
NUBO	225-15	2.04E-04	1.04E-06	18.828	0.12	24.964	0.092	0.0175	0.0004	0.0207	0.0003	0.002	6.61E-16	75.51	6.91	0.04
NUBO	225-16	2.04E-04	1.04E-06	59.554	0.178	68.761	0.168	0.0187	0.0003	0.0311	0.0003	0.002	1.35E-15	86.64	21.76	0.06
NUBO	225-17	2.04E-04	1.04E-06	31.642	0.085	33.821	0.079	0.0251	0.0003	0.0073	0.0001	0.004	1.48E-15	93.63	11.59	0.03
NUBO	225-18	2.04E-04	1.04E-06	485.853	1.018	492.383	1.023	0.0208	0.0002	0.022	0.0002	0.003	2.66E-15	98.68	170.29	0.34
NUBO	225-19	2.04E-04	1.04E-06	23.048	0.072	24.564	0.064	0.0156	0.0003	0.005	0.0001	0.002	1.39E-15	93.94	8.45	0.03
NUBO	225-20	2.04E-04	1.04E-06	26.168	0.201	30.287	0.142	0.0164	0.0005	0.0139	0.0005	0.002	4.69E-16	86.48	9.59	0.07
NUBO	225-21	2.04E-04	1.04E-06	67.27	0.334	71.695	0.322	0.0157	0.0005	0.0149	0.0004	0.002	3.49E-16	93.87	24.56	0.12
NUBO	225-22	2.04E-04	1.04E-06	665.37	3.365	671.81	3.384	0.0169	0.0008	0.0217	0.0007	0.002	1.92E-16	99.05	229.36	1.09
NUBO	225-23	2.04E-04	1.04E-06	74.946	0.3	76.967	0.29	0.0135	0.0004	0.0068	0.0003	0.002	4.62E-16	97.41	27.34	0.11
NUBO	225-24	2.04E-04	1.04E-06	2.169	0.158	11.951	0.048	0.0194	0.0005	0.033	0.0005	0.002	4.43E-16	18.19	0.8	0.06
NUBO	225-25	2.04E-04	1.04E-06	20.569	0.168	22.453	0.116	0.0141	0.0006	0.0063	0.0004	0.002	2.65E-16	91.72	7.54	0.06
NUBO	225-26	2.04E-04	1.04E-06	15.683	0.103	18.278	0.08	0.0147	0.0004	0.0087	0.0002	0.002	6.56E-16	85.94	5.76	0.04
NUBO	225-27	2.04E-04	1.04E-06	13.372	0.077	14.475	0.048	0.0135	0.0004	0.0037	0.0002	0.002	5.47E-16	92.56	4.91	0.03
NUBO	225-28	2.04E-04	1.04E-06	44.806	0.228	48.941	0.208	0.0149	0.0005	0.0139	0.0004	0.002	3.20E-16	91.6	16.4	0.08
NUBO	225-29	2.04E-04	1.04E-06	25.998	0.324	45.318	0.241	0.0244	0.0007	0.0653	0.0009	0.002	2.59E-16	57.4	9.53	0.12
NUBO	225-30	2.04E-04	1.04E-06	54.025	0.423	62.786	0.319	0.0184	0.001	0.0296	0.0011	0.002	1.32E-16	86.09	19.75	0.15
NUBO	225-31	2.04E-04	1.04E-06	43.556	0.32	47.839	0.275	0.0151	0.0008	0.0144	0.0007	0.002	1.83E-16	91.1	15.94	0.12
NUBO	225-32	2.04E-04	1.04E-06	22.728	0.1	25.816	0.074	0.0153	0.0003	0.0104	0.0002	0.002	1.07E-15	88.13	8.34	0.04
NUBO	225-33	2.04E-04	1.04E-06	58.757	0.208	64.17	0.2	0.0163	0.0004	0.0182	0.0003	0.002	6.45E-16	91.61	21.47	0.08
NUBO	225-34	2.04E-04	1.04E-06	71.06	0.445	71.993	0.419	0.0132	0.0007	0.0031	0.0005	0.002	1.96E-16	98.74	25.93	0.16
NUBO	225-35	2.04E-04	1.04E-06	250.122	1.989	263.566	2.017	0.0216	0.0013	0.0454	0.0017	0.002	8.07E-17	94.91	89.67	0.7
NUBO	225-36	2.04E-04	1.04E-06	383.064	1.969	383.432	1.951	0.0126	0.0009	0.0012	0.0009	0.002	1.59E-16	99.91	135.58	0.67
NUBO	225-37	2.04E-04	1.04E-06	50.752	0.563	58.655	0.446	0.0176	0.0012	0.0267	0.0014	0.002	8.32E-17	86.57	18.56	0.2
NUBO	225-38	2.04E-04	1.04E-06	64.072	0.268	72.203	0.255	0.0176	0.0005	0.0274	0.0004	0.002	4.67E-16	88.77	23.4	0.1
NUBO	225-39	2.04E-04	1.04E-06	417.901	2.096	447.303	2.194	0.0303	0.0007	0.0994	0.0011	0.002	2.67E-16	93.43	147.42	0.71
NUBO	225-40	2.04E-04	1.04E-06	63.096	0.201	71.849	0.198	0.0178	0.0003	0.0295	0.0002	0.002	1.28E-15	87.85	23.05	0.07
NUBO	225-41	2.04E-04	1.04E-06	60.793	0.479	108.817	0.443	0.0436	0.0009	0.1624	0.0013	0.002	2.57E-16	55.88	22.21	0.17
NUBO	225-42	2.04E-04	1.04E-06	73.644	0.482	78.084	0.444	0.0153	0.0007	0.0149	0.0008	0.002	1.77E-16	94.35	26.87	0.17
NUBO	225-43	2.04E-04	1.04E-06	60.27	0.301	61.66	0.287	0.0134	0.0004	0.0046	0.0004	0.002	2.92E-16	97.79	22.02	0.11
NUBO	225-44	2.04E-04	1.04E-06	44.933	0.208	50.144	0.183	0.0155	0.0004	0.0176	0.0004	0.002	4.66E-16	89.66	16.44	0.08
NUBO	225-45	2.04E-04	1.04E-06	17.789	0.135	20.351	0.099	0.0145	0.0004	0.0086	0.0003	0.002	5.56E-16	87.53	6.53	0.05
NUBO	225-46	2.04E-04	1.04E-06	67.263	0.399	71.632	0.382	0.0155	0.0006	0.0147	0.0006	0.002	2.39E-16	93.94	24.56	0.14
NUBO	225-47	2.04E-04	1.04E-06	66.928	0.643	70.588	0.561	0.0142	0.0011	0.0123	0.0012	0.002	8.26E-17	94.85	24.44	0.23

NUBO	225-48	2.04E-04	1.04E-06	44.853	0.116	54.095	0.115	0.0294	0.0002	0.0312	0.0001	0.004	5.77E-15	82.96	16.41	0.04
NUBO	225-49	2.04E-04	1.04E-06	63.594	0.131	65.306	0.13	0.0137	0.0001	0.0057	0.0001	0.002	6.78E-15	97.42	23.23	0.05
NUBO	225-50	2.04E-04	1.04E-06	51.342	0.174	52.495	0.168	0.0141	0.0003	0.0038	0.0002	0.002	7.08E-16	97.86	18.77	0.06
NUBO	225-51	2.04E-04	1.04E-06	61.452	0.208	71.469	0.206	0.0192	0.0002	0.0338	0.0003	0.002	1.25E-15	86.02	22.45	0.08
NUBO	225-52	2.04E-04	1.04E-06	13.519	0.107	17.266	0.059	0.0147	0.0004	0.0126	0.0003	0.002	4.38E-16	78.43	4.96	0.04
NUBO	225-53	2.04E-04	1.04E-06	74.08	0.367	82.95	0.374	0.018	0.0002	0.0299	0.0002	0.002	2.37E-15	89.34	27.03	0.13
NUBO	225-54	2.04E-04	1.04E-06	77.289	0.307	80.213	0.305	0.0146	0.0003	0.0098	0.0003	0.002	5.63E-16	96.39	28.19	0.11
NUBO	225-55	2.04E-04	1.04E-06	19.311	0.254	20.451	0.127	0.014	0.0008	0.0038	0.0008	0.002	1.30E-16	94.56	7.08	0.09
NUBO	225-56	2.04E-04	1.04E-06	21.443	0.156	22.765	0.097	0.0134	0.0005	0.0044	0.0004	0.002	2.66E-16	94.31	7.86	0.06
NUBO	225-57	2.04E-04	1.04E-06	26.851	0.304	33.833	0.202	0.0176	0.0007	0.0236	0.0009	0.002	1.69E-16	79.43	9.84	0.11
NUBO	225-58	2.04E-04	1.04E-06	59.822	0.481	64.546	0.495	0.0159	0.0003	0.0159	0.0002	0.002	3.21E-15	92.72	21.86	0.17
NUBO	225-59	2.04E-04	1.04E-06	1.982	0.071	3.243	0.013	0.0143	0.0003	0.0042	0.0002	0.002	8.80E-16	61.63	0.73	0.03
NUBO	225-60	2.04E-04	1.04E-06	10.746	0.492	26.946	0.195	0.0252	0.0012	0.0547	0.0017	0.003	9.14E-17	39.92	3.95	0.18
NUBO	225-61	2.04E-04	1.04E-06	48.767	1.664	68.229	1.224	0.0226	0.0034	0.0658	0.0049	0.002	2.34E-17	71.5	17.84	0.61
NUBO	225-62	2.04E-04	1.04E-06	1.402	1.191	24.148	0.336	0.0257	0.0029	0.0769	0.0042	0.002	3.16E-17	5.81	0.52	0.44
NUBO	225-63	2.04E-04	1.04E-06	75.859	0.4	88.147	0.395	0.0198	0.0006	0.0415	0.0006	0.002	3.06E-16	86.09	27.67	0.14
NUBO	225-64	2.04E-04	1.04E-06	2.178	0.339	8.833	0.07	0.022	0.0011	0.0224	0.0011	0.003	1.02E-16	24.74	0.8	0.12
NUBO	225-65	2.04E-04	1.04E-06	75.001	0.797	78.155	0.721	0.0142	0.0012	0.0106	0.0013	0.002	7.07E-17	96	27.36	0.29
PASIGHAT	239-04	2.01E-04	1.26E-06	12.892	0.234	15.872	0.086	0.0144	0.0008	0.01	0.0008	0.002	1.53E-16	81.4	4.68	0.08
PASIGHAT	239-05	2.01E-04	1.26E-06	72.46	0.391	73.531	0.372	0.0135	0.0006	0.0035	0.0004	0.002	2.21E-16	98.6	26.12	0.14
PASIGHAT	239-06	2.01E-04	1.26E-06	57.223	0.315	61.518	0.293	0.0146	0.0006	0.0145	0.0005	0.002	2.79E-16	93.1	20.66	0.11
PASIGHAT	239-07	2.01E-04	1.26E-06	23.053	0.132	23.859	0.099	0.0134	0.0004	0.0026	0.0003	0.002	4.68E-16	96.7	8.35	0.05
PASIGHAT	239-08	2.01E-04	1.26E-06	23.063	0.169	26.402	0.104	0.0142	0.0006	0.0112	0.0005	0.002	2.93E-16	87.4	8.36	0.06
PASIGHAT	239-09	2.01E-04	1.26E-06	51.376	0.429	53.28	0.345	0.0131	0.001	0.0064	0.0009	0.002	1.18E-16	96.5	18.56	0.15
PASIGHAT	239-10	2.01E-04	1.26E-06	73.748	0.877	81.825	0.754	0.0159	0.0017	0.0272	0.0019	0.002	5.98E-17	90.2	26.58	0.31
PASIGHAT	239-11	2.01E-04	1.26E-06	3.936	0.179	14.95	0.058	0.0191	0.0005	0.0372	0.0006	0.002	3.65E-16	26.4	1.43	0.07
PASIGHAT	239-12	2.01E-04	1.26E-06	77.723	0.79	96.786	0.69	0.0243	0.0013	0.0644	0.0018	0.002	1.16E-16	80.3	28.01	0.28
PASIGHAT	239-13	2.01E-04	1.26E-06	2.788	0.17	6.889	0.031	0.0233	0.0008	0.0138	0.0006	0.003	2.44E-16	40.6	1.01	0.06
PASIGHAT	239-14	2.01E-04	1.26E-06	32.858	0.224	36.765	0.187	0.0148	0.0005	0.0131	0.0005	0.002	2.74E-16	89.4	11.89	0.08
PASIGHAT	239-15	2.01E-04	1.26E-06	38.94	0.211	40.425	0.174	0.0161	0.0005	0.0049	0.0004	0.003	3.05E-16	96.4	14.09	0.08
PASIGHAT	239-16	2.01E-04	1.26E-06	1.039	0.087	2.243	0.011	0.0138	0.0004	0.004	0.0003	0.002	3.82E-16	46.9	0.38	0.03
PASIGHAT	239-17	2.01E-04	1.26E-06	16.866	0.331	23.544	0.176	0.017	0.0009	0.0225	0.001	0.002	1.27E-16	71.7	6.11	0.12
PASIGHAT	239-18	2.01E-04	1.26E-06	27.027	0.136	30.644	0.105	0.0149	0.0004	0.0122	0.0003	0.002	7.50E-16	88.3	9.79	0.05
PASIGHAT	239-19	2.01E-04	1.26E-06	26.422	0.174	30.14	0.147	0.0149	0.0005	0.0125	0.0004	0.002	3.71E-16	87.7	9.57	0.06
PASIGHAT	239-20	2.01E-04	1.26E-06	42.433	0.179	46.69	0.166	0.0158	0.0004	0.0143	0.0003	0.002	5.10E-16	90.9	15.34	0.06
PASIGHAT	239-21	2.01E-04	1.26E-06	47.957	0.395	52.466	0.297	0.0167	0.0009	0.0152	0.001	0.002	1.35E-16	91.5	17.33	0.14
PASIGHAT	239-22	2.01E-04	1.26E-06	73.657	0.362	76.609	0.345	0.0142	0.0006	0.0099	0.0005	0.002	2.55E-16	96.2	26.55	0.13
PASIGHAT	239-23	2.01E-04	1.26E-06	70.262	0.312	72.823	0.302	0.0145	0.0005	0.0086	0.0004	0.002	3.57E-16	96.5	25.34	0.11
PASIGHAT	239-24	2.01E-04	1.26E-06	60.706	0.249	64.348	0.229	0.0146	0.0005	0.0122	0.0004	0.002	3.75E-16	94.4	21.91	0.09
PASIGHAT	239-25	2.01E-04	1.26E-06	0.872	0.307	18.653	0.102	0.0238	0.0008	0.0601	0.0011	0.002	1.88E-16	4.7	0.32	0.11
PASIGHAT	239-26	2.01E-04	1.26E-06	42.526	0.258	43.583	0.231	0.0129	0.0006	0.0035	0.0004	0.002	2.81E-16	97.6	15.38	0.09
PASIGHAT	239-27	2.01E-04	1.26E-06	25.607	0.116	27.599	0.102	0.0146	0.0003	0.0067	0.0002	0.002	6.70E-16	92.9	9.28	0.04
PASIGHAT	239-28	2.01E-04	1.26E-06	23.746	0.166	26.671	0.14	0.0149	0.0004	0.0098	0.0003	0.002	4.07E-16	89.1	8.6	0.06
PASIGHAT	239-29	2.01E-04	1.26E-06	0.84	0.075	1.729	0.008	0.0136	0.0004	0.0029	0.0003	0.002	5.08E-16	49.4	0.31	0.03
PASIGHAT	239-30	2.01E-04	1.26E-06	33.337	0.14	36.766	0.122	0.0153	0.0004	0.0115	0.0003	0.002	5.85E-16	90.7	12.07	0.05
PASIGHAT	239-31	2.01E-04	1.26E-06	44.351	0.166	44.984	0.152	0.0122	0.0004	0.0021	0.0002	0.002	5.53E-16	98.7	16.03	0.06
PASIGHAT	239-32	2.01E-04	1.26E-06	45.787	1.389	64.209	0.877	0.0229	0.0029	0.0623	0.0043	0.002	3.22E-17	71.3	16.55	0.5
PASIGHAT	239-33	2.01E-04	1.26E-06	3.697	0.341	11.122	0.072	0.0194	0.0012	0.025	0.0012	0.002	1.12E-16	33.3	1.34	0.12
PASIGHAT	239-34	2.01E-04	1.26E-06	19.602	0.342	31.465	0.162	0.0204	0.0008	0.0401	0.0011	0.002	1.54E-16	62.4	7.1	0.12
PASIGHAT	239-35	2.01E-04	1.26E-06	42.429	0.452	49.543	0.326	0.0171	0.0011	0.024	0.0012	0.002	1.18E-16	85.7	15.34	0.16
PASIGHAT	239-36	2.01E-04	1.26E-06	43.962	0.559	46.967	0.436	0.0129	0.0013	0.0101	0.0013	0.002	7.66E-17	93.7	15.89	0.2
PASIGHAT	239-37	2.01E-04	1.26E-06	48.333	0.332	49.266	0.305	0.0132	0.0006	0.0031	0.0005	0.002	2.07E-16	98.2	17.47	0.12
PASIGHAT	239-38	2.01E-04	1.26E-06	17.114	0.099	18.576	0.063	0.0149	0.0004	0.0049	0.0003	0.002	4.99E-16	92.3	6.2	0.04
PASIGHAT	239-39	2.01E-04	1.26E-06	1.007	0.114	7.694	0.028	0.017	0.0004	0.0225	0.0004	0.002	5.25E-16	13.1	0.37	0.04
PASIGHAT	239-40	2.01E-04	1.26E-06	49.509	0.198	57.753	0.187	0.0178	0.0003	0.0278	0.0003	0.002	7.41E-16	85.8	17.89	0.07

PASIGHAT	239-41	2.01E-04	1.26E-06	53.559	0.28	57.155	0.261	0.0147	0.0004	0.0121	0.0004	0.002	3.62E-16	93.8	19.35	0.1
PASIGHAT	239-47	2.01E-04	1.26E-06	28.046	0.421	31.189	0.245	0.0154	0.0013	0.0106	0.0012	0.002	8.84E-17	90	10.16	0.15
PASIGHAT	239-48	2.01E-04	1.26E-06	36.355	0.245	39.504	0.182	0.0152	0.0008	0.0106	0.0006	0.002	1.96E-16	92.1	13.15	0.09
PASIGHAT	239-49	2.01E-04	1.26E-06	30.865	0.208	30.972	0.149	0.0129	0.0005	0.0003	0.0005	0.002	4.03E-16	99.7	11.17	0.07
PASIGHAT	239-50	2.01E-04	1.26E-06	55.761	0.251	62.125	0.235	0.0159	0.0005	0.0215	0.0004	0.002	4.33E-16	89.8	20.14	0.09
PASIGHAT	239-51	2.01E-04	1.26E-06	21.245	0.157	27.245	0.104	0.017	0.0004	0.0202	0.0004	0.002	6.67E-16	78.1	7.7	0.06
PASIGHAT	239-52	2.01E-04	1.26E-06	21.345	0.2	25.918	0.108	0.016	0.0006	0.0154	0.0006	0.002	2.68E-16	82.4	7.73	0.07
PASIGHAT	239-53	2.01E-04	1.26E-06	25.286	0.177	28.303	0.122	0.0162	0.0006	0.0101	0.0005	0.002	2.72E-16	89.4	9.16	0.06
PASIGHAT	239-54	2.01E-04	1.26E-06	558.463	1.568	561.619	1.574	0.0141	0.0002	0.0106	0.0002	0.002	9.96E-16	99.4	192.19	0.51
PASIGHAT	239-55	2.01E-04	1.26E-06	54.926	0.226	60.037	0.213	0.016	0.0004	0.0172	0.0004	0.002	5.68E-16	91.5	19.84	0.08
PASIGHAT	239-56	2.01E-04	1.26E-06	49.715	0.559	59.286	0.451	0.0192	0.0013	0.0323	0.0014	0.002	9.05E-17	83.9	17.96	0.2
PASIGHAT	239-57	2.01E-04	1.26E-06	16.058	0.116	18.934	0.065	0.0158	0.0004	0.0097	0.0003	0.002	4.31E-16	84.9	5.82	0.04
PASIGHAT	239-58	2.01E-04	1.26E-06	34.137	0.21	76.096	0.182	0.0613	0.0005	0.1419	0.0006	0.006	1.37E-15	44.9	12.35	0.08
PASIGHAT	239-59	2.01E-04	1.26E-06	1.37	0.158	4.763	0.024	0.035	0.0007	0.0114	0.0005	0.006	3.08E-16	28.9	0.5	0.06
PASIGHAT	239-60	2.01E-04	1.26E-06	24.124	0.276	28.678	0.163	0.0155	0.0009	0.0153	0.0008	0.002	1.32E-16	84.2	8.74	0.1
PASIGHAT	239-61	2.01E-04	1.26E-06	75.869	0.4	83.677	0.364	0.0165	0.0006	0.0263	0.0007	0.002	3.27E-16	90.7	27.34	0.14
PASIGHAT	239-62	2.01E-04	1.26E-06	27.2	0.291	34.874	0.166	0.018	0.0008	0.0259	0.0009	0.002	2.42E-16	78.1	9.85	0.11
PASIGHAT	239-63	2.01E-04	1.26E-06	71.371	0.305	84.45	0.301	0.0207	0.0005	0.0442	0.0005	0.002	4.30E-16	84.5	25.73	0.11
PASIGHAT	239-64	2.01E-04	1.26E-06	26.047	0.191	33.039	0.139	0.0179	0.0005	0.0236	0.0005	0.002	4.24E-16	78.9	9.43	0.07
PASIGHAT	239-65	2.01E-04	1.26E-06	29.889	0.249	32.827	0.17	0.014	0.0008	0.0099	0.0007	0.002	1.92E-16	91.1	10.82	0.09
PASIGHAT	239-66	2.01E-04	1.26E-06	14.457	0.35	39.493	0.211	0.0297	0.001	0.0847	0.0012	0.002	1.88E-16	36.6	5.24	0.13
PASIGHAT	239-67	2.01E-04	1.26E-06	1.373	0.176	7.318	0.039	0.0183	0.0007	0.02	0.0006	0.002	2.27E-16	18.8	0.5	0.06
PASIGHAT	239-68	2.01E-04	1.26E-06	351.222	1.515	352.815	1.516	0.0124	0.0004	0.0053	0.0004	0.002	3.43E-16	99.6	123.24	0.51
PASIGHAT	239-69	2.01E-04	1.26E-06	48.12	1.189	73.458	0.941	0.0264	0.0025	0.0857	0.0036	0.002	3.65E-17	65.5	17.39	0.43
PASIGHAT	239-70	2.01E-04	1.26E-06	1.143	0.177	2.882	0.016	0.0153	0.0006	0.0058	0.0006	0.002	2.71E-16	40	0.41	0.06
PASIGHAT	239-71	2.01E-04	1.26E-06	369.376	1.753	372.688	1.759	0.0145	0.0005	0.0111	0.0005	0.002	2.79E-16	99.1	129.38	0.59
PASIGHAT	239-72	2.01E-04	1.26E-06	195.022	0.619	200.347	0.621	0.0161	0.0003	0.0179	0.0003	0.002	8.98E-16	97.4	69.47	0.22
PASIGHAT	239-73	2.01E-04	1.26E-06	18.875	0.133	20.67	0.083	0.0149	0.0005	0.006	0.0004	0.002	3.79E-16	91.4	6.84	0.05
PASIGHAT	239-74	2.01E-04	1.26E-06	0.867	0.105	5.325	0.019	0.0162	0.0004	0.015	0.0004	0.002	4.63E-16	16.4	0.31	0.04
PASIGHAT	239-75	2.01E-04	1.26E-06	0.926	0.138	8.15	0.033	0.018	0.0005	0.0244	0.0005	0.002	3.68E-16	11.4	0.34	0.05
PASIGHAT	239-76	2.01E-04	1.26E-06	75.265	0.252	94.165	0.256	0.0243	0.0004	0.0639	0.0004	0.002	1.12E-15	80	27.13	0.09
PASIGHAT	239-77	2.01E-04	1.26E-06	36.279	0.168	49.485	0.149	0.0216	0.0004	0.0446	0.0004	0.002	8.99E-16	73.4	13.13	0.06
PASIGHAT	239-78	2.01E-04	1.26E-06	25.815	0.389	49.736	0.227	0.028	0.0008	0.0809	0.0013	0.002	1.79E-16	51.9	9.35	0.14
PASIGHAT	239-79	2.01E-04	1.26E-06	177.474	0.89	205.183	0.919	0.063	0.0011	0.0937	0.0012	0.008	2.49E-16	86.5	63.32	0.31
PASIGHAT	239-80	2.01E-04	1.26E-06	47.968	0.578	54.538	0.423	0.0171	0.0013	0.0222	0.0015	0.002	9.58E-17	88	17.34	0.21
PASIGHAT	239-81	2.01E-04	1.26E-06	48.279	0.495	52.36	0.395	0.0169	0.0011	0.0137	0.0011	0.002	9.53E-17	92.3	17.45	0.18
PASIGHAT	239-82	2.01E-04	1.26E-06	36.783	0.377	38.172	0.267	0.0155	0.001	0.0046	0.0009	0.002	1.11E-16	96.4	13.31	0.14
PASIGHAT	239-83	2.01E-04	1.26E-06	68.031	1.146	110.591	1.096	0.0409	0.002	0.144	0.0034	0.002	5.98E-17	61.5	24.54	0.41

Blank corrections

Analyses from 3/31/11 to 5/3/11					Air shot 40Ar/36Ar correction range	
Mean 4 minute extraction system blanks (moles STP)					Min (1σ)	Max (1σ)
40Ar	39Ar	38Ar	37Ar	36Ar		
1.31×10^{-16}	3.81×10^{-18}	3.90×10^{-19}	2.95×10^{-18}	1.35×10^{-18}	290.3 ± 1.0	302.3 ± 2.0
Analyses from 11/7/11 to 11/15/11						
Mean 4 minute extraction system blanks (moles STP)					Min (1σ)	Max (1σ)
40Ar	39Ar	38Ar	37Ar	36Ar		
1.11×10^{-16}	4.97×10^{-18}	2.24×10^{-19}	2.51×10^{-18}	9.05×10^{-19}	304.0 ± 1.2	314.4 ± 1.4
Analyses from 9/14/13 to 10/17/13						
Mean 4 minute extraction system blanks (moles STP)					Min (1σ)	Max (1σ)
40Ar	39Ar	38Ar	37Ar	36Ar		
1.49×10^{-16}	2.25×10^{-18}	1.85×10^{-19}	3.15×10^{-18}	8.32×10^{-19}	268.6 ± 1.5	274.7 ± 1.3

Nuclear interference reactions

McMaster 3		
40Ar/39Ar from K (1σ)	39Ar/37Ar from Ca (1σ)	36Ar/37Ar from Ca (1σ)
0.027945 ± 0.0014354	> 6 mo. Wait, Ca decayed	> 6 mo. Wait, Ca decayed
McMaster 11		
40Ar/39Ar from K (1σ)	39Ar/37Ar from Ca (1σ)	36Ar/37Ar from Ca (1σ)
0.0156325 ± 0.005312	0.000632 ± 0.0000133	$0.0002863 \pm 7.25528E-6$

4.10.6 Model parameters

TABLE A6. One dimensional cooling model parameters**Constants**

Thermal diffusivity (km ² /Myr)	25
Temperature at base of model (deg. C)	875
Temperature at top of model (deg. C)	20
Heat production rate (C/Myr)	7.5
Time step (Myr)	0.2
Length of Model run (Myr)	50

Variables

Time of stepwise change in exhumation rate (t; in Ma)	1 to 15
Increment of t (Ma)	0.5
Final exhumation rate (E _f ; km/Myr)	5 to 10
Increment of E _f (km/Myr)	1
Factor change in exhumation rate (xE)	1 to 20
Increment of change in xE	0.5

CHAPTER 5. Conclusions

5.0 Summary and suggestions for future work

5.0.1 Chapter 2

From the second chapter, I learned that Neogene Siwalik foreland basin units proximal to the Brahmaputra River confluence record a mixed sedimentary provenance from Himalayan sources and Tibetan sources west of the Namche Barwa massif. I interpret this record to indicate that the river has been connected through the eastern syntaxis to Tibetan source rocks since deposition of these units began in the Early or Middle Miocene. While this data do not explicitly exclude the alternative hypothesis that a high-elevation ancestral Yarlung river was captured by a headward eroding Siang River (e.g., Clark et al., 2004), such an event must have occurred prior to deposition of the Lower Siwalik in the Early Miocene and thus is not directly related to increased exhumation of the region in the Pleistocene and Late Pliocene (e.g., Zeitler et al., 2001).

To explain observations of Tibetan zircons in Burmese sedimentary basins prior to this time, I speculate that an additional northern river followed large strike slip fault zones (like the present Yigong, Parlung and Lohit rivers) to join the ancestral Irrawaddy River system. Disconnection from the Irrawaddy may have occurred around ~18 Ma (Robinson et al. 2014), after which this river drained through the Lohit into the foreland basin. Ultimately northward expansion of the Namche Barwa massif led to the capture and reversal of the Parlung River (e.g., Seward and Burg, 2008) greatly expanding the drainage area immediately upstream of the Tsangpo Gorge.

The timing of reversal of the Parlung river remains largely unconstrained. However,

I propose that either glacial lowering of divides between the ancestral Yarlung and a north-draining tributary to the Yigong-Parlung-Lohit River, or spill over of a dammed lake on the Parlung River (perhaps from expansion of the Lhagu Glacier near Renwu, China, see Kingdon Ward, 1934) may have first integrated these rivers in the Quaternary. While the detrital zircons from the Upper Siwalik may be consistent with this capture, detailed provenance and detrital thermochronology of Pleistocene terraces near the Siang confluence should help elucidate the Quaternary record of mountain exhumation.

While our provenance data do not explicitly exclude an alternative connection between the Subansiri River and the upper $\sim 2/3$ of the present Yarlung River drainage (Cina et al. 2009), this explanation is not required to explain the presence of Gangdese-age zircons in ancestral Brahmaputra deposits in Siwalik units downstream of the Subansiri River. The zircons observed by Cina et al. (2009) near and Bhalukpong, Itanagar may simply have been derived from an integrated Yarlung-Siang-Brahmaputra River like those observed upstream of the Subansiri River confluence near Likabali and Pasighat. Moreover, if the Subansiri River had a substantially greater drainage area at some time in the Miocene I would expect the correspondingly increased erosion to have focused uplift within the Subansiri valley instead of the Tsangpo Gorge. It may be possible that the morphological record of this erosion (i.e., a knickpoint) has disappeared if the river has since readjusted to more recent tectonic uplift, however I would still expect to observe locally increased metamorphic grade, local anatexis or a similar “bullseye” of relatively young cooling ages around the connection point in the upper Subansiri River, as seen in the Tsangpo gorge. Preliminary detrital sampling within the Subansiri drainage (like that of Stewart et al., 2008) might further evaluate this

hypothesis directly.

5.0.2 Chapter 3

A well preserved record of moraine and landslide debris in the immediate headwaters to the Tsangpo Gorge are acknowledged to have dammed rivers entering the gorge in the Quaternary (Montgomery et al., 2004; Korup and Montgomery, 2008). In fact, recent examples of such damming occurred on the Yigong River in ~1900 and 2000 (Evans and Delaney, 2011). Such damming may aggraded sediment upstream of the gorge, inhibitingupstream migration of the knickpoint, and focusing erosion within the gorge during the Pleistocene and Late Pliocene.

In the third chapter, I learned that upstream dams episodically (and potentially catastrophically) failed, draining enormous lakes through the Tsangpo Gorge. These megafloods may have generated substantial channel and hillslope erosion by transporting debris from the gorge downstream along the Siang River. I interpret enigmatic sedimentary units up to ~150 m above the modern Siang River as slackwater deposition from these Quaternary megafloods. Detrital zircon U-Pb geochronology from flood deposit samples confirm a mixed Himalayan and Tibetan provenance, and comparison with analyses of modern sediment and known flood deposits from the 2000 Yigong River event demonstrate that megaflood deposits are considerably more enriched in both ~500 Ma Himalayan zircons and Neogene anatectic zircons uniquely attributable to the Namche Barwa massif. I interpret this enrichment to indicate that megafloods preferentially scoured and transported material from massif bedrock within the Tsangpo Gorge, potentially by inducing contemporaneous landsliding on gorge adjacent hillslopes.

I exclude the alternative interpretation of these units as accumulation of alluvium behind landslide dams (c.f., Oiumet et al., 2007) along the Siang River based on the height of these deposits above the river, the relationship of deposits to existing topography, and sedimentological comparison with modern alluvium. Modern alluvium is considerably coarser, clast-supported gravel-cobble conglomerate while flood deposits are typically medium to fine laminated sand. Additionally, the more recent identification of deposits with similar characteristics and elevation in a subsequent field season apparently correlate with hydrodynamically favorable conditions for slackwater depositions (e.g., protected reaches of the river).

Our calculations of shear stresses experienced in the gorge following a catastrophic megaflood are admittedly simplistic and intended to provide a first order estimate of floodwater competence, demonstrating that the enormous discharge resulting from a dam-burst flood could effectively transport any landslide debris out of the gorge. Additional, more detailed hydrodynamic modeling of catastrophic flooding, perhaps calibrated with observations from the 2000 Yigong River event could significantly improve estimation of the erosional impact of a single flood event and the capability of floods to deposit sediment up to ~150 meters above the downstream river channel. Furthermore, single grain Hf analyses, bulk Nd analyses, or complimentary zircon fission-track dating of <300 Ma zircons from these deposits might better constrain source region provenance within the Tsangpo gorge specifically.

5.0.3 Chapter 4

In the fourth chapter I revisit Siwalik foreland basin units to extend the exhumation

history of the eastern Himalayan syntaxis into the Late Miocene. I complement the existing detrital zircon U-Pb geochronology with detailed stratigraphic measurements, fission-track analyses coupled to previously U-Pb dated detrital zircons and new muscovite $^{40}\text{Ar}/^{39}\text{Ar}$ thermochronology. I combined lithostratigraphic, magnetostratigraphic and detrital thermochronologic observations to correlate a Siwalik section proximal to the Brahmaputra River confluence to a well dated section along the Kameng River (Chirouze et al., 2012). Thermochronological analyses provide valuable insight to the exhumation history of the syntaxial source area as thermochronologic lag time may indicate attainment of an exhumational steady state (e.g., Bernet and Garver, 2005). In the second chapter I determined the sedimentary provenance of these units to represent deposition from the ancestral Brahmaputra River connected to Tibetan source rocks through the eastern Himalayan syntaxis, and I assume that the youngest cooling ages from detrital thermochronology should reflect rapid cooling of the Namche Barwa massif, if rapid exhumation had begun by the depositional age of these units. In fact, the youngest cooling ages are within the range uniquely attributed to the Namche Barwa massif today, demonstrating that a contribution from a rapidly exhuming source region has been maintained since the Late Miocene.

I interpret the up section decrease in detrital lag time to indicate that exhumation rates have been increasing in the syntaxial source area since the Late Miocene. Using a simple one-dimensional thermal model, I quantitatively constrain the time and magnitude of this increase, assuming the end-member scenario of a simple piecewise change in exhumation rate. Our observations are best matched to models employing a ~5-10 fold increase in exhumation rate between 5-7 Ma.

Lag time estimation is strongly dependent on accurate determination of depositional age. Unfortunately, our limited magnetostratigraphy in this chapter only permits a tentative correlation from our proximal section to a previously dated section along the Kameng River (Chirouze et al., 2012) and not direct correlation to the Geomagnetic Polarity Reversal Timescale. While I do not anticipate further paleomagnetic analyses to alter the conclusions of this work, additional analyses (potentially paired with detailed biostratigraphy) would permit more robust interpretation of the data, and potentially provide additional, independent constraints on the accumulation rate of these units.

5.1 Synthesis of results

This thesis approached three research objectives: to determine when a river initially drained through the eastern Himalayan syntaxis, to assess the impact of Quaternary glacial damming of drainages upstream of the Tsangpo gorge, and to extend the exhumation history of the syntaxis into the Late Miocene. In the previous section, I summarized the conclusions of the chapters that address each of these objectives with an emphasis on where future research can make useful additions. In total, this research demonstrates the potential for and persistence of rapid exhumation within the eastern Himalayan syntaxis.

Our results favor a model by which the eastern Himalayan syntaxis has been progressively denuded by a large, antecedent river system that was capable of sustaining elevated surface erosion rates despite episodic damming in the Quaternary. Simpson (2006) emphasized the importance of sustained rapid exhumation concurrent with tectonic uplift for the development of a positive thermo-mechanical feedback between surface erosion and rock uplift. I propose that an integrated Yarlung-Siang-Brahmaputra

River provided the sustained rapid exhumation necessary to initiate such a feedback in the eastern Himalayan syntaxis in the Late Cenozoic, potentially since the Late Miocene. In particular, our observations of decreasing detrital lag time in Siwalik units proximal to the Brahmaputra confluence indicate that exhumation rates have increased within the syntaxial source region since the Late Miocene, a prediction of this positive feedback (Zeitler et al., 2001; Koons et al., 2013).

I emphasize that it is the antecedent drainage of a large river system that may play the key role in developing this positive feedback during Himalayan uplift by initially maintaining rapid surface erosion coincident with early rock uplift (Simpson, 2006). While transverse drainages develop in response to tectonic uplift, a relatively large antecedent river may match rates of rock uplift from the onset of uplift, focusing erosion to a specific portion of the orogen that may ultimately lead to the development of a localized thermo-mechanical feedback between surface erosion and rock uplift.

In Chapter 4 I compared similar lag time studies from across the Himalaya. This exercise demonstrated that a history of accelerating exhumation is only observed in foreland basin units proximal to the syntaxes (Cerveny et al., 1988; Bernet and Garver, 2005; and results from chapter 4). Lag time studies from Siwalik units deposited by transverse rivers along the main Himalayan front in Nepal (Bernet et al., 2006; Chirouze et al., 2012b), and the western (Jain et al., 2009) and eastern Indian Himalaya (Chirouze et al., 2013b) all indicate relatively constant, or slightly decelerating exhumation histories. If the constant exhumation across the Main Himalayan indicates attainment of an exhumational steady state (Willet and Brandon, 2002), then the acceleration exhumation of the syntaxes may alternatively be evidence of the development of thermo-mechanical

feedbacks in the syntaxes (Zeitler et al., 2001).

Subsequent rock uplift will locally steepen river channels (Whipple and Tucker, 1999) and increase topographic relief until relief approaches an upper limit constrained by rock strength and valley spacing (Montgomery and Brandon, 2002). Both local channel steepening (e.g., Finlayson, 2002; Finnegan et al., 2008) and steep topographic relief (Larsen and Montgomery, 2012) are presently observed within the eastern Himalayan syntaxis potentially indicating that the regional is near the maximum limit of topographic relief. If rock uplift of the region has been increasing since the Late Miocene, such steep topography may have been sustained over a similarly prolonged timescale.

Moreover, increasing rock exhumation may have correspondingly increased the sediment discharge from the eastern Himalayan syntaxis, biasing the downstream sedimentary record toward this region. Presently, nearly half of detrital zircons carried into the foreland basin are sourced from this ~3% of the Yarlung-Siang-Brahmaputra River drainage area (e.g., Stewart et al., 2008; Enklemann et al., 2011) and I might expect a similar biasing as long as rapid exhumation has been present in the syntaxis. Distal sedimentary archives from the Bengal fan record relatively short lag times after ~9 Ma (Copeland and Harrison, 1990) that are not also observed from potential sources along the Main Himalayan front (e.g., White et al., 2002; Szulc et al., 2006). Alternatively, I propose that such young lag times could reflect preferential exhumation from the eastern Himalayan syntaxis.

5.2 Loose ends

The eastern Himalayan foreland is ripe for further research. In contrast to the

western and central Himalaya, there are remarkably few published sections with unfortunately few constraints on depositional history. This thesis is both a contribution to this body of work and an aspiration for future contributions. While conducting this work, I explored multiple avenues for alternative projects that, for a variety of reasons remain unresolved. Here I briefly outline several of those projects.

This research has demonstrated the value of coupled geochronological and thermochronological single grain analyses in the interpretation of detrital lag time. Complimentary detrital geo-thermochronology of Lower Siwalik units along the Siji River, or in nearby tributaries with potentially better exposure (recent road expansions and dam construction in Arunachal Pradesh have provided new and interesting road cuts) would be a valuable addition to the research presented in the second and fourth chapters, potentially extending the eastern syntaxial exhumation record through the Middle Miocene. Furthermore, detailed measurement and sampling of thick alluvial terraces with potential intercalated flood deposits near the Siang River confluence (Srivastava et al., 2008) would expand our understanding of Quaternary megafloods, documented and discussed in the third chapter.

While this research focused on the application of specific provenance indicators (e.g., U-Pb age), additional isotopic measurements (Hf and Nd specifically) may also be valuable indicators of sedimentary provenance that could additionally permit differentiation between Gangdese and Bomi-Chayu or Northern Plutonic provinces at the eastern and northern margins of the syntaxis and clarify our interpretation for Late Miocene drainage patterns in the second chapter. Complimentary modal analysis of framework and heavy mineral suites would also be a useful addition to this work, though

our preliminary work indicates that this approach is less sensitive than in-situ single-grain analyses.

Constraining the depositional ages of eastern Siwalik units has proven to be challenging, but not impossible with a significant number of analyses and high-resolution temperature steps during thermal demagnetization. Though it will likely require a considerable amount of additional work, detailed magnetostratigraphy (ideally coupled with isotopic analysis like Chirouze et al., 2012 or biostratigraphy) would be an invaluable contribution to the interpretation of these units.

There is surprisingly little published work from within the Lohit River drainage, despite a substantial sediment load and at least four large thrust faults within ~50 km of the mountain front. Our reconnaissance of this portion of the Lohit River demonstrates the significant potential for rapid erosion near the mountain front, which could potentially be investigated with detrital sampling across this reach, as in the approach of Stewart et al. (2008).

5.3 A note on persistence

I end with a brief note on the importance of persistence in scientific work. Some unfortunate complications may have dramatically hindered the completion of this work (e.g., injury, illness, threat, theft, politics and bureaucracy) were it not for the dedication and persistence of the researchers involved. I take from these collective experiences that good scientific research may sometimes be only achieved through a thoughtful, diligent, and persistent approach. As I mentioned, this thesis is both a contribution to a broader understanding of the eastern Himalayan syntaxis as well as an aspiration for continued

work in the future. To those future researchers, I wish to convey the value of persistent study, for without it I would not have been successful in this work. Good luck.

5.4 References

- Bernet, M., Garver, J.I., 2005. Fission-track analysis of detrital zircon, in Reiners, P.W., Ehlers, T.A., *Reviews in Mineralogy and Geochemistry, Low-Temperature Thermochronology: Techniques, Interpretations and Applications*, 58, 205-238.
- Bernet, M., van der Beek, P., Pik, R., Huyghe, P., Mugnier, J-L., Labrin, E., Szulc, A., 2006. Miocene to recent exhumation of the central Himalaya determined from combined detrital zircon fission-track and U/Pb analysis of Siwalik sediments, western Nepal. *Basin Res.* 18, 393-412.
- Brandon, M.T., 1992. Decomposition of fission-track grain-age distributions. *Am. J. Sci.*, 292, 535-564.
- Cervený, P.F., Naeser, N.D., Zeitler, P.K., Naeser, C.W., Johnson, N.M., 1988. History of uplift and relief of the Himalaya during the past 18 million years: Evidence from fission-track ages of detrital zircons from sandstones of the Siwalik Group, in Kleinspehn, K.L., Paola, C. (eds). *New perspectives in basin analysis*, Springer, New York. 43-61.
- Chirouze, F., Dupont-Nivet, G., Huyghe, P., van der Beek, P., Chakraborti, T., Bernet, M., Erens, V., 2012a. Magnetostratigraphy of the Neogene Siwalik Group of far eastern Himalaya, Kameng section, Arunachal Pradesh, India. *J. Asian Earth Sci.* 44, 117-135.

- Chirouze, F., Bernet, M., Huyghe, P., Erens, V., Fupont-Nivet, G., Senebier, F., 2012b. Detrital thermochronology and sediment petrology of the middle Siwaliks along the Muksar Khola section in eastern Nepal. *J. Asian Earth Sci.*, 44, 94-106.
- Chirouze, F., Huyghe, P., van der Beek, P., Chauvel, C., Chakraborty, T., Dupont-Nivet, G., Bernet, M., 2013b. Tectonics, exhumation and drainage evolution of the eastern Himalaya since 13 Ma from detrital geochemistry and thermochronology, Kameng River section, Arunachal Pradesh. *Geol. Soc. Am. Bull.* 125, 523-538.
- Cina, S.E., Yin, A., Grove, M., Dubey, C.S., Shukla, D.P., Lovera, O.M., Kelty, T.K., Gehrels, G.E., Foster, D.A., 2009. Gangdese arc detritus within the eastern Himalayan Neogene foreland basin: Implications for the Neogene evolution of the Yalu-Brahmaputra River system. *Earth Planet. Sci. Lett.* 285, 150-162.
- Clark, M.K., Schoenbohm, L.M., Royden, L.H., Whipple, K.X., Burchfiel, B.C., Zhang, X., Tang, W., Wang, E., Chen, L., 2004. Surface uplift, tectonics and erosion of eastern Tibet from large-scale drainage patterns. *Tectonics*, v. 23, TC1006.
- Copeland, P., Harrison, T.M., 1990. Episodic rapid uplift in the Himalaya revealed by $^{40}\text{Ar}/^{39}\text{Ar}$ analysis of detrital K-feldspar and muscovite, Bengal fan. *Geology*. 18, 4, 354-357.
- Enkelmann, E., Ehlers, T.A., Zeitler, P.K., Hallet, B., 2011. Denudation of the Namche Barwa antiform, eastern Himalaya. *Earth and Planet. Sci. Lett.* 307, 323-333.
- Evans, S., and Delaney, K., 2011. Characterization of the 2000 Yigong Zangbo River (Tibet) landslide dam and impoundment by remote sensing. In *Natural and Artificial Rockslide Dams*, S.G. Evans et al., (eds.), Springer-Verlag, Berlin, Heidelberg, p. 543–559.

- Finlayson, D.P., Montgomery, D.R., Hallet, B., 2002. Spatial coincidence of rapid inferred erosion with young metamorphic massifs in the Himalayas. *Geology*. 30, 219-222.
- Finnegan, N.J., Hallet, B., Montgomery, D.R., Zeitler, P.K., Stone, J.O., Anders, A.M., Liu, Y., 2008. Coupling of rock uplift and river incision in the Namche Barwa–Gyala Peri massif, Tibet, China. *Geol. Soc. Am. Bull.* 120, 142–155.
- Jain, A.K., Lal, N., Sulemani, B., Awasthi, A.K., Singh, S., Kumar, R., Kumar, D., 2009. Detrital-zircon fission-track ages from the Lower Cenozoic sediments, NW Himalayan foreland basin: Clues for exhumation and denudation of the Himalaya during the India-Asia collision. *Geol. Soc. Am. Bull.*, 121, 519-535.
- Kingdon Ward, F., 1934. The Himalaya east of the Tsangpo. *Geograph. J.*, 84, 369-394.
- Koons, P.O., Zeitler, P.K., Hallet, B., 2013. Tectonic aneurysms and mountain building, in: *Treatise on Geomorphology*. Owen, L.A., (ed.), 5, Elsevier, Amsterdam, 32 pp.
- Korup, O., Montgomery, D.R., 2008. Tibetan plateau river incision inhibited by glacial stabilization of the Tsangpo gorge. *Nature*. 455, 786-789.
- Larsen, I.J., Montgomery, D.R., 2012. Landslide erosion coupled to tectonics and river incision. *Nature Geos.* 5, 468-473.
- Montgomery, D.R., Brandon, M.T., 2002, Topographic controls on erosion rates in tectonically active mountain ranges. *Earth and Planet. Sci. Lett.* 201, 481-489.
- Montgomery, D.R., Hallet, B., Yuping, L., Finnegan, N., Anders, A., Gillespie, A., Greenberg, H.M., 2004. Evidence for Holocene megafloods down the Tsangpo River gorge, southeastern Tibet. *Quat. Res.* 62, 201-207.

- Najman, Y.M.R., Pringle, M.S., Johnson, M.R.W., Robertson, A.H.F., Wijbrans, J.R.,
Laser $^{40}\text{Ar}/^{39}\text{Ar}$ dating of single detrital muscovite grains from early foreland-
basin sedimentary deposits in India: Implications for early Himalayan evolution.
Nature, 25, 535-538.
- Ouimet, W., Whipple, K., Royden, L., Sun, Z., Chen, Z., 2007. The influence of large
landslides on river incision in a transient landscape: Eastern margin of the Tibetan
Plateau (Sichuan, China). *Geol. Soc. Am. Bull.* 119, 1462-1476.
- Robinson, R.A.J., Breznia, C.A., Parrish, R.R., Horstwood, M.S.A., Oo, N.W., Bird, M.I.,
Thein, M., Walters, A.S., Oliver, G.J.H., Zaw, K., 2014. Large rivers and orogens:
The evolution of the Yarlung Tsangpo-Irrawaddy system and the eastern
Himalayan syntaxis. *Gondwana Res.*, 26, 112-121.
- Seward, D., Burg, J-P., 2008. Growth of the Namche Barwa Syntaxis and associated
evolution of the Tsangpo Gorge: Constraints from structural and
thermochronological data. *Tectonophys.* 451, 282–289.
- Simpson, G., 2006. Influence of erosion and deposition on deformation in fold belts, in
Willet, S.D., Hovius, N., Brandon, M.T., and Fisher, D., (eds.), *Tectonics,
Climate and Landscape Evolution: Geol. Soc. Am. Special Paper 398*, p. 267-281.
- Stewart, R.J., Hallet, B., Zeitler, P.K., Malloy, M.A., Allen, C.M., Trippett, D., 2008.
Brahmaputra sediment flux dominated by highly localized rapid erosion from the
easternmost Himalaya. *Geology*. 36, 711-714.
- Srivastava, P., Bhakuni, S.S., Luirei, K., Misra, D.K., 2008. Morpho-sedimentary record
at the Brahmaputra River exit, NE Himalaya: climate-tectonic interplay during the
Late Pleistocene-Holocene. *J. Quat. Sci.*, 24, 175-188.

- Szulc, A.G., Najman, Y., Sinclair, H.D., Pringle, M., Bickle, M., Chapman, H., Garzanti, E., Ando, S., Huyghe, P., Mugnier, J-L., Ojha, T., DeCelles, P., 2006. Tectonic evolution of the Himalaya constrained by detrital ^{40}Ar - ^{39}Ar , Sm-Nd and petrographic data from the Siwalik foreland basin succession, SW Nepal. *Basin Res.*, 18, 375-391.
- Vermeesch, P., 2012. On the visualisation of detrital age distributions. *Chem. Geol.* 312-313, 190-194.
- Whipple, K.X., Tucker, G.E., 1999. Dynamics of the stream-power river incision model: Implications for height limits of mountain ranges, landscape response timescales, and research needs. *J. Geophys. Res.* 104, 17661-17674.
- White, N.M., Pringle, M., Garzanti, E., Bickle, M., Najman, Y., Chapman, H., Friend, P., 2002. Constraints on the exhumation and erosion of the High Himalayan Slab, NW India, from foreland basin deposits. *Earth and Planet. Sci. Lett.* 195, 29-44.
- Willet, S., Brandon, M.T., 2002. On steady states in mountain belts. *Geology.* 30, 175-178.
- Zeitler, P.K., Meltzer, A.S., Koons, P.O., Craw, D., Hallet, B., Chamberlain, C.P., Kidd, W.S.F., Park, S.K., Seeber, L., Bishop, M., Shroder, J., 2001. Erosion, Himalayan geodynamics, and the geomorphology of metamorphism, *GSA Today*, 11(1), 4-9.